Proceedings
of the
8th American Water Jet Conference

Volume II

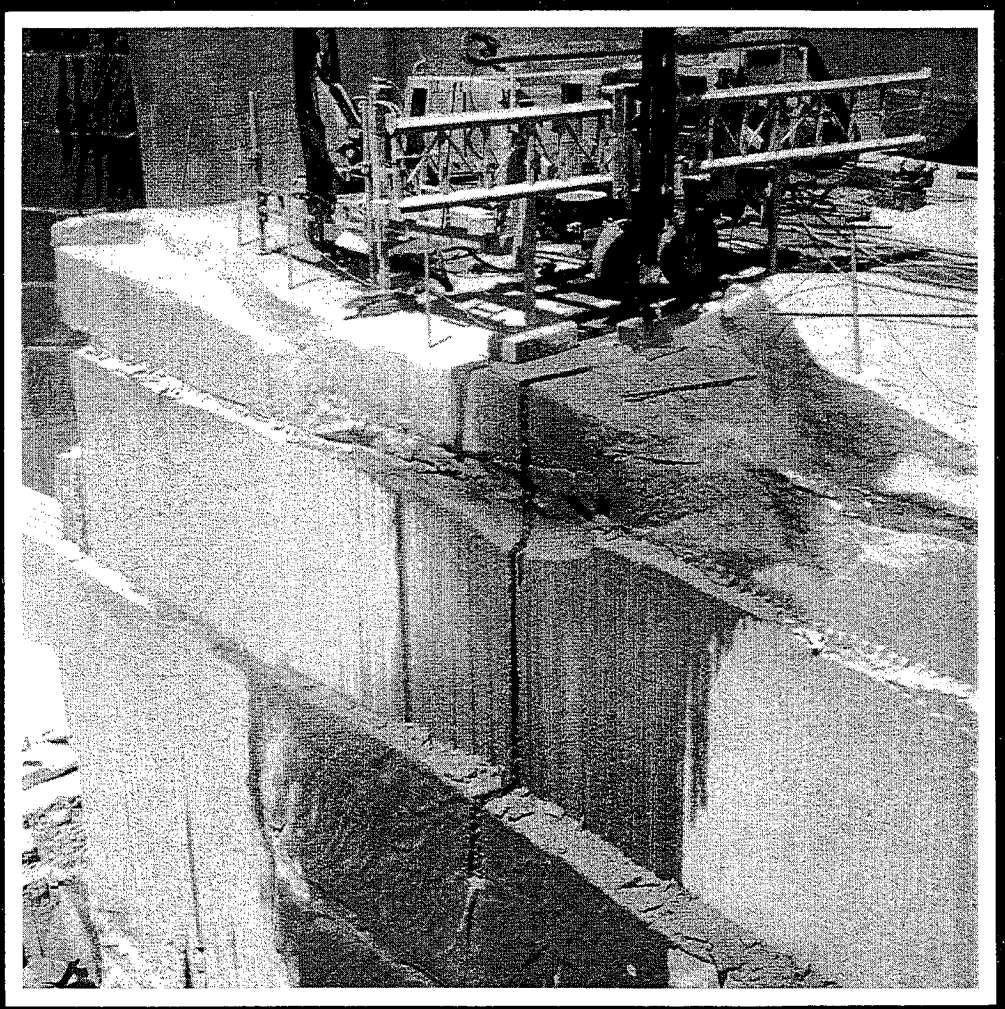

August 26-29, 1995

Houston, Texas

Edited by Thomas J. Labus

Proceedings of the 8th American Water Jet Conference

Volume II

August 26-29, 1995
Houston, Texas

Edited by

Thomas Labus

Published by the

Water Jet Technology Association

Cover photograph: Slot cutting in a granite quarry using a water jet. Photograph reprinted courtesy of Ned Jet Cutting Systems, Inc., Worcester, Massachusetts.

Proceedings Of The 8th American Water Jet Conference

Published by the

Water Jet Technology Association
818 Olive Street, Suite 918
St. Louis, MO 63101-1598 USA

ISBN: **1-880342-06-5** (Volume II)
1-880342-07-3 (2 Volume Set)

Printed in the United States of America
August 1995

Copies obtainable from:

Water Jet Technology Association
818 Olive Street, Suite 918
St. Louis, MO 63101-1598 USA
Telephone: (314)241-1445
Fax: (314)241-1449

Price: $150 (payable in advance)

Forward

Read on if you wish to learn the present state of the art of water jet technology. This volume contains the considered thoughts of some of the leading authorities in the field as expressed at the 8th American Water Jet Conference. These authors assembled in Houston, Texas in August of 1995 to share their thoughts and thereby gain new insights on how water jet technology can be advanced even further.

The Water Jet Technology Association offers this volume, the eighth in a series of *Proceedings of American Water Jet Conferences*, as evidence that water jet technology is contributing significantly to man's ongoing and comprehensive effort to enlarge human power and safeguard human welfare.

George A. Savanick, Ph.D.
President, Water Jet Technology Association

In 1983, when the Water Jet Technology Association (WJTA) was just formed, there were only few charter members. In 1989, when I became the vice president of the Association, the membership was 327 (including corporate members). Now, when I am leaving WJTA as chairman of the board, the membership stands at 535, an indication of truly remarkable growth and interest in the varied applications of ***Fluid Jet Technology***. Similar trends can be noticed in other major associations/societies in the world, for example, the Water Jet Technology Society of Japan. The fact that the International Society of Water Jet Technology (ISWJT) has recently become a Federation of National Associations/Societies in the world confirms that there is a genuine interest for international understanding and collaboration for enhancing the spread of the ***Technology for beneficial uses***.

Yes, we should all be proud. Through our persistent endeavors, we have made noteworthy contributions to advance the ***Technology*** which, in turn, has made the world a somewhat better place to live by increasing productivity and abating pollution that occurs in many industrial processes.

I am certain you will learn a great deal from your participation at this Conference. You will make new acquaintances and friends. You will continue to improve the ***Technology*** to address serious problems (for instance, safe disposal of nuclear waste) of the 21st century. I have friends all over the world and I sincerely thank each and every one of them for giving me the opportunity to serve the ***Fluid Jet Community*** in a modest way. I wish you all the best in your future endeavors.

Mohan M. Vijay, Ph.D.
Chairman of the Board, Water Jet Technology Association

Organizing Committee

Mr. George Rankin (Chairman)
Aqua-Dyne, Inc.
Houston, Texas

Dr. Andrew F. Conn
Conn Consulting, Inc.
Baltimore, Maryland

Dr. Mohamed Hashish
QUEST Integrated, Inc.
Kent, Washington

Dr. Thomas Kim
University of Rhode Island
Kingston, Rhode Island

Prof. Thomas Labus
University of Wisconsin
Fontana, Wisconsin

Mr. William Lees
Parker Hannifin Corporation
Houston, Texas

Mr. Richard Paseman
American Powerlance
Houston, Texas

Mr. Joe Phillips
Phillips Machining And Repair Service
Federal Way, Washington

Dr. George Savanick
Bureau Of Mines
Minneapolis, Minnesota

Mr. Forrest Shook
NLB Corporation
Wixom, Michigan

Dr. David Summers
University of Missouri-Rolla
Rolla, Missouri

Dr. Mohan Vijay
National Research Council Of Canada
Ottawa, Ontario

Mr. John Wolgamott
StoneAge, Inc.
Durango, Colorado

Mr. Bruce Wood
MPW Industrial Services Inc.
Hebron, Ohio

International Advisors

Australia:	Howard Mendel
Austria:	Franz H. Trieb
Canada:	Daniel Bernard
China:	Shougen Hu, Ph.D.
Czech Republic:	Jaroslav Vasek, Ph.D.
England:	Edward J. Bloomfield
France:	Claudie Merle, Ph.D.
Germany:	H. Louis, Ph.D.
Hungary:	Elemer Debreczeni, Ph.D.
India:	Minoo F. Engineer
Italy:	Roberto Groppetti, Ph.D.
Japan:	Ryoji Kobayashi, Ph.D.
Korea:	W.H. Kang
Norway:	Ola M. Vestavik, Ph.D.
Poland:	Leszek Jarno
Portugal:	Rosa Maria M. Miranda
Romania:	Andrei Magyari, Ph.D.
Republic Of Singapore:	Reginald B.H.Tan, Ph.D.
South Africa:	Hendrik Kusten, Ph.D.
Sweden:	Claes Magnusson, Ph.D.
Taiwan:	Bill Wang
Ukraine:	G. Atanov, Ph.D.

Preface

Fluid jet technology continues to be a dynamic growth area in the 1990s. The papers in these *Proceedings* provide insight into the areas that are the future of the technology. New types of fluid jets and new uses for the standard jets continue to be developed. Trends identified in the 7th American Water Jet Conference (i.e., nuclear decontamination, hazardous waste removal, and demilitarization) have continued to develop and to achieve commercialization.

The advent of abrasive suspension jets and improvements in standard aspiration-type abrasive jets have moved the technology toward a competitive position versus traditional machining operations. This area continues to evolve as evidenced by the number of papers in these *Proceedings* addressing machining processes, theoretical and experimental investigations of the cutting process, and integration of fluid jets into intelligent machining systems. These trends should continue through the balance of the 1990s. Improvements in abrasive nozzle life, the amount of abrasive used, and cut quality control will drive the adaptation of fluid jets into traditional machining operations. In some fields such as paper processing, fluid jets are the standard against which all other technologies are measured.

Construction and mining applications still have not utilized the potential of fluid jet technology. Several papers in these *Proceedings* address fields such as soil/ground stabilization, hydrodemolition, bore hole mining, and tunnel boring. These areas of application need equipment designed for mobile use that is rugged, has a high reliability, and low capital and operating costs. Some of these issues are addressed in papers in these *Proceedings*.

The evolution of any technology depends heavily on the free exchange of information on research and applications issues. This Conference provides a forum for such an exchange. It is due to the willingness of the authors to share their information and views that this Conference takes place. I would personally like to thank all the authors for their contributions. This Conference continues to be international in nature with 27 of 70 papers submitted for consideration being from international authors. I would like to thank this group of authors for taking time to prepare a paper, and for supporting the conference with their attendance.

Sincere thanks go to Dr. Andy Conn, Dr. Tom Kim, and Mr. Bruce Wood who reviewed all the paper abstracts, which aided in developing the overall technical paper content of the conference. Thanks also goes to Dr. Tom Kim, Mr. Bruce Wood, and Dr. Mohamed Hashish who edited the submitted papers. They executed this time consuming task with diligence and dedication to maintaining a high quality program. Finally, but certainly not the least, the staff at Birenbaum & Associates needs to be recognized.

Mark Birenbaum and Ken Carroll provided guidance and counsel as related to the overall Conference goals. Ms. Jan Tubbs and Rhonda Stevens administered the development of these *Proceedings*. They did an outstanding job. Ms. LeAnn Hampton supported the short course and made it a success. I also wish to express my sincere thanks to all participants for making this Conference a success.

Thomas J. Labus
Editor, *Proceedings of the 8th American Water Jet Conference*
Vice President, Water Jet Technology Association

TABLE OF CONTENTS

Volume 1

Paper # Page #

APPLICATIONS SESSION III

RESEARCH SESSION IV

APPLICATIONS IV

Volume II

Paper # Page #

RESEARCH SESSION VIII

MISCELLANEOUS PAPERS

ADDITIONAL SUBMISSIONS

8th American Water Jet Conference
August 26-29, 1995: Houston, Texas

Paper 32

EFFECT OF OFFSET BORES ON THE PERFORMANCE AND LIFE OF ABRASIVE WATERJET MIXING TUBES

Madhusarathi Nanduri, David G. Taggart, Thomas J. Kim
Waterjet Laboratory, University of Rhode Island
Kingston, RI

Eric Ness
Dow Chemical Company
Midland, MI

Ed Risk
Boride Products, Inc.
Traverse City, MI

ABSTRACT

It is well known that in abrasive waterjet (AWJ) machining systems, the shortest lived component is the mixing tube or nozzle. Recent advances in ceramic technology have led to significant improvements in mixing tube life. For instance, the composite carbide nozzle ROCTEC 100 manufactured by Boride Products, Inc. has an average life of approximately 80 hours with garnet abrasive. The process of boring these nozzles from either end can result in a step in the bore that may be visible to the naked eye. Although quality control procedures in manufacturing maintain this step in the bore to less than 0.025 mm (0.001 inch), the effect of this small step on nozzle performance has not previously been systematically studied. In this paper, the effect of the offset bore on the AWJ machining process is investigated through nozzle bore wear and weight loss. Experimental results demonstrate that the offset bore adversely affects the nozzle wear and hence nozzle performance only when the measured bore offset is greater than approximately 0.2 mm (0.008 inch). A nozzle with an offset less than 0.2 mm performs as well as a nozzle with zero offset.

Organized and Sponsored by the Water Jet Technology Association.

1. INTRODUCTION

Nozzle wear and performance characterization are receiving increased attention in an effort to produce longer lasting mixing tubes for use with hard abrasives such as aluminum oxide and silicon carbide (Ness et al., 1994 and Schwetz et al., 1994). Some observations on the wear of mixing tube materials were also made by Hashish (1994). Abrasive waterjet nozzle wear depends on many parameters that can be categorized as

- Geometric parameters
- System/process parameters
- Material parameters

Figures 1 and 2 illustrate the geometric and system parameters respectively. Material parameters that affect nozzle wear are hardness, toughness, elastic modulus, compressive/tensile strength and material microstructure.

In order to completely characterize, model and predict nozzle wear, the effect of each of these parameters and their interactions must be thoroughly understood. This paper is a small step in that direction; dealing with the effect of the parameter e, the nozzle eccentricity or offset.

Standard wear tests to characterize nozzle performance involve exit and entrance diameter measurements. The exit diameter increase is often approximated as a linear function of time. Nozzle life is determined by setting an allowable limit on the deviation of exit diameter from the initial value, generally 10 - 25% depending on the application. Our experimental results demonstrate that the exit diameter increase is non-uniform over short time intervals. Over the entire life of the nozzle, however, the exit diameter may be approximated as a linear function. The nozzle weight loss data, on the other hand, for fixed operating parameters such as abrasive type and size, abrasive flow rate, water pressure, orifice/nozzle combination, is almost perfectly linear throughout the life of the nozzle (Nanduri et al., 94-1 1994). Therefore, nozzle performance can be better characterized and nozzle life more accurately predicted by weight loss data.

1.1 What is an Offset Nozzle?

The manufacturing process of an abrasive waterjet mixing tube or nozzle can be thought of as a two step process. First, a cylinder of diameter and length equal to the required outer diameter and length of the nozzle is manufactured. Then it is bored to a diameter equal to the inner diameter of the nozzle. The process of boring these nozzles from either end can result in a step in the bore that may be visible to the naked eye. Although quality control procedures in manufacturing maintain this step in the bore to less than 0.025 mm (0.001 inch), the effect of this small step on nozzle performance has not previously been systematically studied. A sketch of a typical offset nozzle is shown in figure 3.

1.2 Objective and Strategy

In this study the offset nozzles were characterized by comparing their performance to standard, zero offset nozzles. Exit diameter increase and nozzle weight loss per unit time were used for comparison.

The nozzle chosen in this study was the composite carbide nozzle ROCTEC 100 manufactured by Boride Products, Inc. ROCTEC 100 nozzles were selected due to their high wear resistance and consistent and repeatable performance with standard commercial abrasives.

The strategy for this systematic study of offset bore nozzles was as follows. (1) To conduct baseline wear tests on standard ROCTEC 100, zero offset nozzles. These tests would include one nozzle wear test each with garnet and aluminum oxide abrasive. A typical wear test is explained in the next section. (2) Conduct wear tests on the offset nozzles with garnet abrasive. (3) Conduct accelerated wear tests (Nanduri et al., 94-2 1994) on the offset nozzles with aluminum oxide abrasive to confirm results obtained in step 2.

2. EXPERIMENTATION

Tests on offset nozzles were conducted at the University of Rhode Island (URI) Waterjet Laboratory. The abrasive waterjet system at URI consists of Flow International Corporation's Model 9XD-55 Dual Intensifier pump capable of delivering water pressurized to 379 MPa (55 ksi) at a maximum flow rate of 4.69 lpm (1.24 gpm); Flow's PASER II abrasive cutting head and abrasive delivery system; Flow's 404 X-Y cutting system; a robotic unit that controls the motion of the abrasive cutting head and capable of machining two dimensional designs in the horizontal plane. The motion control of the system is done through a CNC controller. The unit is a microprocessor based numerical control system.

2.1 Offset Nozzle Data

The offsets selected for study were zero, 0.05 mm, 0.13 mm, 0.2 mm and 0.25 mm (0, 0.002 inch, 0.005 inch, 0.008 inch and 0.01 inch). The zero offset nozzles served as basis for comparison. Table 1 gives the values of intended offset, offset via pinning and offset via mold for each of the offset nozzles selected for study. The intended offset is the actual value by which the boring machine was offset while boring from one end with respect to the other. The offset via pinning is the value of offset obtained by noting the diameter of the largest gage pin that went all the way through the bore. This value was always lower than the intended offset due to the fact that the gage pins could bend around the step and hence not detect the offset accurately. The third column shows values of the offset obtained by measuring the offset from a mold of the inside of the nozzle. The molds of the inside of the nozzles were prepared by using dental mold. These values are closer to the actual intended offsets.

2.2 A Typical Wear Test

The exit diameter of the nozzle is recorded prior to testing using 50 mm long steel dowels (gage plugs) which range from 0.28 mm (0.011 inch) to 6.35 mm (0.250 inch) in diameter with a 0.025 mm (0.001 inch) increment. The weight of the nozzle is recorded using an electronic scale with 0.0001 gram accuracy. The nozzle is installed and the stream aligned. Alignment consists of creating a fine, low pressure (34.5 MPa) stream that is centered through the nozzle using three adjustment knobs. This crucial step ensures normal, smooth wear. The abrasive flow rate is calibrated and water pressure is adjusted. The wear test is conducted and timed by a Heuer stopwatch. There is no target material in the path of the jet and the jet is simply allowed to impinge on the steel balls in the catcher tank for energy dissipation. At predetermined intervals the test is stopped. The exit diameter and weight of the nozzle are recorded, the operating parameters adjusted if necessary and the test continued.

2.3 Operating Parameters

Operating parameters for regular garnet tests as well as accelerated aluminum oxide tests were set as follows:

Abrasive flow rate:	7.6 grams/second (1.0 lb/min)
Water pressure:	310 MPa (45,000 psi)
Jewel:	0.33 mm (0.013 inch)

Abrasive type for the garnet tests was Barton Mines Corporation's Garnet # 80 and for the aluminum oxide test was Norton Company's Dynablast # 80. Nozzle length and exit diameter for all the nozzles tested were 76.2 mm (3 inches) and 1.0 mm (0.040 inch) respectively.

3. RESULTS AND DISCUSSION

3.1 Regular Garnet Tests

The results of tests on the 0, 0.2 and 0.25 mm offset nozzles with garnet abrasive are shown in Figures 4 and 5. Figure 4 shows the exit diameter increase as a function of time. In the case of the zero offset nozzle, there was no measurable increase in the exit diameter until the 8th hour. In ten hours the exit diameter increase was just 0.025 mm. In the case of the 0.2 mm offset nozzle, the increase in exit diameter was 0.05 mm in ten hours and there was a 0.15 mm increase in 5 hours for the 0.25 mm offset nozzle. Since our measurement resolution is 0.025 mm (0.001 inch), it is hard to say if the initial increase observed (first half hour) in the 0.2 mm offset nozzle exit diameter is significant. For example, if the initial exit diameter was 1.036 mm (0.0408 inch, close to 0.041 inch), pinning would record it as 1.0 mm (0.040 inch). In other words, using gage plugs, following the first 0.025 mm (0.001 inch) increment recorded, subsequent exit diameter increases measured will be significant. After the first half hour the 0.2 mm offset nozzle exhibited identical wear behavior as the

zero offset nozzle. The 0.25 mm offset nozzle, however, after 3 hours of similar, although not identical, stable behavior (in terms of exit diameter wear) as zero offset nozzle, wore out much faster. The test on this nozzle was discontinued due to the high wear rate exhibited.

The nozzle weight loss results are shown in figure 5. The average weight loss rate (excluding the first half hour of testing) of the zero and 0.2 mm offset nozzles was 0.23 grams/hour. In the case of the 0.25 mm offset nozzle, the weight loss rate was 0.5 grams/hour. All the nozzles exhibited an increased weight loss in the first half hour or one hour of testing. We believe that the removal of the material residue left over after boring the nozzles adds to the initial weight loss measured. This phenomenon is observed in the weight loss data of the zero offset nozzle to a lesser degree. In the case of offset nozzles, we believe that the increased weight loss in the first half hour of testing is due to initial smoothening of the edges of the step in the nozzle. This primary difference apart, the zero and the 0.2 mm offset nozzles have almost identical weight loss rates corroborating the results obtained in the exit diameter wear aspect as shown in figure 4. In the case of the 0.25 mm offset nozzle, the weight loss rate is much higher (about twice as much), again confirming the result in the exit diameter wear plot. The trends obtained in the exit diameter wear and nozzle weight loss measurement are similar. A higher weight loss rate suggests a higher exit diameter wear rate and vice versa. A one to one correspondence between the two is evident. This also implies that the life of the nozzle, which is based on exit diameter wear, can be predicted using the extrapolated weight loss curve. The advantage in using the weight loss data is due to linearity of the weight loss curve. This allows one to run a short test on a nozzle with a certain abrasive and predict the useful life of that nozzle with a good deal of accuracy. Hence, the ambiguity in nozzle life is eliminated and the choice of a particular nozzle material for a given cutting application is facilitated. Extended testing time for nozzle life prediction is also obviated.

The direct correlation between weight loss and exit diameter wear (and hence, useful life of the nozzle) has some limitations. It is not applicable when the flow pattern within the nozzle is non uniform, whereby the exit diameter wear is eccentric and erratic. It is applicable only to the nozzle and abrasive combination in question. If either is changed, another short test should be run. The question whether weight loss data of an accelerated test can be used to predict life of the nozzle with any other abrasive is currently under investigation.

3.2 Accelerated Aluminum Oxide Tests

After conducting the regular garnet tests described above, we decided to conduct accelerated tests using aluminum oxide abrasive instead of garnet on 0.05 mm and 0.127 mm offset nozzles. Intuitively, the weight loss and exit diameter wear trends for these two nozzles were expected to lie in between the zero and 0.2 mm offset nozzle data.

Tests were conducted on zero, 0.05 mm, 0.13 mm, and 0.2 mm offset nozzles with aluminum oxide #80 abrasive. The results of these tests are shown in figures 6,7.

The exit diameter wear of the zero, 0.05 mm, 0.13 mm and 0.2 mm offset nozzles was almost identical. The average weight loss rate of all the nozzles tested was the same, being

approximately 0.035 grams/minute. As mentioned above in the section on garnet tests, a slightly increased initial weight loss phenomena was observed also in the accelerated tests.

3.3 Discussion

It is noteworthy to mention a few qualitative remarks based on visual observation regarding the garnet test on the 0.25 mm offset nozzle. At the beginning of the test, the jet lacked coherency. The jet stream was in no way comparable to the zero and 0.2 mm offset nozzles. (The 0.2 mm offset nozzle also exhibited a minor jet incoherency in the first half hour.) In the 0.25 mm offset case, jet coherency improved in the next 2-3 hours and then degraded progressively till the end of the test. This trend corroborates the exit diameter wear trend as shown in figure 4.

Figure 8 reveals the cross-sectional view of the zero offset nozzle at the end of 10 hours of testing with garnet abrasive. Figure 9 shows the sections of the zero offset nozzle after 30 minutes of testing with aluminum oxide abrasive. These are typical wear profiles. A comparison of the wear profiles of the nozzles tested with garnet is shown in figure 10, and wear profiles of the nozzles tested with aluminum oxide are shown in figure 11. Again, the exit diameter wear and nozzle weight loss data trends are matched by the wear profiles. The wear profiles of the offset nozzles are identical to the typical wear profiles with the 0.25 mm offset nozzle being the exception.

The excessive wear of the 0.25 mm offset nozzle as evident from the exit diameter wear, nozzle weight loss data and its wear profile, is a clear indicator of poor nozzle performance. We believe that the primary reason for the poor performance of this nozzle is due to the change in flow pattern within the nozzle effected by the relatively large step of 0.25 mm. The upper portion of this step is visible near the middle of the 0.25 mm offset nozzle in figure 10.

There is an initial smoothening of the step in the case of 0.25 mm offset nozzle similar to the other offset nozzles as mentioned before. However, the 0.25 mm offset could be a critical step size, above which a permanent change in flow pattern is effected. A change in flow pattern would mean changes in the mixing conditions, abrasive velocities and angles of attack within the nozzle. These changes would result in increases/decreases in nozzle weight loss, non uniformity of exit diameter wear and eccentric wear profiles. In the present case, there is an increase in the weight loss and increased wear in the lower 1/3 portion of the nozzle that can be seen in figure 10. Factors affecting the different flow patterns within the nozzle and hence nozzle wear, are being studied.

4. CONCLUSIONS

- The effect of a small step (offset) on nozzle performance was systematically studied.
- The offset nozzles were characterized by comparing their performance to standard, zero offset nozzles. Exit diameter increase and nozzle weight loss per unit time were used for comparison.

- Baseline wear tests with garnet and aluminum oxide abrasive were conducted on standard ROCTEC 100, zero offset nozzles.
- Wear tests were conducted on the offset nozzles with garnet abrasive.
- Accelerated wear tests were then performed on the offset nozzles with aluminum oxide abrasive to confirm the results from garnet tests.
- Wear profiles of the offset nozzles were examined.
- Experimental results demonstrate that the offset bore adversely affects the nozzle wear and hence nozzle performance only when the measured bore offset is greater than approximately 0.2 mm (0.008 inch).
- A nozzle with an offset less than 0.2 mm performs as well as a nozzle with zero or no offset.

5. ACKNOWLEDGMENTS

The support of Dow Chemical Corporation for this study is greatly appreciated.
The authors would like to thank Mr. Joel Kahn for his assistance in conducting the tests.

6. REFERENCES

Hashish, M., "Observations of Wear of Abrasive Waterjet Nozzle Materials," *Journal of Tribology*, vol. 116, pp. 439-444, July 1994.

Nanduri, M., Taggart, D.G. and Kim, T.J., "Nozzle Weight Loss as a predictor of Nozzle Wear and Life," *Technical Report 94-1*, Waterjet Laboratory, University of Rhode Island, 1994.

Nanduri, M., Taggart, D.G. and Kim, T.J., "Stability of Accelerated Aluminum Oxide Wear Tests," *Technical Report 94-2*, Waterjet Laboratory, University of Rhode Island, 1994.

Ness, E.A., Dubensky, E., Haney, C., Mort, G. and Singh, P.J., "New Developments in ROCTEC Composite Carbides for Use in Abrasive Waterjet Applications," *12th International Conference on Jet Cutting Technology - Applications and Opportunities*, Mechanical Engineering Publications, London, 1994, pp. 195-211.

Schwetz, K.A., Greim, J., Sigl, L.S., Pontvianne, P.M., Ehlbeck, U., Basile, G., Raissi, K. and Slotte, P., "Research on Design and Application of Industrial Scale Hydro-abrasive Jet-cutting Nozzles," *12th International Conference on Jet Cutting Technology - Applications and Opportunities*, Mechanical Engineering Publications, London, 1994, pp. 165-175.

7. NOMENCLATURE

a	=	Abrasive Parameter (type, size, shape)
d	=	Original Inner Diameter
d_e	=	Exit Diameter Wear
d_i	=	Inlet Diameter Wear
d_w	=	Orifice Diameter
e	=	Bore Eccentricity
l	=	Nozzle Length
l_e	=	Exit Zone Length
l_i	=	Inlet Depth
l_m	=	Mixing Zone Length
l_o	=	Orifice - Nozzle Distance
l_p	=	Preliminary Mixing Zone Length
m	=	Mixing Chamber Parameter
m_a	=	Abrasive Flow Rate
P	=	Water Pressure
s	=	Wear Profile Parameter
α	=	Inlet Angle

Table 1. Offset Nozzle Data

Intended offset (mm)	Offset via pinning (mm)	Offset via mold (mm)
0.0	0.0	0.0
0.05	0.0	0.025
0.13	0.0	0.10
0.20	0.05	0.15
0.25	0.20	0.23

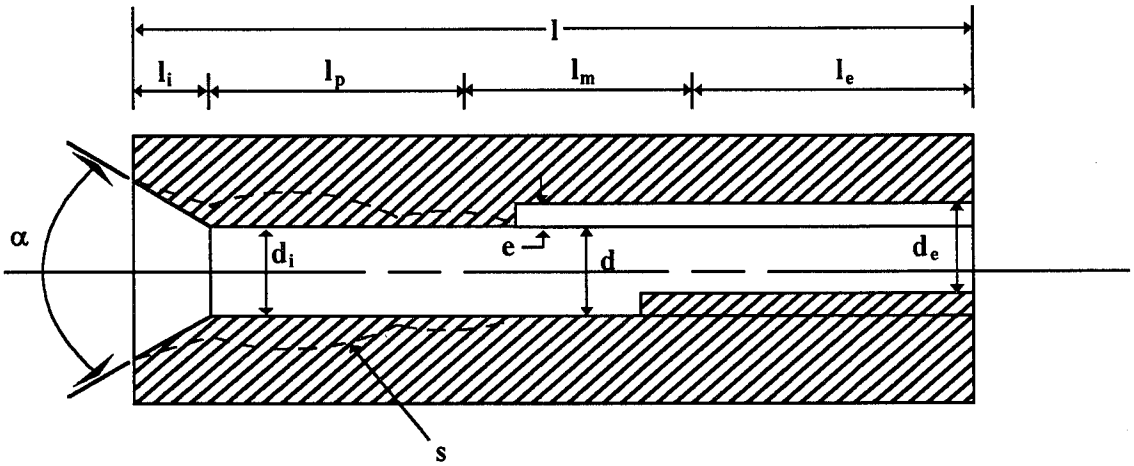

l = Nozzle Length
l_i = Inlet Depth
α = Inlet Angle
d = Original Inner Diameter
d_e = Exit Diameter Wear
d_i = Inlet Diameter Wear
s = Wear Profile Parameter
m = Mixing Chamber Parameter
l_p = Preliminary Mixing Zone Length
l_m = Mixing Zone Length
l_e = Exit Zone Length
e = Bore Eccentricity

Figure 1. Abrasive Waterjet Nozzle Wear; Geometric parameters.

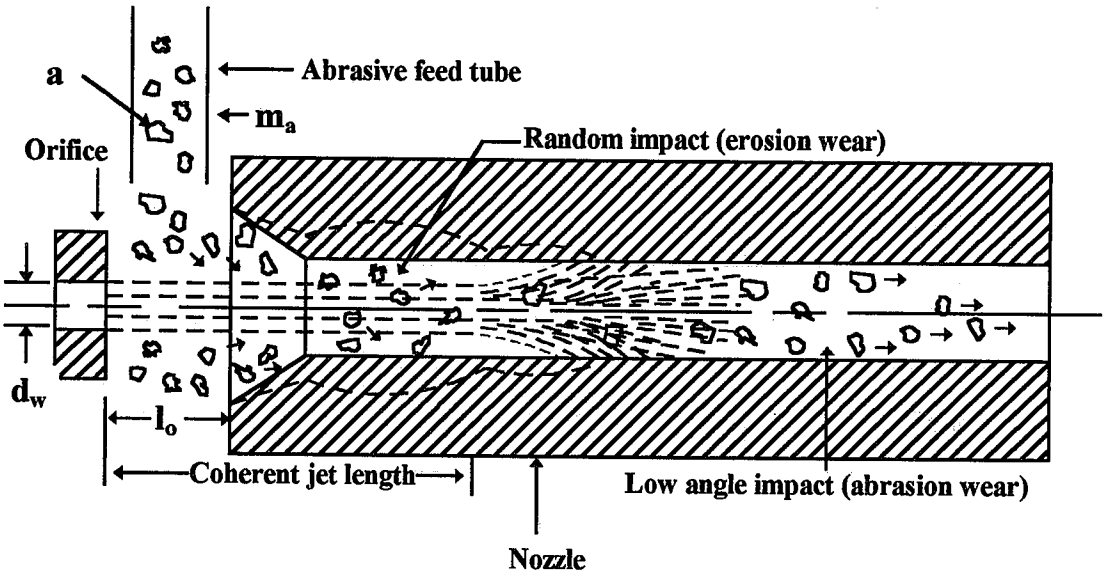

P = Water Pressure; d_w = Orifice Diameter; m_a = Abrasive Flow Rate; a = Abrasive Parameter (type, size, shape); l_o = Orifice - Nozzle Distance

Figure 2. Abrasive Waterjet Nozzle Wear; System / Process Parameters.

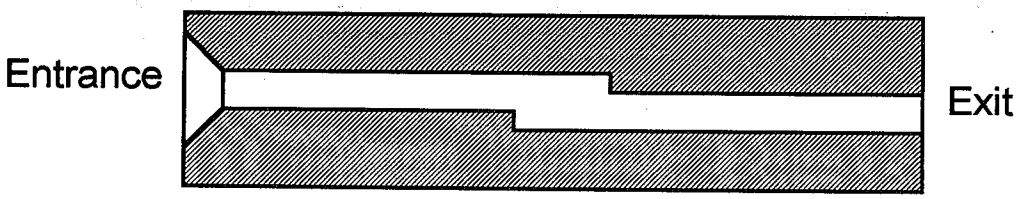

Figure 3. Cross Section of an Offset Nozzle

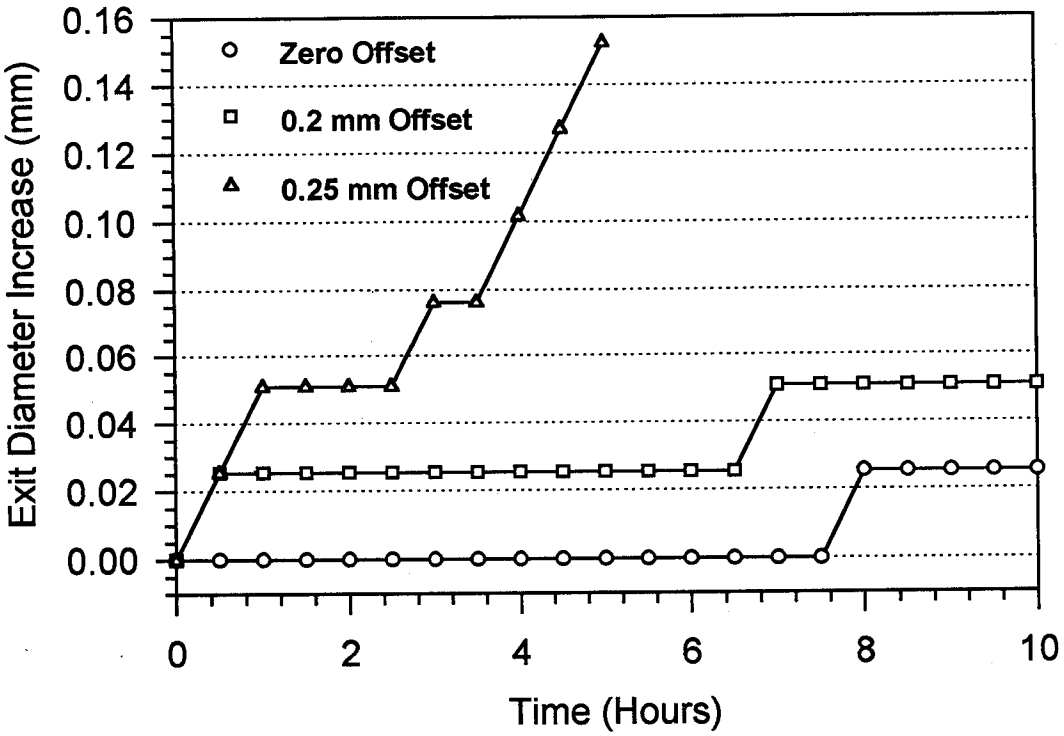

Figure 4. Exit Diameter Wear (Garnet Tests)

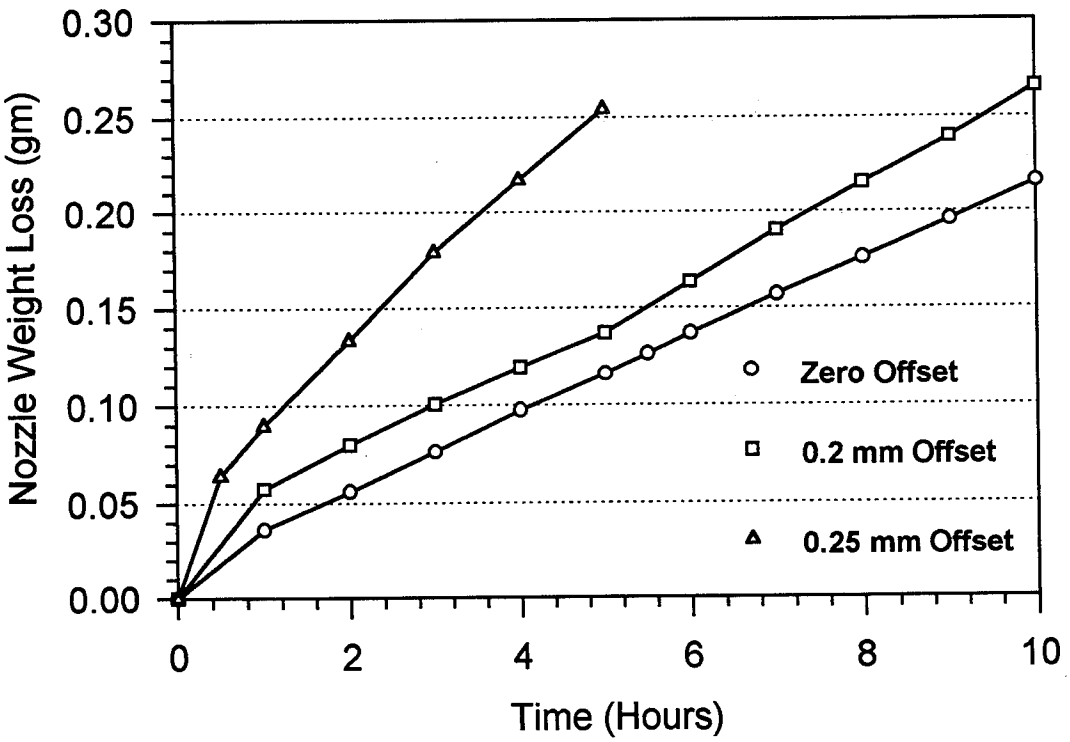

Figure 5. Nozzle Weight Loss (Garnet Tests)

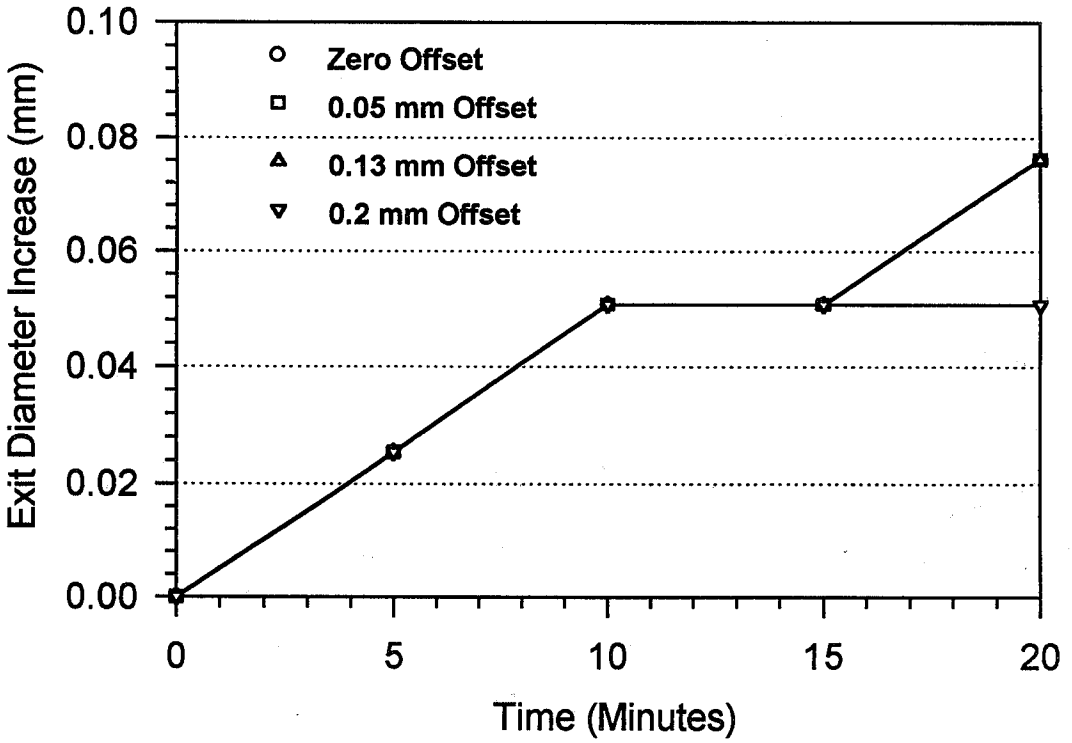

Figure 6. Exit Diameter Wear (Aluminum Oxide Tests)

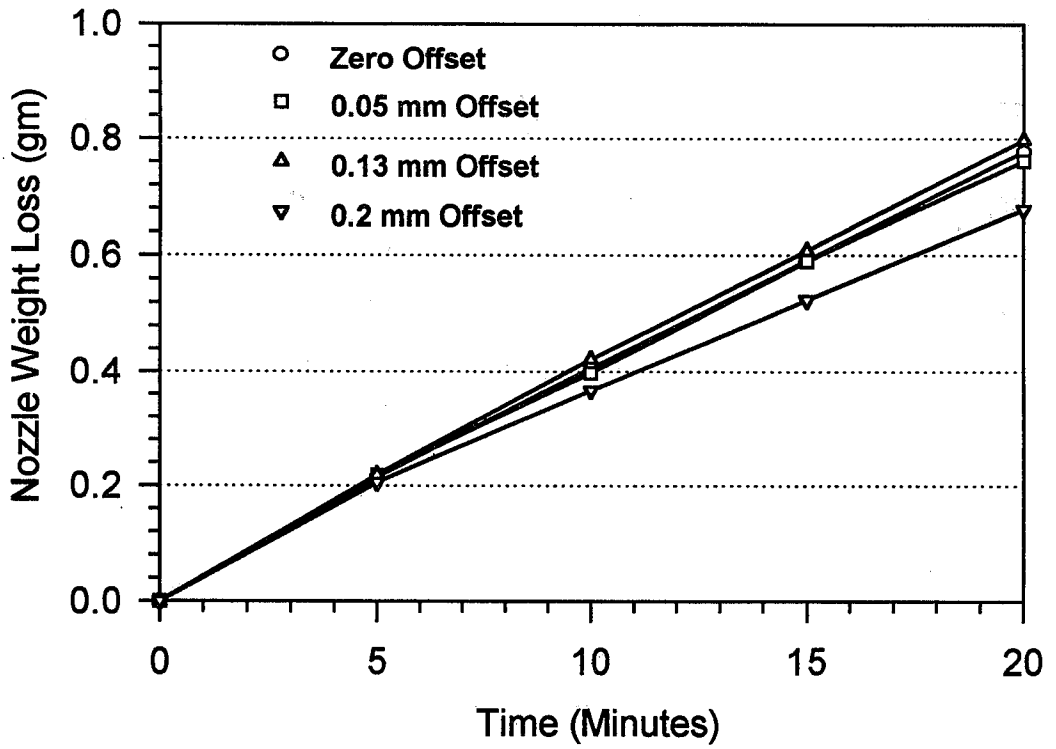

Figure 7. Nozzle Weight Loss (Aluminum Oxide Tests)

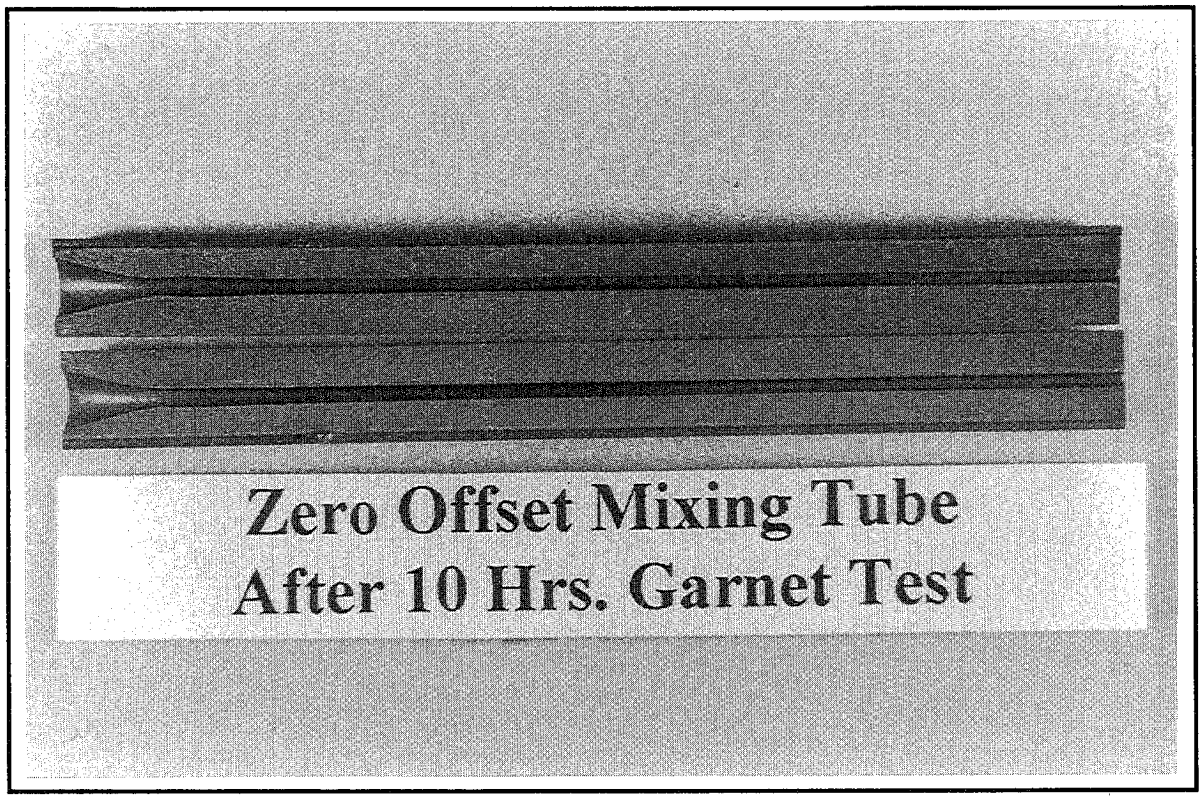

Figure 8. Typical Wear Profile of ROCTEC 100 Nozzle with Garnet Abrasive.

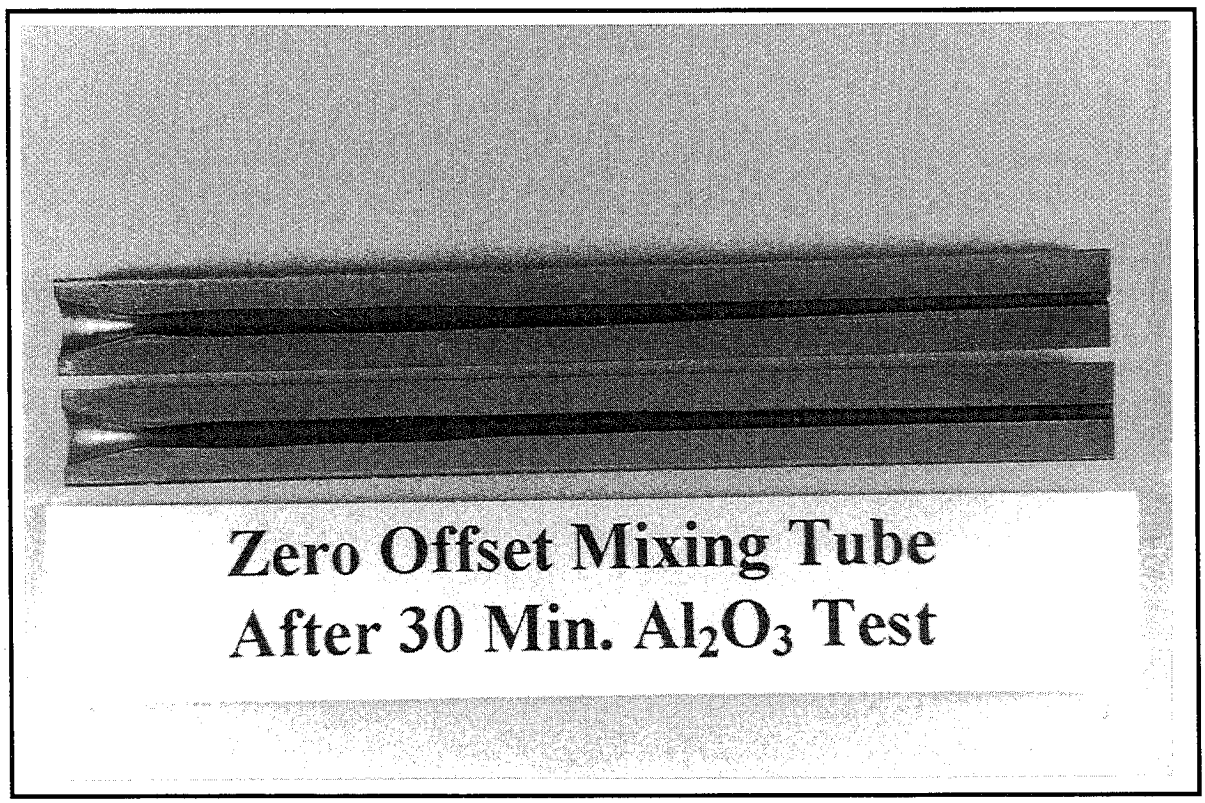

Figure 9. Typical Wear Profile of ROCTEC 100 Nozzle with Al_2O_3 Abrasive.

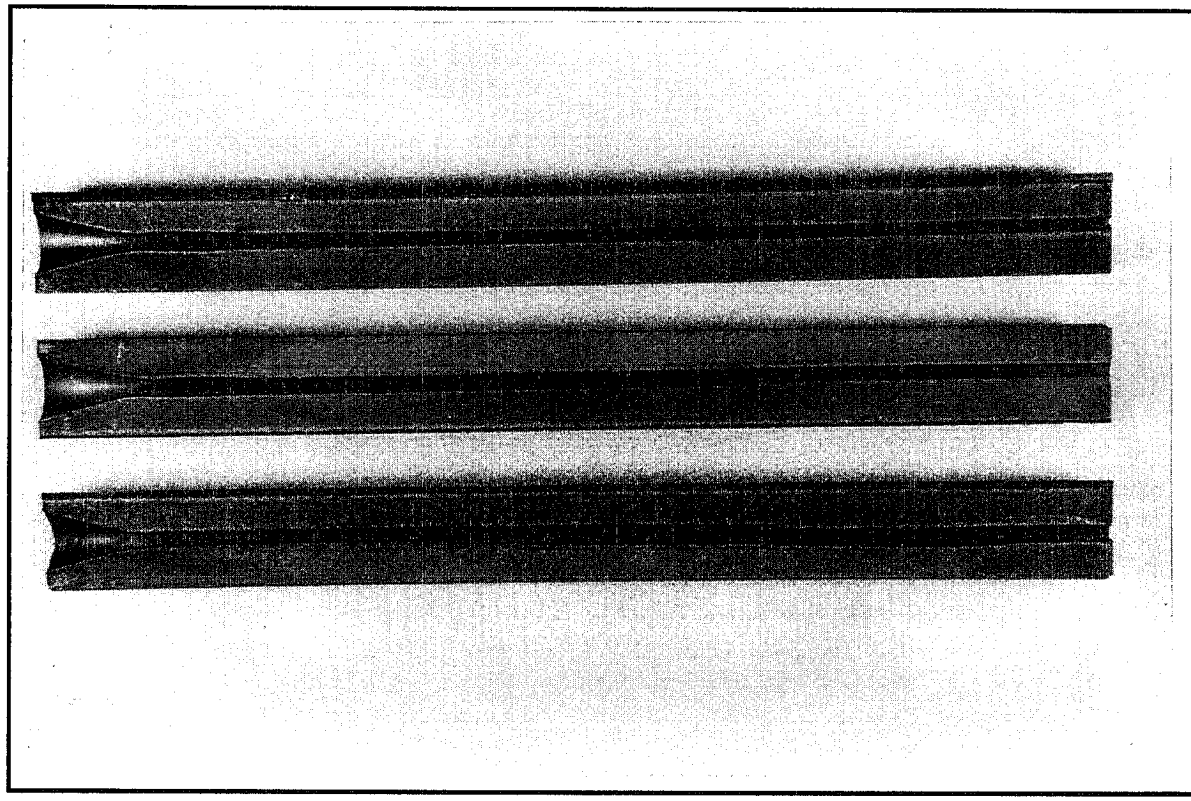

Figure 10. Garnet Test Wear Profiles. From Top: 0, 0.2, 0.25 mm Offset Nozzles.

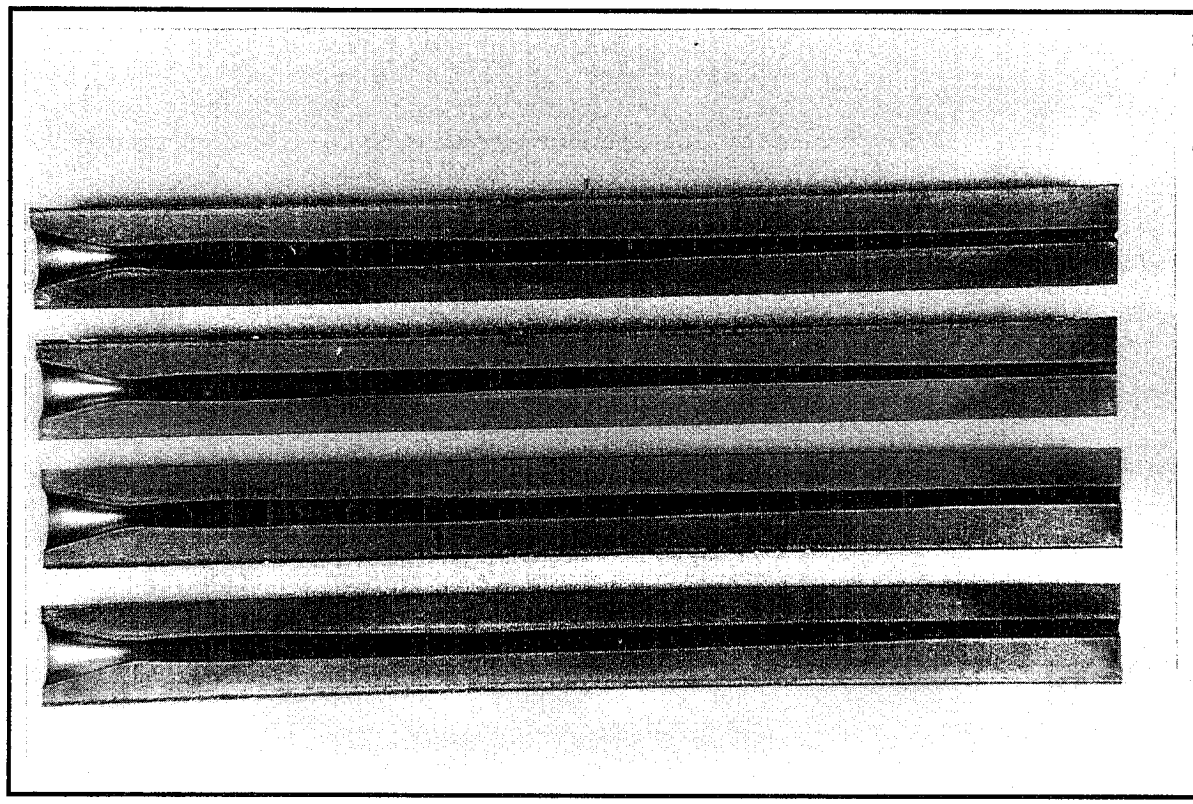

Figure 11. Al_2O_3 Test Wear Profiles. From Top: 0, 0.05, 0.13, 0.2 mm Offset Nozzles.

8th American Water Jet Conference
August 26-29, 1995: Houston, Texas

Paper 33

WATER PEENING — AN ADVANCED APPLICATION OF WATER JET TECHNOLOGY

H.K. Tönshoff, F. Kroos, and M. Hartmann
Institute for Production Engineering and Machine Tools
University of Hannover, Germany

ABSTRACT

This paper deals with investigations on surface hardening by water peening as an advanced application of water jet technology for improving surface integrity and fatigue strength of components.

The effect of water peening parameters on residual stresses and structural changes are discussed. X-ray measurements proved that high compressive residual stresses can be induced in surface layers even in hard materials and in the notch root of kerfs with high notch acuity. Furthermore, experiments were conducted to describe the characteristics of water jets which are beneficial to the water peening process.

Rotating bending tests with notched and non-notched specimens were carried out to determine the effect of water peening on fatigue strength.

Based upon these results, the paper defines the conditions for a promising use of surface treatment by water peening to increase fatigue strength of components in industrial applications.

Organized and Sponsored by the Water Jet Technology Association.

1. INTRODUCTION

From investigations on rain erosion (Beutin, 1975) and cavitation (Hetz, 1987) the application of high velocity water jets for surface hardening was derived. The application of water jet technology for surface treatment aims at improving surface properties analogous to the well known shot peening process. Thereby, it is characterized by the following advantages: As discussed by Tönshoff et al. (1994) workpieces with complex geometry and kerfs of high notch acuity can be treated by water peening. Moreover, a complete coverage of the surface is guaranteed. In contrast to shot peening, investigations provided no change of roughness after water peening (Tönshoff et al., 1995). The small number of process parameters and the constant quality of water simplify process control. Low costs for the preparation of the water are an economical advantage compared to shot peening. Besides surface hardening, water peening can simultaneously be combined with cleaning or other operations such as burr removing (Brinksmeier et al., 1991). These features are forcing the current development of the water peening process at the Institute for Production Engineering and Machine Tools.

2. EXPERIMENTAL CONDITIONS

The jetting-pump used for the investigations on surface hardening by water peening has a power of 75 kW and is characterized by a maximum pressure of 105 MPa and a water flow of 39 dm^3/min. A detailed description of the experimental set-up for water peening was given by Tönshoff et al., 1994.

The geometries of nozzles used in the presented investigations are described in Fig. 1. Besides a round nozzle with a conical nozzle bore (type 1), a nozzle characterized by a cylindrical nozzle bore and a sharp edge at the elliptical aperture (type 2) was tested to study the influence of different jet characteristics on the surface properties after water peening. Furthermore, investigations with so-called flat nozzles were performed. Due to the elliptical aperture the jet is spread and its characteristics are decisively different compared to round nozzles. The jet has a nearly rectangular cross section on the workpiece surface of several mm^2. The coefficient of expenditure evaluated by Tönshoff et al. (1994) is comparable between round and flat nozzles described in Fig. 1 and amounts about 0.8.

The investigations on surface hardening by water peening were carried out on case hardened steel SAE 5115 (german specification: 16 MnCr 5) with a surface hardness of 60 to 62 HRC. The material offers a thickness of the case hardened layer of about 0.7 mm and an edge oxidation of 10 to 20 μm thickness.

Besides peening experiments on non-machined case hardened specimens with edge oxidation, finished samples too were used to investigate the influence of surface properties on structural changes due to drop impingement. Two series of ground and two series of turned case hardened cylindrical specimens were machined which differed significantly in their close-to-surface structural properties and residual stress states. However, the surface roughness values were comparable. The results of the metallographic examinations, X-ray residual stress and contact stylus measurements, are shown in Fig. 2.

For every finishing process one set of samples was characterized by beneficial surface properties, i.e., compressive stresses and the other one by thermal surface damage. The latter one showed rehardening zones combined with tempered structure beneath. Thereby, structural changes with higher extension were observed after turning while the chosen grinding conditions led only to local white layers along the circumference of the samples. These structural changes were found for both finishing processes to appear together with tensile residual stress states in the surface layer due to critical process temperatures. X-ray phase analysis proved that the amount of retained austenite in the rehardening zones is increased compared to the bulk material by more than 25%. However, the case thickness of 0.6 mm after grinding and turning, respectively, is still sufficient for the rotating bending tests.

3. JET CHARACTERISTICS AND NOZZLE GEOMETRIES

The general structure of turbulent-free jets in air according to investigations described by Yanaida (1974) consists of three parts: the *initial region* with a constant jet axial dynamic pressure and continuous flow characteristic, the *main region* with constant jet axial velocity and the *final region*, where diffusion occurs. In the main region, the so-called droplet flow region, the continuous jet falls into pieces.

In general, the dynamic pressure of the continuous flow jet within narrow nozzle-to-surface distances does not exceed the strength of the material. On the contrary, impact of drops in the droplet flow region causes peak loads (Rochester et al., 1974), which suffice to deform even material of high strength plastically and induce residual stresses a in the spot of impact. This jet region is used for surface treatment by water peening.

In the following the influence of nozzle geometry on the effect and the efficiency of the process due to the specific jet characteristics is described. First, Fig. 3 shows the influence of nozzle-to-surface distance s on surface residual stress state for nozzles with different diameters but the same nozzle angle α_D. On one hand, compressive residual stresses show maximum level for a range of distances s where droplet flow in the jet occurs, Fig. 3. On the other hand, the maximum compressive residual stress level increases from about -350 MPa for a nozzle diameter D of 0.8 mm to more than -500 MPa for D = 1.5 mm. This can be explained by taking the number of drop impingements per unit area into account which cause impact pressures higher than local yield strength of the workpiece material. Higher flow rates as well as increasing peening duration t_s go along with an increasing coverage of the workpiece surface and more plastic deformation in the surface very similar to the shot peening process.

The effect of nozzle angle α_D on the residual stress state after water peening case hardened samples with edge oxidation, is described in Fig. 4. It was found for flat nozzles that maximum compressive residual stresses of about -500 MPa appear at lower distances with increasing nozzle angle. Using round nozzles ($\alpha_D = 0°$) leads to a significant lower compressive residual stress level at much higher nozzle-to-surface distances for the same pressure p_s of 75 MPa and almost the same nozzle diameter D. But if the pressure is

increased up to 100 MPa the maximum residual stress level of about -500 MPa which can be reached by water peening in the surface of a cased hardened steel with edge oxidation appear over a wide range of nozzle-to-surface distances. Therewith, the extension of droplet flow region and the optimum distance to nozzle depends strongly on the nozzle geometry.

Investigations were performed to study the effect of drop impingement within the cross section of the jet on the surface residual stress distribution (Fig. 5). For a flat nozzle (α_D = 20°, D = 1,5 mm) a very even compressive residual stress state was measured by X-ray diffraction method after water peening within an area of 3 x 11 mm^2. This was found to be valid for all flat nozzles described in Fig 1. Obviously, it is possible by using flat nozzles to produce a water jet with equal characteristics within its cross section more suitable for surface treatment than round nozzles.

A comparison of nozzle geometries concerning their efficiency in water peening can be performed by evaluating the specific peening energy per unit area W'' required for reaching a certain level of compressive residual stress. W'' can be calculated from the flow Q, the pressure p_s, the effective cross section area of the water jet A_{eff} derived from examinations exemplary described in Fig. 5 and the peening duration t_s.

$$W'' = \frac{Q \cdot p_s}{A_{eff}} \cdot t_s \quad with \quad A_{eff} = a \cdot b_{eff}$$

The right chart of Fig. 6 shows the compressive residual stresses due to water peening versus specific peening energy W'' for peening with flat nozzles. With increasing nozzle diameter, i.e., flow Q, the required specific peening energy per unit area W'' to reach maximum surface residual stress state of about -500 MPa is strongly decreasing. Thereby, no significant difference in process behavior was found between a nozzle angle of 10° and 20°.

The left drawing in Fig. 6 shows the different results for round nozzles described in Fig. 1. The results obtained with a round nozzle with conical bore are characterized by a lower ascent of compressive residual stresses with increasing peening energy W'' compared to the second nozzle. Although the diameter of both nozzles is slightly different, the main reason for the different results is seen in the different jet structure. The sharp edge at the aperture disturbs the continuous jet in the initial region. On one hand, the droplet flow region appears at lower nozzle-to-surface distances. On the other hand, within a bigger part of the cross section of the jet at the optimum nozzle-to-surface distance drop impingement occurs and causes local plastic deformation in the spot of impact. Therefore, efficiency of the process increases. Nevertheless, flat nozzles are still more efficient than round nozzles due to their beneficial jet structure.

4. SURFACE PROPERTIES AFTER WATER PEENING

The properties of machined surfaces can vary in a wide range depending on the machining process and its parameters. Usually, the finishing process for components of hardened steel is grinding. But in more and more industrial applications, turning of hardened steel is used as finishing process too (Tönshoff et al., 1994). After turning the surface properties differ from those after grinding. Furthermore, tool wear or any kind of disturbances of the machining process can cause surface or sub-surface damage like tensile stresses, tempering zones or even rehardening zones, the so-called white layers. These changes in surface layers can lead to a significant deterioration of strength properties (Syren, 1975; Wohlfahrt, 1978; and Brinksmeier, 1991).

Based upon the experimental studies on jet characteristics beneficial for the water peening process, a suitable nozzle geometry was chosen (α_D = 20°; D = 1,5 mm) for further investigations on water peening finished surfaces with different surface integrity (Fig. 2). This research work aimed at finding a suitable peening duration for achieving maximum compressive residual stresses in the surface (left drawing of Fig. 7).

For each peening duration nearly the same compressive residual stress state was obtained for ground and turned specimens. The maximum residual stress value of more than -800 MPa which is evidently higher than that after water peening of specimens with edge oxidation occurred for a peening duration t_s of 15 s. For this peening condition, the residual stresses after water peening of all states described in Fig. 2 are shown in the right part of Fig. 7. In all cases the same high compressive residual stress state was obtained independent of the initial surface residual stresses and structural differences between the sets of samples described above.

It hardly makes a difference referring to the maximum residual stress value after water peening whether there are high or low tensile residual stresses in the initial state. The extension of layers under compressive residual stress obtained at this peening conditions amounts to approximately 20 μm. The increase in compressive residual stresses as well as the increase in hardness is partly due to a strain caused transformation of retained austenite within the same distance to surface (Tönshoff et al., 1995).

Another important aspect of water peening is described in Fig. 8. Surface roughness measurements for several peening durations t_s verify that no change in roughness values occur as a result of water peening. The removal of white layers due to drop impingement which was detected in metallographic examinations is too little to deteriorate surface roughness. Even the results of SEM investigations do not point to any significant change in topography for ground and turned surfaces as well.

5. FATIGUE STRENGTH TESTS

Rotating bending tests were performed for turned non-notched specimens (α_k=1,0) with and without surface damage to investigate the influence of the structural changes in surface layers by water peening on fatigue behavior.

In case of no surface damage after the turning or grinding process, crack initiation occurs beneath the surface within a distance of 150 to 200 μm at local structural irregularities (carbides) for all tested specimens. Therefore, the rotating bending strength remains almost on the same level of about 900 MPa, independent of whether the specimens were peened or not. The modified surface layer by water peening is too thin to have any effect on fatigue behavior. These conditions change if unfavourable properties in surface layers like tensile stresses or local rehardening zones due to, e.g., tool wear, during the finishing process occur (Fig. 9). The rotating bending tests showed a significant decrease in fatigue strength for samples with surface damage which causes a crack initiation directly at the surface. Due to water peening the same level of fatigue strength of 900 MPa was reached compared to the set of samples without surface damage after turning because crack initiation can be shifted below the surface by generating beneficial properties in surface layers.

Notches cause stress concentration under mechanical load. With increasing concentration factor, the tensile stress in the notch root and the stress gradient below surface increase. Therefore, the properties of the surface are getting more important for fatigue strength than deeper sub-surface regions. Rotating bending tests which were carried out to evaluate the increase of fatigue strength of notched specimens with a concentration factor α_k = 2,0 due to water peening show an increase of fatigue strength of more than 31%. This is due to the fact that crack initiation in notched components usually takes place at the surface, even after a surface treatment (Kloos et al., 1988).

6. CONCLUSIONS AND OUTLOOK

The working mechanism of water peening is drop impingement. Due to the impact pressures in the spot of impact, local plastic deformations cause high compressive residual stresses and an increase in dislocation density in surface layers. Using pressures up to 100 MPa and a high flow, it is possible to treat considerable surface areas.

The beneficial effect of water peening on fatigue strength is mainly based on the increase in compressive residual stresses in surface layers. An increase in hardness was only detected for the case hardened steel with a content of retained austenit. Higher dislocation densities, which were detected after water peening in normalized or quenched and tempered steels by evaluating peak-diffraction width from X-ray measurements and TEM (Transmission Electron Microscopy)-investigations in previous studies (Tönshoff et al., 1993) do not lead to a measurable increase of micro hardness.

From the results of experimental investigations the field of application of the water peening process for increasing fatigue strength can be defined by taking two aspects into

consideration. First, the beneficial properties like high compressive residual stresses have to be stable over the life time of a component. While residual stresses in steels of low hardness are reduced significantly during the first cycles of loads, compressive residual stresses in hardened steels remain almost on a high level even for high amplitudes and cycles of loads due to their high yield strength (Wohlfahrt, 1978). When talking about notched components it has to be taken into account that residual stresses have a higher stability due to the multi-axial-stress state in the root of the notch where crack initiation occurs. That's why recently performed rotating bending tests with notched specimens out of normalized steel even showed an increase of fatigue strength of more than 20%.

According to the concept of local strength described for example by Velten (1984) and Starker (1981), a local fatigue strength value versus distance from surface can be evaluated from the surface properties. Fatigue of the material appears if tensile stresses due to external load exceed the local fatigue strength. Therefore, the gradient of stress in surface layers has a strong influence on the effect of surface treatment by water peening.

For non-notched components, the decrease in tensile stress versus distance from the surface is small, almost linear and symmetrical to the neutral axis. For that reason it depends on the surface integrity before water peening whether this process has any effect of fatigue behavior of a component. If surface damage exists and leads to a crack initiation at the surface like presented above, improving surface integrity by water peening shifts the crack initiation below the surface combined with an increase in fatigue strength.

If already beneficial surface properties exist before water peening within the surface layer of about 20 μm, the extension of structural changes due to water peening is not sufficient for non-notched components.

Notches cause stress concentration under mechanical load. With increasing concentration factor, the tensile stress in the notch root and the stress gradient below the surface increase. Therefore, the surface properties are more important for fatigue strength than deeper sub-surface regions and water peening can improve fatigue strength evidently.

Taking all these results into account, water peening appears to be a suitable process to "repair" surface damages with negligible influence on surface roughness. In addition, it is an efficient process to increase fatigue strength of finished notched components. Therefore, water peening complements the established mechanical surface treatment processes like shot peening and deep rolling.

7. REFERENCES

Beutin, E.F., "Flüssigkeitsschlag, Grundlagen der Beanspruchung und ihre technische Nutzanwendung," Dr.-Ing. Diss. TU Hannover, 1975.

Brinksmeier, E., "Prozeß- und Werkstückqualität in der Feinbearbeitung," Habilitationsschrift Univ. Hannover, 1991.

Brinksmeier, E., and Kroos, F., "Hochdruck-Wasserstrahlen - Ein aussichtsreiches Verfahren zur Steigerung der Betriebsfestigkeit," Moderne Fertigungstechnologien zur Lebensdauersteigerung, 17. Vortragsveranstaltung des DVM-Arbeitskreises Betriebsfestigkeit, Schaffhausen, Schweiz, 1991.

Hetz, F., "Randzoneneigenschaften von Chrom-Nickel-Stählen nach Schleifen und Kavitationsbelastung," Dr.-Ing. Diss. Univ. Hannover, 1987.

Kloos K. H., Adelmann J., Bieker G., and Oppermann T., "Oberflächen- und Randschichteinflüsse auf die Schwingfestigkeitseigenschaften," VDI Berichte Nr. 661, 1988, S.215-245.

Rochester M.C. and Brunton J.H., "Surface Pressure Distribution During Drop Impingement," 4th Int. Conf. on Rain Erosion and Allied Phenomena, 1974.

Syren, B., "Der Einfluß spanender Bearbeitung auf das Biegewechselverhalten von Ck 45 in verschiedenen Wärmebehandlungszuständen," Dr.-Ing. Diss. Univ. Karlsruhe (TH),1975.

Starker, P., "Der Größeneinfluß auf das Biegewechselverhalten von Ck 45 N in verschiedenen Bearbeitungs- und Wärmebehandlungszuständen," Diss. Uni. Karlsruhe 1981.

Tönshoff H.K., Brinksmeier E., and Kroos F., "Surface Bonding by Water Peening," Int. Conf. on Surface Eng., 1993, Bremen, Germany.

Tönshoff, H. K., and Kroos F., "Increasing Fatigue Strength by Water Peening," Intern. Conf. on Residual Stresses, Baltimore, Maryland, U.S.A., 1994.

Tönshoff, H.K., Wobker, H.-G., and Brandt, D., "Hard-Turning-Substitute For Grinding Operations," Eurometalworking, Udine, Italy, 1994.

Tönshoff, H.K., Wobker, H.-G., and Kroos F., "Improving Surface Integrity of Finished Surfaces of Case Hardened Steel by Water Peening," Proc. of the International Symposium For Electromachining, ISEM XI, April 18th-20th 1995, Lausanne, Swiss.

Velten E., "Entwicklung eines Schwingfestigkeitskonzeptes zur Berechnung der Dauerfestigkeit thermochemisch randschichtverfestigter bauteilähnlicher Proben," Diss. TH Darmstadt, 1984.

Wohlfahrt, H., Zum Eigenspannungsabbau bei der Schwingbeanspruchung von Stählen. HTM 28(1973)11, 288-293.

Wohlfahrt, H., "Einfluß von Eigenspannungen." In "Verhalten von Stahl bei schwingender Beanspruchung." Hrsg. W. Dahl, Verlag Stahleisen mbH, Düsseldorf 1978.

Yanaida, K., "Flow Characteristics of Water Jets," Reprints of the Sec. Int. Symp. on Jet Cutting Technology, Paper A2, BHRA, Fluid Engineering, Cranfield, April 1974.

8. FIGURES

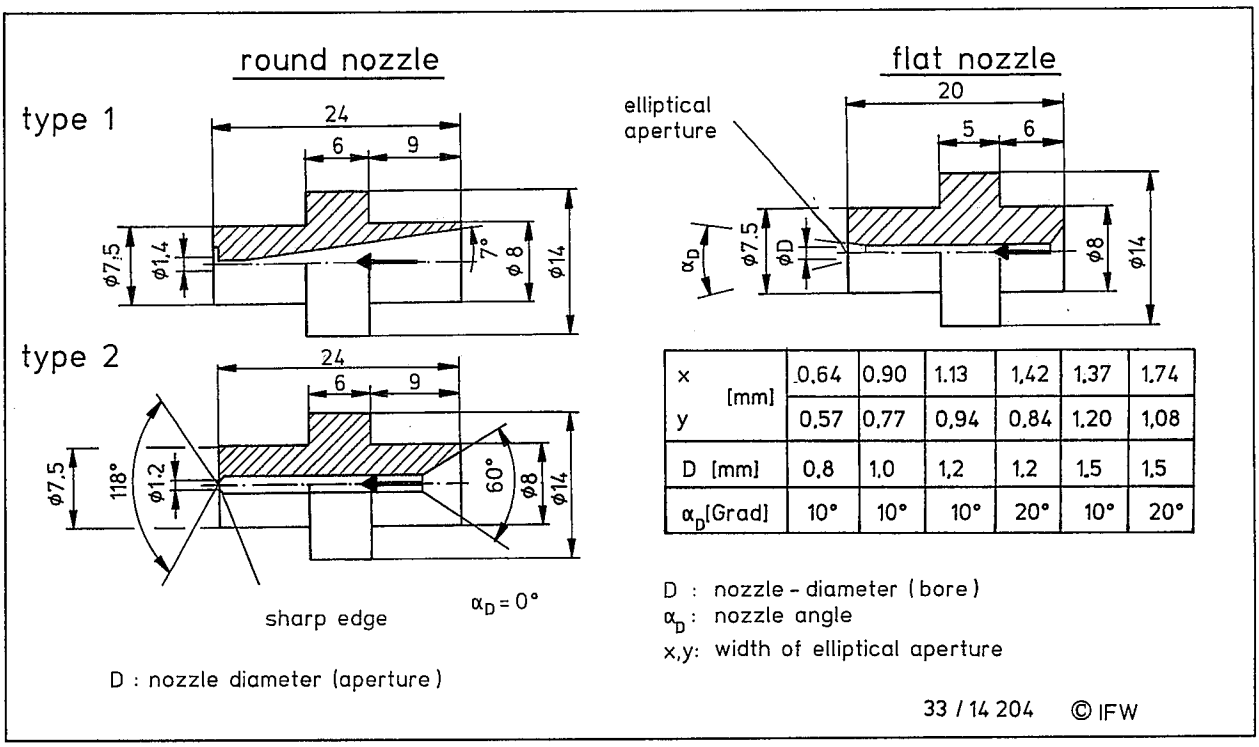

x [mm]	0,64	0,90	1.13	1,42	1,37	1.74
y [mm]	0,57	0,77	0,94	0,84	1,20	1,08
D [mm]	0,8	1,0	1,2	1,2	1,5	1,5
α_D [Grad]	10°	10°	10°	20°	10°	20°

D : nozzle - diameter (bore)
α_D : nozzle angle
x,y: width of elliptical aperture

33 / 14 204 © IFW

Fig. 1: Nozzle-geometries for water peening

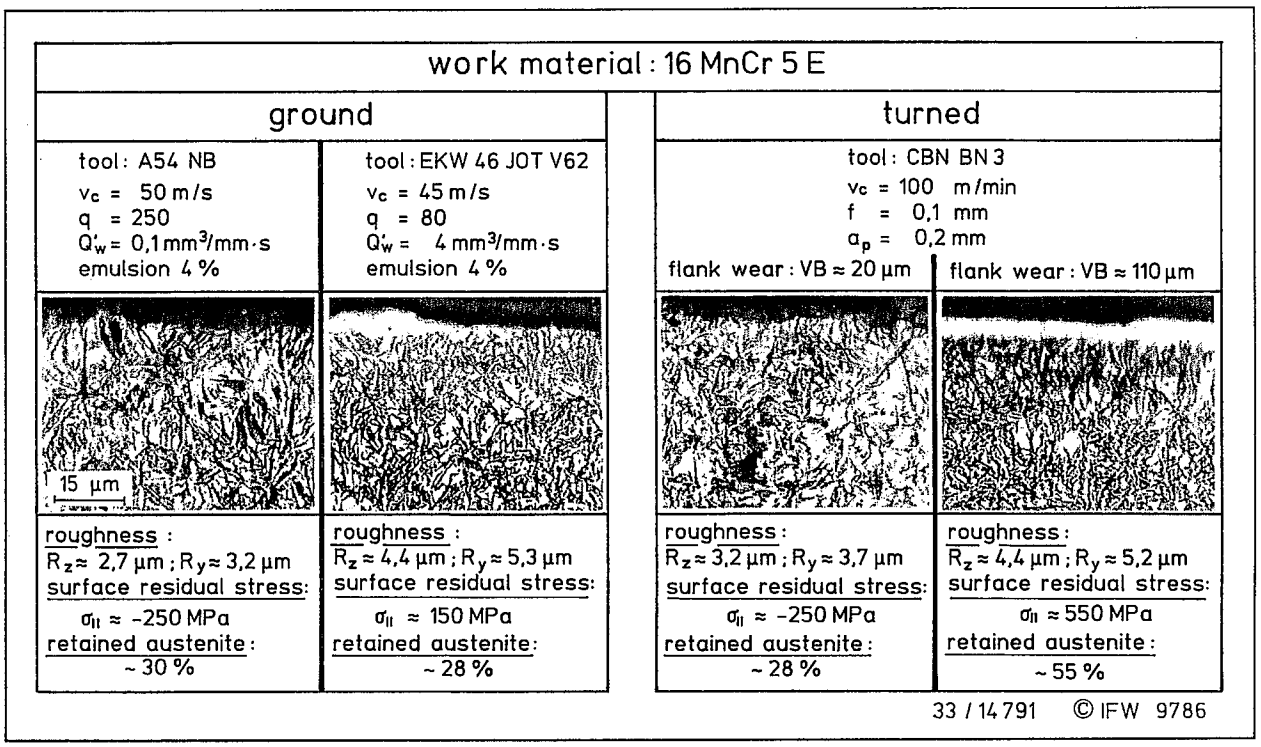

Fig. 2: Structural Properties of finished surfaces before water peening

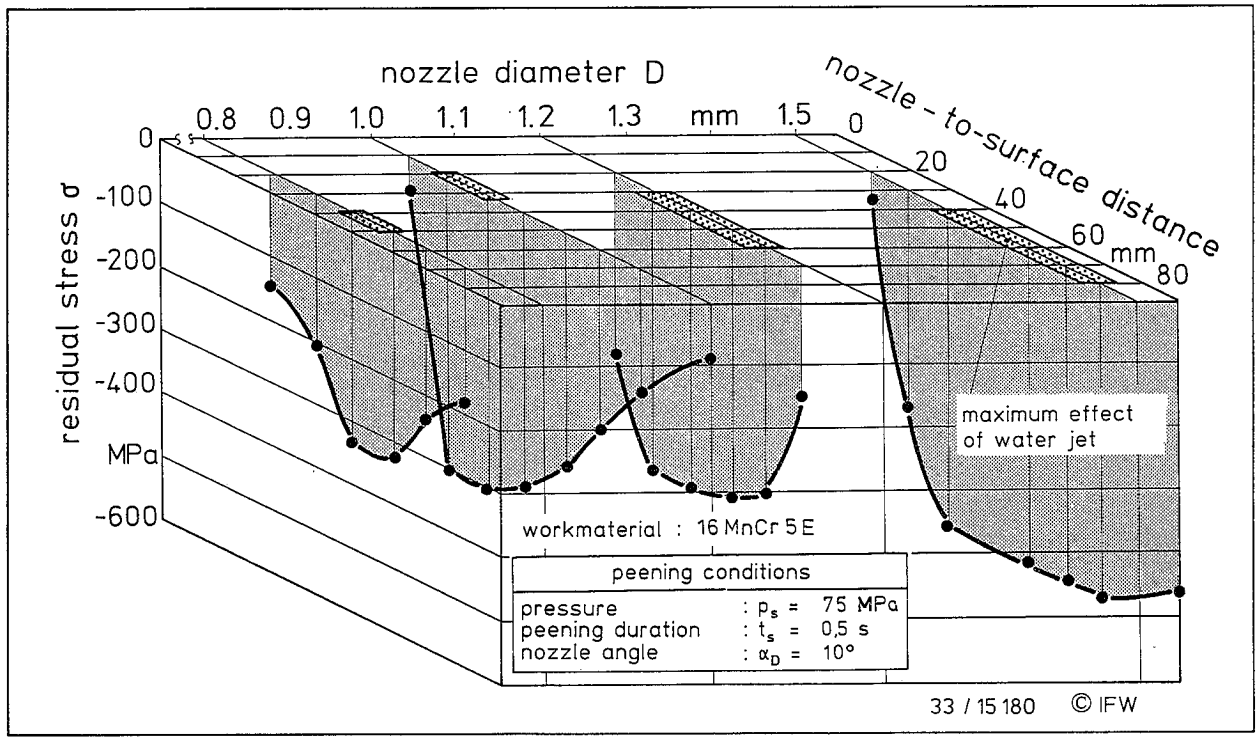

Fig. 3: Characteristics of water jets for different nozzle diameters

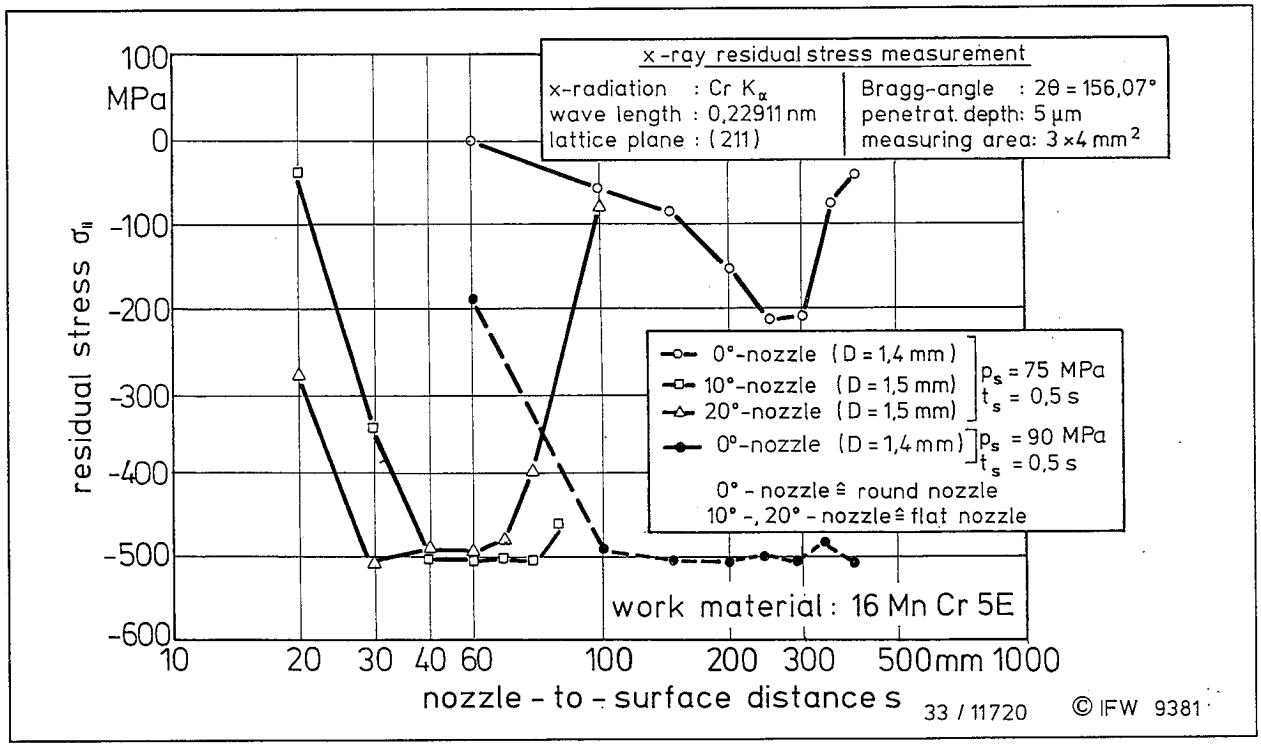

Fig. 4: Characteristics of water jets for different nozzle angles

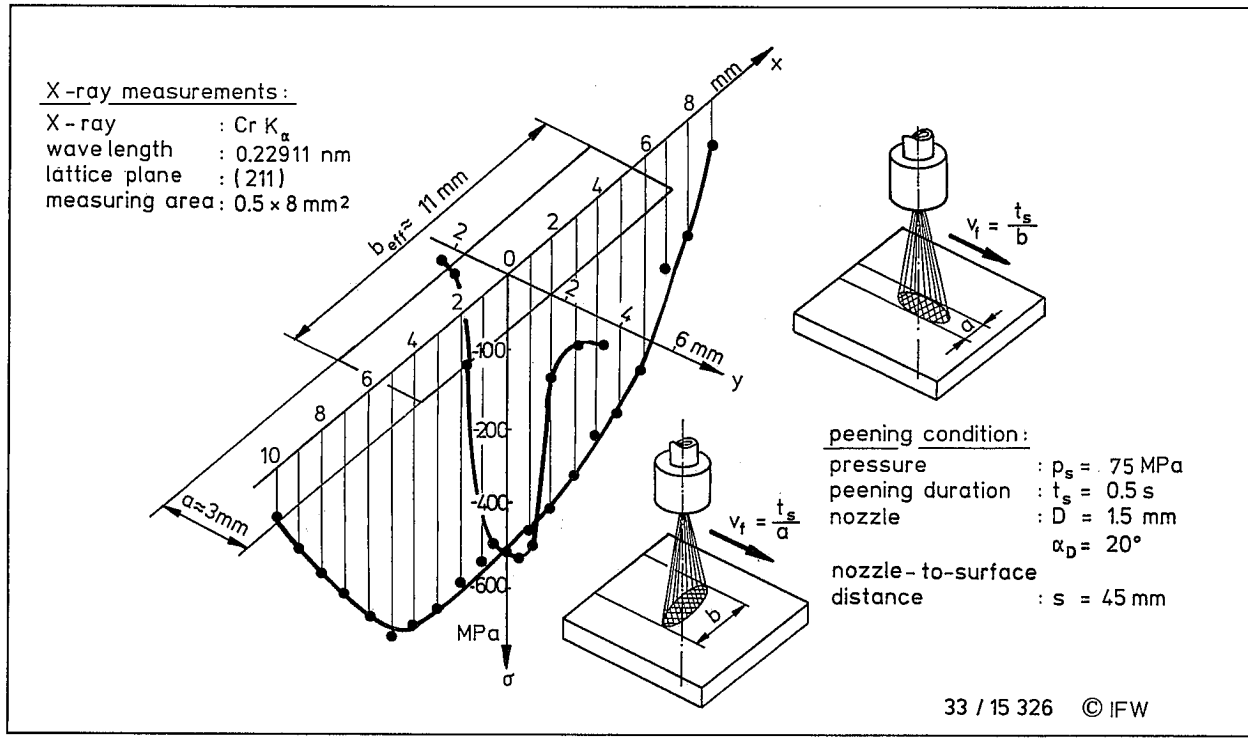

Fig. 5: Residual stress distribution generated by a discontinuous water jet

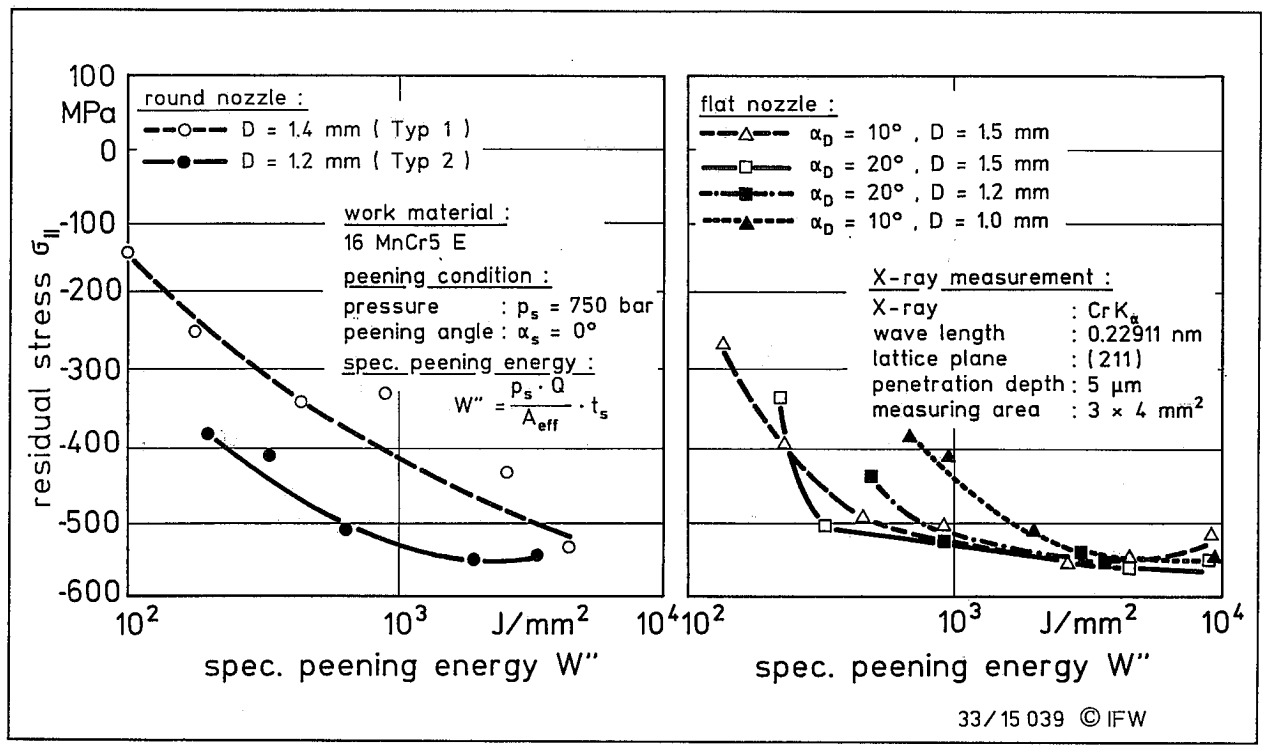

Fig. 6: Residual stresses vs. specific peening energy

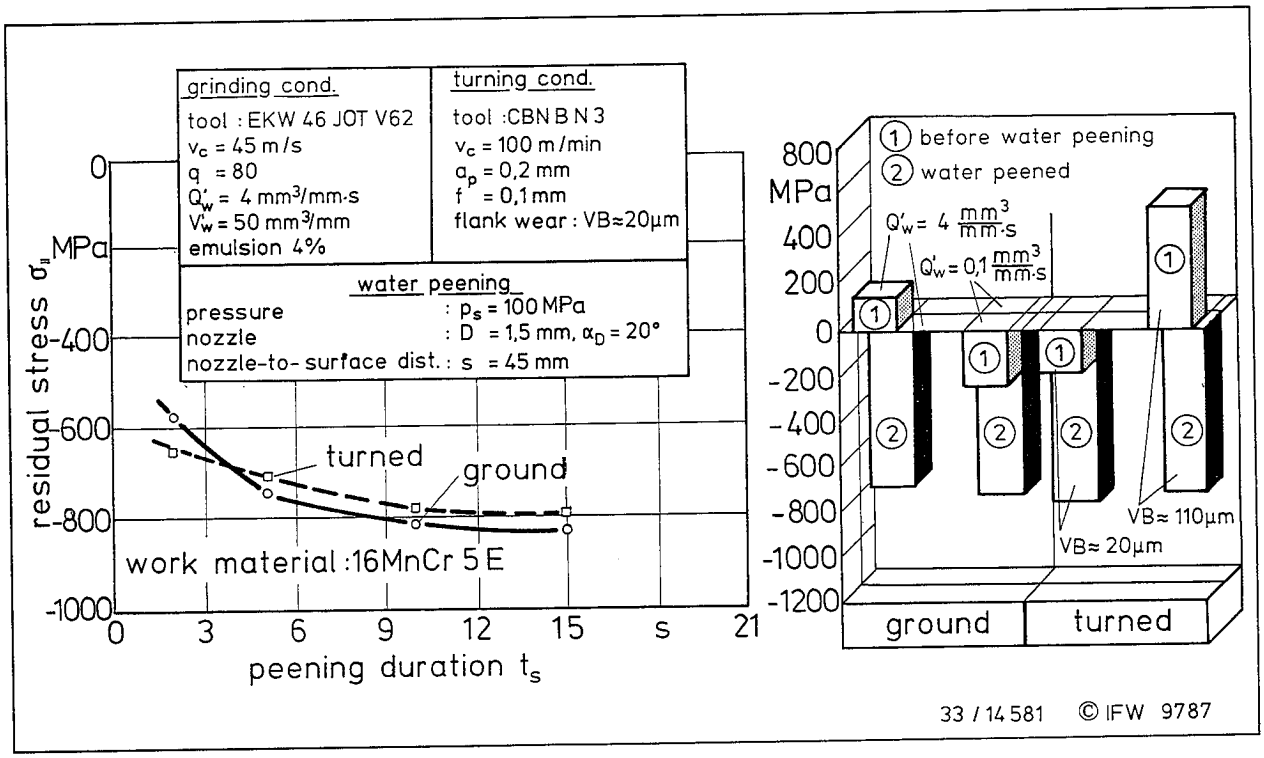

Fig. 7: Compressive residual stresses after water peening

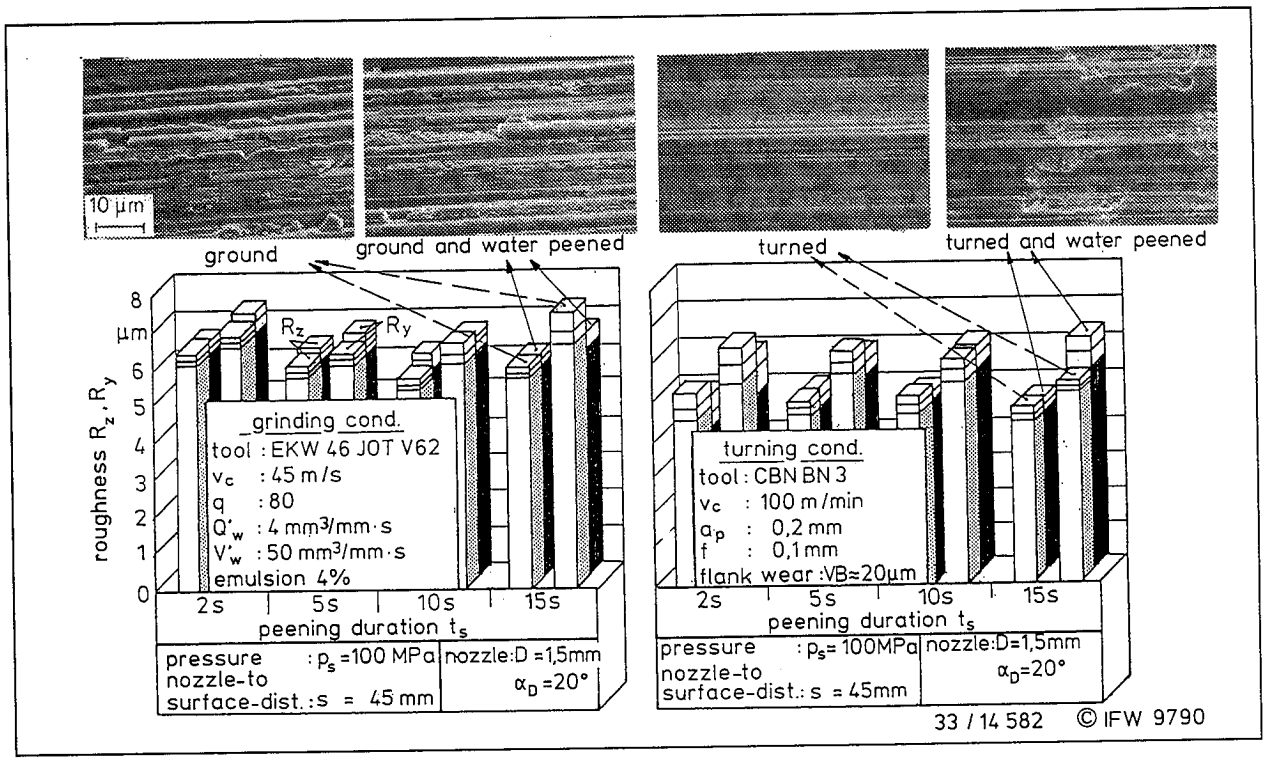

Fig. 8: Surface roughness before and after water peening

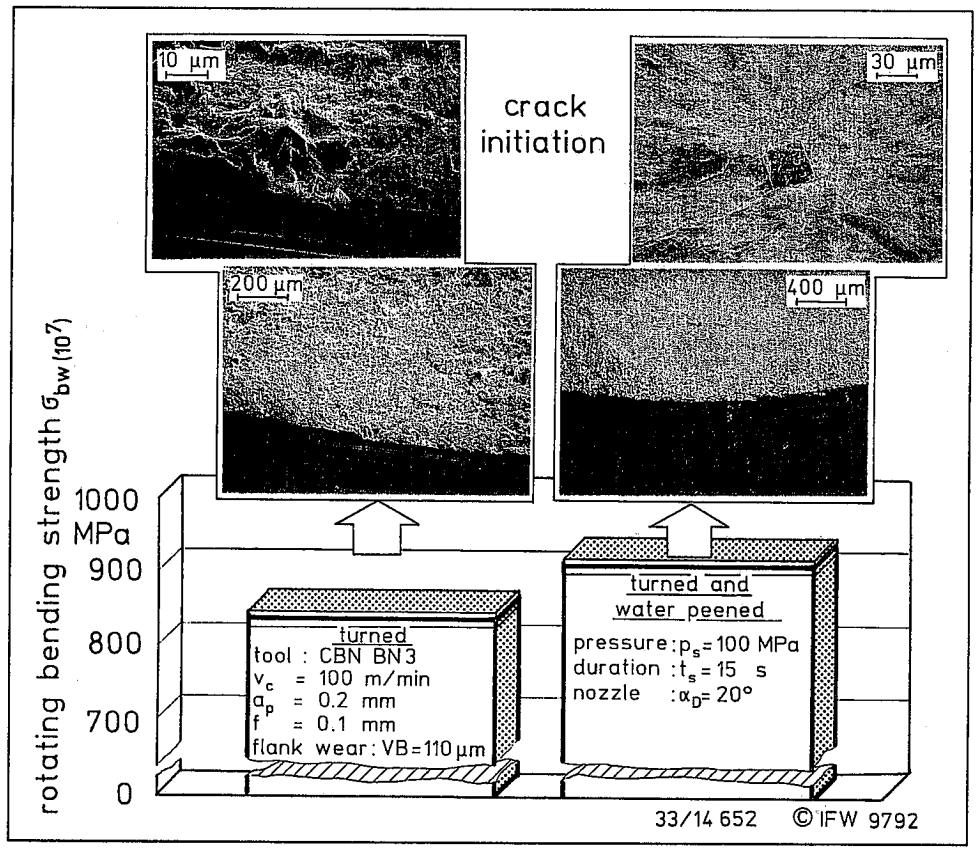

Fig. 9: Repairing surface damage by water peening

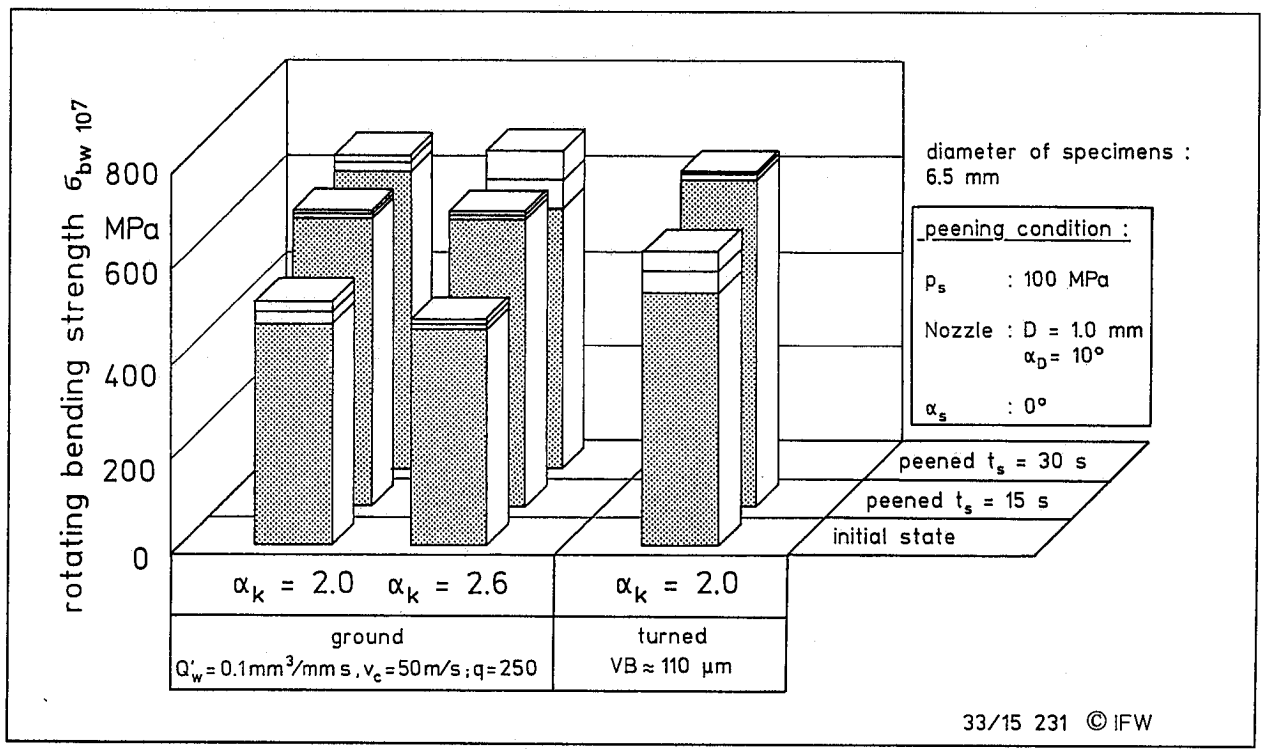

Fig. 10: Increasing fatique strength of notched specimens

8th American Water Jet Conference
August 26-29, 1995: Houston, Texas

Paper 34

ADVANCES IN FLUIDJET BEAM PROCESSING

M. Hashish
QUEST Integrated, Inc.
Kent, Washington, U.S.A.

ABSTRACT

Waterjets and abrasive-waterjets (AWJs) are currently used in a wide range of industrial trimming and shape-cutting applications. This paper addresses three areas of advancement in this technology. These are related to creation of new fluidjet beams, machining applications, and new components.

New fluidjet beams include superpressure (100 ksi) waterjets and AWJs for metal and composite machining, cryogenic jets for zero-added-waste machining, abrasive-cryogenic jets (ACJs), and high-pressure, directly pumped abrasive suspension jets (ASJs). Also presented in this paper are new capabilities of the AWJ tool for machining operations, such as turning, thread and spiral machining, wafer slicing, drilling, and milling, with emphasis on achieving precise results. In general, the AWJ has been demonstrated to be capable of achieving highly precise results within 0.001-inch accuracy. The use of automated, quick-change nozzles, waterjet quality sensors, and abrasive flow rate sensing and feed back control has significantly contributed to achieving precision and high productivity in the industry. These components are also presented in this paper.

Organized and Sponsored by the Water Jet Technology Association.

1. INTRODUCTION

Waterjet beams provide tools for cutting parts out of a wide range of materials such as glass, metals, and composites. These jets can also perform such operations as cutting, turning, milling, surface preparation, and the drilling of holes of different shapes and sizes.

This paper discusses advances in fluidjet beams, processing applications, and enabling components. The discussion in this paper will address:

- Superpressure waterjets
- Superpressure abrasive-waterjets (AWJs)
- High-pressure abrasive suspension jets (ASJs)
- Cryogenic jet (CJ) machining
- Abrasive cryogenic jets (ACJs)
- Polishing
- Spiral machining
- Milling
- Small-diameter hole drilling
- Deep hole drilling
- Three-dimensional machining
- Quick-change nozzles
- Jewel health sensor
- Abrasive flow rate sensor
- Mixing tube sensor
- Vision-assisted machining

2. FLUIDJET BEAMS

2.1 100-ksi Waterjet Machining

Commercially available, high-pressure intensifier pumps provide reliable operations up to 55 ksi. At this pressure many materials can effectively be cut without using abrasives. However, the cutting of metals and composites is limited at these pressures. For example, only thin foils of soft metal can be cut with waterjets and several composites will delaminate when pierced or cut. To overcome these limitations, waterjet pressures need to be increased. Tests were conducted at pressures up to 100 ksi, with significantly improved results. Figure 1 shows the effect of increasing pressure on removing delamination when cutting composites. It was found that a 0.001-inch-diameter jet at 100 ksi is feasible in making thin cuts and small-diameter holes in thin sheet metals. Tests conducted by Raghavan and Ting (1993) showed that there is a threshold pressure for metal cutting with plain waterjets in the range of 40 ksi to 60 ksi. It has also been established that the most efficient working pressure is 3 times the threshold pressure. Accordingly, pressures in the range of 120 to 180 Ksi will be needed for efficient metal cutting. However, the thermodynamic limit for waterjet pressure is about 150 ksi without upstream heating. It is recommended here that pumps in the range of 100 to 150 ksi be developed.

2.2 100-ksi AWJ Machining

The addition of abrasives to 100-ksi waterjets has been explored. The premise is to increase the particle velocity. This will allow reduction of the abrasive consumption to obtain the same cutting performance. Figure 2 shows a 100-ksi AWJ cutting through a 1-inch-thick steel plate. Observe that a vacuum assist line (U.S Patent No. 4,934,111) was used to help entrain the abrasives to the nozzle. The use of a 0.001- and 0.003-inch waterjet in an AWJ nozzle system with a 0.007-inch-diameter mixing tube was also explored. Figure 3 shows some results obtained when cutting a 0.062-inch-thick aluminum plate. It can be deduced from this figure that reducing the waterjet size improves the efficiency of cutting. For example, the power used with the 0.003-inch-diameter waterjet is 9 times that used for the 0.001-inch-diameter jet. The reduction in cutting speed with the 0.001-inch-diameter jet is only half that with the 0.003-inch-diameter waterjet. It is recommended here that further work be conducted on superpressure AWJs with reduced sizes of waterjets and mixing tubes.

2.3 High-Pressure ASJ

Figure 4 shows a high-pressure (50-ksi) continuous ASJ pumping system. Three basic critical components are currently under investigation for developing reliable high-pressure ASJ systems. These are the nozzle, valves, and isolator. The isolator concept was selected to eliminate the need for slurry seal development. This concept showed great reliability and flexibility to controlling effective stroke length and pressure fluctuations without a need for an accumulator. Nozzle materials made out of molybdenum carbide (supplied by Boride Products) and diamond composite show great promise for reliable operation up to 4 hours. However, there is still a need for improved nozzle material. The nozzle geometry was found to be critical in affecting its lifetime and cutting performance. For example, longer nozzles will last longer but are less efficient in cutting. It has been observed that ASJs cut up to 5 times faster than AWJs. Figure 5 shows thin cuts made in aluminum with ASJs. It was also observed that the rheological characteristics of the suspension fluid is of critical importance to the coherency of the ASJ. Hollinger and Mannheimer (1991) found out that the viscoelastic component of the jet controls the penetration depth and width. They indicated that tripling the viscoelastic polymer additive to the water doubled the jet penetration depth.

2.4 Cryogenic Jet (CJ)

The use of liquid nitrogen jets has been demonstrated by the Air Force Armstrong Laboratory (WJTA, 1994) for explosive washout. Also it was reported by the Idaho Energy National Laboratory (INEL) that liquid nitrogen jets have been used to cut several relatively soft materials. Recent tests by Dunsky and Hashish (1994) indicated the need for accurate thermodynamic control of the cryogen. Although not a cryogenic liquid, liquefied CO_2 jets were generated at pressures up to 50 ksi to explore the potential of this technique and to identify the requirements for cryogenic jet development. Figure 6 shows a sample of lexan cut with a 50-ksi CO_2 jet whose performance was found to be comparable to that of waterjets at the same pressure and flow rate.

2.5 Abrasive Cryogenic Jet (ACJ)

The addition of abrasives to cryogenic jets will enhance their performance, as is the case with the AWJ. Entrainment of abrasives in a cryogenic jet, however, is more complex due to possible abrasive feed line freezing and plugging. Tests conducted with entraining abrasives in CO_2 and liquid nitrogen jets showed great promise for the use of this approach. Figure 7 shows an abrasive cryogenic jet using garnet as abrasives. Observe the freezing of the nozzle.

The use of such abrasives as pelletized CO_2 was also explored in a regular AWJ nozzle. It was observed that the produced jet has improved cleaning power, but no improvement in cutting power was observed. Also, a degradation in performance was observed when the CO_2 particles were injected in a relatively long mixing tube AWJ nozzle. This may be attributed to the CO_2 particles not surviving the highly erosive environment during the mixing process.

3. ADVANCED PROCESSING APPLICATIONS

3.1 Polishing

The use of high-velocity free streams of liquid-abrasive jets has been demonstrated for polishing (Hashish and Bothell, 1993). Figure 8 shows a picture of a polished diamond film using silicon carbide abrasives. The rationale for using high-speed particles is to use inertia rather than hardness. In typical lapping processes, the abrasive velocity is limited to few inches per second. In fluidjet polishing, the abrasive particle velocity is over three orders of magnitude higher. The forces on the abrasive particle are transmitted to the workpiece via hydrodynamic loading and not by the contact of the lap.

Recent results show that progressive reduction in grit size to improve surface finish is still required with fluidjet polishing, but the quantitative increments of grit size reduction are significantly different than with conventional polishing.

3.2 Spiral Machining

The use of waterjet beams to produce complex shapes can be accomplished through both kinematic and dynamic control of the traverse and jet parameters. Traversing a waterjet beam parallel (or along) the axis of a rotary part will either result in a turned part diameter or a machined spiral based on the relative magnitudes of the rotational speed and traverse rate. The dynamics of the jet, controlled through hydraulic and abrasive parameters, will affect both the qualitative and quantitative results, but the general geometry may not be affected. Figure 9a shows a double helix spiral being machined with an AWJ using a specially built AWJ lathe. Synchronization of the rotary motion of the part and axial motion of the nozzle is key to producing accurate dimensions, especially for a double helix, which requires forward and backward passes. Figure 9b shows another helical shape machined by an AWJ traveling over the centerline of a rotary part. Inspection of the helical surfaces

produced shows line-of-sight marks extending in the radial direction. Applications in heat exchanger design and screw feeders can greatly benefit from this simple process.

3.3 Milling

The milling of complex shapes was conducted to demonstrate the degree to which the depth of milling can be controlled. This approach involved the use of masks to machine complex patterns, such as isogrid structures (Hashish, 1994), on the inside and outside of cylinders, cones, and domes. Figure 10a shows a part milled to a depth of 0.25 inch with an accuracy of 0.001 inch using this method. The milling of variable-depth pockets can also be achieved by controlling the exposure time of the AWJ over the different areas to be milled. Milling of variable-depth pockets can be accomplished by controlling the exposure time through the traverse rate and number of passes. Milling can also be used for multiple pattern cutting. For example, a large number of holes can be drilled simultaneously by using a mask drilled with the hole pattern. The milling of thin closely spaced slots can be accomplished with or without a mask. Figure 10b shows 0.030 inch wide slots milled with an AWJ.

Similar to polishing, the surface finish of milled parts can be improved by reducing the grit size. The use of a waterjet pass for surface cleaning showed that embedded abrasives can be removed effectively.

3.4 Small Hole Drilling

The drilling of relatively small-diameter (up to 0.25 inch) holes with an AWJ may be conducted using piercing and trepanning either separately or combined, (Hashish, 1994).

The majority of drilled holes in the industry are pierced and trepanned and are over 0.035 inch in diameter. However, recent advances were made to drill holes in the diameter range of 0.015 to 0.025 inch for jet engine applications. Figure 11 shows a 0.003 inch diameter hole drilled in glass. The length of this hole is over 1.5 inch. The use of small-diameter jets and computerized pressure ramping are key to producing high-quality holes both qualitatively and quantitatively. Pressure ramping eliminated delamination, chipping or cracking, and significantly reduces the drilling time. The use of small-diameter jets and ramped pressure requires the use of vacuum assist for abrasive entrainment.

3.5 Lathe Turning

Turning with an AWJ is a relatively simple process. The workpiece is rotated while the AWJ is traversed axially and radially to produce the required turned surface. Work on AWJ turning has addressed the volume removal rate, surface finish control, visualization and modeling (Ansari and Hashish, 1992) of the turning process, and the development of a hybrid AWJ/mechanical lathe.

The depth of cut, which is determined from the radial jet position, is a critical parameter for process optimization. Figure 12 shows trends for the effect of the depth of cut on the machined diameter and the volume removal rate. Typically, the volume removal rate

increases as the depth of cut is increased. Unlike conventional turning, AWJ turning is less sensitive to the original part shape. For example, a highly irregular geometry can be turned in one pass with a relatively large depth of cut to a surface of revolution, as shown in Figure 13. Also, AWJ turning is not sensitive to the length-to-diameter ratio of the workpiece. Long and small-diameter parts have been turned to precise dimensions. Underwater turning has also been demonstrated to significantly reduce the noise on the AWJ.

The processes of turning and cutting can be combined to improve the volume removal rate. With this method, prior to turning a part, a number of linear cuts are made to reduce the initial diameter. A number of experiments were conducted using a 2-inch-diameter magnesium silicon carbide rod in which a three segments were first cut out, resulting in a polygonal shape, and then the rod was turned to its final diameter. Using this approach, the machining time can be reduced by over 50%.

The AWJ was also used to turn threads in glass, as shown in Figure 14. No mechanical tool was used in this case.

3.6 Hybrid Lathe Turning

A hybrid AWJ/mechanical lathe was built by modifying a conventional lathe to allow simultaneous turning with the AWJ and a solid tool, with the solid tool performing the finishing process. The AWJ nozzle can either be mounted on a separate manipulator for flexibility of pattern machining or mounted on the tool carriage when accurate synchronization between the rotational and axial motion is required. Figure 15 shows a rod of Mg/SiC turned on the hybrid lathe. The AWJ was used to produce a diameter 0.25 mm greater than the required diameter. The machined surface was simultaneously finished using a solid single-point tool immediately behind the AWJ. This approach was found to be most efficient to obtain surface finishes better than 200 micro inch.

3.7 Three-Dimensional Machining

Figure 16 shows samples of glass and granite machined automatically using an AWJ. These parts demonstrate the flexibility of the AWJ process for cutting, turning, and drilling using the same setup and the same nozzle. A controller program was written to fully automate the machining process, which includes automatic quick-change nozzles. Also implemented was an intelligent manufacturing process involving parameter changes.

4. ENABLING COMPONENTS

4.1 Quick-Change Nozzles

To automate the AWJ machining process similar to CNC operations, a quick-change nozzle was developed. This nozzle, shown in Figure 17, consists of a nozzle body that attaches to the end effector and cartridges that represent AWJ tools. A cartridge contains the jewel and the mixing tube in an alignable assembly. The alignment of the cartridge was provided to

allow the user to select the proper combinations of waterjet orifices and mixing tubes and also to be able to reuse the cartridge for several applications. The challenge of reliable cartridge operation was to design a small-size, nonmetal-to-metal, high-pressure quick-connect seal with minimal maintenance. Another critical design criteria was position accuracy of the mixing tube tip.

Significant reduction in down time was observed in operations requiring multiple machining operations when the quick-change nozzle was used in the industry (Whalen, 1993).

4.2 Abrasive Flow Rate Sensor

To measure the abrasive mass flow rate directly, a force sensor can be placed in the path of the abrasive particle stream, which free-falls from the metering valve. The force on the sensor is proportional to the change in momentum of the stream of abrasive particles. The change in momentum is in turn a function of the mass flow rate.

A force sensor was constructed for this application. The force sensor is constructed by measuring the deflection of a spring. In this case, the spring is a cantilever beam, with a strike plate at the free end to act as a target for the abrasive stream. Figure 18 shows a picture of the abrasive flow rate sensor. A ceramic strike plate is used to resist the erosion of the falling abrasives.

A differential pair of eddy current displacement sensors is used to sense the beam deflection. The use of differential sensors provides a very stable gain and offset calibration. Of particular importance is the gain stability over time and temperature.

4.3 Jewel Health Sensor

A physical measure of the quality or health of a waterjet is the coherence length. A long coherence length provides the most efficient and stable machining conditions and is therefore most desirable.

Two methods of monitoring the health of the waterjet jewel were selected for evaluation. The first was an acoustics-based approach, looking for changes in the acoustic signature to infer changes in the shape of the waterjet as it forms in the jewel. The second approach was to monitor the vacuum level in the mixing chamber, located just below the jewel in the nozzle. The later method was selected for further development due to its simplicity.

Figure 19 shows a cutaway drawing of the pressure-based sensor and the location of the sensing port in the waterjet head.

Disturbance of the upstream flow produced poor-quality jets to simulate worn-out jewels. Correlation of sensor reading was conducted with the following parameters:

- Waterjet coherence length
- Abrasive feed rate

- Mixing tube diameter
- Waterjet pressure
- Jewel size

Figure 20 is a chart showing the results from one series of tests. These tests were done using a 0.016-inch-diameter jewel, a 0.047-inch-diameter mixing tube, and mesh 60 garnet. Tests for this jewel size were performed at four different abrasive rates, four different coherence lengths, and three different pressures. The figure shows the relationship between coherence length, pressure sensor reading, and abrasive rate. Note the primary relationship between the coherence length and the pressure reading with only a minor dependence on abrasive rate.

4.4 Nozzle Exit Diameter Sensor

The method selected to sense the diameter of the mixing tube is an optically based method. When a measurement needs to be done, the CNC brings the AWJ nozzle to an enclosed measurement station where the end of the mixing tube is imaged onto either a one- or two-dimensional solid state camera. Using very simple image processing techniques, the diameter and shape of the tube can be determined. Front lighting is used to increase the contrast of the tube. This presents a very-high-contrast, easy-to-interpret image to the measurement station.

An OPTCON (inspector series) machine vision sensor was used to evaluate this approach. The sensor consists of an imaging lens, a one-dimensional CCD camera, and pixel mechanic software to control the camera and process the data. The front-lit image of the exit tube is imaged onto the one-dimensional CCD array using a lens of the appropriate focal length to obtain the proper mix of resolution and field of view. The CCD array is aligned with the axis of rotation of the mixing tube. The pixel mechanic software is configured to measure the width of the central dark spot of the image, which represents the mixing tube exit diameter.

4.5 Vision-Assisted AWJ Machining

A new advance has been made in using machine vision to assist AWJ precision machining of out-of-tolerance parts. The part, in the form of a honeycomb grid, needed to be cut with several slots between specific cells without affecting cell walls. The machine vision camera, with the aid of a special lighting scheme, maps the part. The developed software program identifies AWJ beam paths to produce precise, accurate parts. Another software program was also developed to interface the vision software with the manipulator controller and AWJ components. To avoid the harsh environment of the AWJ operation, vision and cutting were performed in separate stations. Calibration was performed to determine the spatial relationship between the two stations and to develop a mathematical transformation function. The transformation function is applied to the vision-generated data.

5. CONCLUSIONS

- Advances in new jetting beams include superpressure waterjets and AWJs, high-pressure ASJs, cryogenic jets, and abrasive cryogenic jets. These techniques have been

demonstrated in the laboratory and are currently under development for industrial use.

- Advances in processing include turning, milling, small hole drilling, polishing, and deep hole drilling. Turning to an accuracy of 0.02 mm was demonstrated. A hybrid AWJ/mechanical lathe has been investigated and shows great promise for optimized turning. Milling can be accomplished to an accuracy of 0.025 mm. Both flat and variable-depth pockets can be machined. Hole drilling can be accomplished to an accuracy of 0.025 mm and a precision of 0.025 mm. Holes with length-to-diameter ratios of 100 can be drilled.
- Advances in hardware include an automated quick-change AWJ nozzle, jewel health sensor, mixing tube sensor, and abrasive flow rate sensor.

6. REFERENCES

Ansari, A. I., and Hashish, M., "On the Modeling of Abrasive Waterjet Turning," *Jet Cutting Technology*, A. Lichtarowicz, ed., Kluwer Academic Publishers, Boston, pp. 555-576, 1992.

Dunsky, C. M., and Hashish, M., "Feasibility Study of Machining with High-Pressure Liquefied CO_2 Jets," *Manufacturing Science and Engineering*, Book No. G0930A, PED-Vol. 68-1, The American Society of Mechanical Engineers, pp. 453-460, 1994.

Hashish, M., "Drilling of Small-Diameter Holes in Sensitive Materials," *Proceedings of the 12th International Conference on Jet Cutting Technology*, N. G. Allen, ed., BHR Group Conference Series, Publication No. 13, pp. 409-424, 1994.

Hashish, M., and Bothell, D., "Diamond Polishing with Abrasive Suspension Jets," WJTA Conference, May, 1993.

Hollinger, R. H., and Mannheimer, R. J., "Rheological Investigation of the Abrasive Suspension Jet," *Proceedings of the 6th American Water Jet Conference*, Houston, Texas, August 24-27, pp. 515-528, 1991.

Raghavan, C., and Ting, E., "Hyper Pressure Waterjet Cutting of Thin Sheet Metal," *Proceedings of the 6th American Water Jet Conference*, Houston, Texas, August 24-27, pp. 493-514, 1991.

WJTA, "Liquid Nitrogen Jets Remove Rocket Propellant," *WJTA Jet News*, G. Savanick, ed., Water Jet Technology Association, St. Louis, Missouri, May, pp. 1-4, 1994.

Whalen, J. M., "Application of Advanced Abrasive Waterjet Machining at GE Aircraft Engines," *Proceedings of the 7th American Water Jet Conference*, Seattle, Washington, August 28-31, pp. 883-897, 1993.

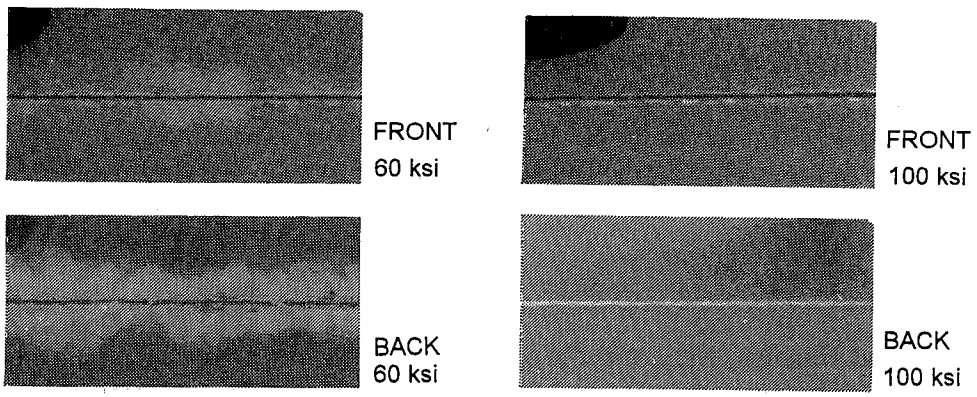

Figure 1. Elimination of Delamination Using 60- and 100-ksi Waterjets.
Orifice diameter = 0.005 in., traverse rate = 175 in./min.

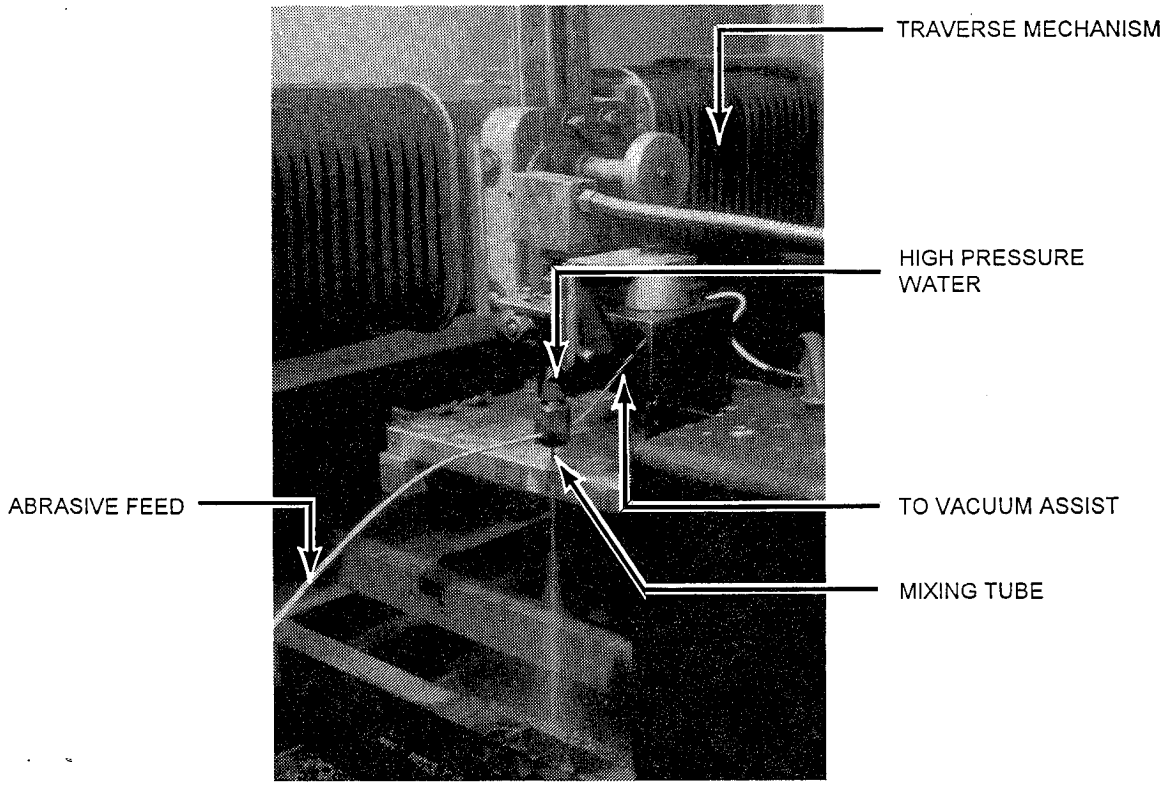

Figure 2. 100-ksi Abrasive-Waterjet Nozzle Cutting Through a 1-Inch-Thick Steel Plate. Nozzle diameter = 0.003 inch, mixing tube diameter = 0.007 inch.

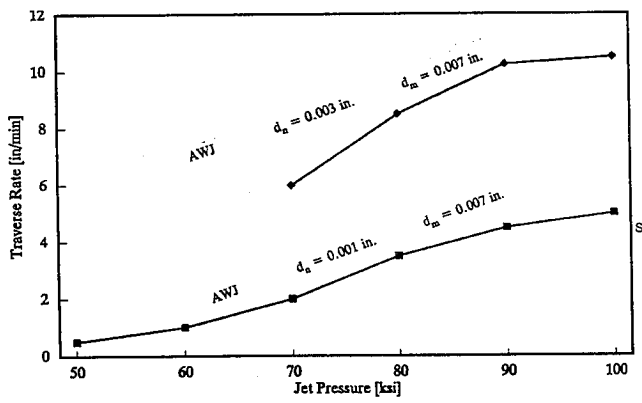

Figure 3. Effect of Pressure on Traverse Rate Using Small AWJ Nozzles

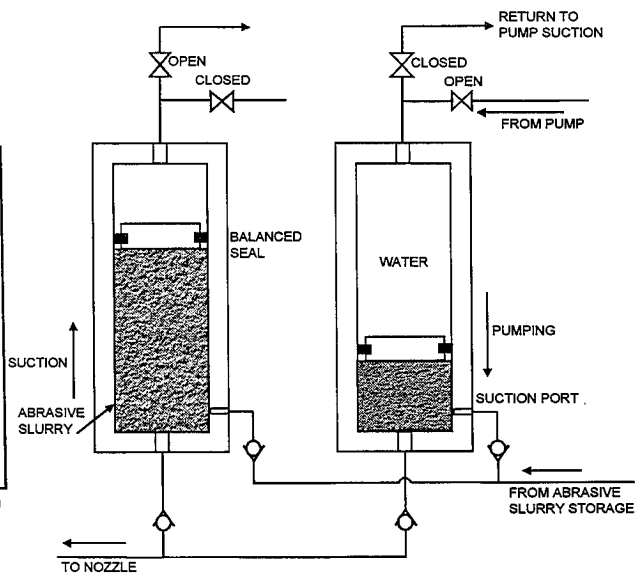

Figure 4. High-Pressure Continuous Pumping System for Abrasive Suspensions

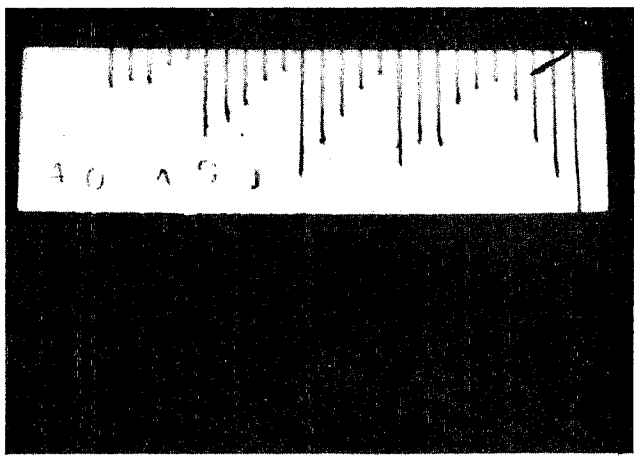

Figure 5. Thin Cuts Made in 1-Inch-Thick Aluminum with ASJs

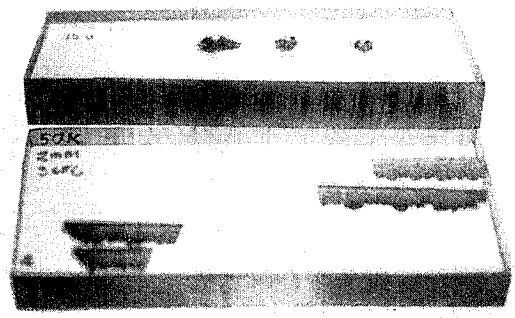

Figure 6. Lexan Coupon Drilled and Cut by 50-ksi CO_2 Jet

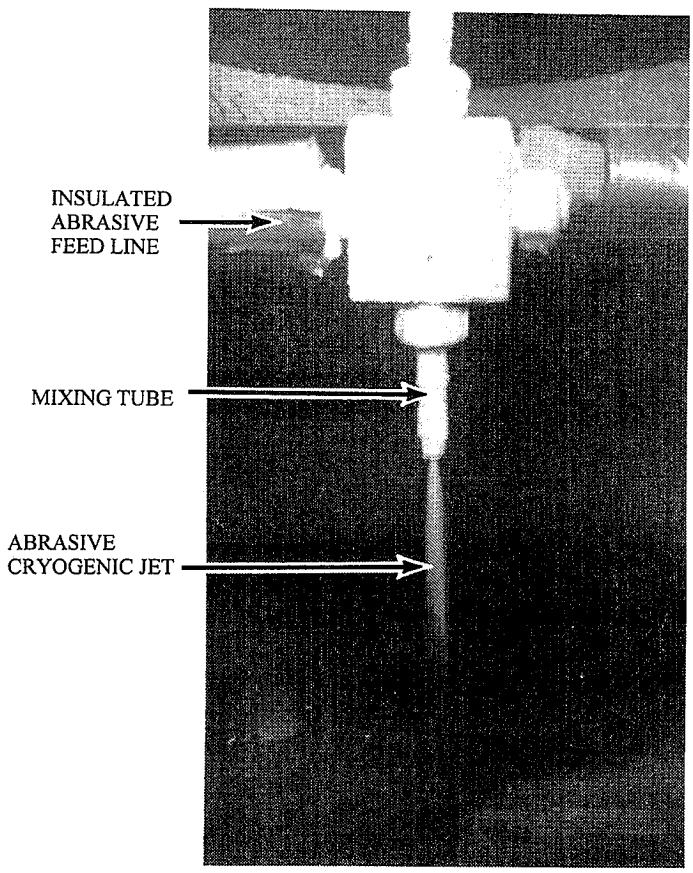

Figure 7. UHP Liquid Nitrogen Jet with Abrasive Entrainment

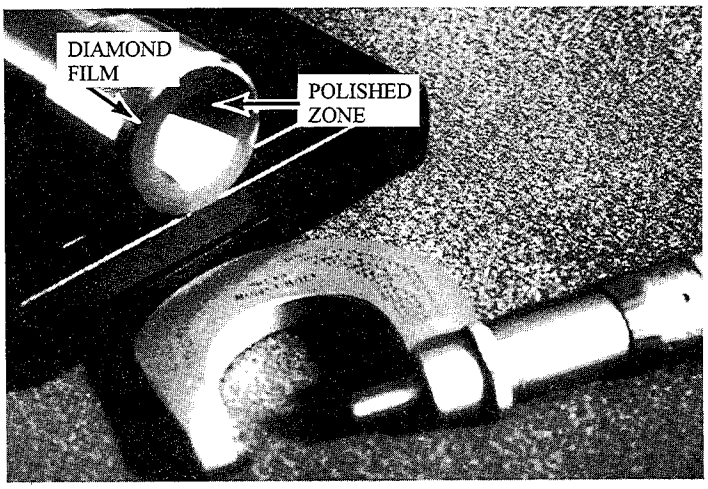

Figure 8. Diamond Film Polished with an ASJ (reflection shows in polished zone)

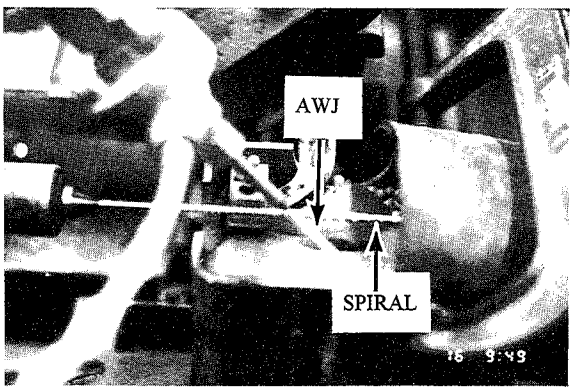

a. Double helix spiral

b. Helical shape machined by an AWJ traveling over the centerline of a rotary part

Figure 9. Spiral Machining on an AWJ Lathe

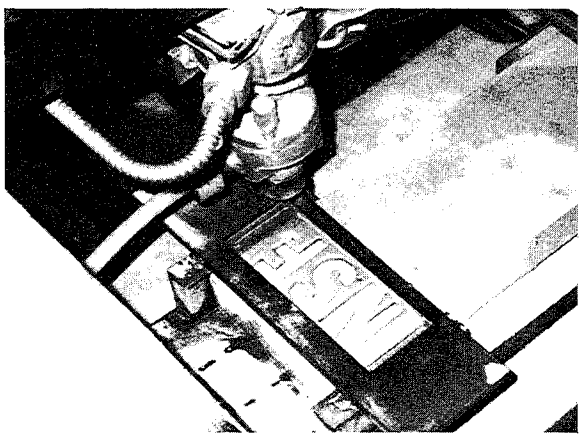

a. Milling pockets

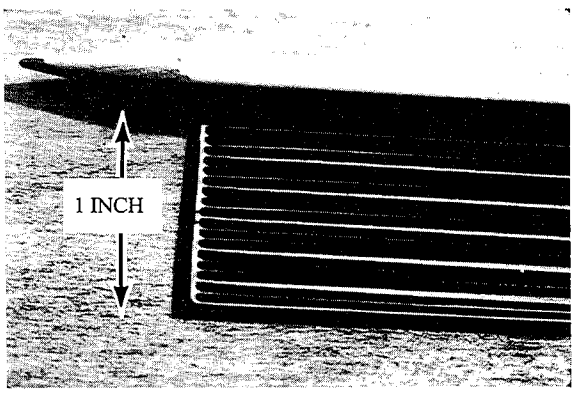

b. Milled slots

Figure 10. AWJ Milling Examples

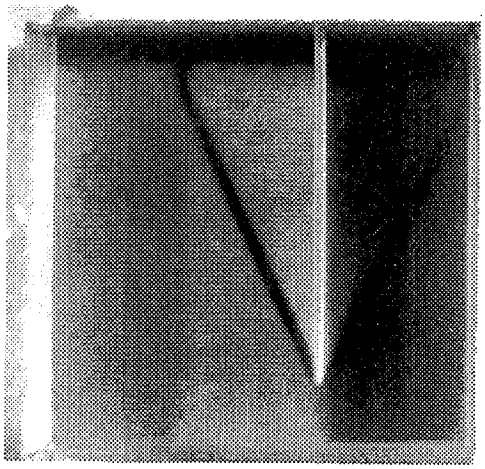

Figure 11. Small-Diameter Hole Drilled in Glass

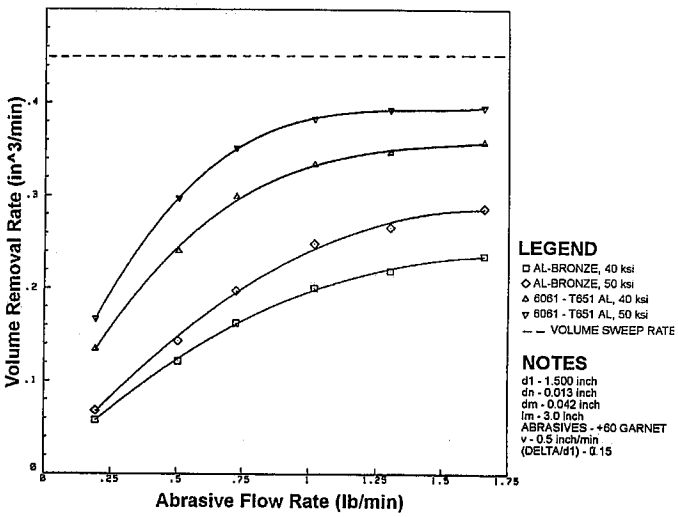

Figure 12. Effect of Depth of Cut on Volume Removal Rate in Turning of Various Materials

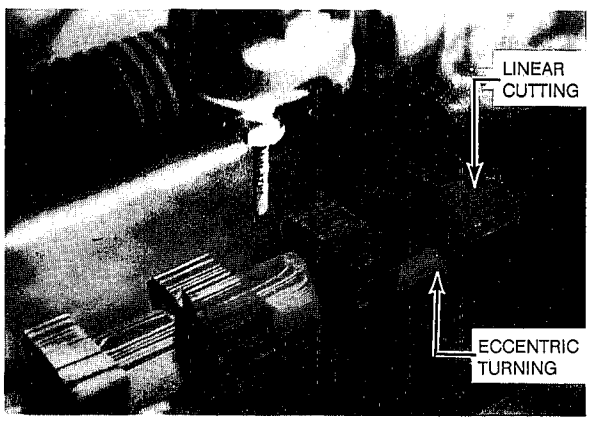

Figure 13. Turning of Irregular Shaped Composite with AWJ

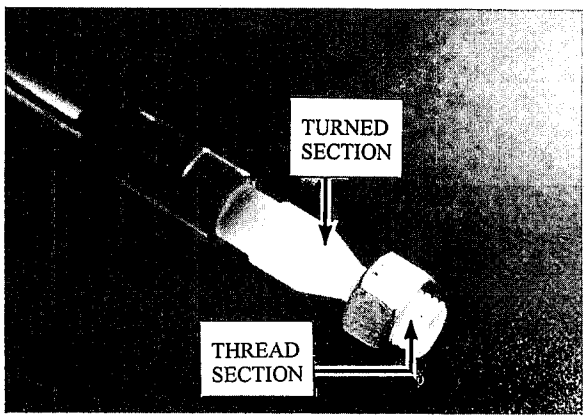

Figure 14. AWJ-Turned Threads in Glass

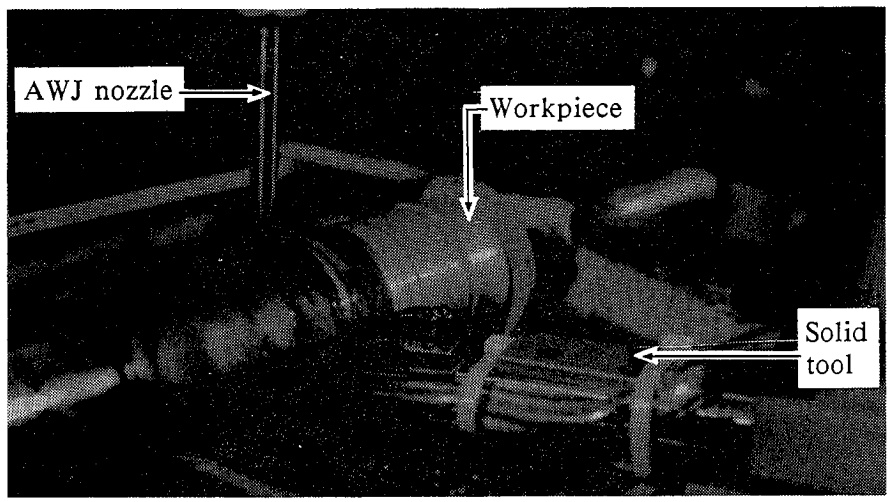

Figure 15. Hybrid Mechanical AWJ Lathe

Figure 16. Example of Three-Dimensional Machining with AWJ

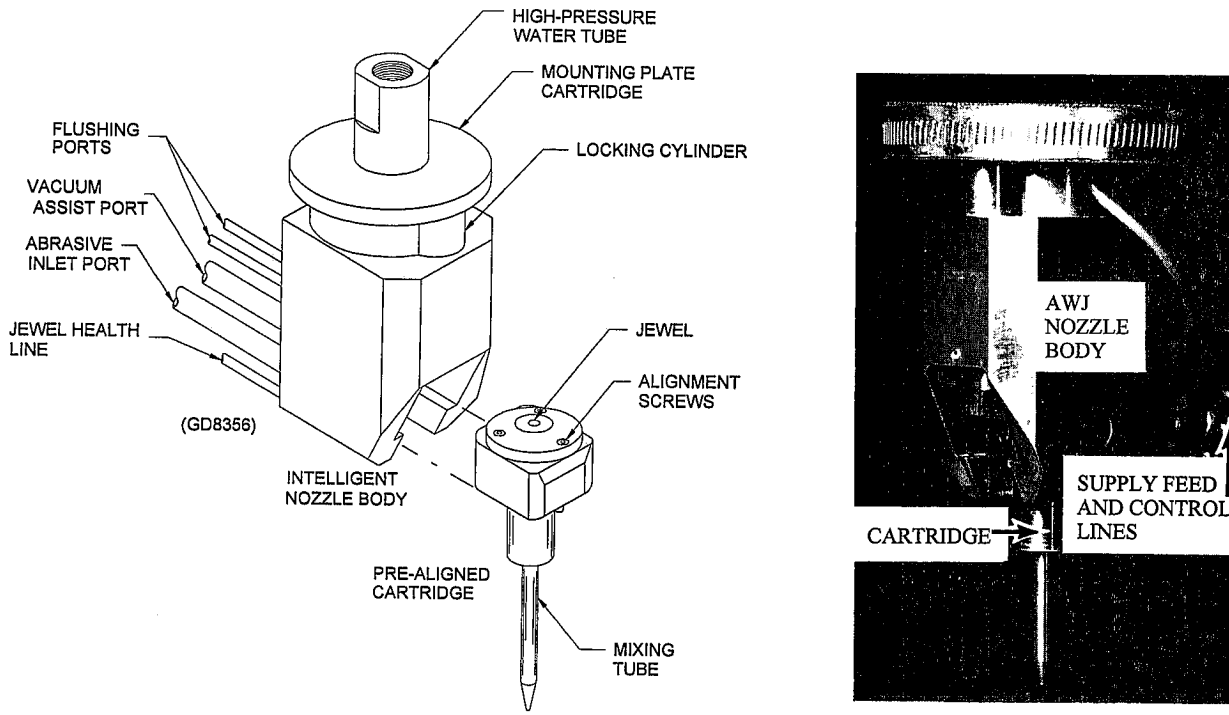

Figure 17. Quick-Change Nozzle

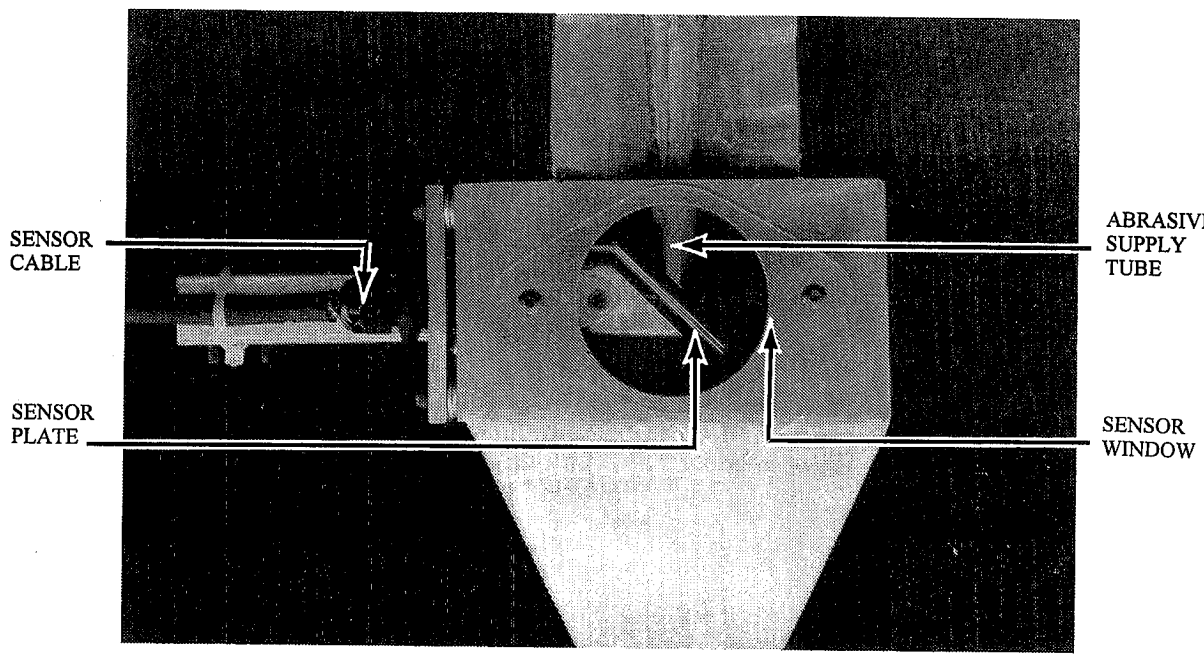

Figure 18. Abrasive Flow Rate Sensor

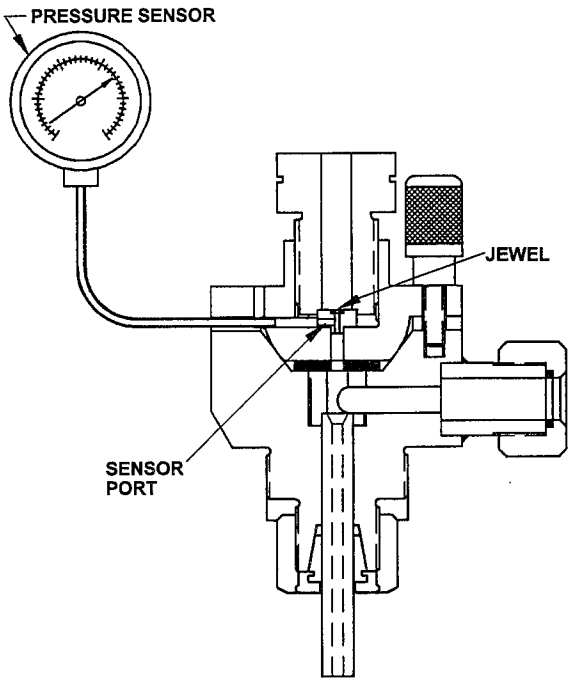

Figure 19. Pressure-Based Jewel Health Sensor

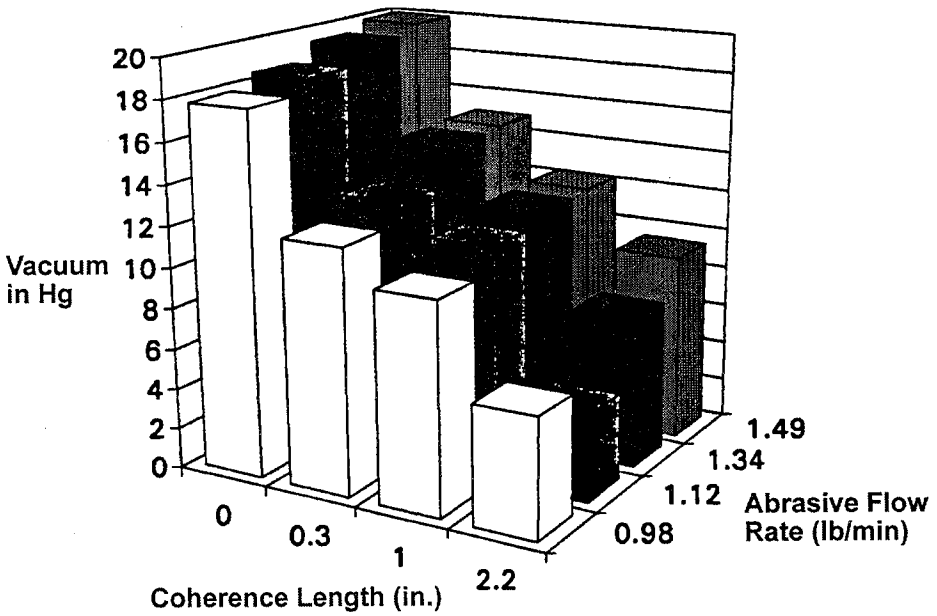

Figure 20. Pressure-Based Jewel Health Sensor Response

8th American Water Jet Conference
August 26-29, 1995: Houston, Texas

Paper 35

FEASIBILITY STUDY OF THE USE OF ULTRAHIGH-PRESSURE LIQUEFIED GAS JETS FOR MACHINING OF NUCLEAR FUEL PINS

C. M. Dunsky and M. Hashish
QUEST Integrated, Inc.
Kent, Washington, U.S.A.

ABSTRACT

This experimental study examined the feasibility of using ultrahigh-pressure (UHP) cryogenic jets for cutting the metal fuel pins for the proposed Department of Energy Integral Fast Reactor. The concept offers all the machining advantages associated with abrasive-waterjet cutting, while eliminating the liquid residue that poses special waste generation and handling problems in hazardous or toxic applications. To establish expertise in handling UHP liquefied gases, CO_2 jets were first investigated. Although liquid CO_2 is thermodynamically unstable at ambient conditions, UHP mixed-phase CO_2 jets were successfully produced in this study at pressures from 70 to 345 MPa. The CO_2 jets were found to have significant capabilities for drilling, cutting, and surface removal of common materials, comparable to that of pure waterjets at similar conditions. After cutting or drilling, workpieces were left clean, cold, and completely dry. The cutting power of the jets was found to decrease rapidly with distance. A subsequent study explored the formation of UHP liquid nitrogen (LN_2) jets at pressures up to 100 MPa. LN_2 was selected as a close, inexpensive simulant of liquid argon. Most tests yielded UHP LN_2 jets with insufficient liquid content for substantial cutting power. Several, however were able to produce shallow cuts in soft materials, such as wood, and surface damage on harder, brittle materials.

Organized and Sponsored by the Water Jet Technology Association.

1. INTRODUCTION

This study was conducted to examine the process parameters required to achieve ultrahigh-pressure (UHP) jets of both liquid carbon dioxide and liquid nitrogen for material removal applications such as cutting, machining, or cleaning. Specifically, we examined the feasibility of developing a liquefied gas (argon) jet machining system for cutting the metal fuel pins for the proposed DOE Integral Fast Reactor (IFR). In the IFR's pyrometallurgical fuel recycle process, fuel pin injection casting and machining operations will be carried out in a heavily shielded cell containing a dry argon atmosphere. All equipment used in fuel recycle processes must therefore be robust, remotely maintainable, and automated or remotely operable. It must also be chemically compatible with the argon atmosphere and the uranium-plutonium-zirconium fuel material itself.

To solve fracture problems encountered with conventional shearing of the highly brittle fuel alloy, jet cutting with cryogenic liquid argon was proposed. The concept offers all the machining advantages commonly associated with UHP abrasive-waterjet (AWJ) cutting, while eliminating the liquid residue that poses special waste generation and handling problems in hazardous or toxic applications.

More generally, liquefied gas jets of substances such as CO_2, N_2, or air have attractive environmental, technical, and economic characteristics. These substances are odorless, inert, and nontoxic, and their density and viscosity are suitable for high-pressure flow conditions and for forming coherent jets. They are also relatively inexpensive and are among the chemical materials most abundantly produced today.

UHP liquefied gas jets offer a number of potential advantages over the use of waterjets or AWJs in cutting or cleaning operations. These include the following:

- Elimination of liquid residue, since these substances are gaseous at room temperature and pressure. This is very desirable, both in environments that must be kept very clean and in applications where the workpiece contains highly toxic or radioactive material. In the former case, workpiece contamination can be minimized, while in the latter, hazardous waste disposal problems may be mitigated.
- Potential extension of jet cutting to applications in which fragile equipment or materials are located downstream of the intended workpiece surface. The cutting power decreases rapidly with downstream location due to the rapid broadening of the jet's axial momentum flux distribution as the liquid vaporizes.
- Potential for the use of volatile solids such as CO_2 as an abrasive material within the jet to augment cutting or cleaning performance, further reducing the volume of residual material to be removed and processed.
- Possible modifications in the failure mode of the workpiece material due to the decrease in its temperature below the ductile/brittle transition temperature.

In the present study, two experimental investigations were carried out, utilizing liquefied CO_2 and liquid nitrogen, respectively. Tradeoffs in the ease of handling and pressurizing these substances were identified, forming the basis for future work in this area.

2. LIQUEFIED CO_2 JETS

In this study, an experimental apparatus was constructed to demonstrate the feasibility of producing UHP jets of liquefied CO_2 and to examine their potential for material removal. Although CO_2 is not compatible with the IFR environment, our objective in this task was to quickly determine the process parameters required to achieve and control a liquefied gas jet of any material and to compare its cutting capability with that of waterjets.

Figure 1 shows a temperature-entropy (*T-S*) chart for CO_2. The critical temperature and pressure are 304.2 K and 7.39 MPa, respectively. In practical terms, this indicates that CO_2 exists in a liquid phase at high (room) temperatures if maintained under pressures of only several hundred psi. This is in contrast to substances such as N_2 (where T_{crit} = 126.2 K and P_{cri} = 3.39 MPa), which must be maintained at much lower temperatures to exist in the liquid phase. On the other hand, Figure 1 indicates that, at atmospheric pressure, CO_2 exists stably in only the solid or gaseous phases. In contrast, substances such as N_2 and air exhibit stable liquid phases at atmospheric pressure if sufficiently cooled. Thus, in choosing to work with liquefied CO_2 rather than liquefied N_2 or air, one gains the advantage of requiring less cooling, which translates to more relaxed requirements on the operating temperature ranges of UHP system components. This benefit, however, is gained at the expense of having to contend with the thermodynamically unstable nature of liquid CO_2 at ambient pressure.

Under relatively low pressure conditions (5-10 MPa), as liquid CO_2 is expelled through an orifice, its expansion to ambient pressure results in an aerosol jet of solid (dry ice) particles in vapor. The change of phase between a liquid and the solid/vapor mixture occurs at some finite rate, however. Under UHP conditions, the jet material is accelerated to high velocities according to the approximate expression

$$u = C_v \sqrt{\frac{2P}{\rho_0}}$$

for incompressible substances, where

u	=	jet discharge velocity
C_v	=	nozzle velocity coefficient (typically close to 1.00)
P	=	upstream (stagnation) pressure
ρ_0	=	upstream (liquid) density

For pressures ranging between 70 and 350 MPa, this yields CO_2 discharge velocities in the range of 360 to 820 m/s. If one wishes to maintain a jet of liquid CO_2 for, say, x mm downstream of the orifice before the phase transition to the solid/vapor mixture is complete, then the phase transition can take no less than $1.2x$ to $2.8x$ μs to occur. If, in fact, the phase transition takes place on time scales longer than tens of microseconds, then it would be possible for liquid CO_2 to emerge from the nozzle and impact a workpiece, with the CO_2

liquid phase existing during the process in a state of *thermodynamic nonequilibrium*. Since it seemed plausible that the phase transition does not occur more rapidly than this, it was decided to attempt jet formation with liquid CO_2. This eliminated the need to qualify for cryogenic service such system components as the liquid transfer lines, the UHP valves, the high-pressure piston seals, the nozzle orifice, and the UHP isolator vessel itself.

2.1 CO_2 Jet Experimental Apparatus

The experimental arrangement, shown in Figure 2, consisted of conventional UHP equipment and a microprocessor-based control system for timing of the valves controlling flow of the UHP working fluid and the liquid CO_2. The heart of the apparatus was a UHP isolator unit, which was comprised of a 15-5 stainless-steel UHP accumulator cylinder fitted with a piston of low thermal conductivity. This configuration allowed the jet material (here liquefied CO_2) to remain isolated from the UHP intensifier pumps by transferring pressure through a water/antifreeze mixture that was compatible with the intensifier hardware.

The isolator unit was placed in a drum container filled with fiberglass insulation. During testing, dry ice was also used instead of the fiberglass and as a cooling jacket surrounding the nozzle. Standard nozzle bodies and sapphire orifices were used to form the jet. Liquefied CO_2 was obtained in a commercially available pressure vessel. Under typical conditions, the liquid CO_2 was drawn from the vessel at about 1.3 to 1.7 MPa.

2.2. Experimental Results and Discussion

A variety of tests were conducted to develop procedures resulting in UHP liquefied CO_2 jets, to assess their material removal capability, and to examine their structure. These tests are described in the following sections.

2.2.1. Liquid-Phase Jet Formation

Preliminary tests were performed to establish the conditions under which the CO_2 jet would emerge from the nozzle with cutting power. The key physical criterion was found to be eliminating any vaporization of the liquid CO_2 as it entered and was pressurized in the isolator. When this did not occur, mixed-phase, intermittent jets with little material removal ability were produced.

2.2.2. Material Cutting Survey

Upon successfully obtaining UHP CO_2 jets, we performed a preliminary survey of their ability to cut or penetrate common materials. Tests were conducted with a 0.64-mm orifice and each consisted of a 5-second run. Results are summarized in Table 1. The tests indicate that these jets have significant material removal capability, comparable to that of pure waterjets at similar pressures.

2.2.3. Parametric Study of Jet Drilling

After establishing the capability of the CO_2 jets to cut the materials in Table 1, a more detailed parametric study of drilling performance was carried out using 12-mm-thick Lexan coupons. Figure 3 shows typical test pieces after cutting and drilling. In general, the holes drilled exhibited near-circular cross sections. Most of the holes, however, featured subsurface "butterfly" fractures, due to pressure buildup in the hole during the test (Figure 3b). In comparison, a waterjet expelled through the same orifice at the same pressure created holes that were somewhat deeper and had no butterfly fractures, but were smaller in diameter and less circular, leaving more rough "burr" material along the hole walls.

Figure 4 shows the penetration depth for the drilling tests plotted against workpiece standoff distance for four pressures. As expected, smaller standoff distances and higher pressures result in deeper penetration of the workpiece. At each pressure, there exists some maximum standoff distance beyond which the jet did not damage the workpiece. Physically, the thermodynamically unstable liquid changes phase to gas and solid as it moves downstream. This causes the jet to expand and decelerate. Eventually, a condition is reached at which the energy flux impinging upon the workpiece is insufficient to remove material. This characteristic could be exploited in applications in which rapid streamwise energy dissipation is desired to avoid damage to materials downstream of the intended workpiece.

Figure 5 shows drilling depth as a function of jet pressure for several test durations. The data indicate a weak dependence of penetration depth on test duration. Doubling the run time increased the depth attained by only 26-34%. However, run-to-run variations in the depth attained at *fixed conditions* were observed to be as large as 15-20%. Drilling depth dependence on pressure is significant, but weaker than linear.

Figure 6 shows the effect of varying the orifice size. The larger orifice appears to give slightly higher material removal rates, but again the variation with orifice size is within the bounds of the run-to-run repeatability. This is consistent with the view that the parameter largely controlling the material removal rate is the rate of energy transfer per unit area of the workpiece. To a first approximation, this parameter is independent of the orifice size.

2.2.4 Parametric Study of Linear Cutting

Lexan. Tests were also conducted in which the Lexan workpiece was traversed beneath the jet. Measurements of the cut depths indicated that they were constant to within about 20% over the length of the test. Kerf walls were near vertical for these relatively shallow cuts, and the kerf widths varied by less than 10% over the length of the cuts. Subsurface butterfly fractures were absent, due to the exit path provided by the kerf for the rebounding jet material, as in standard waterjet cutting.

Figure 7 plots the maximum cutting depth achieved in a particular test against the traverse speed. In each of the four tests performed at 345 MPa, the jet penetrated the thickness of the workpiece for at least one location along the cut. Hence, the figure does not reflect the actual dependence of cutting performance on traverse speed for these tests. The tests

performed at 207 MPa show slight dependence of the cutting performance on standoff distance, with maximum cut depth increasing by 15-25% as the standoff distance was decreased from 4 to 2 mm. As expected, maximum depth decreased as the workpiece was moved more rapidly.

Aluminum. Several tests were conducted in which a 4.8-mm-thick aluminum workpiece was traversed beneath the CO_2 jet. The piece sustained only slight surface damage for jet pressures below 200 MPa, regardless of the traverse speed. Some material removal was produced, however, at 345 MPa. A comparison was made of cut characteristics for 345-MPa CO_2 jets and waterjets at the same conditions. The waterjet was more effective than the CO_2 jet for aluminum cutting, removing material at traverse speeds well above the speed for which the CO_2 jet no longer produced significant damage. The CO_2 and waterjet cuts produced no major differences in the kerf shape or surface roughness.

3. LIQUID NITROGEN (LN_2) JETS

In a second study, experiments were conducted to develop a directly pumped UHP cryogenic liquid jet, such as the liquid argon jet proposed for use in the IFR fuel recycle processes. The objectives here were as follows:

- Demonstrate the feasibility of obtaining UHP cryogenic liquid jets.
- Assess their cutting performance relative to waterjets and the liquefied CO_2 jets.
- Identify areas needing further refinement in order to add abrasive particles to the jet and maximize its cutting power.

3.1 LN_2 Jet Experimental Apparatus

Although LN_2 is thermodynamically stable at ambient pressure, cryogenic temperatures must be maintained throughout the UHP apparatus. Since certification of standard UHP pumping equipment for service at liquid-nitrogen temperatures (77 K) requires significant engineering modifications, a commercially available cryogenic piston-type pump was used to pressurize the cryogen. Pressures up to 100 MPa were achieved with this apparatus.

Figure 8 shows a schematic of the cryogenic jet experiment. Bulk liquid nitrogen was supplied in a 2000-liter horizontal insulated tank mounted on a wheeled trailer. The UHP cryogenic pump and experiment hardware were located in an outdoor workshed so that the lengths of cryogenic feed lines could be minimized. All plumbing, including low-pressure LN_2 supply, vent lines, and UHP lines were jacketed with fiberglass and foam insulation. The pump itself was a single-cylinder reciprocating crosshead design, which creates substantial pressure oscillations at the discharge. To decrease these fluctuations, the pump discharge emptied into a UHP surge chamber in which a portion of the liquid was allowed to vaporize. This formed a gas cushion at the top of the chamber, which functions as a damper. Commercially available UHP plumbing components were used in the high-pressure portion of the apparatus, including standard sapphire waterjet orifices.

3.2. Experimental Results and Discussion

Most tests yielded UHP LN_2 jets with insufficient liquid content for substantial cutting power. Several tests, however, were able to produce shallow cuts in soft materials such as wood, and surface damage on harder, brittle materials. As in the CO_2 study, workpieces were left cold and dry after impact by LN_2 jets. Various mechanisms may have caused vaporization in the liquid flow, leading to loss of cutting power. First, heat transfer from the ambient may have warmed the liquid within the pump or experiment plumbing, in spite of the thermal insulation blanket. Second, restrictions and sharp turns in the UHP fittings and valves, which create pressure losses, may also be sites for cavitation of the liquid as the flow accelerates or becomes turbulent. Finally, as the high-pressure fluid accelerates through the orifice, frictional heating may add enough energy to the flow to cause vaporization when the liquid pressure drops to ambient.

Figure 9 shows N_2 jets obtained with sufficient liquid content for cutting. The jets typically vaporized and dissipated within 100-150 mm of the nozzle. Figure 10 shows wood and Lexan samples cut with these jets. Material removal appeared to be comparable to that caused by CO_2 jets at similar pressures.

Temperature and pressure measurements were recorded just upstream of the nozzle for several lower-pressure (5 - 35 MPa) tests. These jets were observed to spread rapidly and had no significant cutting power, both characteristic of mixed-phase liquid/vapor jets with high vapor content. Subsequent thermodynamic analysis showed that the measured temperatures were typically 20 - 50 K higher than the upstream conditions that would yield a saturated-liquid nitrogen jet in thermodynamic equilibrium at ambient pressure. Active cooling of the UHP LN_2 upstream of the nozzle appears to be necessary in order to reduce the fraction of vapor in the high-velocity jets. With proper upstream thermodynamic conditioning, LN_2 jets with cutting power are apparently obtainable.

4. CONCLUSIONS

Following are the major conclusions of this work:

1. Although liquid CO_2 is thermodynamically unstable at ambient conditions, ultrahigh-pressure, mixed-phase liquid/ vapor/solid CO_2 jets were successfully produced.
2. The CO_2 jets were found to have significant capabilities for drilling, cutting, and surface removal of common materials, comparable to or somewhat inferior to pure waterjets at similar conditions.
3. After being cut or drilled by the CO_2 jets, workpieces were left clean, cold, and completely dry. Materials placed much farther downstream in the jets were left with a small amount of surface moisture condensed from the ambient air.
4. No evidence of cold-induced brittle failure of metallic workpieces was observed in the CO_2 jet experiments.
5. The cutting power of the CO_2 jets was found to decrease rapidly with distance, presumably due to phase change and expansion of the jets. This could be a desirable

characteristic for applications in which damage to materials downstream of the intended workpiece must be avoided.

6. Preliminary investigations of cryogenic LN_2 jets were carried out. We met with some success in creating jets with cutting power. However, careful control of the thermodynamic state of the cryogenic liquid was found to be more important than that required for the liquefied CO_2 jets. Nozzle orifice geometry and the mechanics of abrasive addition to the jets were also identified as areas needing refinement.
7. Thermodynamic analysis indicates that with proper temperature control of the UHP cryogen, LN_2 jets with minimal liquid content are attainable. It is anticipated that with the addition of abrasives, these jets will equal AWJs in cutting performance.

5. ACKNOWLEDGMENTS

The CO_2 jet formation experiments were funded by QUEST Integrated, Inc. The LN_2 jet experiments were carried out under Department of Energy Contract No. DE-F003-93ER81648. The authors thank Mr. David Owens for his help fabricating and operating the experimental apparatus in both studies.

Table 1. Effect of UHP CO_2 Jet on Common Materials

Material	P (MPa)	Approx. Standoff Distance† (mm)	Result
Blue Polystyrene Foam	69	15	Penetrated 20-cm-thick slab.
6-mm Rubber Sheet	69	5	Penetrated.
Wood 2x4	69	5	Penetrated ~2 cm. Splintered large area. Much solid CO_2 embedded in damaged area.
3-mm Plexiglas	104	5	Penetrated. Fractured downstream face.
6-mm Aluminum	104	4-5	Surface damage.
2-mm Aluminum	207	4	Surface damage.
1.3-mm Aluminum	241	4	Penetrated.
0.9-mm Sheet Steel	104	4	No damage.
0.9-mm Sheet Steel	207	4	Surface damage.
0.2-mm Brass Shimstock	138	4	Dented.
0.2-mm Brass Shimstock	207	4	Penetrated. Small hole w/surrounding dent.

†Measured from exit hole in nozzle end-cap, not from sapphire orifice.

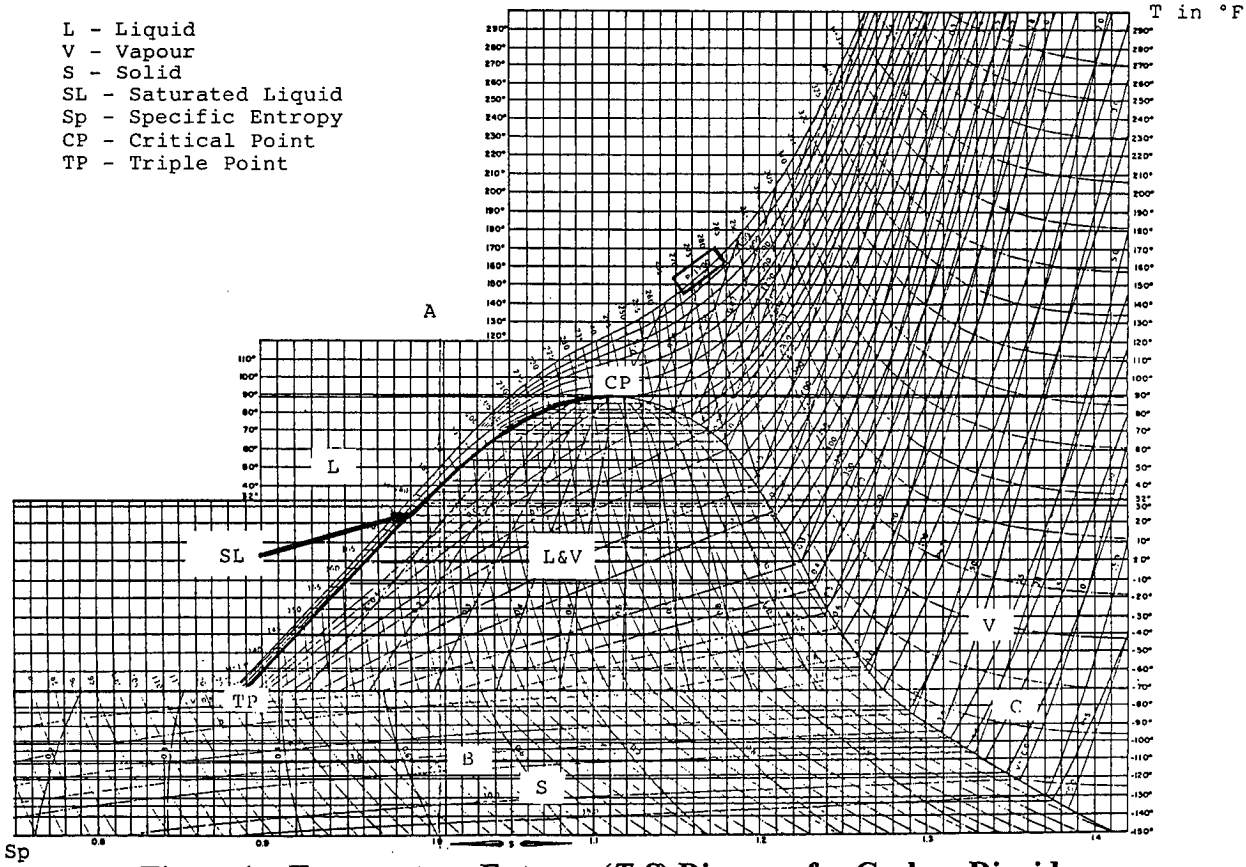

Figure 1. Temperature-Entropy (*T-S*) Diagram for Carbon Dioxide

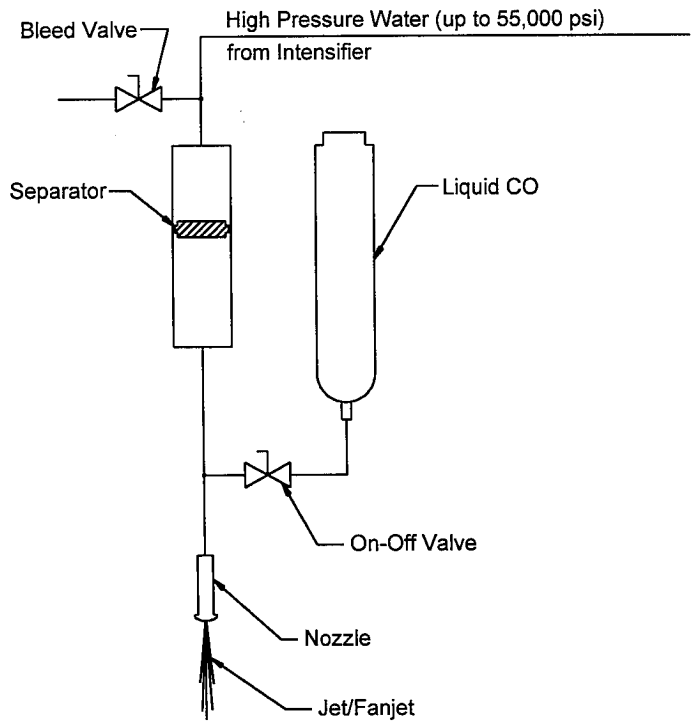

Figure 2. Ultrahigh-Pressure CO_2 Jet System Schematic

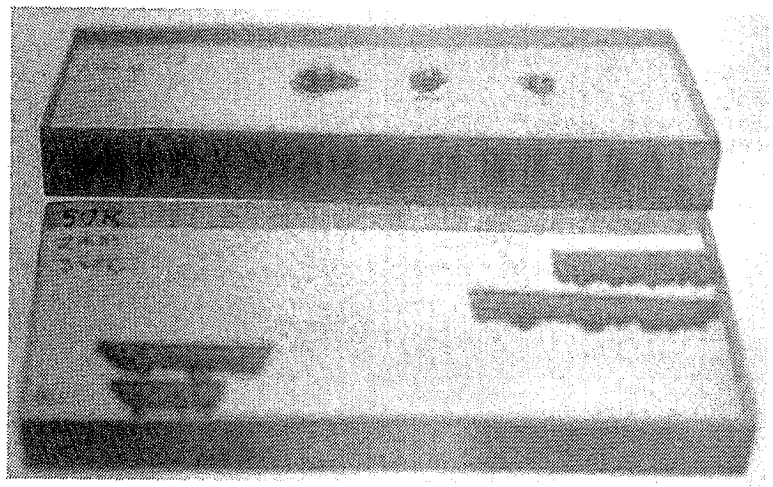

a. Upper coupon shows drilled holes; lower coupon shows test cuts

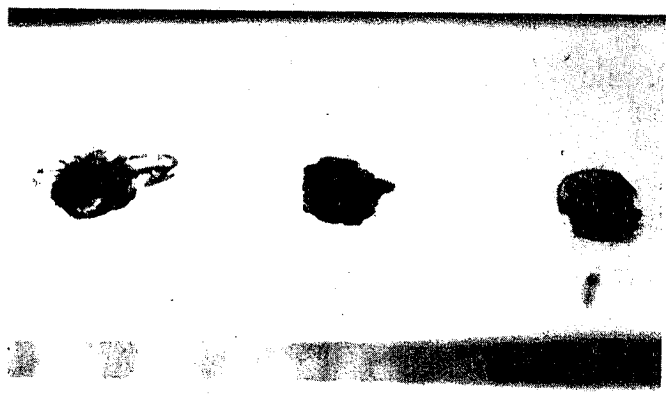

b. Close-up of holes drilled by a 0.64-mm-orifice jet with a 2-mm standoff distance

Figure 3. Lexan Test Coupons Drilled and Cut by 345-MPa (50-ksi) CO_2 Jets. Damaged areas appear larger due to the oblique view through the transparent Lexan, showing subsurface "butterfly" fractures emanating from the holes.

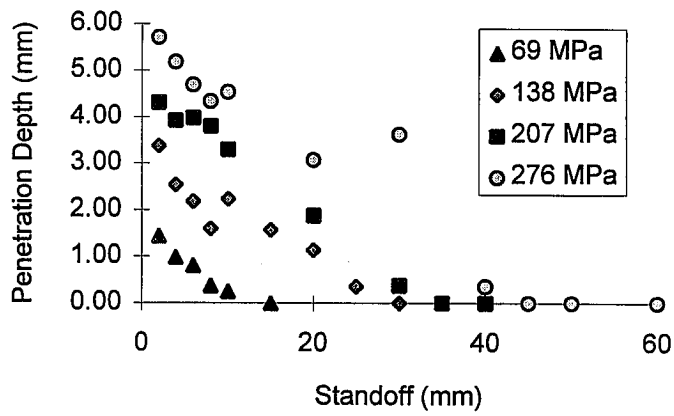

Figure 4. Drilling Tests on Lexan. Material removal increases with higher pressures and smaller standoff distances. At all pressures, a standoff distance is reached beyond which the jet does no damage to the workpiece.

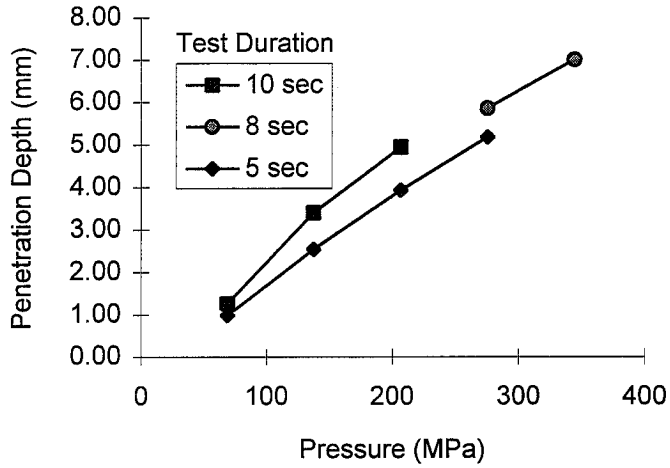

Figure 5. Drilling Tests on Lexan. Material removal increased slightly for longer run times, but nearly the same within the repeatability of the tests. Pressure dependance is weaker than linear.

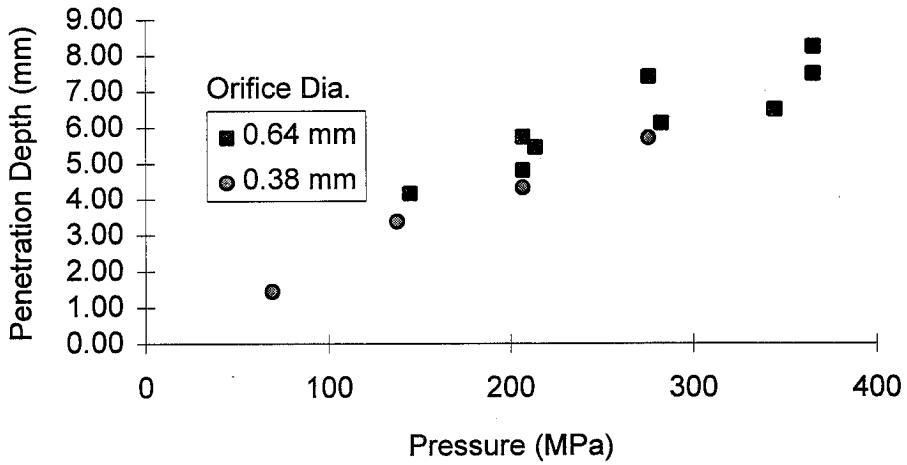

Figure 6. Drilling Tests on Lexan. Material removal increases slightly for larger orifice, but within the repeatability of the tests.

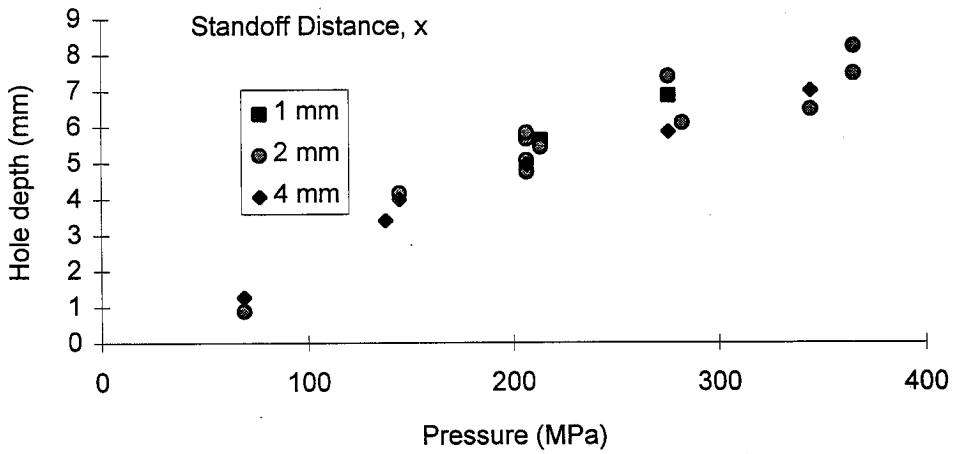

Figure 7. Cutting Tests on Lexan. All tests at 345 MPa penetrated through the workpiece at some location in the cut, so all have a maximum cutting depth equal to the coupon thickness.

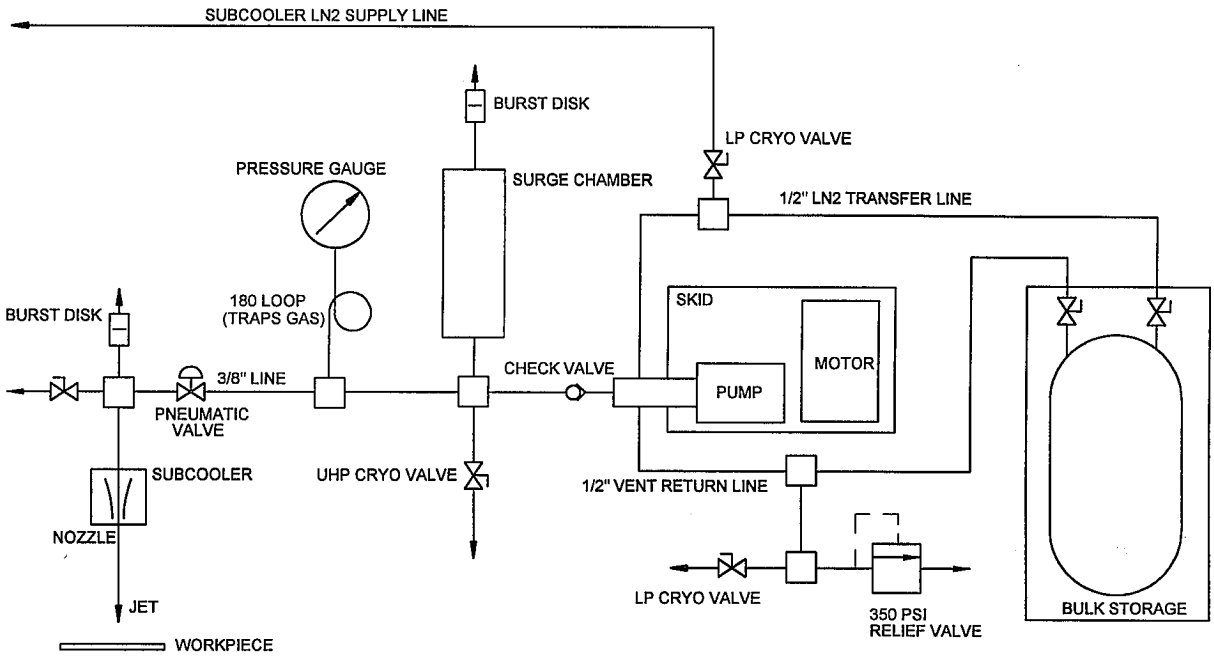

Figure 8. Schematic of UHP LN_2 Jet Experiment

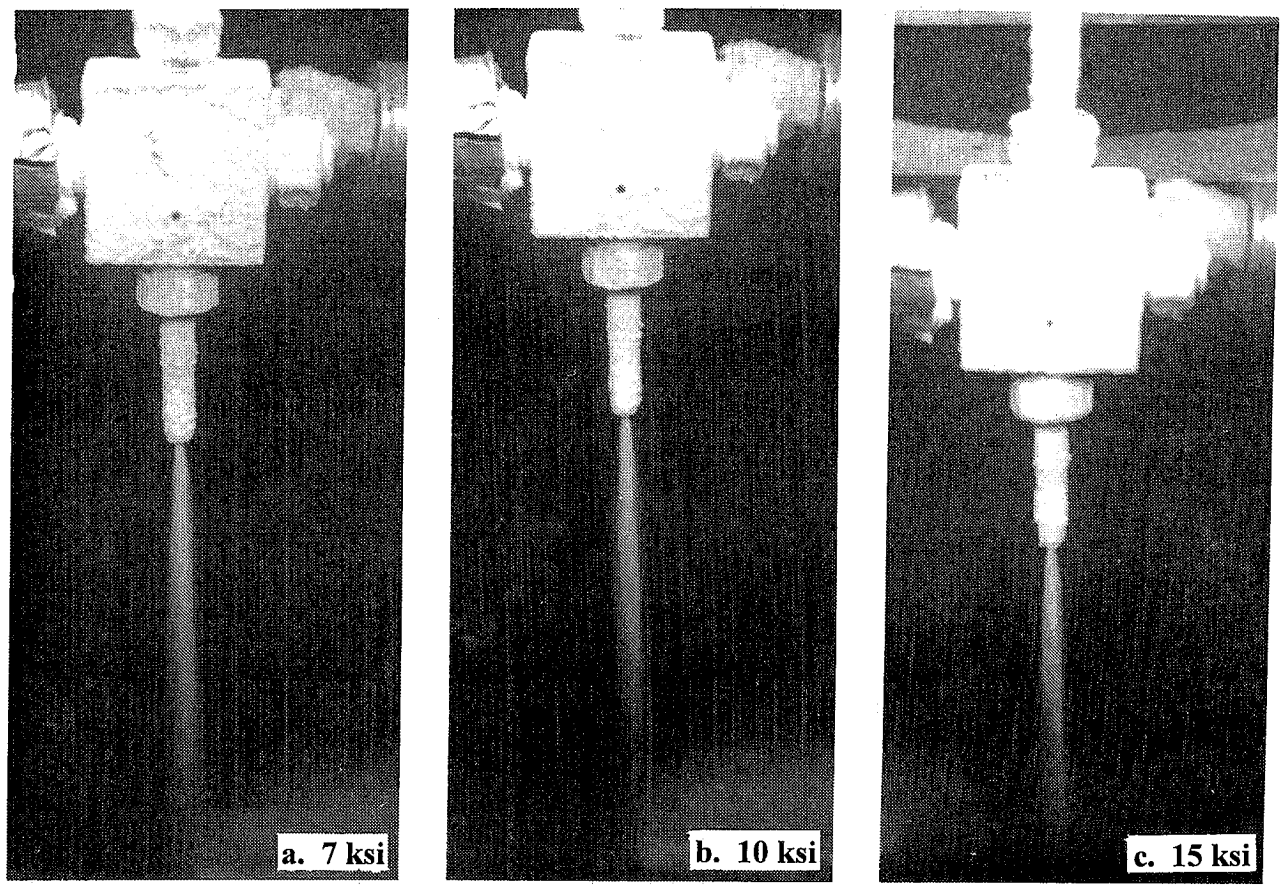

Figure 9. UHP Liquid Nitrogen Jets Obtained with a 0.46-mm. Sapphire Orifice

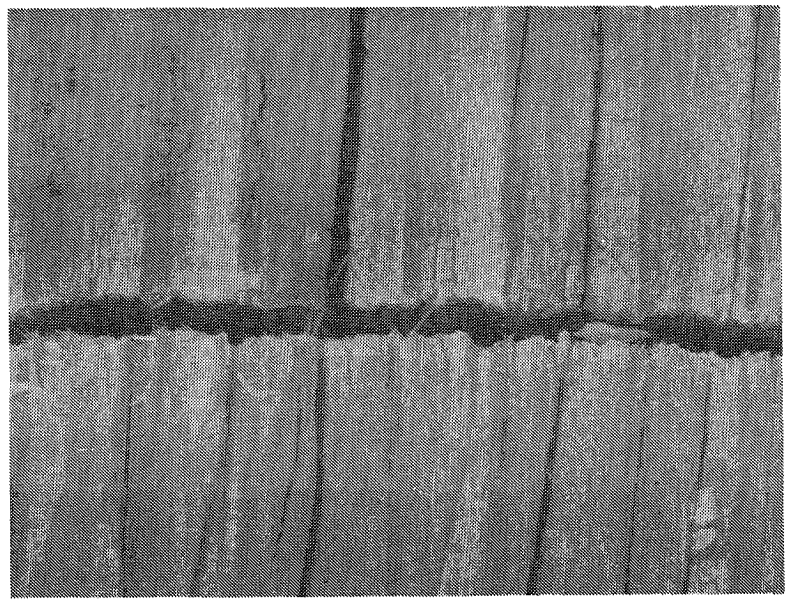

a. Wood 2x4. Kerf is ~1-mm wide and ~5-mm deep

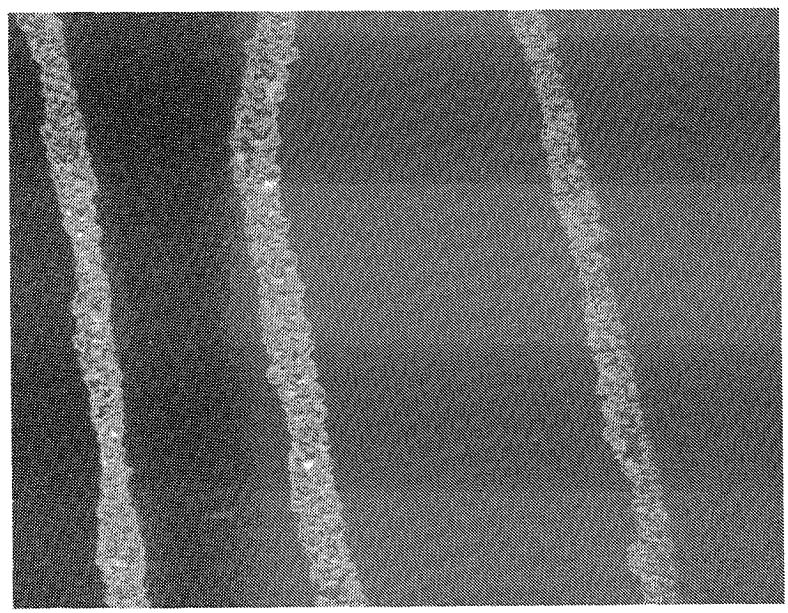

b. Lexan. Workpiece standoff distances are approximately 0, 3, and 6 mm for left, center, and right cuts

Figure 10. Sample Materials Cut with UHP Liquid Nitrogen Jets at 15 ksi with a 0.018-in. Sapphire Orifice

8th American Water Jet Conference
August 26-29, 1995: Houston, Texas

Paper 36

HIGH PRESSURE WATERJET APPLICATION TO IMPROVE PERFORMANCE OF MACHINING OPERATIONS

R. Kovacevic and R. Mohan
Department of Mechanical Engineering and
Center for Robotics and Manufacturing Systems
University of Kentucky, Lexington, Kentucky, USA.

ABSTRACT

Performance improvement in terms of better surface quality, reduced cutting forces, enhanced tool life and improved chip shape has always been the focus in metal machining processes. Detailed investigations conducted by the scientific community have demonstrated that this objective can be better achieved if the thermal/frictional conditions existing at the cutting zone can be controlled effectively. Cutting fluids have been used traditionally as an external means to dissipate the heat produced at the cutting zone and reduce the friction. However, the location of placement, speed and direction of application of cutting fluids are very important factors which determine their effectiveness. In order to improve the performance of two different machining processes namely face milling (where the material removal is due to interrupted cutting by a finite number of cutting edges) and surface grinding (where material removal is initiated by abrasion), suitable cooling/lubrication techniques are developed by the application of waterjet at high pressures. Salient features of these two techniques are presented in this paper. The results obtained indicate that apart from improvement in thermal/frictional conditions at the cutting zone (which was observed for both the processes), effective cleaning and resharpening of the grinding wheel was accomplished thereby improving the overall process performance.

Organized and Sponsored by the Water Jet Technology Association.

1. INTRODUCTION

Fundamentally, metal machining operations can be classified into two types namely, primary operations and finishing operations. In the primary material removal processes such as turning, shaping, milling etc., a tool penetrates into the workpiece and removes the material in the form of big chips through shearing action. This could be achieved either by continuous cutting (turning) or interrupted cutting (milling). In the case of finishing operations like grinding, material removal is accomplished by the abrasive action between the rotating wheel and the workpiece. Similar to other machining processes such as turning or milling, material removal in grinding also takes place in the form of chips, but of a much finer scale. However in grinding, the shearing process of chip formation is performed by a multitude of cutting edges randomly distributed and randomly oriented. In all these processes, a considerable portion of energy is expended in the formation and removal of chips. As a result, a lot of heat is generated at the cutting zone due to friction and plastic deformation. The factors which lead to higher energy consumption cause an increase in the frictional forces, workburn, subsurface cracking, residual stresses, tool/wheel wear, chip burn and poor surface finish. In the grinding process, the debris consisting of the chips and wheel particles have a tendency to adhere to the wheel and fill the pores. This undesirable effect, called wheel loading, causes drastic reduction in the grinding capability leading to the above problems. Frequent wheel dressing needs to be performed in order to remove this debris and resharpen the wheel which affects the productivity. The overall process efficiency of the above machining operations can be improved if the thermal/frictional conditions existing at the cutting zone and wheel loading (in case of grinding) can be controlled. Cutting fluids can be employed to achieve this objective. However, the effectiveness of the cutting fluids in abstracting the heat generated at the cutting zone, reducing the friction at the tool-workpiece interface and reducing the wheel loading effect depends upon the location of placement, rate of flow and direction of application of the fluids.

A flood of fluid directed towards the cutting zone is the conventional way of applying cutting fluids. But, it has been proved that the cutting fluids lose their effectiveness at high cutting speeds and severe cutting conditions. This is because of greater rate of heat generation, inability of the cutting fluids to reach the regions to be cooled and the tendency of the fast moving chips and workpiece to carry the fluid away from the cutting zone. Only 5% to 30% of the cutting fluid is effectively used in conventional flood application in grinding operations (Guo et al., 1992) because of the inability of the cutting fluid to penetrate through the thin air film barrier surrounding the wheel, and the high centrifugal force of the wheel.

Several attempts have been made in the past (Pigott et al., 1952; Ramaiyengar et al., 1965; Sharma et al., 1971; Mazurkiewicz et al., 1989; Lindeke et al., 1991; and Wertheim et al., 1992) to improve the effectiveness of the cutting fluids by employing high pressurized jet. These methods were primarily focused on single edge stationary cutting tool operations like turning and the pressures employed were ranging from 2.75 MPa to 280 MPa. Waterjet and oiljet were used as cutting fluids. The results indicated that cutting fluids injected into the cutting zone increased the tool life more than five (5) times, improved surface finish drastically, eliminated built-up edge, decreased coefficient of friction, reduced cutting force (about 60%) and improved chip shape. It was also concluded that applying cutting fluids

through the rake face of the tool was more beneficial than injecting through a remote nozzle as it reduces secondary shear, lowers interface temperature and changes the chip shape. The present authors have developed (Kovacevic, 1994a; Kovacevic et al., 1994b; and Kovacevic et al., 1995b) a coolant/lubricant system for rotary tool operations (face milling) based on high pressurized waterjet (up to 380 MPa).

Different methods have been adopted in the past to enhance the effectiveness of grinding fluids. Wagner et al. (1948) developed an apparatus for grinding fluid application at lower pressures and higher volume flow rate through a plurality of nozzles. Pigott (1958) developed another apparatus for application of grinding fluids at a pressure of 1.7 MPa so that the discharged jet by the nozzle will be at a speed sufficient to overcome the peripheral speed of the grinding wheel. A liquid coolant applying nozzle that supplies coolant in a direction opposite to the direction of wheel rotation was developed by Klassen (1976) to remove the air film and loose particles from the wheel surface. Apparatus such as air deflection flood nozzle (Werner et al., 1980), radial or spiral grooved grinding wheel (Radhakrishnan et al., 1986), etc. were used to penetrate the air cushion around the wheel; but they were not very successful in overcoming the wheel centrifugal force or providing effective cleaning and cooling/lubrication. Pressurized waterjet upto 2 MPa were used by Borkowski et al., 1989, and Lincoln (1992) for cleaning and cooling the grinding wheel. However, at such low pressures, the waterjet may not be able to provide effective cooling or cleaning of the grinding wheels. Thus, an effective technique needs to be developed to provide proper cleaning, cooling/lubrication and dressing/resharpening of the wheel. Towards this end, a technique has been developed (Kovacevic et al., 1995a) to deliver grinding fluid at ultra-high pressures (up to 165 MPa).

This paper discusses the salient features of the ultra-high pressurized waterjet based coolant/lubrication system developed for face milling and surface grinding operations. The effectiveness of the developed system for face milling operation is evaluated in terms of the cutting force, surface finish, chip shape and tool wear. The technique developed for ultra-high pressurized waterjet based grinding operation is evaluated by measuring the grinding force, surface finish and acoustic emission (AE) signal. The workpiece material stainless steel AISI 304 is used for investigation.

2. EXPERIMENTAL SETUP AND PROCEDURE

A schematic of the designed high pressure waterjet coolant/lubricant system in conjunction with face milling operation is shown in Fig. 1. Water from a high pressure intensifier pump capable of supplying cutting fluids up to 380 MPa is directed to the main flow channel in the cutter through a rotary swivel which provides sealing up to a rotational speed of 2000 rpm. The main flow channel directs the cutting fluid through a plurality of radially extending feed channels, a sapphire orifice and the EDM drilled hole in the insert. The jet of water is delivered to the tool-chip interface through the rake face of the insert at about 2.5 mm from the tool tip and oriented in such a way that it hits the underside of the chip as it gets formed. The number of radially extending feed channels depends upon the number of inserts mounted in the cutter. The experimental setup also includes a four component dynamometer, charge

amplifiers, A/D converter and a computer with suitable software. Cutting force components in X, Y and Z directions were acquired at a sampling frequency of 2 KHz using the dynamometer. In order to study the effectiveness of the high pressure waterjet cooling system, the experiments were performed by changing the hydraulic parameters namely water pressure and orifice diameter, keeping the conventional parameters such as cutting speed, feed and depth of cut constant. The process parameters adopted for these experiments are given in Table 1. The surface roughness was measured and the chips produced were collected for analysis.

A schematic of the experimental setup used for evaluating the ultra-high pressure waterjet coolant/lubricant system developed for the surface grinding operation is shown in Fig. 2. The cutting fluid that can be pressurized up to 380 MPa using a high pressure intensifier pump is brought through a flexible hose towards the grinding wheel. The pressure energy of the high pressure cutting fluid is converted into kinetic energy using a sapphire orifice placed at the end of the flexible hose. Suitable fixturing is provided to facilitate easy manipulation of the angular position of the waterjet and the stand-off distance of the nozzle from the grinding wheel. Orifice diameter (0.46 mm) was chosen such that the complete width (10 mm) of the grinding wheel can be covered by the ensuing waterjet. This design can be easily extended for higher wheel widths by providing a row of nozzles. The experimental setup also includes a horizontal spindle surface grinding machine, a four component dynamometer, charge amplifier, A/D converter, AE sensing unit (consisting of an AE sensor, pre-amplifier and oscilloscope), a computer with suitable software and the workpiece. The experiments were performed by varying the water pressure keeping the conventional parameters namely workpiece traverse speed and depth of cut constant. In order to quantify the influence of waterjet with progressive wheel wear, grinding force components and acoustic emission signals (at 1MHz sampling frequency) were monitored at four different stages of grinding time namely 2.5, 5, 7.5 and 10 minutes. A newly dressed wheel is used for experiments conducted at each water pressure setting. The process parameters for these experiments are also given in Table 1.

3. RESULTS AND DISCUSSION

3.1 High Pressure Waterjet Assisted Milling

3.1.1 Cutting Force Components

Typical cutting force components in the X, Y and Z directions for flood cooling are given in Fig. 3. The different stages of intermittent cutting namely idle period and cutting period can be noticed in the time domain signal very clearly. Fig. 4(a) shows the plot of average cutting force components in the X, Y, and Z directions with changes in water pressure and Fig. 4(b) shows the changes with orifice diameter. Zero water pressure and zero orifice diameter indicates flood cooling. The presence of a high pressure waterjet has led to a reduction of about 30% to 50% in the cutting forces. All three component forces steadily decrease with an increase in water pressure. Whereas with an increase in orifice diameter, the cutting force components initially reduce steeply and then remain more or less steady. This indicates that

after an optimum value, further increase in the volume flow rate of water does not benefit the machining process. Placement of the high velocity jet at the rake face close to the tool tip causes a hydraulic wedge by the jet lateral flow after impingement on the chip bottom surface (Kovacevic, et al., 1995b). This hydraulic wedge causes the tool-chip contact area to decrease which reduces the secondary shear and lowers the interface temperatures. The effectiveness of the hydraulic wedge improves with increase in flow rate which causes the cutting force components to reduce.

3.1.2 Surface Finish

The surface roughness quantified in terms of R_a is plotted in Fig. 5 with change in water pressure and orifice diameter. The flood cooling condition is represented by zero water pressure and zero orifice diameter. The presence of a high pressure waterjet leads to a reduction in R_a of about 35% to 50%. An increase in water flow rate caused by an increase in water pressure or orifice diameter, results in steady reduction in R_a. Lowering of interface temperatures and secondary shear caused by the presence of a waterjet close to the cutting zone leads to a reduction in tool wear. This reduction in tool wear is responsible for improvement in surface finish.

3.1.3 Tool Wear

The effect of a high pressure waterjet on tool wear can be better understood from the photographs of the carbide inserts at different stages of their lives. A new insert and the inserts used in conjunction with flood cooling and high pressure waterjet cooling after 30 minutes and 50 minutes of operation are shown in Fig. 6. It can be noted that the width of the flank wear which is used as a measure of tool wear is much less in the case of inserts used with high pressure waterjet cooling compared to that of flood cooling, indicating that the wear rate of flood cooling inserts is much higher.

3.1.4 Chip shapes

Being an intermittent cutting operation, even though chip handling is not a very critical issue in the case of milling, study of the chip shapes gives us a better understanding of the role of a waterjet in the material removal process. It is known that a considerable portion of the energy is consumed in the formation and removal of chips. The chips produced for flood cooling and high pressure waterjet cooling are shown in Fig. 7. The chips produced in flood cooling were found to be bigger in size, more serrated (indicating the intense shearing action), and blackened due to the extreme heat generated at the tool-chip interface. As the heat generated during flood cooling was primarily conducted away by the chips, they could not be physically handled immediately after machining. The chips produced by high pressure waterjet cooling were smooth without burrs, thin, small, spirally and folded over. These chips had longitudinal channels along the surface in contact with rake face (Kovacevic et al., 1995b) through which the cutting fluid was exiting. Similar observations were made by Sharma et al. (1971). Chips produced by a high pressure waterjet have bright surfaces indicating that they were not burnt. Thus the presence of a high pressure waterjet at the tool-

chip interface promotes the self breaking effect of the chips and improves the thermal/frictional conditions existing at the cutting zone.

3.2 High Pressure Waterjet Assisted Grinding

3.2.1 Grinding Force Components

The tangential and normal grinding force components are plotted in Fig. 8 for different water pressures and progressive grinding time. The magnitude of the grinding force components increase with increase in grinding time for both flood cooling and high pressure waterjet assisted cooling. As grinding proceeds, the grains on the wheel surface are subjected to gradual attritious wear. This reduces the cutting capability of the grains and leads to an increase in grinding force. With the application of high pressure waterjet the magnitude of the grinding force components are reduced by almost 50%. This could be due to several reasons. The high pressure waterjet is converted to high velocity waterjet by the sapphire orifice. This high speed jet is capable of overcoming the centrifugal force of the rotating wheel and breaking the air shield surrounding the wheel. The high velocity waterjet is also capable of dislodging the workpiece particles and debris which adhere into the pores of the wheel surface performing an effective cleaning action and reducing the wheel loading effect. The waterjet stream also provides a dressing/resharpening effect on the wheel by removing a layer of grains from the wheel surface exposing new grains. Due to its high velocity, the jet is able to penetrate into the wheel-workpiece interface providing an effective cooling/lubrication action. All these actions lead to a reduction in grinding forces, wheel wear and work burn, consequently improving the performance of grinding operation. The high flow rate of the grinding fluid prevents complete evaporation of the fluid film at the wheel-workpiece interface which is desirable.

3.2.2 Acoustic Emission

Acoustic emission (AE) signals in grinding are stress waves primarily resulting from a combination of attritious wear, grain fracture and bond fracture (Hundt et al., 1994). Recently a lot of attention has been focused on AE sensing technique for grinding process monitoring and control because of its capability to detect the abrasion process effectively. AE signals are acquired to understand more about the role played by the high pressure waterjet in the grinding process. Fig. 9 shows a plot of frequency domain AE signals acquired for different cooling/lubrication conditions after ten (10) minutes of grinding time. Note that the peak frequency for all the grinding conditions is around 150 KHz. As these AE signals are after ten (10) minutes of grinding, the effect of grain fracture and bond fracture on the AE signal can be eliminated. The peak amplitude is highest for flood cooling conditions indicating the presence of high attritious wear of the wheel. With the introduction of a high pressure waterjet at 55 MPa, the peak response at 150 KHz drops down drastically by about 40% due to reduction in attritious wear. No other frequency component is affected. Whereas with a further increase in water pressure, the amplitude of the frequency domain AE signal drops down through all the frequency ranges. This is because, the positive effect of reduction

in attritious wear is contributed by the resharpening of the wheel by the high pressure waterjet. The resharpening effect increases with increase in water pressures.

The overall effect of the combination of attritious wear, grain fracture and bond fracture occuring in the grinding wheel as grinding progresses, can be evaluated from the plot of AE_{RMS} vs. grinding time shown in Fig. 10. As expected, the AE_{RMS} corresponding to flood cooling is higher for different grinding time. An increase in water pressure tends to reduce the AE_{RMS} throughout the grinding process. These trends support the previous observations made regarding the positive role played by a high pressure waterjet in the reduction of wheel wear, improvement in the cleaning effect, reduction in wheel loading, improvement in cooling/lubrication of the cutting zone and resharpening of the wheel.

3.2.3 Surface Finish

Any factor which has a positive effect on the grinding wheel should contribute to an improvement in the surface finish of the workpiece. Fig. 11 shows a plot of R_a vs. grinding time for flood cooling and high pressure waterjet cooling. With progressive grinding time, the surface finish deteriorates. As water pressure increases, the quality of the surface improves for all grinding time. Stainless steel has a tendency at higher temperatures to undergo metal adhesion to the wheel due to chemical bonding. The presence of wheel and workpiece particles on the workpiece surface also affects the surface finish. These effects are eliminated in high pressure waterjet assisted grinding. As a result of this and previously mentioned reasons, the R_a of the ground surface is reduced with high pressure waterjet cooling assistance by more than 50%.

4. CONCLUSIONS

The salient features of the techniques developed for the coolant/lubricant systems based on ultra-high pressure waterjet face milling and surface grinding operations are discussed. The following conclusions can be deduced based on the evaluation of these systems.

In a high pressure waterjet assisted milling operation the cutting force components in the X, Y, & Z directions reduce by about 30% to 50% with an increase in water pressure and orifice diameter. This is caused by the improved effectiveness of the hydraulic wedge, created by the jet lateral flow, with increase in water flow rate. Presence of waterjet close to the cutting zone causes a reduction in tool-chip contact area and improvement in cooling/lubrication effect. This reduces the tool wear and leads to about a 50% improvement in R_a. The chips produced by high pressure waterjet cooling were small, without burrs, thin, folded over and have bright surfaces. In contrast, chips produced by flood cooling were blackened, large in size and more serrated.

The tangential and normal grinding force components are reduced by almost 50% by the application of a high pressure waterjet. The jet stream, due to its high velocity is capable of

penetrating through the air barrier surrounding the wheel, overcoming the centrifugal force, and causing an increase in the fluid flow rate through the grinding zone. The high pressure waterjet is also very effective in removing the adhering debris from the wheel surface, thus reducing the wheel loading effect. As the high pressure waterjet is capable of resharpening the wheel, the number of wheel dressings required is reduced. The positive role played by the high pressure waterjet in reducing wheel wear and wheel loading, improving the cooling/lubrication of the cutting zone and the resharpening of the wheel serve to reduce the R_a by more than 50%, and improve the quality of the surface. Presence of a high pressure waterjet at the grinding zone reduces the AE signals by more than 50%. At lower water pressures, the reduction in attritious wear plays a prominent role, whereas at higher pressures the resharpening effect of the waterjet also contributes in the improvement of the overall process performance.

5. ACKNOWLEDGMENTS

The authors would like to thank the Center for Robotics and Manufacturing Systems, University of Kentucky for the financial support in executing this project, Flow International Inc., Kent, Washington, for providing the waterjet cutting system & other required waterjet components, and Kennametal Inc. for providing the milling machine and tools.

6. REFERENCES

Borkowski, J., and Mazurkiewicz, M., "Aluminum Grinding with High Pressure Waterjet Assistance," *Proceedings of the 5th American Waterjet Conference,* pp.253-261, Toronto, Canada, 1989.

Dornfield, D. and Cai, H.G., "An Investigation of Grinding and Wheel Loading Using Acoustic Emission," *ASME Journal of Engineering for Industry,* Vol. 106, pp. 28-33, 1984.

Engineer, F., Guo, C. and Malkin, S., "Experimental Measurement of Fluid Flow Through the Grinding Zone," *ASME Journal of Engineering for Industry,* Vol. 114, pp. 61-66, 1992.

Guo, C. and Malkin, S., "Analysis of Fluid Flow Through Grinding Zone," *ASME Journal of Engineering for Industry,* Vol. 114, pp. 427-434, 1992.

Hundt, W., Leuenberger, D., Rehsteiner, F., and Gygax, P., "An Approach to Monitoring of the Grinding Process Using Acoustic Emission (AE) Technique," *Annals of the CIRP,* Vol. 43, pp.43-46, 1994.

Klassen, William P., "Grinding Wheel Coolant Nozzle," *US Patent No. 3,978,625,* 1976.

Kovacevic R., "Apparatus and Method of High Pressure Waterjet Assisted Cooling/Lubrication in Machining," *U.S. Patent No. 5,288,186.*, 1994a.

Kovacevic, R., Mohan, R., and Cherukuthota, C., "High Pressure Waterjet as a Coolant/Lubricant in Milling Operation," *ASME, PED* Vol. 64, pp. 733-748, 1994b.

Kovacevic, R., and Cherukuthota, C., "Improved Grinding Process Efficiency by High Pressure Waterjet Assistance," *Proceedings of the 1st World Congress on Intelligent Manufacturing Processes and Systems,* Mayaguez/San Juan, Peurto Rico, Feb. 13-17, pp. 1003-1013, 1995a.

Kovacevic, R., Cherukuthota, C. and R. Mohan, "Improving Milling Performance with High Pressure Waterjet Assisted Cooling/Lubrication," to be published in *ASME Journal of Engineering for Industry,* Vol. 117(2), 1995b.

Lincoln, H., "Method and Apparatus for Cleaning and Cooling a Machine Tool and Workpiece," *U.S. Patent No. 5,140,780,* 1992.

Lindeke, R.R., Schoenig Jr., F.C., Khan, A.K. and Haddad, J., "Machining of Titanium with Ultra-High Pressure Through the Insert Lubrication/Cooling," *Transactions of NAMRI/SME,* pp. 154-161, 1991.

Mazurkiewicz, M., Kubala, Z. and Chow, J., "Metal Machining With High-Pressure Water-jet Cooling Assistance — A New Possibility," *ASME Journal of Engineering for Industry,* Vol. 111, pp.7-12, 1989.

Pigott, R.J.S. and Colwell, A.T., "Hi-Jet System for Increasing Tool Life," *SAE Quarterly Transactions*, Vol. 6, No. 3, pp. 547-564, 1952.

Pigott, R.J.S., "Application of Cutting Fluids in Grinding Operations," *U.S. Patent No. 2,818,696,* 1958.

Radhakrishnan, V. and Achyutha, B.T., "A Method for Reducing the Corner Wear in Plunge Grinding," *Proc. Inst. Mech. Eng.,* Vol. 200, No. B1, pp. 19-27, 1986.

Ramaiyengar, H.S., Salmon, R., and Rice, W.B., "Some Effects of Cutting Fluids on Chip Formation in Metal Cutting," *ASME Journal of Engineering for Industry,* Series B, Vol. 87, pp. 36-38, 1965.

Sharma, C.S., Rice, W.B., and Salmon, R., "Some Effects of Injecting Cutting Fluids Directly into the Chip-Tool Interface," *ASME Journal of Engineering for Industry,* Vol. 93, pp. 441-444, 1971.

Wagner, H.W. and Wickstrom, G.J., "Method and Apparatus for Grinding," *U.S. Patent No. 2,434,679,* 1948.

Werner, P.C. and Shmaltz, L., "Advanced Application of Coolant and Prevention of Wheel Loading in Grinding," *Proc. International Symposium on Metal Working Lubrication, ASME,* pp. 228-235, 1980.

Wertheim, R., Rotberg, J. and Ber, A., "Influence of High-Pressure Flushing Through the Rake Face of the Cutting Tool," *Annals of the CIRP,* Vol. 41(1), pp. 101-106, 1992.

Table 1. Process Parameters

Face Milling		Surface Grinding	
Workpiece material	- SS (AISI 304)	Workpiece material	- SS (AISI 304)
Diameter of the Cutter	- 50.8 mm	Wheel Material	- Al. Oxide (WA543-731-556106)
Max number of Inserts	- 5	Wheel Speed	- 30 m/s
Number of Inserts Used	- 1	Wheel width	- 10 mm
Type of the Insert Used	- TPG322 (K313)	Wheel Dia.	- 300 mm
Geometry of the Insert	- Rake Angle = 0° Nose radius=0.8 mm Clearance angle 11°	Cross Feed	- 0.81 mm/pass
		Orifice Dia	- 0.46 mm
Type of Cooling Used	- Flood & High Pr. Waterjet	Type of Cooling Used	- Flood & High Pr. Waterjet
Cutting Speed	- 71.8 m/min	Traverse Speed	- 120 mm/s
Depth of Cut	- 0.89 mm	Depth of Cut	- 0.062 mm
Cutting Feed	- 8.9 mm/min	Range of Water Pr.	- 0 to 165 MPa
Length of the Cut	- 75 mm	Grinding Time	- 2.5, 5, 7.5, 10 min.
Range of Water Pr.	- 0 to 110 MPa		
Range of Orifice Dia.	- 0 to 0.45 mm		

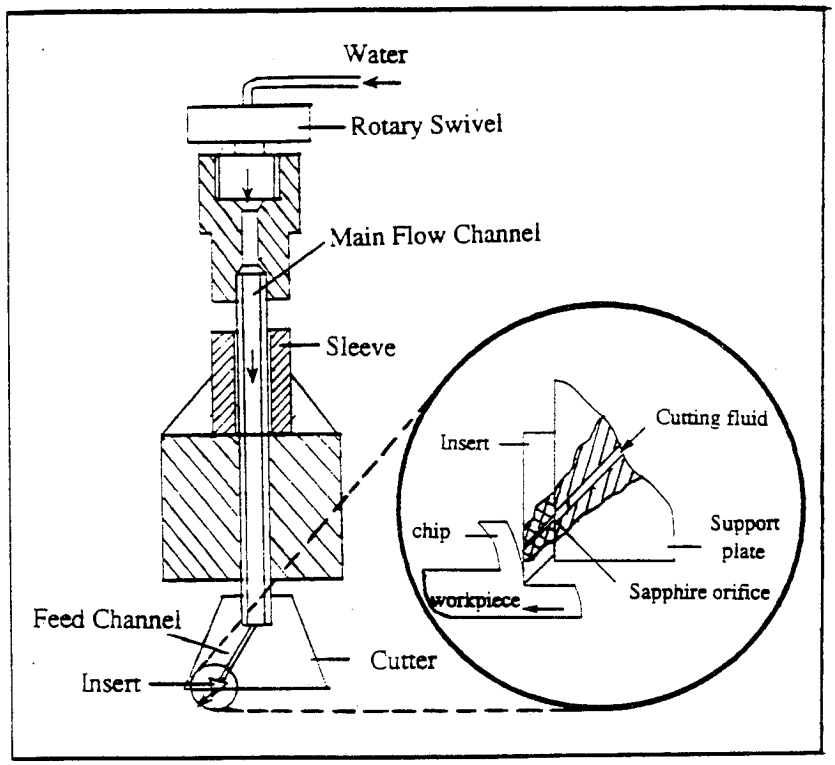

Fig. 1. Design of High Pressure Waterjet Coolant/Lubricant System for Milling

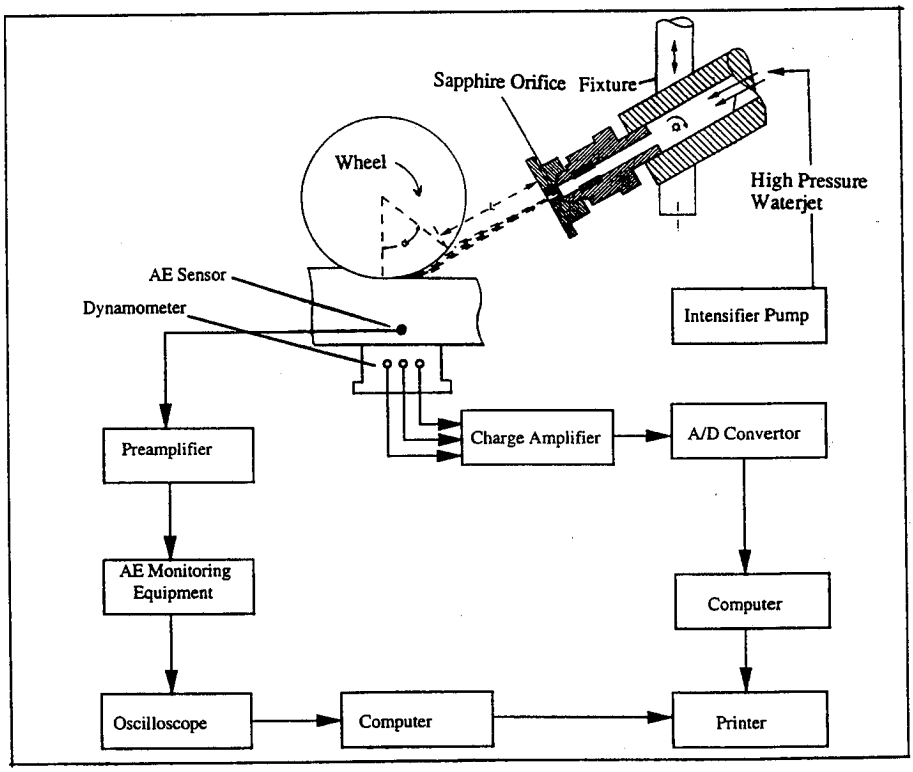

Fig. 2. Experimental Setup for Ultra-High Pressure Waterjet Assisted Grinding Operation

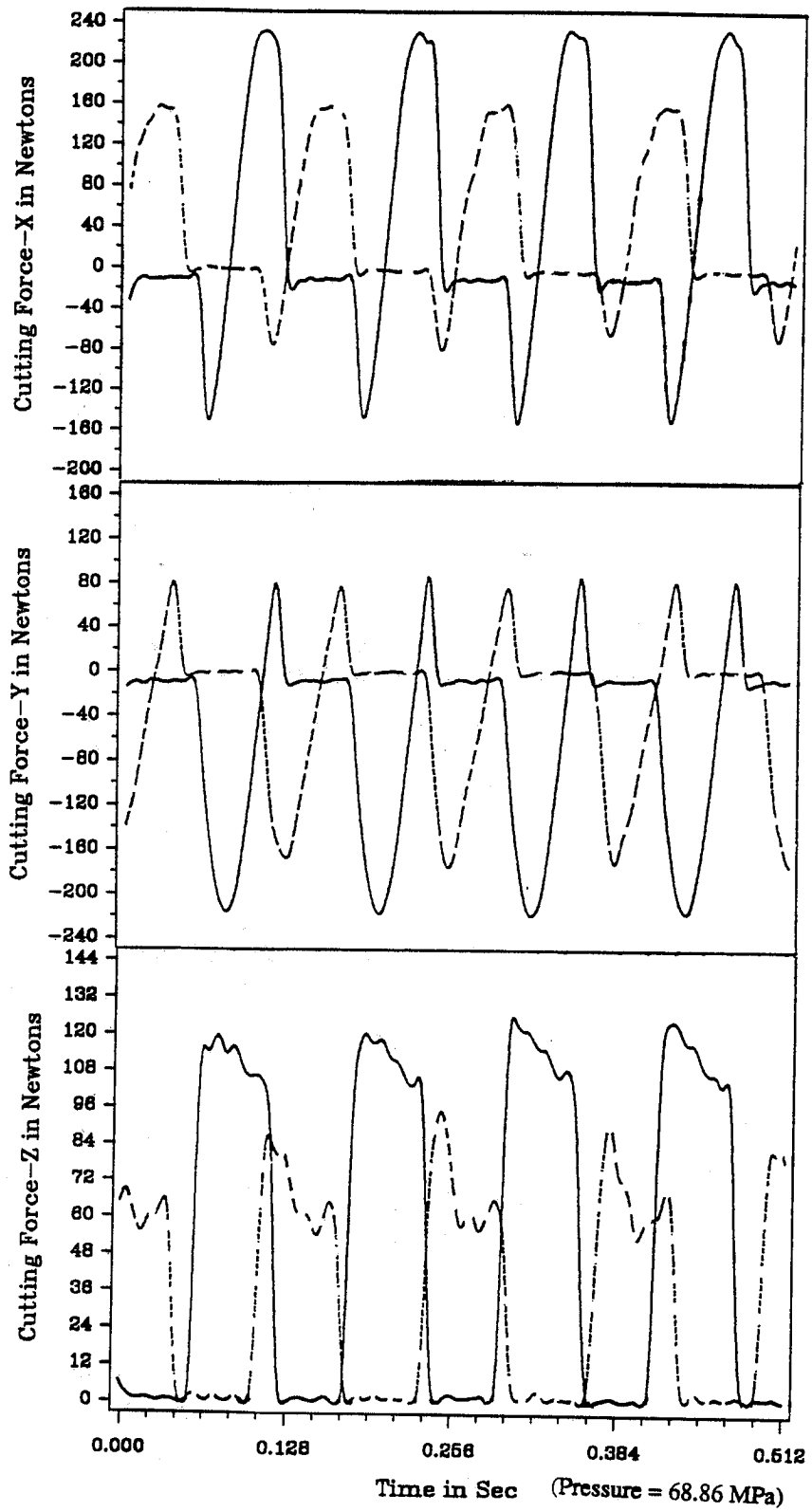

Fig. 3. Typical Cutting Force Signals in Milling

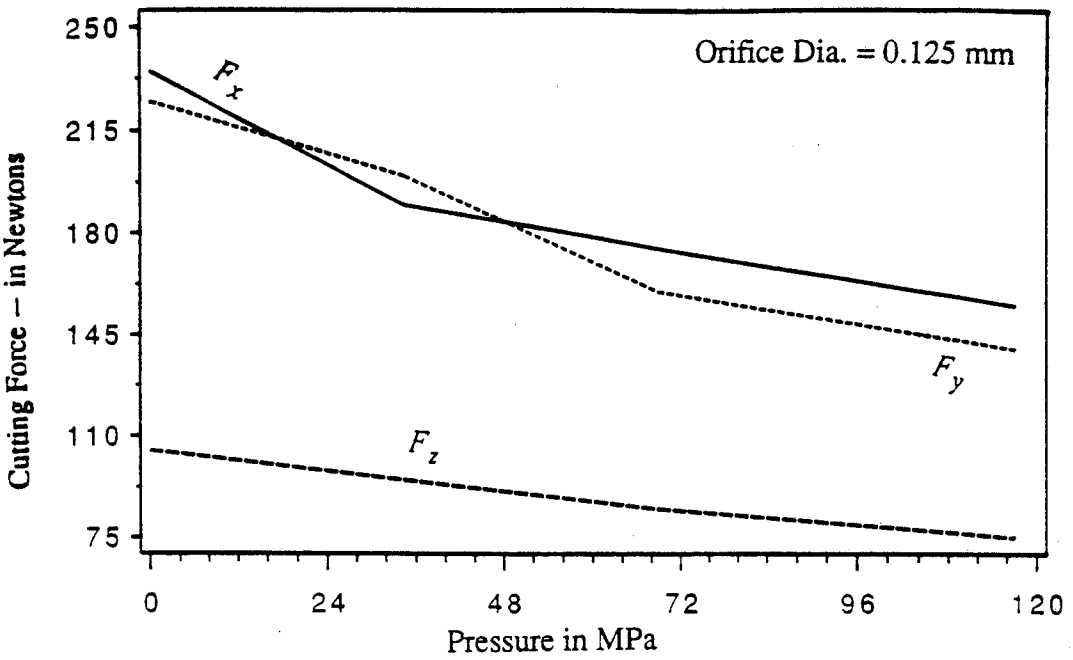

(a) Water Pressure

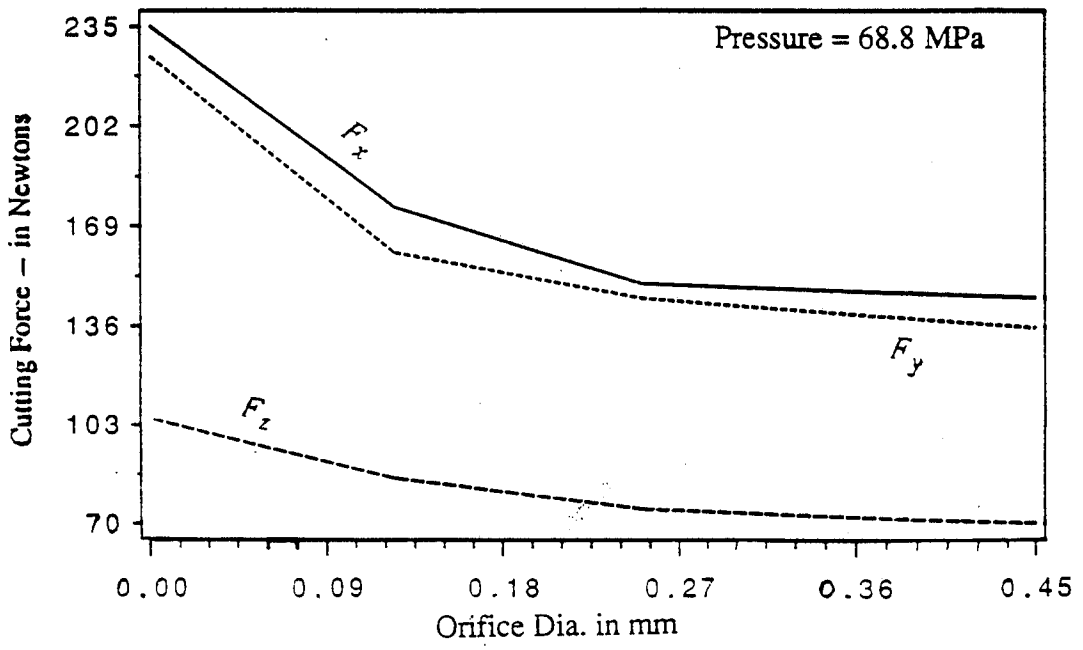

(b) Orifice Diameter

(Speed=71.8 m/min, Feed=8.9 mm/min, Depth=0.89 mm)

Fig. 4. Cutting Force Components vs. Water Pressure and Orifice Diameter in Milling

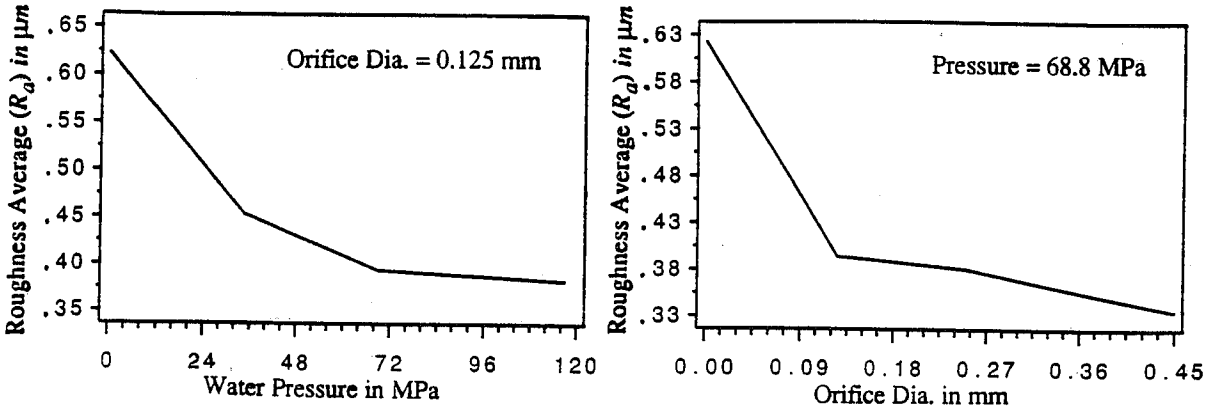

(a) Water Pressure (b) Orifice Diameter

(Speed=71.8 m/min, Feed=8.9 mm/min, Depth=0.89 mm)

Fig. 5. R_a vs. Water Pressure and Orifice Diameter in Milling

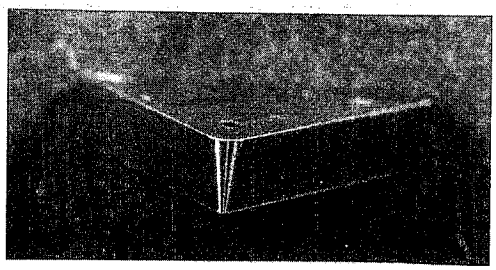

(a) New Insert

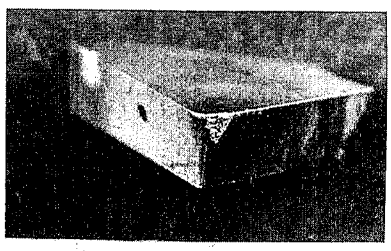

(b) Flood Cooling

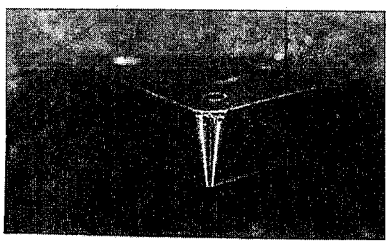

(c) High Pressure Waterjet Cooling

Worn Insert after 30 minutes of Operation

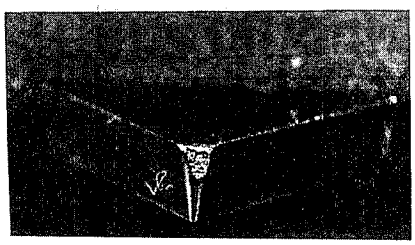

(d) Flood Cooling

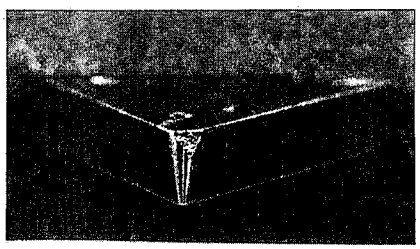

(e) High Pressure Waterjet Cooling

Worn Insert after 50 minutes of Operation

Fig. 6. Progressive Wear of Insert in Milling

(a) Flood Cooling

(b) High Pressure Waterjet Cooling
(Pressure = 34.43 MPa)

(c) High Pressure Waterjet Cooling
(Pressure = 68.86 MPa)

(d) High Pressure Waterjet Cooling
(Pressure = 117.07 MPa)

(Speed = 71.8 m/min, Feed = 8.9 mm/min, Depth = 0.89 mm)

Fig. 7. Typical Chip Shapes of Milling Operations

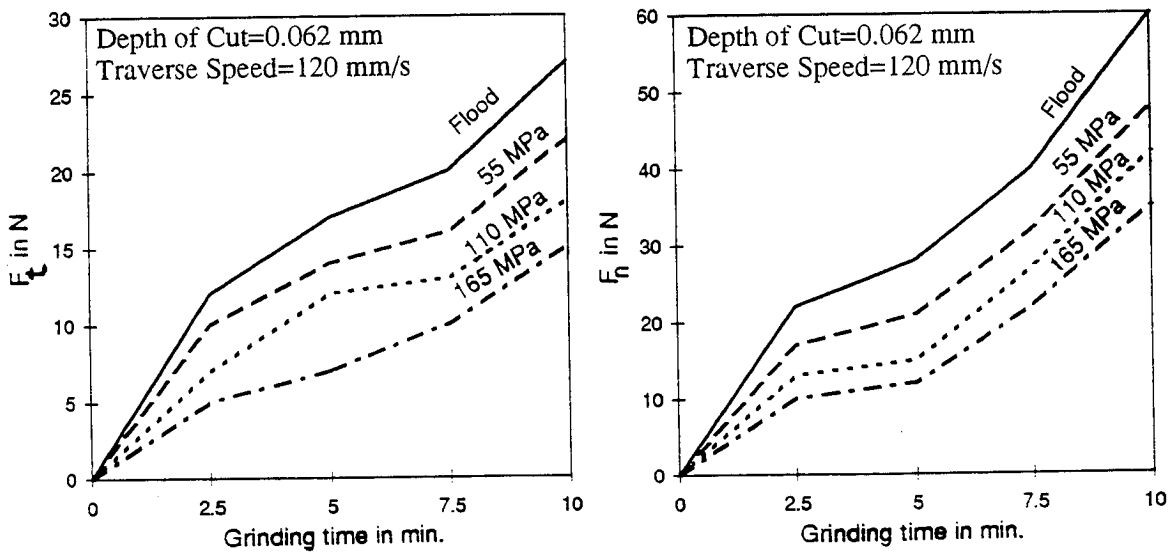

Fig. 8. Grinding Force Components vs. Grinding Time

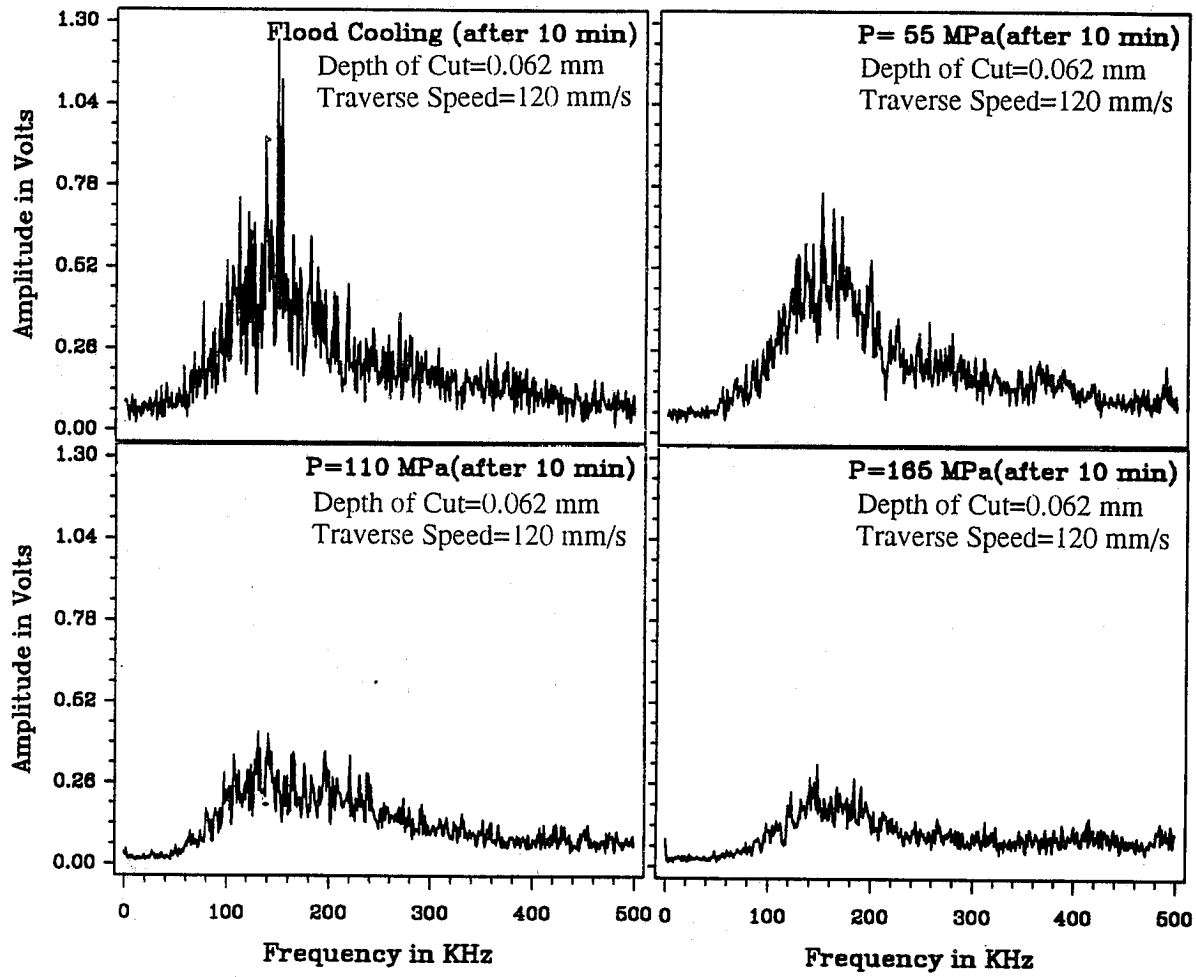

Fig. 9. Frequency Domain AE Signals in Grinding

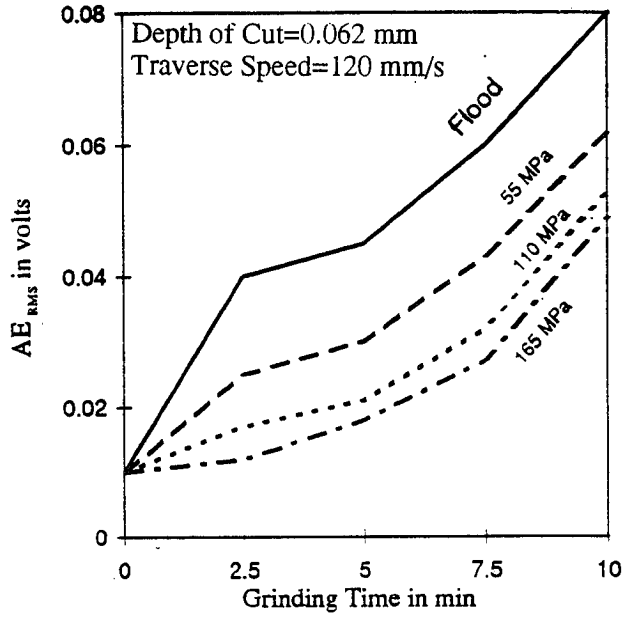

Fig. 10. AE_{RMS} **vs. Grinding Time**

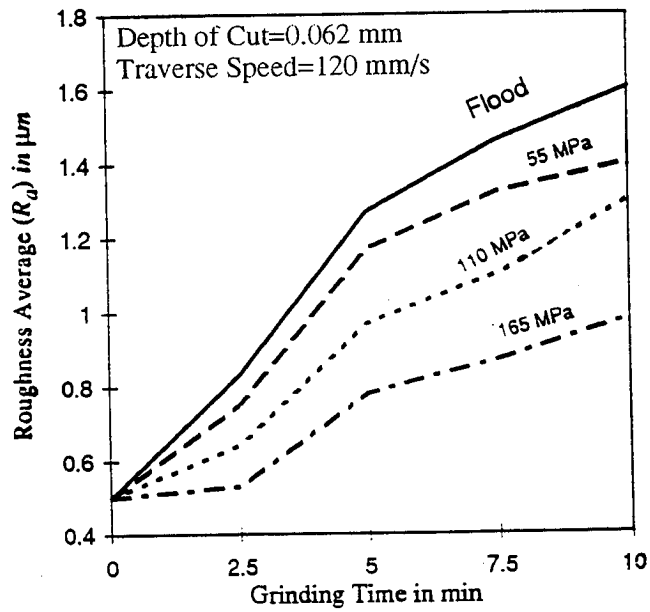

Fig. 11. Surface Roughness (R_a) vs. Grinding Time

8th American Water Jet Conference
August 26-29, 1995: Houston, Texas

Paper 37

DIRECT DRIVE PUMPS IMPROVE COMPETITIVENESS OF ULTRAHIGH-PRESSURE WATERJETS FOR SURFACE PREPARATION & INDUSTRIAL CLEANING

by
Rick Schmid
Flow International Corporation
Kent, Washington U.S.A.

ABSTRACT

Increasing environmental restrictions have created a renewed interest in the use of ultrahigh-pressure (UHP) equipment for industrial cleaning and cutting applications. In an effort to respond to this demand, leading manufacturers of UHP pumps have recently introduced a new generation of direct-drive UHP pumps that are more efficient, economical and easier to service than today's intensifier-based systems. This presentation will discuss the recent advancements in direct-drive UHP pump technology, and focus on the advantages of direct-drive ultrahigh-pressure pumps as compared to hydraulic-based intensifier pumps.

Organized and Sponsored by the Water Jet Technology Association.

1. INTRODUCTION

Ultrahigh-pressure waterjet technology was first introduced into the industrial cleaning market in the early 1980s. The adaptation of this technology can in many ways be seen as a response to the demand for a cleaner, more environmentally friendly way of dealing with the problems of the industrial cleaning market.

2. ULTRAHIGH-PRESSURE IN THE INDUSTRIAL CUTTING AND CLEANING MARKET

The term ultrahigh-pressure (UHP) when used with waterjets is technically defined as those pumps having a working pressure in excess of 28,000 pounds per square inch (psi). With the advancement of technology, the term UHP has generally become accepted today as those pumps with an operating pressure ranging from 36,000 psi to 55,000 psi.

The process involves the focusing of highly pressurized water through a small orifice thus forming a cohesive stream of water. Hand-held applications are normally limited to pressures of 40,000 psi and below. If 55,000 psi is needed, the cutting or cleaning tool is normally robotically controlled. The target materials are removed by the pure energy generated by the waterjet stream which moves at speeds of 2,280 to 2,860 feet per second.

The difference between traditional 10,000 and 20,000 psi waterblasting pumps and ultrahigh-pressure pumps is not unlike the difference between a modern attack fighter and a heavy bomber. UHP waterjets are very precise. Using extremely low volumes of water (2 to 7 gallons per minute), they accomplish their mission by striking their target with a highly focused beam of energy. Waterblaster pumps, on the other hand, saturate their target by delivering a high volume (15 to 250 gpm) of energy over a wider target area.

UHP waterjet machines have become the standard method of choice for a specific number of industrial cleaning applications: Tube bundle/heat exchanger cleaning of extra-tough materials (mechanically controlled, some hand-held), surface preparation (normally hand-held), coating removal (normally hand-held), and abrasivejet (cold) cutting (mechanically controlled).

The reasons that UHP water is the "tool of choice" over traditional cleaning and surface preparation methods such as solvents, acid, sandblasting, heat and high-volume waterblasting are:

- Low volume of effluent: A relatively low amount of water is required in proportion to the volume of material to be removed.

- Easy separation of material: In most cases, simple settling tanks will separate the water from the paint or other substances removed.

- ♦ No toxic or hazardous wastes: Besides the material being removed, UHP waterjets produce no toxic, hazardous, or flammable substances that require special handling.

- ♦ No sand or dust: Sandblasting requires large volumes of material to be disposed of, particularly where used on modern paint systems. Also, it is difficult to separate the sand from the material removed, and airborne dust and silt can cause numerous problems.

- ♦ Improved operator safety and health: Because ultrahigh-pressure water produces no dust or other toxic chemicals, the process alleviates workers' exposure to toxic materials. Due to the significantly lower volumes of water generated, UHP hand tools are much easier to handle than the high-volume, high-thrust tools typically used with waterblasters.

3. INTENSIFIER PUMPS OPEN THE UHP CLEANING MARKET

Until recently, the only commercially available ultrahigh-pressure waterjet pumps were hydraulically actuated intensifier pumps. Since their introduction some 20 years ago, intensifier pumps have been well accepted into a wide variety of industrial cutting and cleaning applications.

The most common application for intensifier-based UHP waterjet pumps has been in permanent factory cutting installations. These pumps have proven to be quite reliable in well controlled factory environments. Where good water quality is available and routine maintenance can be scheduled under relatively clean conditions, these pumps are often found working around the clock. In the field however, the situation is quite different.

The performance record of intensifier pumps in field cleaning applications has been less than perfect. Equipment used by industrial service contractors is routinely exposed to the extremes of weather and temperature. Clean facilities for maintenance rarely exist under field operating conditions. Contractors are often supplied with dirty or caustic water sources. The combination of these conditions is a formidable challenge for any type of industrial field machinery. Due to the advanced technology used in intensifier pumps, they are particularly susceptible to failures caused by any one or all of the conditions listed above.

4. HIGH OPERATING COSTS LIMIT THE USE OF UHP EQUIPMENT

Despite the many advantages offered by UHP waterjets, the actual implementation of this technology into industrial cleaning applications has remained somewhat limited. The reason for this limitation is based primarily on economic reasons.

Ultrahigh-pressure intensifier pumps and their accessories have had high purchase prices and relatively expensive operating costs. The higher cost of operation has limited the use of UHP equipment to a specific number of problems that could only be solved by using pressures in excess of 30,000 psi.

In order to remain competitive, the majority of industrial service contractors continue to use conventional lower pressure/higher volume 10,000 and 20,000 psi waterblaster pumps. These pumps are often used in jobs where UHP waterjets could do the same job faster and with less generated waste, but their higher operating costs result in non-competitive bids from the equipment owners.

5. NEW ENVIRONMENTAL PRESSURES OPEN THE DOOR TO UHP

Due to a more aggressive enforcement policy by the Environmental Protection Agency (EPA) and other related governmental agencies, many new restrictions are being placed on traditional methods used for industrial cleaning and surface-preparation work. The use of chemicals in stripping lead paint, for example, has come under intense scrutiny. In many areas of the country, open-air sandblasting, when not heavily restricted, is altogether banned. Regardless of the method being used, acid stripping, bicarbonate of soda, sandblasting, shot peening, or low-pressure/high-volume waterblasters, the trend toward containment of cleaning media, recycling of grit or water and a reduction of waste generation is the same throughout the country.

The problems encountered by today's industrial service contractor lie not so much with the method of coating removal, but rather with the amount of waste that is generated during the process. In some geographic locations, the cost of disposal now routinely equals or exceeds removal costs.

In an effort to respond to this demand, many leading pump manufacturers, both UHP and traditional waterblasters, have charged their design teams by developing a new generation direct-drive ultrahigh-pressure pump that will be more efficient, economical and easier to maintain than intensifier-based systems.

6. NEW DIRECT-DRIVE TECHNOLOGY LEADS THE WAY

In the development of UHP direct-drive pumps, the emphasis is on combining the reliability and ease of service of triplex-plunger pumps with the pressures of UHP intensifier pumps. With operating pressures ranging from 30,000 psi to 40,000 psi, many of these new pumps have already been introduced into the market.

One of the most technically advanced direct-drive UHP pumps to be introduced into the industrial service market comes from a leading manufacturer of intensifier equipment. This new pump produces 6.5 gpm at 40,000 psi working pressure.

7. THE CHALLENGE OF DIRECT-DRIVE PUMPS AT ULTRAHIGH PRESSURES

Two fundamental approaches may be taken when designing a UHP direct-drive pump. One approach is to simply take the existing 20,000 psi pump and modify the components so that

they will withstand the greater operating pressures. This approach generally takes the standard operating conditions found in 10,000 and 20,000 psi pumps and increases the wall thickness and size of the components in order to withstand the higher operating pressures.

Because traditional waterblaster pump bodies are designed with low-pressure/high-volume operational characteristics, the larger size of the pump components limits the speed at which the pumps can operate. Since the majority of prime movers, whether diesel or electric, turn at relatively high revolutions per minute (rpm), the waterblaster style of pump normally requires some type of gear reduction between the engine and the pump. The average working cycle of these pumps is 400 to 600 rpm. The design criteria for bringing a waterblaster pump up to ultrahigh operating pressures is basically: the slower the rpm and the higher the pressure, the larger the size of the pump components.

Another challenge faced by waterblasting pumps at ultrahigh pressures is the design of the high-pressure seals. Most 10,000 and 20,000 psi triplex pumps are equipped with a multi-element packing or seals. The design of the packing becomes even more complicated when dealing with pressures greater than 28,000 psi.

8. SMALL COMPONENTS ALLOW FOR HIGH RPM OPERATION

In the case of the 40,000 psi direct-drive pump, thousands of hours of testing of high rpm pumps was successfully combined with an in-depth knowledge of ultrahigh-pressure materials and components. This combination of technologies led to a patent pending-design which has allowed the pump to have relatively small high-pressure components.

The pump's small-diameter plungers make it possible to operate at much higher rpms than waterblaster pumps are able to handle. It can easily operate at the 1700 to 2100 rpm level found in most prime movers. The ability to run at high rpm means that the pump may be directly coupled to the prime mover, thus eliminating the need for any type of gear reduction.

The high-pressure seal design of the pump takes full advantage of the small plunger diameter and the ability to control the length of the plunger stroke. The seals in the pump are very similar to the elastomer and polymer combinations found in the high-pressure seal design of most ultrahigh-pressure intensifier pumps.

The check valve of the pump is sealed with a simple metal to metal seal that eliminates the possibility of extrusion or erosion. The plunger seal or "dynamic" seal is made of a polymeric material and is located at the back end of the plunger.

9. PRESSURE COMPENSATION, A LEAP FORWARD IN DIRECT-DRIVE PUMPS

The feature that most distinguishes the pump from the group of modified medium-pressure triplex plunger pumps is its unique pressure-compensation system.

Pressure compensation as it is applied to pumping technology basically means that the output flow rate of the pump will be adjusted to maintain a given constant pressure. When dealing with ultrahigh-pressure pumps, pressure compensation may also be defined as volume control. In order to have pressure compensation it is first necessary to sense a given pressure and then have the pump respond to it. The latter is especially critical when running multiple tools with numerous on/off functions.

In the case of hydraulic-actuated intensifier pumps, the pressure compensation system is based on sensing and adjusting hydraulic oil pressure. During compensation hydraulic oil pressure is sensed and once regulated, acts upon the swash plate of the hydraulic pump thus, changing its displacement. The change in the volume of hydraulic fluid to the intensifier lowers the stroke rate of the intensifier. The reduced stroke rate in turn lowers the output volume of water while maintaining the preset working pressure.

If an intensifier pump is placed in an idle or dead-head mode (where working pressure is maintained but the output flow is stopped) the pressure compensation mechanism will adjust the displacement of the hydraulic pump. Hydraulic fluid will be delivered to the intensifiers so that the high-pressure plungers will only move enough to make up for any leakage of water past the high-pressure seals.

The fact that positive-displacement pumps do not have a hydraulic circuit to control makes the challenge of pressure compensation much more difficult. In the case of the 40,000 psi direct-drive pump, instead of adjusting the output displacement of the pump, a mechanical device is used to prevent the pumping of the fluid which is charged on the inlet plunger stroke.

The pressure compensation device of the pump is a patent-pending mechanism that allows the pump to deliver only the required amount of pressurized water. The amount of water is determined by the pressure setting of the pump and the size and number of orifices at the toolpoint.

The pressure-compensation device of the pump works by adjusting volume to maintain pressure. Working pressure is defined by the amount of flow through a nozzle, much like an electrical current through a resistor that establishes a certain voltage. Just as the current through a resistor may be changed to maintain a voltage drop, in the pump the flow through an output nozzle is adjusted in order to maintain a constant pressure.

In order to illustrate this concept, let us assume that an operator is using a pump which has an output flow rate of 6.5 gpm @ 40,000 for a hand-held cleaning job. The operator has loaded the hand tool with a nozzle combination which allows 5 gpm of flow. The question is: What happens to the other 1.5 gpm of flow?

The pump has a built-in mechanism which is designed to sense the output pressure. If the operating pressure of the pump has been set at 40,000 psi, it will try to force all 6.5 gpm of water through the output nozzles which are set at 5 gpm. Since not all of the output flow is able to exit the nozzles, the pressure will start to increase. As soon as the pressure starts to

rise, the pump immediately senses it and begins to compensate by holding the inlet check valve open as described above.

The water that is in excess of the set discharge rate determined by the output nozzle size is recirculated through the pump's internal plumbing system. It is important here to note that no water is discharged in this process.

If for any reason the pressure compensation mechanism of the pump should fail to react to a pressure build-up, the pump is equipped with a resettable pop-off valve. This valve will automatically open if the pressure exceeds a given level. The valve is easily reset by lowering the pressure of the pump back to idle pressure (approximately 10,000 psi). Once idle pressure is reached, the valve automatically resets and the pump may be brought back up to full operating pressure.

10. UNLOADER VALVES THE ONLY ALTERNATIVE TO PRESSURE COMPENSATION

All hydraulic-powered intensifier pumps have pressure compensation systems based on the control of the hydraulic pump as described above. The pump is the only ultrahigh-pressure direct-drive positive displacement pump available with full internal pressure compensation. The majority of 30,000 psi direct-drive pumps have dealt with the problem of pressure compensation by developing various types of pressure by-pass valves.

Also known as dump valves or unloader valves, these units are fairly complex in design. Valves of this type are used regularly with lower pressure pumping equipment. Unloader valves are a high maintenance item even when used with 5,000 psi pressure washers. When pressure losses occur during operation, operators are often tempted to adjust the unloader valve rather than fix the real problem (worn packings or nozzles). Improper adjustments, poor maintenance and excessive wear of by-pass valves can create significant safety problems.

Ultrahigh-pressure positive-displacement pumps that do not have internal pressure-compensation require the use of very complex pressure by-pass valves. Because of extremely high operating pressures and relatively large output volumes the unloader valves for these pumps are often quite massive in size. The seats of these ultrahigh-pressure dump valves are subject to extreme erosion and washout problems causing them to be a high maintenance item.

11. ENVIRONMENTALLY FRIENDLY CLOSED LOOP COOLING SYSTEM

Many of the new direct-drive pumps address the need to limit the amount of cooling water required by typical intensifier pumps. In some models of intensifier units, up to 6 gallons of water per minute may be run through the pump and subsequently dumped for cooling requirements. In most of the new direct-drive UHP pumps, the cooling systems are closed-loop.

In the case of the 40,000 psi direct-drive pump, the cooling system has been made to operate in a closed-loop zero-discharge mode. The crankcase lubrication oil is cooled on the pump by means of a forced air heat exchanger mounted in front of the radiator. The cooling water of the pump is recirculated through the high pressure heads and only leaves the pump when it is discharged through the nozzles for cleaning and cutting purposes.

12. EFFICIENCY OF OPERATION

Although positive-displacement ultrahigh-pressure pumps have only been on the open market for two and a half years, they are rapidly becoming the new industry standard for mobile cleaning applications. The primary reason for this rapid acceptance is their simple design and ease of maintenance. With the elimination of the entire hydraulic power circuit, these pumps are cheaper to operate and easier to repair than intensifier pumps. For the owners of these new UHP plunger pumps reduced down-time and lower operating costs translate directly into higher profits.

Another important reason that positive-displacement pumps are being readily accepted by industrial cleaning contractors is the absolute increase in efficiency of operation that they offer. Due to energy loss through the hydraulic loop, the average intensifier pump has an overall efficiency level of 60 to 65 percent. Positive-displacement pumps produce an impressive efficiency rating of 90 to 95 percent.

Efficiency can be expressed in several ways. A direct benefit will be a significant fuel savings realized when operating a direct-drive pump versus an intensifier pump. Of greater importance to the operator are larger output flow rates and higher nozzle horsepower.

For industrial cleaning contractors, nozzle horsepower directly impacts surface cleaning and coating removal rates. The greater the nozzle horsepower, the faster, thicker and harder the type of material that can be removed.

13. GREATER EFFICIENCY & INCREASED FLOW RATES OPEN NEW APPLICATIONS FOR ULTRAHIGH-PRESSURE WATERJETS

New applications for UHP waterjets are opening up because of improved efficiency and relatively large increases in output flow rates of ultrahigh-pressure positive-displacement pumps.

The combination of higher water volume with greater nozzle horsepower makes these pumps well-suited for use with multiple hand-held tools as well as large-volume robotic cleaning heads.

Faster removal rates combined with stricter environmental regulations are making UHP waterjets one of the key methods currently being evaluated in each of the following applications:

- ♦ Nuclear decontamination and decommissioning
- ♦ Lead-based paint abatement
- ♦ Automotive paint booth cleaning
- ♦ Large surface coating removal (such as ships, bridges and storage tanks)
- ♦ Factory cleaning applications to replace solvents

14. CONCLUSION

Technology progression of the direct drive pumps must move parallel with new accessories and other equipment to complement the pumps. New lightweight UHP hand tools have been introduced as well as flexible high-pressure hose capable of withstanding ever-increasing working pressures.

As new types of tools and robotics are perfected for field use, the acceptance of UHP waterjet technology will continue to expand into new application areas. Currently, more than 100 direct drive, ultrahigh-pressure waterjet pumps are in service.

Under the new administration, environmental regulations are expected to become much more strict. This fact combined with the greater efficiency and ease of operation of ultrahigh-pressure direct-drive pumps will guarantee that this new technology will be accepted as the preferred method of industrial cleaning and coating removal in a wide variety of industries and applications.

15. REFERENCES

Sepe, R. and Schmid, R., "Ultrahigh-Pressure Waterjet for Surface Preparation," *Products Finishing*, June, 1993.

8th American Water Jet Conference
August 26-29, 1995: Houston, Texas

Paper 38

TEST RESEARCH OF SUPER HIGH PRESSURE RECIPROCATING SEAL UNDER 300 MPa

S.X. Xue, W.P. Huang, Z.W. Chen
General Machinery Research Institute
Hefei, Anhui, P.R.C (230031)

D.J. Shi, Y.H. Yang
Jian Yang Test Pump Factory
Jianyang, Sichuan, P.R.C (641402)

ABSTRACT

Operational reliability of water jet cutting equipment is dependent on the super high pressure reciprocating seal. A design for a seal under 300 MPa: the combination of conical bushing and packings is described. Elastic deformation of the conical bushing under high pressure causes a gap between the plunger and the bushing which creates a large pressure drop, and then it is sealed by packing which is made of soft metal. A metal incline seal is used as static seal. Equipment parameters are pressure: 300 MPa, flow rate: 2 L/min, medium: pure water plus 3～5% emulsion, nozzle diameter: 0.25 mm.

Organized and Sponsored by the Water Jet Technology Association.

1. INTRODUCTION

As a new technology of material cutting, super high pressure water jet technology is attached more and more interests by the international field of engineering. Because of its following advantages: no destruction to the inner structure of machined material, narrow and smooth cutting gap, copy-cutting ability and no selectivity of machined material. High pressure water jet is widely used for cutting, polishing, burr removal, stripping, drilling and so forth. While the key problem of super high pressure water jet equipment is its operation reliability. The unit reliability is mainly dependent on the reciprocating seal of high pressure pump or intensifier. Various types of seal can be used. As discussed by Fuchs (1981), floating bushing seals with pressure dependent clearance deformation can be used for sealing plungers of piston pump especially in high pressure applications. By means of the finite element method with respect to geometry, pressure drop, flow and self-centering, a special type of elastrohydrodynamic bushing seal was theoretically analyzed and a useful result was given for technical practice [1].

X.S. Xue (1989) Introduced the pump for high pressure water jet [2] and the complete metallic viscous elastic seal which is similar to Fuchs' was applied to high pressure intensifier by H.P. Xu (1993), the working pressure was up to 1200 MPa [3]. This paper describes the new design of this type of seal used in high pressure pump and its experimental results. Different structure, material, processing are considered, its achievements make the super high pressure water jet unit can operate continuously and become more merchantly.

2. EXPERIMENTAL SYSTEM OF SUPER HIGH PRESSURE

The experimental system of super high pressure is used to test the working ability and reliability of the seal. As it consists of super high pressure pump, control mechanism and executive body (cutting head), material cutting under different condition can be also done. Scheme of the system is shown in Fig.1.

Test is done under 250～300 MPa pressure and the required operation condition is controlled by the manual restrictor which can adjust the pressure sensitively by the overflow of part of the working fluid return to the tank. The cutting head is fixed on the working table and can be moved up and down to keep the optimum distance from the material surface. Brown aluminum oxide or garnet is used as abrasive respectively. Abrasive which is sucked into the nozzle, is controlled by the sand valve to adjust its capacity per unit time. The exhausted water jet is collected by the catcher to eliminate its noise and splash. Operation stability of the pump is determined by measuring its flow rate and pressure at specified operation speed. High pressure reciprocating seal or static seal is considered fail while flow rate under rated pressure decreases 15% compared to what under standard atmosphere. And thus the pump must be disassembled to check and to determine if the test can be continued. Experimental parameters pressure: 250～300 MPa, flow rate 2 L/min, plunger diameter: 12/14 mm, pump speed: 230 /140 min^{-1} , working fluid: water plus 3～5% emulsion, diameter of water nozzle: 0.2 /0.25 m, diameter of sand nozzle: 1/1.2 mm, material of abrasive: 60# brown aluminum oxide or garnet, motor power: 15KW.

Tri-plunger reciprocating pump is used as source equipment of high pressure, compared to intensifier, it is of low cost, small pressure fluctuation, convenient disassembling. However the speed is relatively high, this is harmful to the duration of reciprocation seal. Inlet and discharge valves are fundamentally the same as those of intensifier, they are arranged vertically. Three high pressure cylinders are arranged separately with two layers fitting and self strengthen technology to bear the required super high pressure. The pressure gauge is at one end of the pump head and the protective valve at the other.

Executive body consists of cutting head, abrasive system and cutting table. Fig. 2 shows the head structure of abrasive jet. Vacuum is created by the high speed jet and abrasive is sucked into the chamber of water jet, behind the outlet of jet nozzle, it is mixed with jet. At the outlet of sand nozzle, high speed abrasive jet with cylindrical cross section is formed. Air compressed sand feed assisted by a mini-compressor can be also used to guarantee sand feed. To provide the accuracy of the jet from water nozzle into the sand nozzle, coupling with spherical body and two dimensional adjusting are considered in the fit of sand nozzle. Cutting table is a kind of two dimensional mechanism which can provide the motion of cutting head along different line with different velocity.

Control of over-load, discharge of high pressure fluid and condition of the pump operation is performed by the control valve which is infact a three passage valve, fluid is in and out horizontally and overflow vertically. In addition, mechanical safety and protecting mechanism is also set in the unit.

3. STRUCTURE OF SUPER HIGH PRESSURE RECIPROCATING SEAL

The design criterion of super high reciprocating seal is such that the super high pressure pump can operate continuously and steadily with clean water as medium. Depending on this, four problems as: hermetic sealing, wear resisting, lubrication and leakage should be considered. All this is infact the duration and reliability of the seal.

It is proved by experience that to seal super high pressure water with nonmetallic packing is impractical while combination seal of the metallic bushing and packing is widely used. The most important to be considered is the gap which should be proper. Principle of bushing seal is that with very small gap between the plunger and the bushing to create a large pressure drop. Optimum gap should keep the seal to have a maximum pressure drop and rational leakage of fluid for lubrication and cooling. Usually external surface of the bushing is designed to be conical. High pressure acts on the external and internal surface of the bushing during compressing stroke. Because of fluid pressure acting on the external surface is relatively static and on the internal surface is steadily decreasing, the conical bushing is deformed and gap which is difficult to be machined is formed. Forces acting on the bushing and the resulted deformation are shown in Fig. 3. To help the formation of a relatively uniform clearance, a hole is drilled at the end of the plunger and this causes its expanding under high pressure.

As the gap is quite small, any bending or tilt of the bushing and the plunger will affect the working of the seal, it is not permitted for metal-to-metal friction to occur. It is necessary for the bushing to be "FLOATING" to the plunger. Top of the plunger is pointing connected with cross head and a precompressed spring is put at the front stage of the bushing. In addition, material of the bushing must be highly elastic and highly wear-resistant, here QBe2.5 is selected as the material of bushing. In the internal surface of the bushing, some circular troughs are machined to "RESERVE WATER." One of the scheme of bushing seal is shown in Fig. 4. The bushing is divided into two stages, the front stage is designed to seal the moving plunger and the behind stage to the cylinder. Two stages are connected with conical end. In this plan, the bushing is relatively short and thus is manufactured easily, while the problem is that accuracy of these two conical surfaces is difficult to be provided by machining and grinding, thus their lapping is not very well, so that two conical surfaces are separated under certain pressure and high pressure water discharges from the large gap between the plunger and the behind bushing with little pressure drop, the seal is easily failed.

A single bushing seal is shown in Fig. 5. In this plan, the bushing is relatively long, thus it can provide good hermetic sealing. The bushing is only used to seal the gap between its internal surface and the moving plunger. Sealing of the external surface of the bushing is dependent on the static seal which is fitted by two metallic triangle rings. It is obvious, leakage of working fluid in the gap is hard to avoid, at the same time, it is also effective to lubricate the moving pair and to lower the temperature during continuous operation of the pump. Therefore, behind the bushing, seal of packing is fitted and an out flowing hole is drilled on packing case. The volume of leakage can be estimated by measuring the fluid out flowing from this hole. If the flow rate increases to some extent, the sealing of bushing can be suggested to be failed and it should be replaced.

The bushing and the packing are separated by the packing case. Thus, twisting force acting on the packing will not transform to the bushing. Packing which is made of soft metal, for example lead foil, can assist the sealing of the bushing. As a result, requirement of the gap can be lowered and its duration is prolonged obviously.

The most important for the duration of super high pressure bushing seal is the formation of "water film" between the sealing pair. "Water film" is imaginary according to the "oil film" in the hydraulic equipment. The lubrication is dependent on the imaginary "Water film," bad lubrication is definitely to bring about "HUGGING." Problems listed below must be considered during structure design and assembling of the seal. Surface of the bushing is thoroughly finished. The bushing is "FLOATING" to the plunger which is self-centering to reduce the partial wear between them. WC powder is hot sprayed on the surface of the plunger while its hardness is higher than HRC62. Water temperature should be less than 75°C, and proper pump speed is selected. Another, 3～5% emulsion is added into water.

It is interesting that this plan exists double contradictory — "GAP" and "HUGGING" at the same time. The key of research is to solve them.

4. EXPERIMENT

Test system is shown in Fig. 1. High pressure up to 300 MPa is caused by the small diameter nozzle and the manual restrictor. During the experiment of reciprocating seal, material cutting with water jet and abrasive jet is also done. Such parameters as flow rate, pressure and speed of the pump, temperature and flow rate of the out flowing fluid from three holes are measured.

The seal failed under two circumstances: the first is that flow rate of leaked fluid for one cylinder under rated pressure is more than the theoretical flow rate with a factor of 15%, the second is the hugging of bushing with plunger. This is because the inlet valve of this cylinder failed to suck water and the seal pair is in the condition of dry friction. It is necessary to inspect water inlet of three cylinders during operation, and this can be avoided by adding a centrifugal pump before the inlet of the pump.

It is shown by experiments that leakage of the seal of Plan I (Figure 4) grows up fast for the failure of incline connection. While the leakage of the seal of Plan II is very small for longtime under the same pressure and pump speed. The temperature in the cylinder increases with the decreasing of fluid leakage, and if the temperature is more than 75°C, bushing seal is easily failed for partial steaming of fluid in the gap.

To analyze the effect of pump speed to the duration of the seal, two experiments are done with the bushing seal shown in Figure 5 of different diameters. That is $d = 12$ and 14 mm, to obtain the same flow capacity, the corresponding pump speeds are 230 min^{-1} and 140 min^{-1} respectively. Under the same pressure and leakage, the duration of seal with $d = 14$ mm is 4 times of the seal with $d = 12$ mm. It is obvious that choice of proper pump speed is very important to the bushing seal. Lower pump speed is profitable to decrease the temperature in the cylinder and for the lubrication of the seal.

Although storage vessel should be added in the discharge channel of the pump to reduce pressure pulsation.

Packing made from different materials such as stuffing PTFE, Nylon 1010, and soft lead foil is also used in the test to compare their sealing ability. It is shown that the stuffing PTFE is easily failed for high pressure (up to 80°C) and dry friction. Its duration is less than 40 hours, while with nylon 1010, less than 10 hours for lacking of wear-resistance. Model shaped lead foil is the best, to increase its wear-resistance and self lubricacity, graphite is filled into.

Total operation time of the pump under 200 ~ 300 MPa pressure is more than 300 hours, and the duration of the bushing seal is more than 100 hours. This is relatively satisfied for the cutting equipment. With the experiment of bushing seal, material cutting test is also done, cutting ability under 200 ~ 300 MPa pressure is shown in table 1.

5. CONCLUSION

The combined seal of bushing and packing is effective used for super high pressure reciprocating plunger. Its duration depends on the structure, material, composition of fluid and operation condition. Volume of leakage can be controlled while stuffing seal is used. Lower pump speed can prolong the duration of bushing seal, while choice of material of stuffing is also important.

Bushing seal with two stages cannot be used because of machining and assembling. The alignment of surfaces between the two stages is difficult to be guaranteed.

Water jet and abrasive jet under 200～300 MPa pressure is able to cut various metallic and nonmetalllc materials.

6. REFERENCE

[1] Fuchs, E.H., "An Elastrohydrodynamic Floating Bushing Seal For Reciprocating Plungers," *Proceedings of the 9th International Conference on Fluid Sealing*, PP369～388 BHRA Fluid Engineering, Cranfield Bedford, 1981

[2] Xue Sheng-Xiong, "Pump Used to High Pressure Water Jet," *High Pressure Water Jet*, NO. 4, 1989.

[3] Xu.H.P, Lei. T.J., "Research on New Type Sealing for Super High Pressure," *Journal of Petrolic Chemical Industry Equipment*, No.1, 1993.

Table 1 Cutting ability of the test unit

cutting condition	cutting material	dia.of nozzle
340 MPa clean water jet	30mm thick rubber, plastic plate, asbostos plate, clothes layer	0.2mm
300 MPa clean water jet	20mm thick marble plate cutting speed 80～100mm/min	0.2mm
220 MPa abrasive jet (60# brown aluminium oxide or garnet.	20mm 65Mn steel plate 50mm plexiglass 65mm Al－Mg refractory brick 10mm steeless plate etc.	0.25mm abrasive jet nozzle 1.2mm
300 MPa abrasive jet	50mm thick GCr15, 1Cr18Ni9Ti plate, cutting speed 20mm/min	0.2mm abrasive jet nozzle 1.0mm

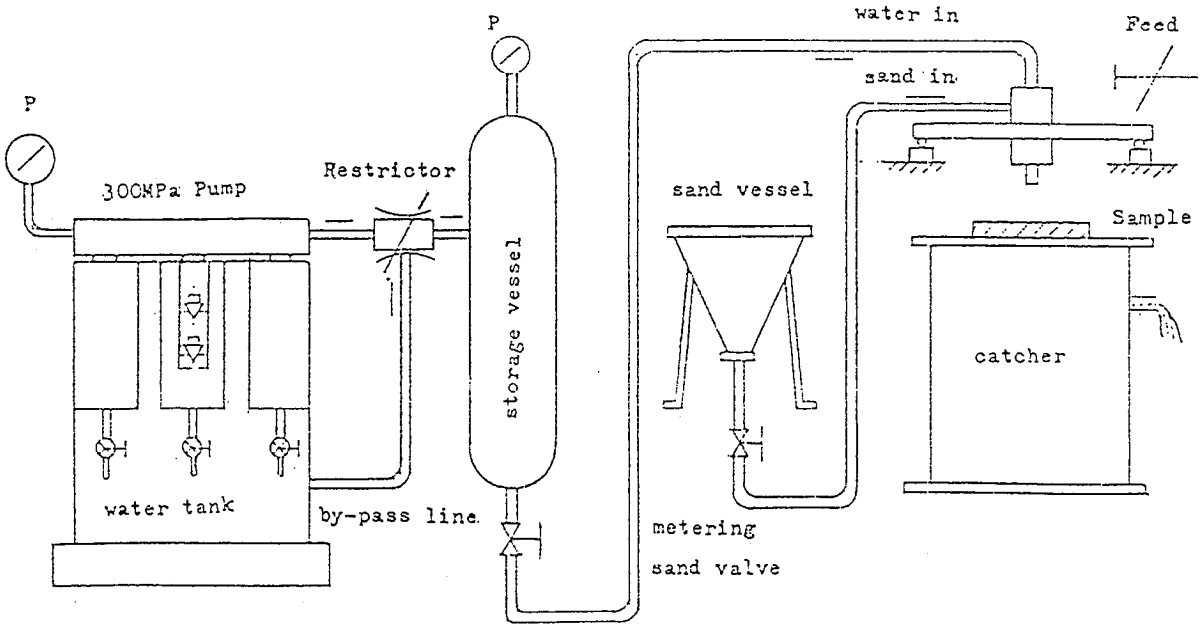

Figure 1. Scheme of the experimental unit of super high pressure water jet cutting

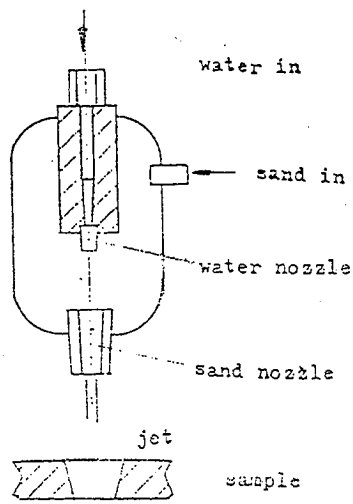

Figure 2. Structure of abrasive jet nozzle

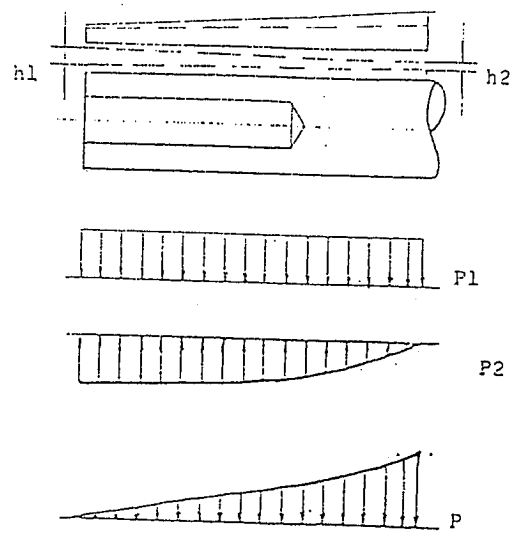

Figure 3. Sketch of forces acting on the bushing and its deformation

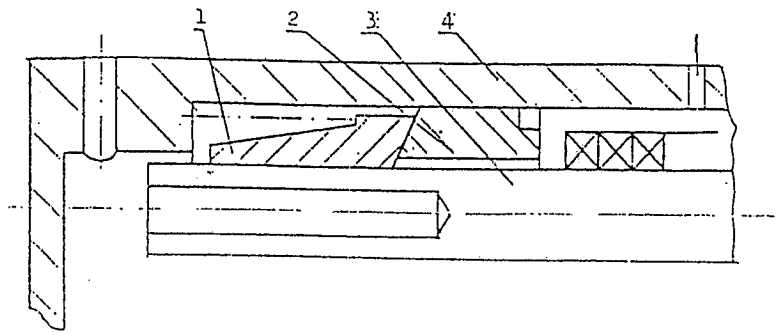

1—front stage 2—behind stage 3—plunger 4—cylinder

Figure 4. Plan I of bushing seal

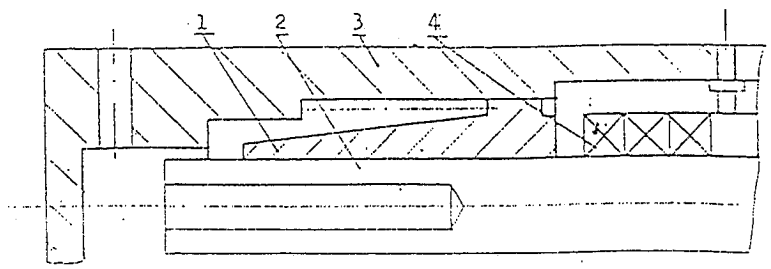

1—bushing 2—plunger 3—cylinder 4—packing

Figure 5. Plan II of combined seal

8th American Water Jet Conference
August 26-29, 1995: Houston, Texas

Paper 39

COMPUTATIONAL FLUID DYNAMIC ANALYSIS AND VISUALIZATION OF HIGH FREQUENCY PULSED WATER JETS

M.M. Vijay, M.K.Y. Lai and M. Jiang
National Research Council of Canada
Ottawa, Ontario, Canada, K1A 0R6

ABSTRACT

High frequency pulsed water jets generated by forced ultrasonic modulation of a continuous stream of water have a great potential for a variety of cutting and cleaning applications. However, the formation of well defined pulses, which are necessary for efficient cutting or cleaning, is a complex function of both configurational and operating parameters of the nozzle. In order to understand the mechanics of pulsed jet formation, visualization experiments and computational fluid dynamics (CFD) analysis are in progress.

The visualization system consists of a high powered pulsed sheet of light produced by a Continuum Surelite Nd-Yag Pulsed Laser with a repetition rate of 10 Hz. The computer code, called herein CODE-PULSE, is for the analysis of two-dimensional, transient, two-phase gas-liquid flow problems with a sharp discontinuity at the interface. The code is based on the numerical solution of the conservation equations of mass, momentum, and the standard k-ε submodel. The surface tension effect is taken into account at the interface and the Fractional Volume-of-Fluid (VOF) method is used to track the dynamics of the interface. It is shown that visualization and the CFD analysis are valuable tools for examining the structure of the pulsed jets and hence in optimizing the nozzle designs.

Organized and Sponsored by the Water Jet Technology Association.

1 INTRODUCTION

The concept of forced modulation of a continuous stream of water to produce high frequency pulsed jets is known for some time (Nebeker & Rodriguez, 1976). However, due to lack of reliable nozzle systems, virtually no attempts have been made to exploit the potential of high frequency pulsed jets for practical applications. Recently, Vijay (1992) introduced the concept of generating high frequency pulsed water jets using ultrasonic waves for modulation (Fig. 1). Further investigations by Vijay, et al. (1993), Vijay & Foldyna (1994) and Foldyna & Vijay (1994) showed clearly that high frequency pulsed water jets produced by this technique are powerful indeed and can be used to cut even metals at fairly low pressures (≈ 69 MPa; Fig. 2). Viewed differently, if one were to use continuous water jets to cut metals such as cast iron (thickness ≈ 6 mm), one would need pressures in excess of 200 MPa. The advantages of pulsed water jets for many other applications (cutting and fragmentation of rocks, demolition of concrete, removal of paints or coatings, etc) are immediately obvious.

Figure 3 shows some basic results obtained with a typical nozzle device (Fig. 1). As explained in detail by Vijay & Foldyna (1994), the results are influenced by both the operating variables (for example, pressure, flow and frequency of oscillations) and the configurational parameters (α_n, α_t, d_t, etc., in Fig. 1). It is clear from Fig. 3 that the peak (optimum) performance (measured in terms of the rate of mass loss of the sample) is strongly influenced by the location of the velocity transformer in the nozzle (parameter "a" or "a_o" in Fig. 1). In other words, the optimum performance of the nozzle is strongly influenced by the configurational parameters.

Since the flow both within and outside of the nozzle is quite complex, it is not possible to optimize the nozzle design by a simple mathematical analysis. Therefore, computational fluid dynamics (CFD) was adopted to analyse the flow. Visualization experiments, using pulsed laser sheet illumination, were conducted to examine the characteristics of the pulsed jets and to validate the CFD results. It should be pointed out however that, in this paper, only preliminary results are presented. In other words, CFD analysis is confined to the modulation of the jet starting from the exit plane of the nozzle (nozzle wall in Fig. 4), disregarding the influence of the nozzle configurational parameters (inner profile of the nozzle, velocity transformer, etc). Visualization results were obtained at fairly low pressures (Maximum: 35 MPa). Nonetheless, it is shown that the visualization technique and more importantly CFD are valuable tools for understanding the characteristics of pulsed jets and hence in optimizing the nozzle designs without resorting to extensive experimental work.

2 CFD ANALYSIS

The solution domain, in an axisymmetric cylindrical coordinate system, used in the CFD analysis is shown in Fig. 4. The CFD methodology is derived from a version of the NRC TURCOM code (Lai, 1987). The computer code thus derived, called herein as CODE-PULSE, is developed for the solution of two-dimensional, transient, gas-liquid flow problems with a sharp discontinuity at interface. The code is based on the numerical solution of the instantaneous ensemble-averaged Navier-Stokes equations. The k-ϵ turbulence submodel (Launder & Spalding, 1974) is used to calculate parameters of the turbulent field. The surface tension effect is taken into account at the interface. The fractional Volume-of-Fluid (VOF) method by Hirt & Nichols (1981) is used to track the dynamics of interface.

2.1 Governing Equations

The flow is assumed to be incompressible. The complete set of instantaneous ensemble-averaged conservation equations of continuity and momentum is expressed, in vector notation, as:

$$\frac{1}{\rho}\frac{D\rho}{Dt} + \nabla\cdot\vec{U} = 0 , \qquad (1)$$

$$\frac{\partial \rho \vec{U}}{\partial t} + \nabla\cdot[\rho\vec{U}\vec{U} + \rho\overline{\vec{u}\vec{u}} + (P + P_s)\vec{I}] = \nabla\cdot\vec{\tau} + \rho\vec{g} \ . \tag{2}$$

The viscous and Reynolds stress tensors are given by

$$\vec{\tau} = \mu[(\nabla\vec{U}) + (\nabla\vec{U})^T] - \tfrac{2}{3}\mu\nabla\cdot\vec{U}\vec{I} \tag{3}$$

and

$$-\rho\overline{\vec{u}\vec{u}} = \mu_t[(\nabla\vec{U}) + (\nabla\vec{U})^T] - \tfrac{2}{3}(\rho k + \mu_t\nabla\cdot\vec{U})\vec{I} \ . \tag{4}$$

The turbulent viscosity, μ_t, is determined by:

$$\mu_t = C_\mu \rho k^2/\varepsilon \tag{5}$$

with k and ε derived from their own conservation equations:

$$\frac{\partial \rho k}{\partial t} + \nabla\cdot[\rho\vec{U}k - \frac{(\mu+\mu_t)}{\sigma_k}\nabla k] = G - \rho\varepsilon \ , \tag{6}$$

$$\frac{\partial \rho \varepsilon}{\partial t} + \nabla\cdot[\rho\vec{U}\varepsilon - \frac{(\mu+\mu_t)}{\sigma_\varepsilon}\nabla\varepsilon] = (C_1 G - C_2\rho\varepsilon)\frac{\varepsilon}{k} \tag{7}$$

and

$$G = \{\mu_t[(\nabla\vec{U}) + (\nabla\vec{U})^T] - \tfrac{2}{3}(\rho k + \mu_t\nabla\cdot\vec{U})\vec{I}\}:\nabla\vec{U} \ . \tag{8}$$

The turbulence model constants (C_μ, C_1, C_2, σ_k, σ_ε) are given by Launder & Spalding (1974).

In the present analysis, viscous effects are neglected at the interface. The surface tension coefficient σ is assumed to be constant and the surface tension pressure P_s is given by

$$P_s = -\kappa\sigma \ . \tag{9}$$

The volumetric continuity equation Eq. (1), called GALA (Gas And Liquid Analyser) formulation by Spalding (1977), is used to prevent numerical problems arising from a discontinuity of density across the interface. This allows flow variables to be computed over the entire flow domain. The pressure and velocity are continuous across the interface.

The values of ρ, μ and μ_t appearing in Eqs. (2-4) are calculated by linear interpolation of the pure (single-phase) values using a liquid volume fraction F:

$$\rho = F\rho_l + (1-F)\rho_g \ , \quad \mu = F\mu_l + (1-F)\mu_g \ , \quad \mu_t = F\mu_{tl} + (1-F)\mu_{tg} \ . \tag{10}$$

F has a value of 1 in the liquid region, 0 in the gas region, and $0 < F < 1$ in the two-phase (air-water mixture) region, and is governed by

$$\frac{DF}{Dt} = 0 \ . \tag{11}$$

This equation is solved to advance the interface location.

2.2 Boundary Conditions (see Fig. 4)

Inlet Plane

The instantaneous velocity of the jet emerging from the nozzle is assumed to be uniform across the inlet plane but periodic about a mean value, expressed as:

$$V = \overline{V} + \Delta V\sin(2\pi ft) \ . \tag{12}$$

The average velocity at the inlet plane is given by

$$\overline{V} = C_D\sqrt{2(P - P_a)/\rho} \ . \tag{13}$$

The pulsed jet calculations illustrated in this paper were obtained under the following assumptions: $0.2\overline{V}$ and $0.5\overline{V}$ for ΔV with zero radial and swirl velocities. Boundary condition for k is calculated using a turbulence intensity of $0.1V$, and prescribing 3% of the nozzle diameter for the length scale of ε. It should be emphasized that these assumptions depend strongly on the horn and nozzle configurations.

Outlet Plane

Zero normal gradient is imposed on all variables.

Axis of Symmetry

Zero normal gradient is imposed on all variables, except the radial velocity which is assumed to be zero.

Solid Wall (Nozzle Wall)

At the nozzle wall, no-slip and impermeable boundary conditions are imposed. Velocities are set to zero. The wall shear stresses and the values of k and ε close to the walls are modelled by the wall function method (Launder & Spalding, 1974). Wall adhesion effect with a prescribed contact angle is assumed.

Entrainment Boundary

The air, through aerodynamic drag, is entrained through this boundary. Zero normal gradients are assumed for all variables, except the prescribed values for molecular viscosity and density for air.

2.3 Solution Procedure

CODE-PULSE solves the finite volume approximations to the governing equations in primitive variables. A fully implicit numerical scheme in time and a hybrid upwind/central differencing in space were used to discretise the equations {Eqs. (1-7)} on a staggered grid. The SIMPLE (Semi-Implicit Method for Pressure Linked Equations) algorithm (Patankar & Spalding, 1972) was employed to obtain the velocity and pressure fields. Each discretised equation was solved sequentially in an iterative fashion using a line-by-line method. During the iteration procedure, the fluid properties were updated according to Eq. (10). The whole iterative procedure was repeated at each time step, taking the results of the previous step for the guessed values. At the beginning of each time step, the surface tension pressure and wall adhesion force were computed in the same manner as in Hirt & Nichols (1981). To preserve the discontinuity property at the interface, the donor-acceptor flux approximation of Johnson (1970) was used to solve Eq. (11).

All the results were obtained using 142x27 grid points in the axial and radial directions, respectively. An under-relaxation factor of 0.5 was used for all variables. Two sweeps for the governing equations were used. The solution was assumed to have converged when the sum of the normalized absolute residuals had fallen below 10^{-3}. One hundred iterations per time step were found to be sufficient for convergence. A time step of 0.55μs was used to ensure numerical accuracy and stability. The CPU time on the SGI Indigo2 workstation was approximately 4s per time step calculation.

3 VISUALIZATION TECHNIQUE

A schematic diagram of the experimental set-up for the visualization of the high frequency pulsed water jets is depicted in Fig. 5. The set-up consisted essentially of an ultrasonic nozzle device to generate the pulsed water jets at 15 kHz issuing in the vertical direction, a jet catcher (a tank partially filled with water), a Continuum Surelite I-10 pulsed Nd-Yag Laser (frequency: 10 Hz, wave length: 532 nm, maximum energy: 200 mJ per pulse in single pulse mode of operation, pulse width: 4-6 ns), optical components for producing a sheet of light (Philbert, et al., 1989 and Vijay, et al., 1991), a 35mm Canon T-70 camera with Canon Macro FD 50 mm Lens (1:3.5) and Kodak Gold 100 coloured films. The advantages of the laser sheet are that its thickness can be controlled and, both axial and cross-sectional views of the jet can be photographed (Vijay, et al., 1991).

Since the location of the camera with respect to the sheet of light was found to be quite important, the camera was placed at one of two locations (Fig. 5). For $P \leq 10$ MPa, the spray around the jet was not too severe and the image on the film was produced essentially by scattering of the laser light. For $P > 10$ MPa, the spray around the jet was quite severe and the quality of the photographs could be improved by locating the camera facing the laser. This required increasing the width of the sheet, by inserting a slit between the laser and the jet, to photograph full size of the pulses. In this case, images were produced by transmission of the light through the jet (almost like a shadowgraph).

The procedure for taking the photographs was quite simple. Tests were conducted in a totally darkened room. When the appropriate operating conditions were set, the camera shutter was kept open and the laser was triggered to produce a pulse of light at the required level of energy. It was necessary to take several photographs of the same jet.

4 RESULTS

4.1 General Remarks

Although a large number of photographs have been taken to examine the structure and characteristics of the ultrasonically modulated pulsed water jets, it is not possible to consider all the minute details in this paper. The most useful information from the standpoint of cutting performance is the break-up length {the distance from the nozzle at which the continuous stream just starts to form bunches (pulses) of water, Vijay & Foldyna, 1994} of the continuous jet, the shape and size of the pulses (see Nebeker & Rodriguez, 1976) produced by a particular nozzle configuration at a given set of operating conditions. Similar arguments apply to the CFD results reported in the paper.

4.2 Visualization Results

Typical photographs of the pulsed jets produced by the ultrasonic nozzle device are depicted in Fig. 6. The operating conditions and other relevant information are indicated on the figures. The photographs clearly demonstrate the formation of pulsed jets by ultrasonic modulation of a continuous stream of water.

4.3 CFD Results

The numerical results were simulated for the nozzle with $d_n = 1.70$ mm ($C_D = 0.94$) at the following operating conditions: $f = 15$ kHz, $P_a = 0.1$ MPa, and two values of $P = 10$ and 35 MPa. Figure 7 shows a magnified view of the shape of the bunch (pulse) and Fig. 8 shows a sequence (snap-shot) of the predicted structure of the water jet outside of the nozzle. Colour (or black-grey-white shading) indicates a prescribed value of liquid volume fraction, F. Other information relevant to the analysis are indicated on the figures.

5 DISCUSSION

5.1 Visualization

A simplified analysis of the mechanism of formation of pulsed jets by modulation is given by Sami & Ansari (1981) and an excellent qualitative description is reported by Neberker & Rodriguez (1976) and Nebeker (1983), except that these authors considered only low frequency (< 5 kHz) water jets. Although the flow mechanism is quite complicated, the characteristics of the pulsed jets observed in the present study generally agree with the observations reported by these authors.

Fig. 6(a) shows a continuous jet emerging from the nozzle at a very low pressure of 0.43 MPa surrounded with small droplets. Fig. 6(b) shows that the surface structure of the jet begins to change even for a small input of ultrasonic power (this could not be measured). Surface waves are visible which start at a distance of approximately 40 mm from the nozzle exit. At the extreme right, initiation of modulation leading to break-up of the jet can be seen. In Fig. 6(c), the appearance of the jet is shown for an ultrasonic power input of 2 kW. Here, as explained by Vijay & Foldyna (1994), one can see four zones of the jet consisting of (i) a continuous segment, (ii) a transition zone where the modulation starts to form bunches of water, (iii) a zone of well defined pulses (slugs), and (iv) disintegration of the pulses into droplets. In fact, the shape of the erosion curve in Fig. 3 is attributed to this changing structure of the jet with the standoff distance, with the peak corresponding to the zone of well defined pulses. Droplets are visible in all the photographs.

In Figs. 6(d) to 6(l), the appearance of the jets is shown at P = 5, 10, 13 & 34.5 MPa, P_U = 2 & 4 kW and "a" = 11, 11.5 & 12 mm all at f = 15 kHz. Due to limitation of the experimental set-up, it was not possible to take photographs for values of P > 34.5 MPa or lengths of jets > 8 cm. The photograph shown in Fig. 6(l) was taken with the camera facing the laser source (Fig. 5). The following observations can be made from these photographs:

At close distances from the nozzle exit ($S/d_n \approx 11$), the jet appears to consist of spherically shaped pulses which are then gradually transformed into a train of mushroom (umbrella) shaped pulses. This can be clearly seen in Figs. 6(c), (e) and (g). The distance at which the spherically shaped pulse is transformed into a mushroom shaped (hemispherically-curved) pulse is a function of the pressure. For $P \leq 15$ MPa, the mushroom shaped pulses can be seen in all the photographs. However, at 34.5 MPa {Fig. 6(k)}, only transition zone is visible and the mushroom shaped pulses probably occur beyond the distance (> 40 mm) shown in the photograph. It should be noted that, from a standpoint of cutting or fragmentation performance, the mushroom shaped pulses are favourable because they impart much higher impact forces on the target than flat faced pulses (Rochester & Brunton, 1972).

The mushroom shape occurs due to the combined effects of surface tension, inertial force and aerodynamic drag. Water droplets at the edges (periphery) of the pulses, which are clearly visible in the photographs, are formed by the aerodynamic drag. According to Nebeker (1983), these droplets, moving at the same mean velocity as the jet, form a shroud around jet's core and thus preserve its effectiveness over a long distance from the nozzle exit (note that cutting performance peaks at S ≈ 160 mm in Fig. 3).

It is clear that the diameter of the pulses increase with standoff distance. However, as the jet eventually disintegrates into droplets {Fig. 6(c)}, the pulse will attain a maximum diameter at a certain distance from the nozzle exit. Once again, due to aerodynamic drag, the maximum diameter is a function of pressure. For example, the maximum diameters at 5 and 10 MPa {Fig. 6(d) and 6(e)} are respectively about $7d_n$ and $5d_n$. Nebeker & Rodriguez (1976) explained that the effectiveness of the pulsed jets, apart from the water hammer effect, is due to this increased area of impact on the target.

The effect of P_U, which is proportional to the amplitude of vibration at the tip of the velocity transformer, at 10 MPa is shown in Figs. 6(f) and 6(j). Theoretically, for a given pressure (average speed of the jet), diameter of the pulses should increase with the increase in the amplitude of modulation (Nebeker, 1983 and Sami & Ansari, 1981; see also CFD Analysis below). In fact, this is the method to use to preserve large size of the pulses as the pressure is increased (see above). There is no evidence of this occurring in these photographs. It appears that an increase in P_U results in the generation of more water droplets than enhancing the diameter of the pulses. A comparison of Fig. 6(f) with Fig. 6(h) seems to indicate, however, that when the value of P_U is increased, the location ("a") of the velocity transformer in the nozzle must also be adjusted. The diameter of the pulse has now increased by about 30%, compared to the value at 2 kW {Fig. 6(j), 4th pulse from the nozzle exit}. Further work is in progress in the laboratory to confirm this observation.

The influence of the configurational parameter "a" on the structure of the pulsed jet can be seen in Figs. 6(i) and 6(j). The diameter of the pulse appears to have decreased by about 20% when the value of "a" was increased from 11.5 to 12 mm. Since the impact force on the target is proportional to the diameter of the pulse, this should have an adverse effect on the performance. The experimental results plotted in Fig. 3 certainly confirm this deterioration in performance.

A close examination of Fig. 6(l) shows that the pulse is a mixture of water, air and probably minute droplets of water (see CFD Analysis below). Furthermore, there is no evidence of toroidal vortices in any of the photographs.

The photographs are useful in extracting the values of parameters other than diameter of the pulses. This is important in validating the CFD results. For example, the wavelength ($L = \bar{V}/f$), which is equal to the distance between two consecutive pulses, is an important parameter. The theoretical (Nebeker, 1983) and measured {Figs. 6(d) and 6(e)} values of L are, respectively: 6.3 & $\approx$ 7 mm (at 5 MPa) and 9 & $\approx$ 8.5 mm (at 10 MPa).

5.2 CFD Analysis

It is obvious from the equations of motion presented in Section 2 that the mechanism of formation of pulsed jets by modulation is quite complex. The characteristics of the pulses are governed by the interaction between turbulence (Reynolds stresses), aerodynamic drag and surface tension forces. Surface tension forces are strong as the sizes of the slugs are small. Simulation results depicted in Figs. 7 and 8 were obtained for arbitrary values of the amplitude of modulation (ΔV). Therefore, comparison between the simulated and the visualized results (Fig. 6) is, at present, only qualitative.

Figure 7 shows a magnified view of the modulated jet at 35 MPa. The pulse is clearly of the mushroom shape containing small amount of air and probably some water droplets (on the periphery of the pulses, $0.5 < F < 1.0$). In Fig. 8 (a, b & c), the simulated results are shown for the conditions listed on the figure. As shown in the visualization photographs at 10 MPa {Fig. 6(e)}, the mechanism of pulse formation starts close to the nozzle wall. Due to the effects of afore mentioned forces, the amplitude of disturbance increases with axial distance from the nozzle wall and towards to the centre of the jet, eventually breaking the jet into pulses. The spacings between the pulses appear to be quite constant. Photographs in Fig. 6 show that the mist (droplet) region increases with downstream distance as a result of air entrainment. However, due to the size of the grid selected in the CFD analysis, it was not possible to predict the small scale mist surrounding the jet. Thus, the increase of the pulse diameter in the axial direction cannot be seen in Fig. 8.

As the pressure increases from 10 to 35 MPa {Fig. 8(b)}, the shear force due to aerodynamic drag becomes a strong component affecting the structure of the pulse. As a result, it becomes elongated. Also, the number of pulses within a given distance from the nozzle wall decreases. These findings are in agreement with the experimental observations {compare, for example, Fig. 6(j) with 6(k)}. The effect of increasing the amplitude

of modulation from 20 to 50% (this is related to ultrasonic power input in the experiments) can be seen by comparing Fig. 8(b) with 8(c). The diameter of the pulse has increased by about 33 percent. This was not obvious in the visualization results as discussed above.

It is possible to estimate the wavelength and the velocity of pulses from the CFD results. The wavelengths at 10 MPa {Fig. 8(a)} and 35 MPa {Fig. 8(b)} are approximately 8.75 and 16.4 mm respectively. These compare favourably with the values 9.0 and 16.8 mm estimated using the definition by Nebeker (1983) and also the value of 8.5 mm (at 10 MPa) estimated from Fig. 6(e). The velocity of the pulses can be calculated using the fact that the time difference (time per frame) between the two successive rows in Fig. 8 is 16.7 μs. The pulse velocities at 10 MPa {Fig. 8(a)} and 35 MPa {Fig. 8(b)} are approximately 150 m/s and 261 m/s respectively (mean speeds of the jet are: 135 m/s and 252 m/s). Obviously, for a given amplitude of modulation, the pulse velocity approaches the mean velocity as the pressure is increased. However, as pointed out earlier, it is possible to circumvent this drawback, as confirmed by the results indicated in Fig. 8(c), by increasing the amplitude of modulation when the pressure is increased (pulse velocity ≈ 305 m/s). Although highly encouraging, further experimental work and refinement in the CFD analysis are required to confirm these interesting observations.

6 CONCLUSIONS

Pulsed jets were generated by modulating a continuous stream of water by ultrasonic waves at 15 kHz. The conclusions from the limited visualization, CFD and erosion results included in this paper are:

- A pulsed water jet, operating at the same pressure as a continuous jet, is more powerful for processing a variety of materials and, retains its cutting ability over a large standoff distance;
- The optimum performance of an ultrasonically modulated jet is a function of both the nozzle configurational and operating parameters;
- There is a reasonable agreement in the observations made by laser sheet visualization technique and the CFD analysis, corroborated to certain extent, by the experimental results;
- Both laser sheet visualization technique and CFD analysis (usually termed computer visualization) are valuable tools for understanding the mechanics of formation of the pulsed jet and hence in optimizing the nozzle design.

7 ACKNOWLEDGMENTS

The authors are thankful to Dr. D. R. Snelling, Mr. G.J. Smallwood and Mr. R.A. Sawchuk of the Institute for Environmental Research & Technology, National Research Council of Canada for valuable discussions on the selection and setting up of the laser light source. It is a pleasure to acknowledge, Mr. E. Debs (University of Ottawa), Mr. S. Fierobin, Mr. S. Jarosz (University of Toronto), Mr. N. Paquette, Dr. R.J. Puchala and Mr. S. Wlodarski for their technical assistance at various stages of the experimental program.

8 REFERENCES

Foldyna, J., and Vijay, M.M., "Potential of Ultrasonically Modulated Pulsed Water Jets for Cutting Metals", *Manufacturing Science and Engineering, ASME 1994*, Vol. 1., PED-Vol. 68-1, pp. 397-404, ASME, New York, NY, USA, 1994.

Hirt, C.W., and Nichols, B.D., "Volume of Fluid (VOF) Method for the Dynamics of Free Boundaries", *Journal of Computational Physics*, Vol. 39, pp. 201-225, 1981.

Johnson, W.E., "Development and Application of Computer Programs Related to Hypervelocity Impact", *Systems Science and Software Report 3SR-353*, 1970.

Lai, K.Y.M., "TURCOM: A Computer Code for the Calculation of Transient, Multi-Dimensional, Turbulent, Multi-Component Chemically Reactive Fluid Flows. Part 1: Turbulent, Isothermal and Incompressible Flow", *Technical Report TR-GD-011 (NRC No. 27632)*, National Research Council Canada, Ottawa, Ontario, Canada, 1987.

Launder, B.E., and Spalding, D.B., "The Numerical Computation of Turbulent Flows", *Computer Methods in Applied Mechanics and Engineering*, Vol. 3, pp. 269-289, 1974.

Nebeker, E.B., and Rodriguez, S.E., "Percussive Water Jets for Rock Cutting", *Proceedings of the 3rd International Symposium on Jet Cutting Technology*, Paper B1, pp. B1-1 - B1-9, BHRA, Cranfield, Bedford, England, 1976.

Nebeker, E.B., "Standoff Distance Improvement Using Percussive Jets", *Proceedings of the 2nd U.S. Water Jet Conference*, pp. 25-34, Water Jet Technology Association, St. Louis, Missouri, USA., 1983.

Patankar, S.V., and Spalding, D.B., "A Calculation Procedure for Heat, Mass and Momentum Transfer in Three-Dimensional Parabolic Flows", *International Journal of Heat and Mass Transfer*, Vol. 15, pp. 1787-1806, 1972.

Philbert, M., Surget, J., and Véret, C., "Light Sheet Technique", Chapter 14, pp. 211-217, *Handbook of Flow Visualization*, Yang, W.J., Ed., Hemisphere Publishing Corporation, New York, USA, 1989.

Rochester, M.C., and Brunton, J.H., "High Speed Liquid Impact of Jets on Solids", *Proceedings of the 1st International Symposium on Jet Cutting Technology*, Paper A1, pp. A1-1 - A1-24, BHRA, Cranfield, Bedford, England, 1972.

Sami, S., and Ansari, H., "Governing Equations in a Modulated Liquid Jet", *Proceedings of the 1st U.S. Water Jet Symposium*, pp. I-2.1-2.9, Water Jet Technology Association, St. Louis, Missouri, USA., 1981.

Spalding, D.B., "The Calculation of Free-Convection Phenomena in Gas-Liquid Mixtures", *Heat Transfer and Turbulent Buoyant Convection*, Ed: D.B. Spalding and N. Afgan, Vol. 2, pp. 569-586, Hemisphere Publishing Corporation, Washington, D.C., 1977.

Vijay, M.M., Zou, C., and Tavoularis, S, "A Study of the Characteristics of Cavitating Waterjets by Photography and Erosion", *Proceedings of the 10th International Symposium on Jet Cutting Technology* (1990), pp. 37-67, BHR Group, Elsevier Applied Science, London, England, 1991.

Vijay, M.M., "Ultrasonically Generated Cavitating or Interrupted Jet", *U. S. Patent No. 5,154,34 7*, October, 1992.

Vijay, M.M., Foldyna, J., and Remisz, J., "Ultrasonic Modulation of High-Speed Water Jets", *Proceedings of the International Conference Geomechanics 93*, pp. 327-332, A.A. Balkema, Rotterdam, 1993.

Vijay, M.M., and Foldyna, J., "Ultrasonically Modulated Pulsed Water Jets: Basic Study", *Proceedings of the 12th International Conference on Jet Cutting Technology - Applications and Opportunities*, pp. 15-35, BHR Group Conference Series Publication No.13, Mechanical Engineering Publications Limited, London, England, 1994.

9 NOMENCLATURE

A	amplitude of vibration of the tip of the velocity transformer
a	absolute position of the tip of the transformer (distance from the tip to the exit plane of the nozzle) (Fig. 1)
a_0	relative position of the tip, $a_0 = a - L_c$ (Fig. 1)
b	clearance between tip and conical part of the nozzle (Fig. 1)
C_D	discharge coefficient of the nozzle
C_1, C_2	empirical constants in the ε-equation, Eq. (7)
C_μ	empirical constant in the turbulent viscosity expression, Eq. (5)
c	annular gap between cylindrical sections of the velocity transformer and the nozzle (Fig. 1)
d_n	nozzle orifice diameter (Fig. 1)
d_t	diameter of the tip of the velocity transformer (Fig. 1)
F	liquid volume fraction
f	frequency of the velocity modulation
G	generation term of turbulence kinetic energy, Eq. (8)
$\vec{g}$	gravitational acceleration vector
$\vec{I}$	unit vector
k	turbulence kinetic energy
L_c	distance between the tip to the nozzle exit for b = 0 (Fig. 1)
Δm_s	rate of mass loss
P	pump pressure or local pressure
P_a	ambient pressure
P_s	surface tension pressure
P_U	ultrasonic power, W
S	standoff distance, mm
t	time
$\vec{U}$	ensemble-averaged velocity vector
$\vec{u}$	fluctuating velocity vector
V	instantaneous inlet velocity
V_{tr}	traverse velocity
$\overline{V}$	average inlet velocity
ΔV	amplitude of the velocity modulation
α_n	angle of conical entry of the nozzle (Fig. 1)
α_t	angle of conical tip of the velocity transformer (Fig. 1)
ε	turbulence energy dissipation rate
κ	interface curvature
μ	molecular viscosity
μ_t	turbulence viscosity
ρ	density
σ	surface tension coefficient
σ_k, σ_ε	effective Schmidt number for k and ε, respectively
$\vec{\tau}$	viscous stress tensor

Superscripts

g	gas
l	liquid
T	transport of tensor
-	(overbar) ensemble-averaged

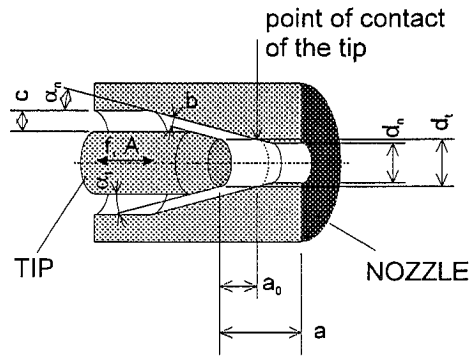

Fig. 1 A schematic sketch of the ultrasonic nozzle device showing the vibrating velocity transformer (tip) in the conical entry nozzle.

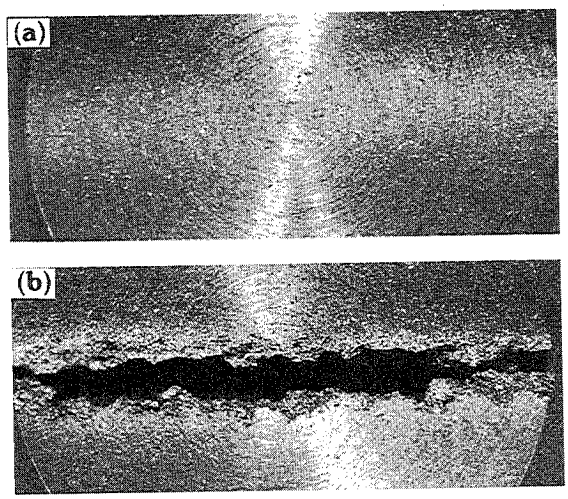

Fig. 2 Comparison of the cutting performance of (a) continuous and (b) modulated high frequency pulsed water jets. Sample: Cast Iron ASTM A48 (3.2 mm thick). d_n = 1.78 mm, P = 69 MPa, P_U = 4 kW, V_{tr} = 37.5 mm/min and S = 220 mm (Foldyna & Vijay, 1994).

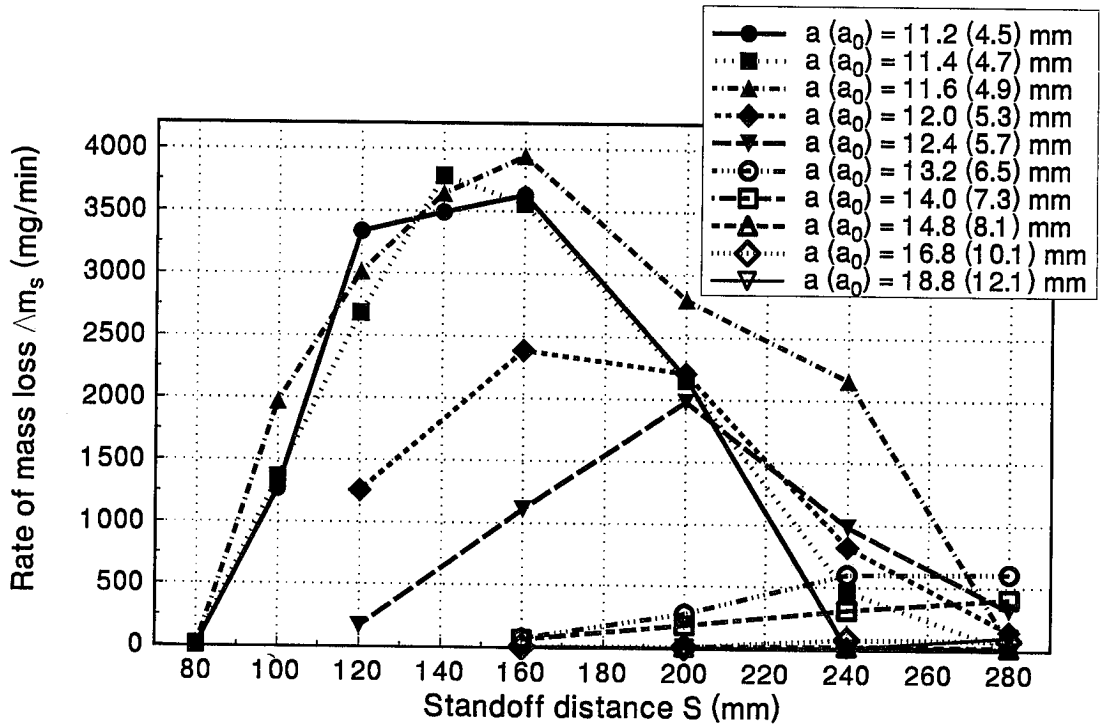

Fig. 3 Effect of the tip position "a" on the performance of ultrasonically modulated pulsed water jet. Plot of rate of mass loss of aluminum samples against standoff distance. P = 34.5 MPa, P_U = 4 kW and V_{tr} = 254 mm/min.

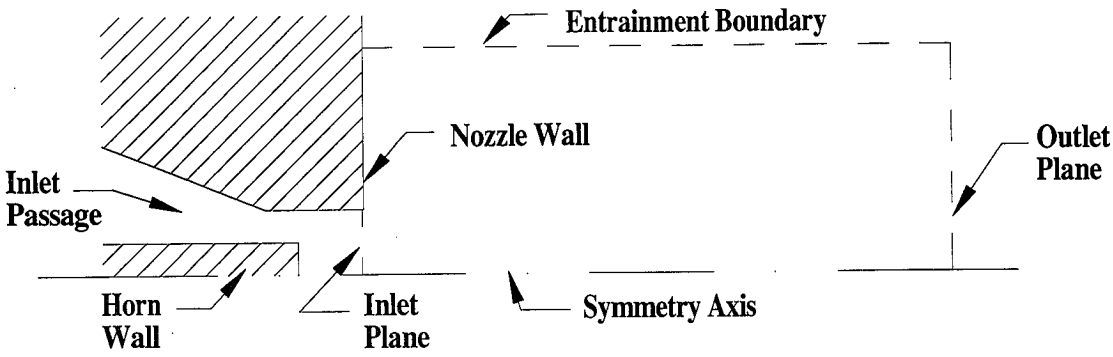

Fig. 4 Solution domain for the CFD analysis of the pulsed water jet nozzle device.

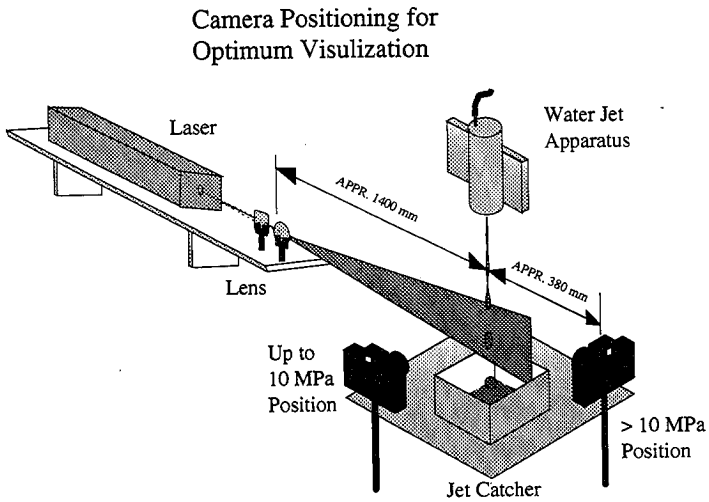

Fig. 5 A schematic diagram of the arrangement for visualization of the high frequency pulsed water jets using pulsed laser light (Nd-Yag) sheet illumination.

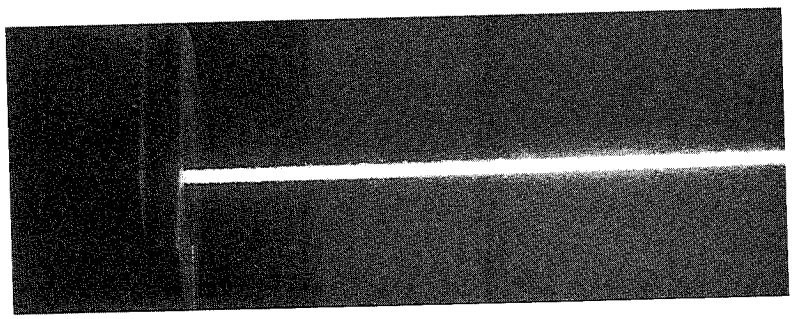

Fig. 6(a) Visualization results obtained with laser sheet illumination.
(a) Continuous jet: d_n = 1.70 mm, d_t = 1.78 mm, a = 13.3 mm, P = 0.43 MPa

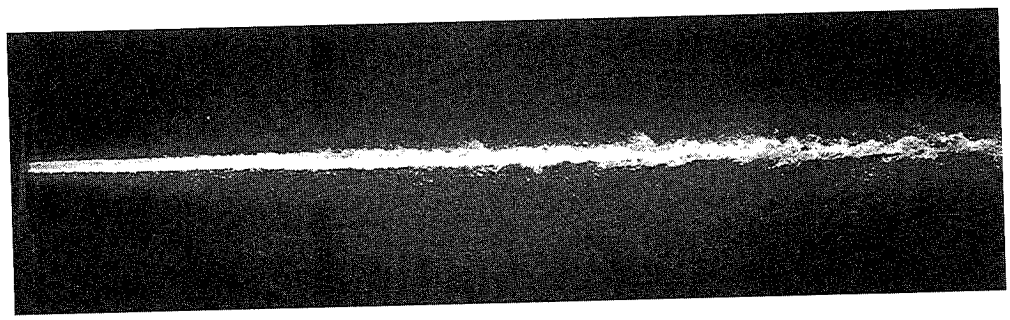

Fig. 6(b) Same as in Fig. 6(a), except P_U slightly $\rangle$ 0 kW.

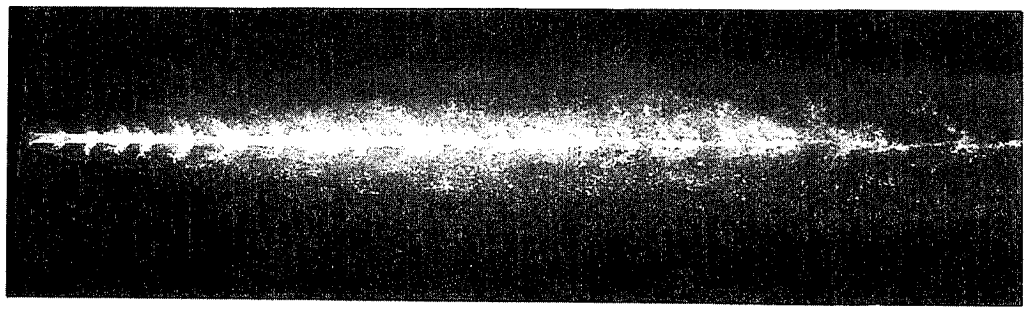

Fig. 6(c) d_n = 1.70 mm, d_t = 1.78 mm, a = 13.3 mm, P = 0.43 MPa, P_U = 2 kW and f = 15 kHz.

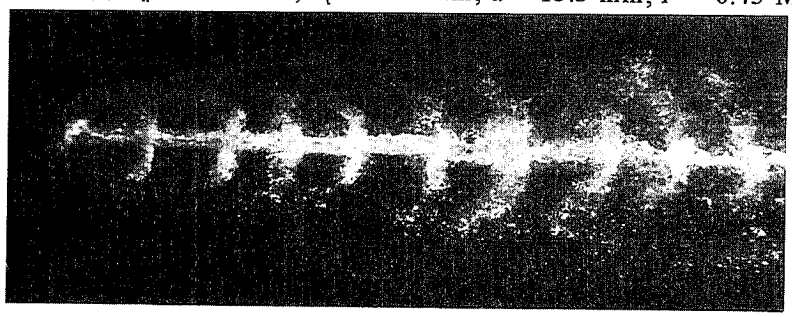

Fig. 6(d) d_n = 1.70 mm, d_t = 2.08 mm, a = 11.5 mm, P = 5 MPa, P_U = 2 kW, f = 15 kHz and M = Magnification = 1.41.

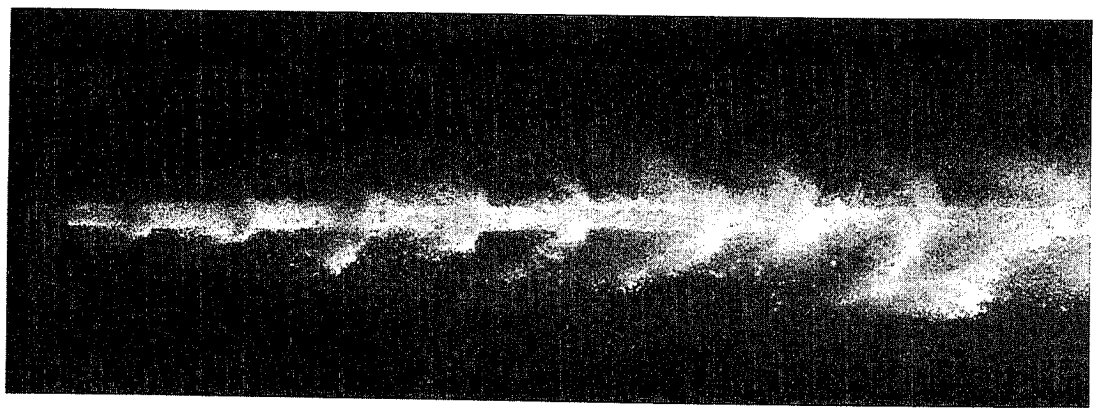

Fig. 6(e) Same conditions as in Fig. 6(d), except P = 10 MPa and M = 1.85

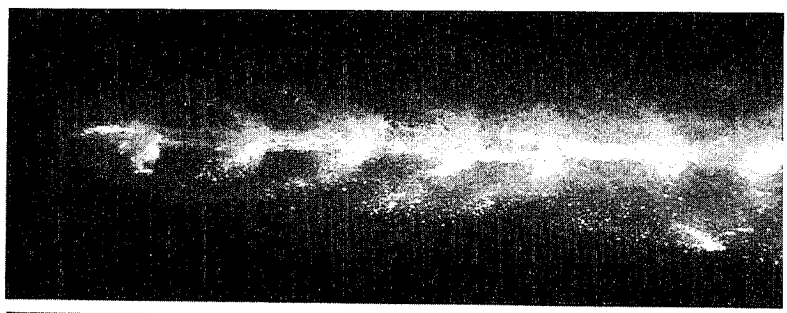

Fig. 6(f) d_n = 1.70 mm, d_t = 2.08 mm, a = 11.5 mm, P = 10 MPa, P_U = 4 kW, f = 15 kHz and M = 1.5.

Fig. 6(g) d_n = 1.70 mm, d_t = 2.08 mm, a = 11.5 mm, P = 13 MPa, P_U = 2 kW, f = 15 kHz and M = 1.41.

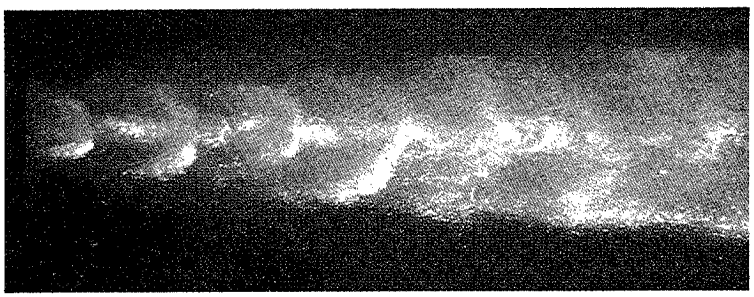

Fig. 6(h) d_n = 1.70 mm, d_t = 2.08 mm, a = 11.0 mm, P = 10 MPa, P_U = 4 kW, f = 15 kHz and M = 1.5.

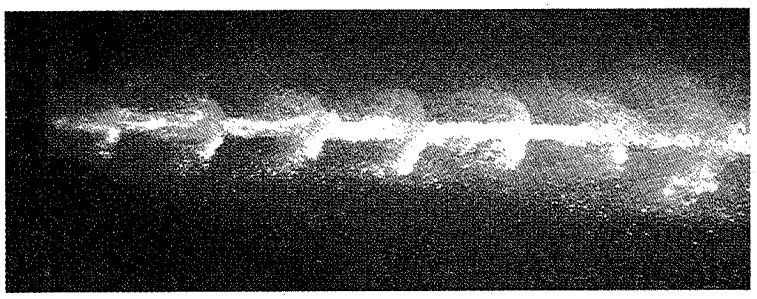

Fig. 6(i) d_n = 1.70 mm, d_t = 2.08 mm, a = 12.0 mm, P = 10 MPa, P_U = 2 kW, f = 15 kHz and M = 1.5.

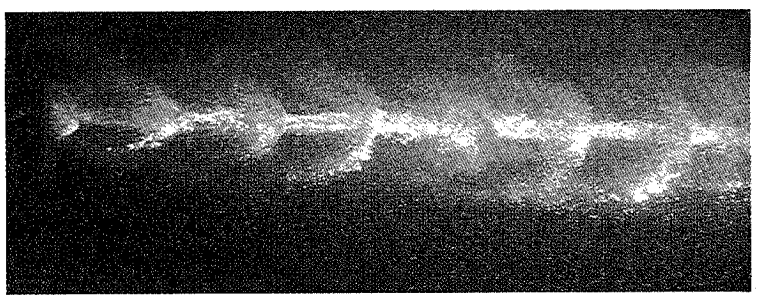

Fig. 6(j) d_n = 1.70 mm, d_t = 2.08 mm, a = 11.5 mm, P = 10 MPa, P_U = 2 kW, f = 15 kHz and M = 1.5.

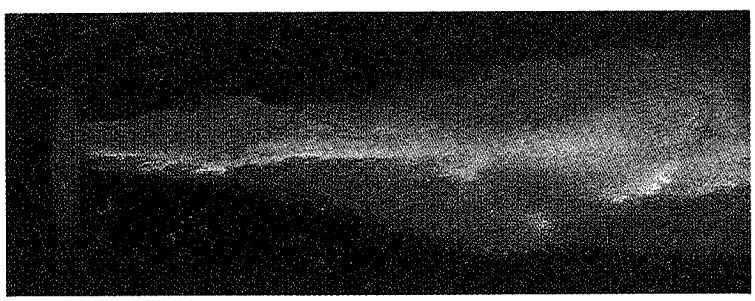

Fig. 6(k) d_n = 1.70 mm, d_t = 2.08 mm, a = 11.5 mm, P = 34.5 MPa, P_U = 2 kW, f = 15 kHz and M = 1.85.

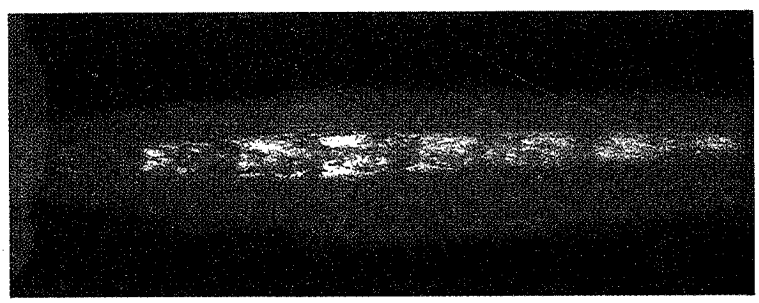

Fig. 6(l) d_n = 1.70 mm, d_t = 2.08 mm, a = 11.5 mm, P = 15 MPa, P_U = 2 kW, f = 15 kHz and M = 1.

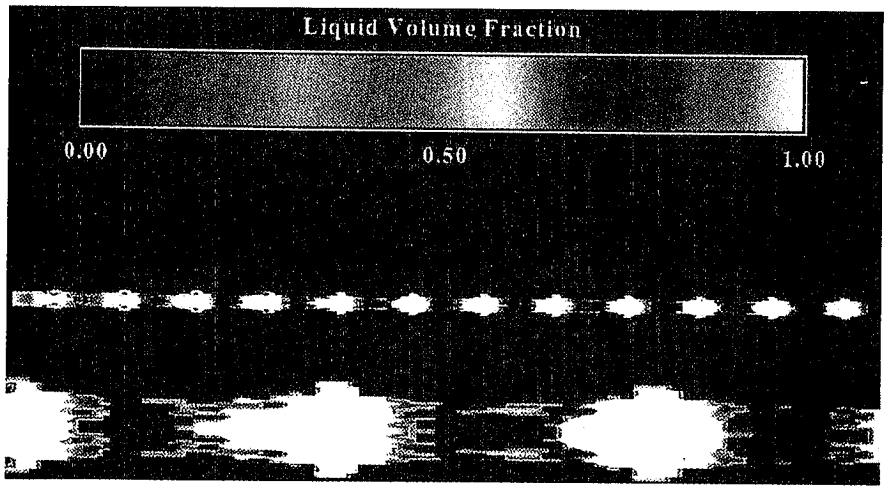

Fig. 7 CFD analysis (simulation) results showing a magnified view of the bunches. Typical appearance of the pulsed jets produced by sinusoidal modulation of a continuous water jet at 35 MPa.

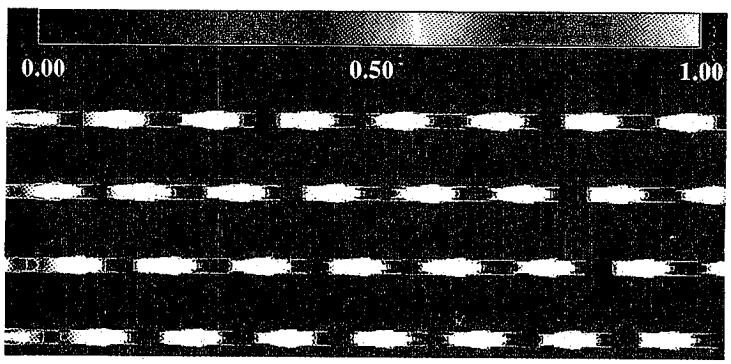

Fig. 8(a) CFD analysis results showing the formation of bunches from the nozzle exit. Total length (from the nozzle exit to the last bunch in the same row) = 70 mm. Time per frame (from one row of bunches to the next) = 16.7 μs. P = 10 MPa, d_t = 1.7 mm, Amplitude of modulation = 20% of the mean velocity.

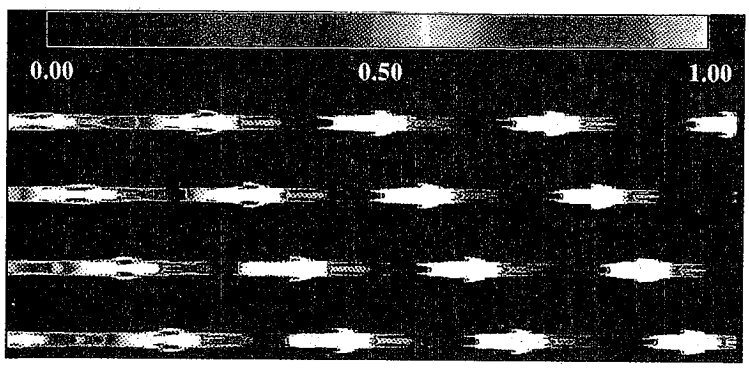

Fig. 8(b) Same conditions as in Fig. 8(a), except P = 35 MPa.

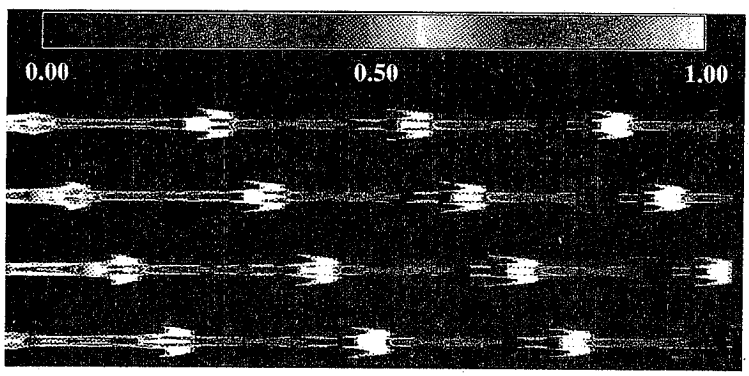

Fig. 8(c) Same conditions as in Fig. 8(b), except amplitude of modulation = 50%.

8th American Water Jet Conference
August 26-29, 1995: Houston, Texas

Paper 40

CFD ANALYSIS OF SUBMERGED TURBULENT JET FLOWFIELD OF ORGAN-PIPE NOZZLE

Wang Zhiming and Shen Zhonghou
University of Petroleum, Beijing
Changping Beijing 102200, P.R. China

ABSTRACT

CFD analysis of submerged turbulent jet flowfield of the axisymmetric jet emanating from the organ pipe nozzle is made with the turbulence κ–ε two equations model, providing the basis for improving its cleaning ability. The flowfield vectors show that there exist absorb phenomenon near the nozzle exit and large scale vortex structure near the shear layer with wavy boundary shape.

Organized and Sponsored by the Water Jet Technology Association.

1. INTRODUCTION

Hydraulic jet cutting and cleaning technology has been applied to perforating, cutting slots in casing, cutting and washing formation, and removing scale from production casing and debris from the old perforated formations resulting in improvement of oil recovery. Hydraulic jet technology, both pure water and abrasive slurry, would be thought of as the most possible and practical one which could enhance the penetration rate of rock bits and result in innovation in drilling and production method among the present advanced technology. Especially in drilling engineering, there exist two ways to increase the penetration rate. One of these is to use ultrahigh pressure water jet aiming at cutting rocks directly.The other is to use new type of jet, such as cavitating jet and pulsating jet, aiming at hydromechanically cutting of rocks or realizing direct hydraulically cuttting under lower pump pressure. It has been confirmed experimentally that organ pipe nozzle can be used to tune the submerged water jet, producing intense pressure fluctuation and strengthening its orderly structure in the shear layer and the cavitation action which opened up broad prospects for its use in rock cutting and cleaning.

The motive of this study is to predict numerically the flowfield of a turbulent submerged axisymmetric incompressible jet emanating from the organ pipe nozzle and impinging on a flat plate and study the effect of the nozzle configuration on the out flowfield of the nozzle which has not been comprehensively elucidated in the papers known to the authors, and optimize the outlet contour of the organ pipe nozzle.

2. THEORETICAL ANALYSIS

2.1 Governing Equation

Axisymmetric jets as one of the prototype classes of free shear layer have been the focus of numerous analytical, experimental, and numerical studies(Ho,C.M. et al 1981;Dimotakis,P.E., et al 1983;James E. Martin et al ,1991). The equations of the most widely adopted turbulence model, turbulence $\kappa-\varepsilon$ two equations model, used for defining the mean flowfield of a turbulent submerged axisymmetric incompressible jet may be written in the following form(R.S.Amano et al ,1984;Z.Q. Jing,1989):

Continuity equation:

$$\frac{\partial}{\partial x}(\rho r u)+\frac{\partial}{\partial r}(\rho r v)=0$$

Momentum equation:

$$\rho\frac{\partial u}{\partial t}+\frac{1}{r}[\frac{\partial}{\partial x}(r\rho u^2)+\frac{\partial}{\partial r}(r\rho uv)]$$
$$=\frac{1}{r}[\frac{\partial}{\partial x}(r\frac{\partial u}{\partial x}\mu_{eff})+\frac{\partial}{\partial r}(r\frac{\partial u}{\partial r}\mu_{eff})]-\frac{\partial p}{\partial x}+\frac{\partial}{\partial x}(\mu_{eff}\frac{\partial u}{\partial x})+\frac{1}{r}\frac{\partial}{\partial r}(r\frac{\partial v}{\partial x}\mu_{eff})$$

$$\rho\frac{\partial v}{\partial t}+\frac{1}{r}[\frac{\partial}{\partial x}(r\rho uv)+\frac{\partial}{\partial r}(r\rho v^2)]$$
$$=\frac{1}{r}[\frac{\partial}{\partial x}(r\frac{\partial v}{\partial x}\mu_{eff})+\frac{\partial}{\partial r}(r\frac{\partial v}{\partial r}\mu_{eff})]-\frac{\partial p}{\partial r}+\frac{\partial}{\partial x}(\mu_{eff}\frac{\partial v}{\partial r})+\frac{1}{r}\frac{\partial}{\partial r}(r\frac{\partial v}{\partial r}\mu_{eff})-2\mu_{eff}\frac{v}{r^2}$$

Turbulent kinetic energy equation

$$\rho\frac{\partial \kappa}{\partial t}+\frac{1}{r}[\frac{\partial}{\partial x}(r\rho u\kappa)+\frac{\partial}{\partial r}(r\rho v\kappa)]$$
$$=\frac{1}{r}\left\{\frac{\partial}{\partial x}[r\frac{\partial \kappa}{\partial x}(\mu+\frac{\mu_t}{\sigma_\kappa})]+\frac{\partial}{\partial r}[r\frac{\partial \kappa}{\partial r}(\mu+\frac{\mu_t}{\sigma_\kappa})]\right\}+\rho P-\rho\varepsilon$$

Turbulent energy dissipation rate equation

$$\rho\frac{\partial \varepsilon}{\partial t}+\frac{1}{r}[\frac{\partial}{\partial x}(r\rho u\varepsilon)+\frac{\partial}{\partial r}(r\rho v\varepsilon)]$$
$$=\frac{1}{r}\left\{\frac{\partial}{\partial x}[r\frac{\partial \varepsilon}{\partial x}(\mu+\frac{\mu_t}{\sigma_\varepsilon})]+\frac{\partial}{\partial r}[r\frac{\partial \varepsilon}{\partial r}(\mu+\frac{\mu_t}{\sigma_\varepsilon})]\right\}+C_1\frac{\rho\varepsilon}{\kappa}P-C_2\frac{\rho\varepsilon^2}{\kappa}$$

where

$$C_\mu=0.09 \quad C_1=1.44\sim1.47 \quad C_2=1.92 \quad \sigma_\kappa=1.0 \quad \sigma_\varepsilon=1.3$$
$$\mu_t=C_\mu\rho\kappa^2/\varepsilon \quad \mu_{eff}=\mu+\mu_t \quad \nu_t=\mu_t/\rho$$
$$P=\nu_t[(\frac{\partial u}{\partial r}+\frac{\partial v}{\partial x})^2+2(\frac{\partial u}{\partial x})^2+2(\frac{\partial v}{\partial r})^2+2(\frac{v}{r})^2]$$

2.2 Boundary Conditions

Boundary conditions for the above governing equations as shown in Fig. 1 are:

(1) Boundary (1), symmetric axis at r=0 :

$$\frac{\partial u}{\partial r}=0 \quad \frac{\partial \kappa}{\partial r}=0 \quad \frac{\partial \varepsilon}{\partial r}=0 \quad v=0$$

(2) Boundary (2), out flow boundary in the -x direction :

$$\frac{\partial v}{\partial x} = \frac{\partial u}{\partial x} = 0$$

(3) Boundary (3), out flow boundary in the r direction :

$$\frac{\partial (rv)}{\partial r} = \frac{\partial u}{\partial r} = 0$$

3. NUMERICAL SIMULATION RESULTS

The computational domain is divided into two blocks separated at nozzle exit x=L. A constant grid system is adopted in both the x direction and the r direction. The velocity profile at x= 0 in the organ pipe nozzle is given as

$$u_{\max} = \frac{Q}{2\pi} \bullet \frac{1}{0.455 r_n^{\ 2}}$$

$$u = u_{\max}[1 - 0.3412(\frac{r}{r_n})^{5.5}]$$

Figure 2 shows that the decay of axial centerline velocity as a function of distance S along the jet centerline is independent of the Reynolds number. The axial velocity in the radial direction is also independent of Reynolds number as shown in Fig.3 (b). Fig.3 (a) shows that the axial veocity profile in the radial direction becomes more uniform with the increase in distance S.

The flowfield vector map in Fig. 4 (a) shows that there exists cross flow in the corner near the outlet contour of the organ pipe nozzle. Fig.4 (b) shows that there exists absorb phenomenon near the nozzle exit and large scale vortex structure near the shear layer with wavy boundary shape which is helpful for improvement of its cleaning ability.

4. CONCLUSIONS

(1) The flowfield vectors show that there exist absorb phenomenon near the organ pipe nozzle exit and large scale vortex structure near the shear layer with wavy boundary shape.

(2) The computation results show that for a organ- pipe nozzle with a given configuration size, the nondimensional axial velocity in the radial direction attenuates more slowly with the increase in distance along the jet, and the nondimensional axial centerline velocity attenuation pattern is independent of Reynolds number.

(3) The computation results show that for a organ- pipe nozzle with a given configuration size, the nondimensional axial centerline velocity attenuates more slowly with the increase in distance between the nozzle exit and the impinging plate.

5. ACKNOWLEDGMENTS

This work is supported by National Education Committee Foundation. We are grateful for helpful comments made by Prof. J.H. Wu in Peking University and wish to express thanks to Dr. W. Wang for his helpful discussions.

6. NOMENCLATURE

U	mean velocity in z direction
V	mean velocity in x direction
P	pressure
ρ	density
κ	turbulent kinetic energy
ε	turbulent energy dissipation rate
μ_t	turbulent dynamic viscosity
μ_{eff}	effective viscosity
ν	turbulent kinematic viscosity
R_e	nozzle Reynolds number
x	coordinate in jet axial direction
r	coordinate in jet radial direction
r_n	organ pipe nozzle radius
Q	flow rate in the nozzle
C_μ, C_1, C_2	coefficients in turbulent model
P	generation rate of turbulent kinetic energy
σ_κ	Prandtl numbers for turbulent kinetic energy
σ_ε	Prandtl numbers for energy dissipation rate

7.REFERENCES

1.Ho,C.M.,Nosseir,N.S,"Dynamics of an impinging jet",Journal of Fluid Mechanics,Vol105, PP.119~142,(1981).

2.R.S.Amano,H.Brandt,"Numerical study of turbulent axisymmetric jets impinging on a flat plate and flowing into an axisymmetric cavity",ASME Journal of Fluid Engineering ,Vol106,PP.410~417,(1984).

3.Dimotakis,P.E.,Miake-Lye,R.C.,and Papantoniou,D.A.,"Structure and dynamics of round turbulent jets",Physics of Fluid,Vol26,PP.3185,(1983).

4.James E. Martin, Eckart Meiburg and Juan C. Lasheras,"Three dimensional evolution

of axisymmetric jets", 《Separated flows and jets》, Springer-Verlag Berlin Heidelberg, PP.629~646, (1991).

5.Z.Q. Jing, 《Numerical solution to the Navier-Stokes Equation and Turbulence Models》, Hehai University Press, PP.174~208,(1989),(in Chinese).

6.Suhas V.Patankar, 《Numerical Heat Transfer and Fluid Flow》, McGraw-Hill, PP.91~160,(1980).

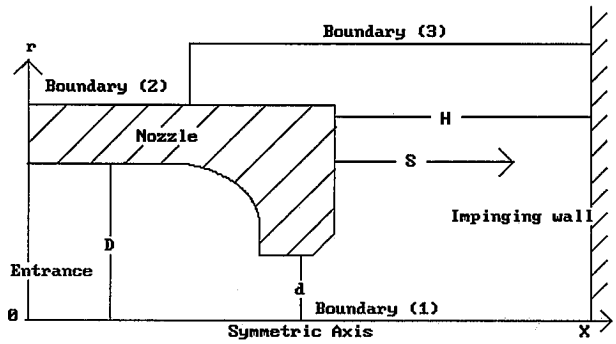

Fig.1 Flow model in and out of nozzle

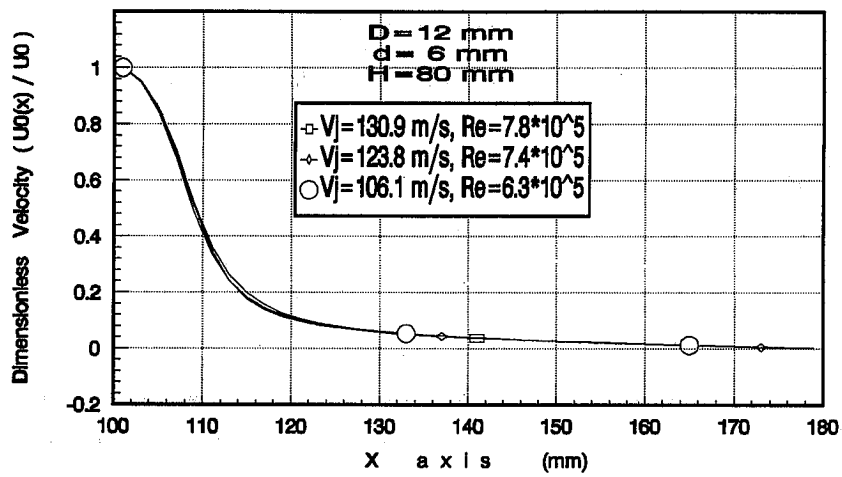

Fig.2 Dimensionless Velocity U0(x) / U0 versus X

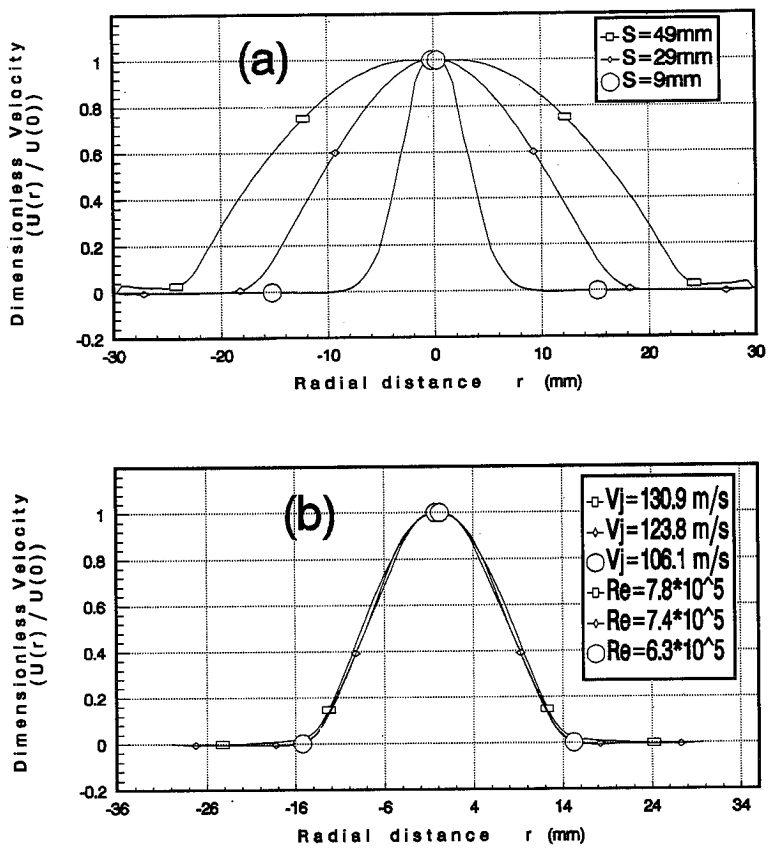

Fig.3 Dimensionless Velocity U(r)/U(0) versus r
(a) Vj=106.1 (m/s) S =variable D=12 (mm) d=6 (mm)
(b) S =19 (mm) Vj=variable D=12 (mm) d=6 (mm)

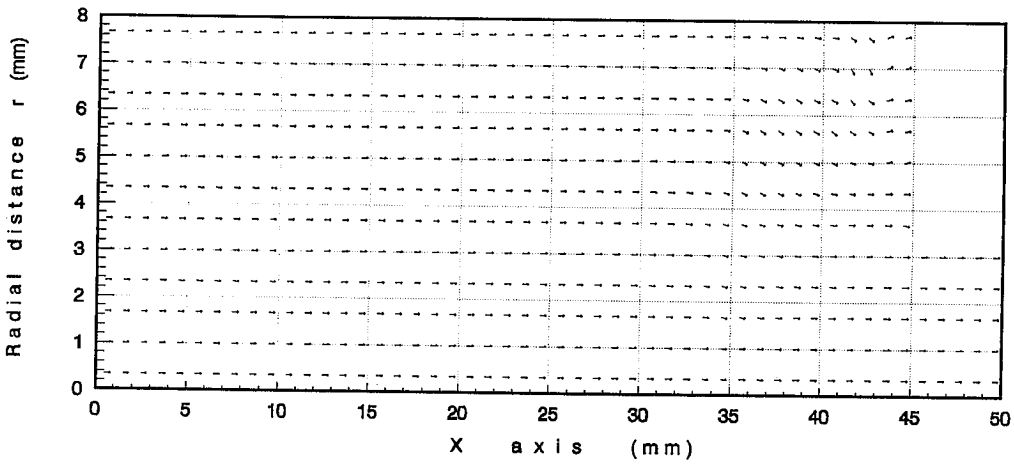

Fig.4 (a) Flowfield vector map in the organ pipe nozzle

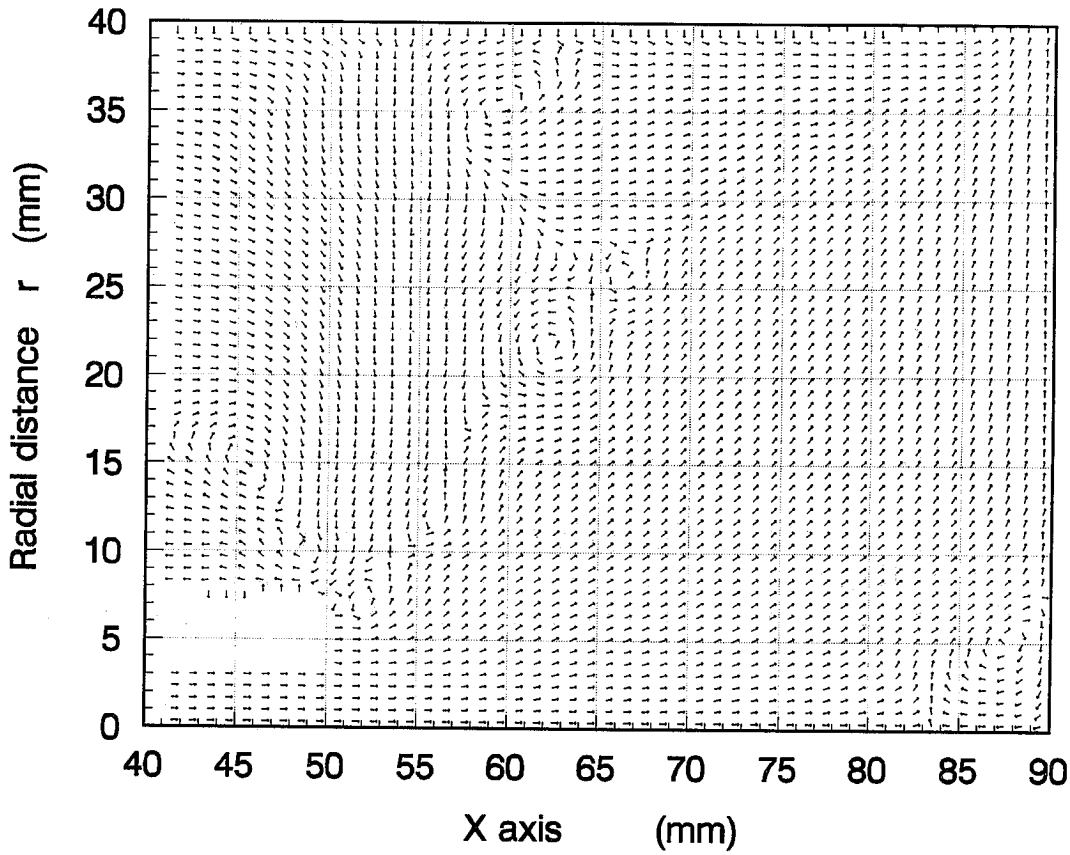

Fig.4 (b) Flowfield vector map out of organ pipe nozzle

8th American Water Jet Conference
August 26-29, 1995: Houston, Texas

Paper 41

SOME ADVANCES IN THE PASSIVE CONTROL TECHNOLOGY OF SUBMERGED WATER JET FLOWFIELD

Wang Zhiming and Shen Zhonghou
University of Petroleum, Beijing
Changping Beijing 102200, P.R. China

ABSTRACT

Characteristic equation of internal hydroacoustics of the jet pipe is established and numerically solved. Computational results show that pressure waves exist with the Strouhal numbers ranging from 0.2 to 1.2; the steps of organ-pipe is requested less than 2 and the exit diameter of the pipe nozzle is requested less than 10 mm, if the nozzle is mounted on tri-cone roller bit within the limited space. The pulsing pressure and velocity due to the hydroacoustic effect can be expressed by fundamental mode waves and their harmonics with different frequencies, damping factors and amplitudes. Measurements of the pulsating pressure signals show that the jet has strong pressure pulsating property and suction pressure, resulting in the cavitation effect and improvement in its cleaning ability. Computational results show that the jet emanating from the nozzle with an elliptic contour and conical exit contour has a well-organized large scale vortex structure.

Organized and Sponsored by the Water Jet Technology Association.

1. INTRODUCTION

Water jet technology has been widely used in many industries, especially in the petroleum industry. Hydraulic jet cutting and cleaning technology has been applied to perforating, cutting slots in casing, cutting and washing formation, and removing scale from production casing and debris from the old perforated formations resulting in improvement of oil recovery. Hydraulic jet technology, both pure water and abrasive slurry, would be thought of as the most possible and practical one which could enhance the penetration rate of rock bits and result in innovations in drilling and production methods among the present advanced technologies. Especially in drilling engineering, there exist two ways to increase the penetration rate. One of these is to use ultrahigh pressure water jet aimed at cutting rocks directly.The other is to use new type of jets, such as cavitating jet and pulsating jet, aimed at hydromechanically cutting of rocks or realizing direct hydraulic cutting under lower pump pressures.

Axisymmetric jets, as one of the prototype classes of free shear layer, have been the focus of numerous analytical, experimental, and numerical studies. Crow & Champagne(1971), by periodically forcing a turbulent jet, were able to demonstrate the existence of a preferred mode leading to the coherent structure having the form of vortex rings. It has been confirmed experimentally (Johnson Jr, V.E. et al., 1982) that several acoustic resonators can be used to tune the submerged water jet, producing intense pressure fluctuation and strengthening its orderly structure in the shear layer, and the cavitation action which opened up broad prospects for its use in rock cutting and cleaning.

Vortex control technology, that is in essence, to organize or reorganize the vorticity structure to meet our technical or performance requirements, has become an important theme of research and development in many industries such as aeronautics. The motive of our research is to understand the oscillating and structuring mechanism of jet flowfield wnich has not been comprehensively elucidated in the papers known to the authors, and optimize the design procedure of the organ pipe nozzle.

2. HYDROACOUSTIC CHARACTERISTICS OF JET PIPE

The theory of passive control technology of water jet flowfield covers several problems which are

1.Hydroacoustic controlling characteristics that means the vortex control technology of jet shear layer and optimization design theory of the jet pipe, covers internal hydroacoustics of jet pipe and interaction between nozzle lip and jet shear layer;

2.Pressure oscillating characteristics means the pressure attenuation law along the jet centerline and radial direction under atmospheric pressure and higher confining pressure, especially pressure distribution on the impinging surface;

3.Large-scale structured characteristics that means vortex dynamics mechanism of jet flowfield, covers linear and nonlinear interference action of instability with different time and space scales;

4.Cavitation characteristics that means cavitation noise frequency analysis, covers cavitation process and affecting factors and efficiency analysis.

Among the above aspects, the hydroacoustics in and out of the jet pipe is the most important one.

Suppose that the flow in the jet pipe is mainly uniform and the pressure and velocity perturbations are P' and V', and Mach number M is low, then continuity equation and momentum equation (T.D.Propson Equations) can be solved with separate variables, then we have

$$P' = e^{st}(C_1 e^{rx} + C_2 e^{-rx})$$

$$V' = -\frac{s}{\rho r C^2}(C_1 e^{rx} - C_2 e^{-rx})$$

where the wave propagation factor $r^2 = (s^2 + f_0 \bullet s)/C^2$, the complex wave frequency $s = \sigma + i\omega$. σ is a factor which indicates unstable attenuation with time if it is a negative value and unstable amplification with time if it is a positive value, ω represents the natural frequency of oscillation. Now we introduce the definition of complex acoustic impedance $Z(x)$ and characteristic impedance Z_c, and that

$$Z(x) = \frac{P'(x,t)}{V'(x,t) \bullet S} = e^{i\varphi} \bullet |Z(x)|$$

$$Z_c = \frac{r\rho C^2}{s \bullet S}$$

where $|Z(x)|$ is the acoustic impedance amplitude, φ is the phase lag between velocity and pressure at x.

In general, the pipe consists of a series of pipes having different cross sectional area $S_i (S_i = \sigma_i + i\omega_i)$, length L_i, wave propagation factor r_i, and characteristic impedance Z_{ci}. Suppose the end acoustic impedance $Z(x) = Z_e$ and that

$$Z_i(x_i)\big|_{x_i=0} = Z_{ui} \qquad Z_i(x_i)\big|_{x_i=L_i} = Z_{di}$$

Let $Z_{ui} = 0$, then we have

$$\frac{Z_{c3} \bullet Z_e + Z_{c3}^2 \bullet T_3}{Z_{c3} + Z_e \bullet T_3} + \frac{Z_{c2}^2 \bullet T_2 + Z_{c1} \bullet Z_{c2} \bullet T_1}{Z_{c2} + Z_{c1} \bullet T_1 \bullet T_2} = 0$$

$$T_i = \tanh(r_i L_i)$$

The above characteristic equation can be numerically solved by Newton's iteration method. Suppose the flow in the pipe is forced by an external force $B \bullet e^{i\omega t}$, then the oscillation equation of the forced system can be written as :

$$\frac{\partial^2 V_2(t)}{\partial t^2} + f_0 \bullet \frac{\partial V_2(t)}{\partial t} - C^2 r^2 V_2(t) = Be^{i\omega t}$$

where the ω is the natural frequency of the free system. If $\omega / \sigma >> 1$, Then the amplification of the forced frictionless system compared to the amplification under the condition of neglecting the inertia and friction term in the above equation can be approximately written as

$$A = -\omega / (2\sigma)$$

It should be noticed that ,if the end impedance $Z_d = Z_e = (2\Delta P) / (V \bullet S)$ where the ΔP is the pressure drop across the nozzle, the design model of one step organ pipe nozzle can be easily written as

$$\frac{L}{d} = \frac{K_n}{S_d \bullet M_j}$$

$$K_n = \begin{cases} \frac{n}{2} when M_j (\frac{S}{S_j} - \frac{S_j}{S}) \le 1 \\ \frac{2n+1}{4} when M_j (\frac{S}{S_j} - \frac{S_j}{S}) \ge 1 \end{cases}$$

where jet Mach number $M_i = V_j / C$, Strouhal number $S_d = f \bullet d / V_j$, n is wave number, V_j is jet velocity, S_j is organ pipe exit cross section and S is the pipe cross section.

For the two step organ pipe nozzle, as shown in Fig. 1, and the configuration:

L_2 =40mm, D_2 =12mm, L_1 =20mm, D_1 =24mm, d = 4mm, the numerical results show that there exist two basic modes , the frequency of the first basic mode increases with the increase in jet speed and the frequency of the second one decreases with the increase in jet velocity, as shown in Fig. 2.

The results , as shown in Fig.3 , show that the oscillating pressure and flowrate due to the hydroacoustic effect can be expressed with the fundamental mode waves and their harmonics with different frequencies and damping factors and amplitudes, which is proved by the numerical solution.

Figure 4 (a) and Fig.4 (b) show that both the Strouhal number $S_d = f \bullet d / V_j$ and amplification A decreases with the increase in jet velocity and there exists a preferred jet velocity at whichthe Strouhal number ranges in our interesting domain 0.3 ~ 0. 6. Thus a program is written that can be used to design the organ pipe nozzle. With the index A and S_d , we can evaluate the performance of the nozzle.

3. NUMERICAL ANALYSIS OF JET FLOWFIELD STRUCTURE

Axisymmetric jets have been the focus of numerous analytical, experimental , and numerical studies. In summary, the combination of experimental and theoretical investigations appears to lead to the conclusion that the mechanism for the emergence and reinforcement of the large scale coherent structure in the jet flowfield

should be essentially inviscid and independent of the Reynolds number. Thus we suppose the flow is an inviscid ,incompressible and irrotational flow. The flow pattern of water jet flowfield can be described as the same as that put forward by Chahine, G.L., et al,1984. Then the stream function Ψ and velocity potential Φ can be written as

$$\Psi = -\frac{\Gamma}{2\pi}(r_1 + r_2)[F_1(\lambda_0) - E_1(\lambda_0)]$$

$$\Phi = \frac{1}{2}\Gamma \bullet a \bullet \int_0^{\infty} e^{-kx} \bullet J_0(kr) \bullet J_1(ka)dk$$

where F_1 and E_1 are respectively complete elliptic integrals of the first kind and second kind , and J_0 and J_1 are respectively Bessel function of order 0 and order 1 , and

$$\lambda_0 = \frac{r_2 - r_1}{r_2 + r_1}$$

The self induced translation velocity of vortex ring is given by solving the above problem with the method of matched asymptotic expansions ()

$$V_{self} = \frac{\Gamma}{4\pi R_0}\left\{\frac{\varepsilon}{\overline{A}}[Ln\frac{8\overline{A}}{\varepsilon} - \frac{1}{2} + \frac{W_s^{-1}}{\Omega_s}] + o(\varepsilon)\right\}$$

where the Weber number W_s and circulation parameter Ω_s can be written as:

$$W_s^{-1} = \gamma / (R_0 P_{\infty})$$

$$\Omega_s = \frac{\rho}{P_{\infty}}[\frac{\Gamma}{2\pi R_0}]^2$$

Numerical simulation of the axisymmetric jet flowfield structure is made by replacing the shear layer and the wall surface of the jet pipe with discrete vortex rings, considering the effect of the nozzle configuration on the vortex shedding process. In order to reflect the real flow pattern, the circulation of vortex ring is given by

$$\Gamma(n) = \Gamma_0[1 + \xi\cos(2\pi f t_n)]$$

The computation results , as shown in Fig.5 where ε=0.001, W_s =200, Ω_s =20, show that jet emanating from the nozzle with an elliptic contour and conical exit contour has a well-organized large scale vortex structure.

4. EXPERIMENTAL RESULTS

Data from the measurement of pressure signals by piezoresistive pressure transducers along the center line of the submerged pulsating water jet show that the root mean square of the fluctuation pressure P_{rms} decreases with an increase in dimensionless standoff distance as shown in Fig.6 (a) where $\Delta P = 120 kgf / cm^2$,

$V_j = 128.1m/s$, $d = 4mm$. Fig.6 (b) shows that the peak pressure P_{peak} first increases with increase in the standoff distance and then fluctuates around the value, and decreases with a further increase in the standoff distance.

5. CONCLUSIONS

(1) The computational results show that there exist pressure waves with the Strouhal numbers ranging from 0. 2 to 1. 2, which meet the requirement for tuning the jet shear layer; the steps of organ-pipe is requested less than 2, and the exit diameter of the pipe nozzle is requested less than 10 mm, if the nozzle is mounted on tri-cone roller bit within the limited space.

(2) As for one step pipe nozzle, there is only one basic hydroacoustic wave and the frequencies of other higher mode harmonic waves are integer times of that of basic mode wave, and the amplitude amplification factor of higher modes are greater than that of lower ones; As for two steps nozzle, there exist two basic hydroacoustic waves,the others are harmonic waves,the frequency of the first mode wave increases with the increase of jet speed, but the frequency of the second decreases.

(3) The pulsing pressure and velocity due to the hydroacoustic effect can be expressed with fundamental mode waves and their harmonics with different frequencies and damping factors and amplitudes.

(4) The experimental results of jet cutting rocks and the measurement results of the pulsating pressure signals show that the jet has strong pressure pulsating property and suction pressure, resulting in the cavitation effect and improvement in its cleaning ability.

(5) The computational results show that the jet emanating form the nozzle with an elliptic contour and conical exit contour has a well-organized large scale vortex structure.

6.ACKNOWLEDGEMENTS

This work is supported by the National Science Foundation and National Education Committee Foundation. We are grateful for the helpful comments made by Prof. J.H. Wu in Peking University and wish to express thanks to Prof. X.S. Liu, Prof. Z.F. Xu, Dr. W. Wang for their helpful discussions.

7.NOMENCLATURE

P_{mean}	mean pressure
P_0	nozzle exit pressure
V	mean velocity
P_a	time average pressure
ρ	density
P_{rms}	root mean square pressure
M	Mach number M = V / C
P_{peak}	peak pressure
C	sound velocity
s	complex wave frequency s= σ +i ω
σ	attenuation factor
$Z(x)$	complex acoustic impedance
ω	natural frequency
$\lvert Z(x) \rvert$	acoustic impedance amplitude
Z_c	characteristic impedance
f	frequency of acoustic wave
Z_e	end impedance
J_0	Bessel function of order 0
Ψ	stream function

J_1	Bessel function of order 1
Φ	velocity potential
M_j	jet Mach number $M_j = V_j / C$
W_s	Weber number
S_d	Strouhal number $S_d = f \bullet d / V_j$
Ω_s	circulation parameter
S_j	organ pipe exit cross section area
λ	friction factor
S	pipe cross section area
A	amplification factor
ΔP	pressure drop across the nozzle
n	wave number
V_j	jet velocity
$P^{'}, V^{'}$	pressure and velocity perturbations
ϕ	phase lag between velocity and pressure at x
F_1	complete elliptical integral of the first kind
E_1	complete elliptical integral of the second kind
r	wave propagation factor $r^2 = (s^2 + f_0 \bullet s) / C^2$
V_{self}	self induced translation velocity of vortex ring

8.REFERENCES

1.Shen,Z.H and Wang, Z.M," Theoretical Analysis of a Jet-driven Helmholtz Resonator and Effect of Its Configuration on water Jet Cutting Property",In BHRA Fluid Engineering,Proceedings of 9th International Symposium on Jet Cutting Technology ,Sendai, Japan, PP.189~201,(1988).

2.Shen,Z.H. Li,G.S, Wang, Z.M and Xu, Y.J,"New Jet Theory and prospects of Its Application in Drilling Engineering", Proceedings of the thirteenth World Petroleum Congress, BuenosAires, PP.397~405,(1991).

3.Johnson Jr., V.E. , Conn A.F. , Lindenmuth , W.T., Chahine , G. L., And Frederick , G.S.,"Selt-resonating cavitating Jets ",6th Int. Symp. on Jet Cutting Technology, PP.1~26,(1982).

4.Wylie E.B, Streeter V.L., 《Fluid Transients》 ,McGraw Hill Inc,New York, PP.158~180, (1978).

5.Lamb,M., 《Hydrodynamics》 ,Dover Publications,New York,PP.230~260,(1967).

6.S.C.Crow,F.H.Champagne," Orderly structure in jet turbulence" ,J.Fluid Mech. ,Vol48 , PP.547~591,(1971).

7.P.F.Genoux,G.L.Chanine, "Simulation of the pressure field due to a submerged oscillating jet impinging on a solid wall" , ASME Journal of Fluid Engineering , Vol106,PP.491~497,(1984).

8.P.G.Saffman,"The velocity of viscous vortex rings" studies in applied mathematics, Vol149, PP.371~381,(1970).

9.Seiji Shimizu, Hitoshi Murai, Shigeo Nishi , "ffect of nozzle lip on structure of two-dimensional sub-merged jets" , 10th Int. Symp. on Jet Cutting Technology, paper B3,(1990).

10.Ghoniem,A.F., "Three dimensional vortex simulation with application to axisymmetric shear layer", AIAA paper 87-0379,(1987).

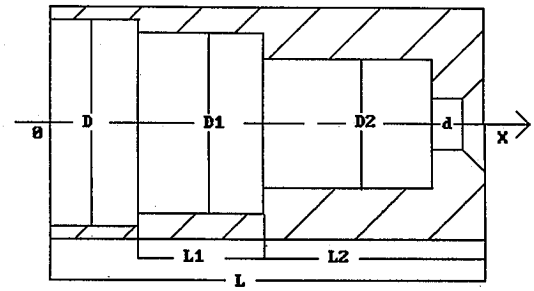

Fig.1 Structure of organ pipe nozzle

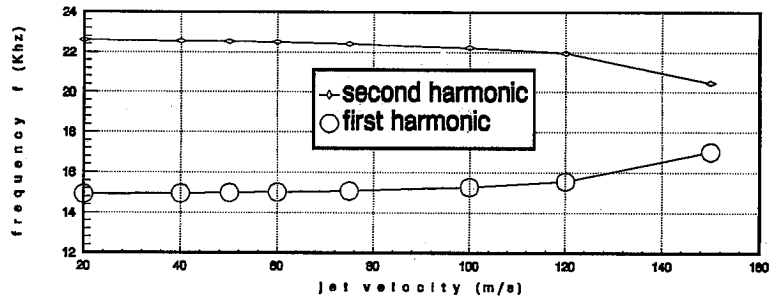

Fig.2 Basic harmonic frequency versus jet velocity

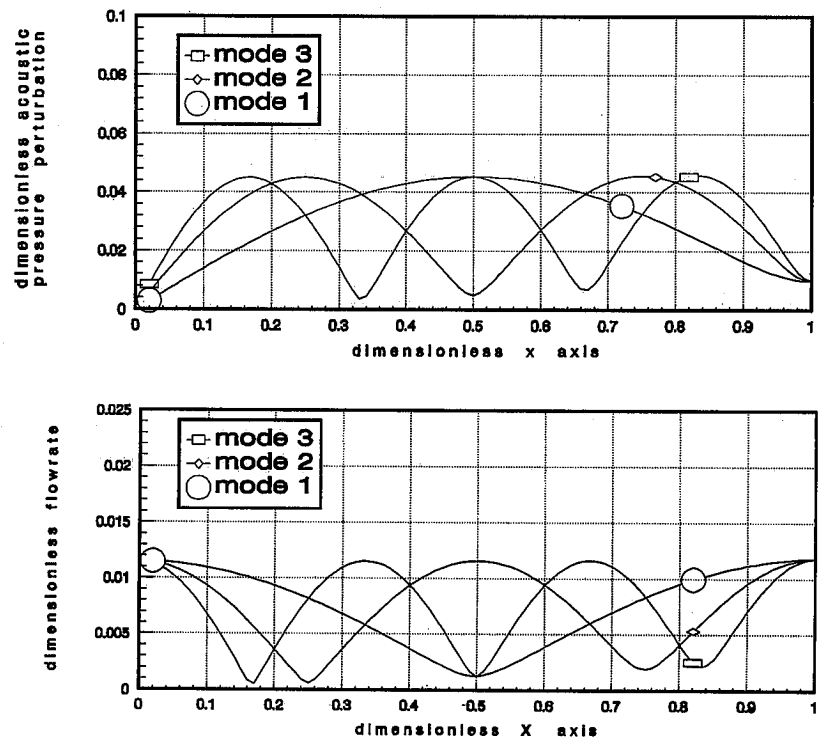

Fig.3 Dimensionless acoustic pressure perturbation or flow rate versus dimensionless X

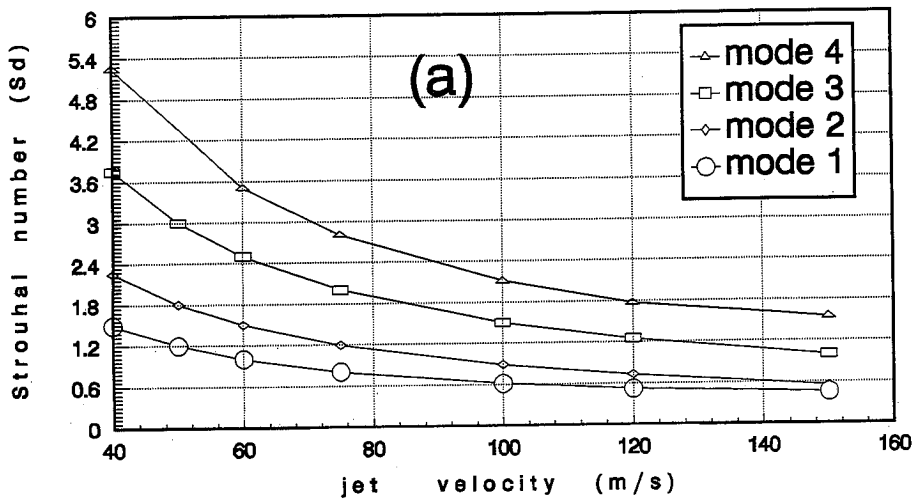

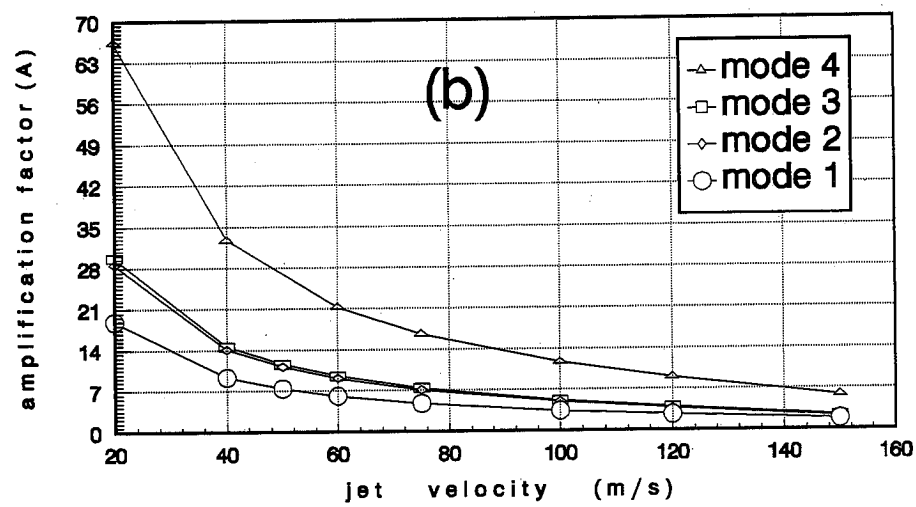

Fig.4 (a) Strouhal number Sd versus jet velocity
(b) Amplification factor A versus jet velocity

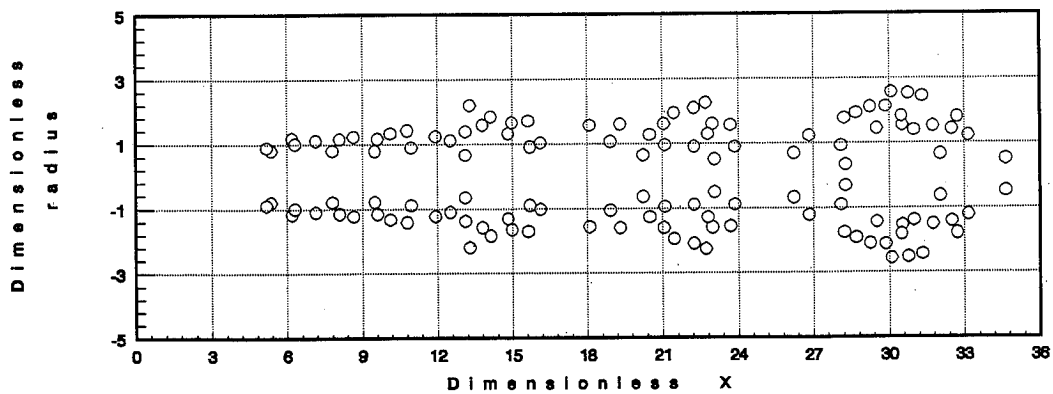

Fig.5 Flow structure of jet flowfield

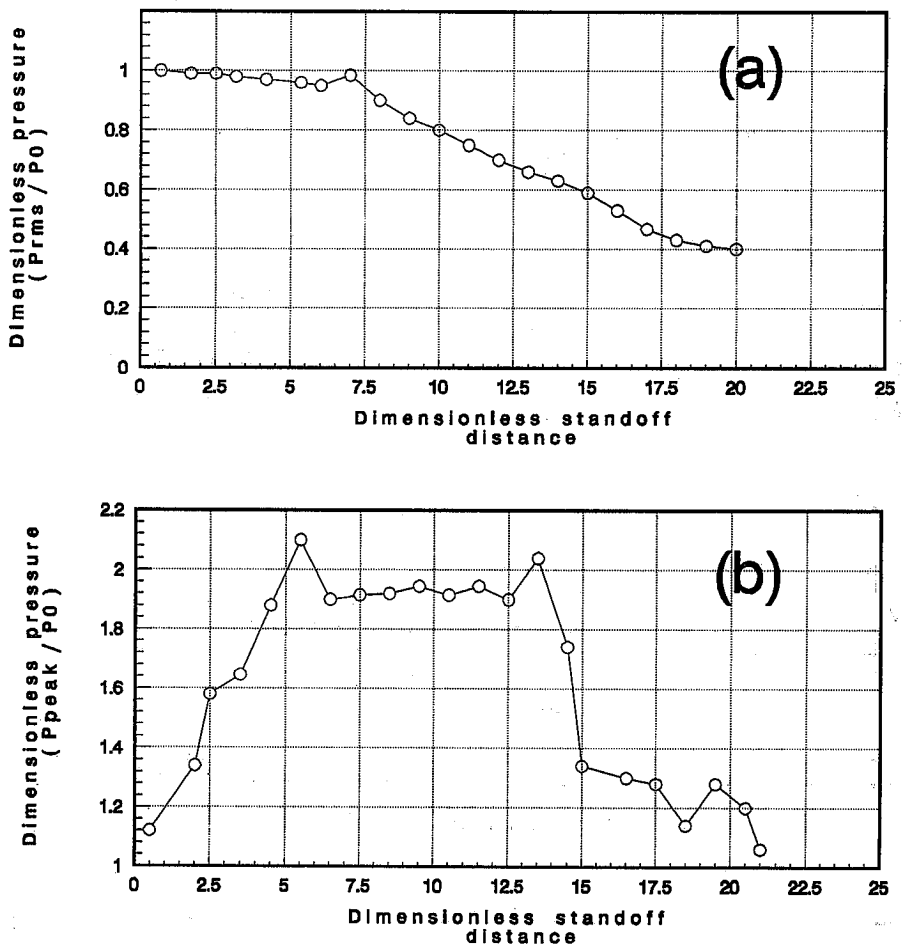

Fig.6 (a)Prms/P0 versus dimensionless standoff distance
(b)Ppeak/P0 versus dimensionless standoff distance

8th American Water Jet Conference
August 26-29, 1995: Houston, Texas

Paper 42

ROCKET PROPELLANT WASHOUT SYSTEM USING A PULSING NOZZLE

M.T. Gracey, B. McMillion
HydroChem Industrial Services, Inc.
Missouri City, Texas U.S.A.

ABSTRACT

A system was designed, built and shipped to a group outside the U.S.A. to remove propellant from rocket motors. A special nozzle technology was used to allow removal of the propellant using lower water jet pressures. The system included a high pressure pump unit, washout mechanism and the auxiliary equipment for capturing the effluent and re-using the water. A remote control console with closed circuit video camera is used to operate the system from a safe location.

Organized and Sponsored by the Water Jet Technology Association.

1. INTRODUCTION

Over three years after the initial contact from an agency outside the USA, a system to wash rocket motors was completed and shipped. The goal of the system design was to incorporate features that would make the system:

* Operate at lower pressures than conventional water jet methods
* Utilize jet velocities well below the levels capable of detonating explosives or propellants
* Provide a "man-in-the-loop" to observe and control the operation
* Integrate automation and simplicity while maintaining safety
* Maintain a flooded mode within the part being cleaned for a safer, more efficient and foam-free process

2. DESCRIPTION OF THE EQUIPMENT

The washout system had some similarities to systems that were developed by Hydronautics to washout artillery shells with the CAVIJET and SERVOJET technology in 1987-88. In 1983, Chahine, Johnson, Conn and Frederick (Reference 1), were developing nozzle technology that included the "SERVOJET" that incorporates a Helmholtz chamber that was tuned to drive an organ-pipe interruption of a water jet. The special nozzle technology enabled the systems designed and built by Hydronautics to remove explosives from obsolete or outdated munitions while providing a safer, more efficient operation. In reference 2, Conn describes an automated explosive removal system using cavitating water jets.

Figure 1 shows the system to washout the rocket motors that could range in size from .5 meters in diameter by 4 meters long to 1 meter in diameter by 6 meters long. The complete system includes:

* Washout Cradle and Lance Machine
* High pressure pump unit
* Control console
* Catch Tank
* Filter Tank
* Make-up water Tank
* Water Chiller
* Filter Transfer Pump
* Filter Tank Pump

3. SPECIAL NOZZLE TECHNOLOGY

The nozzle technology used in the Rocket Washout System is part of the CAVIJET, SERVOJET and STRATOJET family. The CAVIJET is one of the few successful attempts to harness the destructive power of cavitation. Gracey and Conn discuss the use of cavitation erosion for material testing in Reference 3. The basic concept of the nozzle is to induce the

growth of vapor-filled cavities within a relatively low velocity liquid jet. These cavities can be directed to violently collapse on or near the surface of solid materials to produce very small, but extremely high localized stresses. At the same pump pressure and flow, these cavitating fluid jets have a great advantage over a steady non-cavitating jet for removing hard substances and for cutting hard material. The SERVOJET, on the other hand, produces an interrupted or pulsed jet that enhances the rate of cleaning or cutting. Another advancement in the family of cavitating nozzles was the STRATOJET that is basically a SERVOJET that operates underwater (developed for down-hole oil drilling operations). The "self resonating" STRATOJET has proven to be substantially more erosive in applications which involve submerged cleaning or cutting, so it was chosen for the Rocket Propellant Washout System as described in this paper. Figure 2 shows the nozzle used in the system because the pulsing nozzle improves the remove rate because of the following mechanisms:

* Larger impact stresses, due to the water-hammer pressure which increases local erosive intensity.
* Larger outflow velocities across the surface being cut or cleaned which provides an added tendency to open cracks and flaws in the material being washed-out,
* Greater ratio of impacted area to volume of jetted water which exposes larger areas of the surface to the water-hammer pressure,
* Cycling or loading which promotes unloading stresses to enhance the process of de-bonding the propellant,
* Short duration loadings which tend to minimize energy losses within the substrate and the material being cut, improving the material removal per energy input.

4. WATER RECOVERY AND PROCESSING

The effluent from the washout process must be collected and processed by the owner/agency. Figure 3 shows the flow diagram for the water recovery system. In order to reduce water consumption, and to separate as much of the solid material from the water, a system was designed to catch the main bulk of the material, then circulate the water through a filter tank and a bank of filters before entering the water storage tank. There is also a final filter before the water is re-used by the high pressure pump for subsequent washout operations, indicating the water recovery and processing loop.

Other features of the system include a water chiller that is used to remove the heat of the blast water before it is returned to the supply tank. It has a certified capacity of 50 USGPM of water from 96 degree F to 86 degree F entering wet bulb by using a fan motor of 1 horsepower. Air powered diaphragm pumps are used to move the blast water and effluent through the process because of their ability to run dry and to handle large particles along with the water. A supply tank with a float valve is used to store water for use by the high pressure pump while allowing make-up water to enter the system to replace any lost water.

5. SYSTEM OPERATIONAL PROCEDURE

The rocket motor to be cleaned is placed into the cradle shown in Figure 1 for cleaning and the operator is located in a separate room with the control console shown in Figure 4. System start-up procedure is followed to bring the water recovery on-line and to start the high pressure pump which includes manually opening valves and starting the air powered pumps. The high pressure pump unit is shown in Figure 5. Limit switches on the wash-out lance travel are preset for the size of the work. From the Control Console, the operator can operate the following features:

* Air Compressor
* Catch Tank Pump
* Water Chiller
* Water Supply pump
* Observation camera
* High pressure pump
* Nozzle rotation
* Lance extension & retraction
* Pressure up & pressure down

A cleaning cycle includes starting the system and operating the joystick to feed the rotating lance into the work and reversing the lance travel when the indicator light shows that maximum travel has been achieved. The closed circuit camera is located inside the cleaning room while the operator and the monitor are located in a remote location.

6. CONCLUSIONS

A system such as the Rocket Propellant Washout System is a new way of using much of the water jet technology that already exists. The special nozzle technology has been used on a limited basis for specialized system with great success; the water recovery components have been used in various combinations to control effluent discharge and product recovery; and the high pressure pump of this flow & pressure range, is the heart of the wash-out system. The design of the cradle for holding the work and the integration of the existing technology is where the special engineering becomes necessary.

7. ACKNOWLEDGMENTS

The authors want to thank the employees of HydroChem Industrial Services, Inc. that helped design and build the Rocket Washout System. A special thanks to the management of the newly formed HydroChem group for their understanding of our customer's unique requirements.

8. REFERENCES

1. Georges L. Chahine, Virgil E. Johnson, Jr., Andrew F. Conn, Gary S. Frederick, "Cleaning And Cutting With Self-Resonating Pulsed Water Jets," 2nd U.S. Water Jet Conference, Rolla, Missouri, 1983.

2. Andrew F. Conn, "An Automated Explosive Removal System Using Cavitating Water Jets," 22nd DOD Explosives Safety Seminar, Anaheim, California, 1986.

3. Michael T. Gracey and Andrew F. Conn, "Cavitation Erosion Used For Material Testing," 7th International Conference on Erosion by Liquid and Solid Impact (ELSE VII), Cambridge, England, 1987.

Equipment Layout

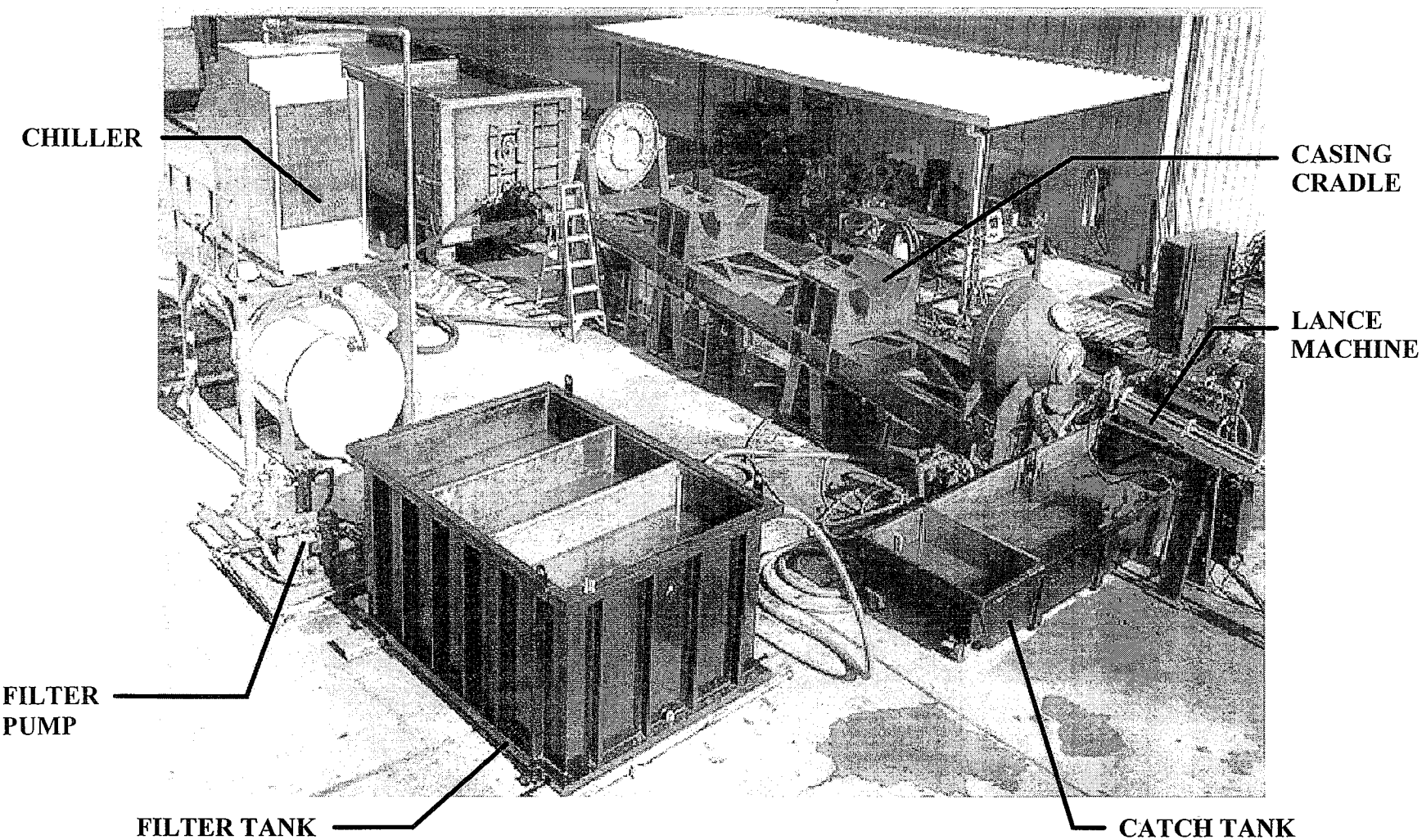

Figure 1

Cavijet Nozzle Assembly

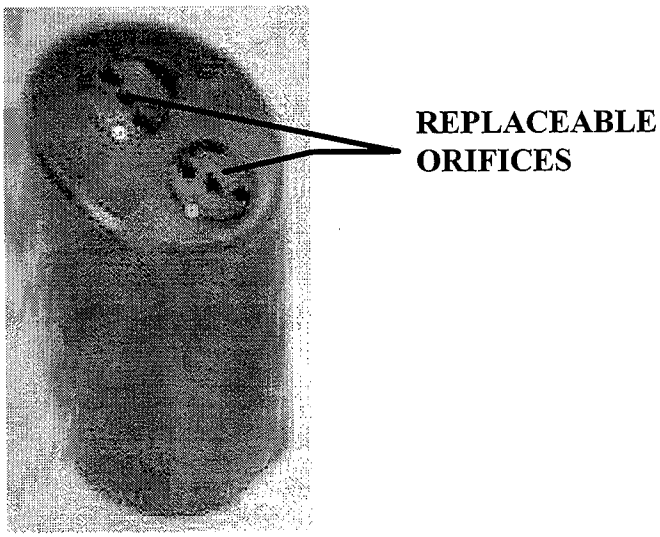

Figure 2

Flow Diagram-Tube Wash System

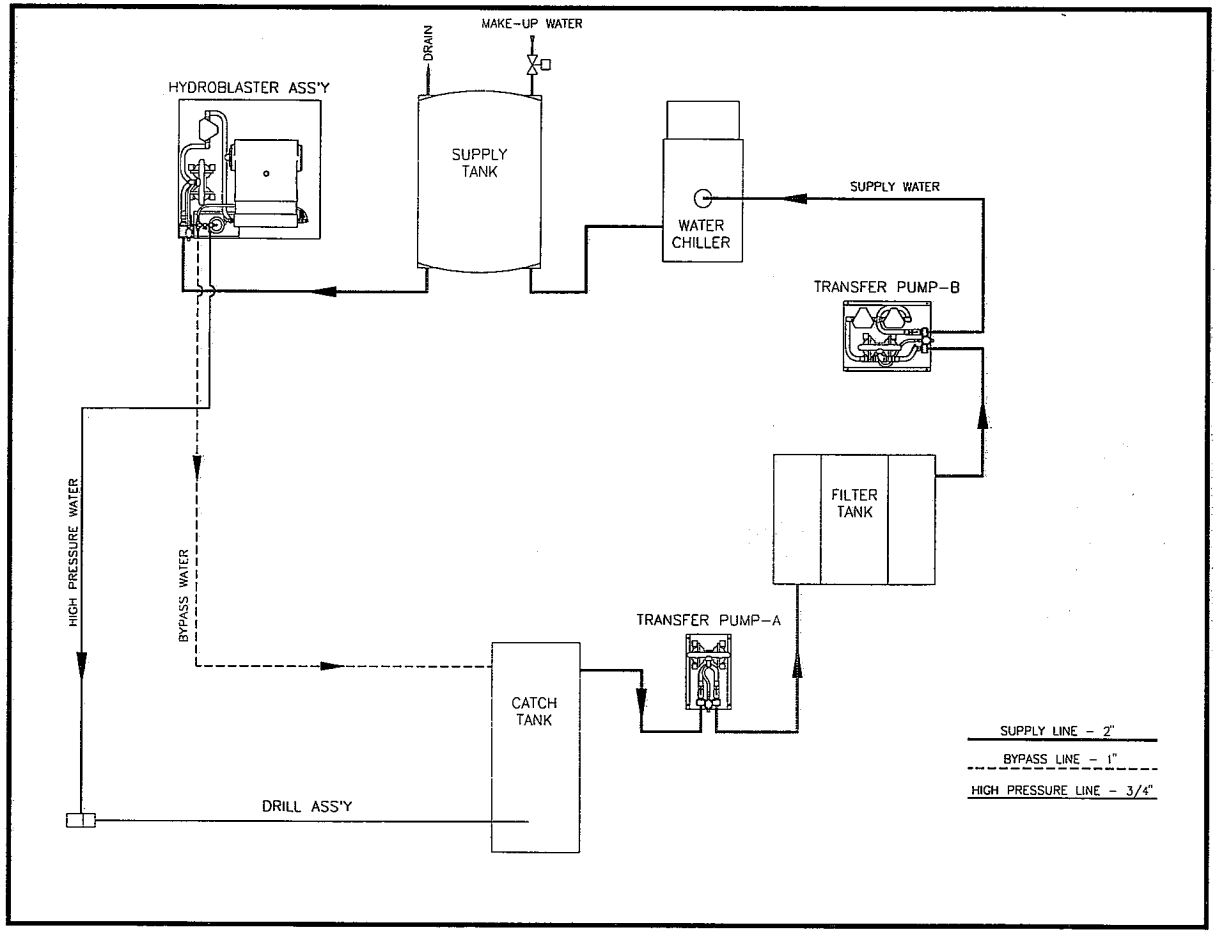

Figure 3

600

Control Console

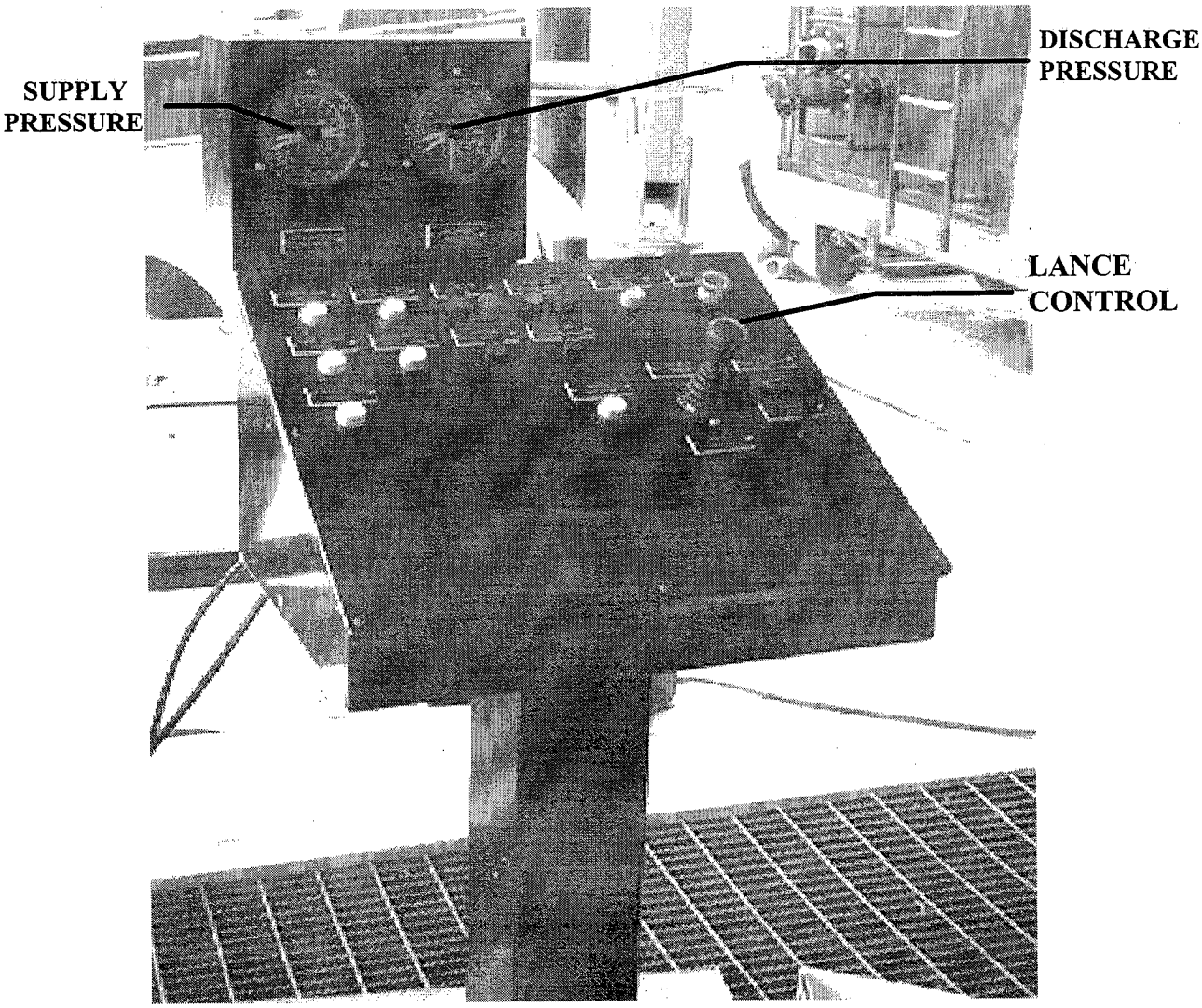

Figure 4

Pump Assembly

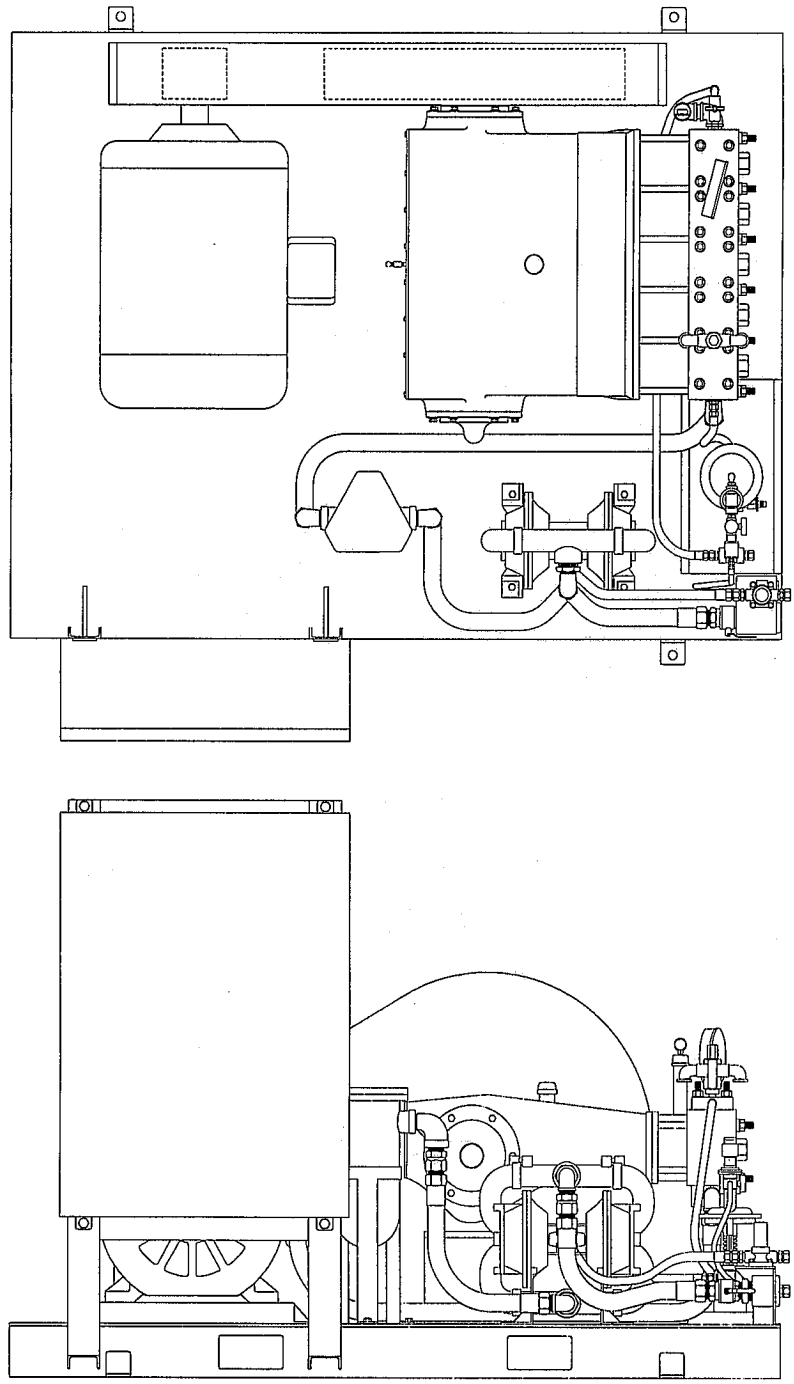

Figure 5

8th American Water Jet Conference
August 26-29, 1995: Houston, Texas

Paper 43

THE DEVELOPMENT OF A PORTABLE WOMBAT FACILITY

R.D. Fossey, D.A. Summers
University of Missouri, Rolla, Missouri

P. Kalim, U. Nejib
Wilkes University, Wilkes Barre, Pennsylvania

Abstract

The development of a high pressure waterjet system for the removal of explosives and energetic materials from ordnance has over the years, led to the development of a waterjet system known as the WOMBAT. Until recently this system has been located at the underground test facility at the University of Missouri, Rolla.

Working with the faculty of Wilkes University, the UMR team have developed a new generation unit which is transportable and capable of being moved from depot to depot to allow demilitarization of small to large quantities of ammunition and projectiles as well as other energetic materials on site. Some flexibility of design is required to accomplish this, and those features will be discussed.

Initial designs for a handling system for the projectiles which will allow a throughput rate of one projectile per minute will also be discussed.

Organized and Sponsored by the Water Jet Technology Association.

1. INTRODUCTION

Thousands of tons of excess munitions are currently stored in military magazines throughout the United States and, indeed, around the world. Many of these have been stored since the 1960,s and are no longer considered viable for their intended use. Previous designs of demilitarization facilities have been mainly stationary with the munitions to be cleaned transported to the facility. With the danger of transporting large quantities of energetic materials in mind, a safe, effective method of demilitarizing these munitions is needed and has been developed at the University of Missouri-Rolla.

2. BACKGROUND

In 1982 the first generation of WOMBAT (Waterjet Ordnance and Munition Blastcleaner with Automated Tellurometry) **Figure 1**, was developed at UMR under the auspices of the Naval Weapons Support Center at Crane, Indiana. This system was proven a safe, effective means of removing a variety of energetic materials from a variety of munition geometries in a remotely controlled facility located in the UMR underground research facility at UMR's Experimental Mine. **Figure 2**.

The initial WOMBAT was designed primarily for the removal of PBXN 4, a relatively soft explosive, from Sparrow air-to-air missile warheads, which have a cylindrical donut shaped casing with a fusing tube running the entire length of the casing in the center **Figure 3**. This system was tested on sixteen different explosives and numerous casing geometries with great success. More recently, rocket motor and gun propellants have been targeted with waterjets in this facility with similar results. Some of the explosives tested required a pressure in excess of 23,000 psi. for efficient removal. It should be noted that this WOMBAT was designed and built specifically as a research tool and not as a production facility. The rate of demilitarization of munitions was constrained by handling of the casing and the energetic material after washout. For a production facility to be effective, a system was needed that could rapidly and continuously remove energetics from casings with safety the uppermost consideration.

3. APPROACH

Safety has continued to be the foremost design criteria for this program at UMR with efficiency and effectiveness close behind. Thus it was determined that transport of a washout system would create less of a hazard to surrounding populations and environments than the transport of live munitions. For efficiency of transport, set-up and operation a modular design was conceived. For effectiveness of cleanout a variable pressure and flow system was incorporated as was a series of sequential washout stations. **Figure 4**.

The safest aspects of the original WOMBAT were retained in the new design. Among these were the obvious, such as the use of waterjets to cut out explosives in the first place and the use of robotics and remote controls for removal of personnel from the immediate area while

jetting is ongoing. Not so obvious, possibly, but of equal importance, is determining the factor of safety from effective cutting pressures to those pressures that can initiate reactions in the target explosive, and explosion-proofing of all electrical and mechanical components as well as using hydraulic or pneumatic power whenever possible.

One of the most advantageous aspects of the original WOMBAT was that it could do a variety of things. It had four degrees of freedom designed into the robotics for precise movement in the three orthogonal directions and controlled rotation of the cutting head at the same time, **Figure 5**. This concept was extremely effective for research, and was very successful for that purpose. Problematic to that design, however, was the need to vary nozzle configurations for sequential cleaning tasks. This was identified as a bottleneck to any production facility as all operations must stop and a partially cleaned shell must be either worked around (a risk to the operators) or removed from the washout station and returned to a safe storage area during the nozzle changeover. The constant stopping and starting of the operation destroys any hope of efficiency as does increased or extended manipulation of the munition. Manipulation of a warhead casing that contains energetic materials should be slow and precise which extends the time taken for a complete cleanout. This problem will be addressed later in the paper.

The solution to the sequential washout was determined to be multiple stations with each having different objectives in the cleaning process. The first station was, in effect, a drilling station that would remove a core from the length of the munition, thereby creating a path for the entrance of the reaming head in the second station that would remove the remainder of the material, **Figure 6**.

The effectiveness of the process continues to be judged by the cleanliness of the washed out casings, **Figure 7**, and the control of the size of solids that are removed from the casing during washout. The incorporation of knowledge obtained from a testing device developed at UMR and known as PETE (Parameter Evaluation Test Equipment) which determines pressure, flow and traverse rate efficiencies on any materials to be cut with a waterjet can be pre-programmed into the new WOMBAT for particulate size control. The importance of sizing is that the washed out material must be recycled for the entire process to be successful, **Figure 8**.

4. DESIGN

A modular approach was taken to the design for a number of reasons. Transportation of the system necessitates that it either be very small, compact, and lightweight or that it can be disassembled for transport, **Figure 4**. It is anticipated that the system will be used in more than one location and that rapid take-down and set-up will be a necessity. The design, then, incorporates this concept and creates a modular system consisting of loading/unloading of shells, shell manipulation, washout, solids manipulation, fluids recycling, and controls, **Figure 10**.

The shell loading/unloading module consists of an x-y table that positions a pallet of shells, a gripper that lifts the shells and transitions them to the proper attitude for the shell manipulator to move them to the washout stations. The shell manipulation module consists of an overhead monorail that is constantly powered with the drives isolated from the environment and a "power and free" drive system.

A series of trolleys that each hold a shell is independently moved or stopped by the monorail drive at precise, predetermined locations for the continuous operation of the washout stations. The washout module consists of two 300 hp diesel driven pumps, supply lines and independent coring and reaming washout stations. The solids manipulation module consists of a gravity collection station, a fluid removal filter, and a solids storage container. The fluids recycling module, **Figure 9**, consists of a hydro-cyclone, course and fine filters, a charcoal bed, and a reverse osmosis chamber as well as storage tanks and pumps for fluid movement.

The controls module, which is the brains of the whole operation, consists of a single driving computer, a series of PLCs and various solenoids, gauges, and valves. It monitors and controls all operations within the entire system and verifies that each of the other modules is performing to specification. The main computer ensures maximum efficiency of coordination between modules to prevent any untoward delays and assure overall production. Concurrently, an interactive training CD is being prepared for ease of integration of the system into normal operational parameters of a military station. It is not UMR's intent to operate the system once installed, but to turn the technology over to either industry or the military.

5. CONCLUSIONS

Major General Dennis L.Benchoff, Commanding general of U.S. Industrial Operations Command has repeatedly stated that there is "One Billion Dollars" available for demilitarizing excess munitions in the United States alone. There is a continuing need to rid our environment of the millions of pounds of stored munitions and waterjets are a safe and effective means. The incorporation of tried and true techniques with state of the art control and communication can effectively remediate this problem. The use of a wholly automated, waterjet de-militarization facility can and will be a solution that is safe to both people and the environment and is economically more advantageous than simply storing ever growing stockpiles of warheads, bombs, and shells.

6. REFERENCES

Benchoff, D.L., Keynote address *Global Demilitarization Symposium*, American Defense Preparedness Association, St. Louis, Missouri, May, 1995.

Blaine, J.G., Fossey, R.D., Summers, D.A., and Tyler, L.J., "Considerations in the Design of a Waterjet Device for Reclamation of Missile Casings," *Proceedings of the Fourth U. S. Waterjet Conference*, pp 51 - 56 Berkley, California, 1987.

Fossey, R.D., Summers, D.A., Short, J., and Craig, L., "Son of Wombat- Lessons learned in the Development of an Automated Explosives Removal System," *Proceedings of the 10th International Symposium on Jet Cutting Technology*, pp 479-485, Amsterdam, The Netherlands, 1990

Fossey, R.D., Summers, D.A., Tyler, L.J., Craig, L., and Short, J., "WOMBAT, A Waterjet Ordnance and Munitions Blastcleaner with Automated Tellurometry," *Proceedings for the Joint International Symposium of Compatibility of Plastics and Other Materials with Explosives, Propellants, Pyroterchnics and Processing of Explosives, Propellants and Ingredients,* American Defense Preparedness Association, New Orleans, Louisiana, 1988.

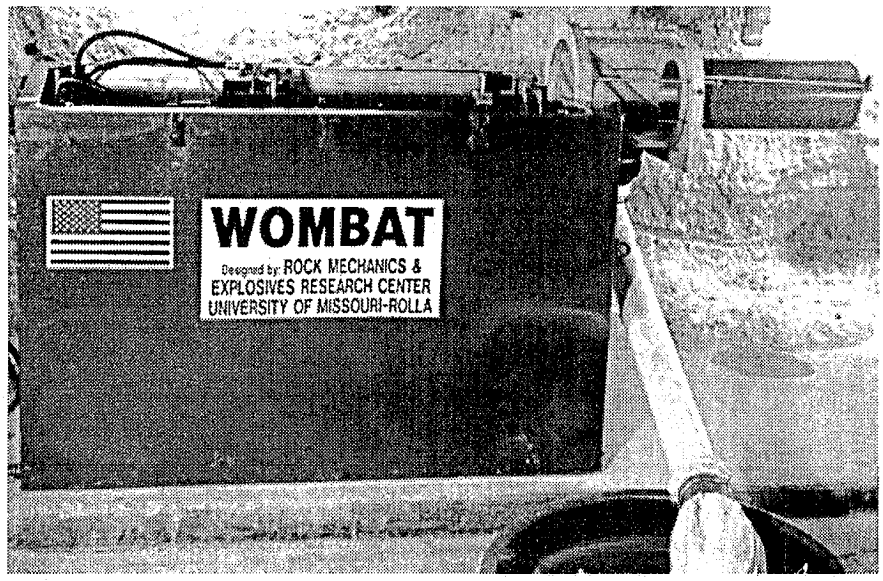

Figure 1. Vintage Wombat

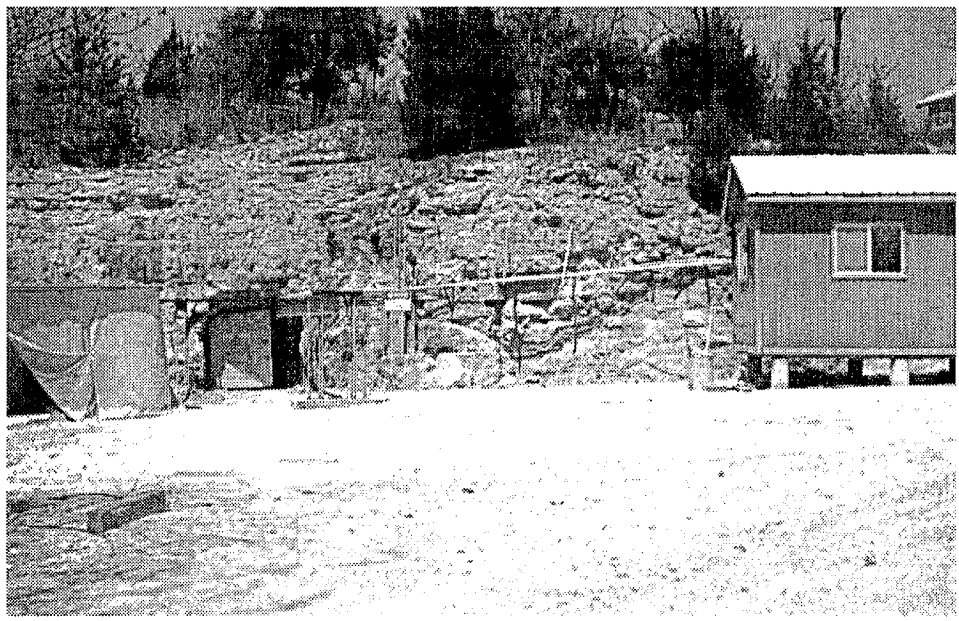

Figure 2. Underground Test facility

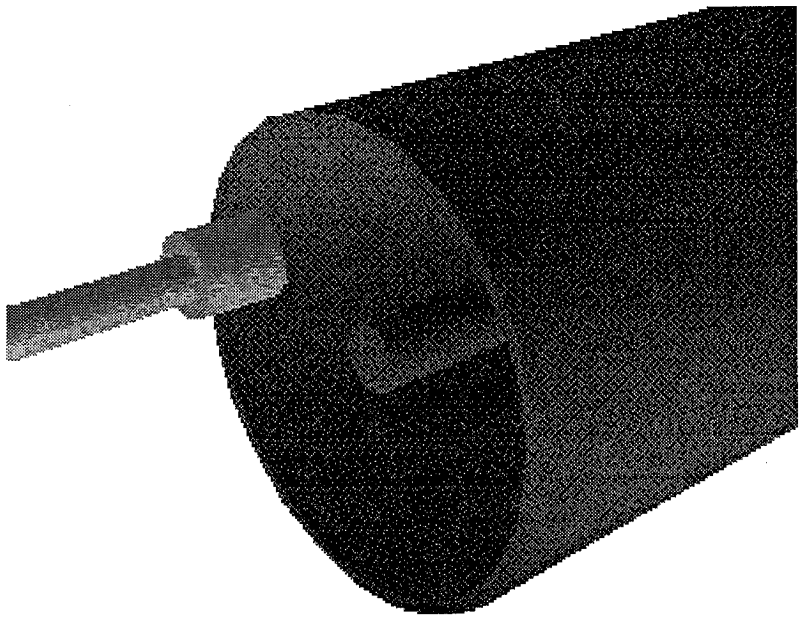

Figure 3. Lance with Sparrow

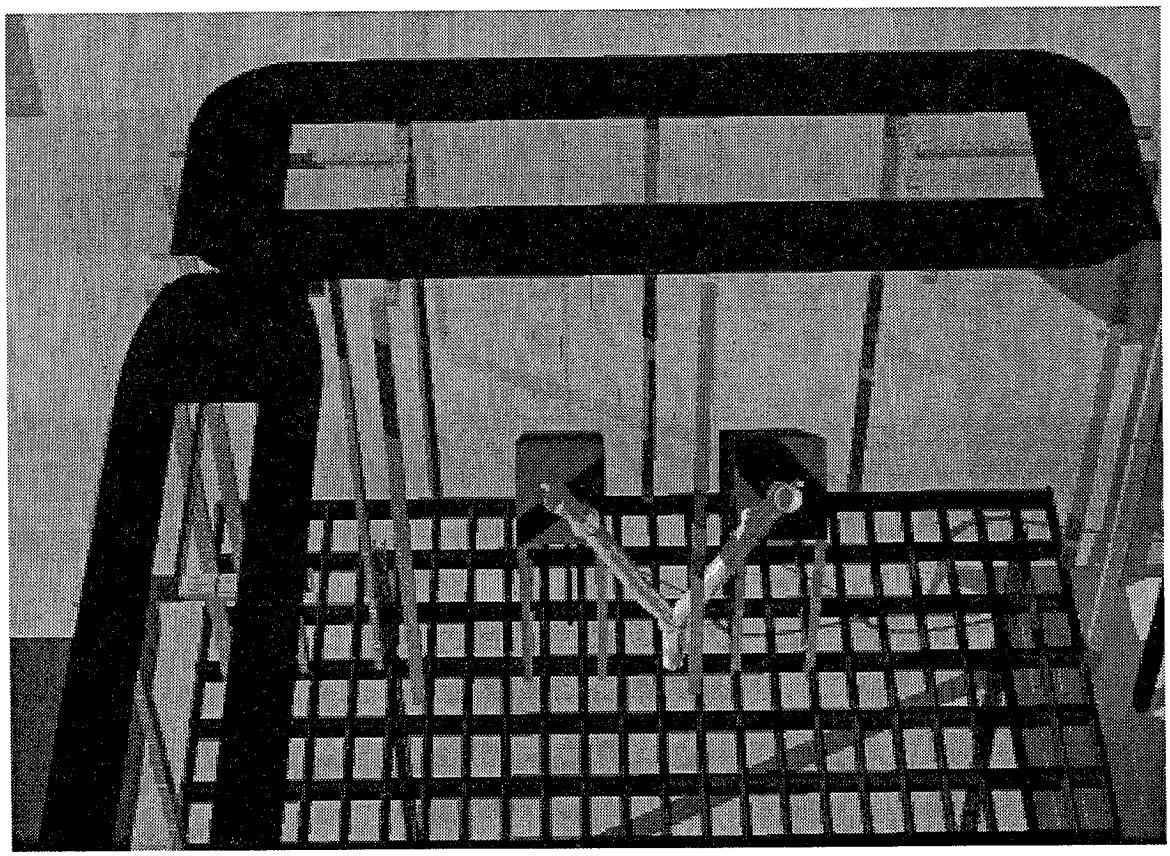

Figure 4. Sequential Washout Stations with "Power and Free" Shell Transport

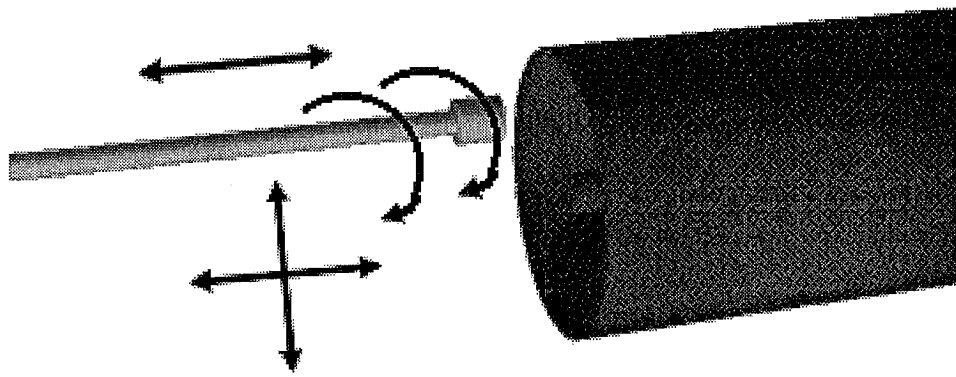

Figure 5. Degrees of Freedom

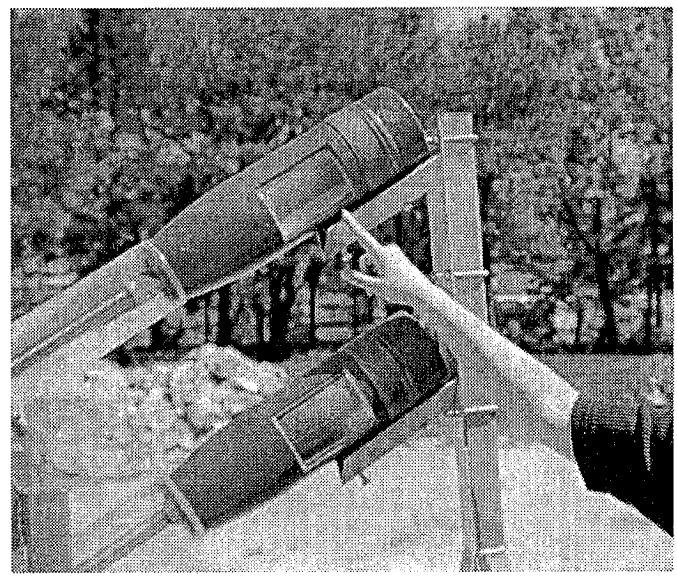

Figure 6. Dual Stations for Cutting and Reaming.

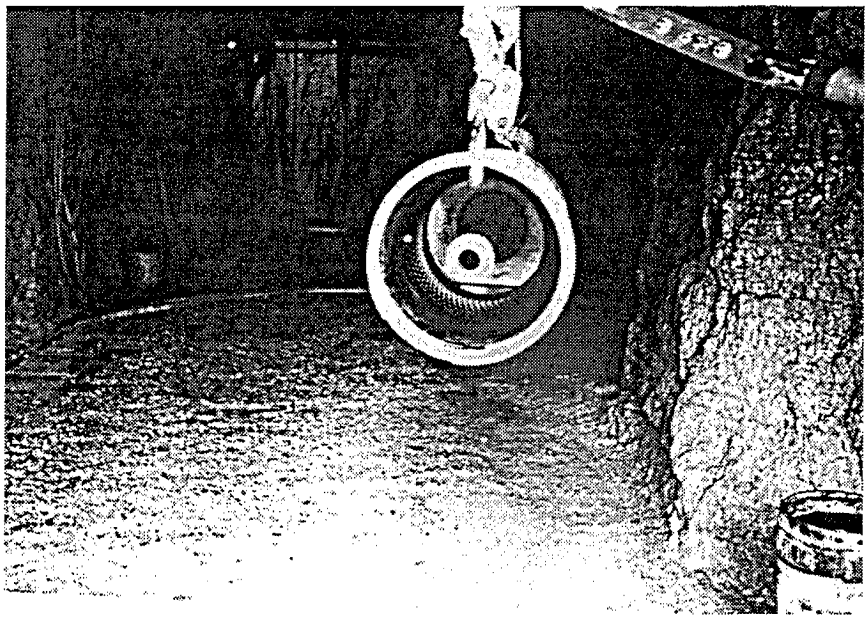

Figure 7. Sparrow Casing Cleaned

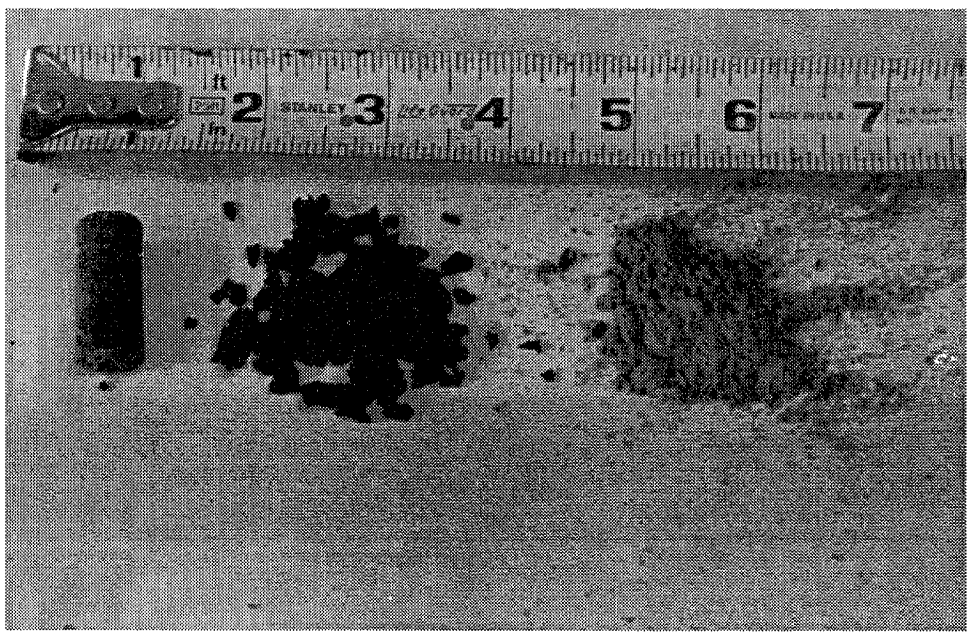

Figure 8. Particle Size

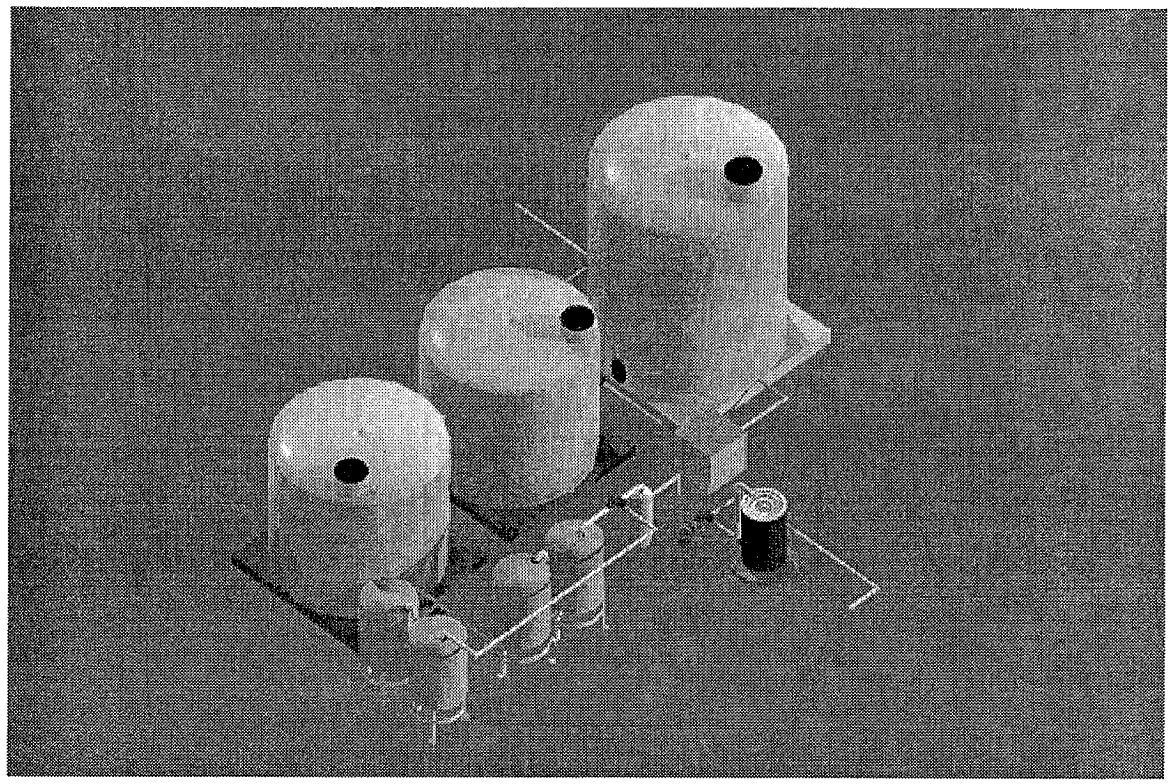

Figure 9. Water Recycling Module

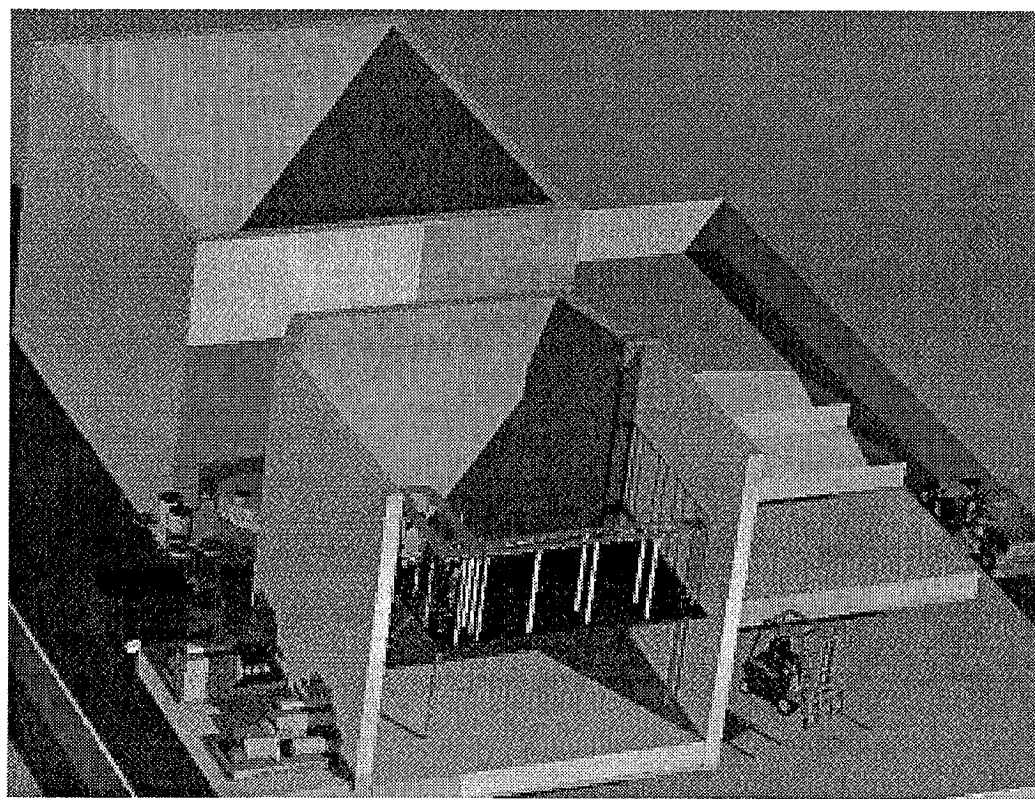

Figure 10. Overall Layout

8th American Water Jet Conference
August 26-29, 1995: Houston, Texas

Paper 44

THERMAL COATING REMOVAL SYSTEM

Darrell Rainey and Greg Reece
Crane Army Ammunition Activity
Crane, Indiana, U.S.A.

ABSTRACT

The thermal protective coating on a large number of U.S. Navy general purpose air-dropped bombs has become defective over the years, developing loose spots and bubbles within the coating. This coating, which contains asbestos, must be removed, and the bombs repainted in order for them to remain in service. Historically, this removal process has been executed using air-driven chisels and wire-wheel brushes. This is an extremely undesirable operation because of the stresses imposed on the operators, as well as the exposure to airborne asbestos fibers. This is also a terribly slow process, requiring up to 60 minutes per bomb.

Crane Army Ammunition Activity is developing a thermal coating removal system, utilizing ultra-high pressure water. The goal is to create a system for performing the coating removal in a more economical manner than the manual method, while reducing health and ergonomic hazards to the operators.

Organized and Sponsored by the Water Jet Technology Association.

1. INTRODUCTION

The purpose of this report is to provide an update (as of May 22, 1995) of work being performed at Crane Army Ammunition Activity (CAAA), evaluating the use of high pressure water for the removal of thermal protective coating from U.S. Navy bombs.

This project has been under consideration at CAAA since January, 1994. At this time we tried blasting an inert bomb skin using a hand-held cleaning wand and waterjet system which CAAA had recently purchased. Although using the wand was cumbersome, the results were encouraging and the idea was planted in our heads. Up to this time the thermal coating had been removed manually with air-driven chisels and wire wheels. Not only was this back breaking work, but it was necessary to do it in protective equipment, including respirators, since the coating contains asbestos fibers.

2. DESCRIPTION OF COATING

The coating is an ablative, thermal insulation which is applied by spraying to Navy explosive ordnance items. The purpose of the coating is to provide protection for the ordnance item from high thermal flux, as would be the case in a ship-board fire. Some of the physical properties of the coating are as follows:

- Ultimate Strength: 35 KG/CM^2 (500 PSI)
- Hardness: 55 Shore D
- Impact Resistance: 18 J (160 IN-LB)
- Application Thickness: 3.175-6.350 MM (0.125-0.250 IN)

3. TESTING

3.1 Testing To Date

On February 28, 1995 CAAA sponsored a demonstration by a commercial waterjet service contractor of their waterjet cleaning capabilities. The purpose was to evaluate an ultra-high pressure, high flow rate pump, using a variety of cleaning heads, for the removal of thermal coating from MK 82 bombs. The testing was attended by representatives from CAAA; Naval Surface Warfare Center, Crane Division; Tooele Army Depot; the University of Missouri - Rolla; and the contractor.

The contractor provided a diesel-driven water jet unit capable of pressures of 276 MPa (40,000 PSI) and 22.7 L/MIN (6 GPM). The contractor also provided several different cleaning heads with a variety of nozzle/orifice installations, as well as their experience and expertise in the waterjet cleaning area. CAAA provided the facility, empty MK 82 thermal coated bombs, waterjet cleaning heads, and a 6-axis robotic arm.

Tests were run with pressures ranging from 241-269 MPa (35-39 KSI) and flow rates from 15.1-20.8 L/MIN (4-5.5 GPM). Results were most favorable when using CAAA's 4 and 8 jet cleaning heads at 20.8 L/MIN (5.5 GPM). Using the 4-jet head sized with 0.305 MM (0.012 IN) orifices, total cleaning time for a bomb (11,730 CM^2 or 1,818 IN^2) was 17.6 minutes. This translates to a coating removal rate of approximately 11.0 CM^2/SEC (1.7 IN^2/SEC). Using CAAA's 8-jet head, a coating removal rate of 17.7 CM^2/SEC (2.75 IN^2/SEC) was attained. We were not able to run an entire bomb using our 8-jet head because of saphire problems. However, extrapolating the removal rate we experienced on the portion of the bomb that we cleaned, the total time would have been in the 11 minute range.

Beginning April 27, 1995 CAAA performed thermal coating removal trials using our waterjet system. This piece of equipment is rated at 276 MPa (40,000 PSI), maximum and 7.6 L/MIN (2 GPM) maximum. As in the earlier tests, the six-axis robotic arm was used to guide the waterjet cleaning head and maintain a constant standoff. Results showed that, predictably, there was a marked lag in performance when compared to the contractor's larger system.

To date, 28 trials have been conducted by CAAA, using our system. The highest effective coating removal rate we have been able to attain is 13.5 CM^2/SEC (2.1 IN^2/SEC) at 241 MPa (35,000 PSI). This was using a circular 5-jet head with 0.356 MM (0.014 IN) orifices in three stations, and the remaining two stations plugged.

Using the same 5-jet head, plumbed with five).254 MM (0.010 IN) orifices, we were able to attain a removal rate of 16.1 CM^2/SEC (2.5 IN^2/SEC). However, at this rate, residual "swirls" of the coating matrix remained over approximately five percent of the bomb surface area. In future trials, we will try the same nozzle setup, but adjust the head rotation speed in order to alleviate this swirling effect.

Our trials showed that the optimum jet angle for removal of this particular coating is approximately 12 degrees (measured from the longitudinal axis of the cleaning head). At larger angles, the energy loss is sufficient to cause incomplete coating removal. At angles closer to perpendicular with the coating, cleaning path width is sacrificed.

3.2 Future Testing

During late May and early July, 1995 CAAA will finish development of our waterjet system for a late summer run of 1,800 bombs. The system utilizes a six-axis robotic arm, on which the waterjet cleaning head and spinner drive are mounted. The bombs are transported on hangers attached to an overhead monorail. As they move through a ventilation booth, the robotic arm directs the waterjet for removal of the thermal coating. The water and removed coating are captured in the booth catch pan and air filtration system. The water is cleaned by means of a filtration system and reused in the waterjet. Previous testing done by the Concurrent Technologies Corporation had shown that flash rusting of the steel bomb bodies could be extreme. Therefore CAAA tested both sodium nitrite and benzoic acid on the bomb skins in a high humidity environment. Our trials showed that a 0.1-0.2% sodium nitrite solution was very effective in inhibiting corrosion on the substrate. Plans are to utilize this inhibitor during production runs.

The waste sludge and filters can be sealed in plastic bags and disposed of at an industrial landfill. As the bombs exit the paint booth, they are dried automatically using an air knife and continue along the monorail to the paint line. Here the bombs pass through priming and painting booths, where they receive a new finish coat.

4. CONCLUSION

The use of ultra-high pressure waterjets has proven to be effective in removing bomb thermal coating. CAAA's thermal coating removal system allows for the processing of a bomb in 25% of the time required by the previous, manual method. When development of the system is finished, the result will be an efficient, non-hazardous process for repairing defective bombs.

5. ACKNOWLEDGEMENTS

The authors wish to express their appreciation for the following people and organizations, who have been extremely helpful: Dr. David Summers of the University of Missouri-Rolla; Concurrent Technologies Corporation; and Hydro-Innovations.

8th American Water Jet Conference
August 26-29, 1995: Houston, Texas

Paper 45

HAZARDOUS WASTE RETRIEVAL STRATEGIES USING A HIGH PRESSURE WATER JET SCARIFIER

B. K. Hatchell, M. W. Rinker
Pacific Northwest Laboratory
Operated by Battelle Memorial Institute
Richland, Washington, U.S.A.

O. D. Mullen
Westinghouse Hanford Company
Richland, Washington, U.S.A.

ABSTRACT

The Waste Dislodging and Conveyance Program is sponsored by the U.S. Department of Energy Office of Technology Development to investigate waste dislodging and conveyance processes suitable for the retrieval of high-level radioactive waste. This program, represented by industry, national laboratories, and academia, has proposed a baseline technology of high-pressure water jet dislodging and pneumatic conveyance integrated as a scarifier as a means of retrieval of waste inside Hanford single-shell tanks. A testing program has been initiated to investigate system deployment techniques to determine appropriate mining strategies, level of control, sensor requirements, and address integration issues associated with deploying the scarifier by a long robotic manipulator arm. A test facility denoted the Hydraulics Testbed (HTB) is being constructed to achieve these objectives and to allow longer-duration, multiple-pass tests on large waste fields using a versatile gantry-style manipulator. Mining strategy tests with materials simulating salt cake and sludge waste forms will be conducted to evaluate the effectiveness of mining strategies, forces related to scarifier and conveyance line, and retrieval rate. This paper will describe the testbed facility and testing program and present initial test results to date.

Organized and Sponsored by the Water Jet Technology Association.

1. INTRODUCTION

The Waste Dislodging and Conveyance Program is sponsored by the U.S. Department of Energy Office of Technology Development to investigate waste dislodging and conveyance processes suitable for the retrieval of high-level radioactive waste. This program, represented by industry, national laboratories, and academia, has proposed a baseline technology of high-pressure water jet dislodging and pneumatic conveyance integrated as a scarifier as a means of retrieval of waste inside Hanford single-shell tanks (Rinker et al., 1994). Waste simulants have been developed to challenge the retrieval process, and this technology has been shown to mobilize and convey the waste simulants at desired retrieval rates while operating within the space envelope and the dynamic loading constraints of the proposed deployment device: a long-reach manipulator (LRM). It has also been demonstrated that the baseline approach has versatility to continuously dislodge and convey a broad range of waste forms, from hard wastes to soft sludge wastes, through the use of rather simple, robust components. Figure 1 provides an overview of the remote retrieval strategy using a scarifier deployed with a long-reach manipulator.

A strategy (Bamberger et al., 1993) was developed to guide an analytical/experimental approach to develop a multi-function scarifier dislodger coupled with a pneumatic conveyance system. Based on the strategy, a testing program has been initiated to characterize aspects of waste dislodging and conveyance processes, evaluate process equipment performance, and address integration issues associated with deploying the scarifier by a long-manipulator arm. The mission of the program is to investigate system deployment strategies to determine appropriate mining strategies, level of control, and sensor requirements. This paper will describe the testbed facility and testing program and present initial test results to date.

2. RETRIEVAL SYSTEM DESCRIPTION

The baseline technology for the waste dislodging is a high-pressure water jet scarifier. High pressure water jet technology has been used by industry for many years for mining, cutting, cleaning, and scarifying materials with a broad range of properties. Proof-of-concept testing has demonstrated that high-pressure water jets can effectively dislodge several diverse waste simulants.

The test scarifier was develop by Quest Integrated, Inc. through collaboration with Pacific Northwest Laboratory (PNL)[1]. This scarifier consists of high-pressure fluid jets mounted on a rotating body and directed at the waste surface. The three rotating jets require approximately 22.7 liters per minute (6 gpm) of water at 344 MPa (50,000 psi). The rotation of the jet carrier is provided by a secondary motion drive, which nominally rotates at 650 rpm. The axis of the secondary motion rotation is normal to the waste surface. The secondary motion drive and jet carrier are contained in an aero-dynamical enclosure mounted concentric

[1]PNL is a multiprogram laboratory operated for the U.S. Department of Energy under Contract DE-AC06-76RLO 1830 by Battelle Memorial Institute.

to and inside the conveyance system inlet shroud. The water jet assembly is encased in a shroud that contains the dislodged waste and water and directs the collected mixture to an air conveyance system.

Figure 2 shows the installation of the scarifier on the gantry mast. To measure dynamic forces due to air suction, inertia, and water jet reaction, the scarifier is attached to a sensor that measures forces and torques along three axes. The sensor is then mounted to a compliant joint, which is attached to the gantry mast and releases in the event of an overload condition. Forces are isolated from the conveyance line by a flexible bellows between the scarifier outlet and the conveyance line. An adjustable spring is used to "zero out" the steady-state moment and forces exerted by the scarifier by providing an alternate load path to the gantry mast.

3. TEST FACILITIES

To demonstrate the scarifier in an actual mining operation, a test facility denoted the Hydraulic Testbed has been constructed to allow longer-duration, multiple-pass tests on large waste fields using a versatile gantry-style manipulator (see Figure 3). A gantry was selected for implementing the mining operation due to its inherent rigidity, programmability, and large load capacity demanded by a technology development program. The actual gantry manipulator selected, provided by PaR Systems, Inc., includes four degrees of freedom to allow rectangular motion plus mast rotation. The control system of the gantry allows sensor data to be used to update the trajectory in real time. This feature allows candidate proximity sensors to be used in the course of an actual mining operation.

The ancillary equipment of the dislodging system includes a high-pressure hose and two high-pressure pumping units. The balance of the conveyance system includes a conveyance line, a wet/dry separator, a collection hopper, and a blower unit.

4. SYSTEM INTEGRATION

The most complete review of previous single-shell tank waste retrieval studies appears in Gibbons et al. (1993). The pertinent conclusions of this review were that hydraulic sluicing should be used to remove the waste inside the majority of single-shell storage tanks, and that arm-based technologies should be the reference system for tanks where net water addition to the tanks is unacceptable. This development work has therefore been based on the assumption that the scarifier will be deployed inside the tank by a long robotic manipulator having a significant degree of both structural and operational flexibility. A long robotic manipulator will have limited positional accuracy in the vertical plane when subjected to erratic dynamic loading. Also, due to kinematic considerations and joint friction, the ability of a long manipulator to maintain a relatively constant transverse velocity will be limited. Table 1 summarizes these key interface issues, their relative ranking, and potential problem areas.

The current retrieval manipulator design consists of a serial dual-arm arrangement with a long-reach manipulator arm used to deliver a short (≈2.5 m) dexterous manipulator to the work area. This configuration provides a high degree of redundancy, allowing the manipulator to thread its way around obstacles in the tank.

5. MINING STRATEGY DEVELOPMENT

5.1 Mining Strategy Functions and Requirements

A process deployment strategy will be required to cope with changes in the surface contours of the waste. This shall include addressing the problems of capturing dislodged waste and spent water over uneven terrain, avoiding collisions with the waste surface, and procedures for maintaining an effective stand-off distance over an uneven waste surface. Initially, it is expected that the topography of the waste surface will be irregular. The mining strategy chosen for the retrieval must be such that a high average retrieval rate is maintained. The overall strategy must effectively retrieve waste over the existing topography and tank hardware as well as any topography created by the scarifier itself, including ridges, knobs of harder material, loose chunks, or leftover ribs from previous passes over the surface.

In order to succeed at removing waste from an underground storage tank, a mining strategy is being developed. The function of the mining strategy is to ensure that mining is conducted in accordance with the following criteria:

- The mining strategy must allow waste removal at the design rate of 136 l/m (30 gpm). 99% of the waste in the tank must be removed as dictated by agreements in place with state and federal agencies.
- No additional water must remain in the tank once mining is completed.
- The tank, waste removal equipment, personnel, and environment must be protected from damage.
- Water should be recovered at the same rate as it is introduced.
- The strategy must specify the waste removal geometry and path such that the end-effectors' required stand-off distance and velocity are observed.

In order to support these functions, the mining strategy must meet the following requirements:

- The mining strategy must minimize the use of gross degrees of freedom of the long-reach manipulator (mast elevation and rotation) by using the dexterous manipulator to implement the mining strategy. Positioning accuracy will be maximized, energy expenditure minimized, and the use of manipulator bracing will be simplified by this requirement. This strategy will dictate dividing the tank into several regions and using the LRM to move from region to region while using the shorter dexterous manipulator to implement the mining strategy.
- The mining strategy must minimize sharp corners and backtracking in the waste removal path due to the robot's inability to abruptly change direction without slowing down.

- The mining strategy must manage the supernatant liquid in the tank. The mining strategy must minimize the loss of cutting fluid and collect existing supernate in the tank.
- The mining strategy must avoid repeated motions with frequencies in the range 0.1 to 5 Hz. These frequencies are near the fundamental natural frequency of the robot.
- The mining strategy must maintain a constant linear velocity. This is required to maximize the efficiency of the waste removing end effectors and to leave the waste surface as clean and smooth as possible.
- The mining strategy must manage hard and soft waste forms; handle variations in topography; and clean the bottom, corner and sides of tank.

5.2 Baseline Strategies

The two baseline strategies illustrated in Figures 4 and 5 are being evaluated: serpentine mining and pit mining. In the serpentine mining strategy illustrated in Figure 4, the end-effector is swept over the waste surface in a regular pattern, removing waste to form horizontal planes. This mining strategy would be the easiest for an operator to implement. In addition, it is the most efficient in terms of cutting rate, since the end effector is cutting waste at all times.

In the pit mining strategy depicted in Figure 5, waste is removed gradually in a pattern that forms a pit. The intent of this approach is to use the pit to manage any excess water that escapes the end-effector. Using this approach, waste is first removed from the inner section of the region to be excavated. Because the scarifier removes only 2.54 cm (1 in.) of waste during each pass, several passes will be required to form the initial pit. As retrieval continues, outer rings of material are removed. It may be required to turn off the water jets as the scarifier is moved from one ring to the other to minimize water losses; this limitation will be brought out during testing. This water management strategy can be augmented by using multiple passes for each ring (to improve efficiency) and by angling the scarifier toward the inside of the pit to facilitate drainage. If multiple passes are not taken at each level, this will lead to a very shallow pit that may have less impact on the flow of water than the existing topography of the waste. Pit mining such as this has been proposed by the University of Missouri as the optimal pattern for waste removal, given the constraints listed above.

6. TESTING FOCUS AREAS

Table 2 provides an overview of the testing program matrix. The first testing segment will verify the ability of the proximity sensors to maintain a constant stand-off distance between the scarifier and the waste surface over various challenging topography. Next, the reaction forces at the scarifier interface plate will be measured separately due to suction, inertia, and jet reactions. This will greatly simplify the force data reduction from subsequent testing. Next, mining strategy tests with salt cake and sludge simulants will be conducted to evaluate the effectiveness of mining strategies, forces related to scarifier and conveyance line, and retrieval rate. Performance of the system during off-normal events and the ability of the system to deal with waste topography will also be evaluated. In addition, tests will also be

conducted to quantify dislodging efficiency as a function of waste stream properties (amount of material, depth of cut, and surface quality).

6.1 Waste Simulant Development

Waste dislodging and conveyance processes will require system qualification tests using actual radioactive waste materials or simulated waste. Testing with radioactive waste has disadvantages involving the volume of material available, significant hazards to personnel, and high cost to run tests. The use of simulated waste is promoted to overcome these strategies. However, the application of simulants is not without its difficulties. Characterization of waste inside Hanford underground storage tanks is very limited and may not span relevant waste properties. Until such time that physical characterization data becomes available for the actual tank wastes, the simulant properties must be carefully designed to expose the limitations of the process and span the range of properties expected to be critical to the processes studied.

Simulants have been designed to capture the essential characteristics of hard salt cake type-wastes and sludges. Salt cake recipes typically contain a water/dynamate or water/dynamate/silica mixture, while sludge recipes contain a water/kaolin or water/bentonite mixture. It is expected that these recipes will bound the critical properties of the actual sludge in the tank.

6.2 Deployment Instrumentation Development

This section of testing will evaluate instrumentation to maintain a constant stand-off distance in an underground storage tank environment. Software will be developed to modify the path of the gantry end effector based on sensor input using the RPM capabilities of the gantry. The instrumentation will be used to modify the gantry position in real time to maintain a constant stand-off distance on hard and soft simulants and various topography.

Lasers and ultrasonic sensors, among others, have been ranked and evaluated in terms of their ability to measure proximity in the hostile tank environment. At this time, ultrasonic sensors appear to be the most promising technology. Two sensors will be installed on the shroud at the leading and trailing edge, and about one 5 cm beyond the shroud. This will allow the system to prepare for abrupt changes in topography without collisions.

Testing will verify the controllability and accuracy of the proximity sensors and control software to maintain a constant stand-off distance. Maintaining a relatively constant stand-off distance is of importance because of constraints imposed by the air conveyance system. Parametric testing has shown that the stand-off distance should be 5.08 cm (2 in.) nominally with an allowable deviation of $\pm$3.8 cm (1.5 in.). If the scarifier is too close to the surface, the vacuum may suck the shroud into contact with the waste surface (known as the smooch effect). Conversely, if the scarifier is too far away, the shroud will not be able to effectively contain the dislodged particles. To maintain the correct stand-off distance with the gantry robot control system, it is only necessary to vary the position of the vertical mast. For the initial testing, the gantry cannot be used to align the scarifier with an angled surface because the robot lacks a wrist necessary to accommodate additional degrees of freedom.

The test series will include abrupt drop-off and rises (Figure 6), inclined surfaces (Figure 7), and rough surfaces. In addition, tests will be conducted to verify controllability of the system over various waste types (salt cake, sludges, water) and in the presence of water jet spray, high velocity air, and noise. Because this is a development program, this approach will help isolate weaknesses in the system and identify needed improvements.

6.3 Test Results To Date

Preliminary testing at Quest has shown that the scarifier can retrieve both hard salt cake and sludges at or above the target retrieval rate of 136 liters/min (30 gpm) for short durations. Construction activities are nearing completion for the HTB to allow mining strategy testing to begin in 1995. Initial testing will determine if the retrieval rate of 136 liters/min rate can be sustained for long periods of time over varying waste types and topography.

The development of the software and instrumentation to maintain a constant stand-off distance is well underway. Two ultrasonic proximity sensors have been installed on the scarifier and tested using data acquisition and control software that receives the sensor position data and updates the trajectory of the gantry. Early results are promising, although testing of the system will continue to verify the operation of the sensors under a variety of simulant surface conditions, scarifier velocities, and in the presence of water jet spray, high velocity air, and noise.

7. CONCLUSIONS

The data generated from these tests are essential to allow the completion of definitive system design of actual in-tank components. Testing of full-scale prototype end effectors, cold testing, operations research, and operator training will be considered as long-range uses for the Hydraulic Test Bed.

8. ACKNOWLEDGEMENTS

The Waste Dislodging and Conveyance Program is sponsored by the U.S. Department of Energy Office of Technology Development.

9. REFERENCES

Bamberger, J. A., Bates, J. M., Keska, J. K., Elmore, M. R., and Lombardo, N. J., *Strategy Plan: Strategy to Develop and Test a Multi-Function Scarifier End Effector with an Integral Conveyance System for Waste Tank Remediation*, PNL-8477, Pacific Northwest Laboratory, Richland, Washington, 1993.

Gibbons, P. W., Sabin, J. C., Prather, M. C., and Kreig, S. A., *Review of Prior Single Shell Tank Waste Retrieval Process Studies*, WHC-SD-WM-ES-252, Revision 0, Westinghouse Hanford Company, Richland, Washington, 1993.

Rinker, M. W., Mullen, O. D., and Hatchell, B. K., *Waste Dislodging and Conveyance Testing Summary and Conclusions to Date*, PNL-10095, Pacific Northwest Laboratory, Richland, Washington, 1994.

10. NOMENCLATURE

HTB	Hydraulic Testbed
LRM	Long Reach Manipulator
WD&C	Waste Dislodging and Conveyance

Table 1. Interface Issues between Scarifier and Long Reach Manipulator

Rank	Key Interface	Problem areas/risk
1	Dynamics	Bound loads due to scarifier and conveyance line
2	Mining Strategy	Develop patterns and sequences that scarifier will move through to extract all the waste. Include considerations for non-uniformity of surface, geometry of cut, and debris
3	Accuracy/Repeatability	Determine accuracy, repeatability, and maneuverability requirements to implement mining strategy and achieve desired retrieval rates.
4	Physical Interface	Define physical interface between LRM and scarifier
5	Sensor Requirements	Define the requirements for instrumentation to maintain a constant stand-off distance over various topography while maintaining the desired retrieval rates and near 100% water recovery.
6	Controls Requirements	Determine the level of control sophistication required to achieve desired retrieval rates. Evaluate the use of tele-operation versus robotic control to implement the desired mining strategy.

Table 2. Overview of the Testing Program Matrix

Test Focus	Test Parameters	Key Data Expected
1. Verity instrumentation to maintain a constant stand-off distance	• Surface Roughness • Traverse Velocity • Angle of Incline • Waste Type	Stand-off distance over various waste types and topography in the presence of water jet spray, high velocity air, and noise.
2. Reaction forces due to separate effects	• Stand-off Distance • Air flow • Position of Gantry • Traverse Velocity • UHP Water Flow	• Reaction forces due to suction, inertia, jet reaction • Pressure drop in conveyance line
3. Initial system checkout & performance verification. • 2 tests	• Simulant type (saltcake and sludge)	• Retrieval rate • Reaction forces • Pressure drop in conveyance line • Air flow rate required to sustain flow
4. Hardpan Testing • 9 tests	• Two salt cake recipes • Two sludge recipes • Mining strategy - serpentine and pit	• Retrieval rate • Reaction forces • Cutting efficiency • Pressure drop in conveyance line • Conveyance line lubrication required
6. Topography/Mixed Waste •5 tests	• Hard and Mixed Waste • Various topography	• Retrieval rates • Reaction forces • Cutting efficiency • Pressure drop in conveyance line • Conveyance line lubrication required

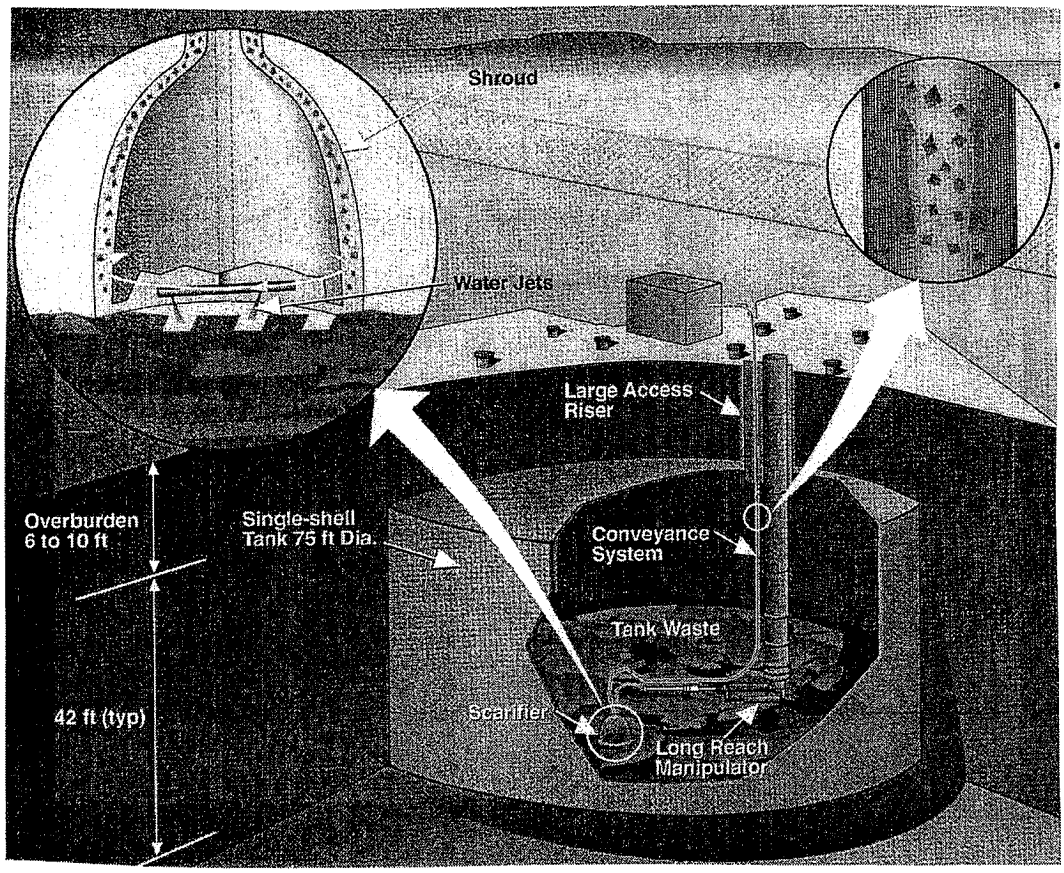

Figure 1 **Retrieving Radioactive Waste from an Underground Storage Tank using a High Pressure Scarifier**

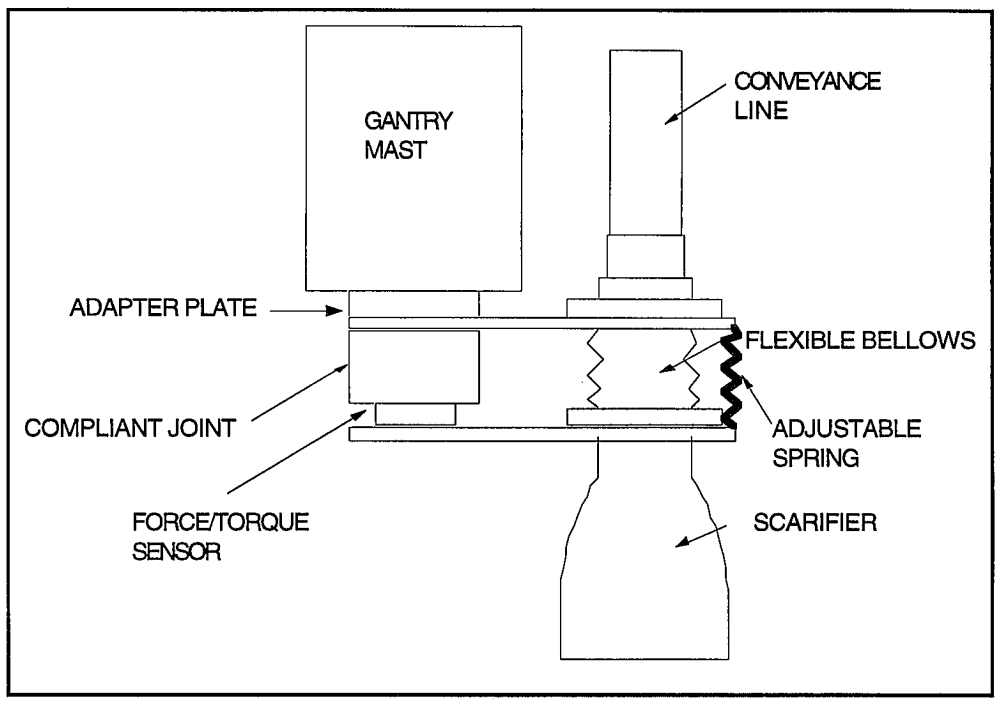

Figure 2 **Scarifier Attachment to Gantry**

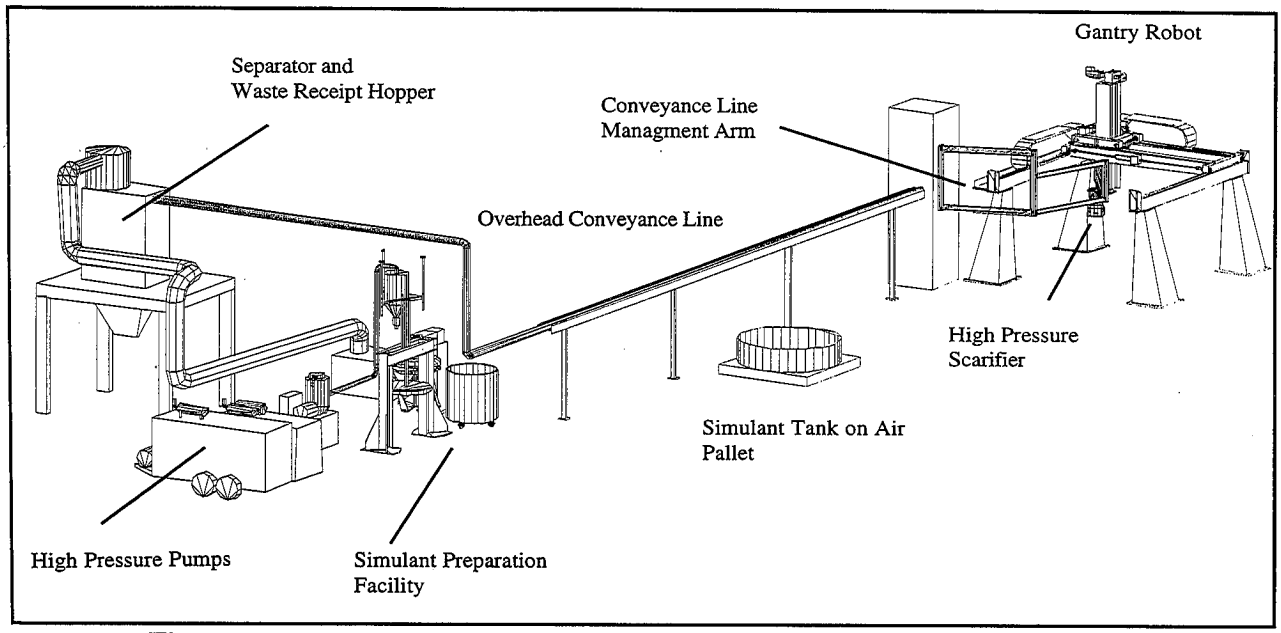

Figure 3 **Waste Dislodging and Conveyance Hydraulic Testbed**

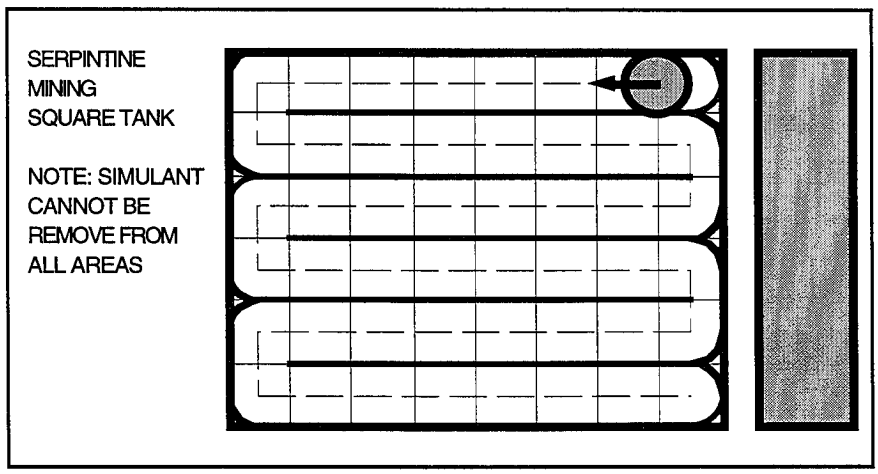

Figure 4 **Serpentine Mining Strategy**

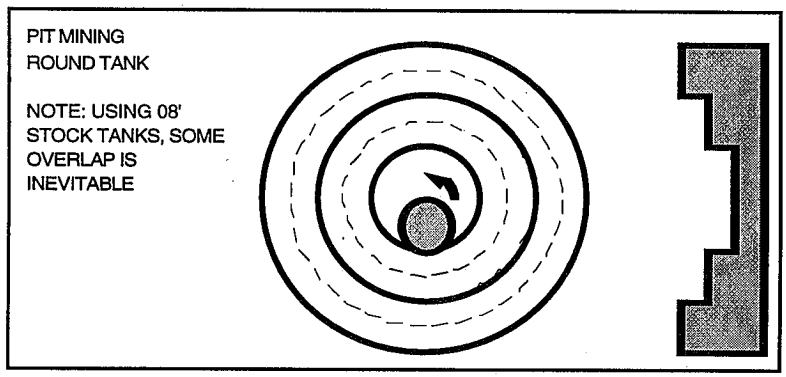

Figure 5 **Pit Mining using a Round Tank**

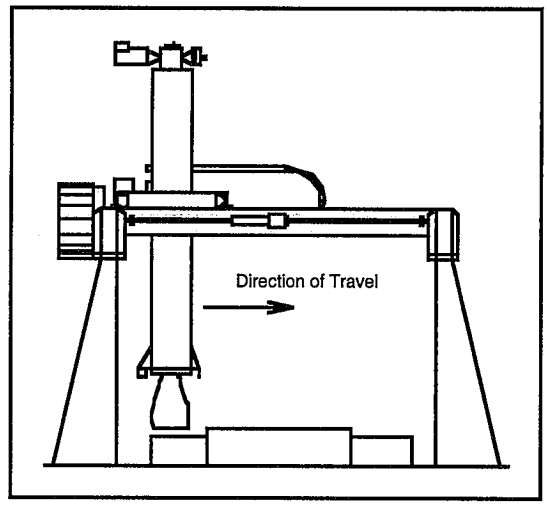

Figure 6 **Abrupt Drop-off Test**

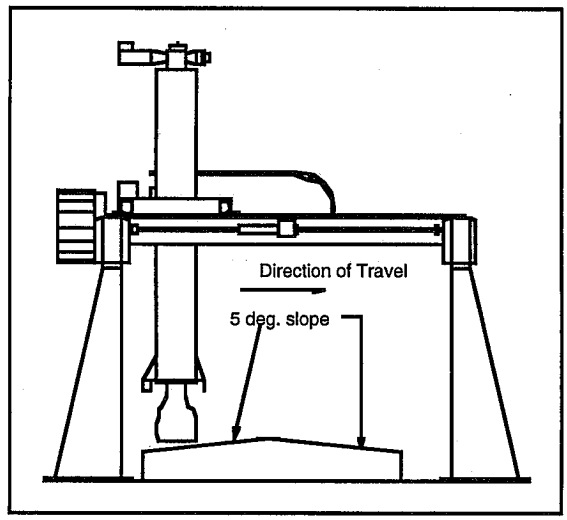

Figure 7 **Inclined Surface Test, 5°**

8th American Water Jet Conference
August 26-29, 1995: Houston, Texas

Paper 46

THE USE OF LOW REACTION DISLODGING TOOLS FOR WASTE RETRIEVAL FROM UNDERGROUND STORAGE TANKS

D. A. Summers, G. Galecki
High Pressure Waterjet Laboratory
University of Missouri-Rolla
Rolla, MO 65401

M.W. Rinker
Batelle Pacific Northwest Laboratory
Richland, WA

C. Christienson
Idaho National Engineering Laboratory

J.D. Randolph
Oak Ridge National Laboratory
Oak Ridge, TN

ABSTRACT

The recovery of highly radioactive waste from underground storage poses significant problems, which vary from location to location with both material stored and tank configuration. Three possible solutions to this retrieval problem illustrate the different approaches which must be adopted for the storage tanks at Hanford, Idaho National Engineering Laboratory, and Oak Ridge National Laboratory. The first must produce up to 30 gpm of mixed waste. A mining strategy to make use of a dual head end effector with a jet pump to extract the resulting fluid is described.

At Idaho the walls of this tank support a series of cooling coils which limit access. A lighter arm is to be used on this site, with limited strength. Initial experiments to clean around the piping and infrastructure are described.

At Oak Ridge the arm has an intermediate capacity. The tool must clean the waste from the gunite walls of the tank without damage, although the jets must have sufficient power to fragment any gunite which has fallen from the walls. The results of the tests to validate the design are described.

Organized and Sponsored by the Water Jet Technology Association.

1. INTRODUCTION

Ever since the beginning of research into the uses of radioactive material, it has been necessary to find ways of storing the resulting waste materials. For much of that time the solution has been to collect this material in underground storage tanks, particularly when the wastes involved have been liquid. The greatest number of the tanks are found on the Hanford reservation in Washington, but there are significant other tank farms at Federal Laboratories in other states.

For a variety of reasons it has now become timely to find ways of removing this material so that it may be separated and treated, and so that those components which remain as hazardous materials may be more permanently treated for long-term storage. Methods of extraction are, however, somewhat limited, given the nature of the storage and the wide range of material to be extracted.

As a general rule access to the tanks is through a series of pipes set into the dome of the tanks, and these pipes, or "risers," are at most some 42 inches in diameter, but may be as narrow as 11 inches. The tanks range in diameter from 25 ft to 75 ft and may contain as much as 500,000 gallons of waste. The waste itself ranges from a liquid form, usually known as "supernate", through a sludge often compared in texture to peanut butter, to a hard solid which has a significant strength and is referred to as a "saltcake." The tool used for the removal must be designed to cope with all the different forms of waste, and a target production rate of 4 cu. ft./min. or 30 gpm. has been set for the removal process.

In order to remove the material in a timely fashion without suffering the problems of working within the waste (whose local construction is widely variable and not well characterized) it has been decided to remove the material using a device (called an "end effector") attached to the end of a remotely controlled flexible arm. The great length of this arm, together with the limitations on its size imposed by the width of the access risers, has, in turn, placed a considerable limitation on the parameters of the end effector. Size, weight and the amplitude and frequency of the force variations exerted through the end effector must be controlled within defined limits for the arm to achieve its most effective operation. These considerations led to the choice of high pressure waterjets as the main tool for dislodging the waste. Two alternative approaches have been developed, in one the system choice has been to use very high pressure waterjets at lower volume flow rates (Hatchell et al., 1995) while the alternative, described herein, has been to use a lower pressure system at higher flow rates.

The choice of flow rate is of some concern since the possibility exists that the tank into which the system must be fielded may be cracked. In such a case there is a risk that, were excessive amounts of water to be added to the tank, that it would then leak out of the tank, carrying with it the contained highly radioactive material. It has thus been a feature of both systems to ensure that all the water used in dislodging the waste, as well as all the dislodged waste itself, is immediately aspirated into a conveyance line which will carry the debris out of the tank. In the higher pressure system this is achieved using an air conveyance line, in the UMR system this is achieved using a modified jet pump (Mann, 1995) based on a

commercially available design (Rankin, 1993). The entire system was then configured about the operational parameters of a specially designed support arm (Figure 1).

2. INITIAL SYSTEM DESIGN

The High Pressure Waterjet Laboratory (HPWL) of the Rock Mechanics and Explosives Research Center (RMERC) at the University of Missouri-Rolla (UMR) is under contract to Battelle Pacific Northwest Laboratories (PNL) to develop a design for use in the storage tanks at the Hanford site, and also for use at the Idaho National Engineering Laboratory (INEL) and at the Oak Ridge National Laboratory (ORNL). To distinguish the different forms of this tool from the alternative device, the UMR tool has been designated the Confined Sluicing End Effector (CSEE).

Initial experiments were carried out to determine the fundamental approach which must be used to develop a tool capable of reaching the preliminary design objectives for the Hanford site. These experiments included the modification of the jet pump to reach both higher material delivery rates, and to deliver it at a greater height above the pump (Mann, 1995). In large measure the experiments were carried out using a recrystallised fertilizer as the simulant for the saltcake, on the premise that a system which could mine the hardest material at the required rate, should also be able to handle the softer materials. This assumption did not prove to be completely accurate since it neglected a critical part of the operation, that of waste mobilization.

The two separate functions of the CSEE, dislodging the waste and carrying it through the conveyance line to the surface could easily be separated and experiments were carried out to define the required system operational parameters (Galecki et al., 1994). These led to the designation of a system in which the cutting head was made up of two modules each of which contained two rotating jet heads (Figure 2).

Each head would remove a one inch layer of material so that the total "bite" of the head would be some 4 inches as it moved over the waste surface. The size of the bite was adjusted to allow some variation in the known position of the head relative to the waste due to the positional accuracy of the arm. In order to further accommodate this variation the head was to be inclined at 15 degrees to the horizontal, and this would give the advantage of allowing the cutting jets to cut outside the perimeter of the surrounding shroud and thus clean to the walls of the tank and around any existing hardware buried within the tank waste.

The jets for the mining head were directed perpendicular to the body of the head, to make sure that the rebounding material would all be collected within the surrounding shroud and thus fed into the conveyance line. This worked well in the major operational function of this head in saltcake, in which the material is resistant to the jet motion and the material is therefore rebounded back out of the cut into the confines of the shroud. Some fluid and debris would not, however, be captured on the initial pass since the variation in the surface contours of the waste and the relative hardness of the target would affect the rebound trajectory. In order to resolve this problem a particular mining strategy was developed which

would allow subsequent collection and removal of any fluid and waste not immediately collected. With this system (Figure 4) the arm moves the CSEE over an oval path with successive passes first deepening and then widening the pit created. In this way the central section of the pattern is the deepest and thus the waste will drain to that location.. By successively returning to the center of the pattern at the beginning of each deepening procedure the head will thus aspirate up all the residual material and fluid and re-establish a dry condition.

However this mining strategy and path orientation has two disadvantages in terms of overall usefulness. The problems arise in dealing with softer but still solid waste (the sludge) and when the tank is almost completely cleaned and the jet is reaching the underlying floor of the tank. The first problem is common to all tanks, while the second has tank specific problems which relate to the differing conditions for the walls at the INEL and ORNL sites.

3. PROBLEMS WITH SOFT SLUDGE MINING

As discussed above, with a relatively resistant target material, a high pressure waterjet will cut into the material and then, having lost the energy for further penetration, will be pushed out of the way, and back up the access slot it has cut by subsequent jet flow. However when the target is soft this cutting range may well extend beyond the range of the suction of the collection shroud (which lies between 0.5 and 4 inches). This is particularly true where the jets are not pointed directly downwards from the shroud. The problem is exacerbated in the soft sludge since when the water is carried deep into the sludge there is very little of it left in the vicinity of the shroud to assist in liquefying the sludge to make it easier to remove. (The analogy usually quoted is that of a blueberry milkshake. It is quite easy to suck up the blueberries in the shake when they are surrounded by fluid - it becomes considerably more difficult when they are lying separately in the bottom of the glass with no more milk present).

The strategy for overcoming that problem requires that the cutting fluid must be retained in the sludge closer to the surface. The three over-riding parameters which control the depth of cut are the jet pressure, the jet diameter and the speed at which the nozzles are being traversed over the surface. It is impractical to change nozzle diameter during a cleanout of the tank on a casual basis, and thus the options are to lower the jet pressure when cutting sludge, and to speed up the rotational speed of the head. When these were tried it proved possible to constrain the cutting fluid to within the effective zone of the suction shroud and the head was able to mine simulated sludge (the simulant was a thick kaolin clay).

4. PROBLEMS WITH APPROACHING THE FLOOR OF THE TANK

The problems of cleaning up the final volumes of waste as the head completes the mining process, are different for the different tank farms which are being addressed. Some of the overall philosophies will remain the same but the geometries of the tanks, and the materials from which they are made, make it important to address the problems in a different way.

The Hanford tanks are made of steel, and while this may be flat there is some evidence that the floor has been bowed by external and internal stresses within this wall during the time of tank operation. There are bracing rings of steel in the walls of the tanks, but no consistent pattern of struts in the floor which would interfere with a cleaning pattern which would be set up for this final operation. At present it is assumed that the waste at the Hanford site will extend to the floor and that the residual clean up will be of a saltcake deposit. No special design changes are currently planned for the final clean-up segment of the tank removal process, although it is likely that the head design will be modified to include some of the concepts developed to deal with the problems at other sites.

5. SPECIAL DESIGN FOR THE INEL

At the Idaho site there are two specific problems which must be addressed. The first of these is that the tank is lined, on its inner surface, with a series of cooling coils which are held away from the walls and floor of the tank by a steel infrastructure (Figure 5). The second is the presence of a gummy contaminant on the surfaces of the tank infrastructure which must be removed as part of the final clean-up. The waste type is also somewhat different from that of the Hanford farm. The nature of the material is a fine granular solid in large part. For the initial parts of this study that material was modeled with a blasting sand. This, while not an accurate simulant, provided sufficient response that the design and approach to solving the problem could be addressed.

The nature of these problems led to a suggestion that they be addressed in separate parts. Because it will be difficult to construct an end effector which can easily move around the contours of the pipes, it is proposed to make use of the slightly abrasive nature of the granular waste and to agitate this up around the pipes and infrastructure in order to abrade away the coating.

For this to be effective there must be a thick level of debris under the pipes which can be agitated and energized so that it will rub against the underlying structures, hidden from direct jet action, and clean the residual coating. Once this coating has been removed then the remaining material can be aspirated up in the same way as with the ORNL system, in a separate series of passes made with the head moving between the pipes to access the underling surfaces.

The metal of the pipes and walls provided a resistant material which was resistant to jet pressure in the ranges anticipated; such was not the case with the Oak Ridge tanks.

6. SPECIAL DESIGN FOR THE ORNL

When the tanks were constructed at Oak Ridge, they were built-up by spraying a concrete material, known as gunite, onto a basic structure assembled from reinforcing bars. Thus the internal surface of the tanks is a concrete, and while gunite has been shown to have a higher

strength than conventional concrete, the exposure of the inner surface to varying fluids over the years may have weakened it.

It is currently planned to remove the majority of the waste in the ORNL tanks using a sluicing technique which has previously been found to be effective (Weeren et al., 1984) in removing all but the last few inches of waste material. The residual material will be cleaned from the tank using a CSEE. However the nature of the residual material is likely to range from very fine particulate matter to pieces of gunite which have fallen from the walls of the tank.

In order to determine how best to configure the head for this cleaning task a special test facility was built at the HPWL. The constraints on the use of this head were that it must produce a force on the arm of less than 70 lb, since the arm to be used would be much smaller than that to be used at Hanford.

For this reason it was decided to begin with only one of the modules which made up the initial end effector. Further, in order to gain a rapid evaluation of the effectiveness of the different concepts for use, tests were carried out on a bed of sand to provide an initial simulant for the waste in the tank.

It rapidly became clear that there are different considerations which must be adopted in carrying out a final clean on a surface which is flat and will not be penetrated by the jet. This is especially true where the solid being removed will "liquefy" in the presence of significant volumes of water and flow evenly over the surface. The reason that this is a problem is that while a jet will rebound almost vertically when it is cutting into a surface it will flow laterally (Figure 7) if it strikes perpendicular to a flat surface which it does not penetrate. In this case it will have sufficient energy to wash all the material from the vicinity of the cleaning head before the suction inlet to the conveyance line has a chance to aspirate the material.

Tests showed that two factors were required in order to overcome this problem. The first, in order to maximize suction at the surface, was to bring the inlet for the suction end of the conveyance line within half an inch of the surface. While this had the advantage of allowing it to attract the material under its path, it made it difficult to advance through waste more than half an inch thick. In order to overcome that problem the cleaning jets were mounted outside the suction port, and designed to rotate with it. At the same time the jets were inclined inwards so that the jets not only cut clearance ahead of the cleaning head, but they also pushed all the material, and water, into the zone of attraction for the suction line (Figure 8). As a result it has proved possible to develop a lighter weight device capable of aspirating a clean line through the waste material in the INEL and ORNL tanks and thus making it possible to effectively program the movements of the arm to ensure that the floor is "swept clean" (Figure 9).

7. REFERENCES

Galecki G., Summers, D.A., Sprung, J., and Yount, J., "Development of a Waste Excavation End Effector," 13th International Symposium on Jet Cutting Technology, Rouen France, October 1994, pp. 637 - 648.

Hatchell, B., Rinker, M.W., and Mullen O., "Hazardous Waste Strategies using a High Pressure Water Jet Scarifier," 8th American Water Jet Conference, Houston, TX, August 1995.

Mann M., "Evaluation of the Performance of a Jet Pump in Waste Retrieval," MS thesis, Mining Engineering Department, University of Missouri-Rolla, 1995 (in preparation).

Rankin G., Performance Specifications of a Jet Pump, AquaDyne Inc., Houston, TX.

Weeren, H.O., Lasher L.C., and McDaniel, E.W., "Cleanout of Waste Storage Tanks at Oak Ridge National Laboratory," Annual Meeting, Materials Research Society, 1984, Boston, Mass.

8. FIGURES

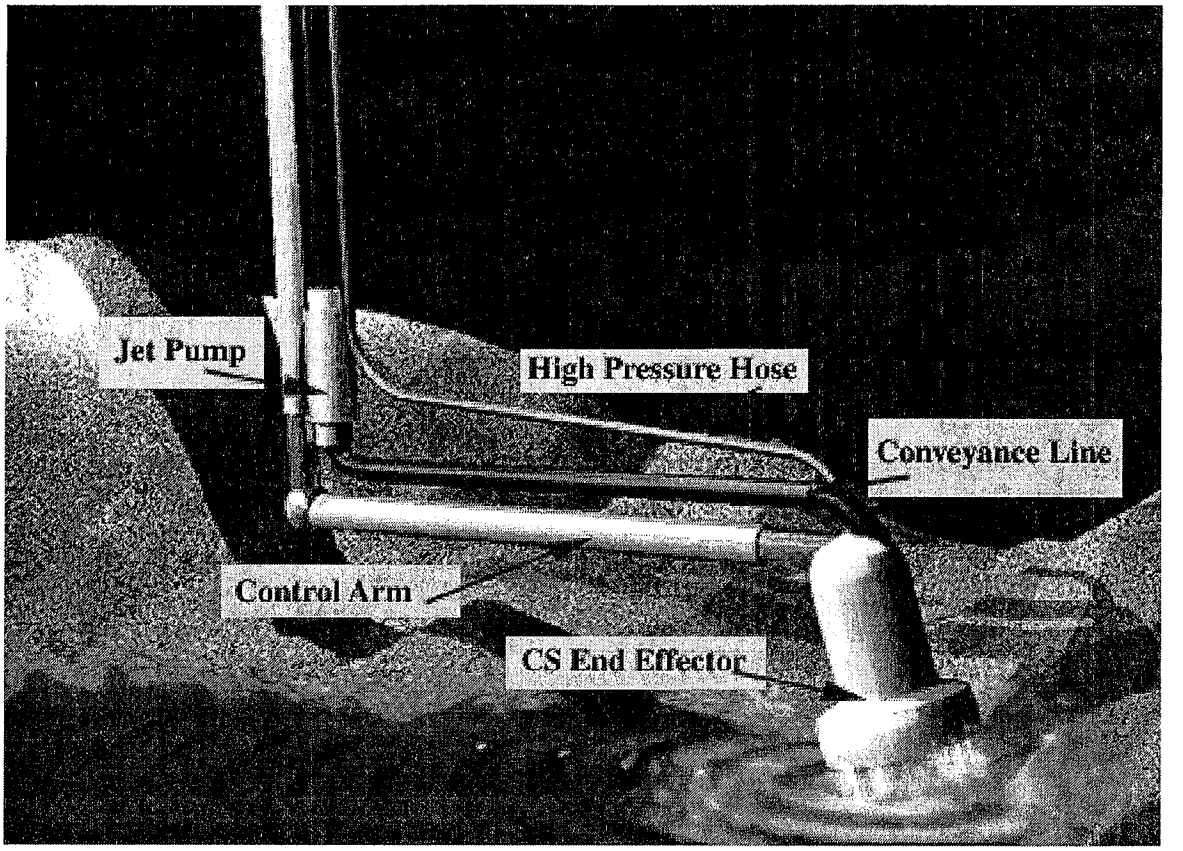

Figure 1. Artists schematic of the components of the UMR CSEE.

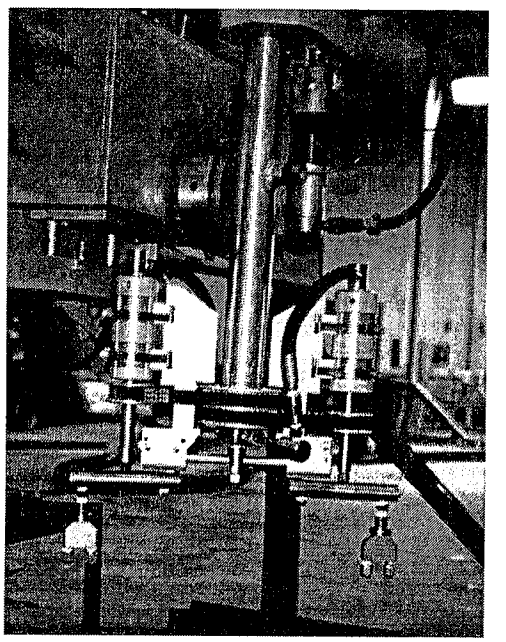

Figure 2. Components for the UMR CSEE.

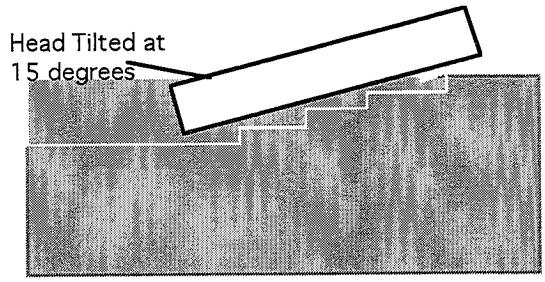

Figure 3. The inclined head used to clean the walls of the tank.

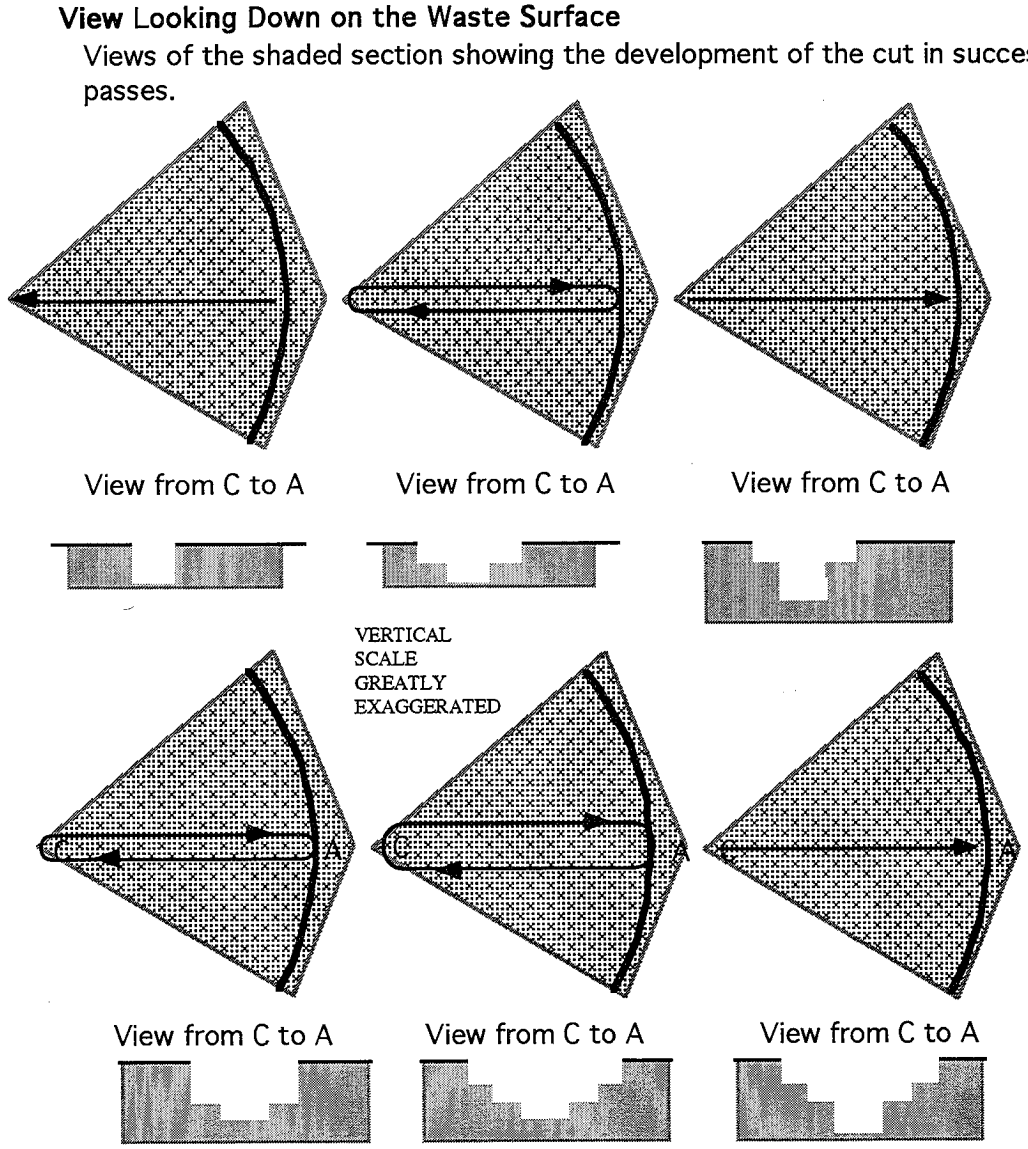

Figure 4. Proposed mining path to collect all the waste and water at regular intervals.

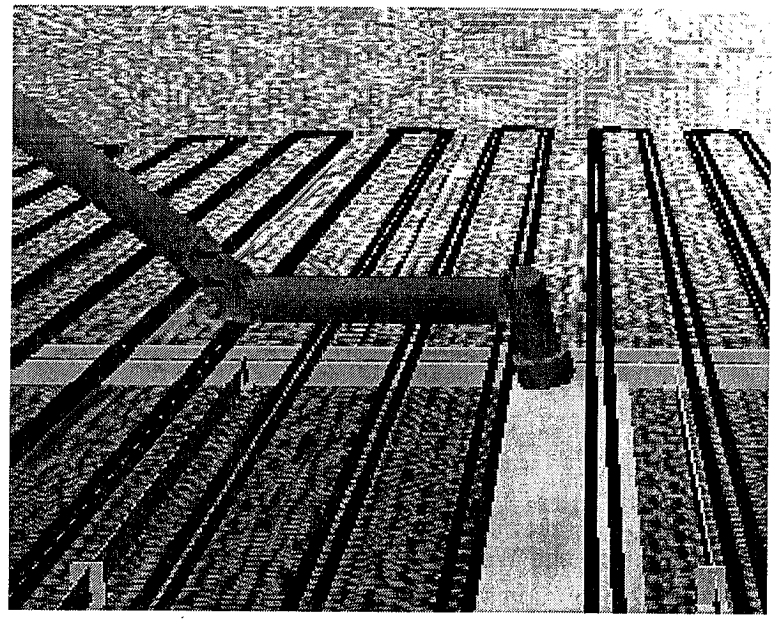

Figure 5. Configuration of the cooling pipes in the INEL tanks.

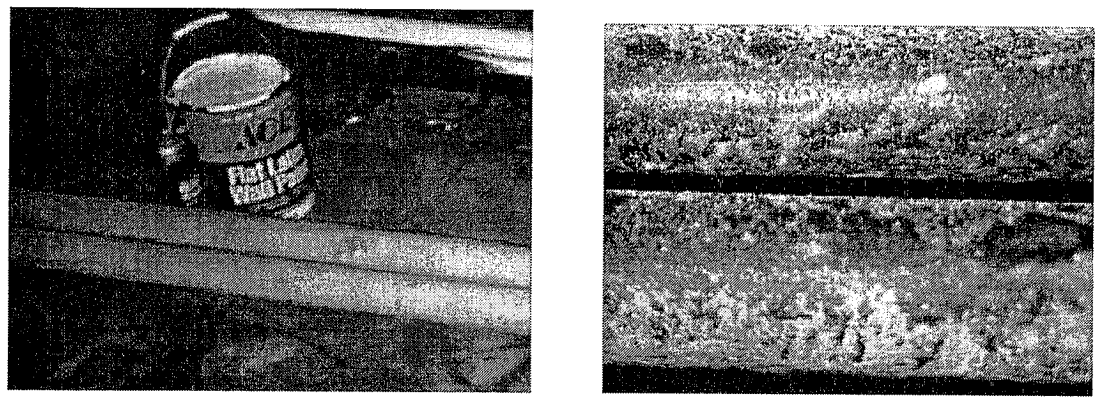

Figure 6. Coating before and after jet and abrasive bed removal of the simulated coating (for the photograph a latex paint was used as the simulant which helps with visualization - a sealing compound was found better able to resemble the likely actual performance of the coating but was less visible.

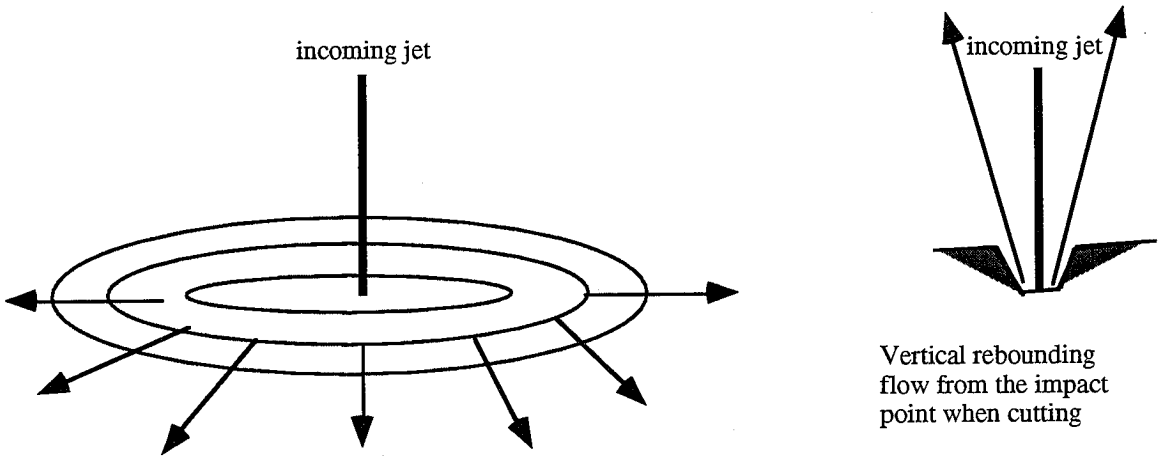

Figure 7. The problems of flow from a vertically inclined jet.

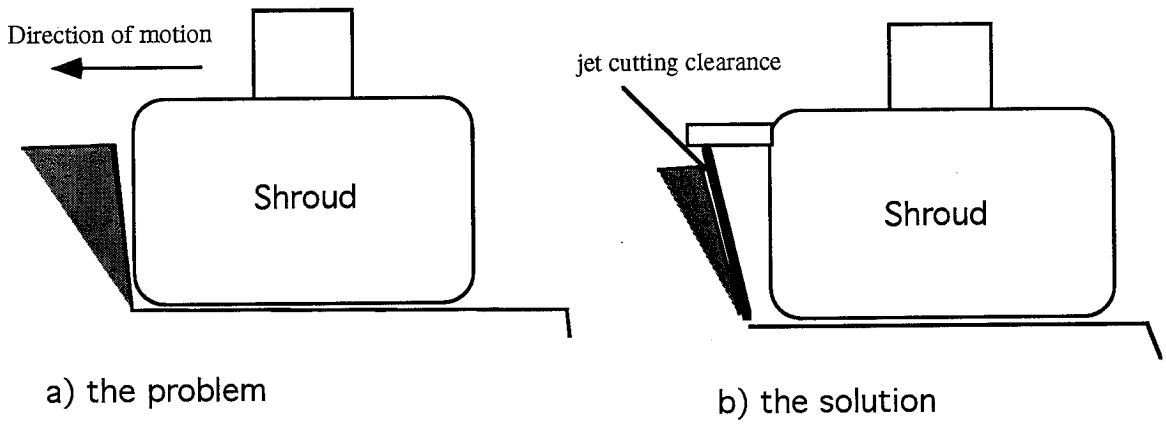

Figure 8. Cutting clearance for the suction shroud.

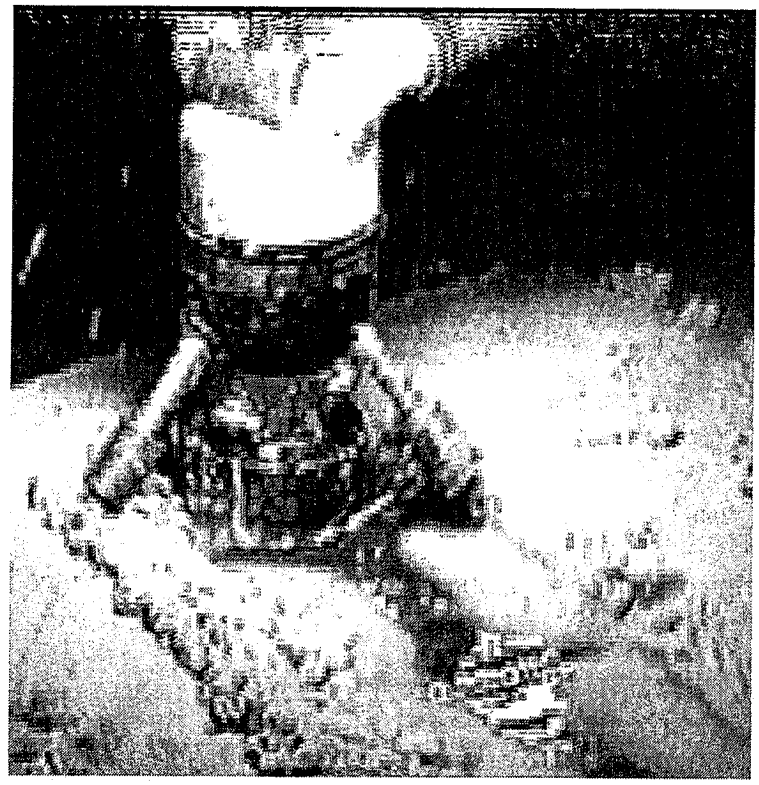

Figure 9. Clean path behind the prototype CSEE - jets are operating at 5,000 psi.

8th American Water Jet Conference
August 26-29, 1995: Houston, Texas

Paper 47

A COMPARISON BETWEEN LASER AND AWJ CUTTING OF PORTUGUESE MARBLES — A PHENOMENOLOGICAL STUDY

R.M. Miranda
Instituto de Soldadura e Qualidade
Lisbon, Portugal

A.J. Mouraz Miranda
Instituto Superior Técnico
Lisbon, Portugal

ABSTRACT

A phenomenological study of precision cutting using CO_2 laser and abrasive water jet (AWJ) was conducted on different types of Portuguese marbles.

Laser cutting is a thermal process that involves thermal gradients and residual stresses in the material adjacent to the cut front. These gradients induce chemical and structural modifications of the material and cracking. This is due to the low thermal conductivity and thermal expansion coefficient of marble. Chemical degradation was investigated under Scanning Electron Microscope (SEM) and X-ray diffraction. $CaC0_3$ was seen to decompose in CaO and CO_2. CaO decomposes either by forming Ca° at high temperature or by absorbing water from environment to form $Ca(OH)_2$. Surface finishing was seen to be dependent on calcite chemical composition and rock hardness.

AWJ cutting gives clean low roughness surfaces, free of cutting, structural, and chemical modifications.

Organized and Sponsored by the Water Jet Technology Association.

1. INTRODUCTION

CO_2 Lasers are in the industrial shop floor since early 70's.

Despite the wide range of applications of lasers, cutting represents about 60% of overall applications. Since the process is easier to control than AWJ, lasers have been used for stone processing both in cutting and in marking.

In the former application, the major advantage of the laser system is its capability to make small kerf widths in cuts of high precision. In other technical advantages, it competes with AWJ.

As far as economics are concerned, though operating costs are higher for AWJ, equipment costs for laser systems are more important. So, in the overall, it can be said that the total cost per hour is in the same order of magnitude in both processes.

2. EXPERIMENTAL PROCEDURE

Three Portuguese calcareous stones were tested with commercial references: Moca Creme, Rosa de Borba and Branco Pardais. Petrographically Moca Creme is biomicritic with clastic argillous matrix; Branco Pardais and Rosa de Borba are crystalline calcitic marbles with medium to fine grain.

Measurements of stone hardness provided the following results:

- Moca Creme: 83 HV
- Branco Pardais: 108 HV
- Rosa de Borba: 103 HV

Laser cutting was performed with 2.5 kW CO_2 laser RF excited, with a Transversal Electromagnetic Mode TEM_{20}, a beam diameter at the ressonator cavity exit of 19 mm and a divergence of 2 mrad.

The following operating parameters were varied: laser power, travel speed, focal length lens, focal point position and assist gas (type and pressure).

Cuts were observed visually and the decomposition products were analysed under SEM and by X-ray diffraction.

AWJ cutting trials were made with a Flow System high pressure pump 9XD-55, varying the water flow rate, water pressure, cutting speed and abrasive flow rate. All other parameters were kept constant and these were:

- sapphire diameter: 0.355 mm
- mixing tube diameter: 1.016 mm
- mixing tube length: 76.2 mm
- abrasive type: Australian garnet

- abrasive grain size: 80 mesh

Cut morphology was observed under SEM and roughness measured at different points in thickness.

3. DISCUSSION OF RESULTS

3.1 CO_2 laser cutting

Natural stones in particular, calcareous stones can be cut by laser. Due to the high energy required to perform the cut, CO_2 lasers are more adequate for the thickness industrially interesting.

Laser cutting process of natural stones, involves a thermal process that consists of rapid and localised heating of the stone, with the formation of a blue colourished plasma at energy densities of about 10^7 W/cm^2 as reported by Oliveira Santos et al. (1991).

The plasma forms a cavity similar to the "key-hole" observed during welding and together with other particles resulting from the stone decomposition, absorbs the energy radiation.

In order to remove the plasma, as well as the molten material, a coaxial gas (neutral or oxidising) is injected.

Besides the effect of expelling the molten material, which originates the cutting, the gas has also a cooling effect on the cut surfaces which decreases the extension of the heat affected zone (HAZ). The shape and movements inside the molten material were previously observed by Pires et al. (1991).

When the laser is removed from the interaction area, rapid solidification of the molten material occurs, leading to a vitrified dross slightly attached to the cut surfaces either in the top and in the bottom. This is due to the pressure vapour that ejects the molten material to the surfaces (fig.1).

Dross quantity and appearance depend on the molten material viscosity and thus on the calcite chemical composition. This was confirmed by Basov et al. (1986) who measured the absorption and transmission coefficients of calcite in the laser wavelength at a temperature of 560°C.

A large quantity of a fine white powder is emitted during cutting. Powder is mainly constituted by CaO which forms during the thermal decomposition of $CaCO_3$ between 896 and 910°C, according to the chemical reaction:

$$CaCO_3 \rightarrow CaO + CO_2 - 42.52 \text{ kcal/mol} \qquad (1)$$

When observing the cut surfaces, one can notice they are covered with a thin layer of white powder with pores and cracks (fig.2). Pores are due to excaping gases (CO_2 and O_2) resulting from decomposition of $CaCO_3$ and CaO, respectively.

$$CaO \rightarrow Ca^{\circ} + 1/2\ O_2 - 151.7\ kcal/mol \qquad (2)$$

This occurs at about 2 570°C. In fact, Pires et al. (1991) measured the temperature in the cut front and this was of about 3 100°C.

Cracks form as a consequence of the sharp thermal cycle and the low thermal expansion coefficient of stones. Under the optical microscope they appear full of an isotropic powder like CaO.

Investigations of this thin layer under SEM revealed the existance of a large amount of cracks and the presence of a cubic like crystal, similar to metallic calcium (fig. 3 and 4).

X-ray diffraction of this powder showed it was mainly constituted by CaO, $Ca(OH)_2$ and metallic calcium (fig. 5). $Ca(OH)_2$ forms according to the chemical reaction:

$$CaO + H_2O \rightarrow Ca(OH)_2 + 15\ kcal/mol \qquad (3)$$

Removing this layer, that is about 0.3 to 0.4 mm thick, the surface is of industrial quality, with low amplitude striations characteristics of laser and AWJ cutting processes.

When investigating the effect of operating parameters it was found that there is an almost linear relationship between laser power and cutting speed for a given stone varying thickness (fig. 6). The maximum cutting speed increases with the laser beam power.

There is also a relationship between the stone hardness and the maximum cutting speed (fig. 7): the harder the stone, the slower the cut.

When cutting sedimentary rocks like Moca Creme, the sedimentation direction affects the cutting speed (fig. 8). Cut is faster in the So direction.

When increasing the focal length lens, the cutting speed slightly increases (see table 1). This is due to the angle the beam makes in the focus that is a function of the beam diameter and the focal length. Depth of field is also greater.

The focal point position plays a minor role in the cutting speed and cutting quality and it should be kept 1 mm below the impinged surface.

As far as the coaxial gas is concerned it was noticed that the type of gas is not so important for the materials tested as the pressure is (fig. 9). Increasing the assist gas pressure, it increases the cutting speed and improves quality because it removes easily the plasma and the molten material and cools the side walls. For economic reasons, compressed air at 5 bar is advised.

When computing the heat input and the specific energy required to remove a unit of material volume it can be seen that the specific energy decreases with the stone hardness (fig. 10), the focal length lens (fig. 11) and the laser beam power, but it increases with the plate thickness.

3.2 AWJ cutting

From the AWJ cutting trials conducted it was seen that depth of cut increases with water flow rate, water pressure and abrasive flow rate.

Maximum cutting speeds for the materials tested are listed in table 2 for an abrasive flow rate of 350 g/min at a water pressure of 340 Mpa.

Cut surface is clean in any case and roughness measured by Ra is lower than 20 μm (fig. 12) depending on the stone. This is due to the mechanism of cut involved in AWJ cutting of calcareous stones.

The AWJ develops a mechanical action on the stone exerting a force that is higher than its tensile strength. So, cutting is originated by wear of abrasive particles on the material and a rapid change of stress fields in the interaction area.

When observed under SEM, the cut surfaces in metamorphic stones like Rosa de Borba and Branco Pardais, show cleavage of calcitic grains, though some plastic deformation exists within the grains (fig. 13).

In Moca Creme, a soft porous rock with a high content of internal cracks, intergranular cracking was seen as well as cleavage through the harder constituents (fig. 14). No significative differences were observed in the morphology of cut between top and bottom faces.

4. CONCLUSIONS

- Cutting speeds are much higher when using AWJ than with laser which makes the former more attractive to industry;
- CO_2 laser cutting leads to poor quality surfaces with a cracked HAZ and dross, especially in calcitic marbles;
- Cutting by laser involves fusion and volatilisation with chemical degradation and decomposition of $CaCO_3$ and CaO;
- Metallic calcium was detected on the surface suggesting the temperature raises to about 3 000°C;
- Rock hardness affects the maximum cutting speed and the surface quality. Crystallinity of rock and chemical composition of calcite has a similar effect: dolomitic marbles present a higher ability for cutting and speed increases;
- Specific energy required to cut marble is in the order of magnitude of 10^7 J/cm^3 and it increases with rock hardness and thickness;
- Cutting by AWJ is achieved by a mechanical process involving cleavage of calcitic grains in metamorphic calcareous rock and intergranular cracking together with calcite cleavage in soft porous sedimentary calcareous stones;
- For the materials tested, AWJ produces cut surfaces of higher quality than laser.

5. ACKNOWLEDGEMENTS

The authors gratefully acknowledge Prof. T. J. Kim from the University of Rhode Island for his technical advice in the field of AWJ cutting. They would like also to thank JNICT and FLAD for their financial support and ISQ and IST for making available the necessary facilities to perform this investigation.

6. REFERENCES

- Basov, N. G., Bakradze, V. N., Glotov, E. P. , Danilychev, V. A., Meparishvili, G. V., Modebadze, O. E., Khachapnridze, T. S., Yugov, V. I., "Experimental study of the laser treatment of marble", *Sov. Phys. Dokl.*, 31(2), pg. 172-173, 1986.
- Miranda, R. M., Lousa, P., Mouraz Miranda, A. J., Kim, T., "Abrasive Water Jet Cutting of Portuguese Marbles", *Proc. of the 7th American Water Jet Conference*, pg. 443-457, Water Jet Technology Association, Seattle, 1993.
- Oliveira Santos, J. F., Quintino, L., Miranda, R. M., *"Processamento de materiais por feixe de electrões, laser e jacto de água"*, ed. ISQ, 1991 (in Portuguese).
- Pires, M. C., Teixeira, R. M., Rodrigues, F. C., "Studies on marble processed by laser", *Proc.of the Int. Conf. on Lasers*, St. Diego, 1991.

Table 1 - Maximum cutting speed for different focal length lenses (mm/min)

Focal length lens (mm)	**Moca Creme**	**Rosa de Borba**	**Branco Pardais**
127	400	275	275
190	460	275	275

Table 2 - Maximum cutting speed (mm/min) by AWJ in thickness of 10 and 20 mm
Abrasive fow rate = 350 g/min; Water pressure = 340 Mpa

Moca Creme		**Rosa de Borba**		**Branco Pardais**	
10 mm	20 mm	10 mm	20 mm	10 mm	20 mm
10 000	3 500	1 600	500	1 600	400

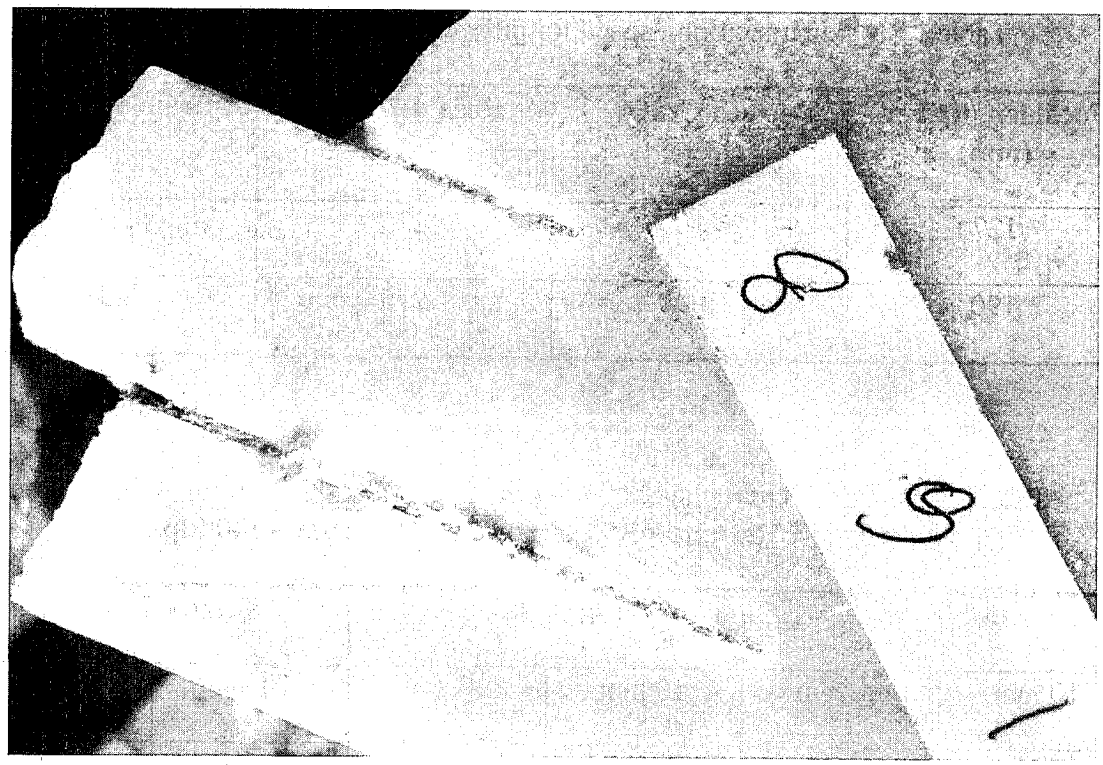

Fig. 1 - Photomicrograph of a bottom face of a CO_2 laser cut in Rosa de Borba

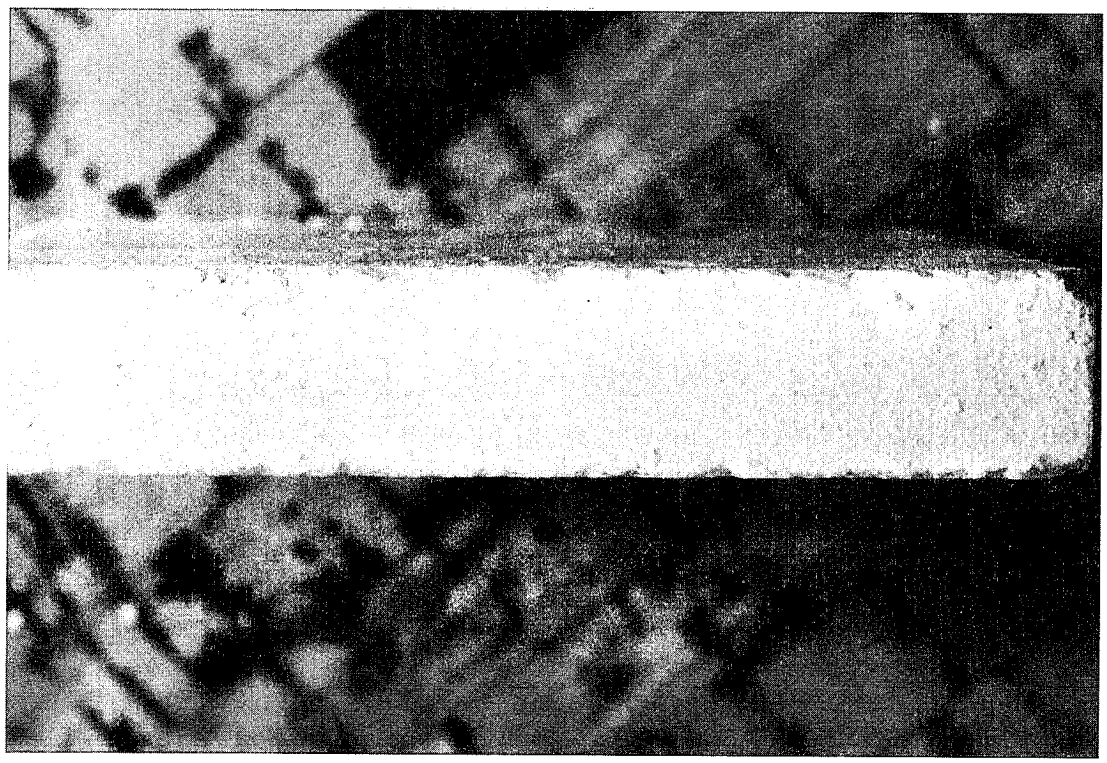

Fig. 2 - Photomicrograph of a laser cut surface

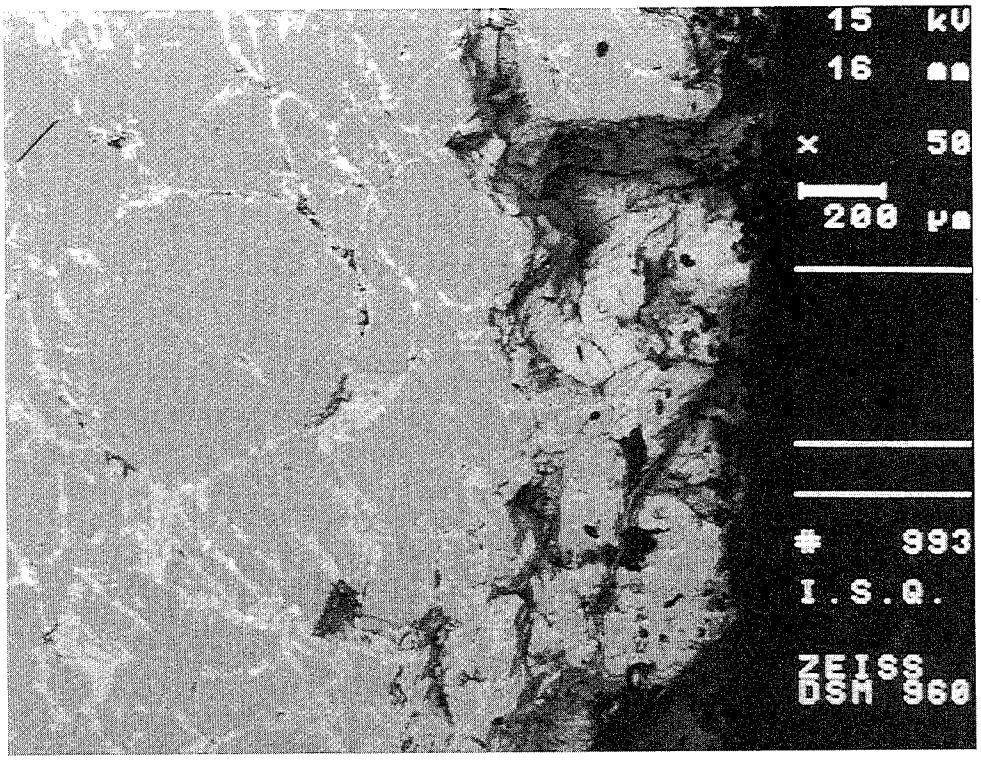

Fig. 3 - SEM photomicrograph of the HAZ of a cut surface

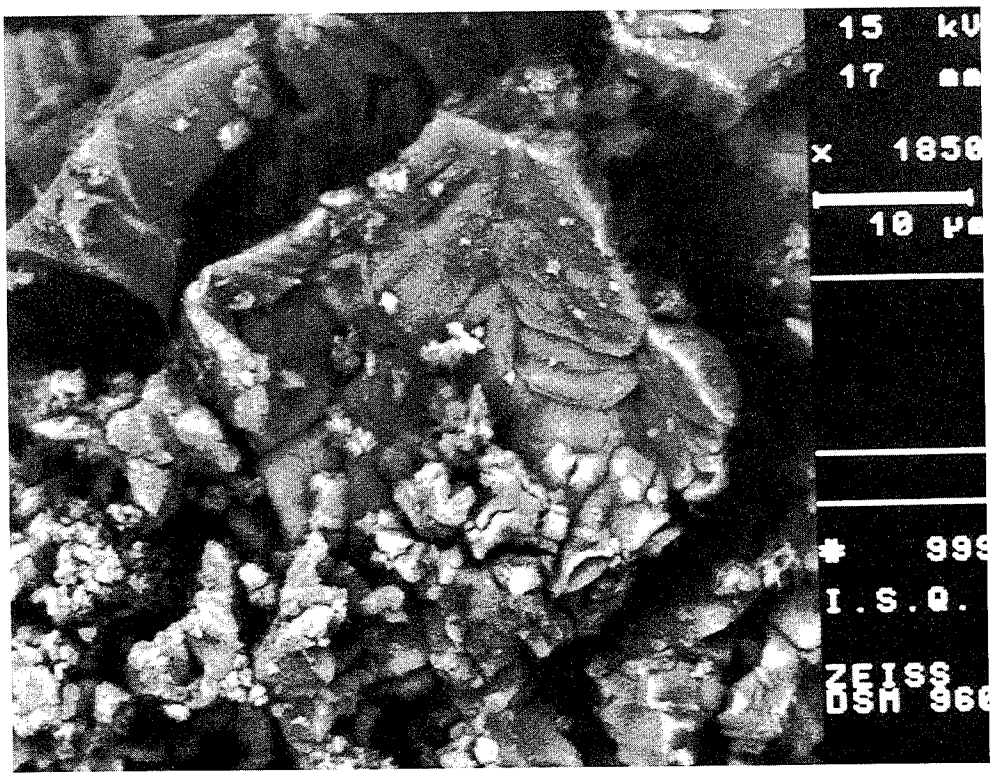

Fig. 4 - Cubic morphology of a Ca° crystal formed during CO_2 laser cutting of Branco Pardais

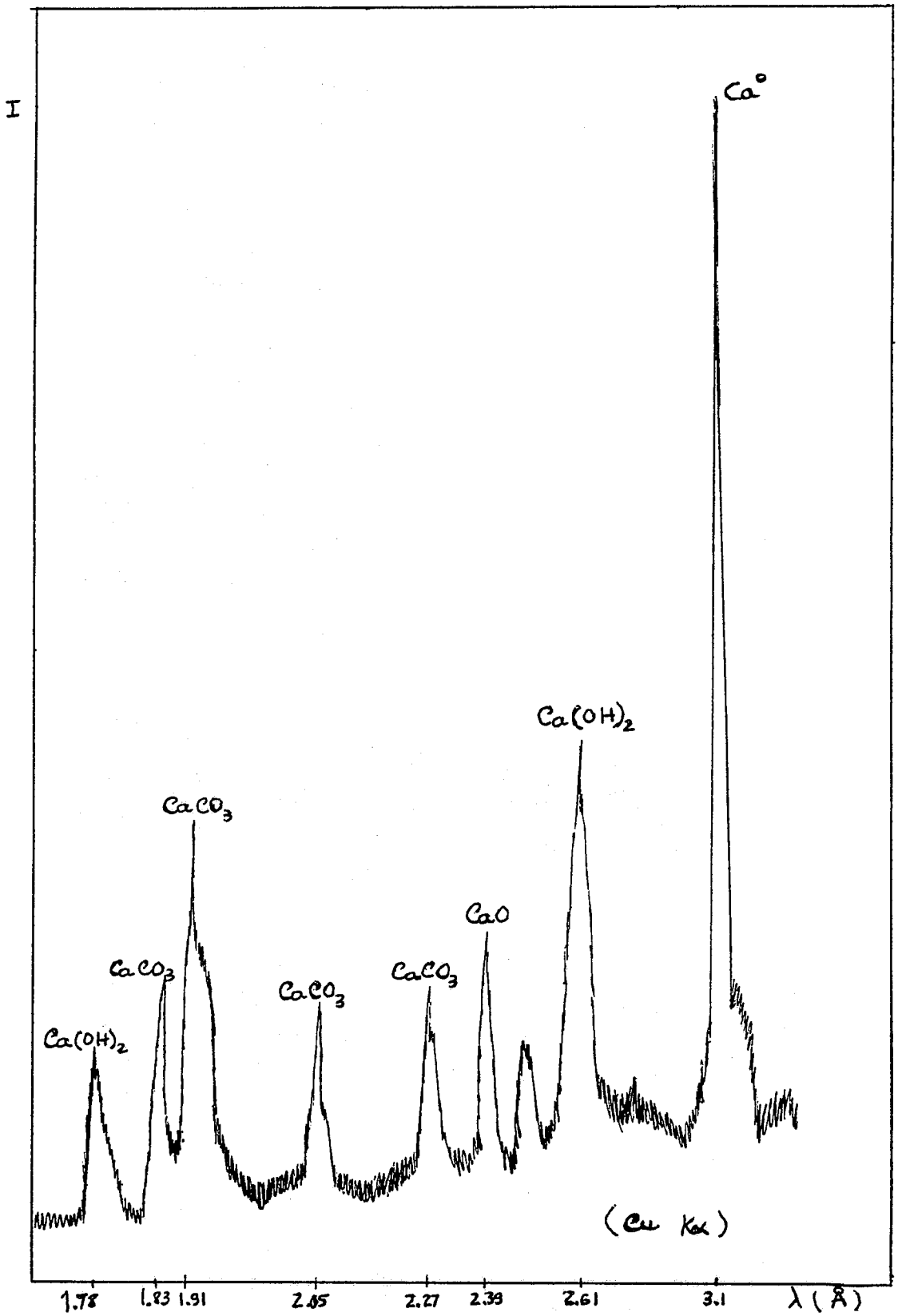

Fig. 5 - X-ray diffraction of powder collected on Rosa de Borba

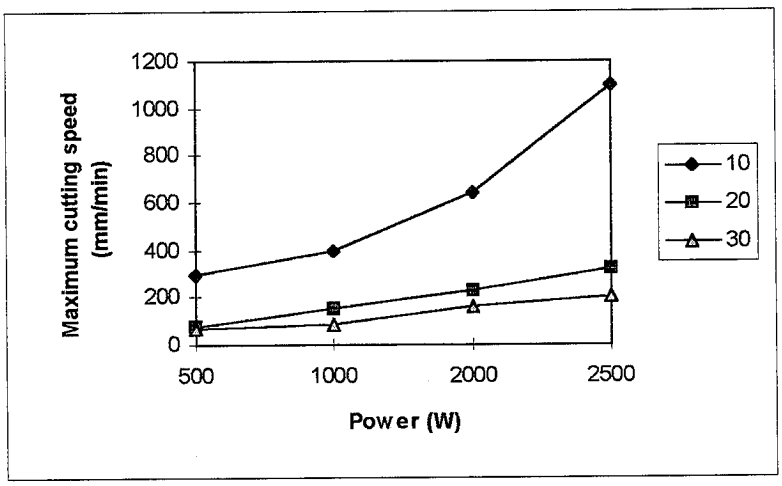

Fig. 6 - Maximum cutting speed vs. laser power for Moca Creme in different thicknesses
Focal length lens: 190 mm
Focal point position: -1 mm
Compressed air at 5 bar

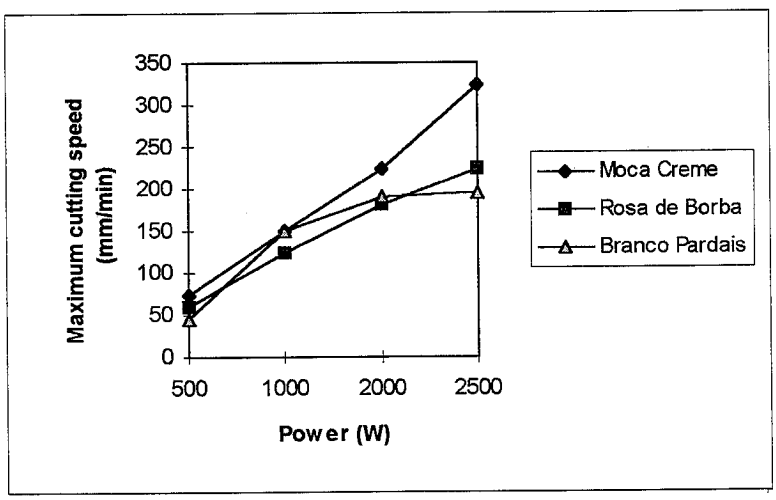

Fig. 7 - Maximum cutting speed vs. laser power for the tested stones
Thickness: 20 mm
Focal length lens: 190 mm
Focal point position: -1 mm
Compresed air at 5 bar

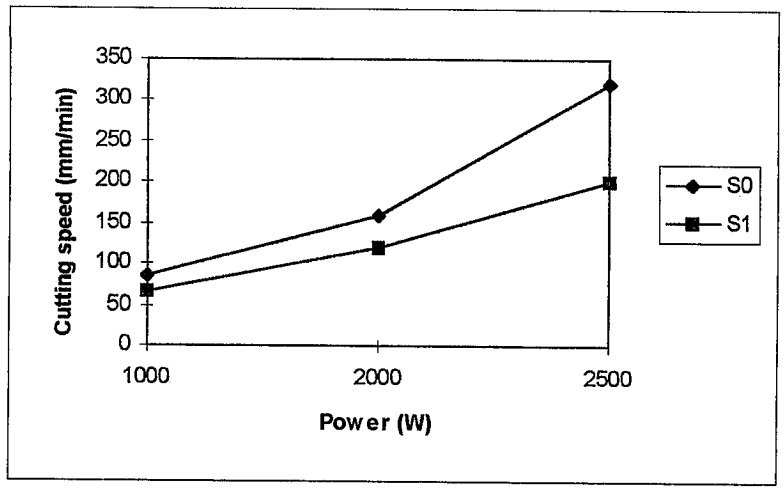

Fig. 8 - Cutting speed vs. sedimentation direction for Moca Creme
Thickness: 30 mm

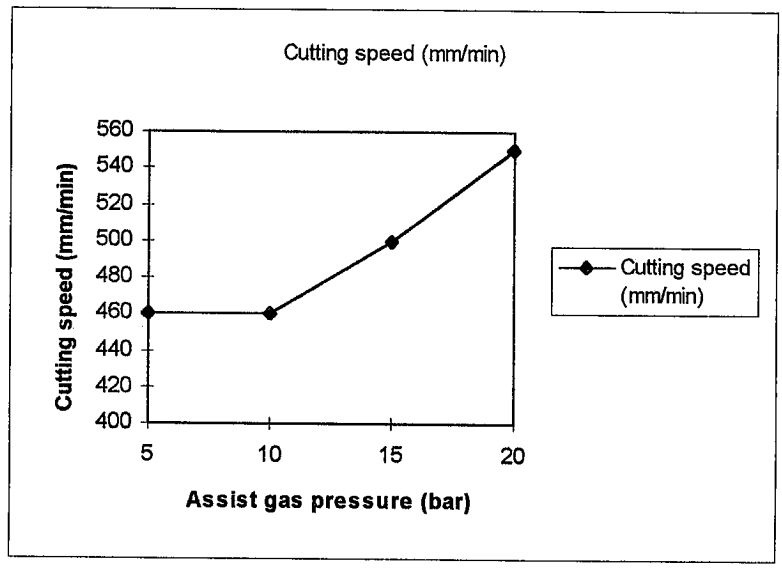

Fig. 9 - Cutting speed vs. assit gas pressure
Stone: Moca Creme, 8 mm thick
Power: 1000 W
Compressed air, 5 bar

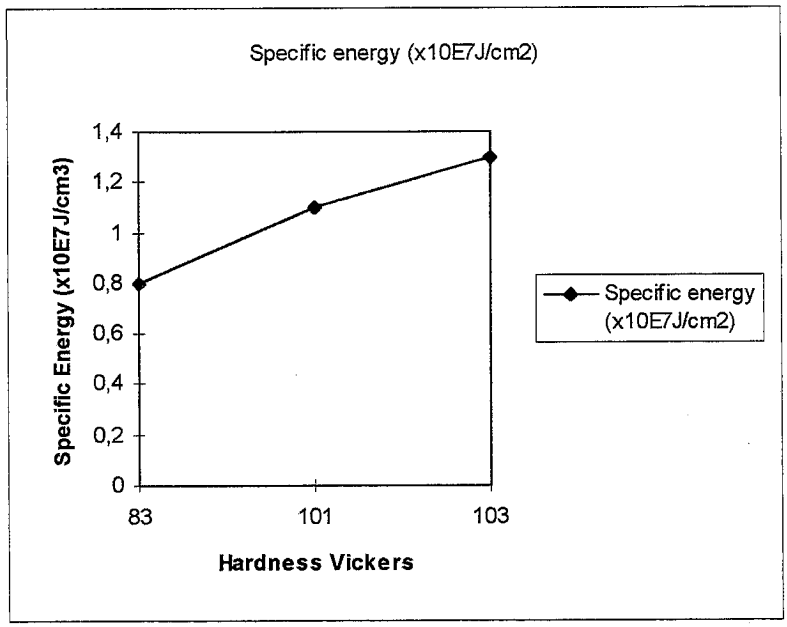

Fig. 10 - Specific energy for CO_2 laser cutting as a fuction of hardness
Moca Creme: 83 HV
Rosa de Borba: 101 HV
Branco Pardais: 103 HV

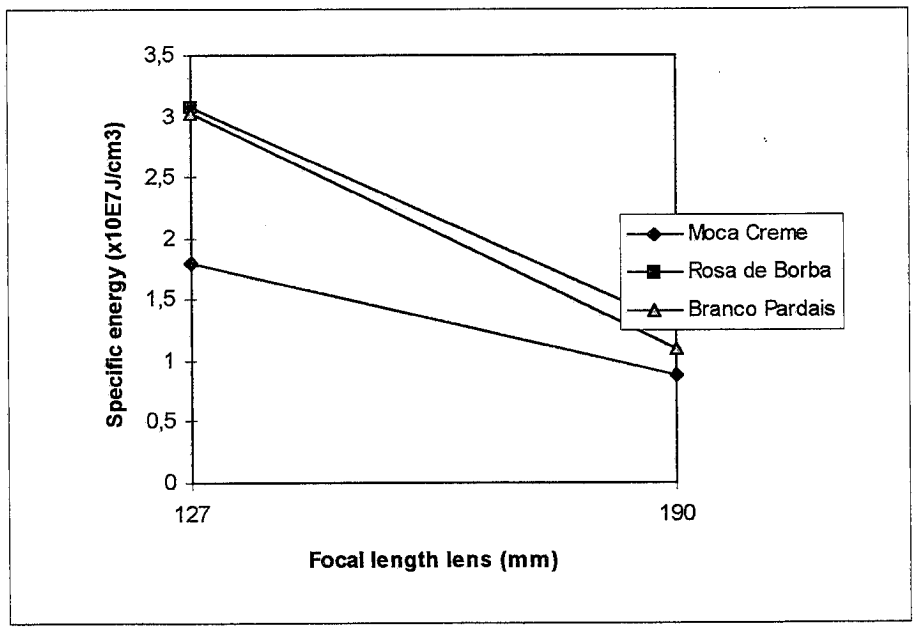

Fig. 11 - Specific energy for CO_2 laser cutting as a fuction of focal length lens

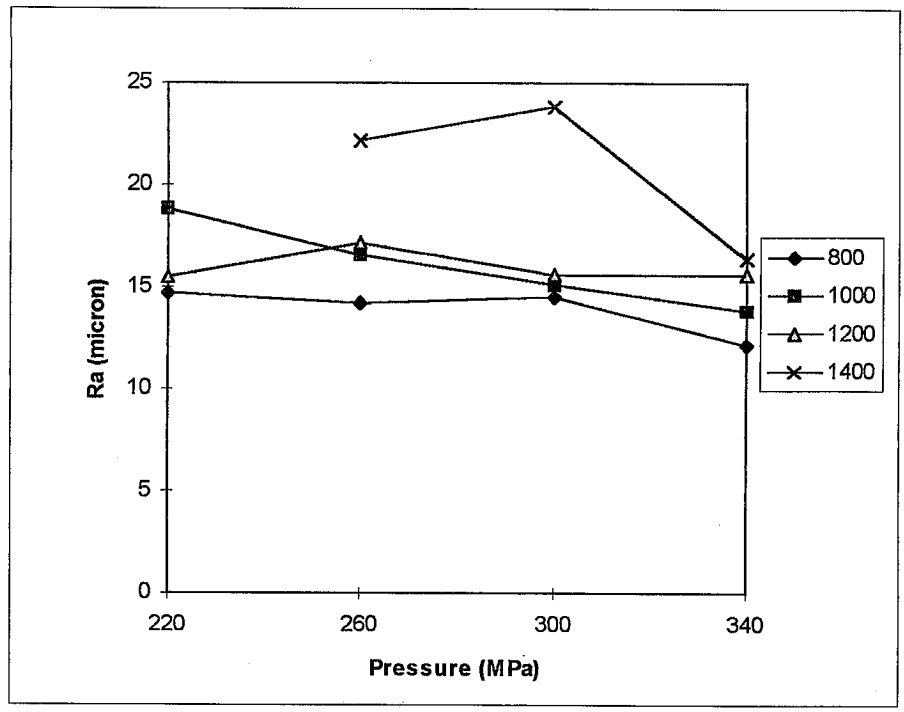

Fig. 12a - Ra as a function of water pressure for different cutting speeds (in mm/min) for Branco Pardais
Plate thickness: 10 mm
Abrasive flow rate: 300 g/min

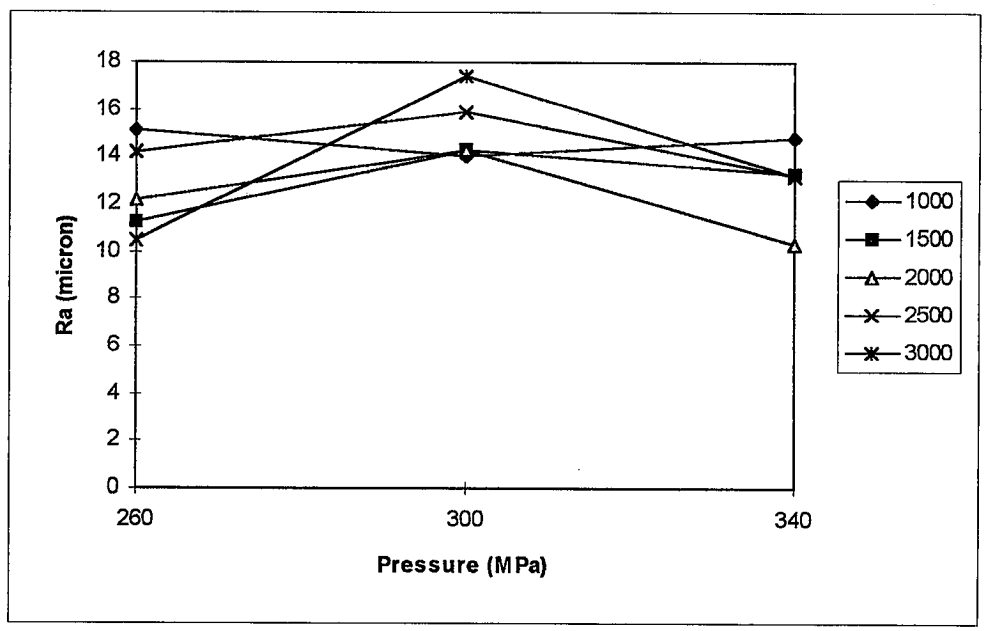

Fig 12b - Ra as a function of water pressure for different cutting speeds (in mm/min) for Moca Creme

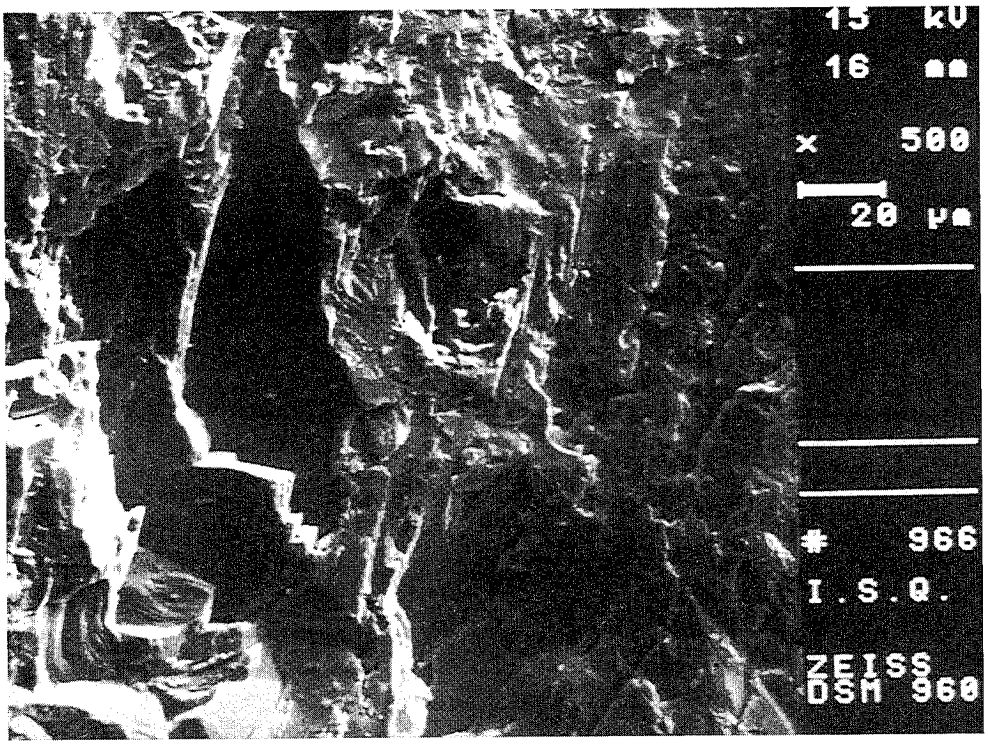

Fig. 13 - SEM photomicrograph of an AWJ cut surface in Rosa de Borba

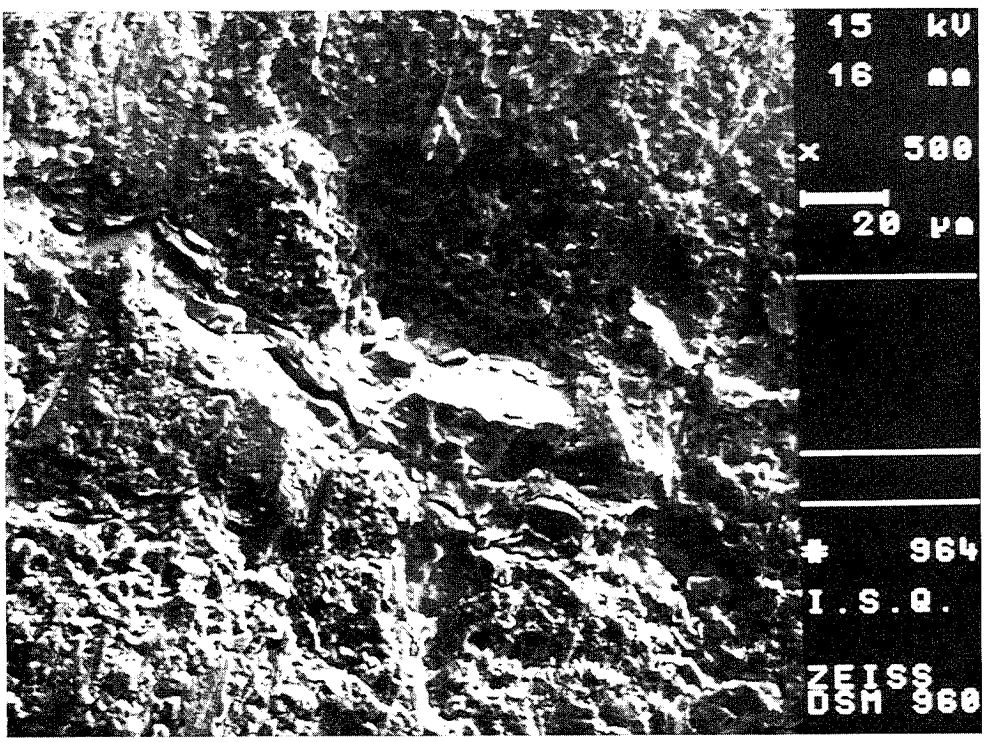

Fig. 14 - SEM photomicrograph of an AWJ cut surface in Moca Creme

8th American Water Jet Conference
August 26-29, 1995: Houston, Texas

Paper 48

NUMERICAL SIMULATION OF STRIATION FORMATIONS ON WATER JET CUTTING SURFACE

Y. Fukunishi, R. Kobayashi and K. Uchida
Tohoku University
Sendai, Japan

ABSTRACT

Numerical simulation is carried out in order to investigate the mechanism by which the striations are formed on the kerf surface in water jet cutting. In the two-dimensional computation, information on temporal movement of the cutting front is acquired and compared with the experimental data obtained by using video pictures in abrasive jet cutting. It is shown that the agreement is satisfactory. From the results of the two-dimensional computations, three-dimensional kerf surfaces are reconstructed. Statistical characteristics of the computed kerf surfaces are in good agreement with those of the real kerf surfaces. It is revealed that the random distribution of abrasive particles within the water jet stream is essential for the formation of the striations. It is shown that the present numerical simulation can be a useful tool for the future investigations to understand and to control the striations.

Organized and Sponsored by the Water Jet Technology Association.

1. INTRODUCTION

In recent years, water jet cutting technology is expanding its area of application to various fields of engineering. When this technology is applied to mechanical engineering field where high precision and smooth cutting surface is required, the striations which appear on the cutting surface becomes a big problem.

The striations were studied through experiments measuring the surface roughness of the specimen, such as Blickwedel et al.(1990) and Kobayashi et al.(1992), and by observation of the cutting process by pictures such as Hashish (1988) and Matsuyama et al. (1991). Kobayashi et al. (1992) showed that the pattern of striations is similar among specimen materials and its character depends mainly on the machining parameters of the jet.

In this study, first, the striation formation process was studied by taking video tape recordings and processing frame-by-frame images in the computer. Then numerical simulations were carried out and compared with the experimental data. It is shown that investigation through numerical simulations may lead us to better understanding of the mechanism by which the striations are formed.

2. VIDEO OBSERVATION OF THE CUTTING PROCESS

2.1 Experimental Setup

A schematic view of the experimental setup is shown in Fig. 1. Acrylic glass (plexiglass) was used as the specimen and video pictures were taken from the side to capture the grooving process. The recorded images were transferred to a computer database through video-capture board. The obtained image data were processed by the workstation and the cutting front curve was extracted from each image. Thus the frame-by-frame movement of the cutting front curve was obtained.

In the experiment, water nozzle of diameter d_w =0.25 mm, abrasive nozzle of diameter d_a=1.09 mm and #60 (particle diameter 250-300 μm) garnet abrasive grain were used. Abrasive feed rate Q was kept constant at Q =0.10 kg/min. The standoff distance from the abrasive nozzle and the specimen was 3 mm.

2.2 Cutting Process Observation and Roughness Measurement

In Fig. 2, locations of the cutting front curve measured every second are shown. Experiment was carried out at discharge pressure P = 100 MPa, nozzle traversing velocity V = 30 mm/min and only the region where distance h measured from the jet-entry-surface of the specimen is between 10 mm and 40 mm is shown in the figure. In the figure, it can be noticed that the cutting front moves at constant speed in the nozzle traversing direction while h is small. However, at large h, locations where several curves overlap can be noticed, indicating little movement of the cutting front for a certain period of time. The intermittent

movement of the cutting front at large h derives from the creation of steps which move downwards as time progresses, as reported by Hashish (1988) and Matsuyama et al.(1991).

Figure 3 shows the relation between the measured roughness R_z and the depth h. Roughness R_z is the difference between the average of the heights of the 5 highest peaks and the 5 lowest peaks as shown below.

$$R_z = \frac{1}{5}\sum_{i=1}^{5} P_i - \frac{1}{5}\sum_{i=1}^{5} V_i \tag{1}$$

It can be found that R_z is small while h is small but starts to increase from a certain depth h .

Figure 4 shows the result of a spectral analysis using Maximum Entropy Method (MEM). It can be found that the peak in the spectra becomes higher as the depth h increases, but the peak location remains the same. This result implies that the roughness in the kerf surface is periodic and the amplitude and the wavelength of the roughness increase with the increase in h.

3. NUMERICAL SIMULATION

3.1 Computational Method

Because it is clear from the experimental results that abrasive action contributes to most part of the machining capability of abrasive jet, only the action of the abrasive particles are taken into account in the computation. The wear caused by abrasive action can be divided into two parts, one is cutting wear and the other is deformation wear as shown in Fig. 5 (a) and (b). In the computation, it is assumed that the total wear W (movement of the surface) caused by each abrasive particle can be expressed by the following equation proposed by Bitter (1963).

$$W = \frac{M\, v_a^2 \cos^2\alpha}{2\,\beta} + \frac{M\, v_a^2 \sin^2\alpha}{2\,\varepsilon} \tag{2}$$

In the equation, M denotes the mass of the abrasive particle, v_a: particle velocity, α: collision angle, β: cutting wear constant and ε: deformation wear constant ($\beta/\varepsilon = 150$). Schematic picture of the process is shown in Fig. 5 (c).

The following assumptions are made in the computation: An abrasive particle makes an inelastic collision on the surface of the material, the coefficient of restriction on bounce being 0.8 (Fig. 6). The nozzle moves a small distance in the traversing direction each time after 30 abrasive particles are ejected from the nozzle (Fig. 7).

The effect of distribution of abrasive particles on the striation formation are tested. The case when particles are ejected in order are compared with the other case when abrasive particles are distributed randomly in the jet.

3.2 Movement of the Cutting Front

Figure 8 is a result of the computation. The distribution of abrasive particles is random. The curved lines represent the location of the cutting front for every 13 time steps (1.95 seconds). It can be found that the distance between the curves are nearly constant at small h, which is an indication of smooth movement of the cutting front. At larger h, the movement becomes intermittent. Creation of steps can be observed as shown in Fig. 9. These results obtained from the present numerical simulation are in good agreement with the experimental results.

Because more detailed data can be obtained in numerical simulations compared to the experiments where resolution of the video camera pictures very often becomes the limiting factor, more information on the movement of the cutting front was obtained. The starting location of the steps could be traced back up to the top.

3.3 Effect of the abrasive particle distribution

The effect of the abrasive particle distribution on the movement of the cutting front was examined. Figure 10 is the case when particles leave the nozzle in order. No creation of the step can be found in this case which is quite different from the result shown in Fig. 8 and the experiment (Fig. 2). This result reveals that the naturally random distribution of the abrasive particles is essential for the generation of steps which leads to the striations on the machined surface.

3.4 Roughness of the Machined Surface

The computational result shown in Fig. 8 shows that the motion of the cutting front is intermittent, sometimes slow and sometimes quick. It is not irrelevant to assume that at locations where the motion is slow, there will be more wear on the side walls, because the sidewalls will be exposed to the jet stream for a longer period of time. Based on this assumption, three-dimensional machined surface was reconstructed from the two-dimensional computation result, which is shown in Fig. 11. In Fig. 11, the amplitude of the roughness is enhanced 10 times.

In Fig. 12, surface facing to the right was shaded for comparison with the photograph of Fig. 13. Fig.13 is a photograph from Kobayashi et al.(1992) showing the machined surface of aluminum A1050. Parameters of the experiment are; water nozzle diameter d_w = 0.25 mm,

abrasive nozzle diameter d_a = 0.76 mm, discharge pressure P = 200 MPa, nozzle traversing velocity V = 20 mm/min and abrasive feeding rate Q = 0.1 kg/min. Parameters for the computations are adjusted to match the experiment. It can be found that the surface obtained by computation looks similar to the actual machined surface.

Figure 14 compares the roughness R_z of the computed surface and the real surface. Although the tendency of the two curves are similar, quantitative agreement is not enough.

Figure 15 compares the wavelength spectra of the surface roughness between computed and real surface. The location of the maximum wavelength is around 1 to 2 mm in both cases. However, overall shape of the spectra especially at long wavelength do not agree well.

4. CONCLUSIONS

Numerical simulation of abrasive jet cutting process has been carried out and was compared with the experimental data. The agreement was satisfactory.

It was found that the random distribution of abrasive particles was essential for the generation of striations on the machined surface.

Three-dimensional machined surface was reconstructed from the two-dimensional computational result. Small discrepancies were found in the roughness distribution and wavelength spectra. This may be the effect of not taking into account the oscillation of the jet perpendicular to the traversing direction at deep locations because the computation is two-dimensional.

5. REFERENCES

Bitter, J.G.A., "A Study of Erosion Phenomena Part 2," *Wear*, Vol. 6, pp. 169-190, 1963.

Blickwedel, H., Guo, N.S., Haferkamp, H. and Louis, H., "Prediction of Abrasive Jet Cutting Efficiency and Quality," *Proceedings of the 10th International Symposium in Jet Cutting Technology*, Paper No. L2, Amsterdam, Netherlands, 1990.

Hashish, M., "Visualization of the Abrasive-Waterjet Cutting Process," *Experimental Mechanics*, pp. 159-169, 1988.

Kobayashi, R., Fukunishi, Y. and Tsuda, M., "Striation Characteristics of Cutting Surfaces Formed by Abrasive Jet," *Proceedings of the 8th Annual Meetings of Water Jet Technology Society of Japan*, pp. 26-35, 1992 (in Japanese).

Kobayashi, R., "Critical Review of Basic Research in Jet Cutting Technology," *Journal of the Water Jet Technology Society of Japan*, Vol. 10, No. 3, pp. 3-20, 1993 (in Japanese), and also *the Proceedings of the 3rd Pacific Rim International Conference on Water Jet Technology*, Invited Paper, Tainan, Taiwan, 1992.

Matsuyama, K., Nishiguchi, K. and Aokura, I., "A study on Ploughing Phenomena of Cutting Front in Abrasive Water Jet Cutting," *Proceedings of the 7th Annual Meetings of Water Jet Technology Society of Japan*, pp. 37-48, 1991 (in Japanese).

6. NOMENCLATURE

d_w	Water nozzle diameter
d_a	Abrasive nozzle diameter
Q	Abrasive feed rate
P	Nozzle discharge pressure
V	Nozzle traversing speed
R_z	Roughness
h	Depth from the top of the specimen
H	Average kerf depth
M	Mass of the abrasive particle
v_a	Particle velocity
α	Particle collision angle
β	Cutting wear constant
ε	Deformation wear constant

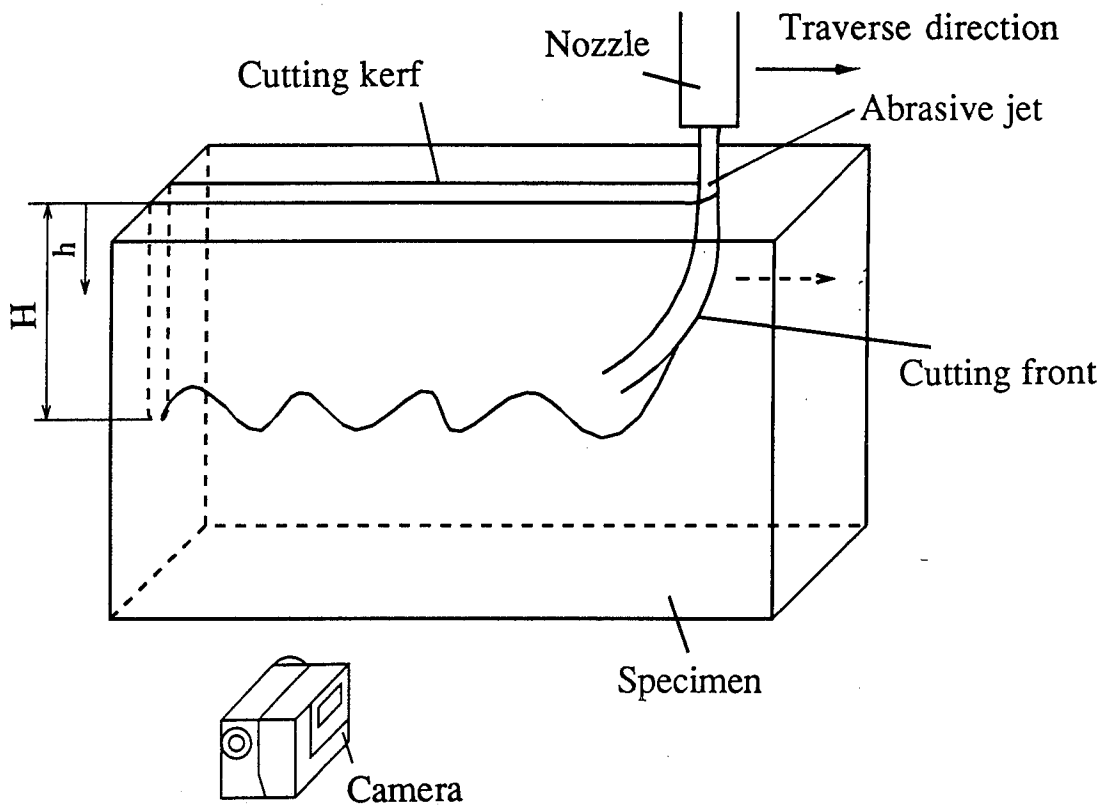

Figure 1. Schematic View of the Experimental Setup.

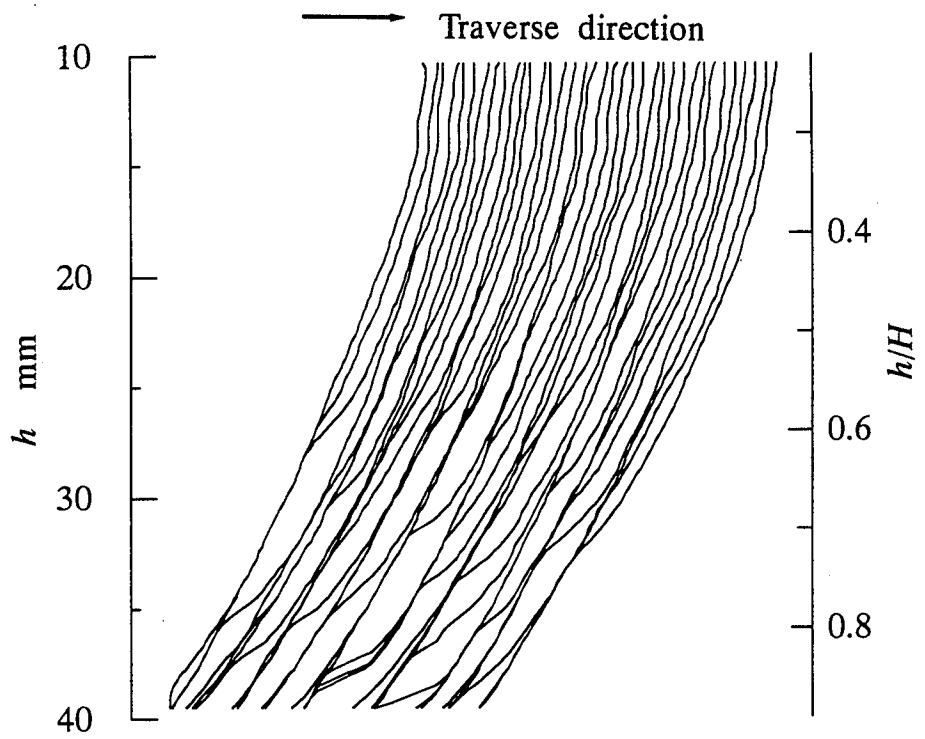

Figure 2. Time Development of the Cutting Front. (Experiment). Every Second, P =100 MPa, V = 30 mm/min, H = 45 mm.

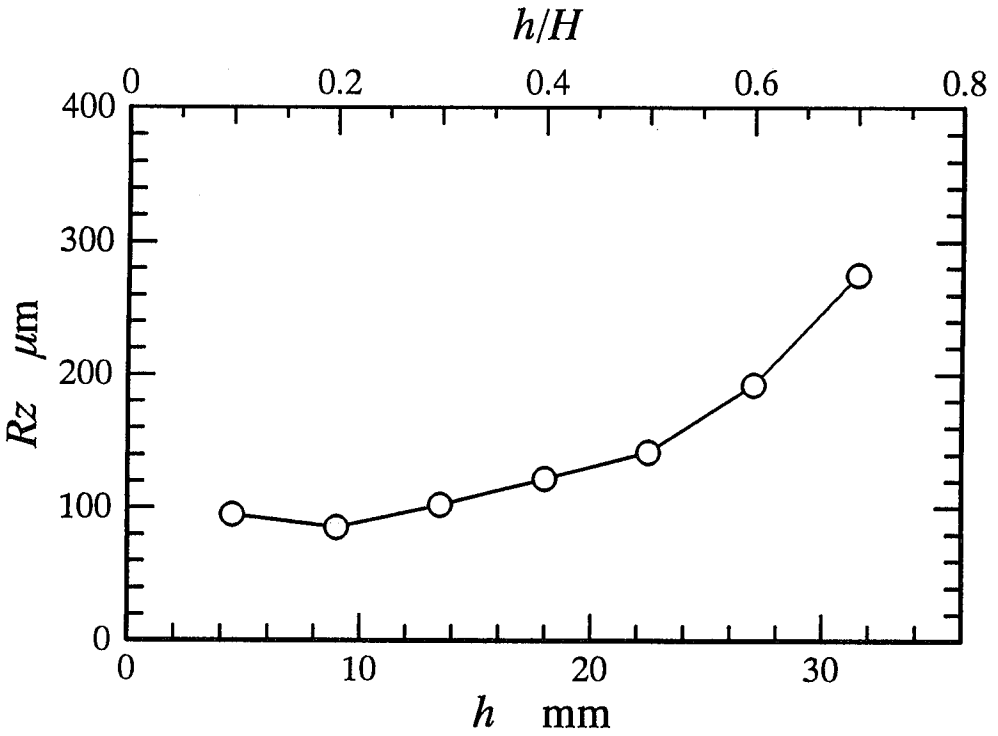

Figure 3. Roughness R_z as a Function of Depth h.
P =100 MPa, V = 30 mm/min, H = 45 mm.

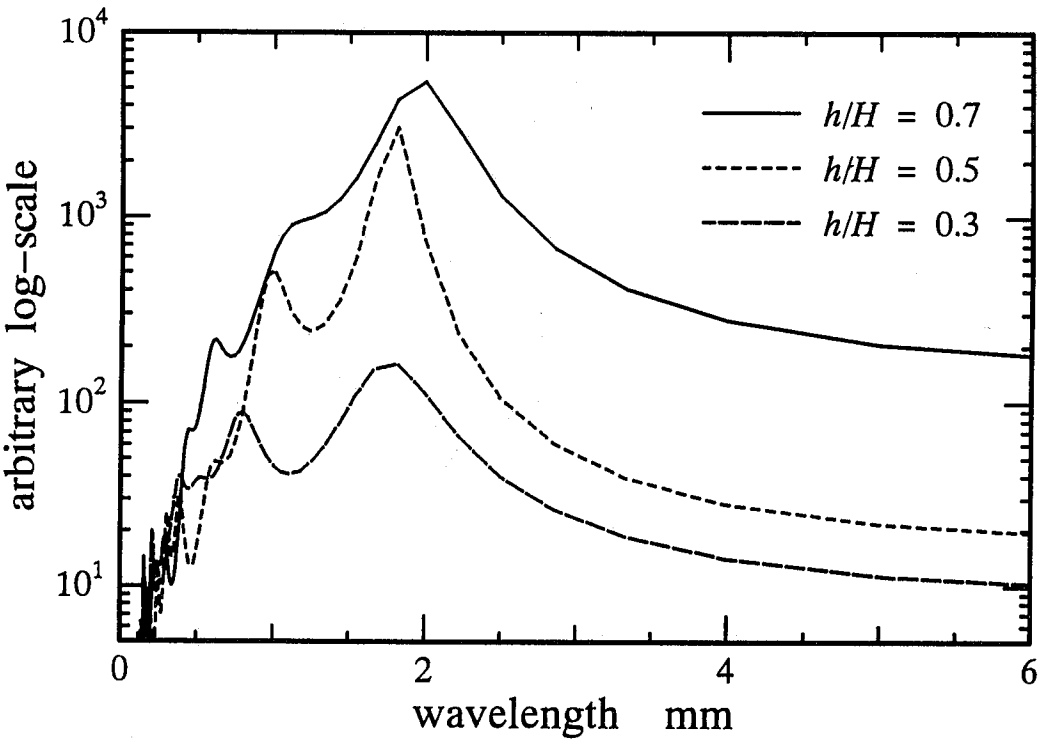

Figure 4. Spectrum of Surface Waviness.
P =100 MPa, V = 30 mm/min, H = 45 mm.

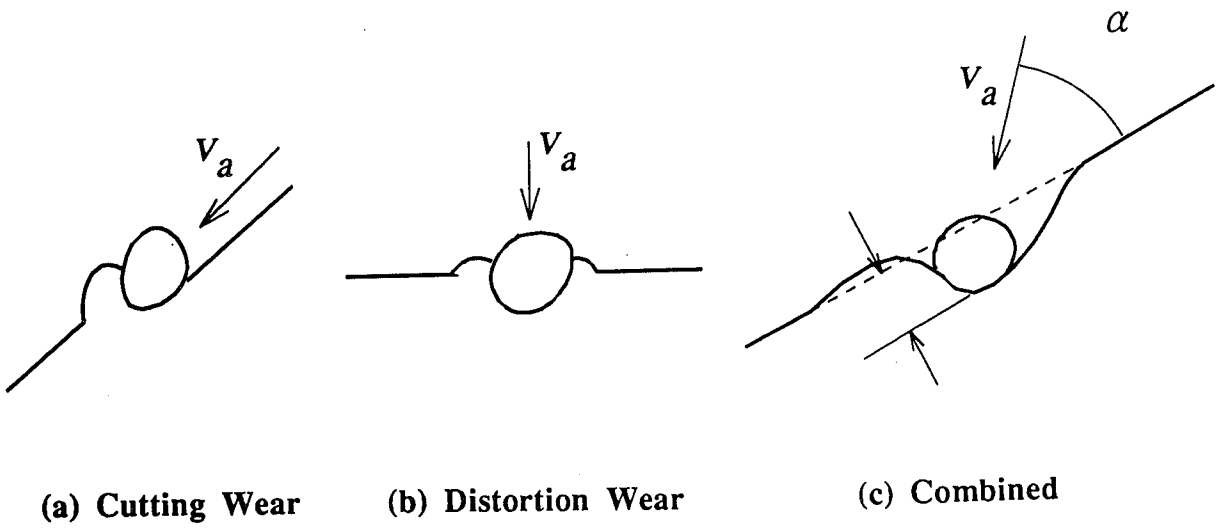

(a) Cutting Wear **(b) Distortion Wear** **(c) Combined**

Figure 5. Schematic Figure of the Wear Process.

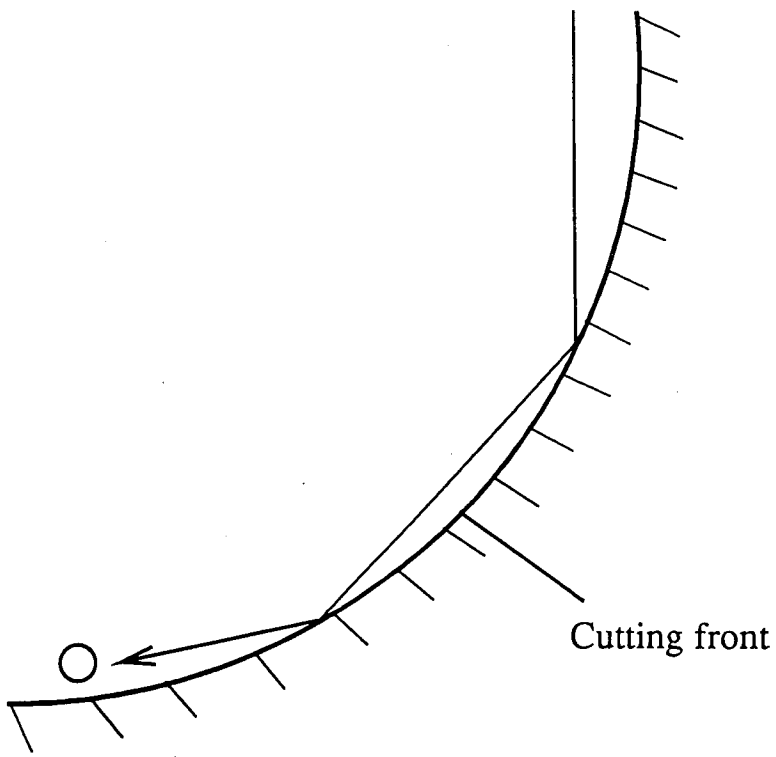

Figure 6. Schematic Figure of the Particle Path.

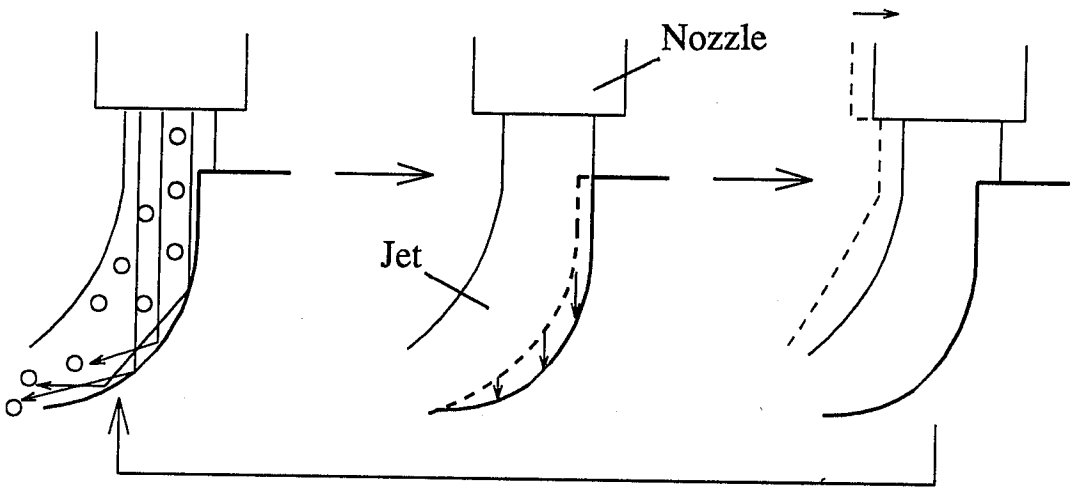

Figure 7. Schematic Figure of the Computational Step.

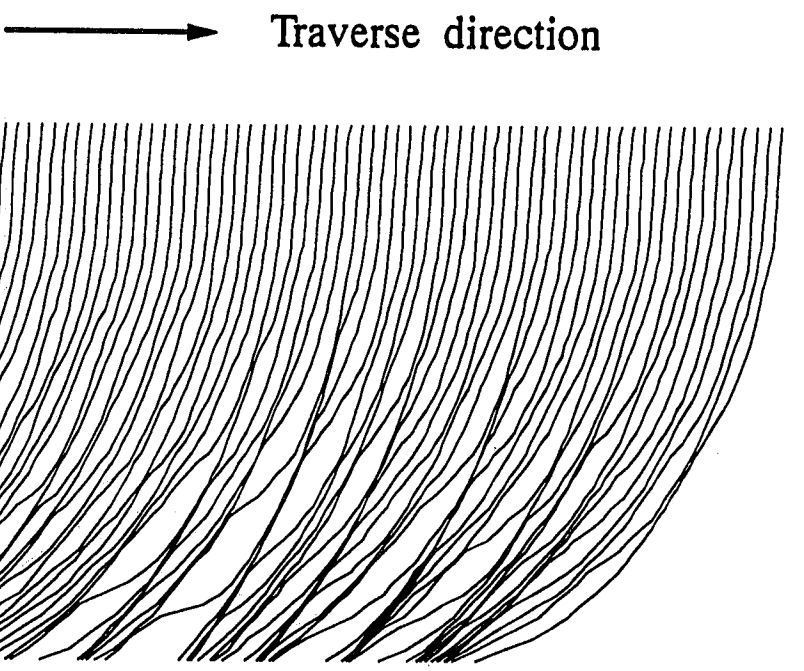

Figure 8. Time Development of the Cutting Front. (Computation).

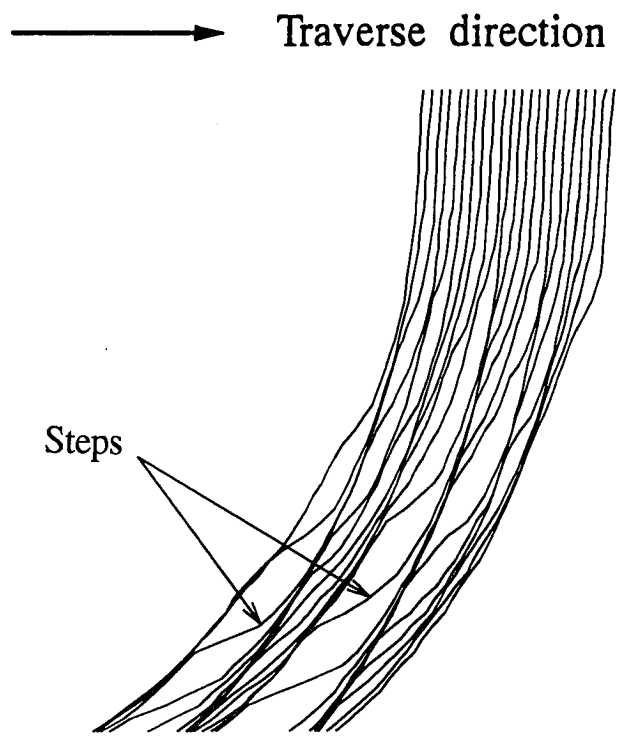

Figure 9. Close Up View Showing the Steps. (Computation).

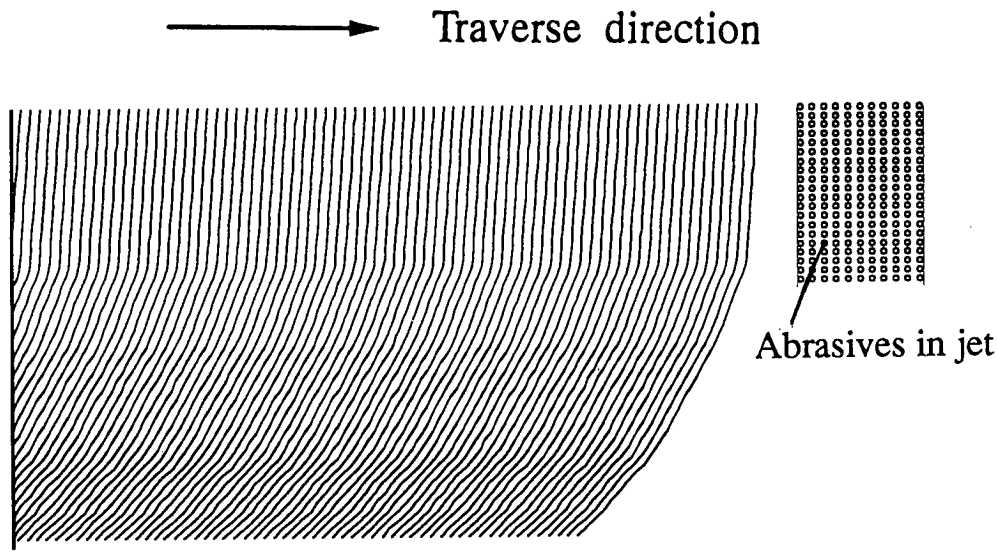

Figure 10. Time Development of the Cutting Front when Abrasive Particles are Ejected in Order. (Computation).

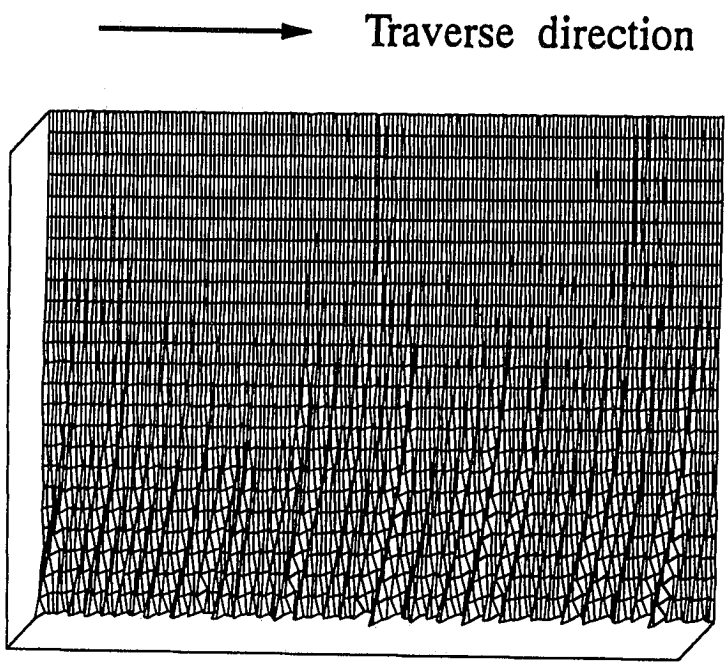

Figure 11. Machined Surface with Striation. (Computation).

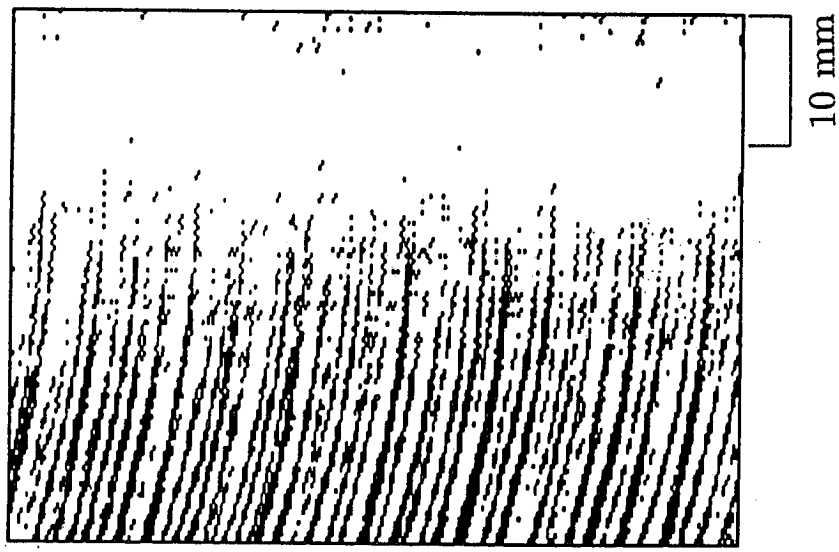

Figure 12. Machined Surface with Striation. (Computation).

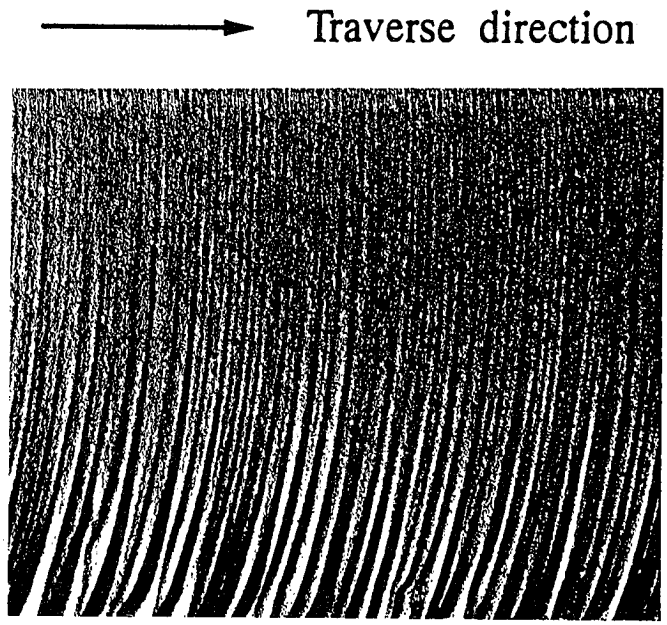

Figure 13. Photograph of a Machined Surface. (Experiment).

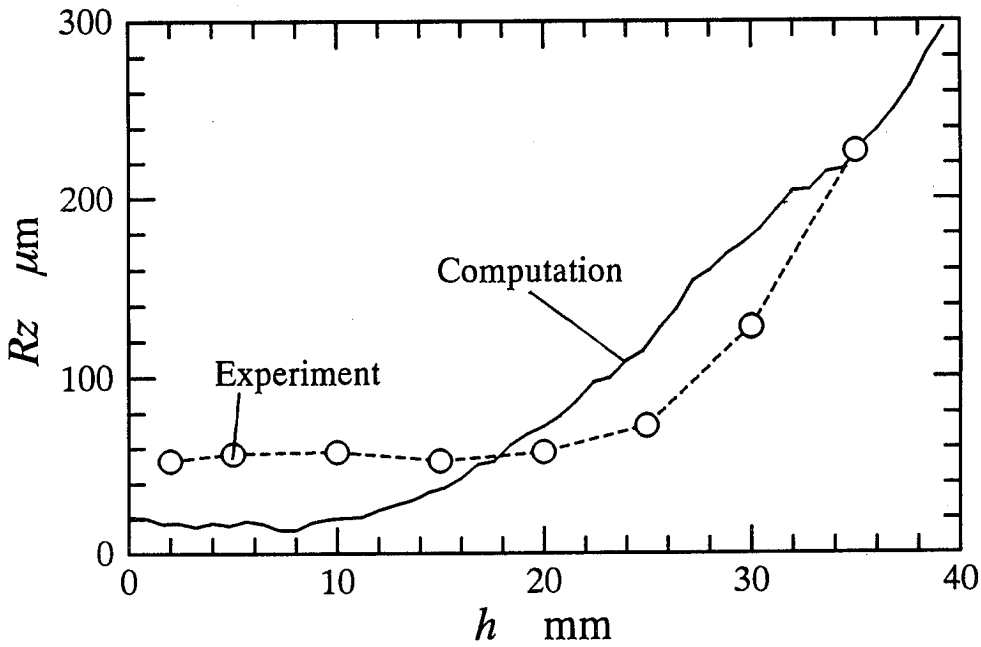

Figure 14. Comparison of Roughness R_z as a Function of h between Computational Result and Experiment.

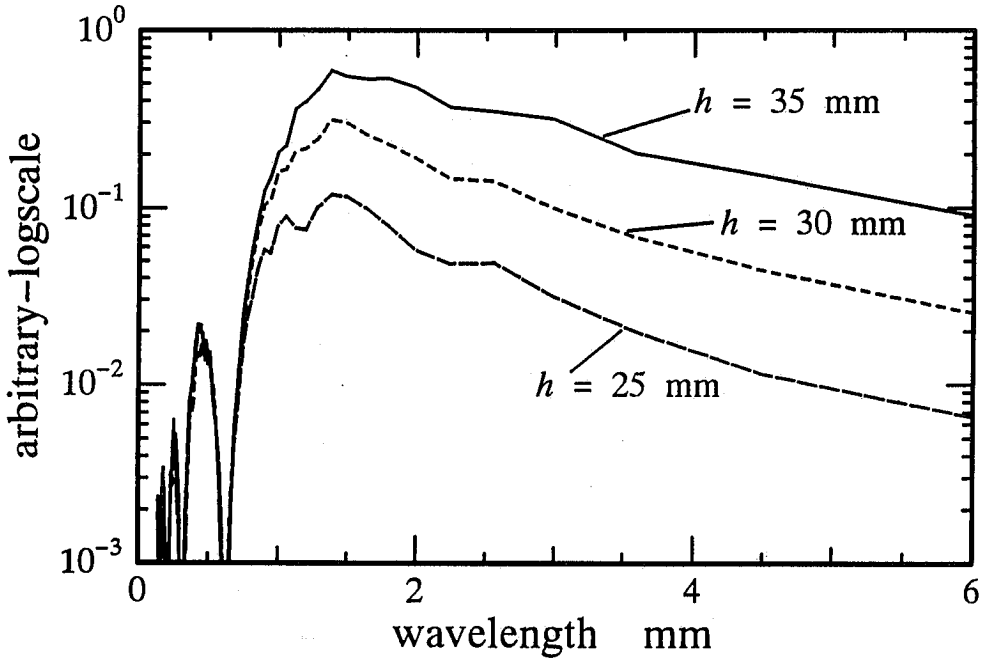

(a) Computational Result

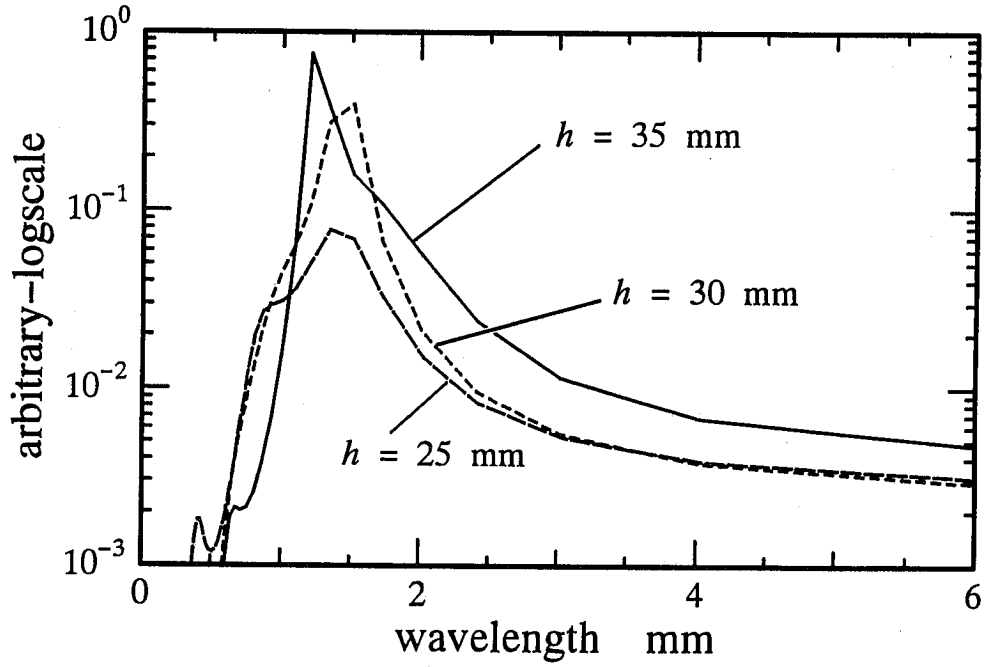

(b) Experiment (Kobayashi et al., 1992)

Figure 15. Comparison of Roughness Spectra between (a) Computational Result and (b) Experiment.

8th American Water Jet Conference
August 26-29, 1995: Houston, Texas

Paper 49

DEVELOPMENT OF ICE JET MACHINING TECHNOLOGY

F. Li, E.S. Geskin, L. Tismenetskiy
Laboratory of Waterjet Machining
Department of Mechanical Engineering
New Jersey Institute of Technology
Newark, NJ 07102, USA

ABSTRACT

Our previous experiments demonstrated the effectiveness of the use of ice particles as a substitute for abrasives. The ice was injected in the water stream via the port for abrasive supply. Experiments, reported in this paper, involved formation of ice particles within the water flow. Water was cooled prior to the booster pump, the nozzle body was inserted in the cooling media and a coolant was injected in the water stream via the port for abrasive supply. At these conditions the ice particles were generated in the water stream. The presence of these particles was demonstrated by the ability of the jet to carry out material removal operations. No surface modification due to water impingement was observed without cooling. The performed experiments demonstrate the feasibility of ice jet formation by cooling a stream of compressed water as well as feasibility of the use of ice jet for machining operations.

Organized and Sponsored by the Water Jet Technology Association.

1. INTRODUCTION

Thermodynamic analysis of material removal and common sense indicate that an ideal tool for material shaping is a high energy beam, having infinitely small cross-section, precisely controlled depth and direction of penetration and no effect on the generated subsurface. The production of the beam should be relatively inexpensive and environmentally sound while the material removal rate should be reasonable high and exceeding the rates of existing material removal techniques. No such beam currently exists. A narrow stream of high energy water, so called waterjet (WJ), comes close to meeting above requirements.

The principal shortcoming of WJ is the low efficiency of the energy transfer between the jet and the workpiece. This results in low productivity. More important, WJ can be applied to machining of comparatively soft materials only. The energy transfer and subsequently the mode of material removal change dramatically by addition of abrasive particles into the water stream. The abrasive waterjet (AWJ) generated as the result of such an addition enables us to machine practically any engineering material. The rate of removal of "hard-to-machine materials" by the use of AWJ is comparative if not superior to other material removal processes. Because of its capability AWJ in a comparatively short time became one of leading machining technologies.

However, AWJ is a mixture of water and particles and this imposes a number of limitations and inconveniences. The energy efficiency of AWJ is still low, although acceptable, mixing of the water and particles imposes a severe limitation on the minimal usable jet diameter, special provisions are required for particles supply and disposal, the addition of abrasive particles increases the cost of processing and its environmental impact.

It would be highly desirable to enhance the productivity of WJ and yet avoid the use of abrasives. This objective can be achieved by replacement of abrasives by ice particles and formation of ice-jet (IJ). The hardness of ice is less than that of the hard abrasives used in conventional AWJ, so IJ can be not that productive as AWJ. However, cost reduction and termination of the negative environmental effects overweight the reduction of the productivity. Most important is the feasibility of the use of IJ for shaping of material in food, electronic, space and other branches of industry where any contamination in the course of processing is impossible. One of the potential applications of IJ is medicine.

IJ can be formed by addition of ice particles into the water stream in a way similar to the abrasive supply. In this case the particles supply system is lightly modified to prevent ice melting, The shortcoming of this system is the necessity to mix ice and water, thus the jet diameter is similar to that of AWJ. This kind of IJ can be used for grinding and shaping of a wide variety of clean materials when the jet diameter of 500 plus micron is acceptable. If the jet diameter should be less than 500 microns, IJ should be formed by the partial freezing of the water during and after acceleration. Thermodynamics of ice formation at a high pressure (Figure 1) allows us to reduce water temperature far below 0^0 C without freezing. For example, at 320 MPa the liquid water exists at -25^0 C indicated by Hobbs. However, ice formation in the course of the isoenthalpic expansion of supercooled water is a complex process. Water enthalpy is reduced during water acceleration in the nozzle, while friction

results in the enthalpy generation. Water temperature increased due to isoenthalpic decompression (Jole-Thompson effect). Most probably, an additional heat removal is needed in order to assure ice generation at an adequate rate. This can be accomplished by heat exchange between the water stream and low temperature medium, such as liquid nitrogen or solid CO_2.

Previous studies of IJ reported by Truchot et al. (1992) and Galeck and Vickers (1982) involved the examination of the both approaches, stream freezing and ice particles supply into the stream. It was reported that addition of ice particles into WJ improves cutting of soft materials, that is the materials which can be cut by a conventional WJ. Because feasibility of IJ machining of hard materials was not explored, our first task was to determine the feasibility and effectiveness of the use of ice particles as a tool for sharing hard materials, such as metals and composites.

2. EXPERIMENTAL PROCEDURE

The preliminary experiments involved cooling of the compressed water prior to the water nozzle. Cooling was accomplished by submerging of the supply pipe into the liquid nitrogen bath and resulted in the improvement of WJ performance. Results of this study were reported by Geskin et al (1995). The further research involved water solidification after the exit from the orifice. The set up was modified to enhance heat removal from the stream and to provide the nuclei for solidification. The modified set up is shown in Figure 2. Dry ice was supplied in the water tank prior to the booster pump. By this way we accomplished reduction of water temperature. In addition , CO_2 bubbles formed at the orifice exit form the solidification nuclei. Water containing the dissolved CO_2 was compressed. After the safety valve and at the immediate vicinity of the nozzle was installed cooling tank 1. This tank was filled with a coolant surrounding a high pressure coil containing compressed water. The coolant consisted of the mixture of car coolant, city water and dry ice. After the cooling tank 1 compressed water was directed to the nozzle. Ingersoll Rand abrasive cutting head was used for the stream formation> The head was submerged into cooling tank 2, filled by dry ice. The major source of cooling was liquid nitrogen supplied into cutting head via abrasive port. A workpiece was installed at a X-Y table located beneath of the nozzle.

Because of this cooling media in both tanks as well as liquid nitrogen in the nozzle body were supplied only after valve was open and compressed water flowed through the system. This prevented water freezing in the coil. However the preliminary tests showed that the cooling power of the system is not sufficient. The adequate cooling was attained only at the orifice diameter of 75 micron (3 mils) and water pressure of 68 Mpa (10,000 psi). At these conditions water flow rate was 0.036 lit/min. It is the minimal possible flowrate of water attainable at our system. The focusing tube diameter was equal to 0.5 mm at the length of 5 mm.

The stream momentum at the conditions above was extremely weak. Jet exiting from the focusing tube did not effect a solid surface in the course of impingement. However, when coolants were supplied in both tanks and in the nozzle penetrative effect of the jet increased

dramatically. The jet acquired the feature of AWJ. This indicates that the flow contained ice particles. The presence of ice was observed only if all four cooling media (dry ice in the water tank, two cooling tanks and liquid nitrogen) were used and dissolved CO_2 provided solidification nuclei. At the absence of any of the factors above no increase in penetrating jet ability, that is no ice formation, occurs.

The temperature distribution in the system at pressure of 68 Mpa (10,000 psi) and Orifice diameter of 75 micron is shown at Figure 3. The temperature was measured by thermocouple inserted in the water at points 1 and 2 and attached to pipe surface at points 3, 4 and 5. Thus T3, T4 and T5 only indirectly indicate temperature of the water. Actual water temperature is unknown.

The jet exiting from the cooled system was used for machining of metal and glass samples. At this stage the samples were guided manually and the traverse rate and stand off distance were estimated visually. The feasibility of material removal by the jet demonstrated the formation of ice particles and it also enabled us to evaluate machining potential of IJ.

3. EXPERIMENTAL RESULTS AND DISCUSSION

The tests of icejet machining included cleaning, drilling and milling operations. Figure 4 shows the removal of the rust deposit from a carbon steel. The traverse rate (estimated) was 0.65 m/min and stand off distance was 7.5 cm. The complete rust removal was attained. The removal of epoxy paint from the grinded surface of a carbon sample is shown in Figure 5. Traverse rate was 0.4 m/min and stand off distance was 5 cm. Again, complete deposit removal was achieved.

Figure 6 depicts icejet drilling of aluminum sample. Process was carried at stand off distance of 2.5 cm during 2 min. The depth of the penetration was 3 mm. The shape of the hole was almost circular. The hole was surrounded by a ring of dimples. Drilling of a plexiglass sample is shown in Figure 7. Drilling was carried out during 3 sec at the stand off distance of 3 cm. The cavity of an irregular form was formed. The depth of cavity was equal to 2 mm.

Figure 8 shows the milling of a wood sample at the travel speed of 1.25 m/min at the stand of distance of 6-7 cm. The depth of the grove was 2 mm and the width was 1.2 cm. The width of the jet exiting the focusing tube was 0.5 mm. Milling of a plastic plate is shown in Figure 9. Travel speed during the test was 0.25 m/min at the stand off distance 1.5 cm. After 3 passes the depth of the groove was 1.2 cm. The width of a V-shaped groove was 1 cm.

The machining experiments were carried 3 times. The duration of each of the experiment was about 2 hours. The results of the observation were consistent.

4. CONCLUDING REMARKS

The performed experiments evidently demonstrate the feasibility to generate ice particles within a high speed water flow if adequate rate of heat removal is assured. More important, the effectiveness of machining by the use of water-ice mixture is shown. The extremely low water speed and irregular shape and size of ice particles reduced machining potential of the stream. Still visible material removal by the cooled jet was consistently observed. No surface modification occurred without water cooling. Increase of the rate of cooling will increase the water velocity, amount of the generated particle and particles size. It is expected that then actual machining of hard materials will become possible. The next stage of our project will include such improvements. However, even at existing conditions the effectiveness of the material cleaning by ice jet is evidently demonstrated.

5. ACKNOWLEDGMENT

This study is supported by NSF grants DDM9315758 and DDM931280. The authors also express their appreciation to Dr. E. Gordon for assistance in the initiation of this work.

6. REFERENCES

Hobbs, Peter V., *Ice Physics*, Clarendon Press, Oxford, 1974.

Truchot, P., Mellinger, P., and Duchamp, P., "Development of Cryogenic Waterjet Technique for Biomaterial Processing Applications," *Processions of 6th Water Jet Technology Conference*, pp.473-480, Houston, USA, Sept. 1992.

Galeck, I. and Vickers, G. W., "The Development of Ice Blasting for Surface Cleaning," *Proceedings of 6th International Symposium on Jet Cutting Technology,* pp. 59-80, BHRA, The Fluid Engineering Center, April, 1982.

E.S. Geskin, L. Tismenetskiy, E. Bakhromi, F. Li "Investigation of Ice Jet Machining," *International Symposium of Electric Machining* pp. 833-890, Lausanne, Switzerland, April, 1995.

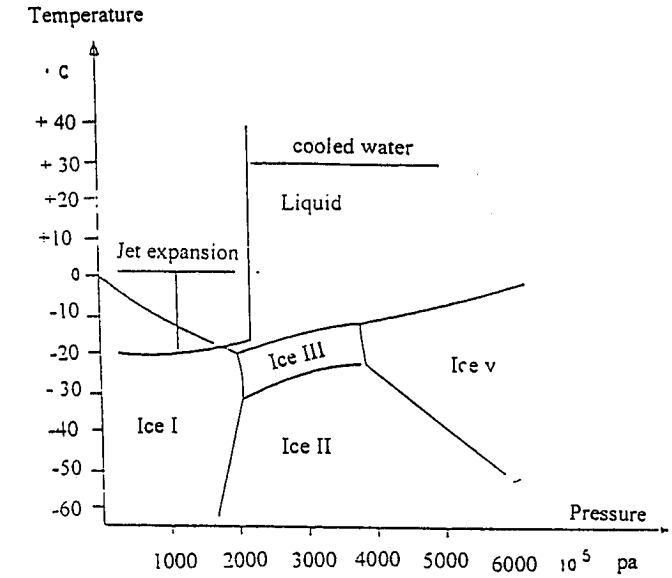

Ice crystallization by expansion

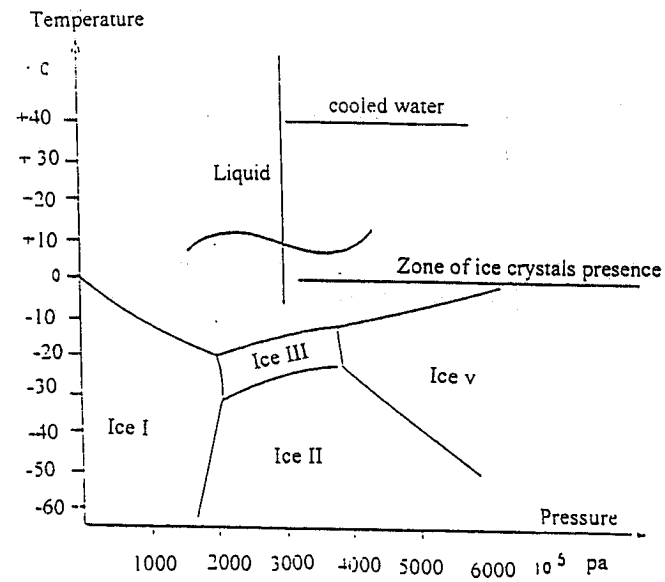

Ice crystals injection

Figure 1. Thermodynamics of Water Freezing

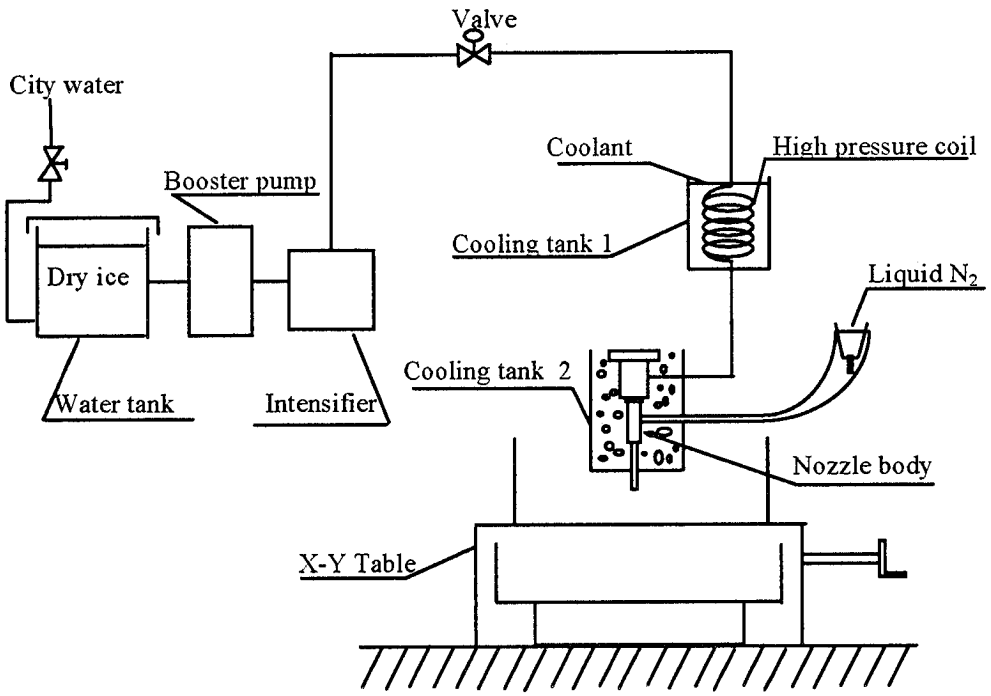

Figure 2. Schematic of Experimental Setup for Study of Ice Jet Machining

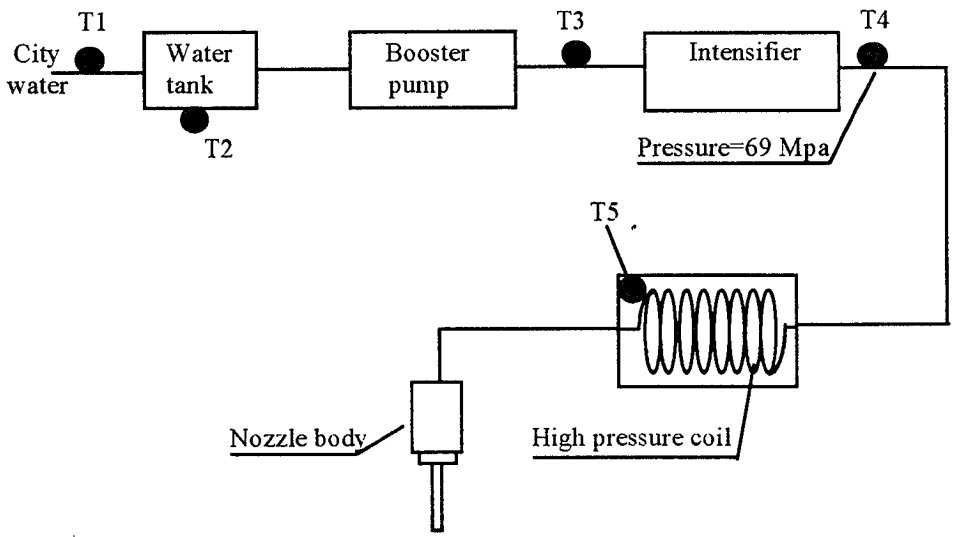

Figure 3. Schematic of Temperature Measurement at Ice Jet Formation
T1=22°C, T2=4°C, T3=6.8°C, T4=23.1°C, T5=-7°C

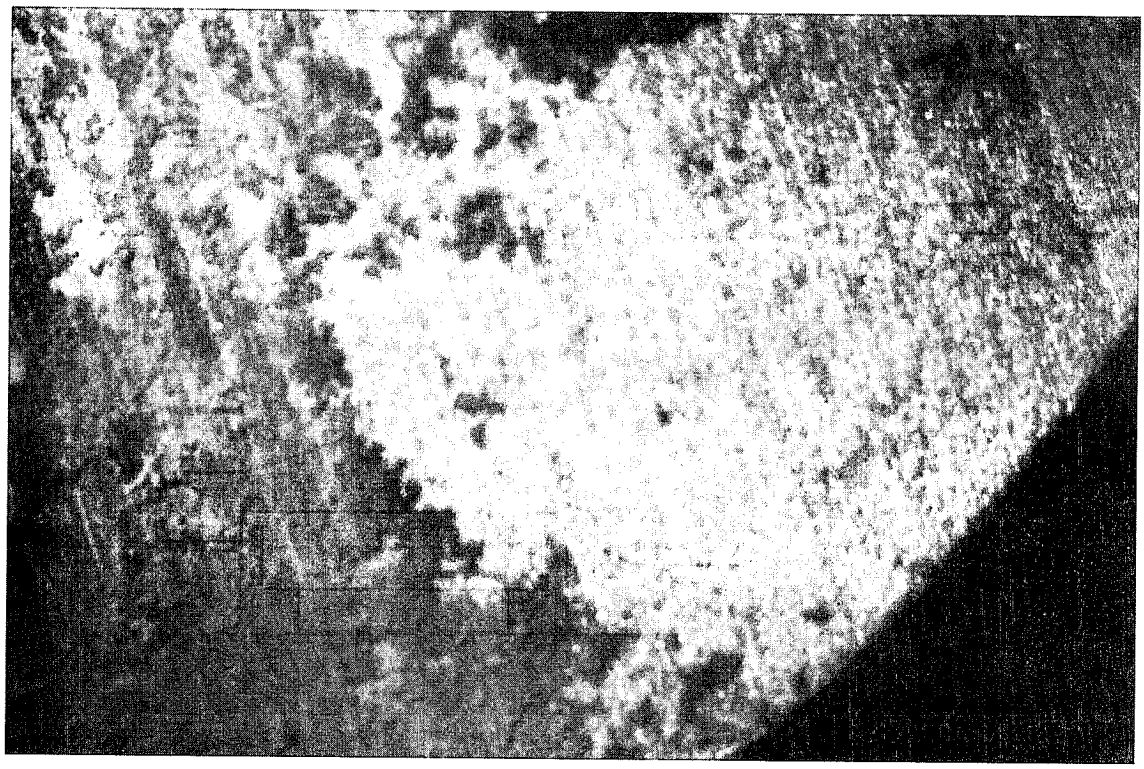

Figure 4. IJ Removing of Carbon Steel Rust
Notice complete rust remove

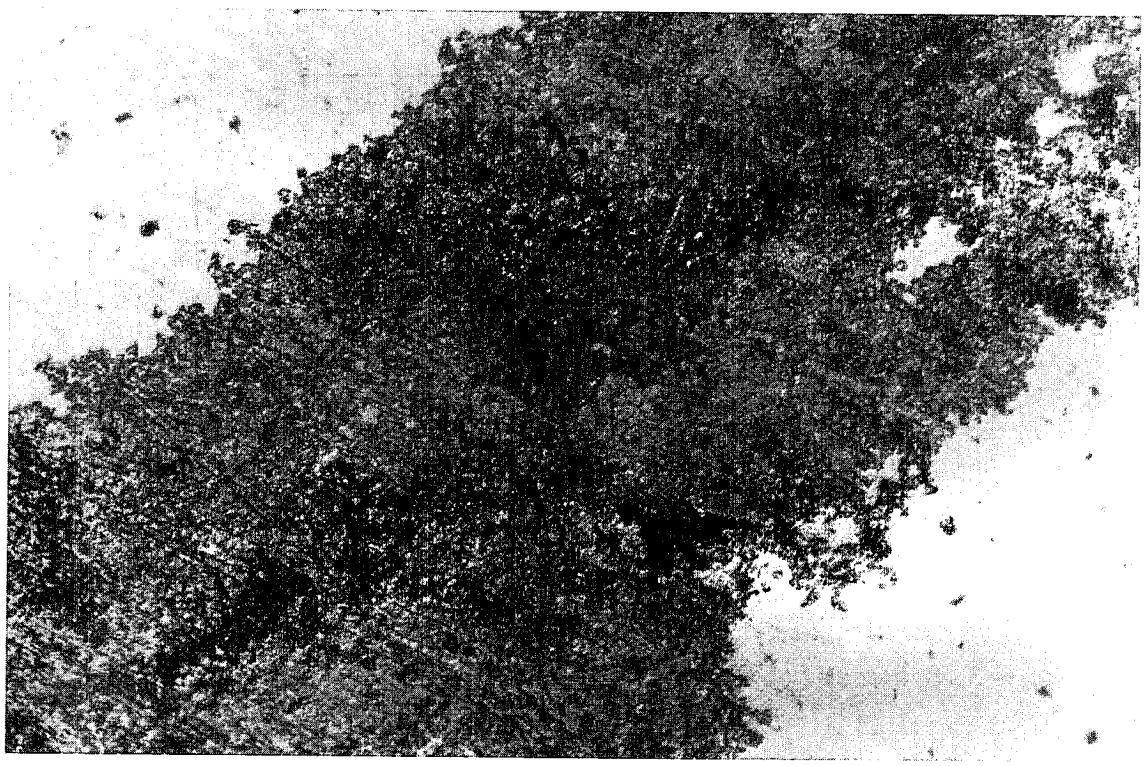

Figure 5. IJ Cleaning of Epoxy Paint on Carbon Steel Surface

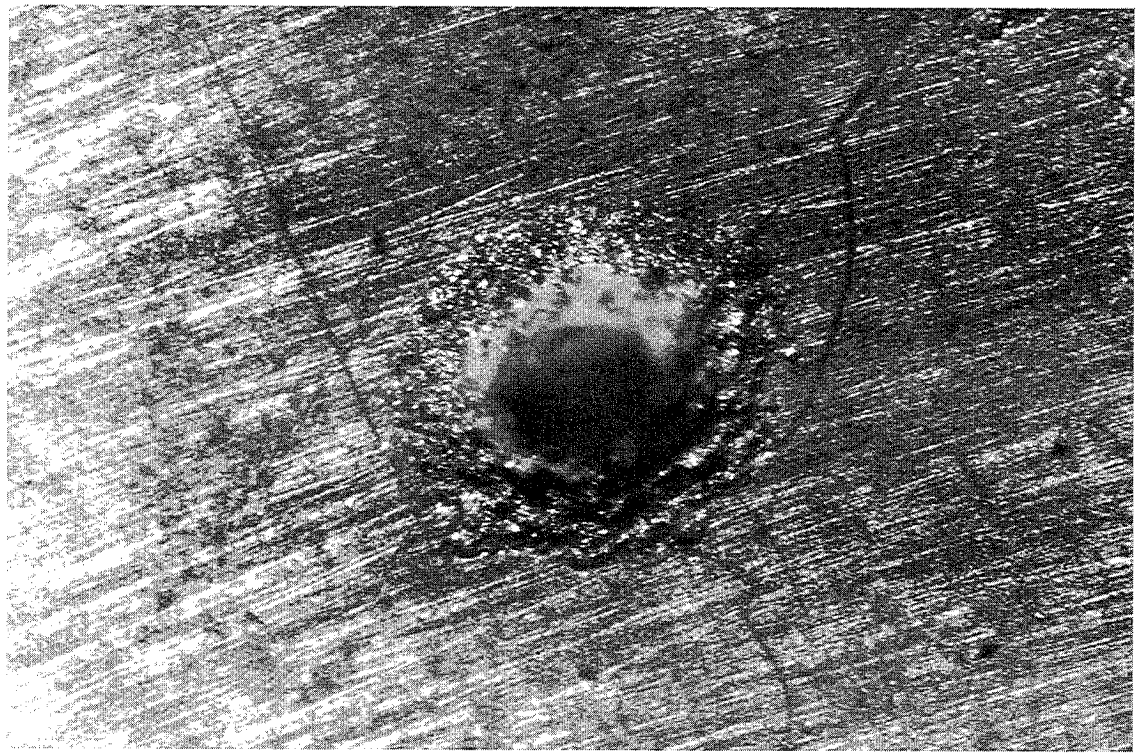

Figure 6. IJ Drilling of Aluminum
Notice a roundness of the generated surface

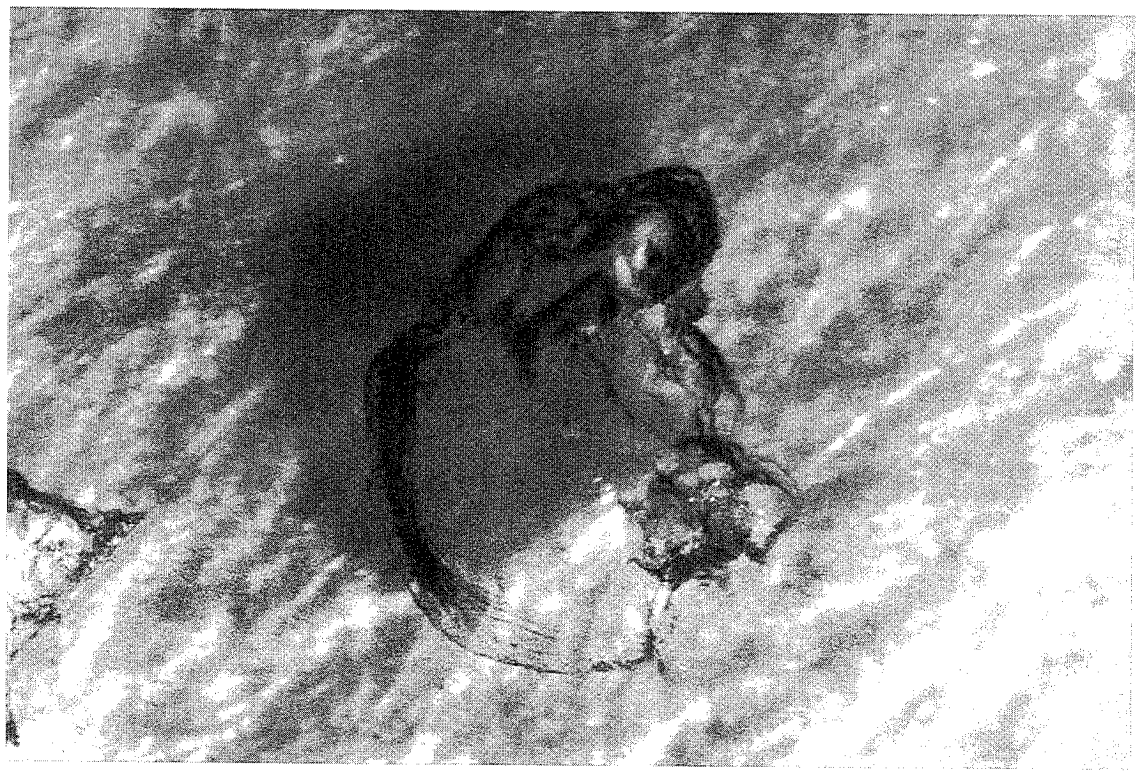

Figure 7. IJ Drilling of Plexiglass

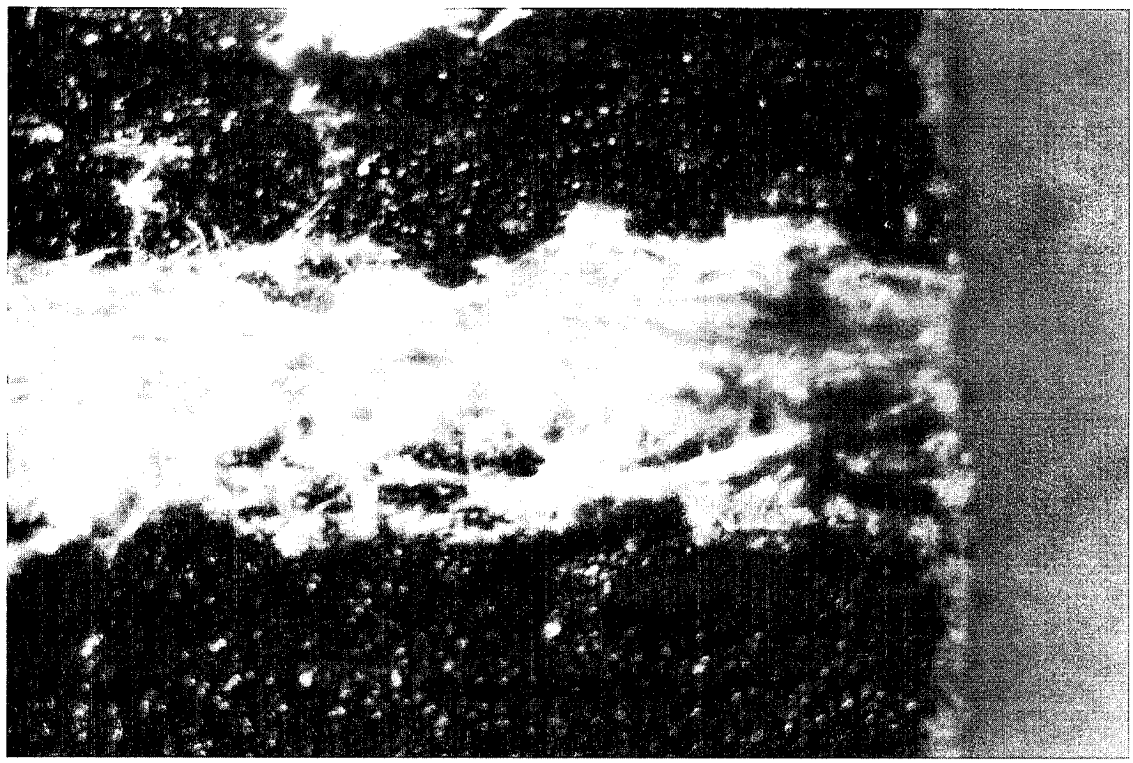

Figure 8. IJ Milling of Wood

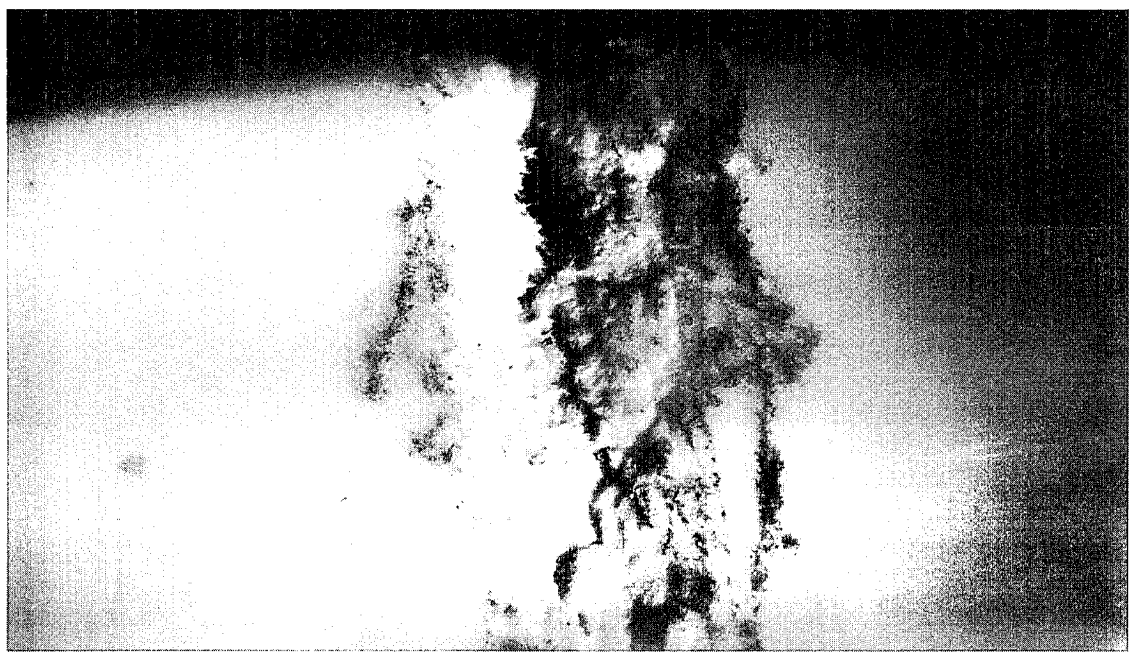

Figure 9. IJ Cutting of Plastic Plate
Notice complete material separation and conventional topography of the generated surface

8th American Water Jet Conference
August 26-29, 1995: Houston, Texas

Paper 50

PHYSICAL ANALYSIS OF THE ENERGY BALANCE OF THE HIGH ENERGY LIQUID JET COLLISION WITH BRITTLE NON-HOMOGENEOUS MATERIAL

L. M. Hlaváč
Institute of Geonics, Academy of Sciences
Ostrava, Czech Republic

ABSTRACT

The paper is devoted to the results of physical analysis of the energy balance of interaction between liquid jet and brittle non-homogeneous material. The problem is studied from several points of view. The classical description of the process by analytical equations is supported by microscopic description of the material element failure and by description based on principles of nuclear physics. The macroscopic approach to the jet energy dissipation problem has been applied first. The analytical equations describing the energy balance in the process of liquid jet origin, its movement through the medium between liquid nozzle and target material and interaction between liquid jet and brittle non-homogeneous material have been derived and proved by experiments. The microscopic approach has been applied next. Knowledge of the material structure behaviour has been used for the derivation of a new equation useful for determination of the depth of disintegration. Finally the procedures based on knowledge from the sphere of nuclear physics have been used the for derivation of the equation for depth of disintegration. The specific energy of the disintegration process has also been derived. All theoretical models are compared with the same database of experimental results.

Organized and Sponsored by the Water Jet Technology Association.

1. INTRODUCTION

This article is aimed at the analysis of the energy balance in the process of interaction between liquid jet of high energy and material. Special attention is devoted to the interaction with brittle non-homogeneous materials. The conclusions of the author are based on the theories set up in the Institute of Geonics Ostrava (Czech Republic) and experiments conducted there as well. Starting from this basis the author tries to summarize the energetic relationships during impact of high energy liquid jets on target material.

2. PHYSICAL LAYOUT OF THE PROBLEM

The basic types of interaction between liquid jets and disintegrated objects are described below in paragraphs a) through c). It is supposed that energy of the liquid jet is sufficient for disintegration processes supposed in described particular cases. However, the input energy of the jet may even be several times higher than those necessary for disintegration. Remaining energy is then absorbed in resulting particles or is wasted.

a) The first case of interaction is characterised by the fact that the jet diameter is significantly smaller compared to the typical dimension of the disintegrated object or relevant basic elements of material. Local disintegration usually occurs in this particular case and a kerf is produced.
b) The second case of great importance can be characterized by the fact that the jet diameter is comparable to the typical dimension of the disintegrated object or relevant basic elements of material. The global disintegration of the target object or element of material usually occurs in this particular case and volume disintegration and excavation of material occurs.
c) The third case is characterized by the fact that the jet diameter is significantly larger than the typical dimension of the disintegrated object or relevant basic element of material. Therefore the drag coefficient of the object (material element) in the liquid flow is significantly lower than in previous cases. The resulting reaction force of the object against the liquid jet is also several times lower and the stress levels inside the object are not sufficiently high for disintegration of material. That is why no disintegration occurs (neither local nor global) and the object is only accelerated and drawn by liquid jet.

All presented considerations are related to the real studied cases that are limited by contemporary technical possibilities. The strength of material of the disintegrated object and its structure also play a very important role in processes studied. Brittle non-homogeneous materials like rocks and concretes are more easily disintegrated than ductile materials (metals) because their partial elements are relatively separated from one another and transfer of energy is very limited. The input energy accumulates easily in the exposed material element until its damage. Ductile materials are much more homogeneous then rocks or concretes. That is why the transfer of energy inside these materials is very good. Therefore they are more resistant against liquid jet impact.

Consumption of energy by the disintegration processes in various materials is a very important parameter for the definition of the appropriate conditions for effective application of liquid jets in practice. The specific energy of disintegration process is determined by ratio of the energy entering the process and the area of cut (thickness of material or depth of kerf multiplied by length of cut). However the appropriate energy entering the interaction with the material has to be determined.

3. EVALUATION OF THE LIQUID JET ENERGY

The energy accumulated in the compressed liquid passes from the static form to the dynamic one through the process of flow development in the liquid nozzle. The efficiency of this transformation of energy is determined both by nozzle parameters (geometric shape, relations among some significant characteristics, roughness of the walls etc.) and by characteristics of the used liquid. The energy losses in nozzle are characterized by nozzle parameter μ.

However the output of the high pressure pumping system is influenced not only by nozzle parameter μ but also by many other technical factors that differ from one pump to another. Therefore the input energy of the pumping system cannot be directly used for evaluation of the specific energy of the disintegration process. For this purpose it is necessary to choose such an energy that is independent of the pumping system configuration and has the same value for the same setting of the liquid and nozzle parameters. These assumptions are fulfilled by kinetic energy of the liquid jet at the nozzle outlet. However the appropriate base for the evaluation of a specific energy of the disintegration process is the kinetic energy of the liquid jet at the target surface. Fortunately the kinetic energy of the liquid jet in any distance from the nozzle outlet is directly related to the kinetic energy at the nozzle outlet and parameters of the medium the jet is passing through. The relationship can be described by a simple equation:

$$v_L = v_o e^{-\xi L} \tag{1}$$

The kinetic energy of the liquid jet at the nozzle outlet is given by the relationship

$$E_{ko} = \frac{1}{2} m_o v_o^2 \tag{2}$$

The mass is determined by the liquid density and the volume flow during certain time. The volume is specified by the following parameters: jet diameter, outlet velocity and time. Since this derivation is performed particularly for extremely high pressures, it is not possible to

neglect compressibility of the liquid. The corresponding liquid density in the pumping system is higher than in normal conditions and it is possible to determine it by the equation

$$\rho_c = \rho_o \gamma_R^{-1} \tag{3}$$

The liquid before the nozzle is characterized by pressure p_o and density ρ_c. The liquid flowing out of the nozzle into the medium with pressure p_m and density ρ_m is characterized by density ρ_o and velocity v_o both determined by pressure difference $(p_o - p_r)$ where p_r is a residual pressure of the liquid and to simplify the analytical equations it is supposed to be equal to the pressure of medium p_m.

The liquid jet velocity is determined by Bernoulli's equation taking into account that density of the liquid accelerated in the nozzle corresponds to the compressed state. When the pressure of the medium at the outlet (residual pressure) is very low (only up to 2% of the liquid pressure before nozzle) the residual pressure can be neglected and the equation can be simplified. The nozzle parameter μ characterizing energy losses has to be inserted into the Bernoulli's equation. The outlet liquid jet velocity can be then determined introducing liquid and nozzle parameters into this basic hydrodynamic equation. Corresponding kinetic energy of the jet is expressed, modifying the relationship (2) in the following way

$$E_{ko} = \frac{\pi d_o^2 \sqrt{2 \mu^3 p^3 \gamma^3}\, t}{4\sqrt{\rho_o}} \tag{4}$$

This equation describes the kinetic energy of the liquid jet at the nozzle outlet without regard to parameters of the medium between nozzle and target and expansion process. Output power of the jet at nozzle outlet is described by the equation

$$P_{ko} = \frac{\pi d_o^2 \sqrt{2 \mu^3 p^3 \gamma^3}}{4\sqrt{\rho_o}} \tag{5}$$

The liquid jet disintegrates itself as a result of expansion of the compressed liquid at the nozzle outlet and interaction with medium between nozzle outlet and material surface. Leaving the nozzle the liquid loses its space limitation and it expands - its density falls down to the value corresponding to the free flow, jet cross-section grows and so does the volume containing the same amount of the liquid; however, the velocity in the flow direction does not grow. On the contrary the growth of volume is possible only thanks to energy loss E_l

determined by the change in density (equation 3). The expansion happens very quickly, therefore it is not necessary to consider other effects connected with energy loss during this time. Another part of energy, marked E_2, is consumed for overcoming the resistance of the medium between nozzle outlet and material surface. Applying equation (1) the energy of the liquid jet at distance L from nozzle outlet is determined by the equation (6):

$$E_{kL} = E_{ko}\, e^{-2\xi L} \tag{6}$$

This energy enters the interaction processes with target material. The corresponding liquid jet power can be calculated from the following equation:

$$P_{kL} = P_{ko}\, e^{-2\xi L} \tag{7}$$

4. SPECIFIC ENERGY OF THE DISINTEGRATION PROCESS

Energy of the liquid jet entering the interaction with target material divided by relative quantity characterizing the output of the disintegration process is considered to be the specific energy of the disintegration process. However the relative quantity can be either area of the kerf made by liquid jet or disintegrated volume. In cases when liquid jet serves particularly for preparing discontinuities in material, i.e. width of the kerf is negligible compared to its depth and length, the area of kerf is used as an appropriate relative quantity for specific energy evaluation. The area of kerf is a product of the kerf depth (material thickness) h and the kerf length s. Substituting the product of traverse rate v_P and time of jet action t for kerf length, equation (8) has been derived for specific energy of target material disintegration:

$$E_S = \frac{\pi\, d_o^2 \sqrt{\mu^3 p^3 \gamma_R^3}\, e^{-2\xi L}}{4\sqrt{\rho_o}\, v_P\, h} \tag{8}$$

In the case of volume disintegration of material the disintegrated volume is used as a relative quantity for specific energy evaluation. However the determination of the disintegrated volume is not so easy as determination of the area of kerf because this parameter depends on many conditions that are very difficult to describe in general. Therefore the most often method for volume determination are experimental measurements.

5. LIQUID JET ENERGY IN THE INTERACTION WITH MATERIAL

The interaction process between high energy liquid jet and material can be studied from the point of view of the law of conservation of energy in the system *LIQUID JET - MEDIUM BETWEEN NOZZLE AND TARGET SURFACE - TARGET MATERIAL*. The situation is schematically drawn in Figure 1. Describing the whole process by analytical equations a great number of physical assumptions and simplifications have been formulated (see Hlaváč and Vašek, 1994).

Description of the energy flowing out of the liquid nozzle and its losses in the medium between nozzle outlet and material surface have been mentioned and specified in previous paragraphs. The energy transfer and dissipation in the interaction process with target object has to be described now.

Energy reaching the target surface is utilized for overcoming the resistance E_W of the material and for acceleration of the elements of disintegrated material E_{kM}. Part of the incoming energy is wasted by friction between liquid and material E_F and part of it is converted into heat E_Q. Certain amount of energy is reflected in the form of the kinetic energy of reflected jet E_{kLR}. The equation of the presented energy balance can be written as follows:

$$E_{kL} = E_W + E_{kM} + E_F + E_Q + E_{kLR} \tag{9}$$

Quantifying all terms under certain physical presumptions and approximations it is possible to express the depth of disintegration by means of basic liquid, material and surrounding medium parameters (see Hlaváč and Vašek, 1994). The resulting equation for depth of disintegration, however, requires supporting equation determining the key parameter of the energy balance in the interaction - parameter α. One more equation is required to describe the total depth obtained after n-passes of the jet. Resulting system of equations based on basic physical analysis of energy transfer and transformation in the interaction between liquid jet and brittle non-homogeneous material is presented here in the complex form including parameters for multiple passes:

$$h_{n+1} = \frac{\pi d_o \sqrt{2 \rho_o \mu^3 p^3 \gamma_R^3 e^{-5(\xi L + \xi^* h_n^*)}} (1 - \alpha_n) \cos\theta}{4 \chi \rho_M \nu^{\frac{\rho_o}{\rho_M}} \left[\alpha_n^2 e^{-2(\xi L + \xi^* h_n^*)} \mu p \gamma_R + \frac{\rho_o}{\rho_M} \sigma \right]} \tag{10}$$

$$\alpha_n = 1 - \frac{C_x^2 \sqrt{2\,\mu^3 p^3 \gamma_R^3}\,\rho_M^* k^*}{8\sqrt{\rho_o}\,\eta\,\sigma_s a\, e^{3(\xi L + \xi^* h_n^*)}} \tag{11}$$

$$h_n^* = h_1 + h_2 + h_3 + \ldots + h_{n-1} + h_n \tag{12}$$

The coefficient α_n characterizes the jet velocity loss in the interaction between liquid jet and target material. Its square α_n^2 expresses the amount of energy left from the original one after the interaction and the difference $(1-\alpha_n^2)$ indicates how much energy has been used for material disintegration. The first attempts to set up this coefficient have been based on macroscopic description of the interaction between liquid jet and brittle non-homogeneous material and the law of conservation of momentum in the interaction. However a lot of empirical or experimentally set up parameters have been introduced in this equation. Therefore, further effort is aimed at the more exact definition of this parameter.

6. DESCRIPTIONS OF THE LIQUID JET

Several representations (physical ideas) of the liquid jet have been considered to describe the liquid flow character. The first model describes the liquid jet in a classical way, i.e. as a continuous flow. The second model is based on the idea that liquid jet can be replaced by a sequence of either spherical or cylindrical drops the volumes of which are determined by jet diameter, average flow velocity and characteristic time. These representations can be used for studying of the interrupted, modulated and pulsing jets as they are not justified for physical behaviour of continuous jets. The third model is based on the knowledge of the cross-sectional distribution of the liquid jet velocity. The magnitude of the velocity across the jet diameter can be determined by many relationships based on empirical, experimental or theoretical description of jet behaviour. The relationship used in our laboratory has been derived by Hlaváč (1994):

$$v_{LC} = v_{LA}\left(1 - \left(\frac{y}{r}\right)^{\log(Re+1)}\right) \tag{13}$$

As generally known, it is very difficult to determine the high energy liquid jet structure with sufficient accuracy using experimental methods. A special type of jet force measurement is

utilized for this purpose in the Rock Disintegration Laboratory of the Institute of Geonics. Both the method and some results were described by Sitek et al. (1994). The first results of those experiments have been compared with the theoretically set curve (calculated from equation 13) by Hlaváč et al. (1995).

7. MICROSCOPIC DESCRIPTION OF THE INTERACTION

To study the interaction between liquid jet and brittle non-homogeneous material from the microscopic point of view it is necessary to schematize the material structure. Two dimensional schematization of the material structure used for mathematical modelling of particles exposed to the liquid jet is presented in Figure 2. A quasi-static two dimensional mathematical model of the liquid jet impact on brittle particle has been tested using the finite element method and the Coulomb criterion of failure. The numerical results obtained using ANSYS software system were published by Hlaváč (1994), Hlaváč and Sochor (1994), (1995) and Hlaváč et al. (1995).

The material elements are considered to be cubes for the purpose of volume evaluations in three dimensions. Analytical description of target material failure starts from the following physical idea: each interaction between liquid jet and target material is characterized by transfer of the kinetic energy of liquid into the internal energy of target objects (basic elements of material - e.g. grains). The increase of the internal energy often results in an increase of the free surface. As a result of this process either new internal failures arise or the object is broken into several parts of the same total volume and larger total surface. The situation can be described by following system of equations partially presented by Hlaváč et al. (1995).

$$E_I = \frac{1}{2} P_{kL} d_o e^{\frac{1}{2}\xi L} v_P^{-1} \tag{14}$$

$$E_{TR} = \frac{1}{2} C_D P_{kL} a_o c^{-1} \tag{15}$$

Equations (14) and (15) determine respectively the total amount of jet energy impacting the material surface and amount of energy transferred into the target object during corresponding interaction times. Derivation has been made supposing that interaction between liquid jet and material at each point on the target surface is limited by the interaction time obtained as a ratio of jet diameter and traverse velocity. Interaction time between liquid jet and material element, on the other hand, is supposed to be a ratio of medium radius of material element and sound velocity. Using the energy transferred into the target material and specific surface

energy of material it is possible to derive the equations for newly created surface and average size of broken particles:

$$P_N = \frac{E_{TR}}{E_{SS}} \tag{16}$$

$$a_n = \frac{6\,a_o^3}{6\,a_o^2 + P_N} \tag{17}$$

Equation (16) determines the average newly developed surface and equation (17) yields the average size of newly developed particles. This theory utilized for evaluation of the depth of disintegration results in the following analytical equation:

$$h = \frac{C_D\,a_o^2\sqrt{2\,\mu^3\,p_t^3\,\gamma_R^3}\,e^{-3\xi L}}{48\sqrt{\rho_o}\,E_{SS}\,c\,(\sqrt[3]{n}-1)} \tag{18}$$

This equation does not include any explicit coefficient of the efficiency of energy transfer into material disintegration. However many parameters in this equation play this role being carefully analyzed from the physical point of view. Discussion of this problem is presented in part 9.

8. JET - MATERIAL INTERACTION STUDIED BY NUCLEAR PHYSICS

Studying the problem of interaction between high velocity liquid jet and material, the principles of nuclear physics have been tried for better understanding of the problem. This physical approach has been fully based on the substitution of the liquid jet by stream of molecules of known mass and velocity. Determination of the kinetic energy of the liquid molecule and the amount of molecules in the interaction with material is utilized for evaluation of the number of broken bonds in material. The bond size together with number of broken bonds and other necessary parameters (jet diameter, diameter of the liquid

molecule, interaction time) make possible to create one more equation for evaluation of the depth of material disintegration:

$$h = \frac{m_M d_o l_B \sqrt{2 \mu^3 p_t^3 \gamma_R^3 e^{-5\xi L}} \cos\phi}{\sqrt{\rho_o^3} E_B d_M v_P} \qquad (19)$$

Analyzing the results yielded by this equation, a better understanding of the energy balance in the interaction between liquid jet and material can be obtained (see part 9.).

9. DISCUSSION

While the theories presented in parts 7 and 8 are still in progress and appropriate coefficients or constants are to be fully justified, the theory presented in parts 3 through 6 has been compared with a large number of experimental results. An example of the comparison of calculated and experimentally set specific energy is presented in Figure 3. Several examples of theoretically set dependence of depth of disintegration on basic macroscopic parameters of liquid jet are compared with experimental results in Figure 4 through 7. However it is necessary to emphasize that this good correlation is obtained due to calculation of the key parameter (dynamic material permeability) from the "testing cut" as it is described by Hlaváč and Vašek (1994). When the material permeability is set from tables or standard tests performed for other material analyses, the coefficient α_n increases and resulting depth of disintegration is nearly ten times higher than corresponding experimental results. On the contrary, the theories presented by equations (18) and (19) in parts 7 and 8 seem to fit experimental values quite well without introduction of any special coefficients (see Figure 8 and 9). On the other hand, it is necessary to admit that coefficient $\cos\phi$ characterizing the effective cross-section of molecule collision with atoms in material lattice plays a very important role and its value determines that only about 10% of impacting energy is utilized for breaking of atomic bonds. While the model based on microscopic study of the interaction processes has not fit the experimental values very well, the theory based on several relationships of nuclear physics yields a very interesting correlation obtained neglecting jet (kerf) width (see Figure 9). Anyway, the most important result of the comparison between theories and experiments is the fact that only about 10% of the initial jet energy is utilized for material disintegration in the case of brittle non-homogeneous materials. This result is directly obtained from equations (8) and (10). For ductile materials the amount of effectively utilized energy is even lower. Improving the energy transfer and utilization is one of the most important future tasks. The introduction of interrupted, modulated and pulsing jets seems to be one of the most effective solutions of this problem.

10. CONCLUSION

Three physical models describing transfer of liquid jet energy to material and utilization of liquid jet energy for material disintegration have been presented and compared with

experimental results: analytical model of liquid jet - material interaction based on classical mechanics, model based on microscopic description of jet - material element interaction and model based on description of liquid molecule - material atom interaction. The energy losses in the medium between nozzle outlet and material surface have been also taken into account. Experiments proved that in spite of many simplifications the process of jet evolution and its impact on target material can be described by any of presented physical models provided that correct values of the respective coefficients are set up.

11. ACKNOWLEDGEMENTS

The authors are grateful to the Grant Agency of the Czech Republic to support the work presented in this paper by grant No. 106/93/2338.

12. REFERENCES

Hlaváč, L., "Physical description of high energy liquid jet interaction with material," *Geomechanics 91*, Z.Rakowski (ed.), pp. 341-346, Balkema, Rotterdam, 1992

Hlaváč, L., "Physical model of jet - Abrasive interaction," *Geomechanics 93*, Z.Rakowski (ed.), pp. 301-304, Balkema, Rotterdam, 1994

Hlaváč, L. and Sochor, T., "A Contribution to the Physics of a High Velocity Abrasive Particle Interaction with Brittle Non-homogeneous Materials," *Proceedings of the 12th International Conference on Jet Cutting Technology*, N.G.Allen (ed.), pp. 117-126, Mech. Eng. Pub. Ltd., London, 1994

Hlaváč, L. and Vašek, J., "Physical Model of High Energy Liquid Jet for Cutting Rock," *International Journal of Water Jet Technology,* Vol. 2, No. 1, pp. 39-50, 1994

Sitek, L., Vala, M., and Vašek, J., "Using of the Physical Model to the Evaluation of an Efficiency of the Tools Creating Multiple-Motions of the Nozzles," *Proceedings of the 12th International Conference on Jet Cutting Technology*, N.G.Allen (ed.), pp. 59-66, Mech. Eng. Pub. Ltd., London, 1994

Hlaváč, L. and Sochor, T., "Modelling of rock excavation by high energy water jet," *Mechanics of Jointed and Faulted Rock*, H.P.Rossmanith (ed.), pp. 847-852, Balkema, Rotterdam, 1995

Hlaváč, L., Sochor, T., Sitek, L., Martinec, P., and Vala, M., "Physical Study of a High Energy Liquid Jet as a Milling Tool," *Proceedings of the 4th Pacific Rim International Conference on Water Jet Technology*, H.KIYOHASHI (ed.), pp. 449-456, Kajima Institute Publishing Co.,Ltd., 1995

13. NOMENCLATURE

α, α_n coefficient of looses in liquid jet velocity during interaction with material ...[-]
a medium size of a basic material structure unit ...[m]
a_o size of a material element - grain ...[m]
a_n size of broken parts of material elements ...[m]
γ_R compressibility factor ...[-]
c sound velocity ...[m.s^{-1}]
C_D drag coefficient ...[-]
C_x coefficient of resistance of material structure to the jet ...[-]
d_o water nozzle diameter ...[m]
d_M diameter of the liquid molecule ...[m]
E_1 kinetic energy losses due to jet flow expansion ...[J]
E_2 kinetic energy losses due to environmental resistance to jet ...[J]
E_B energy of the atomic bonds in material ...[J]
E_F energy losses due to jet friction during disintegration process ...[J]
E_I energy interacting with target material ...[J]
E_{kL} kinetic energy of liquid jet at distance L from nozzle outlet ...[J]
E_{ko} kinetic energy of jet at the nozzle outlet ...[J]
E_{kM} kinetic energy of disintegrated material ...[J]
E_Q energy converted into heat during interaction ...[J]
E_{kLR} kinetic energy of liquid jet reflected from the target ...[J]
E_S specific energy required for disintegration of a unit kerf area ...[J.m^{-2}]
E_{SS} specific surface energy ...[J.m^{-2}]
E_{TR} energy transferred to the target object ...[J]
E_W energy consumed due to material resistance ...[J]
η dynamic liquid viscosity ...[N.s.m^{-2}]
h depth of disintegration in material ...[m]
h_n depth of disintegration made in n-th pass of liquid jet ...[m]
h_n^* total depth of disintegration after n passes ...[m]
Θ angle of incidence of jet measured between a normal line at the point of jet's axis projection through material surface and jet axis ...[rad]
k^* dynamic material permeability ...[m^2]
l_B length of the atomic bond in material ...[m]
L standoff distance ...[m]
μ ozzle discharge coefficient ...[-]
m_o liquid mass flowing out of the nozzle ...[kg]
m_M liquid molecule mass ...[kg]
n number of broken parts of material element ...[-]
ξ coefficient of attenuation of jet caused by resistance of the medium between nozzle and material ...[m^{-1}]
ξ^* coefficient of attenuation of jet caused by resistance of the medium in kerf made in material during previous passes ...[m^{-1}]
p pressure difference p_o-p_m ...[Pa]
p_o liquid pressure before the nozzle inlet ...[Pa]
p_m pressure of the medium between nozzle and material ...[Pa]

p_r remaining pressure ...[Pa]
p_t pressure difference p_o-p_{tr} ...[Pa]
p_{tr} threshold pressure ...[Pa]
P_{ko} output power of the jet at nozzle outlet ...[W]
P_{kL} power of the jet at the distance L from nozzle outlet ...[W]
P_N newly developed surface ...[m^2]
ρ_o liquid density in non-compressed state ...[$kg.m^{-3}$]
ρ_c liquid density in compressed state ...[$kg.m^{-3}$]
ρ_m density of the medium between nozzle and material ...[$kg.m^{-3}$]
ρ_M specific volume weight of material (including pores) ...[$kg.m^{-3}$]
ρ_M^* specific weight of material (without pores) ...[$kg.m^{-3}$]
r radius of the jet cross-section ...[m]
Re Reynolds' number ...[-]
σ material strength ...[Pa]
σ_s material shear strength ...[Pa]
s length of kerf ...[m]
t time ...[s]
v modified traverse rate ...[$m.s^{-1}$]
v_o jet velocity at nozzle outlet ...[$m.s^{-1}$]
v_L jet velocity at the distance L from nozzle outlet ...[$m.s^{-1}$]
v_{LA} jet axis velocity at the distance L from nozzle outlet ...[$m.s^{-1}$]
v_{LC} jet cross-sectional velocity at the distance L from nozzle outlet ...[$m.s^{-1}$]
v_P traverse rate ...[$m.s^{-1}$]
y coordinates in the radial direction perpendicular to the jet axis ...[m]
ϕ angle of molecule - atom collision ...[rad]
χ coefficient of reflected jet expansion due to mixing with disintegrated material ...[-]

14. FIGURES

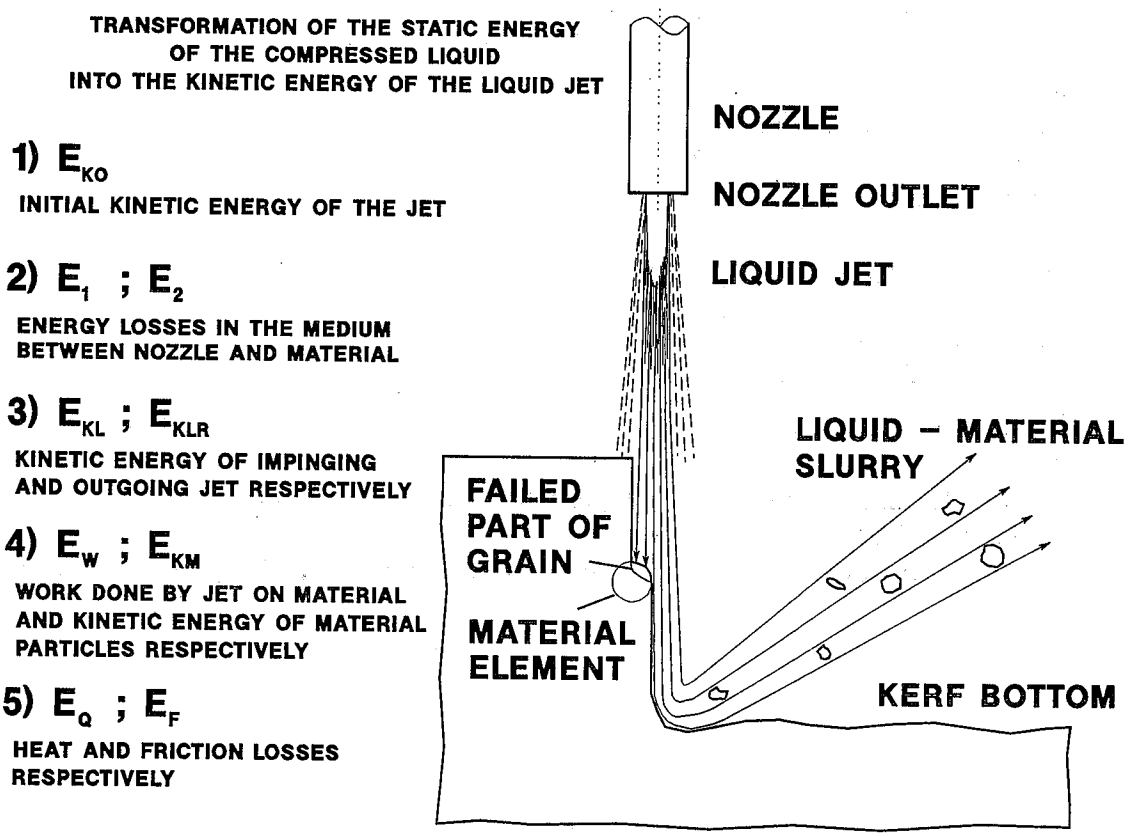

Figure 1. A Scheme of the Energy Balance in the System *LIQUID JET - MEDIUM BETWEEN NOZZLE AND TARGET SURFACE - TARGET MATERIAL.*

BRITTLE NON–HOMOGENEOUS MATERIAL EXPRESSED THROUGH THE ELEMENTS OF VARIOUS SHAPES AND MATERIAL PROPERTIES

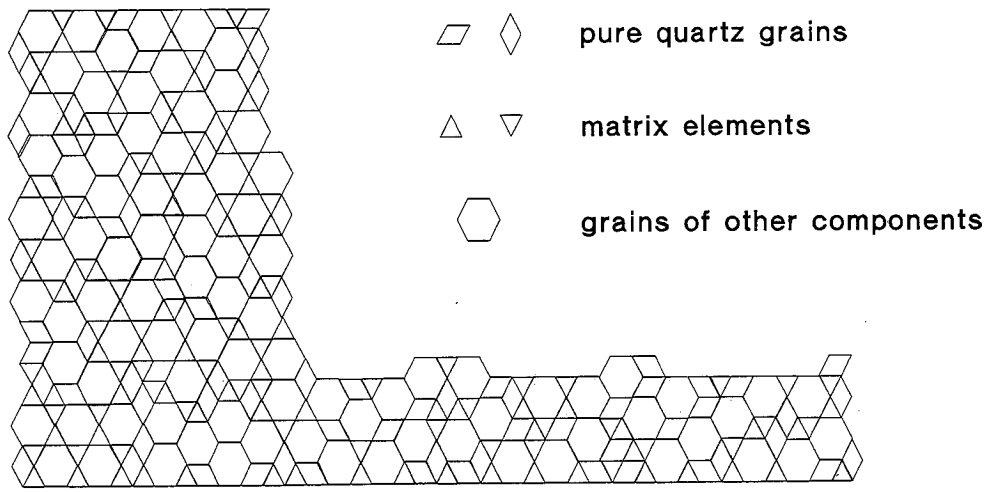

Figure 2. A Two-Dimensional Scheme of the Brittle Non-Homogeneous Material.

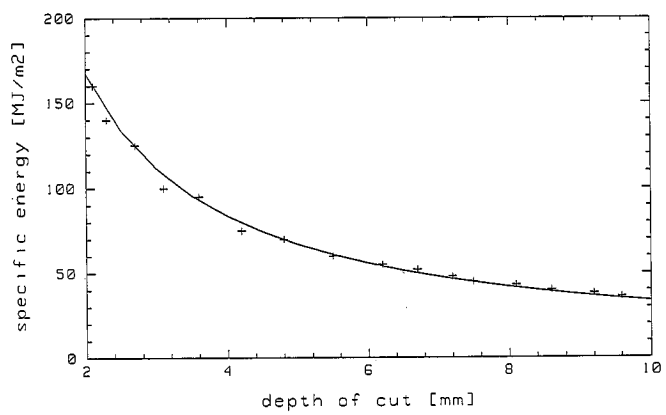

Figure 3. Relation Between Depth of Cut (Disintegration) and Specific Energy.

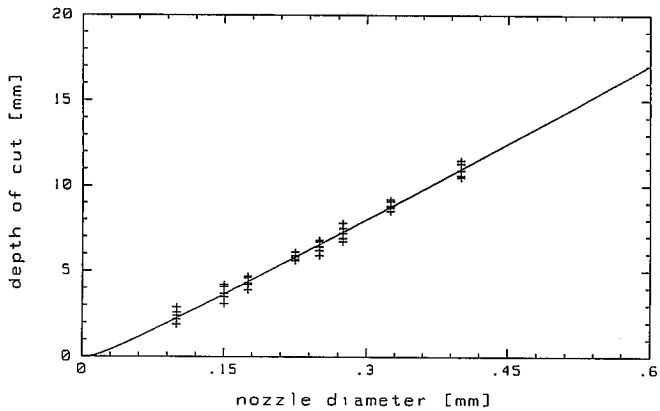

Figure 4. Dependence of the Depth of Cut (Disintegration) on Nozzle Diameter.

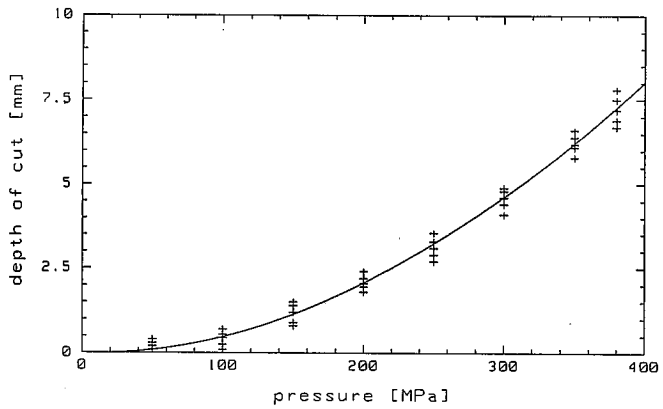

Figure 5. Dependence of the Depth of Cut (Disintegration) on Liquid Pressure.

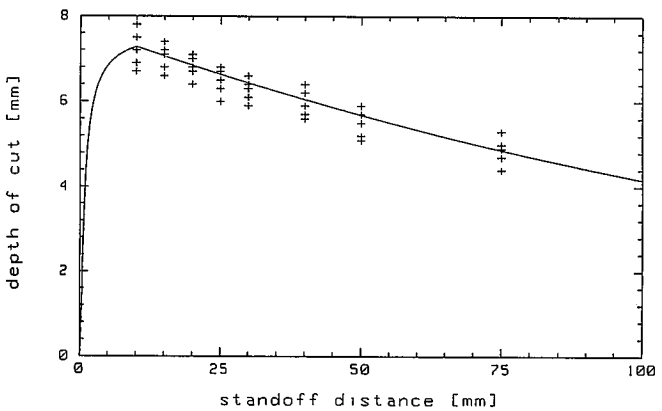

Figure 6. Dependence of the Depth of Cut (Disintegration) on Stand-off Distance.

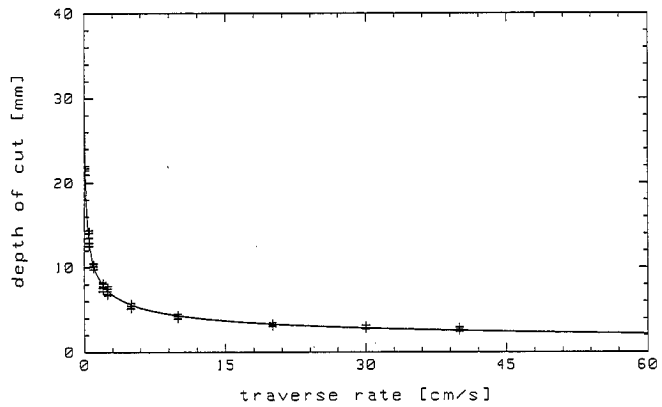

Figure 7. Dependence of the Depth of Cut (Disintegration) on Traverse Rate.

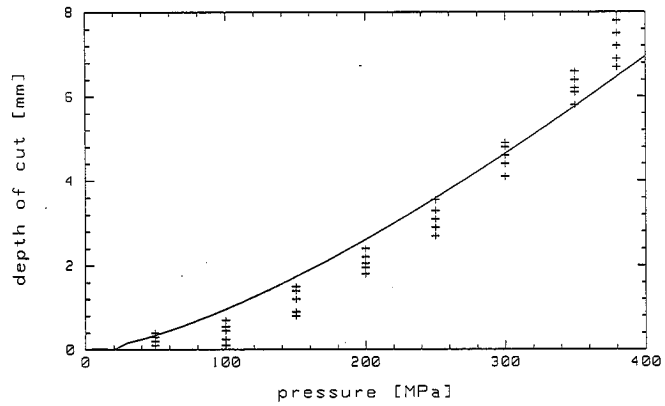

Figure 8. Depth of Cut (Disintegration) Dependence on Pressure Set by Microscopic Model of Jet - Material Element Collision.

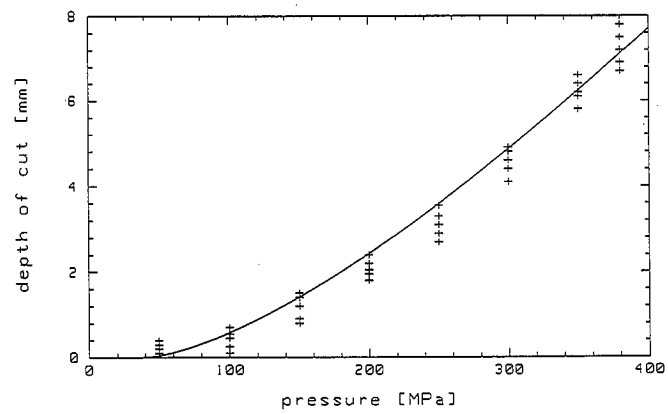

Figure 9. Depth of Cut (Disintegration) Dependence on Pressure Set by Model Based on Liquid Molecule - Material Atom Collision Study.

8th American Water Jet Conference
August 26-29, 1995: Houston, Texas

Paper 51

ULTRAHIGH-PRESSURE WATERJETTING GAINS ACCEPTANCE AS SURFACE PREPARATION METHOD

Rick Schmid
Product Manager
Flow International Corporation

ABSTRACT

Technology advancements and external factors have propelled ultrahigh-pressure waterjetting into the forefront as a surface preparation methodology. Traditionally the domain of abrasive blasting, surface preparation involves removal of paints and industrial coatings from steel substrates. Once limited to industrial cleaning applications, UHP has been gaining acceptance as a tool for surface preparation. Increased productivity rates resulting from pump and nozzle developments and environmental scrutiny of abrasive blast have played a major role in UHP's evolution. This paper will discuss how and why UHP has successfully penetrated the surface preparation industry and advantages of the process for this function.

Organized and Sponsored by the Water Jet Technology Association.

1. INTRODUCTION

Proper surface preparation is critical to the success of any paint job. An improperly prepared surface may lead to coating failure due to corrosion or loss of adhesion. As an alternative to abrasive blasting -- a technology entrenched in the surface preparation industry for nearly 100 years -- ultrahigh-pressure (UHP) waterjetting has recently evolved as a viable tool for commercial applications.

Surface preparation with UHP waterjets involves water pressurized to ultrahigh-levels (> 30,000 psi) to remove a paint or other surface coating in preparation for applying a new coating. A combination of technology advancements and external factors such as increasingly stringent environmental regulations have driven acceptance. This paper will focus on the advantages of UHP for surface preparation.

2. ABRASIVE BLASTING

Abrasive blasting has dominated the surface preparation industry for most of this century, primarily due to economic and performance benefits. High productivity rates, particularly for large area surfaces, reinforced abrasive blasting's popularity with contractors. Industry wide acceptance of a surface prepared by grit blast and familiarity with the process were also factors.

External factors such as environmental and occupational regulations have prompted the surface preparation industry to seek alternatives. Airborne dust generated by grit blast has caused government agencies to scrutinize its impact on the environment. Health problems caused by exposure to toxic airborne dust have also raised concerns.

Grit blasting normally takes place in an open air environment. Air quality regulations constantly change and are growing more restrictive. To satisfy new regulations, grit blast users must build elaborate and costly containment systems to prevent dust from contaminating surrounding areas. Containment devices add to the cost and complexity of a project. Users spend approximately one-third of their time assembling and disassembling containment systems and shoveling abrasive from tarps. Operators must wear respiratory equipment for protection against airborne dust.

The hazards of grit blast are most evident in lead paint abatement applications. Lead paint abatement is one of the industry's most demanding and growing applications. Of the 134,000 bridges in the U.S. in need of repair, more than 90,000 contain lead based paint. Approximately 66% of above ground storage tanks are coated with lead based paint.[1] An SSPC survey conducted in 1991 concluded that 38% of the steel in industrial facilities is coated with lead paint.[2]

Airborne dust produced by abrasive pulverizing lead paint exposes operators to dangerously high levels of lead. The abrasive industry has attempted to address these problems with special containment systems and alternative blast materials.

Disposal of lead-tainted abrasive is another concern. Abrasive blasters use 4 to 10 lbs. of abrasive per square foot. When grit mixes with lead paint, it transforms into a hazardous material. A typical bridge, ship or storage tank project entails preparation of 100,000 square feet of surface, requiring several hundred tons of abrasive. This can significantly increase the cost of disposal. The time and cost of disposing hazardous abrasive waste offset any gain in productivity.

The quality of a grit-prepared surface has also been questioned. Abrasive blast tends to trap contaminants in crevices and folds created by the impact of discreet abrasive particles on the substrate. Previously, the industry believed a new anchor pattern was desirable each time a surface was recoated. Recent research and analysis has shown otherwise.

3. UHP

Traditionally, applications for UHP were limited to removal of heavy, thick layers of material deposits in the industrial cleaning and petrochemical markets. Industrial contractors favored UHP for specific applications where lower pressure applications failed to strip hard, tough deposits from a substrate. Factors prohibiting broader acceptance of UHP included poor reliability, low productivity rates, and excessive capital equipment costs. No singular development has led to the emergence of UHP waterjets for surface preparation. Rather, it is a combination of several factors: technology improvements; lower costs; and environmental factors.

3.1 Productivity

Productivity levels of older hand held UHP lances were once 1/4 to 1/3 that of hand held abrasive nozzles. Commercial coating removal rates generally fell into the 20-30 ft^2/hr per hand held UHP tool, as compared to productivity ranges of 90-120 ft^2/hr per nozzle for abrasive.

Reasons for the lower productivity were numerous. Operating pressures in the 35,000 psi range limited productivity rates. Slow nozzle rotation speeds further slowed removal rates. Maximum rotation speed of UHP swivels connecting nozzles to the wand was 1,000 rpm. Achieving productivity gains necessitated reaching a careful balance between operating pressure and rotation speeds. Simply increasing pressure or nozzle rotation speed did not provide large productivity gains. Only a combination of these parameters would result in faster removal rates.

Technology has rapidly advanced between 1992 and 1995. Pressure ranges have increased to 40,000 psi. Higher nozzle rotation speeds in the 3000-3500 rpm range augmented advancements in operating pressures. Advancements in nozzle technology also improved productivity. By varying orifice sizes, the number of orifices, orifice placement and nozzle geometries, one could increase production rates. Higher pressures and nozzle advancements

have pushed productivity to rates comparable to hand held abrasive blasting. Typical removal rates are 70-100 ft2/hr for UHP versus 90-120 ft2/hr for abrasive blast on similar materials.

UHP offers the following benefits:

Low effluent of water. In contrast to low pressure, high volume (15 to 30 gallons per minute) waterblasters, UHP creates lower volumes of water (typically less than 2.5 gpm per hand tool).

Less waste. Abrasive blast generates 4 to 10 lbs. of waste per square foot. Users must dispose of the aggregate waste material. UHP generates 2 to 3 gpm of water per square foot.

Easy collection, separation and disposal. Water is easier and less expensive to collect and dispose than abrasive. For most applications, paint chips and particulate simply settle out of the water and the water is then mechanically filtered. Users segregate and dispose of the waste separately. Hazardous materials such as leads don't dissolve into the water, so no complex filtration processes are required. Paint chips are sent to a hazardous waste site. The filtered water can be discharged to sewage, in compliance with local regulations.

Lower water consumption. For applications involving hazardous materials or where water consumption must be minimal, water can be collected, filtered and recycled back to the ultrahigh-pressure pump for reuse. Closed loop recirculation systems perform this function.

Improved operator hygiene. UHP reduces worker exposure to toxic materials. Low water volumes make UHP hand tools much easier to handle than high volume, high thrust hand tools.

3.2 Reliability of Equipment

Surface preparation equipment in the field is subjected to harsh conditions such as those found in shipyards and infrastructure rehabilitation work on bridges and storage tanks. UHP equipment previously experienced difficulties withstanding the demands of such environments. Attempts to convert hydraulic intensifier pumps from factory to field applications failed due to unpredictable conditions. Intensifiers were unreliable and complex, requiring well trained technicians to maintain the equipment.

Technical advancements in the past few years have significantly improved reliability. The evolution of positive displacement pumps has been the single most significant development. Positive displacement pumps performing in the 10,000 to 20,000 psi range have been in the field for a number of years. They are much easier to maintain and do not need the clean operating conditions intensifiers require. Ease of maintenance makes positive displacement pumps a popular choice for work in harsh industrial environments. Users don't need to hire or train specialists to operate and maintain the equipment.

Positive displacement pumps capable of 40,000 psi are now operating in the field. To date, more than 100 such pumps are in use. Operation of UHP systems differs little from low pressure waterblasting, a staple for decades in industries such as automotive and marine. Operators familiar with waterblasters can operate UHP systems.

3.3 Capital Equipment Costs

Capital equipment costs for UHP equipment used in surface preparation applications have decreased over the last three years. Positive displacement pumps are less expensive than intensifier pumps per horsepower due to their improved pump efficiency. A 200 brake horsepower intensifier pump operates at 70 percent efficiency or 140 hydraulic horsepower. In comparison, a 200 brake horsepower positive displacement pump operates at 90 percent efficiency or 180 hydraulic horsepower. Simplicity of design -- no hydraulic systems or intricate filtration equipment -- lowers capital cost.

3.4 Environmental & Occupational

The environmental attributes of UHP played a key role in its acceptance. Scrutiny by federal, state and local agencies, along with the cost and time involved with compliance, has led industries to view UHP as a solution to many of their challenges. Another benefit not receiving the publicity but equally as important is improved occupational hygiene.

UHP surface preparation generates no airborne dust, eliminating the necessity to construct containment systems. Operators wear lightweight face masks in place of cumbersome respiratory equipment. No heavy equipment is needed to gather spent abrasive piled on the floor beneath the cleaning area. Expensive disposal costs of spent abrasive are avoided.

Environmental attributes of UHP have broadened markets for the equipment. Shipyards, with their proximity to environmentally sensitive areas, comprise the largest market for UHP surface preparation equipment. Lead paint abatement represents the second largest market for 40,000 psi machines. A recent NIOSH report stated "Ultrahigh pressure waterjetting suppresses the lead based dust by agglomerating the dust into the water droplets. The water may be disposed of through a public sewage system after it has been cleaned and treated."[3]

4. NEW STANDARDS WILL STRENGTHEN ACCEPTANCE

Visual standards for abrasive blast surfaces have existed for many years. The coatings industry recognizes these standards worldwide. Blast operators, foremen and inspectors use simple pocket manuals to conduct visual inspections. Current visual standards only address the resulting surface, not the preparation methodology.

Surfaces prepared by grit blast and UHP share few visual characteristics. The lack of waterblasting standards previously deterred the industry from accepting UHP. Environmental

regulations and economic pressures have impacted the industry to the extent that UHP surface preparation is beginning to overtake abrasive blasting in the marketplace, therefore standards are a necessity.

Professional organizations such as the NACE (National Association of Corrosion Engineers) and SSPC (Steel Structures Painting Council) are moving toward adopting standards for high and UHP water blasting. The industry anticipates release of these standards within the next two years. Visual standards will address the difference between air abrasive blasted and UHP prepared surfaces, along with the level of acceptable residual contaminants allowed to remain on the surface ($< 7\ \mu g/cm^2$ according to NACE and SSPC guidelines). The NACE and SSPC will have to address unfamiliarity with UHP prepared surfaces through education of contractors, inspectors, and coating manufacturers.

Coating manufacturers have also recognized the emergence of UHP. Since coating manufacturers ultimately assume final liability of the coating, it is critical they guarantee coatings for UHP-prepared surfaces. International Coatings, Courtsland, England, has stepped forward to publish interim specifications. Visual specifications provided by International Coatings are now published in the field handbook. Most other major coating manufacturers have also accepted International Coatings' specifications as the standard.

5. FLASH RUSTING

An area previously considered problematic that is now viewed as acceptable is flash rusting. Flash rust is a ferretic oxide which is inert and has no deleterious effect on the applied coating. A UHP-prepared surface will develop flash rust at a specific humidity threshold if corrosion inhibitors are not applied. Industry experts previously viewed flash rusting negatively. Past specifications for steel surface preparation were near white SSPC-SP10 or white metal SSPC-SP5. An inhibitor was required to achieve these visual standards. A UHP prepared surface treated with a corrosion inhibitor looked similar to an abrasive blast surface. Unfortunately, inhibitors were found to cause loss of adhesion and osmotic blistering.

Research conducted recently by major coating manufacturers found flash rusting is actually more conducive to bonding and preventing corrosion than a chemically treated surface. Thus, major coating manufacturers now prefer light flash rusting over a chemically treated surface. Most major coating manufacturers have developed coatings that are flash rust tolerant. Acceptance of a flash rusted surface has truly advanced acceptance of UHP in the surface preparation industry. Elimination of corrosion inhibitors also decreases cost and additional wear and tear on pumping equipment. Flash rusted surfaces can simply be overcoated as long as flash rusting is light and well adhered. Most all major coating manufacturers recognize this fact and now offer warranties on their products over flash rusted surfaces.

6. IMPROVED SURFACE PROFILE ATTAINABLE WITH UHP

To date, factors driving UHP acceptance in the marketplace were environmental- and occupational-related. New information shows UHP offers significant performance-related benefits as well. Recent tests comparing a UHP prepared surface to a grit prepared surface proved conclusively that UHP achieves a superior surface profile to a grit prepared surface.

An abrasive-prepared surface is impacted with many small, discreet abrasive particles that tend to flatten out the sharp peaks created from original profile. On a microscopic level, abrasive particles will actually fold over and trap contaminants such as chlorides and sulfates, affecting the quality of the finished product. Damage to the substrate can also decrease the exposed surface area, adversely affecting bond strength.

Detecting cracks and imperfections is very difficult due to the flattening phenomena. Flattening hides cracks and complicates visual inspections. The importance of a proper visual inspection for cracks increases in magnitude when preparing sensitive pieces of equipment such as steel pressure vessels or natural gas transmission pipelines for recoating.

Surfaces prepared with UHP have less folding and flattening. Thus, coatings bond better to a UHP prepared surface. Texture of a UHP prepared surface features sharp peaks conducive to bonding. More exposed surface area exists for new coating to bond.

Furthermore, abrasive blasting fails to remove all corrosive materials from the substrate. Chloride levels as low as 10 $\mu g/cm^2$ and sulfate levels higher than 20 $\mu g/cm^2$ present on a grit blasted surface can cause blistering of coating films after a few weeks of exposure to condensing humidity.[4] Numerous test conducted have shown that soluble salts still remain at these levels on steel surfaces after abrasive blasting.

UHP removes soluble salts with ease. One major coating manufacturer states, "Wet blasting, particularly ultra high pressure hydroblasting, is a very effective method for removing soluble salts from substrates. Salt removal is perhaps the greatest advantage hydroblasting has over dry abrasive blasting." The company found that if potable water is used for hydroblasting, surface salt levels below the level proposed by the joint SSPC and NACE of 7 $\mu g/cm^2$ are achievable on old rusted and pitted steel.[5] SSPC and NACE have proposed this level in their draft joint standard "Surface Preparation and Cleaning of Steel and other Hard materials by High and Ultra High Pressure Waterjetting Prior to Recoating."

Extensive testing has quantified the differences in residual contaminants on UHP prepared surfaces. All studies to date show conclusively that a much lower level of contaminants remain with waterjet prepared surfaces than grit blasted surfaces. Some of the most extensive analysis was presented at the 1992 NACE Annual Conference and Corrosion Show.

The following table[6] shows the benefits of a UHP prepared surface:

Surface Prep. Method	**Sulfates** $\mu g/cm^2$	**Chlorides** $\mu g/cm^2$
Rusted Water Service Pipe		
Uncleaned	5	28
Abrasive Blasted	2	32
UHP Cleaned	1	1
Coated Water Service Pipe		
Uncleaned	8	6
Abrasive Blasted	4	1
UHP Cleaned	0	1

Detecting contaminants on a surface is difficult, increasing the importance of complete removal. "Water soluble materials probably represent the largest and potentially most detrimental group of contaminants. These materials are frequently colorless in water solution and hence not readily visible when presented in small quantities on the surface of the metal. These quantities, however, are sufficient to initiate the cyclic reaction that may cause extensive persistent corrosion and or blistering under the protective system often leading to complete coating destruction."[7]

7. CONCLUSION

The surface preparation industry now views UHP as an environmentally sensitive alternative to grit blast. Currently, more than one hundred 40,000 psi machines operate in the field. The majority of those machines are used for surface preparation, primarily in the marine industry.

The next major advancement will be automating UHP surface preparation equipment for very large surface area removal. Technology advancements will center around increasing operating pressures and optimizing nozzles and hand tools to achieve higher productivity rates. External environmental factors will also play a key role in accelerating acceptance and broadening markets for UHP.

8. REFERENCES

1. BIRL Industrial Research Laboratory, Northwestern University, published in *American Paint & Coatings Journal*, December 1992, page 16.

2. *Journal of Protective Coatings & Linings* (JPCL), July 1991, page 55.

3. NIOSH study

4. Weldon, D.G., "Salts: Their Detection and Influence on Coating Performance," *Proceedings of the SSPC Annual Symposium,* Pittsburgh Penn., Steel Structures Painting Council (SSPC), 1985.

5. Gilbert, Douglas, International Coatings, "New Hydroblasting and Slurryblasting Standards Issued" *Journal of Protective Coatings and Linings.*

6. Howlett, J.J., Jr., Dupuy, R., *Ultrahigh-Pressure Water*, presented at The NACE Corrosion 92 Show paper 253.

7. NACE Publication 6G186 "Surface Preparation of Contaminated Steel Surfaces."

8th American Water Jet Conference
August 26-29, 1995: Houston, Texas

Paper 52

WATERJET COST EFFECTIVENESS:

CASE STUDIES IN CUTTING AND COATING REMOVAL

J.F. Shunk
Jet Edge
Minneapolis, Minnesota, U.S.A.

ABSTRACT

A customer's decision to purchase high pressure waterjet equipment whether for cutting, coating removal, or hydrodemolition is contingent on many factors including performance, capability, operational effectiveness, maintainability, reliability, and cost. Because of tight capital budgets common in many industries, however, the focus of most decision makers is usually on cost factors. Thus, a key ingredient in marketing waterjet equipment is the ability to show the cost effectiveness of waterjet technology compared to current methods. This paper develops a simple four-step methodology for preparing a cost-effectiveness analysis that includes the following elements:

- Developing a cost and benefit baseline for the current method of cutting, coating removal or hydrodemolition.
- Defining a new baseline for the same tasks using waterjet technology.
- Quantifying the cost and benefit differences between the two baselines.
- Analyzing the results and presenting them in a format suitable for informed decisions by customer management.

The cost effectiveness model developed includes the major cost contributions of labor, materials, waste disposal, and worker safety. Opportunity costs are also included. Other economic factors such as taxes, depreciation, and inflation can also be included, while intangible factors such as company image, improved safety, environmental compliance, etc., are discussed.

Organized and Sponsored by the Water Jet Technology Association.

1. INTRODUCTION

The purpose of this paper is to present - and illustrate with case studies - a simple methodology for constructing a cost effectiveness model designed to compare in economic terms, the value of two comparable methods for performing the same task. Since high pressure waterjet is established as an attractive cutting technology and rapidly gaining acceptance as an alternative to conventional coating removal methods such as grit blasting, machining, chemical treatment, or hand sanding, waterjet will be compared to conventional methods in the analysis. Although waterjet will be used as the replacement technology, the methodology developed is applicable to any evaluation where a sound, economic basis is needed for objectively comparing two or more competing technologies for potential purchase.

Waterjet cutting and decoating systems offer a good example for the use of cost effectiveness modeling since waterjet is still a relatively new technology that potentially offers an alternative to a number of labor intensive, material damaging, or environmentally hazardous methods now in common use in many industries. Being new, however, there is a natural skepticism of its value as well as an inherent difficulty in making a direct process-for-process comparison. In addition, the environmental advantages, in particular, need sound economic evaluation since environmentally acceptable alternatives are perceived as expensive and justifiable only by virtue of their requirements by law.

Waterjet technology provides an excellent example for cost effectiveness evaluations in cutting or decoating because of its speed, low potential for damage to the materials being cut or stripped, and its environmental safety. The only by product of the waterjet process is kerf residue from the material cut, coatings removed from substrate, leached ions from some coatings and substrates, and, of course, the water used in the process. Since most process water is now filtered, reclaimed, reconditioned, and then reused by the high pressure water pump, wastes and associated disposal costs are minimized.

2. OBJECTIVES

The objectives of the cost effectiveness model as it applies to evaluating waterjet technology will be twofold:

- Assess the value of waterjet as a replacement technology in all the areas of comparison that apply.
- Quantify the differences among the competing technologies and provide an economic basis for decision making in an easy-to-understand and logical format.

Although the focus of this paper is on economic factors in view of today's demands for enhancing productivity in a globally competing and interacting business environment, consideration must also be given to intangible - or non-quantifiable - factors to provide a complete analysis for the decision maker. A classic example of an intangible that can override many economic factors is passenger safety in the transportation industry. There may be cheaper ways to refurbish jet engine parts, for example, but if they impact engine reliability and thus impact passenger safety, they are unacceptable to the customer.

The end result will be a simple methodology for comparing competing technologies for either the purchase of new equipment or the replacement of existing equipment.

3. COST EFFECTIVENESS MODEL

A four-step methodology will be used to develop the cost effectiveness model:

I. Establish the current baseline.
II. Develop the potential baseline for waterjet using the same criteria.
III. Quantify the differences and assess the economic value of one method over the others.
IV. Portray the data in a format appropriate to the specific decision makers involved.

In step one, all the elements that contribute to the cost of processing - either cutting or decoating - must be determined. These normally include:

- Labor hours expended and costs per hour
- Material costs
- Operating costs (power, fuel)
- Waste disposal costs
- Maintenance costs

These are usually easy to obtain because they are based upon normal day-to-day operations. In fact, it is these costs that many times contribute to the search for cheaper and more effective alternatives.

In step two, comparable data elements must be obtained for waterjet processing of the identical tasks. These can be obtained from test cuts or coupon decoating or from existing operations where the cutting or decoating tasks are identical or similar. There is a danger, however, in trying to compare actual data from the workplace with "paper data" based on testing or theory. The credibility of the entire analysis rests on the validity of the data used. Step two is clearly the most crucial in the entire analysis.

Step three involves converting the baseline and waterjet costs to comparable time periods, wage rates, workloads, workshifts, and other factors to ensure a meaningful comparison. In step three, another evaluation factor can emerge: opportunity costs. If waterjet processing, for example, were twice as fast as the baseline technology, and all other factors were equal, the customer is presented with many favorable options including increasing workload, transferring man power to other tasks, or needing only half as many waterjet systems as baseline systems. Opportunity costs can be very significant in some specific cases. If waterjet stripping of aircraft, for example, could reduce aircraft "turn time" of a Boeing 747 from six days to three, the additional revenue passenger miles possible if several hundred aircraft were stripped and painted each year is quite significant.

Step four includes presenting the data in terms the client can best interpret to make a decision. The format can be quite variable. In large corporations, for example, the prioritization of capital expenditures is rigorous, formalized, and comparable from one project to another. Commonly used measures of economic value include payback period, return on investment, or internal rate of return. In small job shops or medium-sized businesses, however, the factors of importance can be quite different: speed of operation to meet tight schedules, lower production costs, or even smaller work area requirements. Thus, the process varies from one company to another, one industry to another, one type of equipment to another, and therefore, must be carefully formatted to be useful and persuasive.

5. CASE STUDIES

A series of case studies will be used to illustrate the methodology:

Case I - Waterjet Decoating of Jet Engine Parts

Because waterjet decoating is now operational at most domestic airlines and in many international airlines, there are good data available that compare waterjet decoating with the conventional methods of grit blasting, machining, and manual scraping or heat treatment. Tables 1, 2, and 3 contain actual data from two domestic and one international airline. The current labor hour costs are compared with waterjet processing costs to compute the net savings in labor costs.

Table 1 - Maintenance Data, Major U.S. Airline I

PART IDENTIFICATION	CURRENT (HR)	WATERJET (HR)	SAVINGS (HR)
JT8 BURNER CAN	2.16	0.50	1.66
JT8 1ST STAGE STATOR CASE	46.00	0.50	45.50
JT8 FWD FAN CASE	5.40	0.50	4.90
JT8 REAR FAN CASE	1.20	0.30	0.90
JT8 DIFFUSER CASE	4.00	0.50	3.50
JT8 FWD TURBINE CASE	6.00	0.50	5.50
JT8 REAR TURBINE CASE	5.00	0.50	4.50
JT8 ALUM. 2ND STAGE STATOR CASE	2.00	0.50	1.50
JT8 2ND STAGE COMP. STATOR CASE	2.00	0.50	1.50
JT8 4TH STAGE LPT AIR SEAL RING	2.00	0.50	1.50
JT8 13TH STAGE AIR SEAL RING	2.00	0.50	1.50
JT8 2ND STAGE AIR SEAL RING	2.00	0.50	1.50
JT8 #5 BEARING HOUSING	4.00	0.25	3.75
JT8 REAR COMPRESSOR INLET CASE	3.20	0.50	2.70
JT8 FAN FWD STATOR CASE	5.00	0.50	4.50
GE OUTER COMBUSTOR LINER	3.00	1.00	2.00
GE INNER COMBUSTOR LINER	3.00	1.00	2.00
GE COMBUSTOR ASSEMBLIES	3.00	0.50	2.50
GE FRONT STATOR CASE	2.00	0.75	1.25
GE REAR STATOR CASE	6.00	3.00	3.00
GE 3-9 STAGE COMPRESSOR SPOOL	4.00	1.50	2.50
GE 11-13 STAGE COMPRESSOR SPOOL	3.00	0.50	2.50
GE 14-16 STAGE COMPRESSOR SPOOL	3.00	0.50	2.50
GE 1ST STAGE HPT SUPPORT	2.00	0.50	1.50
GE 2ND STAGE HPT SUPPORT	2.00	0.50	1.50
GE 1ST STAGE NOZZLE IMPINGEMENT RING	2.00	0.50	1.50
GE #4 BEARING SEAL	2.00	0.50	1.50
GE 2ND STAGE NOZZLE	4.00	0.25	3.75
GE 1ST STAGE COMPRESSOR HUB	2.00	0.50	1.50
GE TURBINE MID FRAME	2.00	1.00	1.00

Table 2 - Maintenance Data, Major International Airline

PART IDENTIFICATION	CURRENT (HR)	WATERJET (HR)	SAVINGS (HR)
BOOSTER SHROUD	10.00	0.70	9.30
HPC DISK	5.00	0.10	4.90
SPOOL	12.20	0.80	121.20
HPC STATOR CASE	144.00	0.80	143.20
TURBINE MID-FRAME	5.50	0.70	4.80
COMPRESSOR REAR FRAME	4.00	0.80	3.20
SUMP	3.00	0.70	2.30
THERMAL SHIELD	24.00	0.80	23.20
LOW-PRESS. TURBINE CASE	4.00	1.00	3.00

The third airline assessed the waterjet investment based principally on the processing of inlet fan cases. The environmental concerns associated with the conventional method (heat) combined with high labor costs (scraping) were enough to provide the needed justification.

Table 3 - Maintenance Data, Major U.S. Airline II

PART IDENTIFICATION	CURRENT (HR)	WATERJET (HR)	SAVINGS (HR)
INLET FAN CASE	22.00	2.00	20.00
MISC. PARTS (AVERAGE)	NA	NA	5.00

With two baselines compared, the next step is to establish the economic framework for comparison. Because an automated, robotic waterjet decoating system is a major capital investment, a payback period approach was selected. Most airlines use this method because they can compare a number of different capital funding alternatives at the same time and prioritize them from the lowest to the highest payback period.

Using the data from the three airlines we found:

- The average processing time for waterjet decoating of an engine part was 40 minutes.
- The average labor hour savings for waterjet decoating compared to the conventional method was 4.8 hours per part.

To convert these individual part processing times and savings to a yearly basis requires a number of assumptions and a few simple calculations:

- Assume the waterjet workcell will operate 5 days/week, 52 weeks/year with 260 days of operation per year.
- To obtain the part capacity of the workcell, we assume one 8-hour workshift and the 40 minute/part processing time. All things being perfect, 12 parts/shift could be processed. Only 10 parts/shift were used in the analysis, however, to allow for the "frictional" effects of part setup and work breaks.

To determine the labor savings possible over a year's operation, we calculate:

- Processing 10 parts/shift with 260 days available per year allows 2600 parts to be processed per year. If an average 4.8 labor hours are saved per part, then 12,500 labor man-hours are saved per year with waterjet processing.

- For double shift operations, 20 parts would be processed per day or 5,200 parts per year. At 4.8 hours saved per part, 25,000 hours are potentially saved per year using double shift operations.

With this information, it is now possible to prepare the payback period analysis with a few more assumptions. Table 4 shows a 5-year analysis of the cost factors involved with the waterjet decoating system.

A capital investment of $800,000 is assumed for the waterjet system with an annual maintenance cost of approximately 5% of the purchase price for both parts and labor. An average hourly rate (fully burdened with benefits, etc.) of $20 per hour was assumed as well as double shift operations. This will be varied since $20 per hour may not be representative of other companies.

Table 4 - Cost Summary Analysis

	YEAR1	YEAR 2	YEAR 3	YEAR 4	YEAR 5
MHRS SAVED	25,000	25,000	25,000	25,000	25,000
AVERAGE HOURLY WAGE	$20.00	$20.00	$20.00	$20.00	$20.00
LABOR SAVINGS	$500,000	$500,000	$500,000	$500,000	$500,000
MAINTENANCE COST	($40,000)	($40,000)	($40,000)	($40,000)	($40,000)
WATERJET EQUIPMENT	($800,000)	0	0	0	0
YEARLY SAVINGS	($340,000)	$460,000	$460,000	$460,000	$460,000
CUM. SAVINGS (AFTER PAYBACK)	($340,000)	$120,000	$580,000	$1,040,000	$1,500,000

The yearly labor savings of $500,000 are reduced each year by maintenance costs and, in the initial 2 years, by the cost of the capital equipment itself. For this particular labor cost, the equipment is paid for in 18 months of operation and, by the end of the 5-year period, has earned $1.5 million.

To reduce complexity, several factors such as tax impacts are not included. Depreciation, for example, would provide a tax benefit for several years. On the other hand, the labor savings would accrue to the bottom line and be taxed as additional profits. The value of the out-year dollar savings should also be reduced by inflation since they will be worth less when finally received.

Because the savings shown - and the resulting payback period - are a strong function of the hourly wage, Figure 1 is shown to illustrate the payback period as a function of the average hourly wage rate.

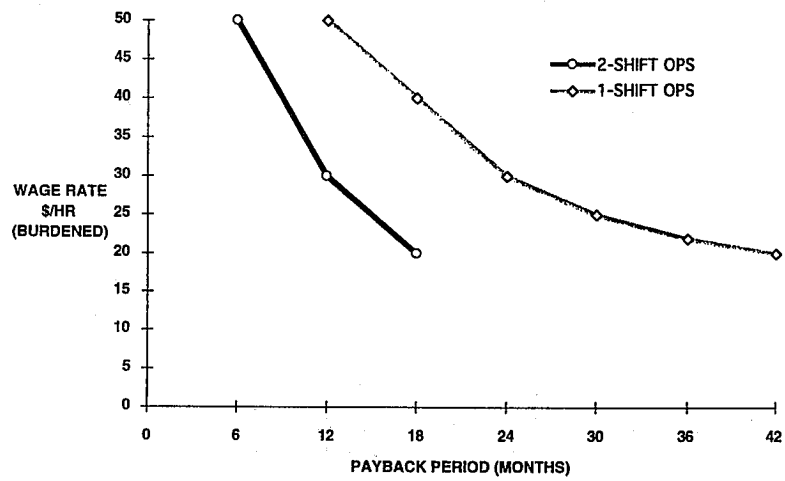

Figure 1 - Payback Period for Variable Wage Rates

The two curves shown allow for calculations of the payback period (for single and double-shift operation) as a function of burdened labor wage rates. For the more typical $35 per hour wage rate in the aerospace/aviation business, a waterjet investment could be paid back in less then one year in double-shift operations, as shown.

There are a number of complicating factors that can be added to the analysis. Tax considerations, for example, can work in different ways. For tax purposes, the capital expenditure can be depreciated over a number of years to provide a tax credit. On the other hand, the money saved using the equipment increases profits which are, in turn, taxed. The future value of money can also be a consideration, since savings received in the out years will be worth less than those saved in the current year because of inflation. Opportunity costs can also be significant in some cases. In our waterjet example, we were able to save 4.8 man-hours, on average, for every part processed. This can translate to additional throughput capacity for the facility allowing them to accept third-party work and further increase profits.

Case II - Waterjet Cutting of Quartz Wafers

The second case study is less complex and involves a decision to purchase conventional cutting equipment or a waterjet cutting system. The material to be cut is a thin quartz wafer - 0.635 mm (0.025 in) thick - used for specialized electronic applications. The conventional method for cutting these type wafers is a diamond saw system. These type saws are relatively slow in operation; however, they are capable of cutting with a very narrow kerf. Conventional diamond cutting saws cost approximately $70,000 each.

Preliminary cutting tests using abrasive waterjet revealed waterjet to be much faster; however, kerf widths were considerably larger than with the conventional diamond saws. By designing a special abrasive cutting head, it was possible to narrow the waterjet cutting kerfs to a range comparable with diamond saws, so the only comparison basis was the cutting speed and system cost. For comparison, the cost of an equivalent waterjet cutting system was approximately $125,000. Other cut characteristics such as edge quality, breakage rates, edge spalling, etc., were found comparable or superior with waterjet.

The cutting data collected for the cost effectiveness analysis are shown below. Several different types of quartz wafers were to be cut and a range of cutting speeds determined:

- Diamond saws operate over a range of cutting speeds for the quartz wafers from 2.54-6.35 mm/sec (0.1-0.25 in/sec)
- Waterjet cutting speeds using the specially designed narrow kerf abrasive head were in the range of 21.1-31.8 mm/sec (0.83-1.25 in/sec)

The wafers to be cut were 101.6 mm (4 in) in diameter. Each wafer requires approximately 26 straight line cuts for a total linear cut length of 1800 mm (71 in) per wafer.

Two economic scenarios were under consideration for capital investment: a new facility capable of cutting 500,000 wafers per year and the modification of an existing diamond saw facility to double the current production rate of 250,000 wafers per year.

To simplify the computations, the following assumptions were used:

- For the range of cutting speeds possible, each diamond saw is capable of cutting between 10,546 and 26,366 wafers per year with an average of 18,500 per year.
- With abrasive waterjet cutting, the potential production rate per waterjet cutting system was 87,535 to 131,831 wafers per year with an average of 110,000 per year.

The first scenario requires a production rate of 500,000 wafers per year using either diamond saws or waterjet. Using the potential rates for each technology shown above, the number of systems and the associated capital costs are:

- Twenty eight (28) diamond saws, each capable of cutting 18,500 wafers per year with a total capital cost of $1,960,000 and a production rate of 518,000 wafers per year.
- Five (5) waterjet systems, each capable of cutting 110,000 wafers per year with a total capital cost of $625,000 and a production capacity of 550,000 wafers per year.

The waterjet alternative is clearly preferable, even though waterjet cutting systems are more expensive to purchase. The net savings in capital costs were over $1.3 million. Maintenance costs, operating costs, and environmental costs were equivalent between the two systems.

The second scenario involves modifying an existing diamond saw facility to double production to 500,000 wafers per year by adding additional saws or using waterjet equipment. The calculations for this scenario are comparable to the first with the objective of determining the least costly method for cutting 250,000 wafers:

- Fourteen (14) diamond saws are needed for a cost of $980,000 and a production rate of 259,000 wafers per year
- Three (3) waterjet cutting systems are needed for a cost of $375,000 and a production rate of 320,000 wafers per year.

Again, the waterjet alternative is most cost effective by saving over $600,000 in initial capital costs.

6. SUMMARY AND CONCLUSIONS

In summary, we have described a relatively simple methodology for developing a cost effectiveness analysis that can be used to compare a potential replacement technology with a conventional one. A complex coating removal example was presented along with a relatively simple cutting application. The end result of using the methodology is an economic basis for justifying the use of a replacement technology, such as waterjet, based on tangible benefits. The basic methodology is expandable to handle the addition of as many other complicating factors as needed to make the case.

Tables

Figures

8th American Water Jet Conference
August 26-29, 1995: Houston, Texas

Paper 53

DEVELOPMENT OF A WINDOWS-BASED EXPERT SYSTEM FOR ABRASIVE WATERJET CUTTING

Pawan Singh
Quantum Industries International, Inc.
Bethlehem, PA 18018

ABSTRACT

The paper describes the development of a PC Windows-based expert system for waterjet cutting and the object-oriented QXpert technology on which the development is based. The expert system integrates many functions and expert aids to help a waterjet system user optimize the system operation. These functions include cutting speed prediction for various materials, guidance on optimal system settings, database development, and cost and investment analysis. Expert aids include system diagnostics, efficient operation tips, hypertext-linked operation manuals and several utilities like communication links and scientific calculator. The expert system can also link to other Windows or DOS applications such as machine controller system, spreadsheet analysis and word processing software. Multimedia applications such as video and audio can be easily integrated with the aid of the underlying QXpert technology. Experience indicates that such expert systems have the potential of providing radical gains in machine productivity and impart a competitive edge to the waterjet technology over competing technologies.

Organized and Sponsored by the Water Jet Technology Association.

1. INTRODUCTION

With increasing growth and commercialization of waterjet technology, there has developed a growing need for simplification and understanding of the best way on how to utilize the technology most efficiently. Like traditional machine tool operators, a waterjet system operator is not interested in intricacies of motor controls or hydraulic circuits. He is mainly interested in how he can get maximum throughput from his system at the lowest possible cost while maintaining the desired quality level.

System manufacturers are responding to these needs in different ways. One system manufacturer has introduced a PC-based control system that almost completely automates the cutting process (Olson, 1994). Other manufacturers have responded by providing guidance on cutting speed and cut quality through PC-based systems (Zeng and Munoz, 1994). One common thread that runs through these various options is the use of PCs to make the task simpler. Since the industry is also gradually shifting toward PC-based control systems, cutting knowledge can then be directly integrated with system operation.

With waterjet cutting, particularly abrasive waterjet cutting (AWJ), an operator has the option to select several parameters to meet his cutting objectives such as speed and quality. These parameters include system pressure, orifice nozzle and focusing tube bores, and abrasive flow rate. Each selection has some constraints either defined by system limits or by performance limits. For example, the selection of orifice nozzle bore is limited by the horse power and flow rating of the high pressure fluid source. The selection of abrasive flow rate is limited by the abrasive loading capacity of the cutting head, and by the deterioration in system performance beyond a certain abrasive flow rate.

For most efficient cutting an operator must be able to develop and employ optimum parameter settings for each cutting job. True optimization for a multidimensional process such as waterjet cutting can be a daunting task. Although Singh and Munoz (1993) have shown that the task can be much simplified through process understanding and local optimization, operator expertise plays a key role in how close the real operation comes to the theoretical optimum. The potential for operating cost savings with optimization is large, as much as 20-30%, according to the author's estimates. Thus any mechanism that can build and disperse expertise can have a huge influence on the waterjet industry by making the waterjet technology more efficient and more competitive. One such mechanism is the use of a computer-based expert system.

2. EXPERT SYSTEMS

2.1 What is an Expert System?

An expert system provides an ability to codify human expertise and knowledge into a computer. It gives the user who may have little product or process expertise himself, tools to come up with best results based on situational analysis. Expert systems are a form of artificial intelligence (AI), although the definition and scope of artificial intelligence have changed

sharply in the last five years. During its formative years, artificial intelligence was closely associated with a special language, LISP, and development of intelligent solutions required special expertise and training. The promoters of AI promised revolutionary changes that never materialized and AI got a bad reputation.

However, the premise behind artificial intelligence, the cloning of human expertise to develop highly productive intelligent business and technical solutions, has never been more popular (May, 1994; Newquist, 1994; Price et al., 1994; Mentzer and Gandhi, 1993; and Kader, 1992). Expert systems are proliferating and expert features are being added to routine software without notice. For example, intelligent features sensing and automatically correcting commonly misspelled words in a word processor software is an example of an expert system.

Unlike the earlier days of artificial intelligence when rigid and complex rules and language prevailed, the greatest push for expert systems comes now from the ease and standardization of building such systems (Fadum, 1993). One recent innovation in software development, object-oriented technology, has been the prime driver for rapid development of expert systems. Other artificial intelligence tools that are gaining popularity are neural networks, case-based reasoning and fuzzy logic.

Object-oriented programming is leading a titanic shift in software development. Instead of the traditional way of writing custom code for each application, a programmer connects a number of objects like an integrated circuit with each object encompassing a function like a resistor or a capacitor. These objects have properties (like resistance of a resistor) that can be changed by the programmer. In expert systems such objects may be rules driven, and may perform extensive calculations to define some of their properties. Since these objects can be re-used like components in an erector set, systems can be reprogrammed or new systems developed at a phenomenal pace.

2.2 Expert Systems and Abrasive Waterjet Cutting

Expert systems are most useful when a system cannot be managed well by rigid rules, and the expertise to manage the system is either not easily available or has a high economic value. Abrasive waterjet cutting fits this definition well. Although the cutting operation itself is relatively simple, determination of an optimal cutting condition for each set of cutting requirements is a very complex task. Based on his experience, an expert waterjet system operator selects system settings that may come very close to the optimal cutting objective. Studies have shown that productivity gains and cost savings of as much as 15-20% can be achieved by optimizing the cutting operation.

What makes the cutting optimization especially difficult is that a host of system parameters influence cutting speed and quality, and the desired result can be achieved by a virtually infinite combinations of these parameters. Of course, only one of these combinations is going to meet the optimization objective and necessary constraints. An expert system operator relies

on experience, past history and knowledge to select system settings. The use of this expertise along with the use of mathematical modeling and optimization techniques offers ideal conditions for development of an effective expert system for waterjet cutting.

Singh and Munoz (1993) have shown that the highly complex mathematical problem of optimization can be simplified by taking advantage of well-established relationships among some of the parameters. The use of such relationships converts the problem of multi-dimensional global optimization to two or three-dimensional local optimization, and the problem can then be solved by linear optimization and other techniques.

The best expert systems use a combination of mathematical modeling and experience-based rules to arrive at decisions (Lausterer et al., 1992 and Gulati and Tanniru, 1993). Sometimes they may offer a choice of decisions along with expected results for each, leaving the selection decision to the user. They provide an explanation on how the decision was arrived at. Like a good waterjet system, they are aesthetically pleasing, uncluttered and functional. They use graphical user interfaces (GUI) that are clear and intuitive. They eschew the temptation of some software designers to smother functionality with multiplicity of colors, charts and clip art. Since technology like waterjet changes rapidly with time, and new knowledge can antiquate yesterday's rules quickly, good expert systems are flexible and modular. Preferably they use object-oriented technology allowing easy upgrades and addition of new features.

3. DEVELOPMENT OF A WATERJET EXPERT SYSTEM

The author's company has developed a waterjet cutting expert system that integrates cutting expertise with enhanced features such as cost analysis, system diagnostics and numerous software utilities. The system is developed using the company's QXpert technology, an object-oriented framework for rapid development of expert systems integrated with standard and custom software tools.

3.1 QXpert Technology

QXpert technology is a platform for rapid development of enhanced expert systems that cuts down development time and cost of such systems by a factor of five to ten. Based on object-oriented software technology and developed by the author's company, QXpert works with Windows 3.x operating system on individual or networked PCs. Using advanced Windows tools such as OLE, DDE, and ODBC, QXpert-based systems can work with existing databases on a host of standard platforms ranging from workstations to mainframes. QXpert also allows seamless integration with other Windows applications such as Excel or Lotus 1-2-3 spreadsheets and Word for Windows or WordPerfect word processors. QXpert can also execute existing DOS-based software, be it a proprietary FORTRAN program or DOS-based AUTOCAD.

QXpert can be used to develop multimedia applications, combining audio, video and graphics with expert software. It offers powerful communications capabilities, allowing machine to

computer and computer to computer communications. It can incorporate data acquisition and analysis systems, yielding on-line real-time diagnostic capability. In summary, using the latest software advances, QXpert can develop powerful software systems that can significantly enhance a machine's capabilities and productivity. Some early studies indicate that QXpert-based expert systems have a payback period of a few months and ROI of 150-200%.

3.2 QXpert Waterjet System Capabilities

Following is a list of the basic capabilities of the expert waterjet system:

Cutting Speed and Settings
- Recommended parameter settings based on specified cutting objective, material selection and system constraints.
- Prediction of cutting speed for most common materials for various quality levels.

Cost and Investment Analysis
- Computation of various cost components and overall cost of waterjet cutting.
- System cost accounting options (depreciation or leasing).
- Computation of cost per inch, based on predicted or actual speed (if known).
- Loan or lease payment calculations including preparation of amortization schedule.

Database Development and Management
- Forms for developing a new or editing an existing cutting database.
- Importing or exporting data from or to spreadsheet software like Excel.
- Direct linking with spreadsheet or database management software for data analysis and graphic output.

Diagnostics and System Information
- Hypertext-linked machine diagnostics in a decision tree format, allowing easy diagnosis of common waterjet system problems and failures.
- Guide to efficient operation of the system in the form of operation tips and expert guidance.
- Extensive communication capabilities, including providing links to system manufacturer computers, bulletin board and data transfer.
- Multimedia capabilities, including video and audio to aid in diagnostics or to supply information.
- Capability to include an on-line operations manual or catalog.
- Fast graphics viewer and marker to view and annotate drawings and digitized pictures and graphics.

Links to Other Applications
- Control cutting operation through CAD/CAM software such as SmartCam.
- Acquire and analyze data through data acquisition software.
- Launch other applications such as AUTOCAD or word processing from QXpert.
- Access to most types of databases and computers through ODBC links.
- Run proprietary applications, including DOS-based software.

Software Utilities
- Communication links.
- Calculator and Notepad.
- File management, including definition of various links.

Usability Features
- Extensive on-line help.
- Context-sensitive help.
- Floating toolbars and use of common icons, wherever possible.

4. WATERJET EXPERT SYSTEM DESCRIPTION

Figure 1 shows graphical user interface (GUI) for the waterjet QXpert system. Characterized by menus, familiar icons and floating toolbars, the interface was selected after extensive research in software usability. Since Windows-based word processing and spreadsheet software are very familiar to most users, QXpert interface was developed to have a similar look. Figure 1 shows the cost profile module.

Based on findings from usability research, several user-friendly features were added. Among them:

- Extensive hypertext-based help routines with contents matching closely to the printed manual.
- Context-sensitive help on every field.
- Expertise-based messages when the user selections are not consistent with normal practice.
- Use of different font colors for input, recommended, recommendation-overridden and calculated values.

Figure 2 shows the cutting speed computation screen. The user first enters intensifier (or pump) ratings which are used as HP and flow constraints. Then the user selects material to be cut, material thickness and a qualitative measure of desired cut quality. Next, the user selects the cutting objective. Based on the selections, the expert software recommends values for system settings such as pressure, abrasive flow rate, and nozzle and focusing tube bore diameters. These settings change if the user changes the default values of the number of cutting heads or the type of abrasive. Also, the user can override the recommended settings.

When the user clicks on the Calculate button, the program calculates predicted cutting speed as well as fluid HP and Flow. If the user has overridden the program recommendations and the HP and flow exceed the intensifier ratings, the program displays error messages. The cutting speed is calculated according to Zeng and Kim's (1993) model, although some of the model's coefficients have been adjusted based on experience and test data.

Figure 3 shows an example of the structure of knowledge base that is available to the users. In this example, diagnostics information is classified under various equipment categories and

it can be further subclassified in a tree-root like structure. The information can also be accessed from keywords and topics through the Help system's search routines.

5. EXPERT SYSTEM APPLICATIONS

QXpert technology described here is a framework for rapid development of expert systems. Such systems have applications in:

- Machine tool operation and automation
- Sales and Marketing
- Machine diagnostics
- Training
- On-line monitoring

It is not necessary to create a separate expert system for each function. An integrated expert system can be used for all the functions described above. For example, the waterjet expert system described in this paper can not only be used as an expert aid for waterjet system operation but also as a productivity tool for waterjet sales and marketing, cutting database development, automated system control and diagnostics.

Experts predict that the greatest source of future increase in machine tool productivity will come from smart software controls (Feldman et al., 1992). In the next ten years, virtually every system software will include expert features as an integral part of the software and the term expert systems will become redundant. It is essential that the waterjet industry becomes a leader in the use of smart software to increase system productivity, as it will be competing with other technologies like laser cutting which are adopting smart controls with great vigor.

6. CONCLUSIONS

The paper describes a framework technology for rapid development of Windows-based PC expert systems and a prototype waterjet expert system developed with the technology. The technology, based on object-oriented programming, creates application modules that are accessed through an intuitively clear graphical user interface. These modules (or objects) can be re-used in other systems or easily modified to adapt to any design changes or upgrades.

The waterjet expert system presented in the paper has multiple capabilities that include cutting speed prediction, cost and investment analysis, database development tools, communications and productivity tools, expert diagnostics and extensive help routines. The system can be integrated with machine controls and on-line data acquisition for automatic machine operation. The system can also be linked to other Windows software and virtually any kind of database.

Expert systems have the potential of creating large gains in machine and business productivity. Waterjet technology must vigorously adopt their use to remain competitive with competing technologies that are actively incorporating expert systems in many applications.

7. ACKNOWLEDGMENT

The author is thankful to the company management for allowing the publication of this paper. Windows is a trademark of Microsoft Corporation and QXpert is trademark of Quantum Industries. Other trademarks mentioned in this paper are the property of their respective owners.

8. REFERENCES

Olsen, J. H., "Structure and Controller for Abrasive-Jet Machine Tools," SME technical Paper No. MR94-252, Presented at Advances in Precision Machine Design Conference, September 12, 1994, Chicago, Illinois, USA, 1994.

Singh, P. and Munoz, J., "Cost Optimization of Abrasive Waterjet Cutting Systems," Proceedings of the 7th American Waterjet Conference, Seattle, Washington, 1993.

Zeng, J. and Kim, T.J., "Parameter Prediction and Cost Analysis in Abrasive Waterjet Cutting Operations," Proceedings of the 7th American Waterjet Conference, Seattle, Washington, 1993.

Zeng, J. and Munoz, J.P., "Intelligent automation of AWJ Cutting for Efficient Production," Proceedings of the 12th International Symposium on Jet Cutting Technology, BHR Group, Rouen, France, 1994.

May, Kenneth M., "Expert Systems in Demand Despite Uneven Past," National Underwriter Life & Health-Financial Services Edition, August 8, 1994 n32 p8 (2).

Newquist, H.P., "It Actually Works! AI Breaks Through in Real-World Apps.," (artificial intelligence), Computerworld, April 18, 1994 v28 n16 p132 (2).

Price, James D., Malley, John C. and Balsmeier, Phillip W., "Expert Systems: Application to Inventory Control and Production Management," Industrial Management, Sept-Oct 1994 v36 n5 p26 (5).

Mentzer, John T. and Gandhi, Nimish, "Expert Systems in Industrial Marketing," Industrial Marketing Management, May 1993 v22 n2 p109 (8).

Kader, Victoria, "Use of 'Expert Systems' Spreads, Particularly in Europe, and U.S. has Technological Lead," Business America, Sept 7, 1992 v113 n18 p18 (3).

Fadum, Ole, "Constructing and Implementing Successful Expert Systems," (Artificial Intelligence, part 2.) Pulp and Paper, March 1993 v67 n3 p87 (5).

Lausterer, G., Ehrler, H. and Zorner, W., "An Expert Approach to Power Plant Optimization," (Control Room Instrumentation). Modern Power Systems, Oct 1992 v12 n10 p33 (3).

Gulati, D. and Tanniru, Mohan R., "A Model-Based Approach to Investigate Performance Improvements in Rule-Based Expert Systems," Decision Sciences, Jan-Feb 1993 v24 n1 p42 (18).

Feldman, Richard M., Lively, William M., Slade, Tom, McKee, L.G. and Talbert, Alan, "The Development of an Integrated Mathematical and Knowledge-Based Maintenance Delivery System," (Technical). Computers and Operations Research, July 1992 v19 n5 p425 (10).

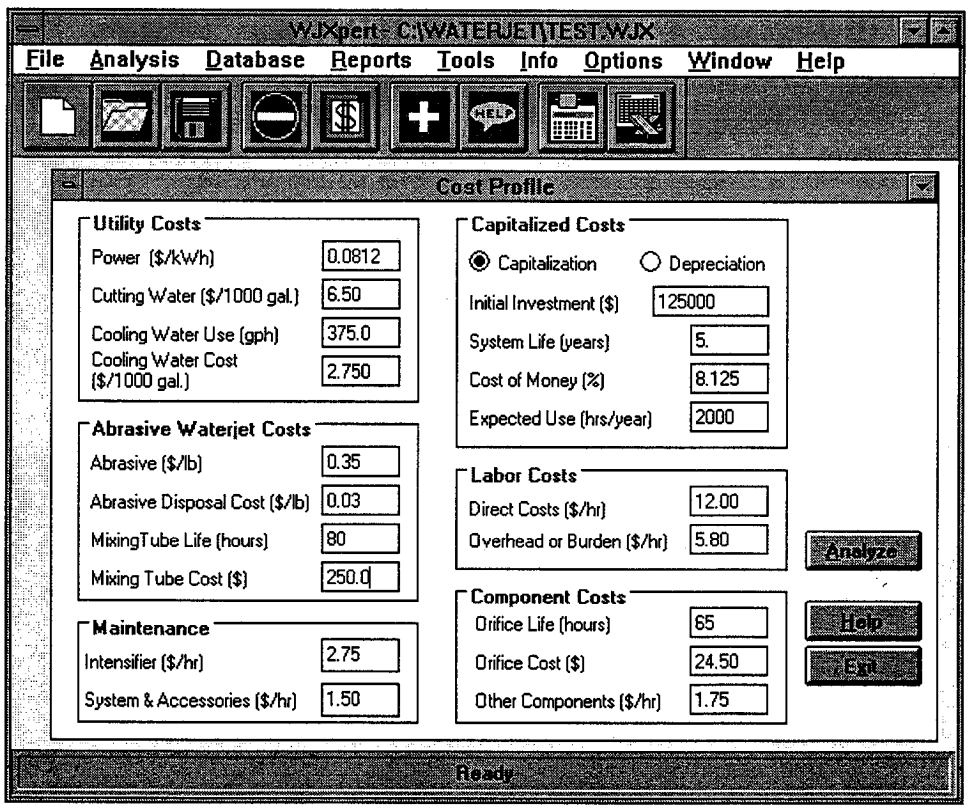

Figure 1: Graphical User Interface for the waterjet QXpert system.

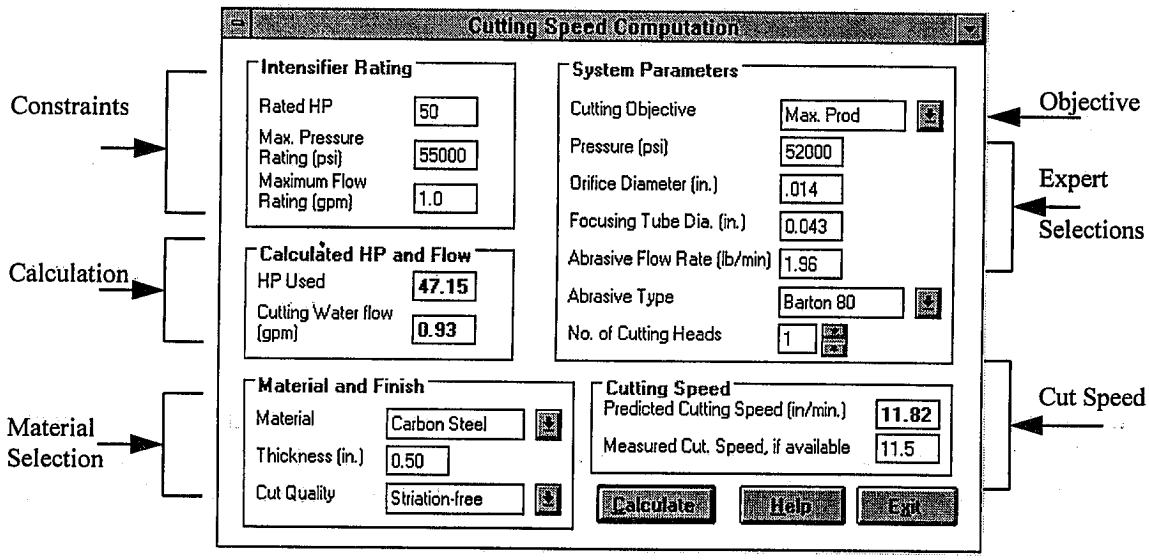

Figure 2: Cutting speed computation form.

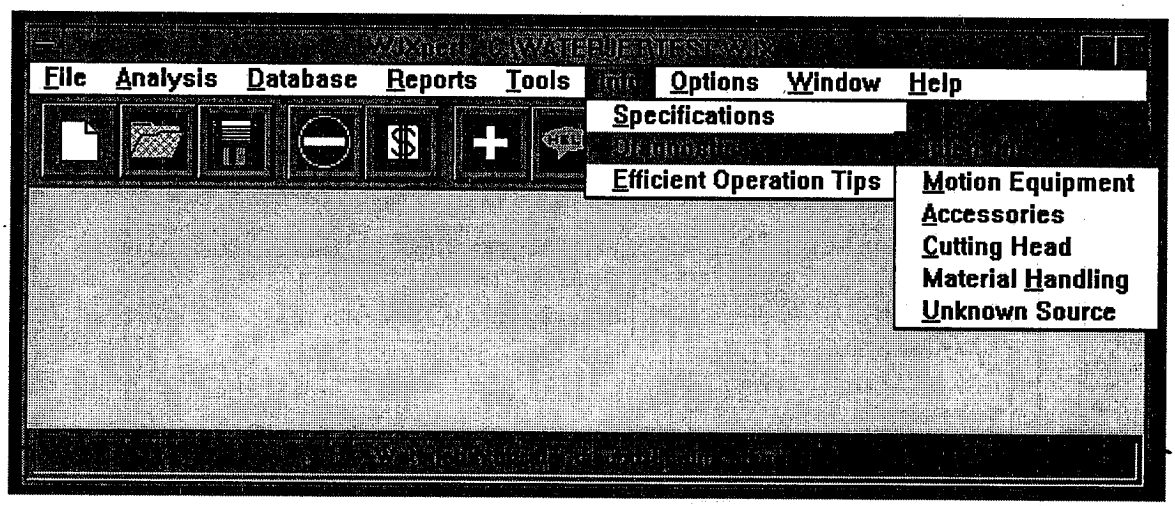

Figure 3: Tree root-like structure of information network.

8th American Water Jet Conference
August 26-29, 1995: Houston, Texas

Paper 54

WATERJET ABRASIVES: EVALUATING COST ANALYSIS PROCEDURES

William A. Ranney, Jr.
Barton Mines Corporation
North Creek, New York

ABSTRACT

With the increasing popularity of abrasive waterjet technology there is a corresponding increase in competitive pressure on operators. Cost effective selection of abrasives is more important than ever. This paper reviews abrasive types and characteristics, and discusses three perspectives from which cost analysis is commonly calculated. An equation for calculating the cost of cutting an inch of material that encompasses both abrasive cost and performance is included for the user's reference.

Organized and Sponsored by the Water Jet Technology Association.

1. INTRODUCTION

Nearly everything written recently on the topic of abrasive waterjet machining opens with a statement that qualifies waterjetting as a technology whose status is rapidly evolving from that of the marginal and esoteric to the level of an accepted, mainstream machining technology.

With this increasing popular acceptance, there is also increasing competitive pressure on waterjet operators, causing many to look hard at ways to optimize operating costs. Abrasives, recognized as one of the larger consumable components of this procedure, often become the focus of attention when calculating the cost of waterjet machining.

The aim of this paper is to examine the ways that abrasive waterjet efficiency is commonly calculated. By isolating the salient elements of the efficiency equation, we hope to assist the user in arriving at a method that suits his or her application best. As the intended audience of this paper is the newer user working in a commercial setting, this paper includes a simple overview of abrasives used in waterjetting applications.

2. WATERJET ABRASIVES. A BRIEF OVERVIEW

Abrasive costs are one of the largest expenses involved in operating a waterjet. While garnet has emerged as the standard, there are variables in cost and quality from one supplier to the next. Other abrasive materials are available for waterjetting applications, also of varying quality and cost, presenting even more for the user to evaluate.

Following are a handful of natural and man-made characteristics that effect abrasive performance in waterjet cutting. Generalizations can be made about the effect of each characteristic, however these assume that the waterjet itself is in good working order. Hardware problems such as insufficient pressure, improper nozzle alignment, etc., may prevent the operator from realizing the full benefit from any abrasive.

2.1 Natural Characteristics

	Mohs Hardness	**Specific Gravity**	**Particle Shape**
Almandite Hard Rock Garnet	8+	4.0	Sharp/Angular
Almandite Alluvial Garnet	7.5	3.9-4.1	Sub-rounded
Olivine	5.5	2.6	Sub-rounded
Slag	6-7	3.2	Angular

2.1.1 Hardness

Harder abrasives often cut faster and deeper. They may also break down less in the process of delivery to the workpiece.

2.1.2 Particle shape

Generally speaking, sharp, angular abrasives cut more efficiently than rounded grains, particularly on difficult or thick materials.

2.1.3 Specific Gravity

All other factors being equal, a heavier particle traveling at the same speed will transfer more energy to the surface and therefore cut more quickly.

2.2 Man-made Characteristics

Other abrasive characteristics are the result of the production process. Some of these include:

2.2.1 Purity

Normally impurities reduce the effectiveness of an abrasive. For example, silica and hornblend are softer and lighter than garnet. A garnet abrasive that has significant quantities of these minerals will not cut as quickly.

2.2.2 Particle Size

With the correct nozzle and pressure, a coarser abrasive will cut faster when speed is the primary concern. On the other hand, a finer abrasive will produce a better surface finish when finish is the chief aim.

2.2.3 Grading and Particle Size

a. Screen and Particle Size
   Mesh size is defined by the number of openings per lineal inch. A series of screens are used to progressively narrow down the particle size distribution for a given grade. An 80 mesh waterjet abrasive is therefore really a range of sizes. The narrower this range, the better the abrasive is for waterjet cutting. A wider range increases the likelihood the operator will encounter oversized particles (called "bricks") and undersized particles (called "fines"), both culprits in clogging and poor performance.

b. Consistency in Distribution and Range
   Different size particles will cut at different speeds. It is therefore helpful to have

consistent particle size distribution for even cutting performance from week to week. A good waterjet abrasive will have consistency both in its distribution (ratio of large to small particles) and its range (the outer size limits at both the fine and coarse ends).

3. DEFINING COST EFFECTIVENESS

The focus of this paper is on calculating efficiency as it relates to choosing abrasives, approached from the perspective of an everyday user operating in a commercial environment. As pointed out by Singh and Munoz in their paper, Cost Optimization of Abrasive Waterjet Systems (Seattle 1993), costs are defined in various ways by various businesses. Engineers, accountants, and business managers all approach the subject with varying needs and expectations. In the current business environment there is often one person who must answer to all of these expectations--the operators or managers of smaller job shops, for example.

Every operator bases decisions regarding abrasives, nozzles, and flow rates on methodology drawn from some combination of training, experience, and/or advice from other operators.

Without delving too far into the vagaries of human behavior it is safe to assert that these users all have a level of (financial) comfort regarding operating costs, which once exceeded trigger a reflex common among all highly evolved bill-paying creatures--panic. This highly effective intrinsic motivator is often the stimulus for examining operating costs, and as a result, the cost effectiveness of their abrasive choice.

How is it then that we determine what is cost-effective and what is not? Starting from abject intuition and moving towards the hopefully scientific, what follows is a fairly simple progression:

3.1 Unit cost

Ranging from cost per pound to cost per truckload, this component of a more comprehensive formula is occasionally as far as some users care to look when attempting to optimize the overall economy of their operation. If all abrasives were equal this reasoning might have some benefit, however, as illustrated by the short description of the various abrasives above it is clear that they are not. Variations in hardware, cutting applications, and operator ability amplify many of these differences even further.

Simply put, your machine may cut material using beach sand as an abrasive, just as your car or truck will run on watered-down fuel. But like your automobile, pinging and sputtering along the shoulder of the road, your waterjet will not cut efficiently--it will take forever to get where you are going. Cheap, yes, but certainly not cost effective.

Cleanliness and consistency of the abrasive has a decided impact on overall efficiency. If your operation suffers inordinate downtime because of clogging or other abrasive related hardware ailments, any savings in unit cost will be quickly eaten up.

3.2 Cost per Hour of Operation

Any complete analysis of overall efficiency requires a careful assessment of hourly operating costs. However, as with unit cost, determining the cost effectiveness of a given abrasive or abrasive/nozzle combination by examining only the cost per hour of operation is at best an incomplete endeavor.

A comprehensive assessment of hourly operating costs would include, but is not limited to, the following factors:

- Capital costs, includes all costs relative to equipment and tooling.
- Labor
- Operating costs, includes:
  - power
  - water
  - filtration
  - maintenance
  - consumables (abrasive, nozzles, etc.)
  - disposal

Given that the total hourly operating costs, in which abrasive costs are included, comprise only approximately 30% of total cost, and that most simple formulas do not account for the possible benefit of increased throughput and/or billable hours due to increased abrasive (cutting) efficiency, this method falls short of the mark for the purpose of accurately evaluating the differences in overall effectiveness.

3.3 Cost per Inch Cut

Both the price per pound (unit cost) and the cutting performance of the abrasive effect the cost of operating an abrasive waterjet. Higher quality abrasives generally cost more because extra effort has gone into producing and refining the product. The additional cost must be weighed against performance.

In any production process the important measurement is the final cost of producing one unit. This can measured by dividing the total cost of production by output.

$$\frac{\text{Total cost}}{\text{Output}} = \$/\text{Unit produced}$$

In waterjet cutting, we can define production as inches cut and measure the cost of cutting one inch:

$$\frac{\text{Total waterjet operating cost per hour}}{\text{Inches per hour}} = \$/\text{inch cut}$$

Total abrasive cost is determined by cost per pound and the amount of abrasive consumed in one minute.

($/lb.)(lbs/minute)(60) = abrasive cost per hour

Therefore an equation calculating waterjet cost would look something like this:

$$\frac{\text{(lbs/hr)(\$/lb)} + \text{equip} + \text{labor} + \text{consumables} + \text{disposal}}{\text{inches cut per hour}} = \$/\text{inch cut}$$

As you are well aware, "in the field" waterjet performance varies from installation to installation due to the many variables involved. The operator can plug numbers into the equation above based on his or her own testing and costs and then determine which abrasive is best in that particular application. I have included a worksheet with this paper which, using this equation, may present this process a little more clearly.

For the sake of illustration, we assumed those other costs to equal $32. and then compared a low cost, low performance abrasive with a higher cost, high performance abrasive. The cut rates are similar to those that might be experienced when cutting 1 1/2 inch thick stainless steel.

Example 1

$$\frac{\text{(60 lbs/hr)(\$.15/lb)} + \$32/\text{hr}}{.8 \text{ in/min} * 60} = \$.85/\text{inch}$$

Example 2

$$\frac{\text{(45 lbs/hr)(\$.40/lb)} + \$32/\text{hr}}{1.25 \text{ inch/min} * 60} = \$\ .67/\text{inch}$$

In these examples, a very low cost abrasive successfully cuts the metal but the higher cost, higher performance abrasive saves a considerable amount of money by its superior performance. The illustration argues that cutting speed is the most important consideration

when selecting an abrasive. Abrasive performance has a greater effect on the final unit cost (that is, the cost of cutting one inch) than does its cost per pound.

3.4 Abrasive Waterjet Cost Analysis Worksheet

COMPANY NAME: DATE:

	ABRASIVE A	ABRASIVE B
Abrasive Info:		
Abrasive Cost:	$/lb	$/lb
Feed Rate:	#/hr	#/hr
Other Costs		
Labor:	/hr	/hr
Management:	/hr	/hr
Equipment:	/hr	/hr
Disposal:	/hr	/hr
Miscellaneous:	/hr	/hr
Total Other:	/hr	/hr
Performance:		
Cutting Speed	in/hr	in/hr

This represents an increase in cutting speed of:

_____ %

Using the formula:

$$\frac{\text{(Abrasive Cost) + (Other Costs)}}{\text{Cutting Speed}} = \text{Cost/Inch}$$

Abrasive A: _____ + _____ = The Cost Per Inch Is: $

Abrasive B: _____ + _____ = The Cost Per Inch Is: $

4. CONCLUSION

There are many variables to consider when selecting an abrasive. Comparisons based solely on unit cost or hourly operating costs do not provide an accurate basis for decisions regarding overall abrasive efficiency.

By using cost per inch cut as a benchmark, we are able to measure the effect of differing unit costs, hourly operating costs, and increased or decreased performance levels when comparing the relative efficiency of different abrasives.

5. REFERENCES

Ohman, J.L., "Abrasives: Their Characteristics and Effect on Waterjet Cutting" *Proceedings of the 7th American Waterjet Conference*, pp. 363-374, Water Jet Technology Association, St. Louis, MO, 1993.

Singh, P.J., and Munoz, J., "Cost Optimization of Abrasive Waterjet Cutting Systems" *Proceedings of the 7th American Waterjet Conference*, pp. 191-204, Water Jet Technology Association, St. Louis, MO, 1993.

Zeng, J., and Munoz, J., "Optimization of Abrasive Waterjet Cutting--The Abrasive Issues" *Waterjet Machining Technology Seminar*, Manufacturing 94, IMTS. Chicago, IL, 12 September 1994.

8th American Water Jet Conference
August 26-29, 1995: Houston, Texas

Paper 55

OBSERVATION OF SUBMERGED ABRASIVE-SUSPENSION JET CUTTING FOR DEEP OCEAN APPLICATIONS

D. Alberts, M. Hashish
QUEST Integrated, Inc.
Kent, Washington, USA

ABSTRACT

An experimental investigation was performed to evaluate the performance of directly pumped abrasive-suspension jets in a test chamber that simulated ocean depths of 0 to 6100 m. Pressure up to 379 MPa was used in the experimentation. This paper discusses the development of the test chamber and specialized abrasive jet heads, the experimental data that was collected under a range of parametric conditions, and the theories behind the phenomena that were found to occur.

Laboratory experiments have shown that the suspension jet cutting performance is not highly dependent on ambient pressures between 17 and 69 MPa, but there is a significant drop in performance between 0 and 17 MPa. Most other operating parameters were found to produce performance trends similar to cutting jets operating in air. It has been concluded that the abrasive jet, particularly the suspension jet, can be developed into a valuable tool for use in many underwater cutting applications.

Organized and Sponsored by the Water Jet Technology Association.

1. INTRODUCTION

Traditional rock cutting, coring, and metal cutting methods for underwater applications have serious technical, safety, and environmental limitations. Cutting methods for deployment via remotely operated vehicles in ocean depths of up to 6000 m with ambient pressures of up to 69 MPa are needed for exploration, mining, and salvage operations. Several related works addressing underwater abrasive jet cutting that have been published include Domann and Aust (1990), Haferkamp et al. (1990), and Surle (1990).

Abrasive-waterjet (AWJ) technology was introduced commercially in 1983. Since then, substantial advances have been made in all facets of AWJ technology, including a basic understanding of the cutting process and hardware improvements. New applications in drilling, turning, and milling are constantly emerging. New jetting processes need to be developed to fill existing performance gaps and extend current machining capabilities, especially in difficult environments. The direct pumping of premixed abrasive-suspensions is an alternative technique that improves upon and extends the capabilities of the AWJ.

An AWJ is typically formed by entraining abrasive particles into a high-velocity waterjet stream in a tubular nozzle (mixing tube). The abrasives are transported to the mixing tube by the inductive jet pump effect produced by the waterjet passing through the mixing tube. Energy is transferred from the water to the abrasive particles in the mixing tube.

In machining with the AWJ, material is removed by the erosive action of impacting abrasive particles. Typically, abrasives strike the workpiece at over one million impacts per second. High levels of particle kinetic power density are delivered to the workpiece; for example, a 1-mm-diameter AWJ operating on a hydraulic power of 15 kW will have about 19 kW/mm^2 power density. However, only a fraction of this power (about 10%) is transmitted from the waterjet to the abrasive particles, which are the main agents of material removal. Only a fraction of the particle's kinetic power (again, about 10%) is used in material removal. In spite of this apparent inefficiency, the AWJ offers great cutting and machining advantages over many other techniques (Hashish, 1984).

The basic limitation of using the AWJ for underwater cutting is primarily related to the reliance on the jet pump concept in achieving high levels of power density. The calculated ratio between the axial particle spacing at the nozzle exit to the particle diameter illustrates that particles are sparse; i.e., there are relatively large distances between particles in the AWJ. If these distances were filled with high-velocity particles, greater cutting capabilities would be expected. Due to the jet pump characteristics of the AWJ nozzle, only limited amounts of abrasives can be entrained. It may not be possible to obtain the desired density of abrasive particles in an entrainment nozzle. In addition, the particle velocity in an entrainment AWJ decreases as the abrasive mass flow rate increases.

It has been intuitively known that an efficient method of forming an abrasive-fluidjet would be to directly pump a premixed suspension through a nozzle to form an abrasive-suspension jet (ASJ). However, hardware complications, especially at high pressures, have limited the development of the ASJ method to low-pressure (up to 70 MPa) commercial systems.

Hashish (1982) reviewed the different methods of forming abrasive jets, including the direct-pumping approach and the advantages and disadvantages. Fairhurst et al. (1986) developed a low-pressure (up to 69 MPa), batch-pumping ASJ system. The relatively low pressure was compensated for by using relatively high abrasive flow rates (to 0.18 kg/s). Hollinger et al. (1989) conducted tests using an ASJ at pressures up to 104 MPa to demonstrate the thin kerf cutting capability. They observed that the nozzle (diameter ~ 0.254 mm) would become plugged if the suspension concentration exceeded about 10%. Also, at a pressure of 104 MPa, the ASJ cuts had less depth than those produced by a lower-pressure (69 MPa) ASJ. This decrease in depth was attributed to the jet's loss of coherency at higher pressures. A prototype ASJ pumping unit that can handle pressures of up to 379 MPa has been developed at QUEST for laboratory use and commercial system development. This pump is capable of continuous and batch mode pumping of abrasive-suspension mixtures. A simplified analysis of the ASJ process is presented by Hashish (1989).

In the research effort presented here, abrasive jet cutting equipment was adapted for testing with a hyperbaric test chamber to simulate deep ocean atmospheres. A direct-pumped ASJ system was used in the testing program. Nozzle pressures of up to 379 MPa were analyzed in the experiments. The cutting parameters that were investigated include abrasive concentration, particle size, nozzle pressure, nozzle size, nozzle length, traverse rate, and sample material.

2. EXPERIMENTAL APPARATUS

2.1 ASJ System

A high-pressure abrasive-suspension pump was prepared for testing. This pump was developed for continuous 379 MPa operation using two reciprocating isolators (Figure 1). With this configuration, ultrahigh-pressure (UHP) water is used to pump a pre-mixed abrasive-suspension using SUPER-WATER® as a suspension media. The UHP water is supplied by an intensifier pump. The water flows through on/off valves to the ASJ pump unit; the valves are selectively controlled to direct the UHP water to either of the isolator vessels. In each isolator vessel is a piston, or isolator, which is acted upon by the UHP water, thus pressurizing the slurry and forcing it out of the vessel. The suspension then passes through a discharge check valve and out of the nozzle.

After the power stroke of the isolator, a transfer pump moves the slurry from the suspension storage tank, through a suction check valve, and into the isolator. The piston is forced up and the isolator is charged with fresh suspension mixture. Vent valves release the water above the isolator while the piston is rising during the charging stroke. The vent valves are automatically controlled. Check valves are used to prevent the UHP suspension from entering the low-pressure charging loop.

® SUPER-WATER is a registered trademark of Berkeley Chemical Research, Inc.

A two-isolator system is used to supply continuous nozzle pressure. A control system times the opening and closing of the on/off valves to maintain continuous power (down) stroking of one or the other isolator pistons to produce continuous flow. This requires that a piston begin the power stroke before the power stroke of the other piston is completed. The charging stroke needs to be faster than the discharge time to provide time for both pistons to stroke, momentarily, in the same direction.

The nozzles used were of the straight or unshaped orifice type.

2.2 Hyperbaric Test Chambers

Two hyperbaric test chambers were developed for simulating 6000-m water depths (69 MPa back pressure). Figure 2a shows a chamber employing a rotating rod on which the test specimen is mounted. Circular cuts can be made in specimens at different traverse rates, depending on the rotational speed. The process of generating circular kerfs with this apparatus involved complex kinematic jet-material interactions, which were difficult to analyze.

Figure 2b shows an alternate chamber containing a slotted indexing rod, linked to a control motor, to hold and linearly translate test specimens under the nozzle. The chamber openings for the indexing rod passage are sealed with special UHP rod seals and scrapers. The test chamber is held at the desired operating pressure by a secondary water input, which is relieved via a high-pressure relief valve. Filters protect the relief valve from wear and erosion by abrasive particle passage. A filter back flush loop facilitates a means by which the filter elements and chambers can be cleaned after every test run. The chamber fluid exchange rate has been made large enough to prevent erroneous data caused by abrasive buildup in the chamber fluid. A photograph of a cut specimen is shown in Figure 3.

3. SIMPLIFIED ANALYSIS

The cutting performance achieved in the AWJ tests (Alberts et al., 1994) was optimal at high jet power levels and with high abrasive consumption. A 1-mm-diameter nozzle producing a 45-kW jet containing 0.048 kg/s of 80-mesh garnet abrasive achieved a cut depth of 46 mm in an ambient pressure of 60 MPa and traverse rate of 0.85 mm/s. This result was obtained with a 190-MPa, 0.37-l/s jet, which has a relatively low pressure and high flow rate when compared to the parameters of the ASJ. If the jet power (Power $\propto$ Flow Rate $\times$ Nozzle Pressure) is held constant, the nozzle pressure is increased and the flow rate is reduced (by reducing the jet diameter), the power intensity and performance of the jet is increased. The ASJ, which utilized higher nozzle pressures, achieved results similar to the AWJ with about one-half the power and abrasive consumption. ASJ nozzles tested ranged in size from about 0.35 to 0.6 mm in diameter.

The power efficiency, η, is defined as the ratio of the kinetic power of the abrasive particles to the hydraulic power used to accelerate the particles. The derived expression (Hashish, 1989) for this efficiency, η, is given below:

For AWJ:
$$\eta = (\eta_m C_v)^2 [r/(1+r)^2] \quad (1)$$

For ASJ:
$$\eta = C_{vs}^2 [r/(1+r)] \quad (2)$$

Where η_m is the energy transfer efficiency from the waterjet to the abrasive particles, C_v is the velocity coefficient for liquid flow, C_{vs} is the velocity coefficient for slurry flow, and r is the particle mass ratio emerging from the nozzle. Typical values for these factors are as follows:

η_m = 0.8 (in air)	C_{vs} = 0.7
η_m = 0.2 (submerged)	r = 0.12-0.25 (AWJ)
C_v = 0.99	r = 0.12-0.5 (ASJ)

η_m is an important limiting factor for the AWJ, especially in underwater applications. The value for η_m for the AWJ is substantially lower when the nozzle is used underwater with a slurry feed than when it is in air with air abrasive conveyance. The slurry that is fed to the underwater AWJ is about 50% water by mass, which absorbs a considerable amount of the momentum from the accelerating waterjet. It is estimated that η_m drops by about 50% due to the liquid carrier fluid in the slurry that is fed to the mixing tube. An additional drop of 25% is estimated due to drag that is introduced by the water-filled mixing tube in underwater applications. These values need experimental verification. The values for C_v and C_{vs} have been experimentally determined.

The efficiency of the entrainment AWJ system peaks at $r = 1$, although this is an impractical case for abrasive suction and transport. The efficiency decreases at a slow rate for $r > 1$. For the direct-pumping ASJ system, the efficiency increases as r increases. This also has practical limitations due to the fact that highly concentrated slurries will settle, which results in transport problems.

From the above equations, it can be calculated that the energy density ratio can reach 20, which is a major advantage of the ASJ over the AWJ.

3.1 ASJ Test Results

The results have shown the ASJ to have an advantage over the AWJ for underwater applications. Because of this, the ASJ performance will be discussed in some detail here.

3.1.1 Nozzle Pressure Effects

The effects of the ASJ nozzle pressure were investigated by making test cuts with nozzle pressures of 276, 310, 345, and 379 MPa. Test cuts were made for each nozzle pressure at three standoff distances and six different ambient cutting environments. Ambient environments tested include cuts made in air and cuts made with the nozzle and specimen submerged in water pressurized to 0, 17, 34, 52, and 69 MPa (gauge pressure). The nozzle pressure had varying effects on the cutting performance, depending on the ambient conditions. The cut depth is used as a measure of performance.

Figures 4 through 7 show plots of the cut depth as a function of the ASJ nozzle pressure and standoff distance under different ambient conditions. Figure 8 shows the comparison of nozzle pressure effects for several ambient conditions, including cutting in air. The cutting performance shows consistent improvement with increases in nozzle pressure. It appears that the nozzle pressure effect is nearly independent of the standoff distance and ambient pressure with similar performance curve shapes at each standoff and ambient condition when plotted against the nozzle pressure.

3.1.2 Ambient Pressure Effects

Figure 8 indicates a significant performance reduction with increasing ambient gauge pressure between 0 and 34 MPa. The cuts in air and in unpressurized water show similar behavior, with the air cuts going 3 to 6 mm deeper. The cuts made with elevated ambient pressures show similar characteristics to one another, but are markedly shallower from those made in air and unpressurized water. This could be evidence of cavitation occurring on a greater scale in unpressurized water, allowing the jet to have nearly the effectiveness that is seen in air. When the ambient pressure is elevated 17 MPa, the cut depth shows a reduction of 10 to 15 mm. Figures 8 and 9 indicate that ambient pressures tested above 17 MPa do not affect the cutting performance and that the loss in performance can not be attributed to reductions in nozzle pressure drop alone.

3.1.3 Nozzle Standoff Distance

The nozzle standoff distance is the distance from the nozzle exit to the workpiece. Standoff was varied in the parametric testing to distances of 0.9, 3.4, and 6 mm. It appears, on examining Figures 4 through 7, that the standoff distance effects were somewhat independent of the nozzle pressure. The standoff effects were, however, dependent on the ambient conditions that the cuts were made in. Figures 4 and 5 indicate a small standoff effect on the cut depth for cuts made in air and in unpressurized water. The cut depth in these tests varied about 2 to 3 mm over the range of standoff distances tested. The effect of standoff on the cut depth was significant in the tests run at elevated ambient pressure conditions (Figures 6 and 7). The cut depth variation due to standoff changes was about 10 to 15 mm in these cuts. Again, these data indicate that the jet is degrading sooner after emerging from the nozzle as the ambient gauge pressure is increased from 0 and 17 MPa.

3.1.4 Cavitation

Cavitation is typically expected to occur in jet flow with conditions in which the cavitation number (σ), as defined in Equation (3), is below about 0.5.

$$\sigma=(P_a-P_v)/\Delta P \tag{3}$$

Where P_a is the ambient pressure, P_v is the vapor pressure of water, and ΔP is the nozzle pressure drop. Figure 10 is a plot of the cavitation number for the tests that were run with a 345 MPa nozzle pressure over the entire range of ambient pressures that were tested. All of the ambient pressures that were tested appear to be within the range of parameters that would theoretically support the occurrence of cavitation.

Laboratory evaluations of cavitation under the extreme pressure conditions that were evaluated in this study are rare. Studies that have been published present relatively mild conditions (Ball, 1960 and Lienhard, 1966). In contrast to the findings of this study, one might expect the cutting performance to go up with increases in ambient pressure due to reduced jet breakup caused by cavitation. It could be postulated that cavitation is assisting the cutting process, but in the cuts made up to 17 MPa (the region in which the performance dropped) are well within the cavitation region reported elsewhere.

The cavitation number has an effect on the distance from the nozzle at which cavitation will occur. Lichtarowicz and Scott (1979) developed a relation for predicting the optimal standoff distance for cavitation damage:

$$L_m/d=a\sigma^{-m} \tag{4}$$

Where L_m is the optimal standoff, d is the nozzle diameter, m is an exponent (set at .81), and a is a coefficient (set at about 1.6). The distance L_m is the axial location in the stream at which the cavitation is developed enough to create damage, but not to the point at which the jet would be deteriorated by the cavitation activity. Figure 11 is a plot of L_m and can be interpreted to indicate that the jet will be relatively undisturbed by cavitation at the point that it enters the material for cuts made with a standoff of less than 2.5 mm. The cuts made in the data presented in Figure 9 had a standoff of 3.4 mm and should also be undisturbed by cavitation activity in ambient pressures below 17 MPa.

The reduction of performance that was experienced with ambient pressures between 0 and 17 MPa can not be explained by theoretically predicted cavitation activity as discussed here. An investigation that focuses on evaluating cavitation under the conditions that were present in this study may prove useful in providing an answer to the problem.

4. CONCLUSIONS

- The ASJ has proven to be of great advantage over the entrainment-type abrasive-waterjet in the underwater environment.
- The ASJ is a feasible and promising method of cutting any material at ocean depths, which create ambient pressure conditions of up to 69 MPa.
- Data trends indicate that the ASJ will continue to perform well in pressures exceeding the 69-MPa testing limit.
- Elevated ambient pressures affect the cutting performance. It may be advantageous to develop some form of jet shroud or shielding device.
- Further investigations into cavitation phenomena at extreme pressure conditions would be of value.
- Many underwater cutting performance trends caused by variations in cutting parameters were qualitatively similar to the performance trends that are encountered in an air environment.
- The test results strongly indicate that the ASJ can be developed into a tool for use in many underwater cutting applications.

5. ACKNOWLEDGMENTS

This work was funded by grant Number 111-9261475 from the National Science Foundation.

6. REFERENCES

Alberts, D. G., Hashish, M., and Lilley, R. (1994) "Experimental Studies on Deep Ocean Cutting with Abrasive Jet Systems," *1994 International Symposium Proceedings,* BHRA, March.

Ball, J. W. (1960) "Cavitation Effect on the Discharge Coefficient of the Sharp Edged Orifice Plate," *Journal of Basic Engineering*, Trans. ASME, Series D, Vol. 82.

Domann, H., and Aust, E. (1990) "Experimental Research on Jet Cutting for Subsea Applications," *Proceedings of the 10th International Symposium on Jet Cutting Technology*, Amsterdam, BHR Group.

Fairhurst, R. M., Heron, R. A., and Saunders, D. H. (1986) "DIAJET - A New Abrasive Water Jet Cutting Technique," *Proceedings of the 8th International Symposium on Jet Cutting Technology*, Durham, England, BHRA, The Fluid Engineering Center.

Haferkamp, H., Louis, H., and Meier, G. (1990) "Deep Sea Applications of Abrasive Waterjets: Feasibilities and Limitations," *Proceedings of the 10th International Symposium on Jet Cutting Technology*, Amsterdam, BHR Group.

Hashish, M. (1982) "Steel Cutting with Abrasive-Waterjets," *Proceedings of the 6th International Symposium on Jet Cutting Technology*, University of Surrey, U.K., BHRA Fluid Engineering.

Hashish, M. (1984) "Cutting with Abrasive-Waterjets." *Mechanical Engineering*, March, pp. 60-66.

Hashish, M. (1989) "Comparative Evaluation of Abrasive-Fluidjet Machining Systems," *Proceedings ASME 1989 Winter Annual Meeting*, PED-Vol. 41, pp. 13-21.

Hashish, M. (1990) "Abrasive-Fluidjet Machining Systems: Entrainment Versus Direct Pumping," *Proceedings of the 10th International Symposium on Jet Cutting Technology*, Amsterdam, BHR Group.

Hollinger, R. H., Perry, W. D., and Swanson, R. K. (1989) "Precision Cutting with a Low Pressure, Coherent Abrasive Suspension Jet," *Proceedings of the 5th American Water Jet Conference*, Toronto, Canada, U.S. Water Jet Technology Association.

Lichtarowicz, A., and Scott, P. J. (1979) "Erosion Testing with Cavitating Jet," *Proceedings of the 5th International Conference on Erosion by Liquid and Solid Impact*, Cambridge England.

Lienhard, J. H. and Stephenson, J. M. (1966) "Temperature and Scale Effects upon Cavitation and Flashing in Free and Submerged Jets," *Journal of Basic Engineering*, Trans. ASME, Series D, Vol. 88.

Surle, R. J. (1990) "Hyperbaric Abrasive Waterjet Cutting Trials for Offshore Industrial Application," *Proceedings of the 10th International Symposium on Jet Cutting Technology*, Amsterdam, BHR Group.

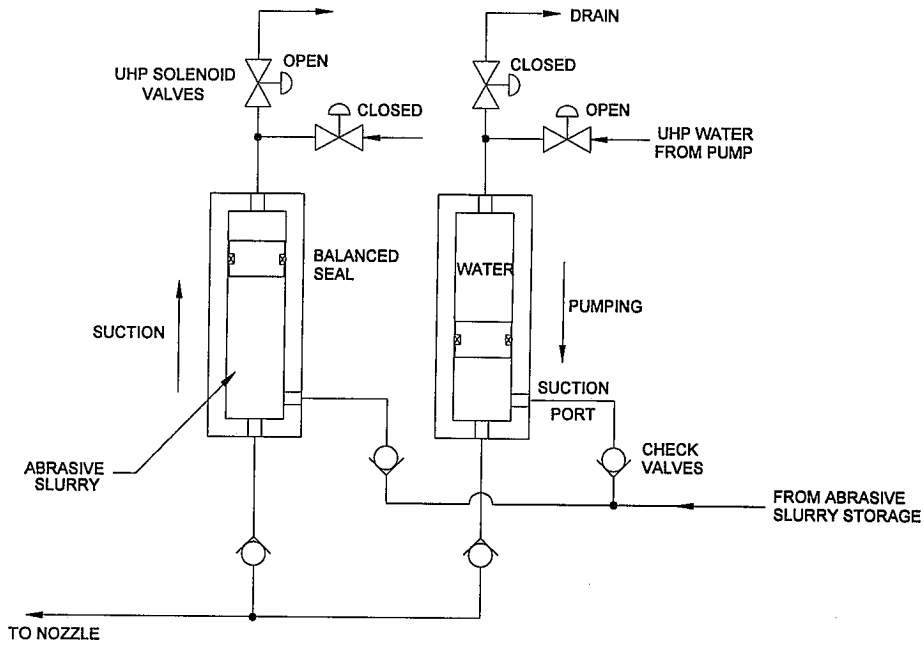

Figure 1. Schematic of Continuous-Pumping ASJ System

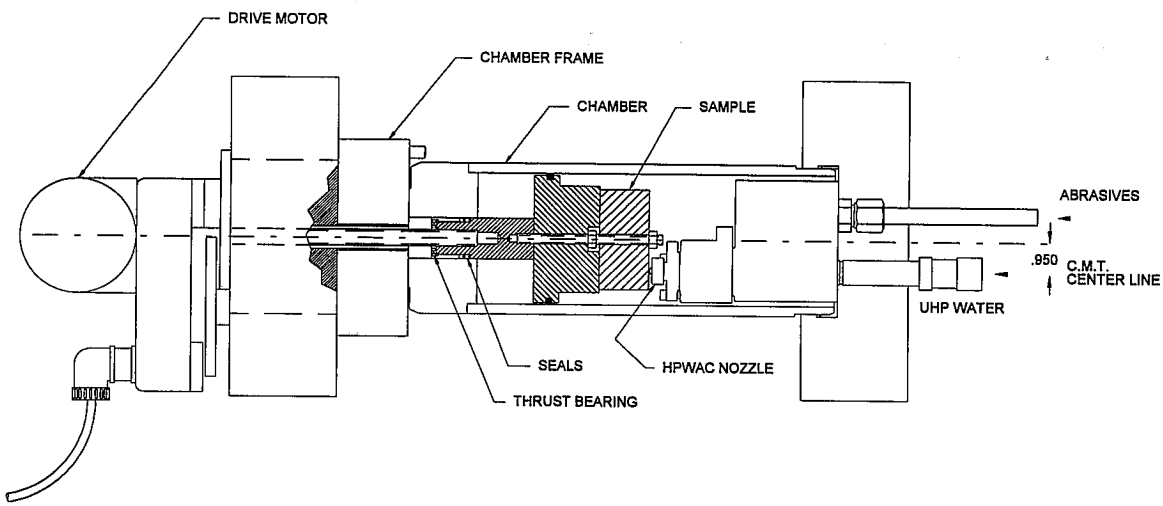

a. Hyperbaric chamber with rotary traverse

Figure 2. Experimental Test Chambers

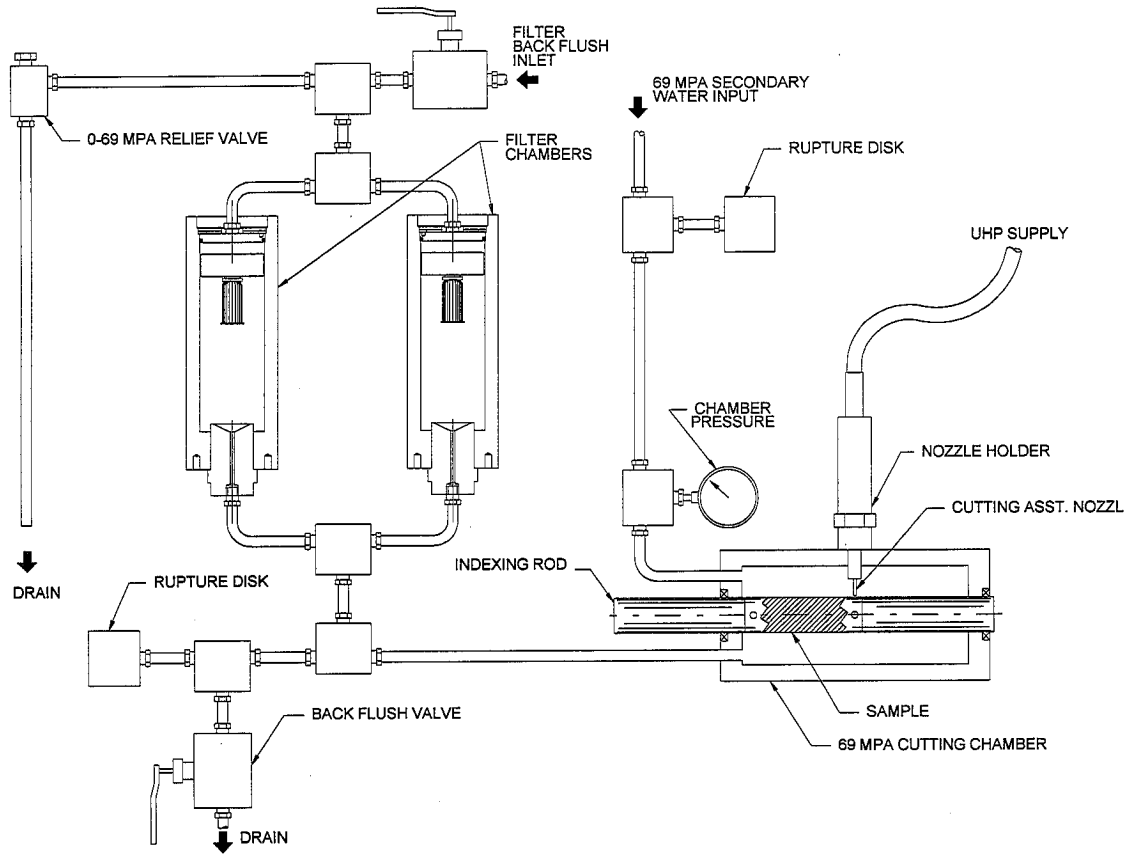

b. Schematic of deep ocean cutting simulation apparatus

Figure 2. Experimental Test Chambers (Cont.)

Standoff Distance (mm)	Depth (mm)	Width (mm)
1	30	0.40
3.5	24	0.51
6	16	0.64

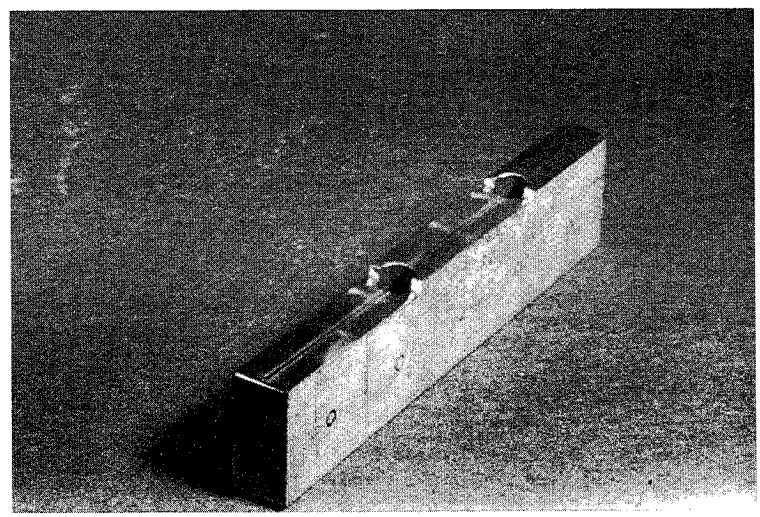

Figure 3. Stepped Stainless Steel Sample Cut with AWJ to Provide a Range of Standoff Distances. 6000 m under water with 0.46 mm-diameter nozzle.

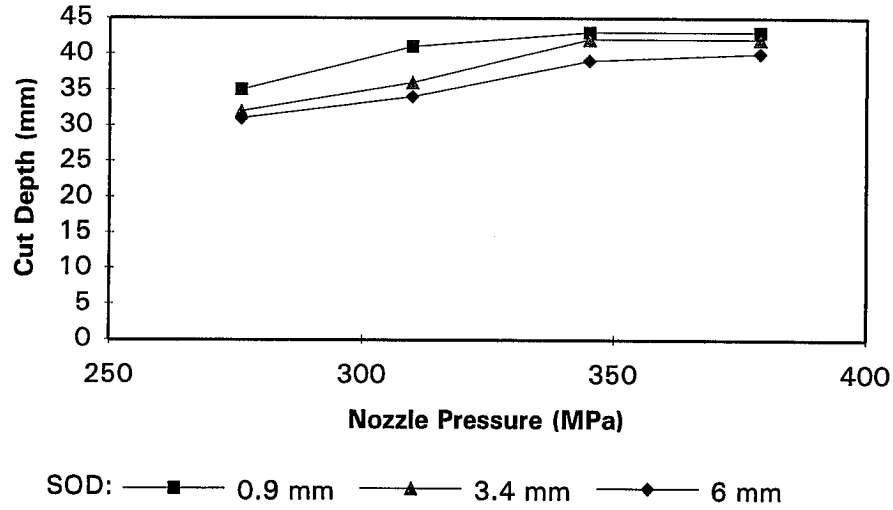

Figure 4. Effect of Nozzle Pressure and Standoff Distance on Depth of Cut. Cuts made in air, 11% mass ratio, #220 garnet abrasives; nozzle = 0.457 mm in diameter.

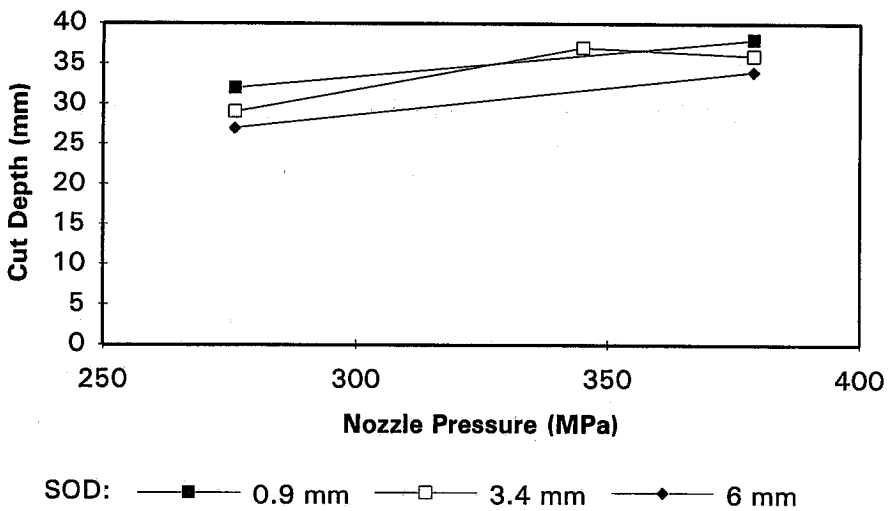

Figure 5. Effect of Nozzle Pressure and Standoff Distance on Depth of Cut. Cuts made in unpressurized water, 11% mass ratio, #220 garnet abrasives; nozzle = 0.457 mm in diameter.

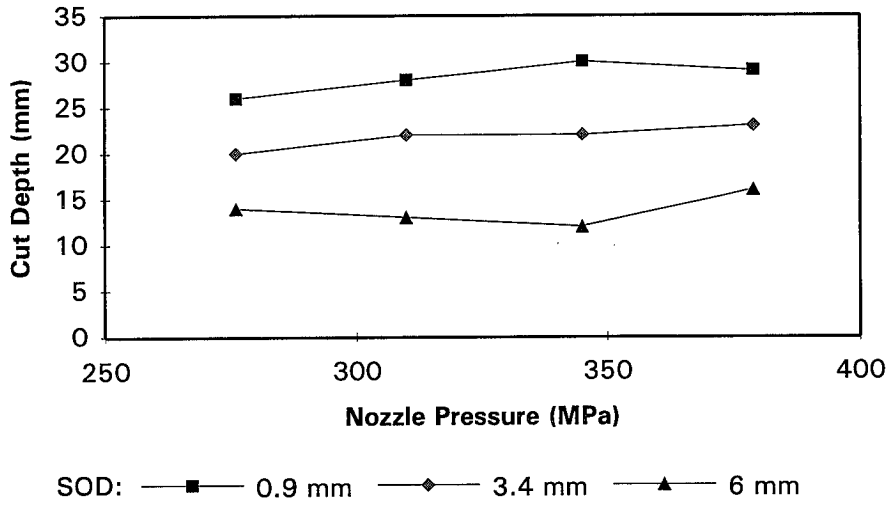

Figure 6. Effect of Nozzle Pressure and Standoff Distance on Depth of Cut.
Cuts made in 35 MPa water; 11% mass ratio, #220 garnet abrasives;
nozzle = 0.457 mm in diameter.

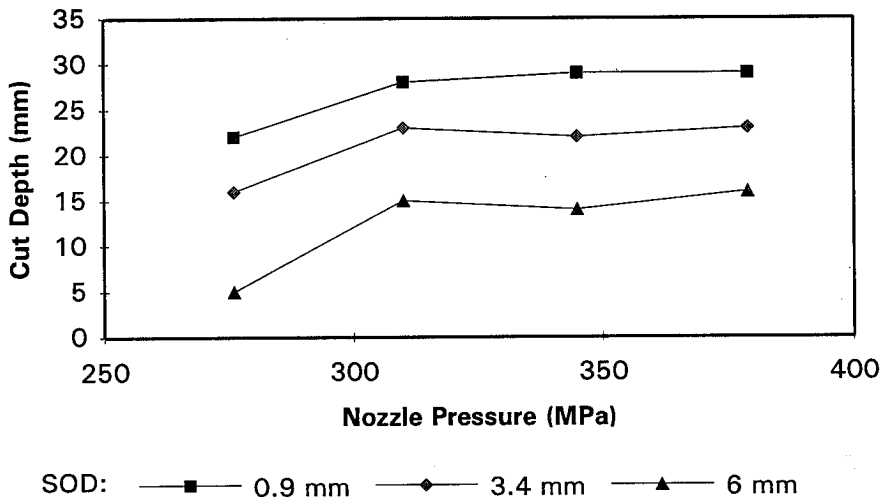

Figure 7. Effect of Nozzle Pressure and Standoff Distance on Depth of Cut.
Cuts made in 69 MPa water; 11% mass ratio, #220 garnet abrasives;
nozzle = 0.457 mm diameter.

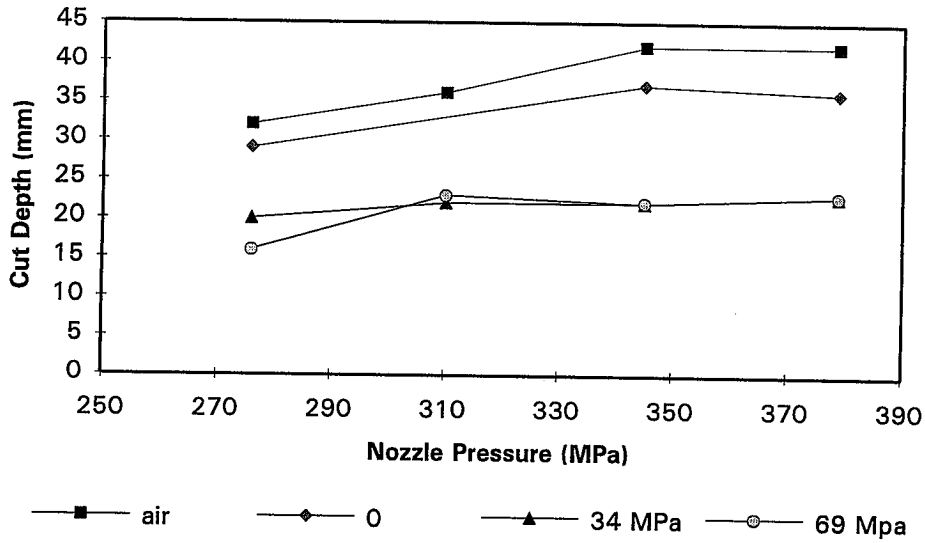

Figure 8. Effect of Nozzle Pressure and Ambient Conditions on Depth of Cut. 11% mass ratio, #220 garnet abrasives; nozzle = 0.457 mm in diameter; nozzle standoff = 3.4 mm.

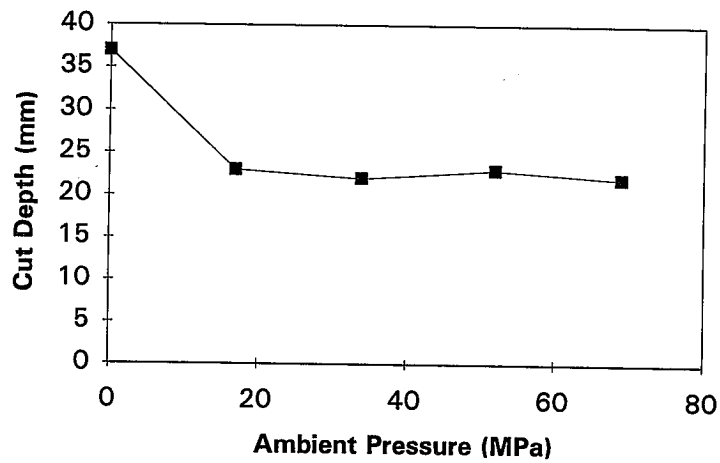

Figure 9. Effect of Ambient Pressure for Submerged ASJ Cutting. Nozzle pressure = 345 MPa; 11% mass ratio, #220 garnet abrasives; nozzle = 0.457 mm in diameter; nozzle standoff = 3.4 mm.

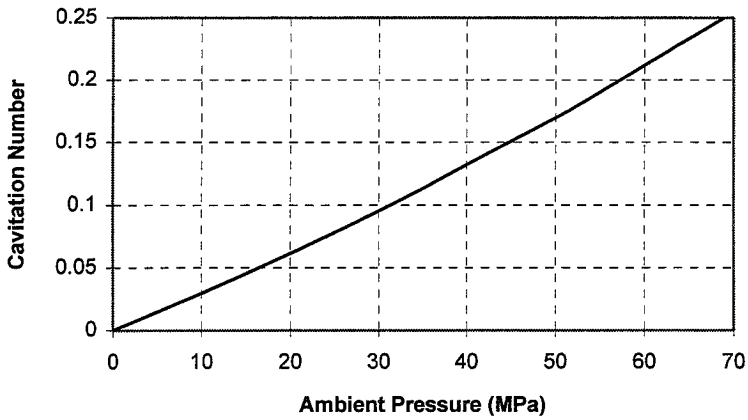

Figure 10. Cavitation Number for 345 MPa Nozzle Pressure.

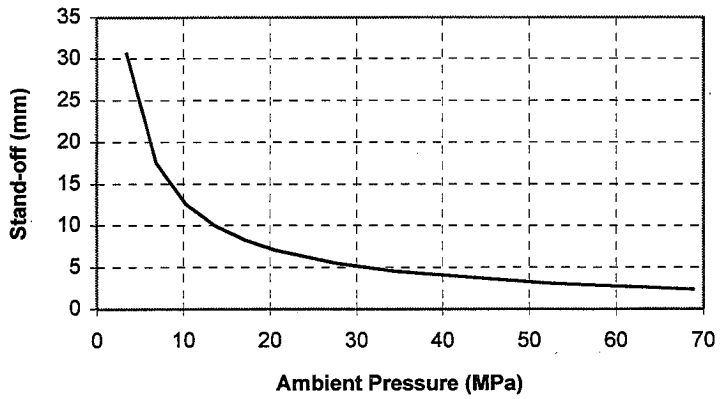

Figure 11. Theoretical Optimal Standoff for Cavitation Damage for 345 MPa Nozzle Pressure.

8th American Water Jet Conference
August 26-29, 1995: Houston, Texas

Paper 56

IMPROVEMENT OF THE WATERJET BASED PRECISION CLEANING TECHNOLOGY

P. Meng, E.S. Geskin, L. Tismenetskiy, M.C. Leu
Laboratory of Waterjet Technology,
Department of Mechanical Engineering
New Jersey Institute of Technology
Newark, New Jersey, 07102

ABSTRACT

A technology for precision cleaning of metal and glass surfaces which eliminates the use of ozone depleting substance is discussed. This technology involves the impingement of a high speed water stream at the surface to be processed. The impingement conditions assure a desired degree of surface quality without subsurface damage. The paper shows correlation between operational conditions and evaluates the effect of these conditions on the process results.

Organized and Sponsored by the Water Jet Technology Association.

1. INTRODUCTION

Cleaning constitutes the reduction of the concentration of soils, that is, undesirable materials on the part surface. The surface cleanliness is estimated by the soil mass per unit of the surface area and by maximum size of soil particles. Precision cleaning assures extremely low values of both characteristics. For example, the surface of spacecraft parts should contain less than 1 mg of soil per square feet. The largest permissible particle size in a class 100 clean room is 0.5 micron.

The established precision cleaning technologies are based on the use of special chemical compounds. Recently, it was found that these compounds contain components hazardous to environment and human health. Particularly, highly dangerous ozone depleting substances such as clorofluorocarbons (CFC) and Ozone-Depleting Solvents (ODS) constitute the principal agents used for precision cleaning. The environmental regulations mandate industry to eliminate manufacturing processes which use these chemicals by 1996. Such diverse products as circuit boards, semiconductors, optical devices, computer disc drivers, a variety of machine parts have been traditionally cleaned by CFC and ODS. Kennedy Space Center, for example, use more than 25,000 kg of CFC per year for precision cleaning and surface verification.

It is quite clear that elimination of CFC and ODS will have a profound impact on metal working, precision manufacturing, electronics as well as some other branches of industry. Although such technologies as plasma or CO_2 cleaning are available, the most practical way to eliminate the use of hazardous solvents is to replace them by pure water or non-hazardous solutions. By eliminating the use of solvents, waterjet impingement has the potential to dramatically reduce the cost of cleaning, to minimize the emission during cleaning operations, and to significantly reduce the volume of the liquid waste stream which must be treated.

The use of waterjets for custom cleaning purposes is not a new technology (Adams, 1979, Schikorr et al., 1982). Waterjet cleaning has been used for various specialty applications such as street and car washing, scale removal from hot steel in the course of rolling, removal of paint, rust, etc. Unfortunately, the experience acquired in existing cleaning operations can not be directly extended to the precision cleaning which presents a more demanding set of application considerations. Water consumption in conventional water cleaning operations is not limited, while both environmental and economical consideration dictate minimization of water consumption in the course of cleaning. More important, conventional techniques do not necessarily assure complete deposit removal which is the most important consideration in the precision cleaning. The reliability of cleaning at a substantially lower water volume can be attained using a higher water pressure, for example 340 MPa. It is quite obvious that an increase in the flow momentum enhances the rate and completion of the material removal. More importantly, there is a change of the material removal mechanism as the water velocity increases.

Material removal by a continuous jet is due to the stagnation pressure in the impact zone as well as to the shear stresses developed between the material surface and water flowing out of the impingement zone. In the case of the high speed impact of solid or liquid particles,

material removal is caused by the high frequency stress waves that are generated by impinging particles. The superposition of these waves results in material fatigue and subsequent spallation. These phenomena constitute the base of the material removal in the course of waterjet and abrasive waterjet machining. There is, however, a critical particle velocity below which the above phenomena do not occur. This velocity depends on the size and material of the droplets as well as the workpiece material.

Bonds between a deposit and a bulk material are weaker than that in the bulk. Thus, spallation of the soil due to the impact of liquid or solid particles precedes erosion of the bulk. Optimal water cleaning is accomplished at operational conditions (droplets size and velocity) which assure destruction and separation of the deposit and no damage to the bulk.

Existing practice as well as the physics of the jet-solid interaction indicates the feasibility of complete deposit removal from surface without causing glass damage. So far various cleaning applications by using high speed waterjets have been reported. Louis et al. (1984) discussed a mechanism of polymeric model layers removal, three samples of real waterjet cleaning applications were reported by Conn (1992), removal of such hard-to-separate material as thermal deposits by high pressure waterjet by Singh et al. (1992) and Watson et al. (1993), and deposit removal with substrate free of damage was discussed by Leu et al. (1994) and Geskin et al. (1995). Optimization of high pressure waterjet cleaning was discussed by Saunders et al. (1986), and Conn (1992). The problem of how to process the wastage after waterjet material processing was evaluated by Remisz (1993). Conn (1985) gave an economic analysis of waterjet cleaning.

Although existing experience indicates the possibility and potential effectiveness of waterjet cleaning, a comprehensive body of experimental data is necessary in order to demonstrate the feasibility of the waterjet precision cleaning without surface and subsurface damage and to define the range of its applications. The acquisition of such an information is the objective of the presented work. Although the goal of the work is the development of precision cleaning technology, the obtained results will be used for more common applications, such as improvement of the existing cleaning and washing machines, fabrication of composites, in-situ cleaning of materials and equipment, etc.

2. EXPERIMENTAL PROCEDURE

The study was carried out at the Ingersoll-Rand made robotic facility of NJIT waterjet laboratory. In order to evaluate the degree of removal of various deposits, water, oil, epoxy paints and rust were used in process examination. Painted surfaces provided a "base-line" contamination material against which the cleaning or removal of other material can be judged. The study involved paint and rust removal at various operational conditions. Steel and glass test coupons used for the study of paint removal were painted and cured at least during 24 hours. Rust removal was studied by cleaning of rusted steel samples. The tested nozzles (Fig. 1) included:

a. Conventional water nozzle of Ingersoll-Rand Co.

b. Modified nipple block nozzle
c. Spiral jet nozzle

The design of the nozzles b and c is shown in Figure 1. The process variables included water pressure, travel speed, stand off distance, nozzle diameter, diameter of the focusing tube and angle of attack. The degree of deposit removal constituted the criterion for process evaluation. Optical microscopy and SEM of the treated surface were used for estimation of the residual surface contamination. The results of cleaning were also evaluated by the ability of the generated surfaces to retain a water layer. This test enables us to determine the ultimate cleanliness of the surface exposed to an impinging waterjet.

The first series of experiments involved identification of a critical standoff distance, that is the standoff distance which assures generation of a surface which does not include contaminated spots. The existence of such spots was determined by microscopic examination and water testing. The critical standoff distance (CSD) was determined for various process conditions and presented as a function of the traverse rate. Then available rate of decontamination and required water consumption were estimated for the same operational conditions which were used to evaluate the CSD, however the standoff distance in the course of these experiments was equal CSD - 5 cm. In this manner, we evaluated almost minimal process productivity and maximal water consumption. It is clear that if stand off distance is reduced these process characteristics will be improved. The correction of 5 cm was used to assure stability of the experiments.

3. EXPERIMENTAL RESULTS AND DISCUSSION

Painted and rusted steel samples subjected to jet cleaning are shown in Figures 2-4. These figures indicate the feasibility of complete paint and rust removal by an impinging waterjet. The effect of process conditions on the critical standoff distance is shown in Figures 5-8. As it follows from these figures, the factors determining the state of the stream (water pressure, diameter of focusing tube, nozzle design) have strong effect on the critical standoff distance. While the conventional and modified nozzles behave almost identically, the spiral insertion reduces CSD significantly. The variation of the water pressure in a range between 130 and 200 MPa has practically no effect on the critical standoff distance (Figure 7). This phenomenon is determined by the peculiarities of the jet formation by the sapphire nozzle. It was also found by Cao (1995), that the velocity of the jet exiting the sapphire nozzle has an identical peculiarity, that is no change in water velocity at the pressure range of 130-200 MPa was observed. This unusual behavior will be explored in our future study. The travel speed above 5 m/min. has practically no effect on the critical standoff distance, while this distance increases dramatically when the travel speed is reduced below 5 m/min. The effect of the strength of the paint adhesion is not substantial. The critical stand off distance for different paints (water, oil, epoxy) as well as for different substrates (steel, glass) is practically the same. However the mode of adhesion, (rust or paint) has a visible effect (Figure 5).

Specific water consumption and productivity of cleaning at semi-critical conditions (standoff distance is CSD-5 cm), depend on travel speed, water pressure and to a lesser extent on the conditions of the jet formation. The correlation between water consumption and operational conditions is shown in Figures 9-11. The water consumption is evaluated by the amount of water in m^3 spent per 1 m^2 of cleaned surface and presented by the inverse travel speed (1m/ travel speed). This parameter indicates the dwell time of the jet in the course of cleaning. Because the experimental conditions assure surface decontamination, the water consumption is directly proportional to the dwell time. The effect of other process variables including water pressure is limited.

Process productivity (Figures 12-14) is proportional to the travel speed. The increase of the water pressure correspondingly increases the process productivity except in the region 130-200 MPa. Nozzle design is also an effective factor in enhancing productivity. The highest removal rate is attained by the use of a spiral nozzle, while the productivity of the conventional nozzle is minimal. The effect of the type of deposit is insignificant for these two paints.

The acquired information enables us to suggest the following mechanism of the soil removal by a high speed water stream. The stream is disintegrated from the focusing tube and the generated droplets impinge on the target surface and form a pack of stress waves. If superposition of the waves occurs at the bulk-deposit boundary, separation takes place even with strong adhesion. If, however, there is no such superposition at the soil-material interface, no separation occurs.

4. CONCLUDING REMARKS

The performed research demonstrates that a generic precision cleaning technology can be developed by the use of high pressure waterjet. The feasibility of the replacement of volatile cleaning solvents used for precision cleaning of various parts with high pressure low volume water jets is shown.

The conditions of jet formation and impingement can assure reduction of the deposit amounts down to the acceptable level while a guidance system should assure complete coverage of the deposit accumulation area. The application of the high speed jets is comparatively simple and does not require special conditions. It is much less expensive than ultrasonic cleaning and much more productive and environmentally benign than low pressure sprays. Thus, the use of high pressure waterjet enables us to develop an effective precision cleaning technology which meets existing and pending environmental regulations and enables us to generate a desired surface quality at an acceptable cost.

In two years the environmental legislation will force industry to eliminate those manufacturing processes which use ozone depleting chemicals. Currently these chemicals constitute the principal precision cleaning agents. Thus, the use of pure water for precision cleaning becomes a matter of surviving for various operations. It is realistic to assume that high speed waterjet will become the principal tool for precision cleaning.

5. ACKNOWLEDGMENTS

The presented work was supported by grants of Emission Reduction Research Center and Center for Manufacturing systems. The authors express their appreciation to Mr. F. Li for his participation in the performed experiments.

6. REFERENCES

Adams, P. B., "A Systematic Approach to Glass Cleaning," *Surface Contamination, Genesis, Detection and Control,* pp. 327-331, V. I, edited by K. L. Mittal, Plenum Press, New York, 1979.

Conn., A., "Water Jet Cleaning for In-Factory Application," *Proceedings of 11th International Symposium on Jet Cutting Technology*, Kluver Academic Publisher, pp. 443-450, Dordrecht, The Netherlands, 1992.

Conn., A., and Chahine, G. L., "Ship Hull Cleaning with Self-Resonating Pulsed Water Jets," *Proceedings of 3rd Water Jet Conference,* pp. 44-62, Water Jet Technology Association, The University of Pittsburgh, Pennsylvania, USA, 1985.

Geskin, E., Leu, M., Meng, P., Uschitsky, M., and Tismenetsky, L., "Waterjet In-Situ Equipment Cleaning," *Progress Report to ERRC*, NJIT, April 13, 1995.

Geskin, E., "Feasibility Study of Abrasive Waterjet Machining for Manufacturing Precision Optical Components," *Report of ORNL/Sub/91-SE192/1,* Oak Ridge National Laboratory, February, 1991.

Leu, M., Geskin, E., Meng, P., Uschitsky, M., and Tismenetsky, L., "Waterjet In-Situ Cleaning." *Report at IAB Meeting of the ERRC*, November, 1994.

Louis, H., Haferkamp, H., and Schikorr, W., "Jet Cleaning Investigations on Polymeric Model Layers," *Proceedings of 7th International. Symposium on Jet Cutting Technology,* pp. 119-134, BHRA, The Fluid Engineering Center, Ottawa, Canada, 1984.

Singh, P. J., Munoz, J., and Chen, W. 1., "Ultra-High Pressure Waterjet Removal of Thermal Spray Coating," *Proceeding of 11th International Symposium on Jet Cutting Technology,* Kluver Academic Publisher, pp. 461-480, Dordrecht, The Netherlands, 1992.

Remisz, J., and Remisz, W., "Hydrodemolition: Why 'Yes' and Why 'No,'" *Proceedings of 7th American Water Jet Conference,* Vol. 2, pp. 573-581, Water Jet Technology Association, Seattle, Washington, USA, 1993.

Saunders, D. H., and Barton, R. E. P., "The Use of Fan-Shaped Water Jets in Preference to Straight Jets to Remove a Paint Coating," *Proceedings of 8th International Symposium on Jet Cutting Technology*, pp. 353-361, BHRA, Durham, England, 1986.

Schikorr, W., and Louis, H., "Fundamental Aspects in Cleaning with High Speed Water Jets," *Proceedings of 6th International Symposium on Jet Cutting Technology*, pp. 217-228, BHRA, The Fluid Engineering Center, University of Surrey, The United Kingdom, 1982.

Watson, J. D., "Thermal Spray Removal with Ultrahigh-Velocity Waterjets," *Proceedings of 7th American Water Jet Conference,* Vol. 2, pp. 583-597, Water Jet Technology Association, Seattle, Washington, USA, 1993.

7. NOMENCLATURE

CSD = critical standoff distance, that is the standoff distance which assures complete soil removal at given operational conditions

FT = focusing tube number corresponding to the tube diameter in milliinches

MSN = modified sapphire nozzle, that is the nozzle shown in Figure 1b

OD = orifice number corresponding to its diameter in milliinches

P = water pressure prior to the orifice in MPa

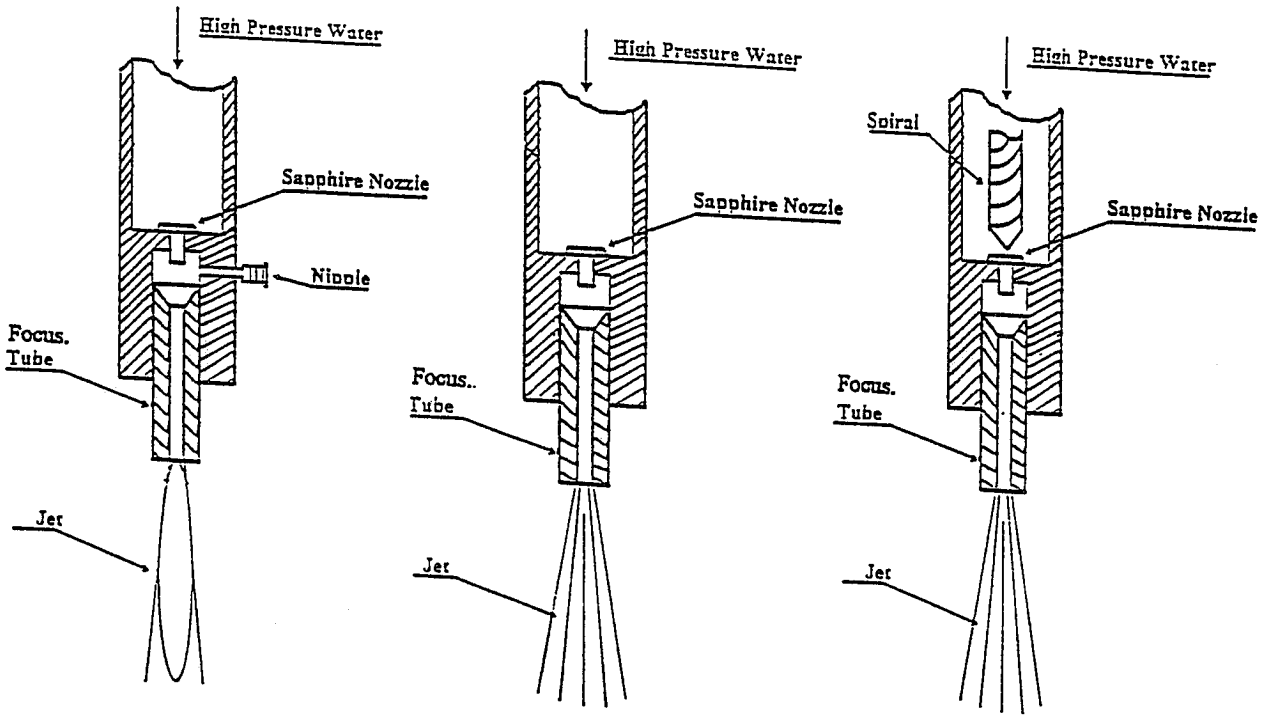

Figure 1. Schematic Of The Nozzle Assemblies Used For Precision Cleaning. a) Ingersoll-Rand Nozzle Assembly b) Modified Nozzle Assembly (MSN). Notice that abrasive port is sealed. c) Spiral Nozzle. Notice a spiral insertion prior to the orifice.

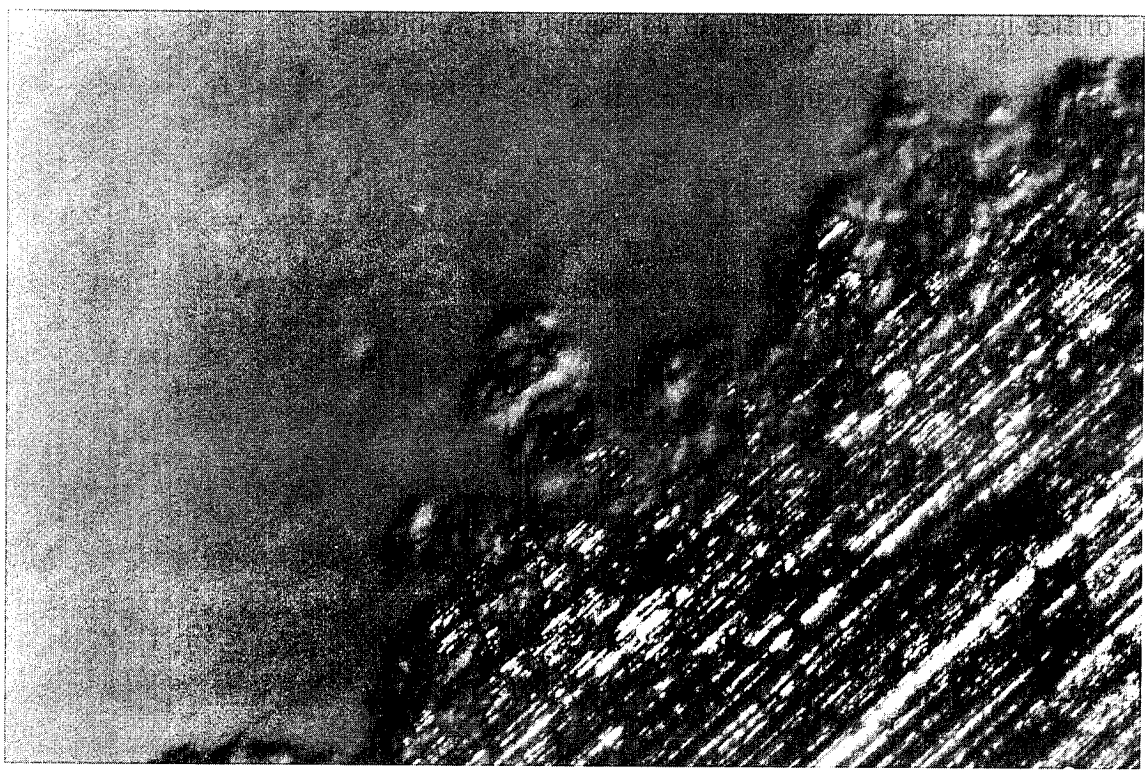

Figure 2. Removal of the Epoxy Paint by the MSN Impinging Jet. Notice complete paint removal.

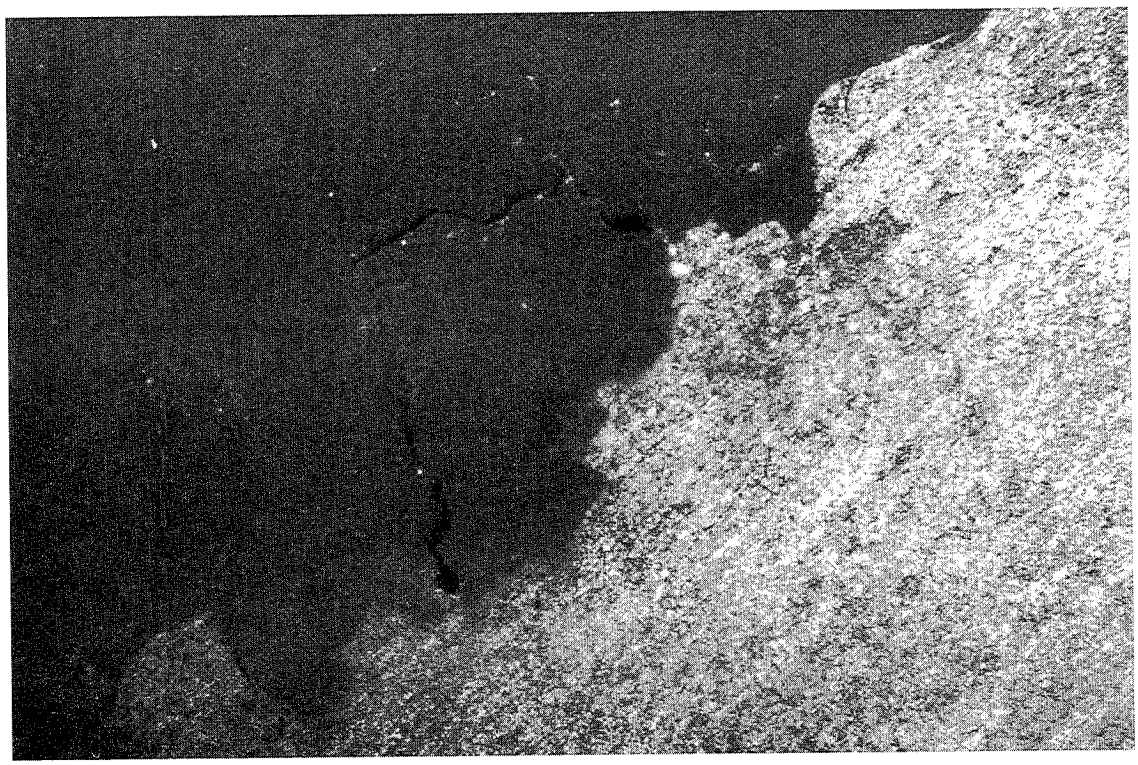

Figure 3. Removal of the Oil Paint by the MSN Impinging Jet. Notice complete paint removal.

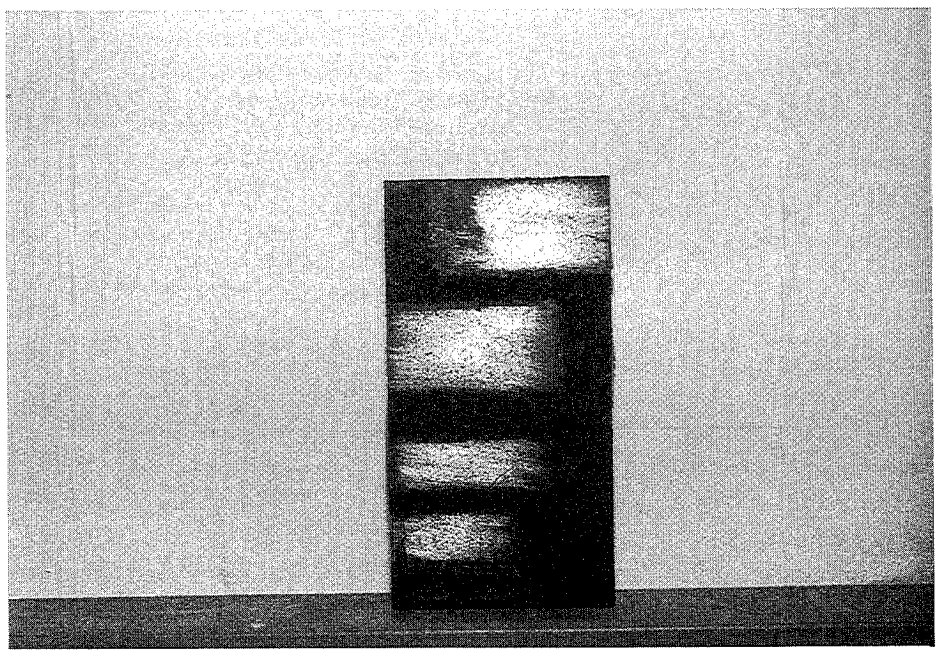

Figure 4. Rust Removal by the MSN Impinging Jet. The black spots at the cleaned area represent eroded spots.

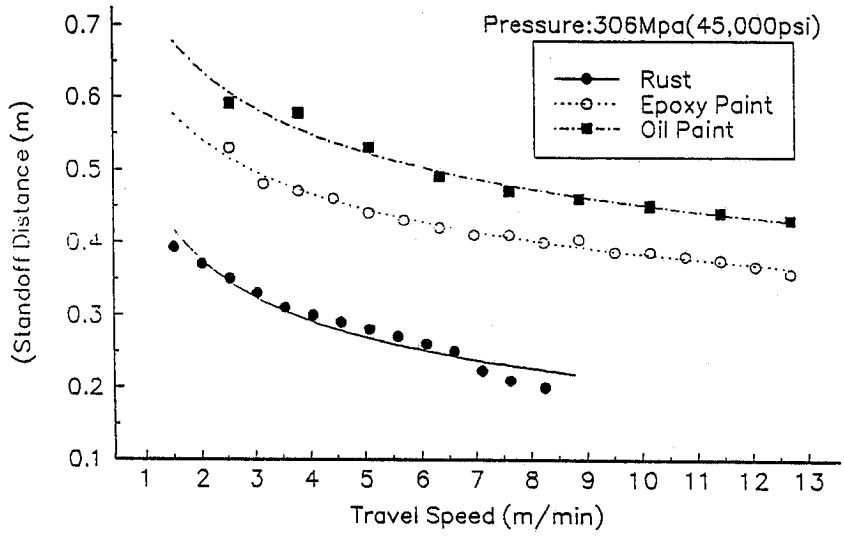

Figure 5. Correlation Between Critical Standoff Distance and Travel Speed. Nozzle in Figure 1a is Used. OD = 10, FT = 30. Notice the difference between CSD at paints and rust removal.

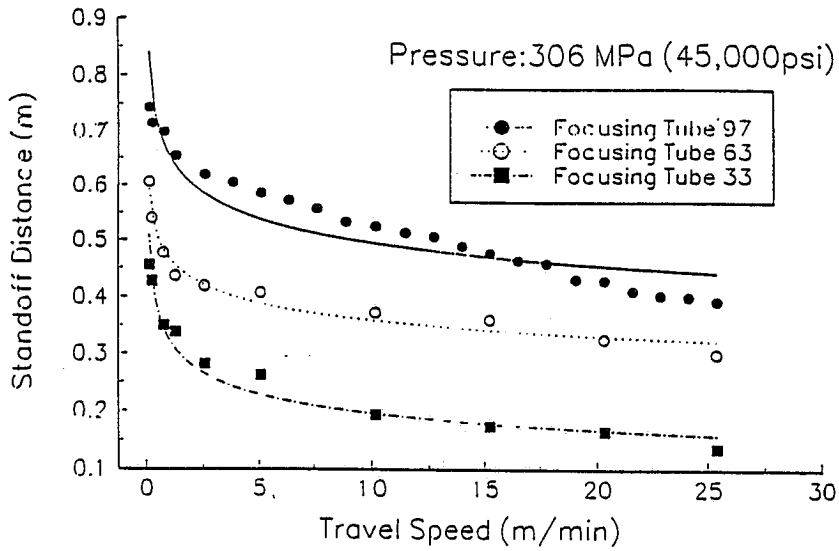

Figure 6. Correlation between CSD and Travel Speed at Oil Paint Removal by MSN Nozzle. OD = 12. Notice limited effect at travel speed above 5 m/min., and strong effect at the travel speed below 5 m/min.

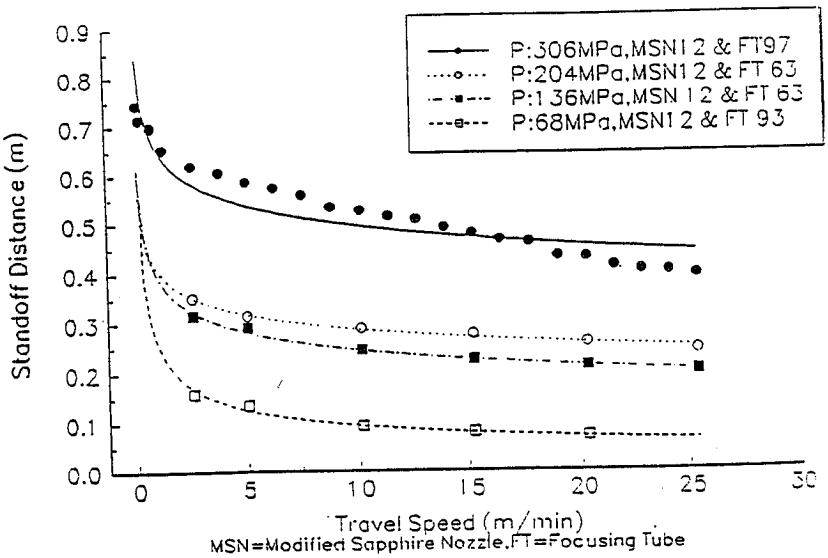

Figure 7. Correlation between CSD and Travel Speed at Oil Paint Removal. OD=12. Notice limited effect at travel speed above 5 m/min., and strong effect at travel speed below 5 m/min. Notice limited pressure effect at the range of P=136-204 MPa.

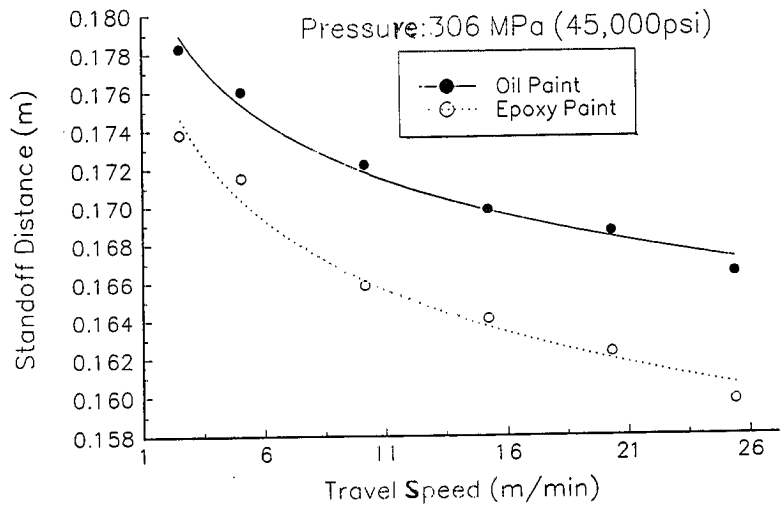

Figure 8. Correlation between CSD and Travel Speed of Spiral Nozzle at Oil Paint Removal OD = 12, FT = 97, Notice a limited effect of the kind of paint.

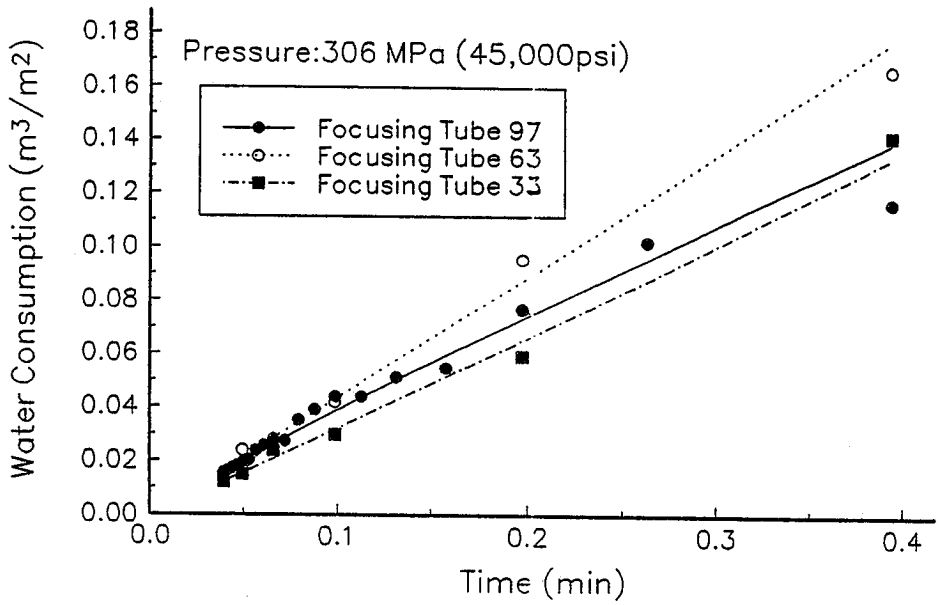

Figure 9. Correlation between Water Consumption and Process Conditions of MSN Nozzle. OD = 12. Dwell time is determine as 1m/travel speed. Notice a limited effect of FT.

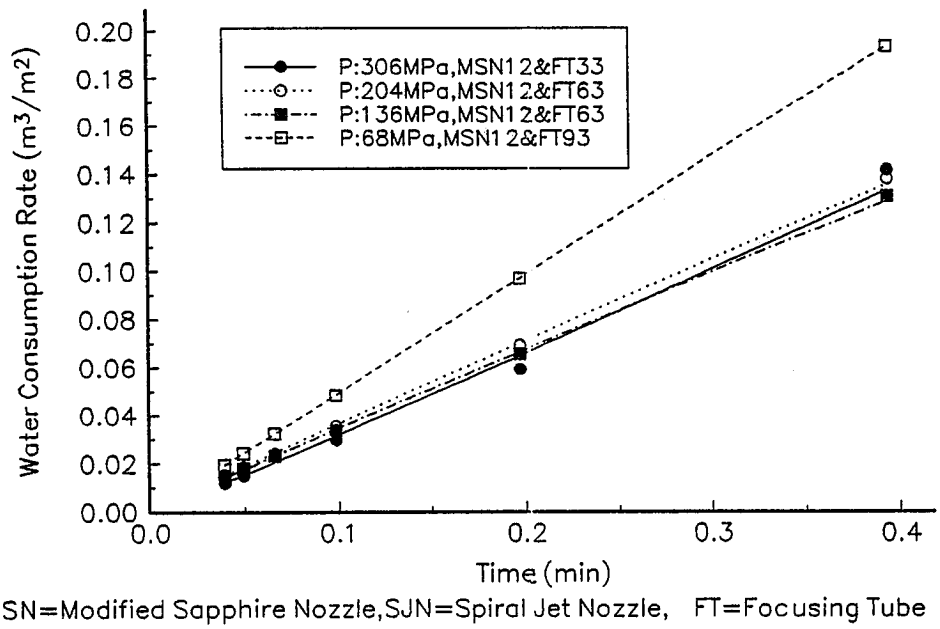

MSN=Modified Sapphire Nozzle,SJN=Spiral Jet Nozzle, FT=Focusing Tube

Figure 10. Correlation between Water Consumption and Process Conditions of MSN Nozzle. OD = 12. Notice limited effect of FT and P at P more than 136 MPa.

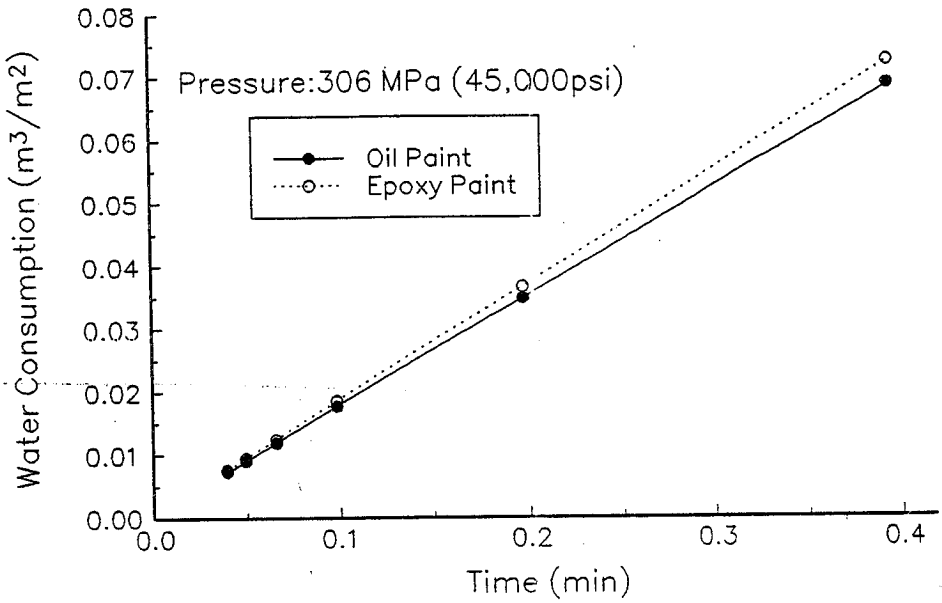

Figure 11. Correlation between Water Consumption and Process Conditions of Spiral Nozzle. OD = 12, FT = 97. Notice reduction in the water consumption due to the use of the spiral nozzle and limited effect of the kind of paint.

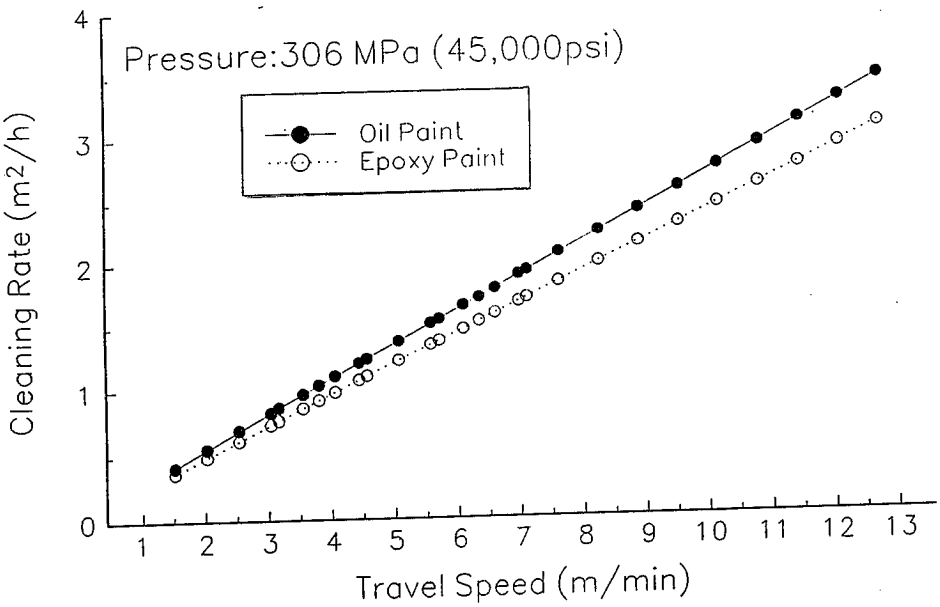

Figure 12. Correlation between Cleaning Productivity and Travel Speed of Nozzle 1a. OD = 10, FT = 30. Notice limited effect of the kind of paint.

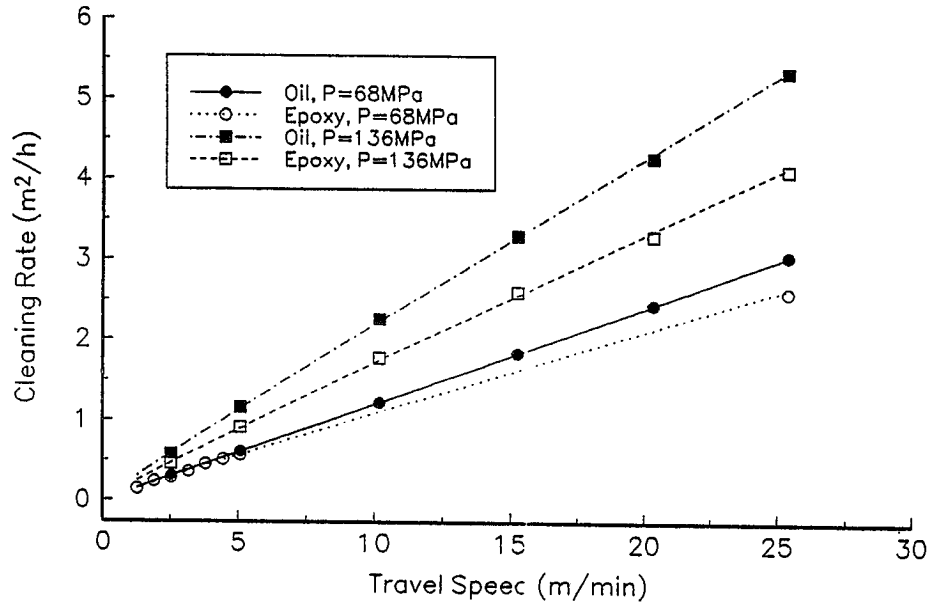

Figure 13. Correlation between Cleaning Productivity and Travel Speed of MSN Nozzle. OD = 12, FT = 97. Notice an effect of the kind of paint on the productivity at low pressure.

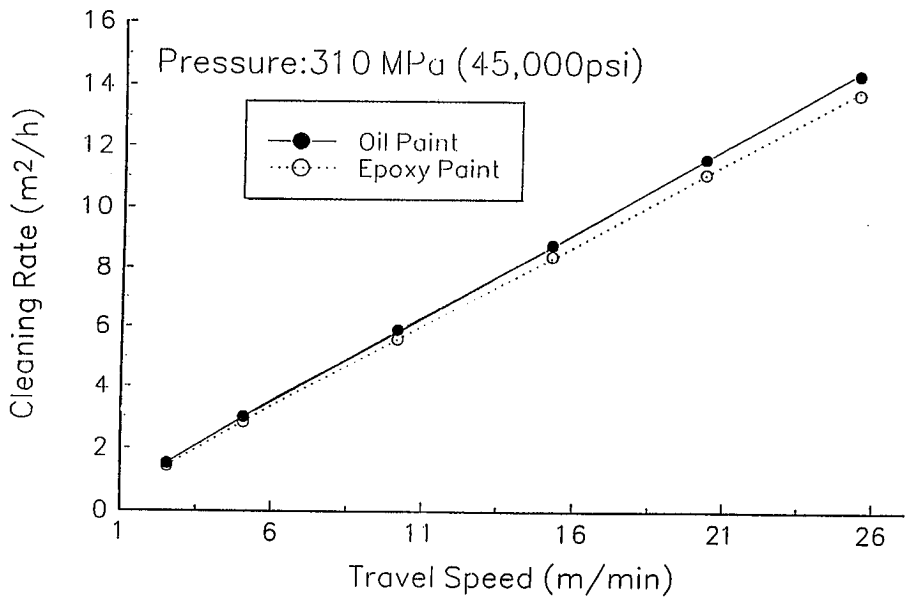

Figure 14. Correlation between Cleaning Productivity and Travel Speed of Spiral Nozzle. OD = 12, FT = 97. Notice a limited effect of the kind of paint.

8th American Water Jet Conference
August 26-29, 1995: Houston, Texas

Paper 57

THE USE OF SELF-RESONATING CAVITATING WATER JETS FOR ROCK CUTTING

G. L. Chahine, K.M. Kalumuck, and G.S. Frederick
DYNAFLOW, INC.
7210 Pindell School Road
Fulton, MD 20759

ABSTRACT

The performance and erosive power of the STRATOJET™ self-resonating cavitating jet was investigated for drilling in rock at various depths and pressures. Such jets show significant performance increases, especially in harder rock and at larger depths, over conventional water jets operated at the same pressures and flow rates. The self-resonating cavitating jet uses a passive acoustic resonance tuned to the preferred Strouhal number of the submerged jet to cause the large scale turbulent motions of the jet to structure into a series of vortex rings whose cores cavitate under specific operating and ambient conditions.

Performance evaluations were conducted in the DYNAFLOW High Pressure Cell at ambient pressures up to 19.3 MPa (2800 psi) for jet pressures up to 69 MPa (10,000 psi) and spanning a broad range of the cavitation number. Performance was found to depend on cavitation number, standoff, rock properties, jet pressure (compared to the rock strength) and nozzle geometry details.

Direct performance comparisons between the STRATOJET™ and a conventional Smith type nozzle were conducted in controlled rock cutting experiments. At very low jet pressures, neither jet erodes the rock. As the jet pressure increases, the self-resonating jet begins to erode the rock before the Smith does, such that its relative performance is initially orders of magnitude greater. As the pressure drop increases further, the performance of both jets improves, and, as the impact pressure of the jets exceed the rock strength, the improvement of the self-resonating cavitating jet over the Smith becomes less. These results of translating experiments performed over a broad range of nozzle pressure drops and ambient pressures provide a map of the relative performance of the two nozzle types. The details of this comparison vary with rock type.

Organized and Sponsored by the Water Jet Technology Association.

1. INTRODUCTION

Cavitation is mainly known for its harmful effects, namely, loss of performance, erosion, and noise. The usual procedure to prevent these deleterious effects is to avoid the phenomenon by proper design and by limiting the operating conditions. However, attempts to induce and harness cavitation for useful purposes have been increasingly successful. Ultrasonic cavitation methods take advantage of the erosive power of cavitation for cleaning, emulsification, and mixing. In water jets, cavitation has for some time now been purposely induced in order to increase jet erosive power.

Experimental observations of submerged jets show the tendency of the turbulent eddies in their shear layer to organize in large structures. Excitation of a turbulent air jet with periodic acoustic signals produced upstream of the nozzle by transducers or loud speakers shows a remarkable change of the jet structure into discrete ring vortices when the excitation frequency, f, matches the predominant natural frequencies of the non-excited jet. This corresponds to a Strouhal number, $S_{d,}$, close to 0.3 or one of its integer multiples. The Strouhal number is defined as

$$S_d = \frac{fd}{V}, \tag{1}$$

where V and d are the velocity and the diameter of the jet. This natural tendency of a submerged jet to organize into large structures is of great interest in aerodynamics for air jet studies. Crow and Champagne (1971) studied this phenomenon extensively and showed experimentally that forced excitation of the jet at the preferred frequency ($S_d \approx 0.3$) enhances the structuring. The vorticity is then mainly concentrated in ring-shaped large structures.

The potential of this phenomenon for submerged water jets was recognized and utilized to develop useful submerged jets having very high amplitude, periodic, oscillatory discharge without the use of moving parts in the supply system. (See, for example, Johnson et al., 1984 and Chahine et al., 1984a and b.) The passive excitation is obtained hydroacoustically and structures the shear layer of the jet into discrete, well defined ring vortices when the excitation frequency, f, matches the jet's preferred value. This can be obtained by feeding the final jet-forming nozzle with various types of acoustic chambers (for example, Helmholtz chambers or organ-pipe tubes) tuned to resonate at the desired frequency; and by shaping the nozzle so as to feed back the pressure oscillations which occur at the exit. Such devices are forms of "whistles" which self-excite and thus are totally passive. These jets are termed STRATOJET™s[1] and have shown enhanced erosivity from increased cavitation activity. The large pressure oscillations associated with the intensification of cavitation, with resonance in the nozzle assembly, and with the production and disappearance of large vortical structures greatly improve the erosion and cleaning capabilities.

These self-resonating cavitating jets have shown large improvements over conventional jets in both cut depth and volume removal in selected laboratory settings and a range of cavitation conditions. The amount of improvement depends on the rock strength relative to the jet erosive

[1] U.S. Patents: 4,262,757 4,389,071 4,474,251 4,508,577 4,681,264 4,716,849

strength, cavitation conditions such as the ratio between ambient pressure and jet pressure, and the ability to achieve resonance. The relative improvement in the cutting rate due to the introduction of cavitation increases with rock hardness, making this class of jets particularly attractive for use in medium to hard rock formations. At deep depths, cavitation is suppressed in conventional jets. Self resonating jets produce cavitation for even higher ambient pressures thus enabling operation at deeper depths and producing good performance at lower nozzle pressures than conventional jets.

The work presented in this paper summarizes efforts at DYNAFLOW, INC. to investigate the performance and erosive power of various water jet nozzles for drilling in hard rock at a range of depths and nozzle pressures.

2. PRINCIPLES OF OPERATION OF SELF RESONATING CAVITATING JETS

One possible type of STRATOJET™ configuration is shown in Figure 1. It uses an organ-pipe acoustic chamber whose resonant frequency is selected to match the desired structuring frequency defined by the critical Strouhal number of the jet. This concept offers the simplest system design and has been used successfully for erosion studies and noise generation (Chahine and Johnson, 1985; Chahine et al., 1984b; Chahine et al., 1986; Chahine et al., 1987).

2.1 Acoustic Resonance

Acoustic resonance is achieved in the nozzle feed-tube assembly when a standing wave forms in the "organ-pipe" section (length: L, diameter: D). Peak resonance will occur when the fundamental frequency of the organ-pipe is near the preferred jet structuring frequency. The exact resonance frequency is dependent on the contractions at each end of the organ-pipe, and the first mode resonance in the pipe will occur when the sound wavelength in the fluid is either two or four times L.

The principles of operation of an organ-pipe STRATOJET™ are schematically represented in Figure 1. Two predominant sources of pressure fluctuations can be distinguished in addition to the classical unexcited turbulent shear layer between the jet and the surrounding liquid. One of these sources corresponds to the volume fluctuations of the moving vortex bubble rings formed in the center of the large structures of the self-excited jet. The other source of pressure fluctuations is more complex and relates to the exit area of the jet where high amplitude oscillations of the main flow characteristics are interrelated with the shear layer-nozzle lip interaction. The acoustic signals from both areas are forcing functions to the resonating chamber in the nozzle assembly. These signals strongly interact; they are both fed back and amplified by the organ-pipe.

2.2 Effects of Jet Structuring on Cavitation Inception

The dimensionless parameter characterizing cavitation is the cavitation number, σ,

$$\sigma = \frac{P_a - P_v}{1/2\rho V^2}, \tag{2}$$

where P_a is the ambient or far field pressure, P_v is the vapor pressure of the liquid, ρ is the liquid density, and V is the characteristic velocity, the jet mean velocity. In deep-hole drilling, the ambient pressure is hydrostatic and directly related to hole depth. In the case of high-pressure submerged jets used in deep-hole drilling, $P_a >> P_v$, and for well-designed nozzles $1/2\rho V^2$ may be approximated by the pressure drop, ΔP, across the nozzle. Thus

$$\sigma \approx \frac{P_a}{\Delta P}. \tag{3}$$

The particular value at which cavitation is incipient is defined as

$$\sigma_i = \left(\frac{P_a}{\Delta P}\right) \text{ at inception.} \tag{4}$$

Thus if the operating conditions for a submerged jet are such that $\sigma/\sigma_i < 1$, cavitation will occur, and as σ/σ_i continues to decrease below unity the amount of cavitation will increase. When a cavitating jet impinges against a surface, the cavities formed in the jet collapse on that surface and produce very high local pressures due to the formation of very high speed microjets. (As an example, Figure 2 presents the results of a numerical simulation we conducted of high speed microjet formation on bubble collapse. Shown are a close up of the microjet and the resulting velocity field.) The resulting pressures are much greater than the jet stagnation pressure ($1/2\rho V^2$), and the resulting cleaning or cutting action is substantially greater than when the jet is not cavitating. A great advantage of the STRATOJET™ class of jets is an increase in σ_i over conventional jets by a factor of 3 with current designs. This means that at a given depth, *cavitation can be generated with only 1/3 as large a* ΔP, or conversely, for a given ΔP, *cavitation can be achieved at three times the depth of a conventional jet.*

The increase in σ_i is due to the decreased pressures at the core of the structured vortices generated. The resulting vortex ring cavities can be seen in Figure 3. This figure presents a strobe photograph from a large scale visualization study at a value of σ=0.21.

3. EXPERIMENTAL SETUP AND PROCEDURES

Experiments were conducted in DYNAFLOW's High Pressure Cell (HPC) capable of ambient pressures up to approximately 19.3 MPa (2800 psi). A photograph of the HPC is presented in Figure 4. The HPC is a cylindrical pressure vessel with inside dimensions of approximately 24 cm (9.5 inch) diameter and 71 cm (28 inch) length with three quartz view ports circumferentially spaced and located near its mid length. Constructed for studies of deep hole drilling with cavitating jets, it includes a fixture in which rocks are placed and rotated at various speeds for cutting beneath the jet. Another fixture enables the rock to advance at a controlled rate towards the nozzle thus enabling actual drilling. The rock surface being cut is visible in the view ports.

The fixture can also be translated to simulate advancement of the jet into the rock. Ambient pressure is adjusted and maintained by a choke plate which acts as a back pressure valve in the outflow line. The jet flow is driven by a Weatherford five piston positive displacement pump capable of up to 76 liters/min (20 gpm) at 69 MPa (10,000 psi).

Nozzle acoustic resonance was checked with the aid of Piezotronics 101-A04 pressure transducers (5 mv/psi sensitivity) located in the HPC wall and used to measure the fluctuating component of the pressure, P'. The output of the transducer was monitored with both a digital rms meter to obtain the rms value of the fluctuating pressure component and with a Nicolet 660B FFT analyzer to ascertain the frequency content of the fluctuations and determine the peak (resonant) frequencies of the nozzles. (Typically, this was in the range of 10-60 kHz.) These measurements were used to determine whether or not a particular self-resonating nozzle had achieved good acoustic resonance - an important factor in achieving good performance.

Important experimental variables include the nozzle pressure drop, ΔP, the ambient pressure, P_a, the cavitation number, σ, the standoff, and the translation velocity of the jet over the target, as well as details of the nozzle geometry. The cavitation number is an important parameter in determination of the occurrence and behavior of cavitation phenomena. Thus all testing should be conducted under conditions that match the value(s) expected in practice.

Both STRATOJET™ and conventional non-resonating (e.g., Smith type) nozzles were designed and fabricated to produce comparable flow rates when operating at the same ΔP and were then comparison tested under the same conditions. The organ-pipe length for the self-resonating nozzle was "tuned" to the jet exit velocity (i.e., to ΔP).

A series of static translating cutting tests were conducted in aluminum (6061-T6) plates. Aluminum was selected for the initial work because it provides a good measure of the performance of a water jet, is a very homogeneous material, and simulates a very hard, nonporous rock. In the nozzle development stage, this removes questions of target sample property variation on nozzle performance and enables one to focus on obtaining a good nozzle design. It is thus very useful as a development and screening tool.

The standoff distance of the jet from the plate was varied to determine optimum standoff for each nozzle type under each set of operating conditions with static exposure times of 5-10 min. in aluminum. Results were assessed both by measuring the maximum cut depth, area (footprint) and volume removed. The latter was obtained by measuring the amount of water (mixed with a surfactant to reduce surface tension) needed to fill the crater. In subsequent tests, each jet type was typically operated at its optimum standoff.

For rock cutting tests, samples of Indiana limestone and Utah granite in the form of 6 inch cubes were obtained from a Utah quarry. The bedding plane direction was marked, and the jets were directed onto faces parallel to the bedding planes (sample "top" or "bottom"). A steel cover plate that exposed 1/4 of the rock face was employed to enable multiple tests on the same sample face and direct comparison of the performance of different jet types.

4. RESULTS AND DISCUSSION

4.1 Cuts in Aluminum

Figure 5 presents a typical set of results of the influence of standoff on the performance of STRATOJET™ and conventional Smith type nozzles at a value of $\sigma \approx 0.4$. Shown in this figure is the measured volume removed from an aluminum plate during a 5 min. static exposure as a function of jet standoff distance. The STRATOJET™ is seen to possess a rather broad optimum between approximately 0.7 and 3.2 orifice diameters. The optimum distance for the Smith nozzle is seen to be the smallest tested - 0.7 diameters. The performance of the STRATOJET™ is seen to be substantially better than that of the Smith.

The performance increase of the resonating nozzle relative to the Smith nozzle is summarized in Table 1 which presents the ratios of cut depth and volume of the resonating to Smith nozzles at their respective optimal standoffs for a range of test conditions. These ratios range from 6 to 20 in volume and 3 to 58 in depth. When no ratio is listed in this table, the Smith nozzle produced no measurable erosion.

Figure 6 presents photographs of the results a 5 min. exposure of an aluminum plate to two different STRATOJET™ designs and a conventional nozzle. This figure illustrates both the improved performance obtained with the STRATOJET™ and the sensitivity of that performance to the design geometry. This is further illustrated in Figure 7 which presents the ratios of cut volumes and depths for these two resonating nozzle designs to that of the conventional nozzle for three different ambient pressures (σ =0.63, 0.19, 0.31) at ΔP=55 MPa (8000 psi). As can be seen, for both designs, these ratios increase with increasing σ as any cavitation present in the conventional nozzle is suppressed. The improvement in cut depth is a factor of 15 at the highest ambient pressure (σ =0.31).

Results of translating cuts at 0.1 in/s in aluminum at the optimal standoffs found in the static test are presented in Table 2 for 6 different conditions tested. This table presents the number of passes required to achieve the onset of visible erosion. For the Smith at ΔP=30.4 MPa (4400 psi) and σ = 0.22, this required 30 passes while the resonating nozzle required only 4. Thus *the onset of erosion occurs 7.5 times faster* with the resonating nozzle than with the Smith. At ΔP=30.4 MPa (4400 psi) and σ = 0.5, the Smith produced no visible erosion (only surface discoloration without roughening). At the other conditions, for the resonating nozzle, between 2 and 8 passes were required for the onset of erosion to occur, with this occurrence being faster at lower σ and higher ΔP.

4.2 Rock Cutting

Figures 8 presents example results obtained from translating cuts at 0.3 m/s (12 in/s) in Indiana limestone. Shown is the percentage improvement in cut depth and volume removal rate of the resonating nozzle to the conventional Smith nozzle. The data were taken at a fixed ambient

pressure of 17.3 MPa (2500 psi) and span a range of ΔP of 17.9-45.5 MPa (2600-6600 psi) corresponding to a range of σ of 0.96-0.38. The resonating nozzle is seen to consistently outperform the Smith over the entire range. At ΔP = 17.9 MPa (2600 psi), the improvement is of the order of 1,000%. Since the performance of both nozzle types improves with increasing ΔP, the *relative* performance increase of the resonating nozzle decreases as the tensile strength of the rock is approached by the stagnation pressure generated by the conventional Smith jet. However, at 45.5 MPa 6600 psi, there is still an improvement in the volume removal rate of 40% and a cut depth improvement of 26%. These curves would be shifted toward higher ΔP for harder rock and toward lower ΔP for softer rock depending on the relative values of the erosive power of the jet and the strength of the rock.

Example results of translating cutting of Utah granite 0.3 m/s (12 in/s) are presented in Figure 9 at a fixed ambient pressure of 17.3 MPa (2500 psi). Presented is the measured cut depth for the STRATOJET™ and Smith nozzles over the range of ΔP = 4.1-45.5 MPa (600-6600 psi). Again the relative improvement of the resonating nozzle over the Smith is seen to vary with ΔP. At the lowest pressure drops, neither jet significantly erodes the rock. At the highest pressure drops, performance is comparable at this translation speed. However, at intermediate pressure drops, the resonating jet significantly outperforms the Smith. At ΔP = 34.5 MPa (5000 psi), the resonating nozzle produces a four fold increase in cut depth relative to the Smith.

5. CONCLUSIONS

Results of a series of studies of the performance of self-resonating cavitating STRATOJET™ nozzles for rock cutting have demonstrated their ability to substantially outperform conventional nozzles, such as the Smith, in both volume removal and cut depth. Initial screening data of candidate nozzle designs can be obtained by erosion of aluminum plates. Subsequent testing in actual rock can then be used for confirmation and quantitative measurement of cutting rates. Results of testing in aluminum, Indiana limestone, and Utah granite demonstrate that the relative performance increase is a function of operating conditions. At an ambient pressure of 17.3 MPa (2500 psi), the self-resonating cavitating jet produces a 10 fold increase in cut depth and volume relative to the Smith in Indiana limestone at ΔP = 17.9 MPa (2600 psi). At the same ambient pressure, the self-resonating cavitating jet produces a four fold increase in cut depth relative to the Smith at ΔP = 34.5 MPa (5000 psi) in granite.

6. ACKNOWLEDGMENTS

The results presented here are based on work supported by DYNAFLOW as well as by various R&D contracts. We would like most particularly to thank Telejet Technologies, Inc. for its support.

7. NOMENCLATURE

D, organ-pipe diameter
L, organ-pipe length
P_a, ambient pressure

P_v, vapor pressure of the liquid
ΔP, nozzle pressure drop
S_d, Strouhal number defined in equation (1)
V, jet velocity
d, orifice diameter
f, frequency
ρ, liquid density
σ, cavitation number defined in equation (2)

8. REFERENCES

Crow, S. and Champagne, T., "Orderly Structure in Jet Turbulence," *Journal of Fluid Mechanics,* vol. 48, August 1971.

Chahine G.L., Genoux, Ph. F., and Liu H.L., "Flow Visualization and Numerical Simulation of Cavitating Self-Oscillating Jets," *7th International Symposium on Jet Cutting Technology,* Ottawa, Canada, June 1984.

Chahine G.L., Genoux Ph. F., Johnson V.E. Jr., and Frederick G.S., "Analytical and Experimental Study of the Acoustics and the Flow Field Characteristics of Cavitating Self-Resonating Water Jets," *Sandia National Laboratories, Albuquerque, NM, Contractor Report SAND84-7142,* September 1984.

Chahine G.L., and Johnson V.E. Jr., "Mechanics and Applications of Self-Resonating Cavitating Jets," *Proceedings of the International Symposium on Jets and Cavities, ASME, WAM*, Miami, FL, November 1985.

Chahine G.L., Genoux Ph. F., Liu, H. L., and Johnson V.E. Jr., "Analytical and Experimental Study of Self-Resonating Jets: Nozzle-Jet and Wall-Jet Interactions," *Sandia National Laboratories, Albuquerque, NM, Contractor Report SAND86-7124*, September 1986.

Chahine G.L., Johnson V.E. Jr., Kalumuck K.M., Perdue T.O., Waxman D.N., Frederick G.S., and Watson R.E., "Internal and External Acoustics and Large Structures Dynamics of Cavitating Self-Resonating Water Jets," *Sandia National Laboratories, Albuquerque, NM, Contractor Report SAND86-7176*, July 1987.

Johnson, V. E., Jr., Chahine, G. L., Lindenmuth, W. T., Conn, A. F., Frederick, G. S., and Giacchino, G. J., "Cavitating and Structured Jets for Mechanical Bits to Increase Drilling Rate, Part 1: Theory and Concepts; Part 2: Experimental Results," *Journal of Energy Resources Technology,* vol.106, June 1984.

RATIO OF STRATOJET TO SMITH PERFORMANCE 5 MIN. STATIC CUTS IN AL. AT OPTIMUM STANDOFFS				
Delta P (MPa)	Pamb (MPa)	Sigma	Cut Volume Ratio (VStrato/VSmith)	Cut Depth Ratio (DStrato/DSmith)
30.4	6.9	0.2	21.0	3.1
30.4	15.2	0.5		
36.6	7.9	0.2		3.6
36.6	18.3	0.5		13.0
45.7	10.2	0.2	6.4	3.2
45.7	17.8	0.4	20.3	58.0

Table 1

TRANSLATING CUTS NUMBER OF PASSES FOR ONSET OF VISUAL EROSION IN Al. AT 0.254 cm/s			
CAVITATION NUMBER	NOZZLE PRESSURE DROP (MPa)		
	30	37	46
RESONATING NOZZLE			
0.22	4	2	2
0.4-0.5	8	4	3
Smith Nozzle needed more than 30 passes. Only tested at 30 MPa.			

Table 2

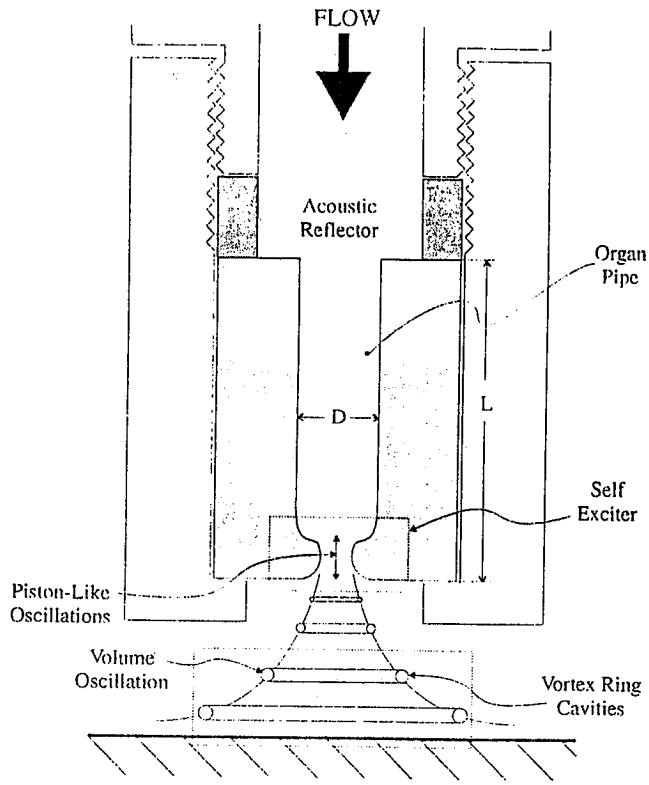

Figure 1: Schematic of Principle of Operation of an Organ-Pipe STRATOJET™.

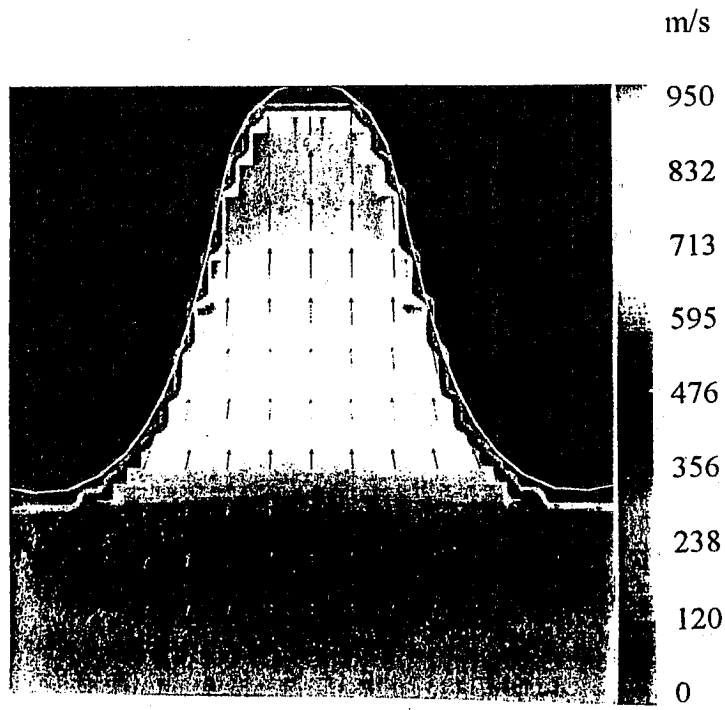

Figure 2: Results Of Numerical Simulation Of Bubble Collapse And Formation of High Speed Microjet at an Ambient Pressure Of 17.3 Mpa (2500 Psi) Using DYNAFLOW's 3D Code, 3DynaFS. Shown are Computed Velocity Vectors and Contours.

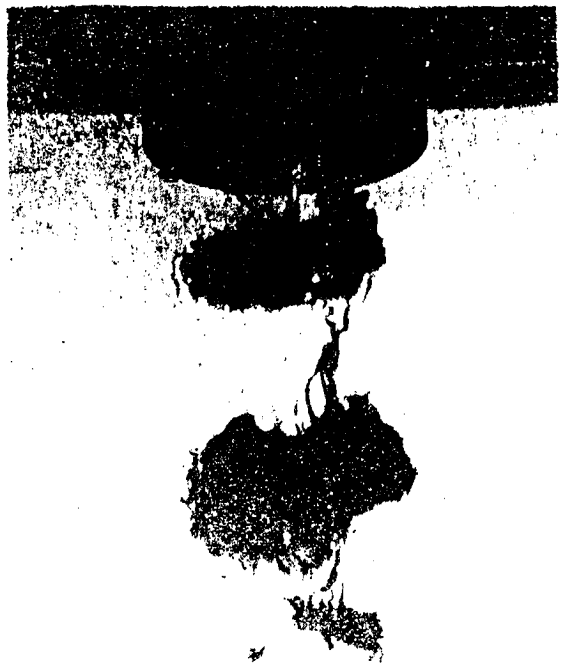

Figure 3: Large Scale Visualization of STRATOJET™. $\sigma = 0.21$.

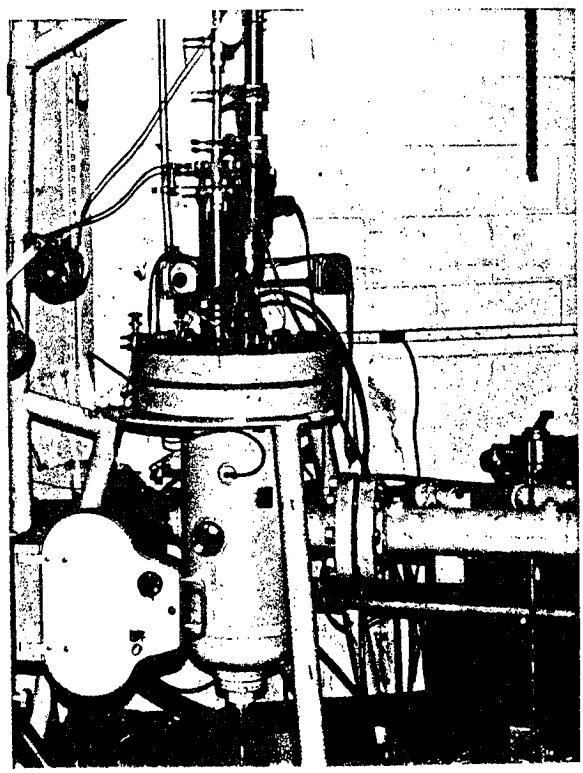

Figure 4; High Pressure Cell (HPC) Capable of Ambient Pressures Up to 19.3 MPa (2800 psi).

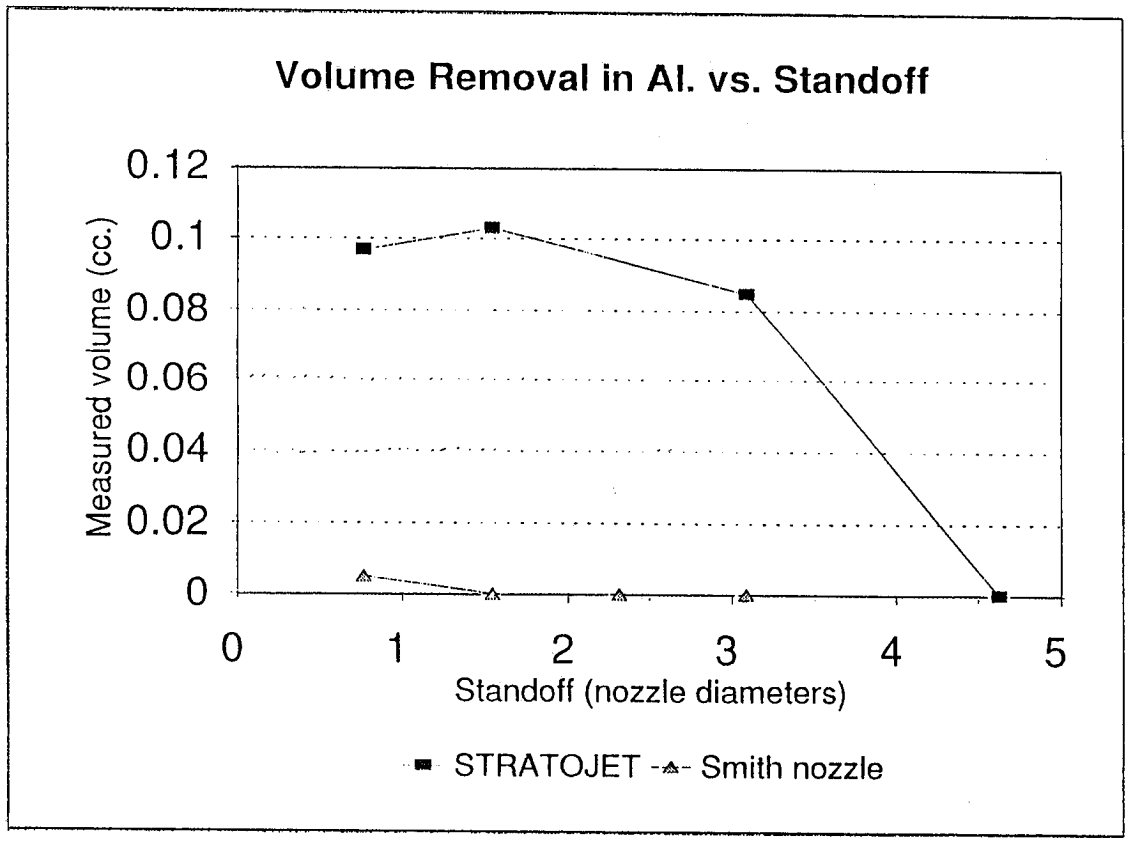

Figure 5: Influence of Standoff Distance on Volume Removal in Aluminum for STRATOJET™ and Smith Nozzles. ΔP = 45.7 MPa (6620 psi), P_a = 17.8 MPa (2580 psi), 5 min. Exposure.

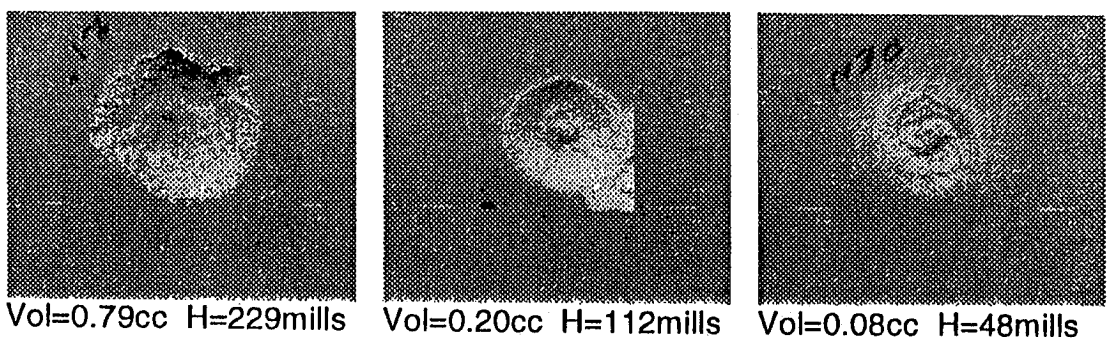

Figure 6: Comparison of Erosion of Aluminum Plate by 2 STRATOJET™ Designs (Left and Center) and a Conventional Nozzle (Right Most Photo). Vol = Volume Removal; H = Depth of Erosion.

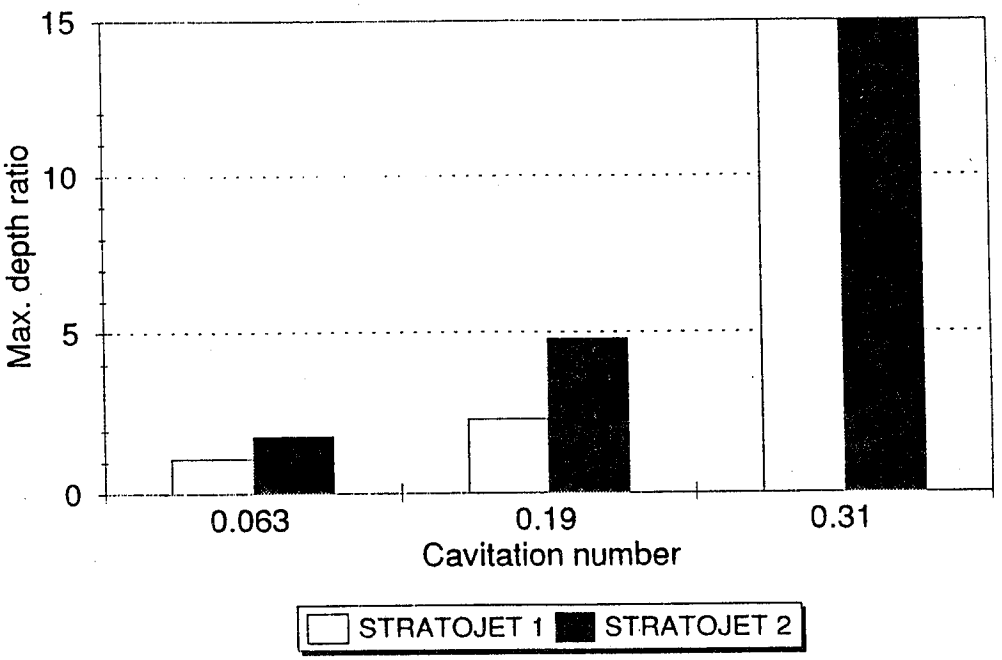

a) Ratio of Cut Depths.

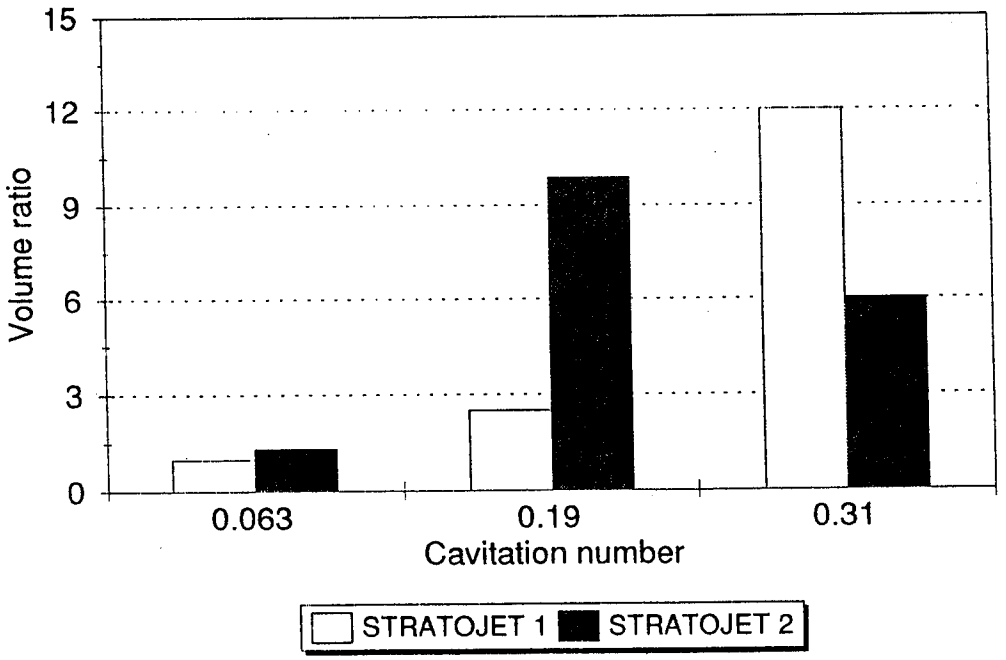

b) Ratio of Cut Volumes.

Figure 7: Comparison of the Performance in Aluminum of 2 STRATOJET™ Designs and a Conventional Nozzle at Different Cavitation Numbers. ΔP = 55.2 MPa (8,000 psi).

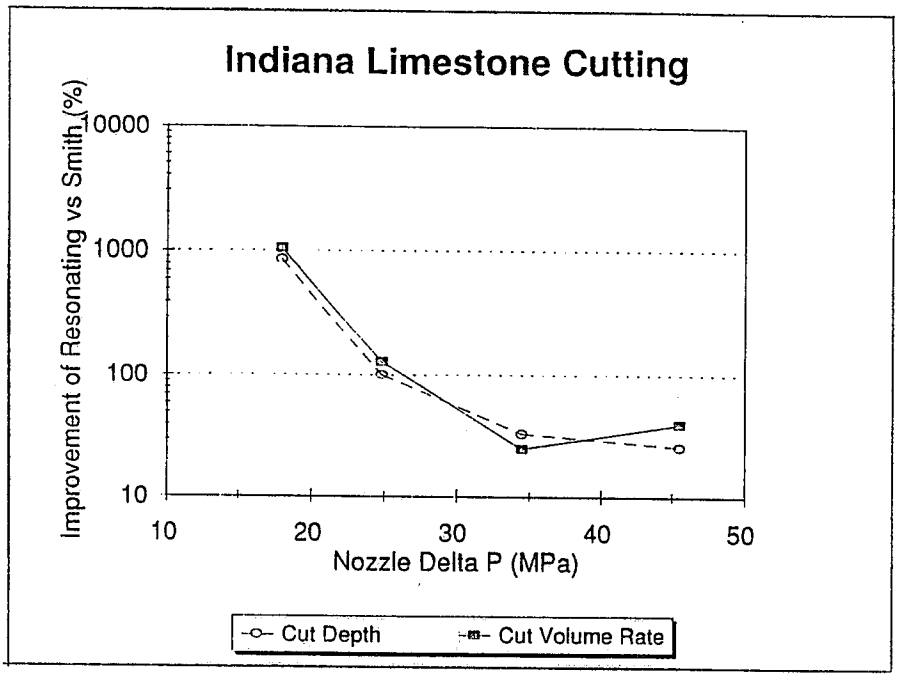

Figure 8: Improvement in Cut Depth and Volume Removal Rate of STRATOJET™ Over Smith Nozzle in Indiana Limestone. Pa = 17.3 MPa (2500 psi), Translation Velocity = 0.3 m/s (12 in/s).

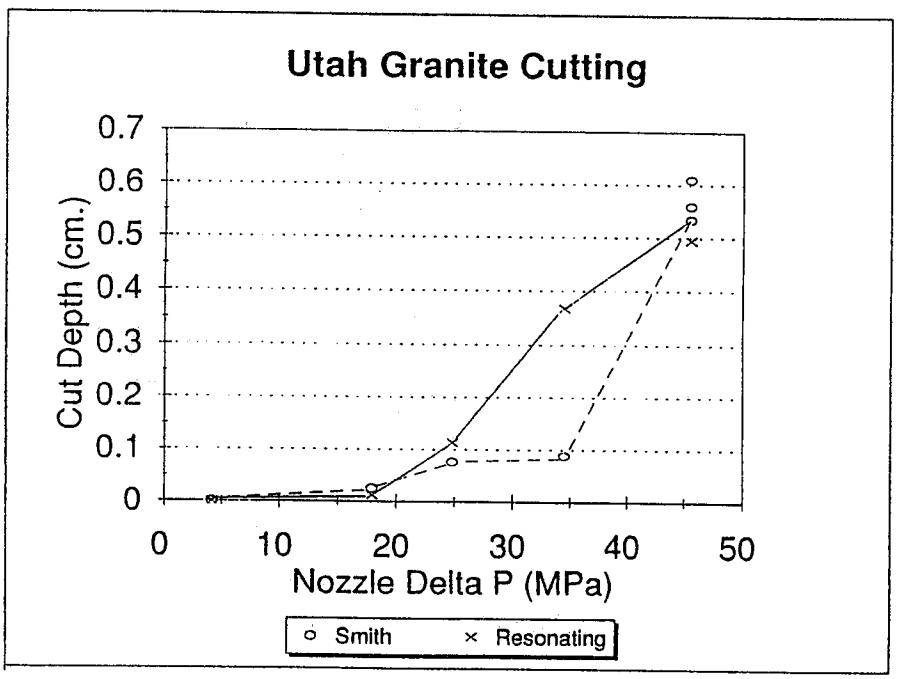

Figure 9: Influence of ΔP on Translating Cut Depth in Utah Granite for STRATOJET™ and Smith Nozzles. Pa = 17.3 MPa (2500 psi), Translation Velocity = 0.3 m/s (12 in/s).

8th American Water Jet Conference
August 26-29, 1995: Houston, Texas

Paper 58

AN APPLICATION STUDY OF PLAIN WATERJET PROCESS FOR COATING REMOVAL

Samuel S. Wu* & Thomas J. Kim
Department of Mechanical Engineering
University of Rhode Island
Kingston, Rhode Island, U.S.A.

ABSTRACT

A series of erosion tests by a high pressure waterjet was conducted to gain a thorough understanding of the mechanisms of a plain waterjet used for coating removal as well as cutting applications. It is well known that the waterjet can effectively be used in cleaning and coating removal without damaging the substrate of target materials. However, the efficiency of removal is greatly dependent on the jet process parameters including the geometry of jet impingement. The experimental results demonstrate that process optimization can be achieved by proper selection of jet system parameters.

* Present address: Aqua-Dyne, Inc.,
3620 W. 11th Street
Houston, TX 77008

Organized and Sponsored by the Water Jet Technology Association.

1. INTRODUCTION

Waterjets have been utilized successfully in industries for many years. During our study on the topic of plain waterjet erosion, it was determined that a thorough understanding of plain waterjet and liquid impact mechanisms will benefit the application of plain waterjets, especially in cutting and coating removal.

In the plain waterjet process, the critical operating parameters are jet structure, orifice (nozzle) size, pressure, traverse speed, and standoff distance. Many researchers (Pai, 1954, Yanaida et al., 1980, Eddinfield et al., 1981) contributed to the study of jet structure. Jet structure can be divided into three flow regions, (a) initial region, (b) main region, and (c) final region. The jet stream becomes wider along the jet axis, while the momentum of the jet remains constant. The velocity profile and the pressure profile of the jet changes from an initial narrow bell-shaped distribution to a flat-shaped distribution. Therefore, different flow regions may result in different cutting profiles and related material removal mechanisms. Previous research and experiments show that the nozzle or orifice geometric structure and pressure have great influence on the jet structure. In other word, these two parameters are the determining factors of jet structure. Traverse speed more or less influences production efficiency. Standoff distance produces different flow regions and therefore, plays a role in determining the material removal mechanism.

The influence of standoff distance on waterjet cutting was carried out by Franz (1974). Optimum standoff distance was found to exist in depth of cut and width of cut. One peak was observed. But only one traverse speed was used. The effect of standoff distance was also tested using zero traverse speed (Kobayashi et al., 1988). Two peaks were found on the mass loss curve. It was believed that the excavation force of the waterjet plays an important role at the first peak, while the impact force due to impingement of lumps and droplets contributed to the second peak. Material erosion by waterjet was performed by means of penetration (Murai et al., 1989). Two peaks were found on the weight loss curve, too. Many researchers (Beutin et al., 1974 and Li et al., 1992) contributed to waterjet material erosion knowledge.

In our study of plain waterjet processes, it was realized that complete erosion experiments and through understanding of waterjet processing mechanisms are necessary in order to employ waterjet technology in industrial applications efficiently, leading to reduced power use, increased production rates and enhanced cutting quality.

2. EXPERIMENTAL PROCEDURE AND SETUP

A series of experiments were carried out to examine the effects of varying the jet stream under various operating conditions. The target material chosen for these tests was aluminum 6061-T6. The process parameters varied included pressure, orifice size, standoff distance and traverse speed. The experiments were carried out by using Flow 9XD-55 dual intensifier pump and 414 X-Y shapecutter with DYNAPATH controller.

For the width and depth measurements a Nikon UM-2 measurescope was used. The width data reported below represents the average width of the cut for each test condition. The mass loss was measured using a Mettler AE163 scale.

The following range of parameters were evaluated:

Material: Al 6061-T6
Orifice: 0.152, 0.254 & 0.381 mm in diameter (0.006. 0.010 & 0.015 inch)
Pressure: 140-345 MPa (20-50 ksi)
Traverse Speed: 0.42-105.83 mm/s (1-250 ipm)
Standoff Distance: 6.35-127 mm (0.25-5 inch)
Cut Length: 12.7 mm (0.5 inch)

3. EXPERIMENT RESULTS AND ANALYSIS

3.1 Results

Mass loss, erosion width and depth versus standoff distance are shown in Figures 1-3. Both mass loss and erosion depth reach an optimum at a certain standoff distance. Variation in erosion width at low standoff distance is observed in Figure 2.

Mass loss, erosion width and depth versus traverse speed can be found in Figure 4-6. It is observed that an increase in traverse speed (below or equal to 10 in/min), reduces the mass loss, erosion width and depth rate sharply. When the traverse speed (larger than 10 in/min) is increased, the mass loss, erosion width and depth become much lower than that of at traverse speeds below 10 in/min and change little.

As expected, when the pressure is increased, the three measured values show an increase (see Figure 7-9). Mass loss and erosion depth have the similar characteristics, their curve slopes depend on the traverse speed. However, the curve slope of erosion width shows no difference among the varied traverse speeds.

It is not strange that larger orifices cause larger mass loss and erosion width as shown in Figures 10 and 11. The increase in orifice size does not cause much increase in depth except when traverse speed is very low (Figure 12). At high traverse speeds, the erosion depth even decreases as the orifice size is increased.

Material removal rate shows an increase when the traverse speed is increased (Figure 13). This implies that in a cutting and cleaning job using waterjet, high traverse speed and multiple passes generate high production rate and efficiency.

Based on the erosion experiment, tests on decoating and derusting were also performed in laboratory by inclining a jet to workpiece (see Figure 14 and 15). Decoating width by a jet normal to workpiece is larger than that by a jet at inclining angles to the workpiece. High traverse speed also produces high production rate.

3.2 Analysis

In a waterjet application, one can classify the jet into three categories: continuous jet, mixed jet and impact jet (Erdmann-Jesnitzer et al., 1980) depending upon processing parameters. The resulting pressure from the continuous jet loading is constant. The pressure resulting from the mixed jet reaches a peak and drops sharply to a constant, lasting for some time, and eventually decaying to zero. The resulting pressure of the impact jet reaches a peak and then goes to zero very quickly. Therefore, these jet structures lead to different loading behavior. The continuous jet results in static loading and the impact jet results in dynamic loading. The mixed jet leads to combined static and dynamic loading. It is also found that the number of jet pulses and intensity of pulses increase with increases in the pressure and standoff distance. The dynamic loading effect of waterjet was investigated (Konig et al., 1984). In fact, the stagnation force of waterjet consists of two components: static and dynamic loading. The static component of the force rises proportionally to the pressure increase, as expected from theory. In addition to the increase in the static component, the dynamic component also grows with pressure. Keeping the pressure unchanged and varying the standoff distance, the static portion of the stagnation force remains constant, while the dynamic portion increases rapidly with increased standoff distance. This is the reason why at a certain standoff distance, mass loss and erosion depth reach an optimum. Erosion width variation was observed at low standoff distance and some traverse speeds because of viscous shear effects on the waterjet (see Figure 16). At low standoff distances, the jet is more continuous and less pulsated and therefore cannot cut any deeper. The ratio of the effective jet diameter to actual jet diameter at this situation is large. This large ratio means more water took part in the material removal in certain area and resulted in more water deflected from the bottom of the kerf. The defected jet has a velocity of 2-10 times the impact jet velocity. At this point, the jet could not cut deeper. However, the deflected radial jet had enough energy to damage the target by tearing off pieces of material, perhaps through crack initiation and propagation.

4. MECHANISMS OF WATERJET IMPACT

The Reynolds number at the exit of a high pressure waterjet nozzle is relatively high. For example, at 140 MPa (20 ksi), orifice diameter 0.381 mm (0.015"), Re = 199410. The jet is turbulent. Especially at great distance, the jet is totally composed of droplets.

For the water drop impingement, it is believed (Adler, 1979) that there are four primary damage modes: direct deformation, stress wave propagation, lateral outflow jetting, and hydraulic penetration. One or more of these loading conditions on a material surface exposed to single or multiple water drop impacts are responsible for initiating damage and subsequent material removal. For brittle and semibrittle materials, the most obvious damage is the development of cracks from impact velocities above the fracture threshold. Fractures usually develop in zones of high tensile stresses. Tensile stresses arise at the boundary of the depressed zone and in the vicinity of the target surface away from the impact site due to stress wave propagation. The near-field wave structure is primarily compressive, but once the shear wave separates from the contact zone, tensile stresses of relatively high magnitude extend over significant radial distances.

It has been observed that material removal will occur in materials exposed to multiple liquid impacts at mean impact pressures well below the yield strength levels, or compression strength in metals. This indicates the role of material microstructure in the damage initiation process. Once fractures, grain tilting, and or other microstructural surface irregularities are present on the surface, lateral outflow jetting produced during the collapse of the drops onto the surface can interact with the displaced edge of these cracks or other surface irregularities to initiate and propagate fractures. The effectiveness of the lateral outflow jets (whose velocity is several times the impact velocity) in extending preexisting cracks depends on the height of the mismatch between the opposing edges of the crack once it is formed. This property is material dependent and can be influenced by the state of initial stress in the surface layer of the target. Lateral outflow jetting will not contribute to the initiation or extension of damage unless there is a preexisting surface irregularity with which it can interact. When cracks are formed on the specimen's surface due to deformation or due to stress wave propagation, there is typically a height differential between the opposing faces of the crack due to incomplete crack closure.

The effectiveness of lateral outflow jetting depends on the proximity of subsequent drop impacts in the vicinity of these cracks. Drop impacts on the same side as the raised edge are ineffective in producing further damage by this erosion mechanism. Even after many drops impact in the same region, the raised edge of the crack shows the effects of subsequent impacts, while the opposing face remains sharp and unaffected.

Hydraulic penetration of the water in a drop impacting over a preexisting crack or erosion pit is the most damaging mode for material removal, since it has the capacity to propagate submicrometer size cracks and surface pits to measurable dimensions, on the order of several millimeters, and is effective throughout the material removal process. The presence of a pit can also induce the formation of high-velocity jets which can further enhance the pit depth. On the other hand, material removal is often associated with a fatigue process which is attributed to the repetitive direct pressure pulse applied to a metallic surface.

In the high velocity impact of a waterjet, it was suggested through SEM examination (Mazurkiewicz et al., 1978) that because the local power density is very high, the dominant fracture mechanism is crack propagation due to high local power density. For the fracture mechanism of brittle materials, it was found (Erdmann-Jesnitzer et al., 1978) that at small distance, the discontinuities of the mainly continuous jet are sufficient enough to initiate microcracks and participate in the propagation of existing microcracks to critical lengths. The continuous part of the jet and its steady state pressure propagate the critical cracks and are also very effective in excavating the crystalline parts out of the samples. But at larger standoff distances, microcracks are produced or partly propagated.

5. OPTIMIZATION IN COATING REMOVAL

Erosion tests on aluminum by a high pressure waterjet showed that optimal results can be achieved at given operation parameters. Mechanisms of material removal and impact by a high pressure waterjet depend on selection of operating parameters. Optimization is strongly

related to materials, coating properties, operating parameters, and user's decision. In fact, it is difficult to give exact parameters in optimization process because there are so many different coating removal jobs which may differ greatly, e.g., from grease removal to high strength bonded thermal spray coating removal. However, understanding of erosion and impact mechanisms by a high pressure waterjet and fundamental aspects in cleaning (Louis et al., 1982), provide the fundamentals and guidelines in optimization of coating removal by a high pressure waterjet.

5.1 Coating Materials

Coating materials range from enamel, scale, deposits, inorganic layers, ceramics, plastics, metals, and rubber. They may be brittle or ductile. Efficient removal of these materials requires different jets which result in various mechanisms.

5.1.1 Ductile materials

These include plastics, rubbers, most metals and deposits. These materials posses the ability to deform under the influence of externally applied forces. Before failure, they would have an elastic elongation and a plastic elongation. Upon waterjet impact, a state of deformation is reached where intense local concentrations of dislocations develop. At these locations the internal stresses exceed the fracture strength of the material and a crack is formed. Because of material elastic and plastic deformation properties, a lot of energy is needed by deformation. Crack propagation needs similar loading as crack opening. Thus, in ductile material coating removal, droplet (impact) jet or mixed jet(partly impact and partly continuous) may have a large removal area or width since the resulting pressure from impact jet is ρcv, much larger than static pressure from continuous jet $(1/2)\rho v^2$ (where v is jet velocity, ρ is density of water, c is velocity of sound in water). In other words, instead of a low standoff distance, a relative high standoff distance should be used to perform the cleaning job. But the standoff distance should not exceed effective distance for the coating to be removed.

5.1.2 Brittle Materials

These are scale, ceramic, and enamel. Due to their brittleness, when waterjet impacts on the layers of these materials, cracks are initiated and propagated with the absence of a deformation area at the crack tip. To remove these layers, it is important to produce crack and crack propagation. When two cracks or more are crossing, a piece of coating will be torn off. With little plastic deformation or without plastic deformation, crack propagation is quick and needs less energy. There are two ways to create a crack, 1. taking advantage of a microstructure on the coating, mini crack, a void or defect; 2. using dynamic or impact loading of waterjet. Once a crack is opened, letting the continuous jet and radial outflow jet to open up and propagate crack. If cracks are initiated and run a short distance, a small piece of coating is removed. If cracks are initiated and run a long distance, a large piece of coating or scale is removed. Creation of a short crack or long one depends on coating or scale thickness and their adherence on the substrate.

5.2 Pressure

Pressure determines jet velocity, Reynolds number, turbulent properties, and loading of jet. Determination of pressure level depends on coating and power available, as well as manual or machine operation. Pressure should be selected so that the coating can be easily removed with less loading time and without damaging the substrate. If high pressure and large water volume are used, a machine-moved cleaning nozzle head should be preferred, with a fast rotation and traverse speed to generate high coating removal rate without risk of damaging the substrate. If hand gun equipment is used, pressure should be selected so that a man can move the gun around the workpiece at a comfortable speed and check if the coating is being removed satisfactorily without damaging the substrate. If the pressure of a machine is fixed, increased flow rate with low pressure can perform a tough job that requires a high pressure or ultra-high pressure because of increase in power use.

However, it should be noted that there is a threshold pressure at which a coating can be removed. Below that pressure, no matter how large the flow and how long the load time is, no coating removal occurs. Such a pressure is obtained principally from testing and experimental data. Usually, manufacturers have that information and can direct their customers to select a jetting system.

5.3 Nozzle

There are many kinds of nozzles, some nozzles produce long cohesive jet, some short cohesive jet. Some generate a wide and flat jet (fan jet) in order to create a large cleaning area. Some form a jet cone by design or by rotation of nozzles.

5.3.1 Nozzle types

a. Long cohesive:

If a piece of work is restricted for access, a long cohesive jet should be used to perform the job so that jet reaches the coating without losing the energy which is required to remove the coating. Otherwise, a much higher pressure or a larger water volume has to be used. This kind of nozzle is also good for brittle coating or scale removal, especially thick brittle coatings and scales.

b. Fan jets

Fan jets are good for large area cleaning and easy-to-remove coatings such as grease, oil layers and thin layers of contamination or dirt. It is found (Xu et al., 1994) that fan jets work better at low traverse speeds compared to round jets.

c. Rotating jet

Rotating jets (nozzles) are designed for large area coating removal, without fan jet's shortcomings. Rotation speed is crucial, usually, faster the better. Fast rotation speed will

generate more passes in a given time which generally creates the efficiency as discussed in Section 3. Jet overlapping is easily achieved by fast rotation speed. It should be also noted that jet traverse speed is $v = \pi dn$. This speed should allow the waterjet to satisfactorily remove the coating. In other words, sufficient loading time to remove the coating at given operating parameters. Thus, n should be chosen according to arm's length or the distance between two nozzles or visa versa.

5.3.2 Nozzle size

Nozzle size determines power use at a given pressure. Increase in nozzle size can decrease the pressure level to perform the coating removal job. At a given pressure large nozzles are more efficient than smaller nozzles. For efficient power use, multi-nozzle system is more effective than a single large nozzle system (Waltson et al., 1993) because a larger nozzle creates a larger cleaning area than a smaller nozzle, however, for same power use, cleaning width of two smaller nozzles is larger than the one by a single large nozzle.

5.4 Standoff Distance

Standoff distance determines the type of jet impacting on the coating, either continuous or impact or mixed. There is an optimal standoff distance at a given pressure, nozzle type and size, at which most efficient coating removal occurs. It is also related to the properties of coating material, since certain jet impact mechanisms are most effective for certain coating materials as discussed in Sec. 5.1. It is difficult to give an optimum standoff distance here for universal use because so many parameters affect its determination.

5.5 Optimization Process

Generally, all cleaning jobs involve removal of unwanted layers or coatings without damaging the substrate or minimizing the damage. For most applications, a system is available. If it is not the case, a manufacturer should propose a system which works well with the customer's requirement. There are several steps in the optimization of coating removal.

1. Job size, coating materials, substrate materials, and the degree of cleaning have to be known.
2. Based on the information obtained in 1., determine the threshold pressure for coating or scale removal and for substrate damage.
3. Select an operating pressure which is larger than the coating removal pressure and lower than the one damaging the substrate so that even dynamic impact loading would not damage the substrate surface.
4. Select a nozzle/nozzles size to suit your system capability and nozzle type to have the most efficient production rate.
5. Standoff Distance selection. Based on your nozzle selection and your coating properties, an effective standoff distance can be determined.

6. CONCLUSIONS

1. There is an optimum standoff distance for mass loss and depth of cut depending on orifice or nozzle geometric structure and material properties.

2. Mass loss, width and depth of cut change little when traverse speed is larger than 4.23 mm/s (10 in/min) for aluminum A16061-T6.

3. In coating removal applications, optimization process can be achieved through understanding of coating materials and their effective removal mechanisms, as well as careful selection of a jetting system and operating parameters.

7. REFERENCES

Adler, W. F., "The mechanisms of Liquid Impact," *Treatise on Materials Science and Technology, Volume 16, Erosion*, edited by Carolyn M. Preece, Academic Press, 1979.

Beutin, E. F., Erdmann-Jesnitzer, F., and Louis, H., "Material Behavior in the Case of High-Speed Liquid Jet Attacks," *Second International Symposium on Jet Cutting Technology*, 1974.

Beutin, E. F., Erdmann-Jesnitzer, F., Hassen, A. M., and Louis, H., "A New Technique in the Application of High Speed Water Jet," *Third International Symposium on Jet Cutting Technology*, 1976.

Eddingfield, D. L., Evers, J. L. and Setork, A., "Mathematical Modeling of High Velocity Water Jets," *First American Water Jet Conference*, 1981.

Erdmann-Jesnitzer, F., Louis, H, and Wiedmeiser, J., "Material Behavior, Material Stressing, Principle Aspects in the Application of High Speed Water Jets," *Fourth International Symposium on Jet Cutting Technology*, 1978.

Erdmann-Jesnitzer, F., Lewis, H. and Wiedemeier, J., "The Action of High Speed Water Jets on Materials," *Fifth International Symposium on Jet Cutting Technology*, 1980.

Franz, N. C., "The Influence of Standoff Distance on Cutting with High Velocity Fluid Jets," *Second International Symposium on Jet Cutting Technology*, 1974.

Kobayashi, R. and Arai, T., "Local Structure of Water Jet and Related Erosion Process of Metallic Materials," *9th International Symposium on Jet Cutting Technology*, 1988.

Konig, W. and Wulf, Ch., "The Influence of the Cutting Parameters on Jet Forces and the Geometry of the Kerf," *Seventh International Symposium on Jet Cutting Technology*, 1984.

Li, H. L., Geskin, E. S. and Gordon, E. I., "Investigation of the Pure Waterjet-Workpiece Interaction," *Eleventh International Symposium on Jet Cutting Technology*, 1992.

Louis, H. and Schikorr, W., "Fundamental Aspects in Cleaning with High-speed Water Jets," Paper E3, *6th International Symposium on Jet Cutting Technology*, 1982.

Mazurkiewicz, M., Sebasten, Z. and Galecki, G., "Analysis of the Mechanism of Interaction Between High Pressure Waterjet and Material Being Cut," *Fourth International Symposium on Jet Cutting Technology*, 1978.

Murai, H. and Nishi, S., "Structure of Water Jet and Erosion of Materials," *5th American Water Jet Conference*, 1989.

Pai, S.I., *Fluid Dynamics of Jets*, D. Van Nortrand Company, Inc., 1954.

Schlichting, H., *Boundary-Layer Theory*, McGraw-Hill Book Company, 1979.

Szekely, J., *Fluid Flow Phenomena In Metals Processing*, Acamedic Press, Inc., 1979.

Watson, J.D., "Thermal Spray Removal With Ultrahigh-Velocity Waterjets," Paper 42, *7th American Water Jet Conference*, August 28-31, Seattle, Washington, 1993.

Xu, J. and Summers, D.A., "Experimental Evaluation of the Performance of Fan Jet Systems," *12th International Symposium on Jet Cutting Technology*, Page 37-46, France, Oct. 25-27, 1994.

Yanaida, K. and Ohashi, A., "Flow Characteristics of Water Jets in Air," *Fifth International Symposium on Jet Cutting Technology*, 1980.

8. NOMENCLATURE

OD -- orifice diameter
P -- pressure
SD -- standoff distance
U -- traverse speed

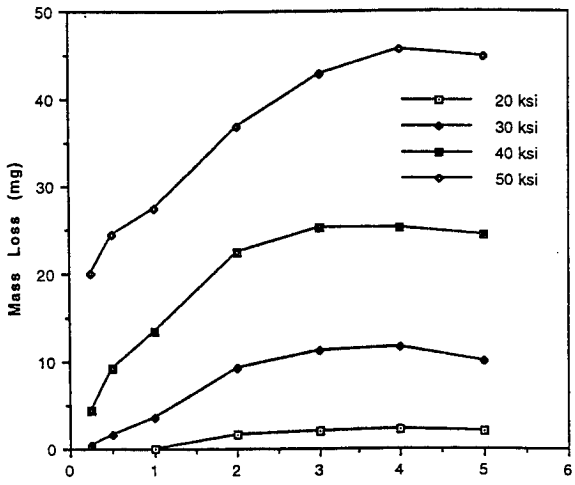

Figure 1 Mass Loss vs Standoff Distance

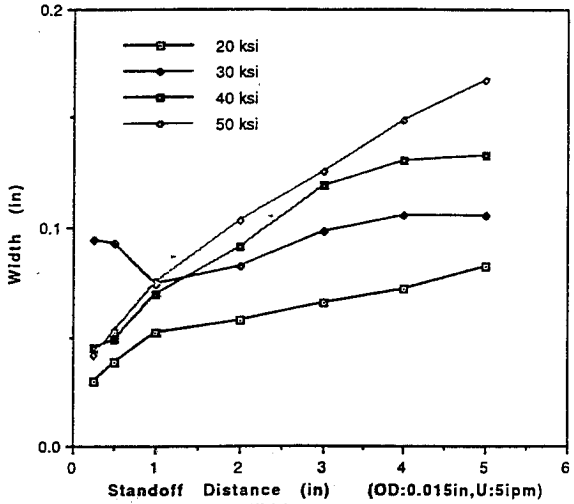

Figure 2 Width vs Standoff Distance

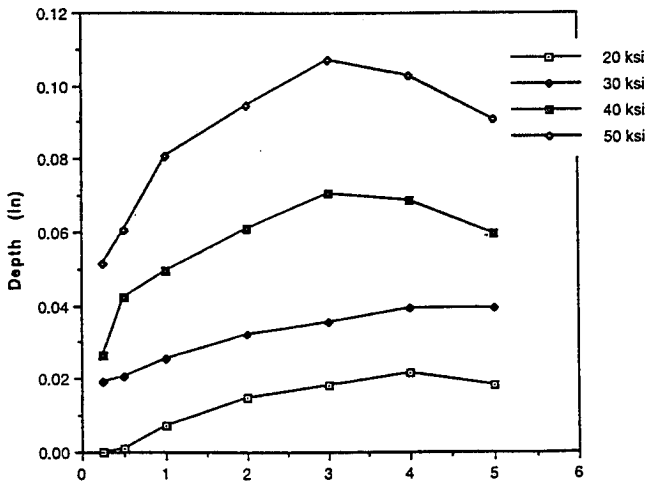

Figure 3 Depth vs Standoff Distance

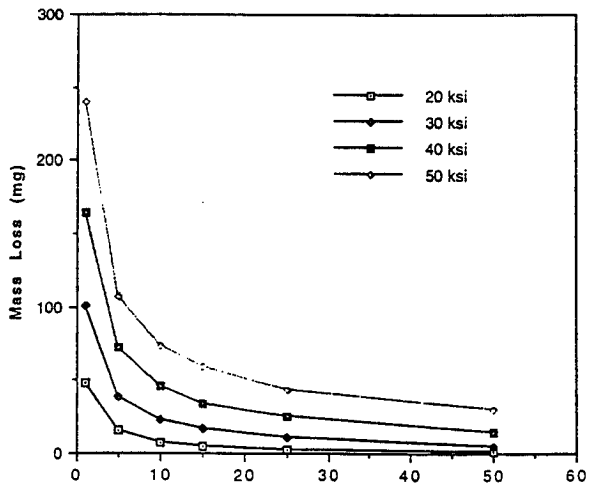

Figure 4 Mass Loss vs Traverse Speed

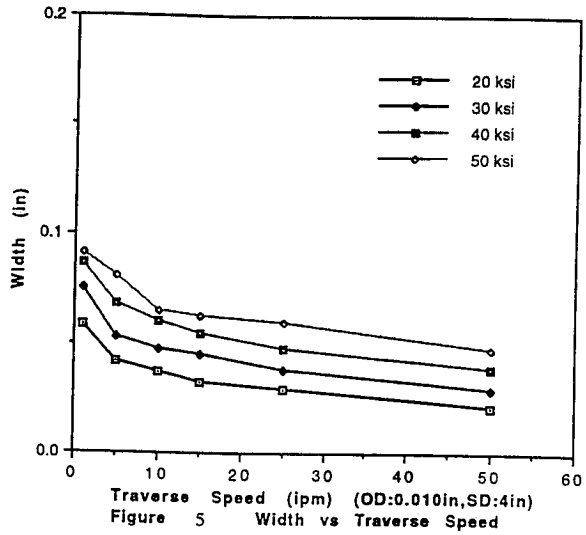

Figure 5 Width vs Traverse Speed

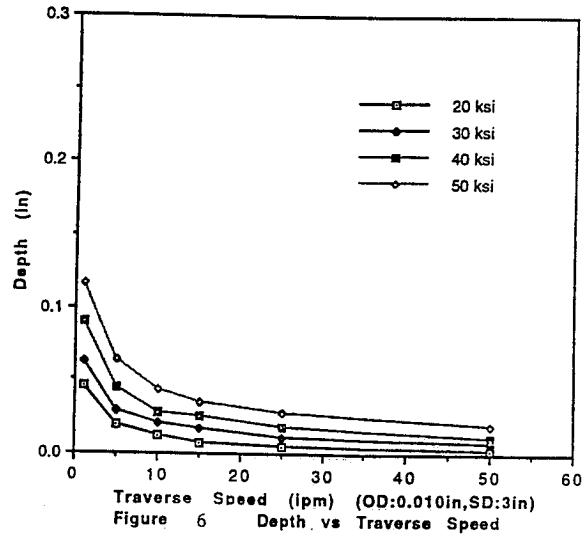

Figure 6 Depth vs Traverse Speed

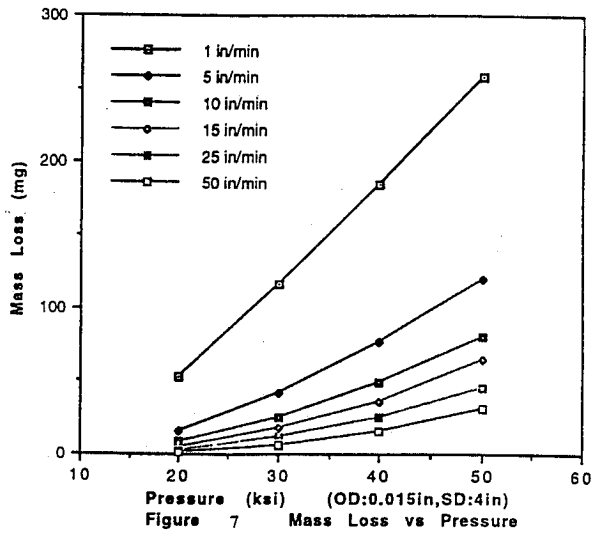

Figure 7 Mass Loss vs Pressure

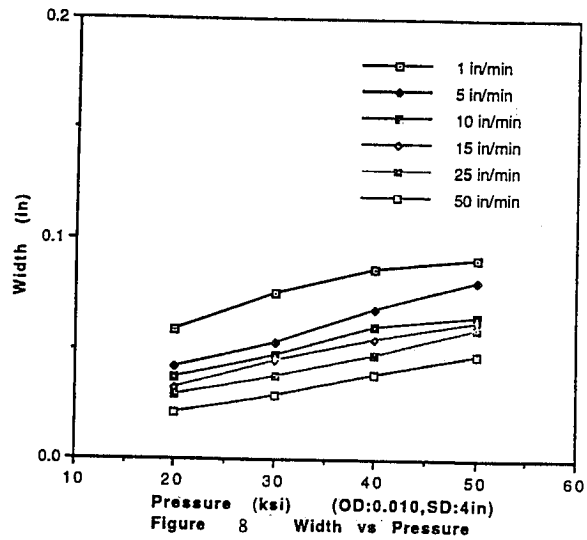

Figure 8 Width vs Pressure

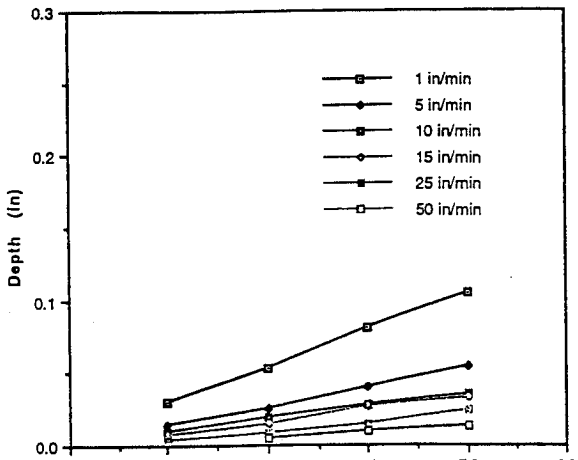

Figure 9 Depth vs Pressure

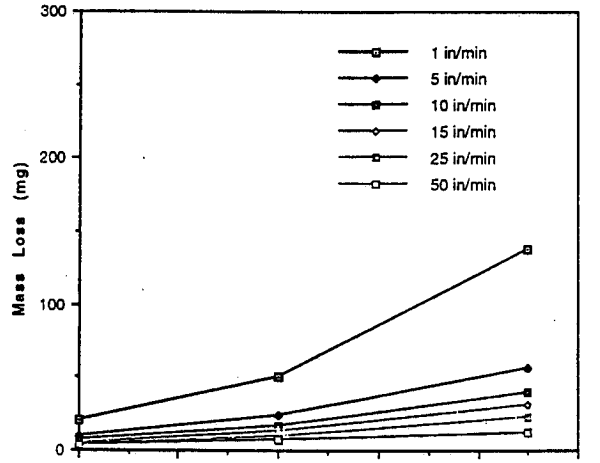

Figure 10 Mass Loss vs Orifice Diameter

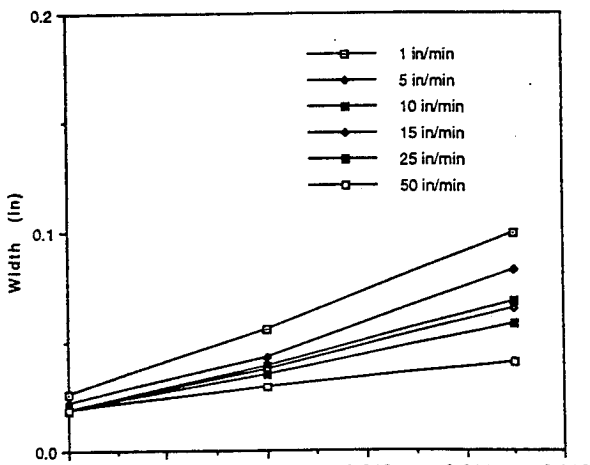

Figure 11 Width vs Orifice Diameter

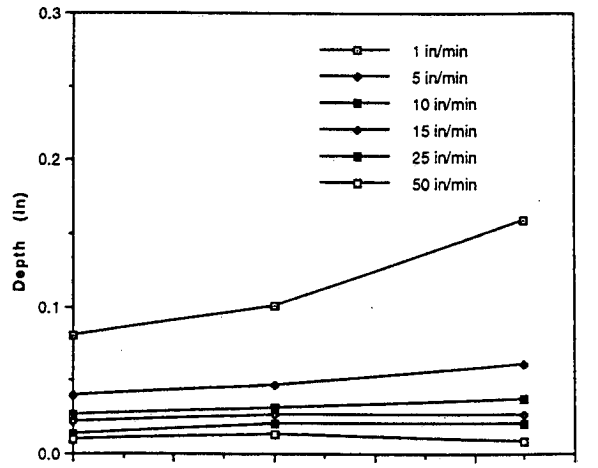

Figure 12 Depth vs Orifice Diameter

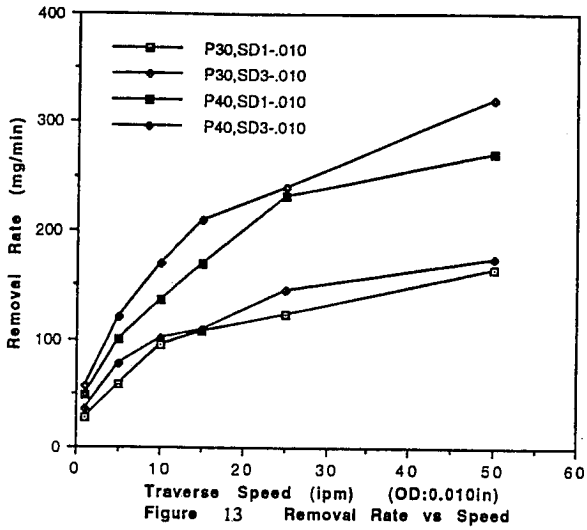

Figure 13 Removal Rate vs Speed

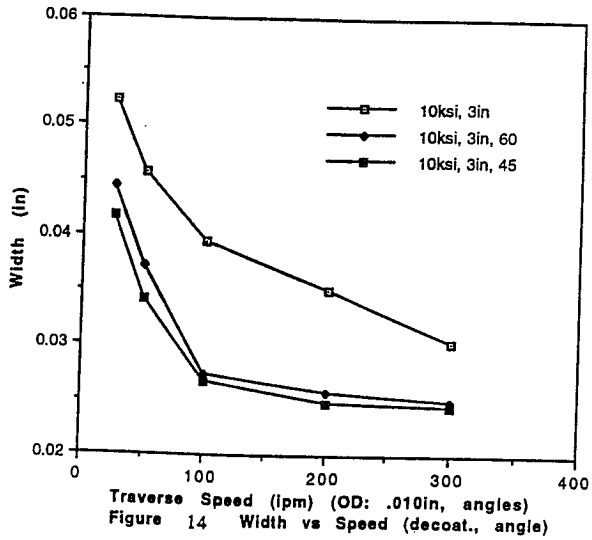

Figure 14 Width vs Speed (decoat., angle)

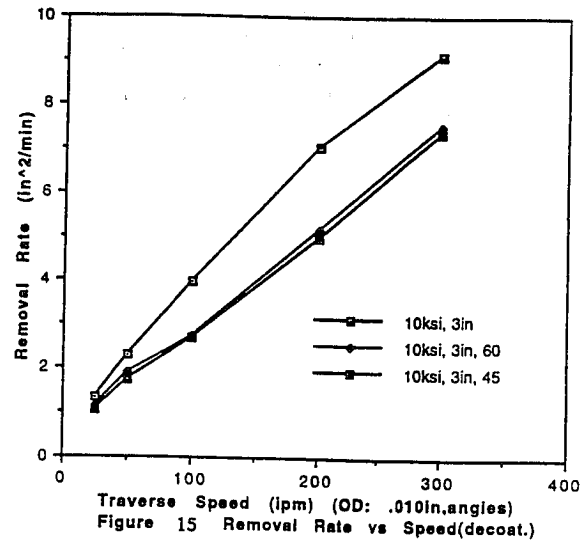

Figure 15 Removal Rate vs Speed(decoat.)

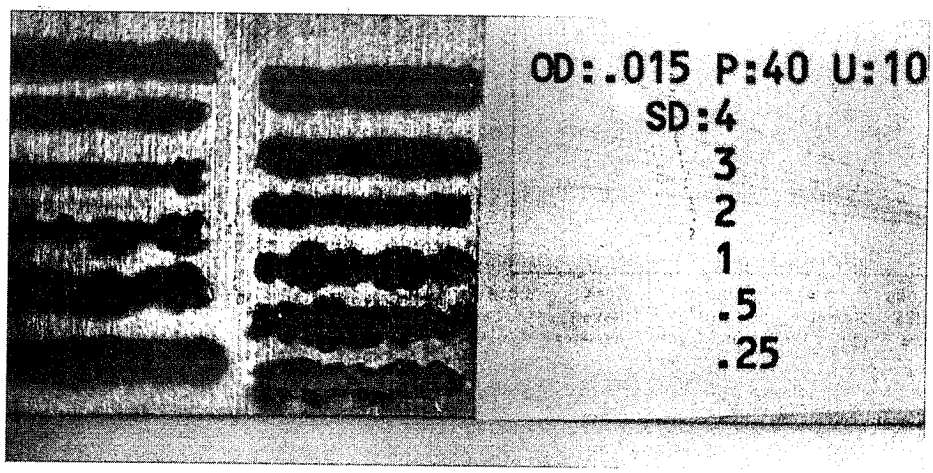

Figure 16 Cutting Profile at P:40ksi,OD:.015,U:10ipm

8th American Water Jet Conference
August 26-29, 1995: Houston, Texas

Paper 59

INFLUENCE OF ASSISTANCE OF HIGH-PRESSURE WATER JET IN THE PROCESS OF ROCK CUTTING UPON THE TEMPERATURE, WEAR, CUTTING FORCE AND DUSTINESS OF THE SHEARER PICK EDGE

A. Klich, K. Kotwica, J. Res
University of Mining and Metallurgy
Cracow, Poland.

ABSTRACT

Paper presents the results of research conducted on a laboratory stand at the University of Mining and Metallurgy, Cracow during cutting of artificial samples of rock with and without cutting process assistance of a high-pressure water jet. During the research the temperature, pick edge wear, pressure and adjacent force and dustiness were measured under several selected mining parameters. The research used Rapid 85 shearer radial picks and the adjacent Alpine picks. The cutting with radial picks was assisted with a high-pressure water jet from the front and back whereas the adjacent picks cutting was assisted only from the front. For cutting with assistance of a high-pressure water jet the Saphintec type nozzles of d = 0.3; 0.55 and 0.8 mm diameter and water pressure of p = 1; 20; 40 and 60 MPa were used.

Organized and Sponsored by the Water Jet Technology Association.

1. INTRODUCTION

Process of coal and hard rock cutting faces the greater problems now, because of mining of lower seams in more difficult mining and geological conditions. It is connected with cutting of harder rocks in worse mining conditions like methane or coal dust explosive conditions caused by a scintillation of cutting instruments.

The coal and hard rock cutting assisted by the high-pressure water jet allows to extend a range of applications of mechanized machinery for rock cutting. Moreover through decreasing of pick edge temperature and watering it prevents from arising of scintillation, thus also gas and coal dust explosions.

Taking under consideration these remarques the attempt of definition of pick edge temperature influence upon its wear during the rock cutting has been elaborated. From the results of theoretical calculations the dependences enabling the pick edge temperature definition have been given for rock cutting and also the laboratory test results for an artificial rock sample cutting have been shown. During this tests dustiness was also measured.

Independent of this tests pressure and adjacent force measurements during the "dry" cutting and with the assistance of high-pressure water jet were made.

2. MEASUREMENT COURSE AND RESULTS.

2.1 Test Stand and Cutting Tools.

The tests have been carried out with dry rock cutting as well as in case of water jet cutting assistance. They were made on a testing stand for individual cutting tools at the Laboratory of the Department of Mining Machines and Waste Utilization Equipment, University of Mining and Matallurgy in Cracow. In Figure 1 there is a view of this stand.

These tests have been carried out on concrete samples made of mixture of cement and high-silica sand of strength of R_c = 26.5 MPa unixial compression. For the tests the concrete ring shape sample of external D_z = 1200 mm diameter and internal D_w = 500 mm diameter and height equal to h = 450 mm were used.

These tests were carried out with two, the most frequently used picks of longwall shearers and continuous miners with the RAPID 85 radial pick and the Alpine conic and rotary pick. During the tests beside the temperature and pick wear measurements the forces operating on pick during the cutting and dustiness have been recorded. For the radial picks the measurements were made during the "dry" cutting and with the assistance of high-pressure water jet in front of it and in back of pick position and with adjacent pick at "dry" cutting, only with a front assistance of jet water. In the case of front assistance a nozzle was in pick axis at a distance of about 50 mm and 2 mm before a cutting edge. In the case of back assistance of water jet the nozzle was placed at a distance of about 65 mm of pick point and the water jet was adjacent to the plane of shear to a distance of about 5 mm from a cutting edge. This picks with two gauges for temperature measurements are shown in Figure 2.

2.2 Theoretical Dependences on Pick Edge Wear and Temperature Description

In addition an attempt of description of the shearer pick edge wear and heat transfer in the edge by theoretical formulae was done. Because of lack of proved dependences for a definition of wear and temperature of shearer pick edges in mining the experiences from the field of metal machining were applied.

After a formula analysis of metal machining and substitution there data getting from rock cutting and carrying necessary transformations the theoretical dependences for a calculation of edge wear value and its temperature were obtained. Assuming a pick wear scheme as in Figure 3, the pick wear expressed by upper value of edge grinding from a VB plane of application can be recorded as following:

$$VB = \sqrt{\frac{(1 - tg\alpha \cdot tg\gamma) \cdot 2 \cdot A_p \cdot \mu \cdot P_d \cdot v \cdot t}{l_k \cdot tg\alpha}} \quad [\text{mm}] \qquad [1]$$

It allows to describe the pick edge wear in given conditions or tool operating time according to the allowed grinding value. Naturaly it is possible having earlier stabilization of cutting conditions, it means of pick clamp force constancy, cutting velocity and wear coefficient, and first of all edge temperature area, because it has a deciding influence upon its wear value.

However the temperature at arbitrary chosen edge point one can obtain using the following dependence:

$$T_{(R)} = \frac{\mu \cdot P_d \cdot v}{2 \cdot \pi \cdot \lambda \cdot R} \quad [^\circ\text{C}] \qquad [2]$$

The formula enables the pick edge temperature calculation during the rock cutting after μ and λ value definition. On the basis of present experiences one recommends an assuming for calculations $\mu = 0.15 \div 0.2$ and $\lambda = 2.15$ J / m·s·°C.

2.3 Pick Edge Temperature Measurement

The wear and pick edge temperature measurement was carried out in five series assigned as following: Prs - "dry" radial pick, Prw - front assistance, Prwt - back assistance, Sts - adjacent "dry" pick, Stw - front assistance. In every series a new pick was used.

The temperature measurement of cutting edge has been carried out with two gauges: PT resistant thermoelement and Ni - Cr - Ni thermocouple. These gauges were placed in special openings into pick [Figure 2]. The PT resistant thermoelements were placed directly in a carbide allowing a temperature measurement at a distance of about 16 mm from the cutting edge, but a Ni - Cr - Ni thermocouples were soldered on distance of about 4 mm from the edge and measured the temperature of this place. The measurement in two different points enables an approximate definition of real temperature distribution. Using the formula [2] and

substituting into it pick clamp force value and cutting value according to the measured values of those parameters during the tests, the theoretical values of temperature on edge have been defined. Having the temperature values theoretically calculated and measured by gauges the attempt of temperature evaluation near the edge for R = 1 mm was done.

Five series of measurements with different measured picks have been carried out. For cutting with assistance of high-pressure water jet the Saphintec type nozzle of d = 0.6 mm diameter was used and water pressure of p = 1; 20 and 40 MPa. The view of pick ready to temperature measurement was shown in Figure 4. The measurement was carried out till edge temperature constancy (at measured points). Chips were made at a constant cutting pitch, t_s = 10 mm and cutting velocity v = 2 m/s.

The results of measurements are shown in Table 1 and in Figure 5. An exemplary temperature transfer measured to a distance of 4 mm from the cutting edge for a radial pick has been shown in Figure 6.

It was found that there was a sharp temperature decrease with application of high-pressure water jet assistance. The decrease was growing up with increasing of the jet pressure. The most important decrease of temperature was gained at p = 40 MPa pressure, the best effects of cutting assistance were obtained in a case of front one against pick. For the radial pick even at the water pressure of p = 1 MPa the temperature was lowered nearly three times.

In Table 1 the distribution of temperature into pick edge at a distance 16, 4 and 1 mm from cutting edge was shown. Besides the temperature calculated by formula [2] as well as values measured in course of measurements were given. Comparing given temperature values one can notice very close temperature values calculated according to the theoretical formula and those measured for radial pick cutting "on dry."

In theoretical distribution the temperature taken by "chips" and put into air was taken under consideration. It can assume that admitted theoretical distribution was near to real one.

Comparing the temperature at the cutting edge for R = 1 mm and cutting velocity v =2 m/s you can see that an introduction of high-pressure water jet assisting the cutting of p = 20 Mpa pressure allows to diminish the edge point temperature from about 3200 °C to temperature nearly under 1000 °C for radial pick. For the adjacent pick the edge temperature from 2300 °C lowered below 1000 °C.

It seams that in real conditions the temperature close to cutting edge will be lower because of emission of some quantily of heat by radiation and scintilation. This lowered temperature near cutting edge has a great influence not only for sparking arising after the pick (or even for its uninitiation) but first of all on pick edge wear.

2.4 Pick Edge Wear Measurement

The pick edge wear measurement during cutting was made by the drawing outlines of profiles of edges under microscope at 20 times magnification before and after cutting finishing.

According to the getting profiles the rate of pick edge grinding was assigned from the VB plane of shear (or D grinding diameter for adjacent picks) and h_n edge shortening. The cutting was assisted by high-pressure water jet of p = 20 MPa pressure.

The exemplery results which been obtained were presented in Figure 7. The profile of new edge was assigned by full line and wear by break line. The measurement were carried out at comparable cutting like depth, velocity and a way of cutting.

In Table 2 all cutting parameters are given and the measurement results from the obtained profiles like: VB rate of edge grinding (or D diameter of grinding for adjacent pick), h_n edge shortening and V volume of grinding materials. By a measurement of P_s tangent force it has also been assigned the A_p real grinding output, so a relationship between grinded materials to accomplished work.

Comparing obtained results (Figure 8) one can see that pick wear applying high-pressure water jet front assistance for the radial pick as well as for adjacent pick lowered about 6.5 times. The back assistance of cutting of radial pick lowered its wear about 2.5 times. The A_p coefficient calculated on the test basis has also decreased for radial pick of about 6 and 2.5 times and for the adjacent pick according about 4 times.

2.5 Dust Concentration Measurement

For a dust concentration measurement during rock cutting without and with a high-pressure water jet assistance, an aerosol filtration suction apparatus type Barbara-3 was used. The direct method was used for dust measurement.The dustfall, i.e dust amount which has accumulated on surface in time period, is measured using measurement plates.

The dust concentration point was situated at a distance of about 1.2 m from cutting pick near the center of dust stream. For cutting only with front assistance of high-pressure water jet nozzle of d = 0.30; 0.55 and 0.80 mm diameter and water pressure of p = 1; 5; 10 and 20 MPa were used.

The results of measurements are shown in Table 3 and in Figure 9. The best results for both picks were obtained using nozzle of d = 0.80 mm diameter and water jet pressure of p = 20 MPa. The dustiness, in comparision to "dry" cutting, was reduced for radial pick of about 96.6% and for adjacent pick of about 92.8%. The satisfactory results (dust reduction of about 80.0%) were obtained for radial pick yet with nozzle diameter of d = 0.55 m and water jet pressure of p = 5 MPa and for adjacent pick with the same nozzle diameter and water jet pressure of p = 10 MPa. For small nozzle diameter and low water jet pressure the obtained results were not satisfactory (dust reduction of 13 ÷ 38%).

2.6 Force Measurement

The force measurement of the cutting pick was carried out on the special tensor head, where the independent pressure force P_d and tangent force P_s were measured.

For cutting with assistance of high-pressure water jet the nozzle of d = 0.30; 0.55 and 0.80 mm diameter and water jet pressure of p = 20; 40 and 60 MPa were used. The measurements were carried out with three different cutting depths g: for radial pick of g = 4; 7 and 10 mm and for adjacent pick of g = 6; 9 and 12 mm.

The exemplary force measurement courses and results of measurements for both picks have been shown in Figure 10 ÷ 15.

The best results were obtained for the greatest nozzle diameters and water jet pressure. The following values of force decreasing were noted: for radial picks for all cutting depths and for water jet pressure of p = 60 MPa was noted for nozzle diameter of d = 0.30 mm decrease of tangent force P_s of 7% and pressure force P_d of 3% and for d = 0.80 mm - P_s force of 15% and P_d force of 9%.

For water jet pressure of p = 20 MPa and all nozzle diameters and cutting depth of g = 7 and 10 mm was observed the increase P_s force of 1.5% for nozzle diameter of d = 0.80 mm and 3.5% for d = 0.30 mm and P_d force of 0.2% for d = 0.80 mm and 3% for d = 0.30 mm. For cutting depth of g = 4 mm was not noted the greater change of P_s and P_d force value.

For adjacent picks the decrease of bath forces for all cutting parameters was obtained. The best results were noted for cutting depth of g = 6 mm. For nozzle diameter of d = 0.80 mm, water jet pressure of p = 60 MPa the reduction of force value: P_s force of 23% and P_d force of 26%. For cutting depth of g = 12 mm the decrease of P_s force of 19.5% and P_d force of 25.7% was obtained. For nozzle diameter of d = 0.30 mm the decrease was for P_s force of 10% and for P_d force of 16%. For water jet pressure of p = 20 MPa was obtained a very little force reduction of about 0.5% for both forces.

3. CONCLUSIONS

The presented formulae for wear calculations and shearer pick edge temperature definition have been proved in the laboratory tests. Having the coal or rock cutting parameters one can assign the pick edge temperature as well as forseen wear or life of picks.

An application of water assistance can be of more importance like a factor lowering the pick edge temperature and wear and increasing safety of work than like factor causing an increasing of rock cutting effectiveness or lowering the forces operating on pick during the cutting.

The water assistance application diminishing the pick edge temperature has a deciding influence upon their wear. This application with water jet of p = 20 MPa pressure allowed to decrease the pick edge wear nearly 6.5 times for both picks at the front assistance and 2.5 times at the back assistance with radial pick.

It seams that the presented formulae and laboratory test results would be helpfull for construction of new generation of cutting elements of longwall shearers and continuous miners. The application of high-pressure water jet assistance allows for diminishing of pick wear in

greater rate thus for the increasing of their durability so for decreasing of costs of their purchase.

At the same time an introduction of water jets into cutting pick areas causes the temperature lowering of edges, dust reduction and enlarges the safety of work of cutting machinery provided with high-pressure water jet assistance into drums and heads with picks.

4. REFERENCES

Betanelli, A. J., "Prochnost i nadezhnost rezushchego instrumenta," Izdatelstvo "*Sobchota sakartvelo,*" Tbilisi, 1973 (in Russian).

Dmochowski, J., "Podstawy obróbki skrawaniem," PWN, Warszawa, 1978 (in Polish).

Kaczmarek, J., "Podstawy obróbki wiórowej, sciernej i erozyjnej," WNT, Warszawa, 1970 (in Polish).

Klich, A., Kotwica K., and Ptak J., "Influence of temperature and cutting conditions upon shearer pick edge wear according to the laboratory test basis," *Tribologia*, Warszawa, 4/1994.

"Poradnik spawalniczy," WNT, Warszawa, 1970 (in Polish).

"Cutting elements of mining machines based on non-conventional mining technologies - Part 2," Report of research work Dept. of Mining Machines, Univ. Min. and Metall., Kraków, 1993 (unpublished, in Polish).

5. NOMENCLATURE

A_p - real capacity of grinding, [mm^3/J];
d - nozzle diameter, [mm];
D_w - internal concrete sample diameter, [mm];
D_z - external concrete sample diameter, [mm];
g - cutting depth, [mm];
h - concrete sample height, [mm];
h_n - edge shortening, [mm];
l_k - edge cutting breadth, [mm];
λ - heat conduction coefficent, [J/m·s·°C];
μ - coefficent of friction of pick against rock;
p - water jet pressure, [MPa];
P_d - pressure force, [N];
P_s - tangent force, [N];
R - distance of tested point from heat source, [mm];
R_c - compressive rock strenght, [MPa];
t - cutting time, [s];
t_s - cutting pitch, [mm];
T - edge temperature, [°C];
v - cutting velocity, [m/s];
V - volume of grinding materials, [m^3].

Table 1. Results of temperature measurements

	Prt 1	Prs 1	Prw 1	Prw 2	Prw 3	Prwt1	Prwt2	Prwt3	Sts 1	Stw 1	Stw 2	Stw 3
	1	2	3	4	5	6	7	8	9	10	11	12
p [MPa]	0	0	1	20	40	1	20	40	0	1	20	40
g [mm]	9.5	9.5	10	10	9.5	10.8	11.5	11.8	10.5	9.4	10	9.5
v [m/s]	2.04	2.04	2.06	2.01	1.98	2.08	2.03	1.98	2.08	2.04	2.01	1.98
T_{R16} [°C]	241	207	73	65	62	113	90	69	191	109	91	86
T_{R4} [°C]	963	808	276	239	227	428	337	257	583	339	279	258
T_{R1} [°C]	3855	3232	1104	956	907	1710	1347	1027	2330	1355	1105	1033

Table 2. Results of pick edge wear measurement

	g [mm]	v [m/s]	P_s [kN]	L [m]	VB/D [mm]	h_n [mm]	V [mm^3]	Ap $*10^{-8}$ [mm^3/J]
	1	2	3	4	5	6	7	8
Prs	6.2	2.04	2012	1238.4	4.78	3.45	64.32	2449.7
Prw	5.8	2.01	2.04	1208.4	4.59	0.98	10.13	411.2
Prwt	5.9	2.07	2.11	1256.1	3.74	2.01	25.41	962.9
Sts	6.9	1.99	3.48	1237.8	2.95	0.52	1.19	27.5
Stw	6.1	2.02	2.33	1262.7	1.51	0.31	0.19	6.3

Table 3. Results of dust measurement

d [mm]	p [MPa]	Radial pick RAPID-85		Adjacent pick Alpine	
		Dustiness [mg/m^3]	Dust reduction %	Dustiness [mg/m^3]	Dust reduction %
0	**0**	426.6	0.00	383.3	0.0
0.30	**1**	309.6	27.43	332.7	13.2
	5	213.7	49.91	238.3	37.83
	10	118.6	72.20	151.4	60.50
	20	76.4	82.09	93.3	75.66
0.55	**1**	193.2	54.71	240.7	37.20
	5	53.3	87.51	116.6	69.58
	10	36.8	91.37	73.8	80.75
	20	24.1	94.35	36.4	90.50
0.80	**1**	154.7	63.74	197.1	48.58
	5	40.1	90.60	84.2	78.03
	10	26.6	93.76	58.9	84.63
	20	14.3	96.65	27.4	95.85

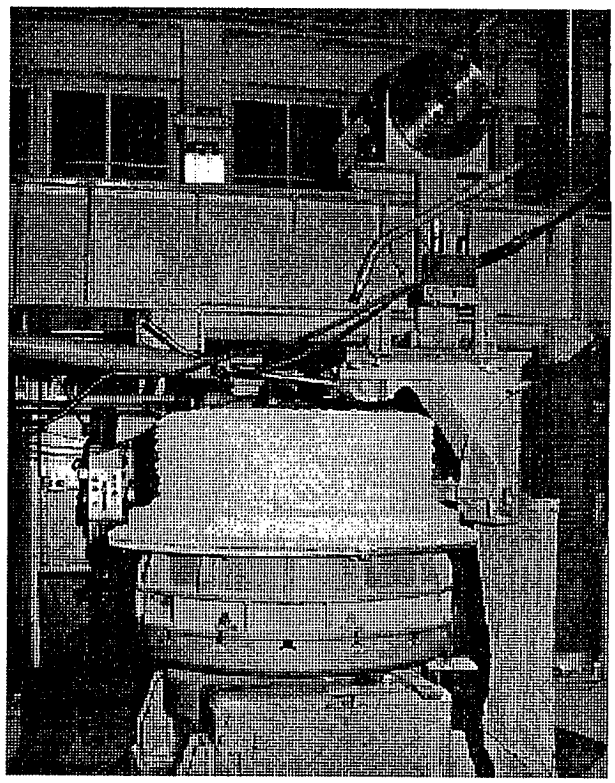

Fig. 1. Testing stand for individual cutting tolls

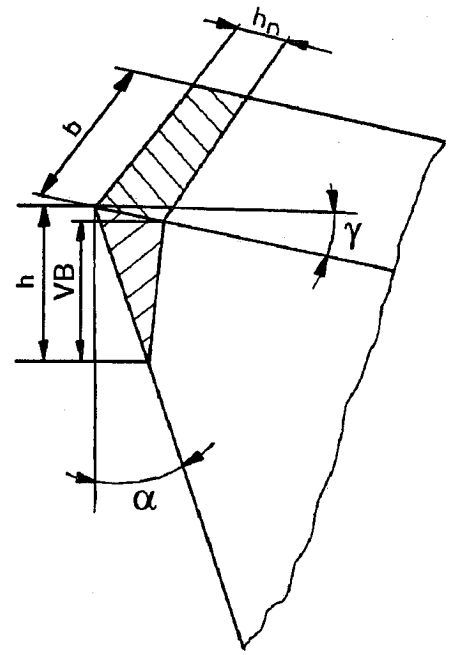

Fig. 2. Scheme of pick wear

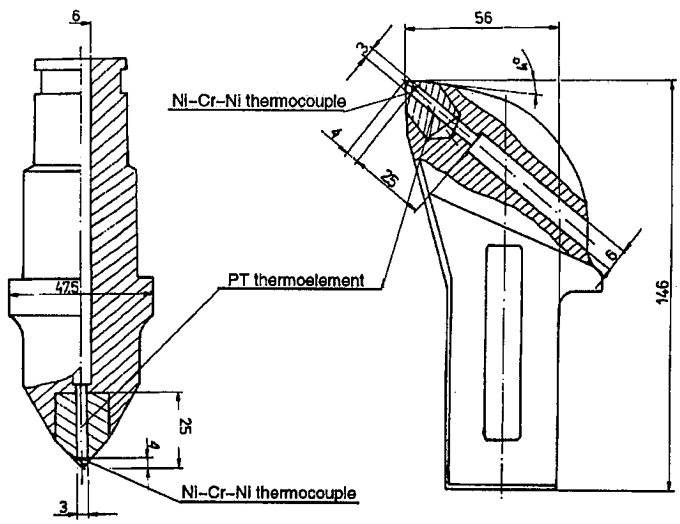

Fig. 2. Scheme of placement of temperature gauge into Alpine and Rapid-85 picks

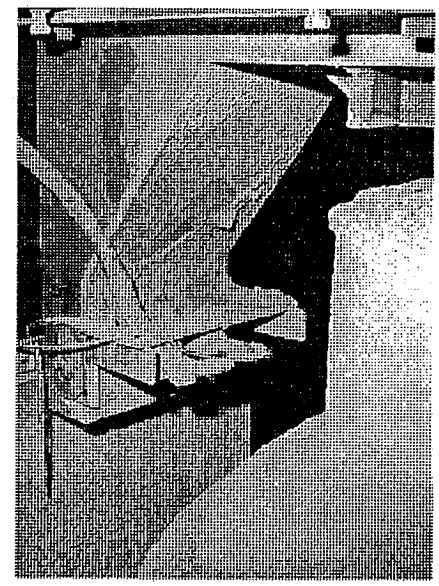

Fig. 4. Pick holder with radial pick and nozzle

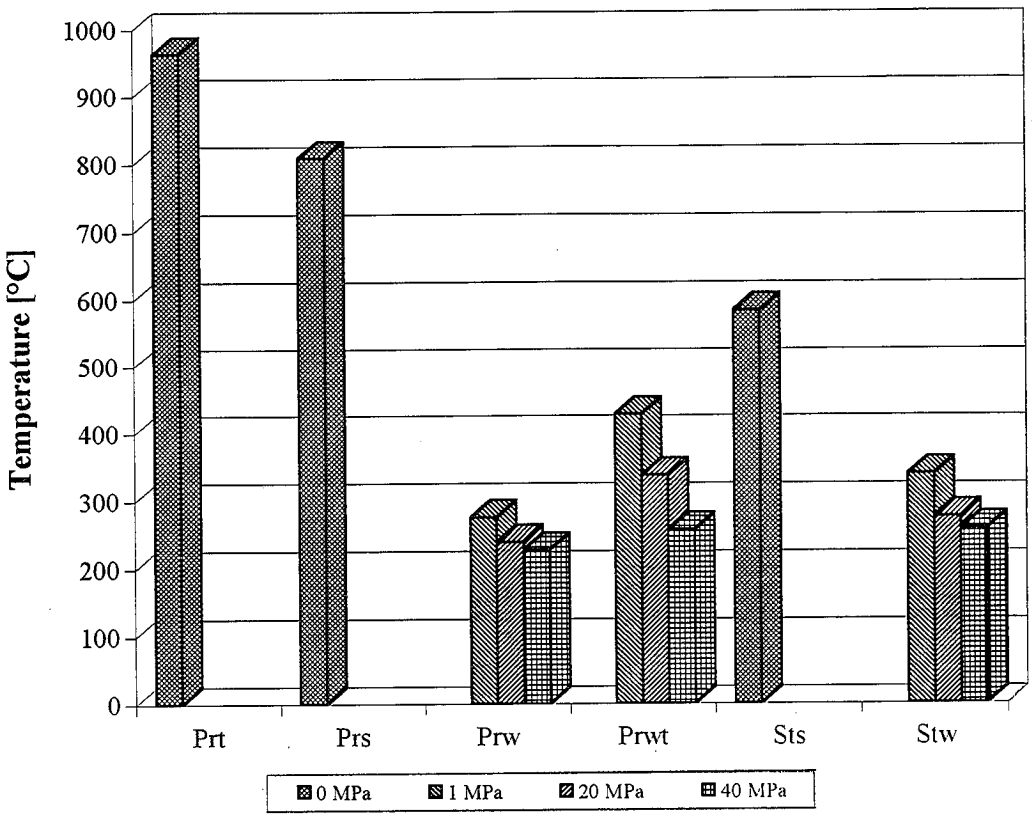

Fig. 5. The temperature of pick edge at v = 2 m/s velocity

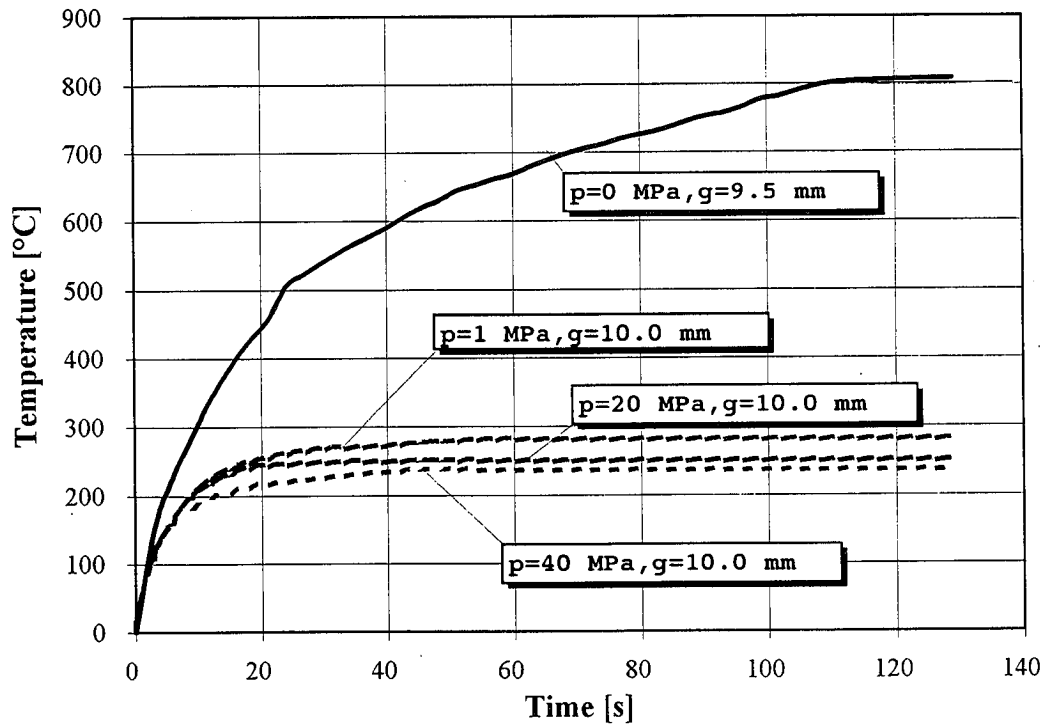

Fig. 6. The temperature transfer measured at a distance of 4 mm from the cutting edge during "on dry" cutting and with front assistance with high-pressure water jet

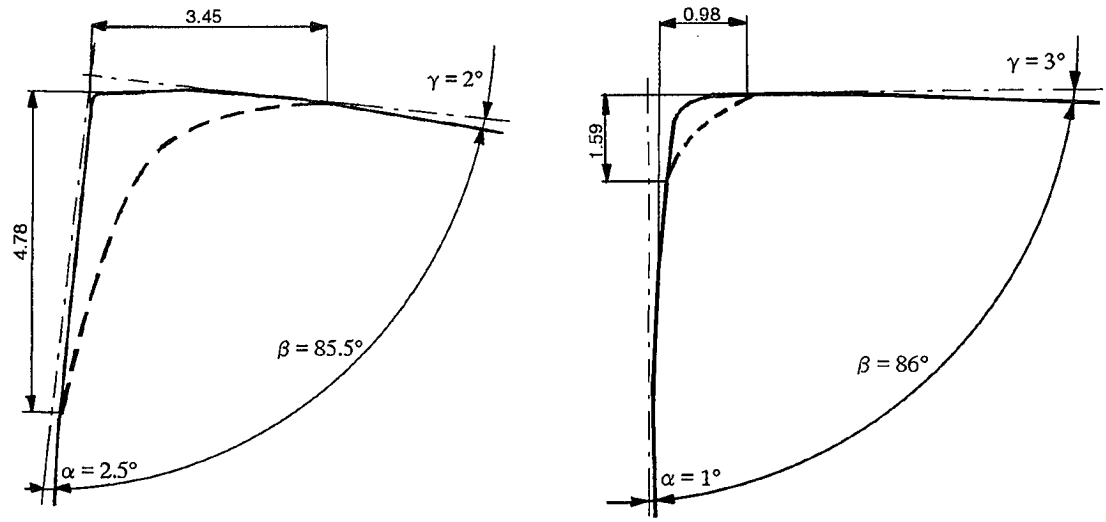

Fig. 7. Scheme of pick edge wear of Rapid-85 pick during „on dry" cutting (left) and with front assistance and high-pressure water jet (right)

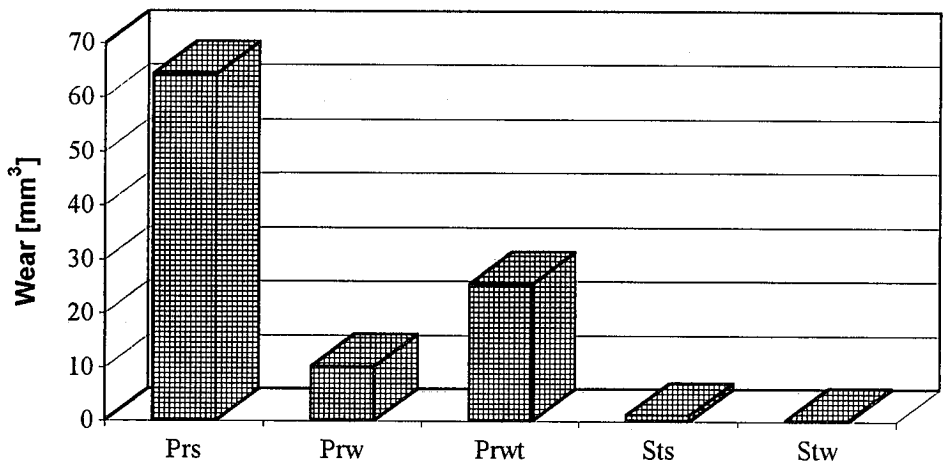

Fig. 8. The wear of pick edge at v = 2 m/s velocity and p = 20 MPa pressure

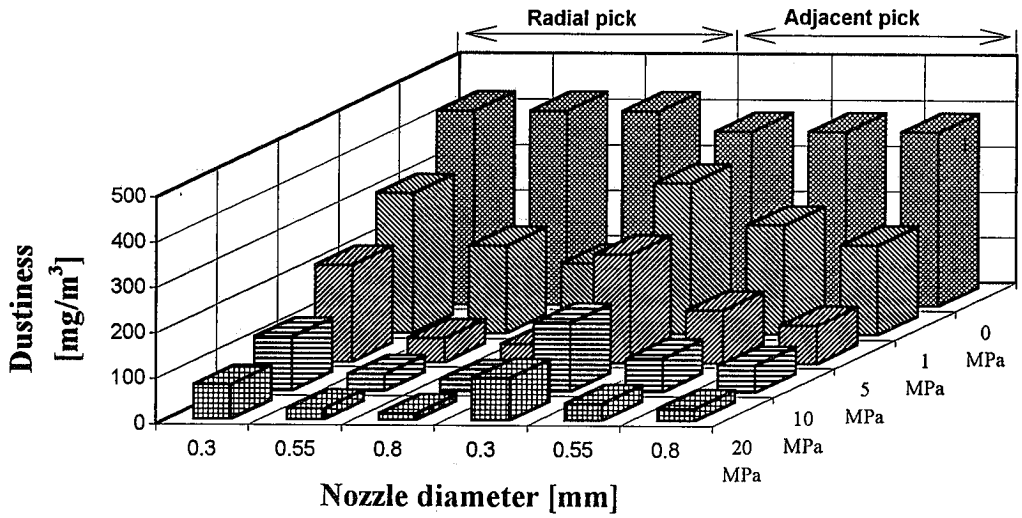

Fig. 9. The dustiness during rock cutting in dependence of water jet pressure and nozzle diameter

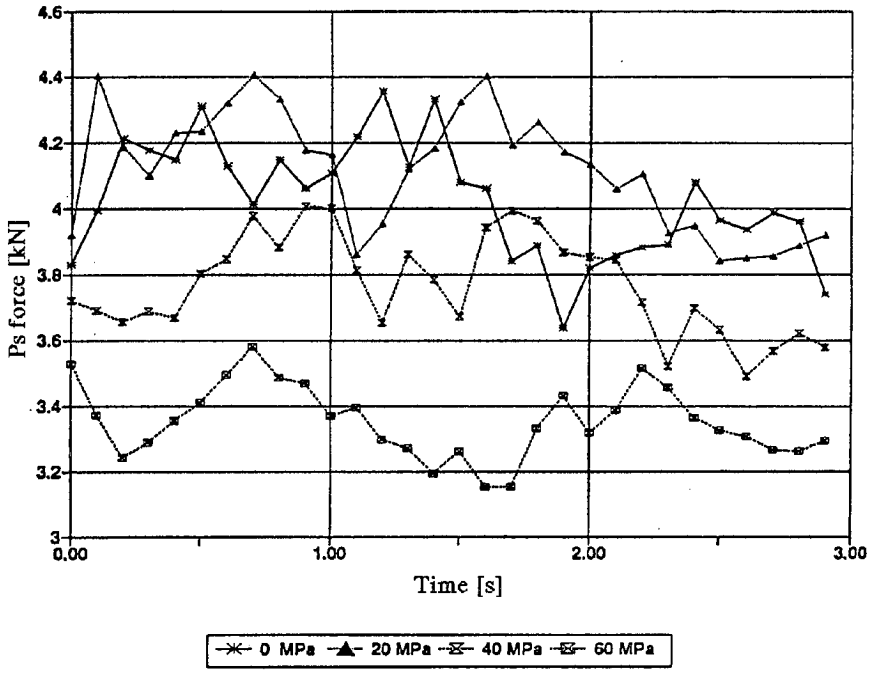

Fig. 10. The course of Ps force during the rock cutting with Rapid-85 pick with cutting depth of g =g 10 mm and nozzle diameter of d = 0.80 mm

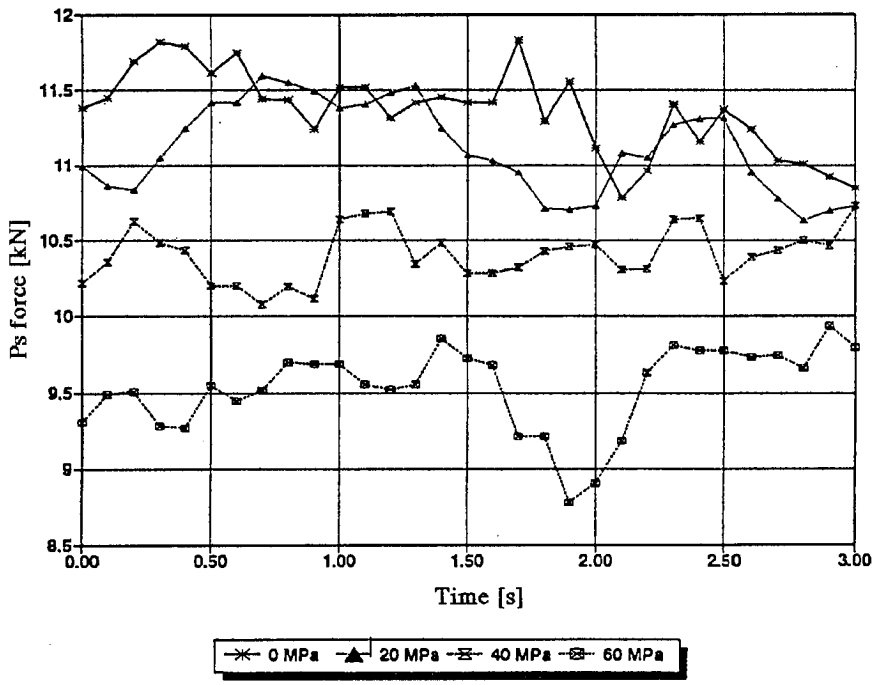

Fig. 11. The course of Ps force during thr rock cutting with Alpine pick with cutting depth of g = 12 mm and nozzle diameter of d = 0.55 mm

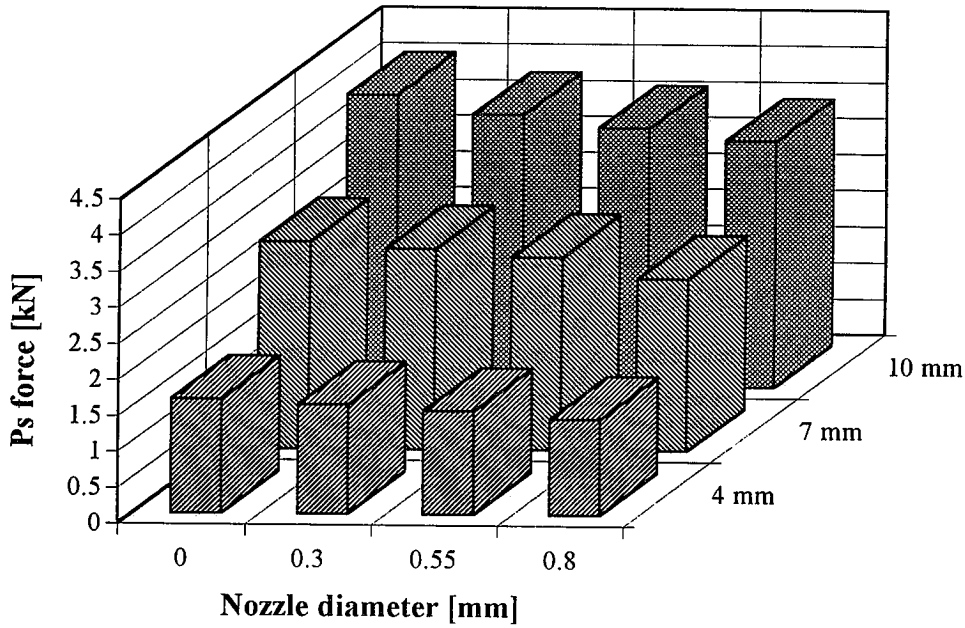

Fig. 12. The Ps force during rock cutting with Rapid-85 pick with water jet pressure of p = 60 MPa in dependence of rock cutting and nozzle diameter

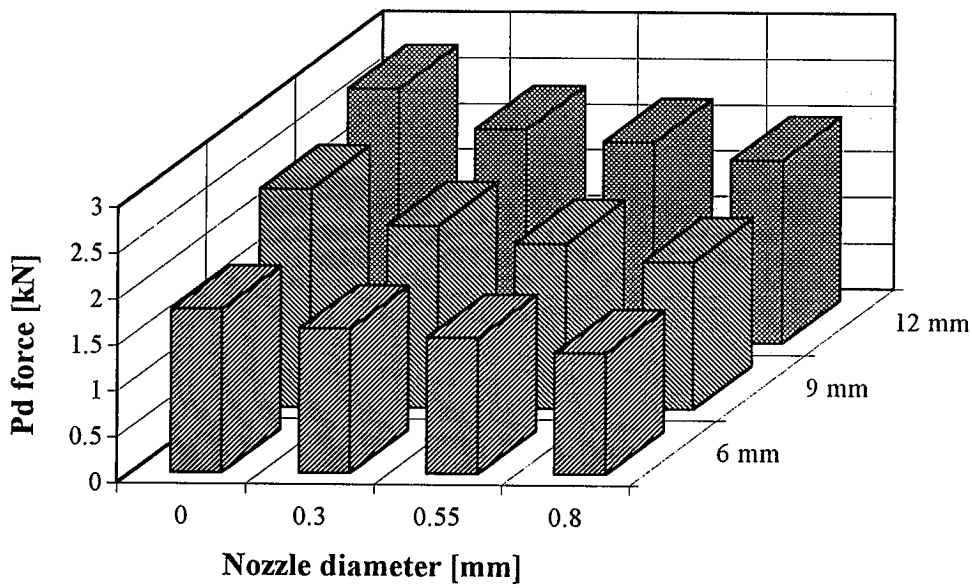

Fig. 13. The Pd force during rock cutting with Alpine pick with water jet pressure of p = 60 MPa in dependence of rock cutting and nozzle diameter

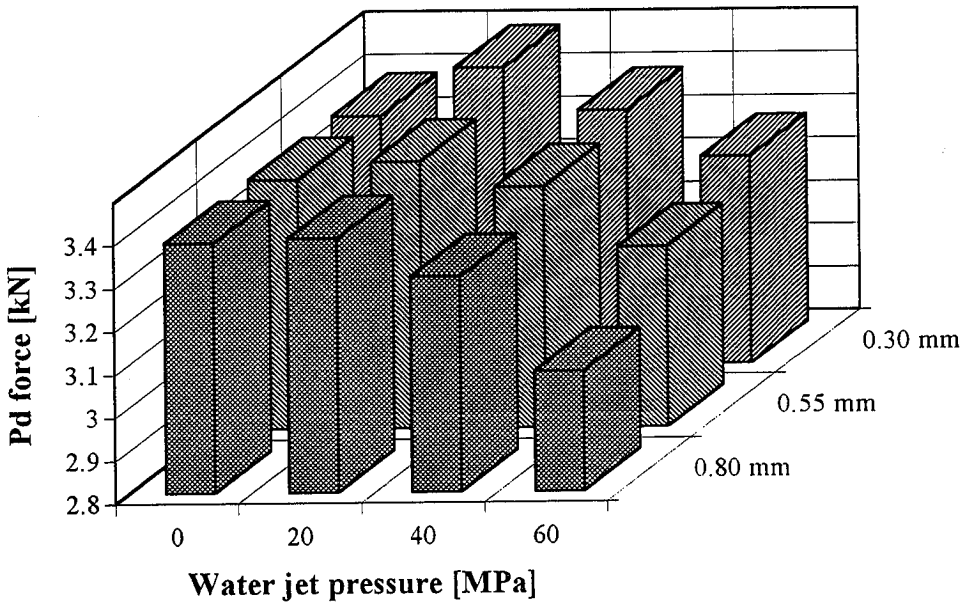

Fig. 14. The Pd force during rock cutting with Rapid-85 pick with rock cutting of g = 10 mm in dependence of water jet pressure and nozzle diameter

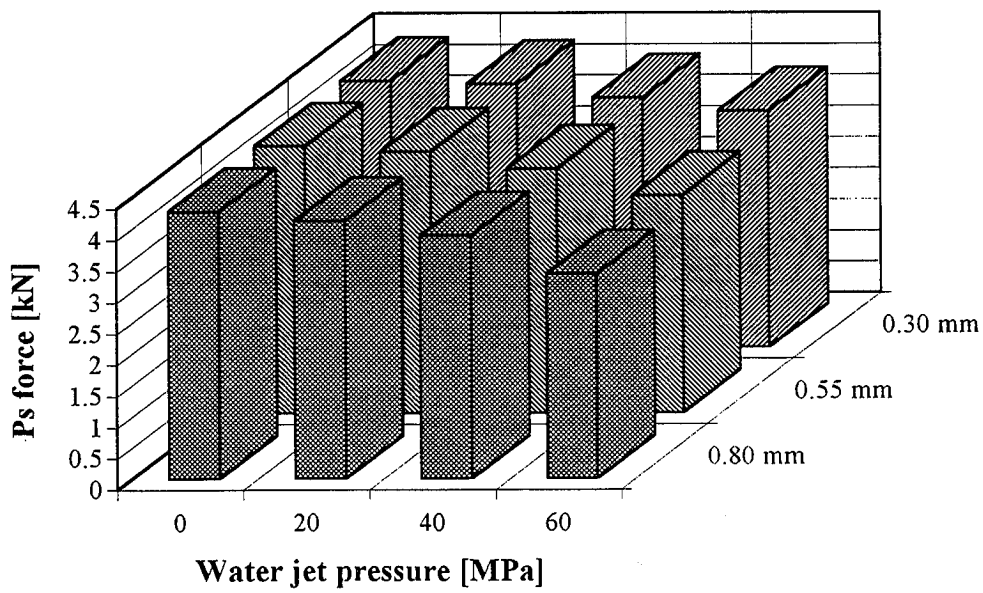

Fig. 15. The Pd force during rock cutting with Alpine pick with rock cutting of g = 6 mm in dependence of water jet pressure and nozzle diameter

8th American Water Jet Conference
August 26-29, 1995: Houston, Texas

Paper 60

A COMPARATIVE STUDY OF CONCRETE BEHAVIOR DURING COMPRESSION TESTING AND WATER JET EROSION

A. W. Momber[1]
WOMA Apparatebau GmbH
Duisburg, Germany

R. Kovacevic
University of Kentucky
Lexington, Kentucky, USA

D. Pfeiffer[2], R. Schünemann[2]
Chemnitz University of Technology
Chemnitz, Germany

ABSTRACT

The paper contains investigations of debris particles from five different concrete mixtures generated during the compression testing and during the erosive wear by high velocity water jets. The energy absorbed during the compressive test of the samples was calculated by estimating and integrating the stress-strain curve up to the ultimate strength for all materials. The particles generated during cylinder compressive tests as well as the particles from water jet erosion tests were collected, dried and analyzed by sieve experiments. Based on the sieve analysis, average grain diameters of the particle samples were estimated. Using simple comminution relations, the authors calculated the specific crack energy of every sample. From the erosion tests, material removal and erosion efficiency were estimated. It is shown that all estimated parameters exhibit a relationship to the energy absorbed during the compressive test. It is further found that a fairly linear relation exists between the average size of the particles generated during the compressive test and the average size of the erosion debris. Observations of the fracture areas of the compressed samples as well as of the water jet erosion sites have shown that the phenomenology of failure for both events is similar. In tendency, the probability of transgranular crack growth during compressive fracture as well as during the water jet erosion process increases with the energy absorption capability of the material. It is concluded that these relations are the result of different paths of fracture propagation through the materials during the generation of a mickrocrack network in compressive testing as well as in water jet erosion.

---

[1] Feodor-Lynen Scholar of the Alexander von Humboldt Foundation, Bonn, Germany, at the Center for Robotics and Manufacturing Systems, University of Kentucky, Lexington, U.S.A.

[2] Visiting students at the Center for Robotics and Manufacturing systems, University of Kentucky.

Organized and Sponsored by the Water Jet Technology Association.

1. INTRODUCTION

The erosion capability of water flowing with very high speed generates serious damage in hydraulic structures, such as concrete covered pipes and channels. However, the material removal capability of high speed water jets can be used successfully to machine concrete. Water jet technology is applied for cleaning, roughening, removal, cutting and fracturing of concrete (Fig. 1). An extensive application review is given by Momber (1993). A possible model for the destruction of concrete by plain high speed water jets is developed in a series of publications (Momber 1992, 1992a, Momber and Kovacevic 1994, 1994a, Momber and Louis 1994, Momber et al., 1994). In these papers, the influences of interfaces, cracks, and inclusions on the failure of concrete materials due to fast flowing water at velocities of several hundred meters per second were investigated. As suggested, the predominant mechanisms of the concrete failure are propagation and intersection of pre-existing microcracks. It was found that the destruction process due to the water flow is introduced in the interface between the matrix and aggregate grains which is characterized by a high degree of porosity and pre-existing microcracks. Inside a crack the water is pressurized, which leads to forces acting on the crack wall surfaces. If the generated stresses exceed critical material values, for example the critical stress intensity factor, the crack starts to grow. The crack growth is controlled by the interaction between crack and aggregate grains. It was shown that inclusions in the material may act as crack arrestors and energy dissipators. The intersection of several single cracks leads to macroscopical material removal. This leads to the generation of fine grained erosion debris. In advanced versions of this phenomenological model a computer-based simulation of the fluid dynamics inside a microcrack (Momber et al., 1994) and a fracture mechanics model for the characterization of the erosion process (Momber and Kovacevic 1995) are presented. The main conclusion from these investigations is that the erosive wear of concrete and similar semi-brittle, multiphase materials, such as, mortars, rocks, and minerals, is a fracture mechanics process which involves the generation, propagation and intersection of cracks. This idea is supported by Werner (1991) who found a good relation between the fracture toughness of concrete and the resistance against water jet erosion.

The mechanical behavior of concrete is usually evaluated by a standardized compression test. It was shown through extensive experimentation by Werner (1991) that neither the compressive strength nor the tensile bending strength can give information about the water jet erosion resistance of concretes. However the compressive strength as an integral parameter obtained on relatively large specimens is also a result of microfracture processes taking place during the test. Every concrete mixture may be characterized by a specific fracture behavior. These mickrocracking processes are illustrated by the stress-strain curve as well as by the generated fracture debris of a concrete material. A typical stress-strain curve for concrete in compression is given in Fig. 2. It is characterized by a non-linear behavior, especially at high stress levels. This shape is discussed in detail by Glucklich (1965). It is well known, that toughening mechanisms, like crack shielding due to microcracks, crack deflection and crack arresting on inclusions, and grain bridging, contribute to this characteristical behavior (Shah and Ouyang, 1993). Several of these mechanisms were observed not only during conventional fracture, but also during the water jet erosion of concrete (Momber and Kovacevic, 1994), which was an indication that compressive failure and water jet erosion

failure of concrete may have a common source. The area under the stress-strain curve is assumed to represent the energy absorption capability of a certain material volume. In the engineering literature this parameter is often termed strain energy or absorbed fracture energy. For concrete as investigated here, the term absorbed fracture energy is used.

In the past, several attempts have been made to relate the stress-strain functions of materials to their resistance against erosive loading. In a model for the solid particle erosion of materials, Bitter (1963) introduced a material constant which describes the plastic-elastic behavior of materials. This parameter is identical to the area occupied by the stress-strain curve. He wanted to illustrate the fact that materials with comparable strength properties show very different erosion resistances. In his model the material removal rate is inversely proportional to the energy absorption capacity. Thiruvengadam (1967) developed a concept for the erosion strength of metals in the case of water drop and cavitation erosion. He also used the energy absorbing capacity of the materials, which can be expressed by the area under the stress strain curve and found a direct relation between this parameter and the volume loss due to cavitation erosion. A very similar approach was made by Kriegel (1968). He related the material resistance against solid particle erosion to the energy absorption of the materials during the tensile testing. Later, Ocepek (1969) discussed a comminution parameter that could describe the resistance against impact fragmentation of minerals, which was based on the ratio between the elastic deformation energy and the total absorbed energy. Medeot (1989) suggested using the energy absorbed during the compressive testing of concrete to define the resistance against plain water jets. This idea was developed by Momber (1992, 1992a) who discussed the efficiency of the water jet cutting process based on an efficiency parameter which is related to the specific energy absorption. For abrasive water jet cutting, Matsui et al. (1991) used simplified stress-strain curves for brittle and ductile materials, respectively, to calculate the depth of cut. Their model failed for rocks which indicates that a simple linear (ideal) brittle behavior does not characterize the behavior of this material group (pre-cracked materials) in the case of abrasive water jet attack.

The fracture debris generated during a compression test can be divided into two groups. One can observe several large pieces with typically conical shapes (Fig 3), and a sample of fine grained material. The properties of these debris, such as shape, size and distribution, should be characteristic for every material or for every fracture process, respectively.

It is assumed in this paper that an analysis of the shape of the compression stress-strain curve as well as of the geometrical parameters of the generated debris particles can give information about the water jet erosion resistance of the investigated materials.

2. MATERIALS, EXPERIMENTAL SETUP AND ANALYSIS METHODS

2.1 Materials

To analyze the behavior of the materials, five different concrete mixtures were designed and investigated. Quartzite grains of different fineness were used as aggregates. Detailed information on the mixtures is given in Table 1. The aggregates were mixed with the

binding agent (cement) in a ratio 2.24:1. The water-cement ratio was varied according to Table 1. After mixing, the compositions were cured and hardened for 28 days under water. After hardening, the mechanical properties of the mixtures were estimated on three cylindrical specimens of every mixture. The specimen dimensions were 30.48 cm in length and 15.24 cm in diameter. The compressive strength was estimated to the ASTM standard C 39. The modulus of elasticity was measured as the static chord modulus according to the ASTM Standard C 469. The stress-strain curve of every mixture was estimated by loading and unloading the specimen 11-times. The results of these measurements are given in Table 1.

2.2 Testing Equipment and Performance

Two cylinders of every mixture were used for the compression fragmentation. The dimensions were 14 cm in height and 5 cm in diameter. These cylinders were subjected to a compressive load in a standardized compression testing unit. The cores were covered by a plastic bag for collecting the fracture debris (see Fig. 4). The high speed water flow attack was simulated by a water jet impact with a velocity of 700 m/s. The high velocity water jet unit consists of a high pressure intensifier, hose system, nozzle holder, nozzle, and x-y-z-positioning table. The experimental conditions are listed in Table 2. The specimens are located inside a closed Plexiglas cell, so that it was possible to collect the removed material. The specimen size for the erosion tests were 15.24 cm in height and 15.24 cm in diameter. Five parallel cuts were generated in each specimen to remove the material. The distance between the cuts was 10 mm. The removed material was collected and dried for 24 hours at room temperature. After that, all grain sample were weighed. The grain size distribution was estimated by sieve analysis using a conventional sieve shaker. Additionally, selected samples of the fractured or eroded material were observed by optical microscopy.

2.3 Analysis Methods

It is assumed in this study that the compressive stress-strain function of a concrete material as shown in Fig. 2 can be approximated by a parabolic equation

$$\sigma(\varepsilon) = A \cdot (\varepsilon - \varepsilon_{cr})^2 + \sigma_C . \tag{1}$$

The energy absorbed during the compression test is simply given by the area under the stress-strain curve, which yields

$$E_{abs} = \int_0^{\varepsilon_{cr}} \sigma(\varepsilon) d\varepsilon . \tag{2}$$

Based on the results of the sieve analyses the specific surfaces and the average grain diameters of the particle samples were estimated. The specific surface was calculated according to Schubert (1988) by

$$S_{sp} = \frac{6}{\Psi} \cdot \frac{\int_{d_u}^{d_o} d^2 f(d_p) dd_p}{\int_{d_u}^{d_o} d^3 f(d_p) dd_p} . \tag{3}$$

The average particle diameter was estimated using

$$d_{av} = \frac{6 \cdot V_M}{\rho_M \cdot S_{sp}}. \tag{4}$$

For further evaluation, the results of Eq. (3) were used to calculate the specific crack lengths using Eq. (5) given by Bond (1964).

$$l_{cr} = \sqrt{\tfrac{1}{2} \cdot S_{sp}} \tag{5}$$

It is possible to relate the specific crack length given by Eq. (5) to the absorbed fracture energy as given in Eq. (2) to calculate the specific crack energy which is the energy required to create a crack network with a given length in the compression specimen. This energy is

$$E_{cr,compression} = \frac{E_{abs}^{dyn}}{l_{cr}}. \tag{6}$$

For the water jet erosion process this parameter can be estimated using Eq. (7).

$$E_{cr,erosion} = \frac{E_W}{l_{cr} \cdot V_M} \tag{7}$$

The results of Eqs. (3) to (7) are the basis for the evaluation of the investigated wear particle samples.

3. EXPERIMENTAL RESULTS AND DISCUSSION

3.1 Energy Absorption and Debris Analysis from Compression Testing

Fig. 5 shows the estimated stress-strain curves of the investigated materials. The parameters of the parabolic regressions are listed in Table 3. The absorbed energy per unit volume was calculated using Eq. (5). The range of the estimated values is between 1.5 MJ/m^3 and 47.6 MJ/m^3, which is of the same order of magnitude as the values published by Medeot (1989) and Momber (1992). The compression test for concrete assumes the condition of pure, uniaxial compression. This is not really true, because of the friction between the ends of the specimens and the plates of the testing unit. Thus, through friction, the plates act to restrain the lateral expansion of the ends of the specimens and introduce a lateral confining pressure (which also introduces shear stress) near the specimen end. The manifestation of this lateral confining pressure is often the appearance of relatively undamaged cones of concrete in samples loaded to failure as shown in Fig. 3. The somewhat different splitting failure mode shown in Fig. 3, too, can be assumed to be a result of secondary tensile stresses. Interestingly, both types of failure are observed during the compression testing. Fig. 6 shows fragments from mixtures #1 and #5, respectively. It is clearly seen that both the mixtures exhibit different failure behavior. Whereas concrete #1 is characterized by the cone-type failure, mixture #5 tends to the splitting mode. Also, mixtures #1 and #2 own cones with base areas identical to the base area of the used cylinder. All the other mixtures show this

geometry as well as cones with base areas smaller than the cylinder base area. It was also very significant that the number of broken aggregates on the surface of these cones depends on the concrete mixture. It is about zero for mixture # 1 and about 100 % for mixture # 5. Beneath these cones a large number of small fracture debris is generated during the compression testing. Sieve analyses of these small fracture debris were used to calculate the average grain diameters and the specific crack lengths of the removed particles.

The results of these calculations are plotted in Fig. 7. It is seen that the energy required to generate a crack network with a given length increases linearly with the absorbed fracture energy. This result is not unexpected and can be used to relate the energy absorption capability of the materials to the microcracking processes during the compression testing. The average debris diameter increases linearly, too, with increasing energy absorption. The average diameters of the particles are between d_{av}=2.3 mm and d_{av}= 4.8 mm. An interesting result is the fact that the differences in the absorbed energies during the compression test are not caused by the different specific crack lengths (they show only a slight decrease with increasing energy absorption), but instead by the path of the cracks. Whereas the cracks run preferably through the interface between the cement matrix and the aggregate grains in samples #1 and #2, their path leads them through the aggregate grains in samples #4 and #5, generating transgranular fracture. This process explains the increase in the specific crack energy with higher absorbed fracture energy. The causes may be the coarser aggregate mixture as well as the higher strength of the matrix of the samples with the higher energy absorbing capacity. It was observed in concrete testing that the work of fracture increases with increasing aggregate size (Wittmann et al., 1988). It was also found that the probability of transgranular fracture increases with increasing cement matrix strength (Reinhardt 1982). Because of the higher specific surface energy of the aggregate grain material which is more than two orders of magnitude higher than those of the aggregate-matrix interface, more energy is absorbed during the fracture at comparable crack lengths.

3.2 Energy Absorption and Debris Analysis from Erosion Testing

Fig. 8 exhibits two samples of the grains removed by water jet erosion. Fig. 9 shows the estimated average wear particle diameters as well as the calculated specific crack energies. The diameter tends to increase linearly with higher values of the absorbed fracture energy. The particle sizes vary between d_{av}=197 μm and d_{av}=415 μm. They are plotted against the average debris diameter from the compression test in Fig. 10. There is a general linear trend between both parameters indicating some analogous failure processes. The specific crack lengths, calculated using Eq. (5), are between l_{cr}=8.5 cm/cm^3 and l_{cr}=12.3 cm/cm^3. As a comparison, a value of about l_{cr}=8 cm/cm^3 is reported for the comminution of cement clinkers (Bond 1964). The specific crack length tends to be lower for the materials with higher energy absorption capability. This is in agreement with the larger wear particle diameters for these materials. Interestingly, observations of the erosion sites show very similar fracture phenomenology as for the compressive test. Two examples are shown in Fig. 11. The amount of transgranular cracking is significantly higher for the concrete sample #5. Also, an intensive splitting took part which led to the complete removal of the ribs between the single parallel cuts. These observations are in good qualitative agreement with Fig. 6a.

3.3 Estimation of the Water Jet Erosion Efficiency

The efficiency of the water jet erosion process can be evaluated from the compressive test by relating the dynamic value of the absorbed energy during the compressive test to the specific energy which is involved in the material removal process during water jet erosion. The absorbed energy values were modified by a factor χ (see Table 3) in order to consider the dynamic character of the water jet erosion process. In the past, some attempts were made to express the "machinability" of rocks by conventional tools by their behavior during the compression test (Hughes 1972, Mellor 1972). For the present case an efficiency parameter F is defined based on Eq. (8).

$$\Phi = \frac{E_{abs}^{dyn}}{E_{sp}} \tag{8}$$

The energy required to remove a certain volume of material by the water jet is given by

$$E_{sp} = \frac{E_W}{V_M}. \tag{9}$$

In this equation E_W is the kinetic energy of the water jet involved in the material removal process which can be calculated using

$$E_W = \frac{\sqrt{2} \cdot \varphi \cdot \pi \cdot d_W^2}{4 \cdot \nu \cdot \sqrt{\rho}} \cdot p^{\frac{3}{2}} \cdot \int_{x=0}^{x=L} dx. \tag{10}$$

The energy portion $(1-\Phi)\cdot E_W$ is partly dissipated in the workpiece due to damping and friction, and is carried away partly by the exiting water-concrete suspension after cutting. The volume removal has to be estimated experimentally by erosion experiments as described before. The calculated efficiency parameters are plotted against the absorbed energies in Fig. 12. The efficiency values lie between $\Phi = 4.8 \cdot 10^{-6}$ and $\Phi = 6.5 \cdot 10^{-5}$. These low efficiency values for water jets reinforce experience from conventional rock cutting (Hughes 1972) which indicates that the efficiency of tools for the removal of rocks and rocklike materials drops significantly with the tool size. For water jets with extremely small tool dimensions (orifice diameter 0.23 mm), the removal efficiency may be comparatively low. It should also be noted here that the used process parameters (pump pressure and orifice diameter) are not typical for hydrodemolition processes. For the concrete mixtures #1 to #4 the estimated efficiency values follow the linear trend suggested by Eq. (8). This trend is an expression of the different crack propagation processes through the materials. As pointed out in paragraph 3.1, the concrete mixtures with the higher energy absorption capabilities show a more brittle behavior which leads to larger fracture debris and to transcristalline fractures. This behavior is valid also for the water jet erosion process as shown in Fig. 11, which shows the erosion sites from two different concrete samples. Whereas the cutting area of the concrete mixture #1 shows about 100% undamaged aggregate grains, the eroded areas of mixture #5 exhibit about 100% transgranular fracture. One can assume that this behavior allows the generation of larger erosion particles in the concretes having higher energy absorption capability during the water jet erosion process. This idea gets some support from measurements carried out by Momber (1994), who found an increasing aggregate fracture probability in concretes eroded

by water jets with increasing loading rate. He explained these results with the fact that an increase in the stress rate leads to a homogenization of the concrete structure, as observed during conventional high rate loading of concrete (Rossi, 1991). The non-linear trend of concrete mixture #5 as seen in Fig. 12 can be explained by the fact that the ribs between the single parallel cuts are completely broken as illustrated in Fig. 11. This situation allows the removal of more material and leads to an unexpected high efficiency. This behavior is in good qualitative agreement with the behavior of this mixture in the compression test, especially with the generation of the large fractured pieces shown in Figs 6a and 6b.

3.4 Estimation of the Volume Removal Rate

The significant influence of the stress-strain functions on the behavior of the investigated materials under water jet attack implies the usage of the energy absorption capability for the construction of a simplified process model which enables the estimation of the possible volume removal rate. An energy balance gives

$$E_{abs}^{dyn} = \Phi \cdot \frac{P_H}{\dot{V}_M} \Rightarrow \dot{V}_M = \frac{p \cdot Q \cdot \Phi\left(E_{abs}^{dyn}\right)}{E_{abs}^{dyn}}. \tag{11}$$

The function $\Phi\left(E_{abs}^{dyn}\right)$ as given in Fig. 12 is approximated by a logarithmic fit. The measured volume removal rates are plotted against the absorbed energies in Fig. 13. The experimental results can reasonably be fitted by Eq. (11) for the samples with medium energy absorption capability. The different material removal rates for these material mixtures at fixed process conditions may be a result of the different capabilities of the materials to dissipate the water jet energy. The increase in the measured volume removal rate in the range of the high energy absorption values is a result of the intensive splitting of material #5. As already reported, the ribs between the parallel cuts are completely broken and removed. This is not considered in Eq. (11). The bad fit for sample #1 may be a result of the very deep matrix removal which was not observed in the other samples.

4. SUMMARY AND CONCLUSIONS

A systematic study on the influence of the energy which is absorbed during the compression test of semi-brittle, multiphase materials on their behavior under water jet attack was carried out. The absorbed energy was estimated by calculating the area under the compression stress-strain curve of five different concrete materials. Additionally, fracture tests in a compression testing unit, and erosion tests with water jets have been carried out to estimate the material behavior. The investigations lead to the following results:

- The amount of absorbed energy during the compression test can be related to crack propagation processes during the fracture process. In materials with high energy absorption capacity the cracks run preferably though the aggregate grains. This process is more energy intensive due to the higher specific surface energy of the inclusions.
- There exists a relation between the energy absorption capability of the materials during the

compression test and their resistance against water jet erosion.

- The average grain size of the wear debris eroded by the water jet is linearly related to the energy absorbed during the compression test.
- The material removal rate during the water jet erosion process is related to the energy absorbed during the compression test.
- The efficiency of the water jet erosion of concrete is about $\Phi = 0.001\%$. The process efficiency increases with the absorbed fracture energy.
- The material removal mechanism depends on the energy absorption capability of the investigated materials. Materials with low energy absorption capability will be removed by intergranular fracture (between the aggregate grains and the matrix). Materials with high energy absorption capability will be removed preferably by transgranular fracture through the aggregate grains.
- The average grain size of the wear debris eroded by the water jet is linearly related to the concrete fracture debris generated during the compressive test.

5. ACKNOWLEDGEMENTS

The authors are thankful to the Alexander von Humboldt Foundation, Bonn, and to the Center for Robotics and Manufacturing Systems, University of Lexington, for financial support. Also, appreciation is directed to Mr. D. Hunsucker from the Transportation Center, Univ. of Kentucky, for conducting the compression tests.

6. REFERENCES

Atchley, B. L., and Furr, H. L., "Strength and Energy Absorption Capability of Plain Concrete Under Dynamic and Static Loading," *ACI Journal*, pp. 745-756, 1967.

Bitter, J.G., "A Study of Erosion Phenomena, Part I," *Wear*, Vol. 6, pp. 5-21, 1963.

Bond, F. C., "Berechnungsmethode zur Feinzerkleinerung," *Aufbereitungstechnik*, pp. 211-218, 1964.

Glucklich, J., 1965, "The Effect of Microcracking on Time-Dependent Deformations and the Long-Therm Strength of Concrete," *The Structure of Concrete*, pp. 176-189, Cement and Concrete Ass., London, 1965.

Hughes, H.M., "Some Aspects of Rock Machining," *International Journal of Rock Mechanics and Mining Science*, Vol. 9, pp. 205-211, 1972.

Kleinschrodt, H. and Winkler, H., "The Influence of the Maximum Aggregate Size and the Size of Specimen on Fracture Mechanics Properties," *Fracture Toughness and Fracture Energy*, pp. 158 to 163, Elsevier, Amsterdam, pp 158-163, 1986.

Kriegel, E., "Der Strahlverschleiss von Werkstoffen," *Chemie-Ingenieur Technik*, Vol. 40, pp. 31-36, 1968.

Matsui, S., Matsumura, Y, Ikemoto, H., Shimizu, H, and Takada, I., "Prediction Equations for Depth of Cut Made by Abrasive Water Jet," *Proceedings of the 6th American Water Jet Conference*, pp. 31-41, Water Jet Technology Association, St. Louis, 1991.

Medeot, R., 1989, "History, Theory and Practice of Hydrodemolition," *Proceedings of the 5th American Water Jet Conf*erence, pp. 99-110, Water Jet Technology Association, St. Louis, 1989.

Mellor, M., "Normalization of Specific Energy Values," *International Journal of Rock Mechanics and Mining Science*, Vol. 9, pp. 661-663, 1972.

Momber, A., "Energetical Aspects of Mass Concrete Removal Using Plain High Speed Water Jet," *Decommissioning and Demolition*, pp. 95-101, Th. Telford Ltd., London, 1992a.

Momber, A., "Untersuchungen zum Verhalten von Beton unter der Belastung durch Druckwasserstrahlen," *VDI Forschungshefte*, No. 109, pp. 1-137, 1992.

Momber, A., "Quecksilberporosimetriemessungen an durch Druckwasserstrahlen beanspruchten Betonproben," *Materialwissenschaft und Werkstofftechnik*, Vol. 42, pp. 283-286, 1992a.

Momber, A., "Handbuch Druckwasserstrahl-Technik," Beton-Verlag, Düsseldorf, 1993.

Momber, A., "Secondary Fragmentation in Water Jet Rock Cutting," *International Jornal of Water Jet Technology*, Vol. 2, pp. 52-55, 1994.

Momber, A., and Kovacevic, R., "Fundamental Investigations on Concrete Wear by High Velocity Water Flow," *Wear*, Vol. 177, pp. 55-62, 1994.

Momber, A., and Kovacevic, R., "The Influence of Material Instabilities in a Brittle Multiphase Material on its Behaviour in High Energy Water Jet Machining," *AMD-Vol.* 183/*MD-Vol.* 50, pp. 327-344, 1994a.

Momber, A., and Kovacevic, R., "Statistical Character of the Failure of Multiphase Materials due to High Pressure Water Jet Impingement," *International Journal of Fracture,* accepted for publication, 1995.

Momber, A., and Louis, H., "On the Behaviour of Concrete under Water Jet Impingement," *Materials and Structures*, Vol. 27, pp. 153-156, 1994.

Momber, A., Kovacevic, R., and Ye, J., "The Fracture of Concrete due to Erosive Wear by High Velocity Water Flow," *Tribological Transactions*, accepted for publication, 1995.

Ocepek, D., "Über die Methoden der Bestimmung des Zerkleinerungswiderstandes," *Aufbereitungs-Technik*, pp. 290-293, 1969.

Reinhardt, H.W., "Concrete Under Impact Loading, Tensile Strength and Bond," *Heron*, Vol. 27, pp. 5-41, 1982.

Rossi, P., "A Physical Phenomenon Which Can Explain the Mechanical Behaviour of Concrete Under High Strain Rates," *Materials and Structures*, Vol. 24, pp. 422-424, 1991.

Schubert, H., "Aufbereitung fester mineralischer Rohstoffe," Vol. 1, Verlag für Grundstoffindustrie, Leip- zig, 1988.

Shah, S. P., and Ouyang, C., "Toughening Mechanisms in Quasi-Brittle Materials," *ASME Journal of Engineering Materials and Technology*, Vol. 115, pp. 300-307, 1993.

Thiruvengadam, A., "The Concept of Erosion Strength," *ASTM STP* 408, pp. 22-35, 1967.

Werner, M., "Einflussparameter und Wirkmechanismen beim Abtrag von Mörtel und Beton mit dem Hochdruckwasserstrahl," PH.D. Dissertation, RWTH Aachen, 1991.

Wiedemeier, J., "Flüssigkeitsfreistrahlen hoher Relativgeschwindigkeit und Bruchkinetik spröder Werk- stoffe," Ph.D. Dissertation, Univ. Hannover, 1981.

Wittmann, F.H., Rokugo, K., Brühwiler, E., Mihashi, H. and Simonin, P., "Fracture Energy and Strain Softening of Concrete as Determined by Means of Compact Tension Specimens," *Materials and Structures*, Vol. 21, pp. 21-32, 1988.

7. NOMENCLATURE

d_{av}	average debris grain diameter	v	traverse rate
d_P	debris grain diameter	V_M	volume removal
d_W	water jet nozzle diameter	$\dot{V}_M$	material removal rate
E_{abs}	absorbed energy per volume during compressive test	Y_M	Young's modulus
		φ	nozzle efficiency parameter
E_{abs}^{dyn}	dynamical absorbed energy	χ	correction parameter for dynamic loading
E_{SP}	specific removal energy		
E_W	water jet energy	Φ	efficiency parameter
L	kerf length	ρ	water density

l_{cr}	specific crack length	ρ_M	material density
p	applied pump pressure	σ	stress
P_H	hydraulic pump power	σ_C	ultimate stress
Q	water volume flow rate	ε	strain
S_{SP}	specific surface	ε_{cr}	ultimate strain
		ψ	grain shape parameter

Table 1. Mix Design and Mechanical Properties of the Investigated Materials.

Concrete mixture	Aggregate*/ Cement**	Sand*** [%]	Water/ Cement	Y_M [GPa]	σ_C [MPa]	E_{abs}^{dyn} [MJ/m³]	ρ_M [kg/m³]
# 1	2.24	80	0.85	10.7	4.0	2.1	1,962
# 2	2.51	70	0.71	24.1	12.5	11.1	2,135
# 3	2.13	60	0.45	33.0	27.1	38.9	2,107
# 4	2.25	50	0.38	34.3	34.2	62.6	2,275
# 5	2.26	40	0.32	42.3	41.1	72.8	2,343

* coarse limestone aggregates (maximum grain size 19 mm) and river sand (maximum grain size 4.7 mm)
** Portland Cement, Type I
*** river sand (maximum grain size 4.7 mm)

Table 2. Experimental Conditions.

Parameter	Unit	Value
pump pressure	MPa	250
flow velocity	m/s	670
nozzle diameter	mm	0.23
standoff distance	mm	15
exposure time	min	92

Table 3. Regression Parameters of the Stress-Strain Curves.

concrete mixture	A	ε_{cr}	σ_C	E_{abs}	$\chi^{1)}$
# 1	-12.5	0.57	4.0	1.5	1.40
# 2	-13.9	0.95	12.5	7.9	1.40
# 3	-12.1	1.50	27.1	27.0	1.44
# 4	-10.6	1.80	34.2	40.9	1.53
# 5	-13.6	1.73	41.1	47.6	1.53

[1)] from Atchley and Furr (1967)

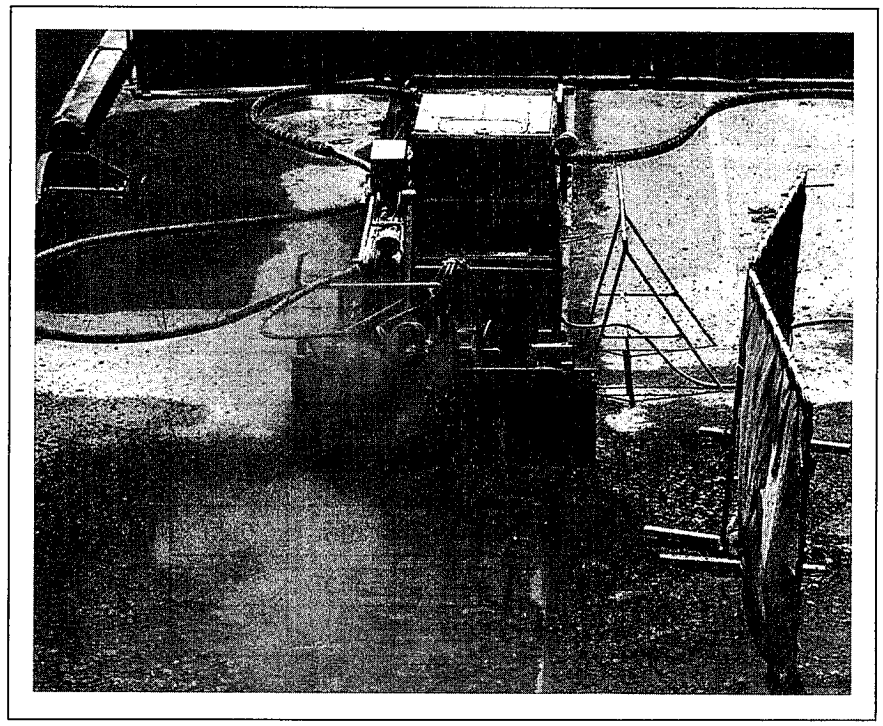

Figure 1. Concrete Removal Using Water Jet Technique.
(Photo: WOMA GmbH, Duisburg)

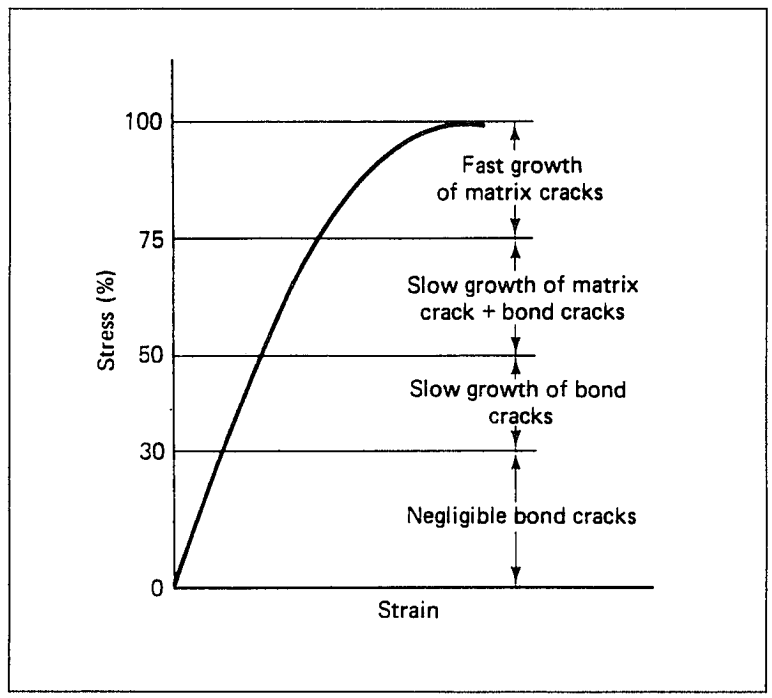

Figure 2. Diagrammatic Stress-Strain Curve for Concrete in Compression.
(Glucklich 1965)

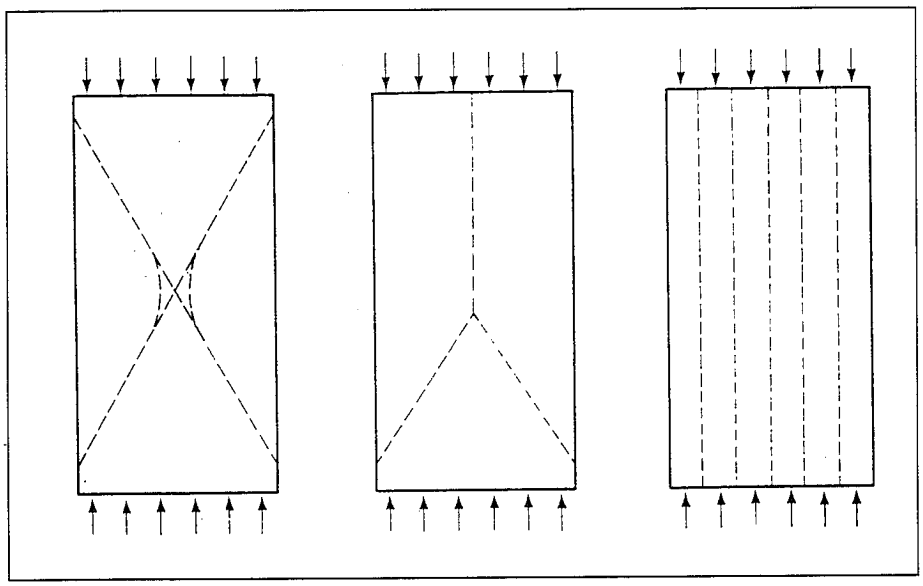

Figure 3. Fracture Types During the Compression Test.
(ASTM Standard C 39)

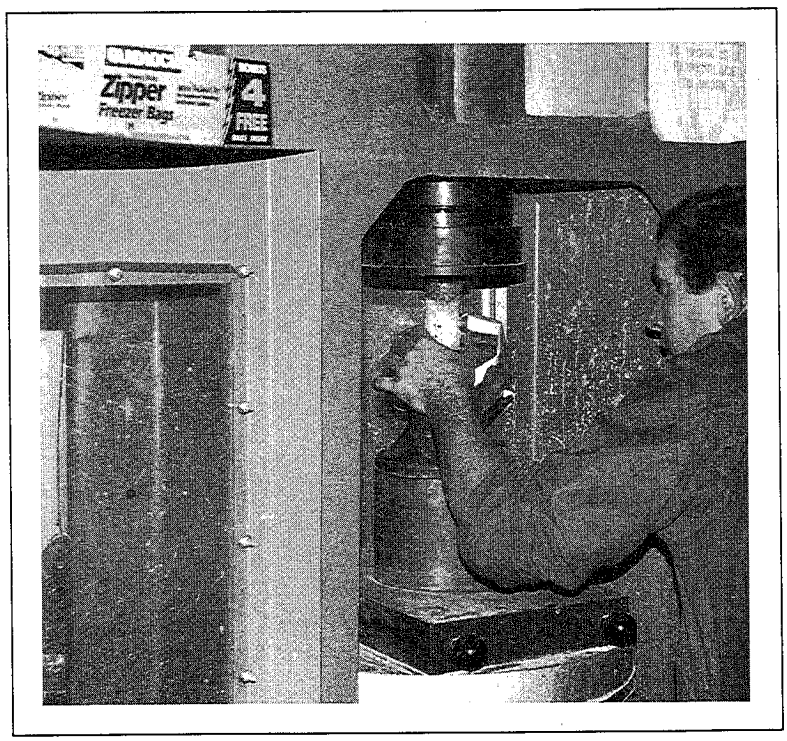

Figure 4. Compression Fracture Test of a Concrete Cylinder.

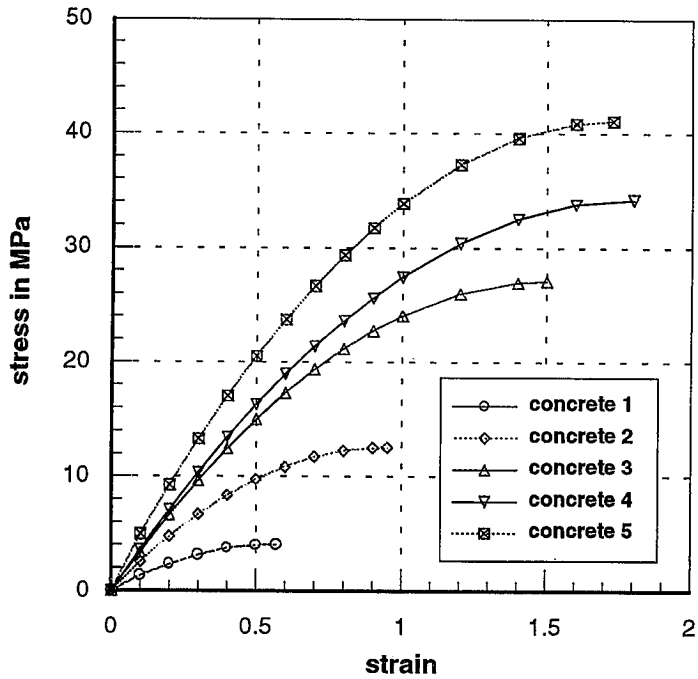

Figure 5. Compression Stress-Strain Curves of the Investigated Concrete Mixtures.

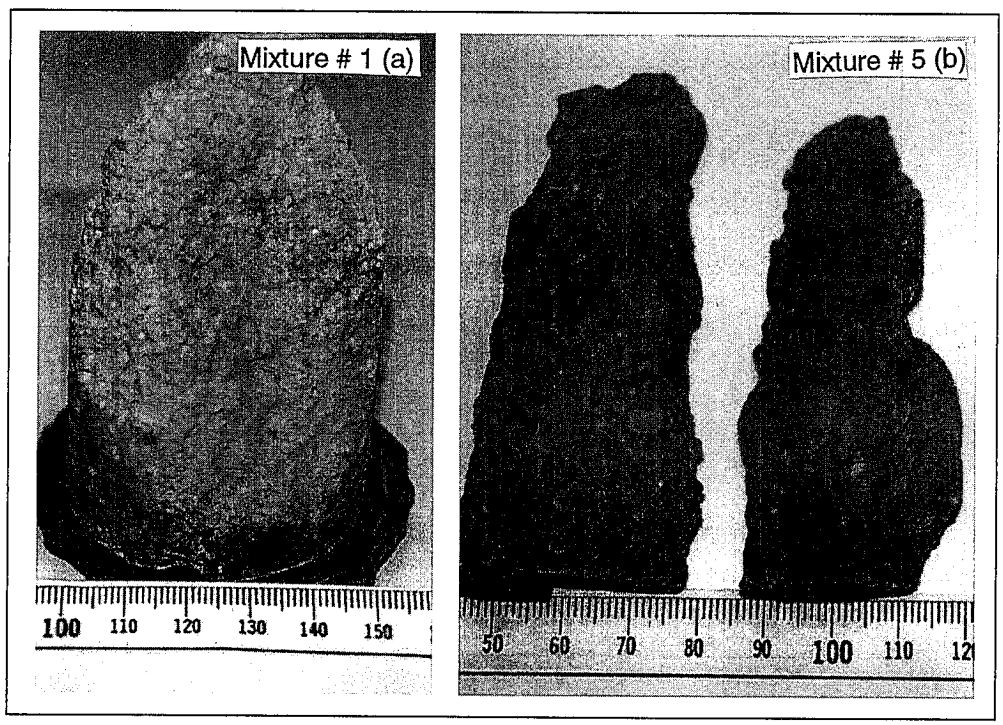

Figure 6. Fracture Mode Resulted From Compression Test.
Concrete Mixture # 1 (a) and Mixture # 5 (b)

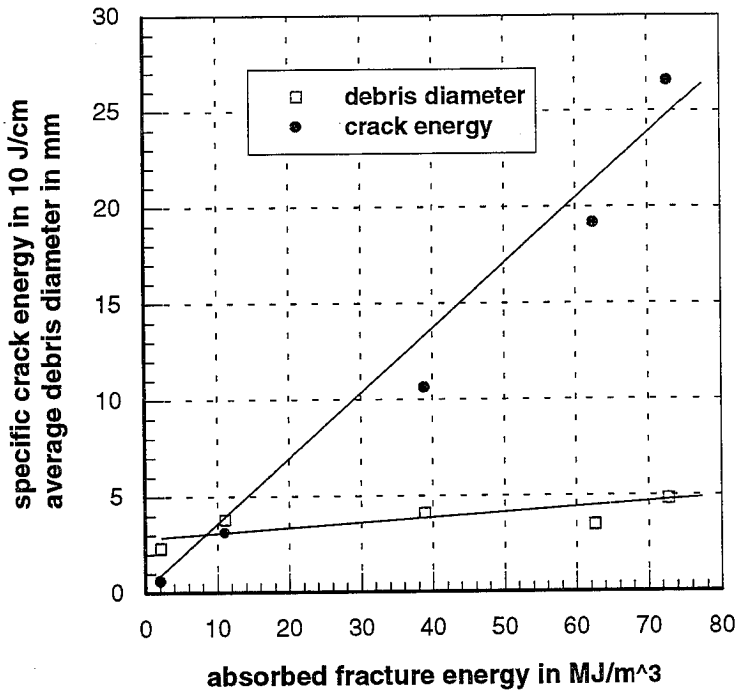

Figure 7. Relation Between Absorbed Fracture Energy, Average Debris Diameter, and Specific Crack Energy. (Compression)

Figure 8. Grain Sample Removed by Water Jet Erosion.
(Sample # 3, Magnification 1:12)

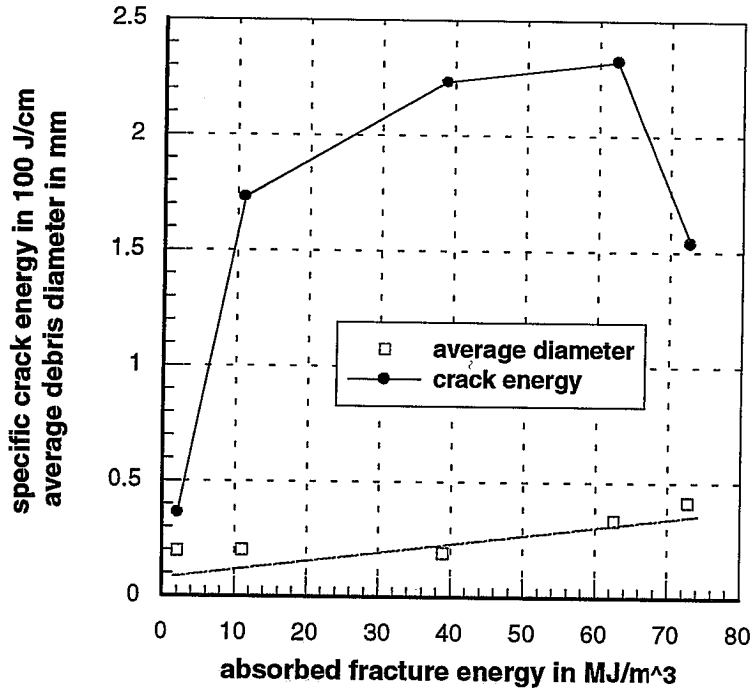

Figure 9. Relation Between Absorbed Fracture Energy, Average Particle Diameter, and Specific Crack Energy. (Erosion)

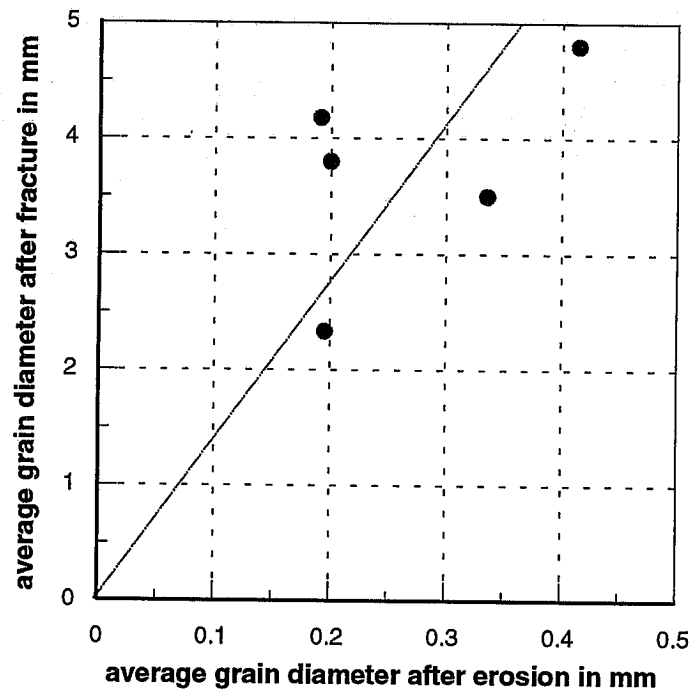

Figure 10. Relation Between Average Debris Diameter (Compression), **and Average Wear Particle Diameter** (Erosion).

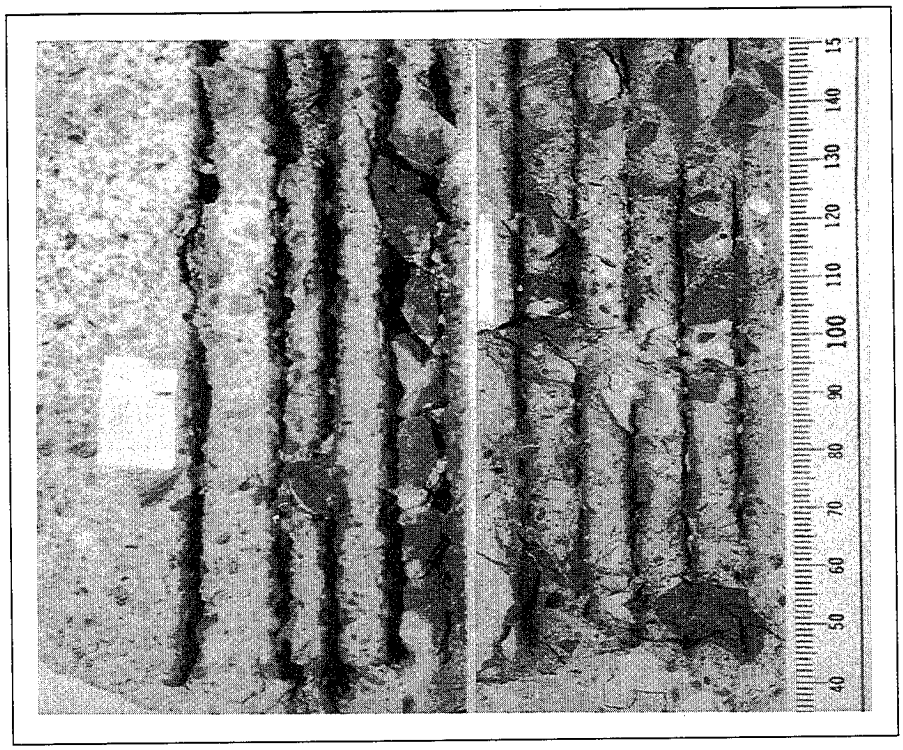

Figure 11. Erosion Sites of Two Specimens.
(Left: Mixture # 1, Right: Mixture # 5)

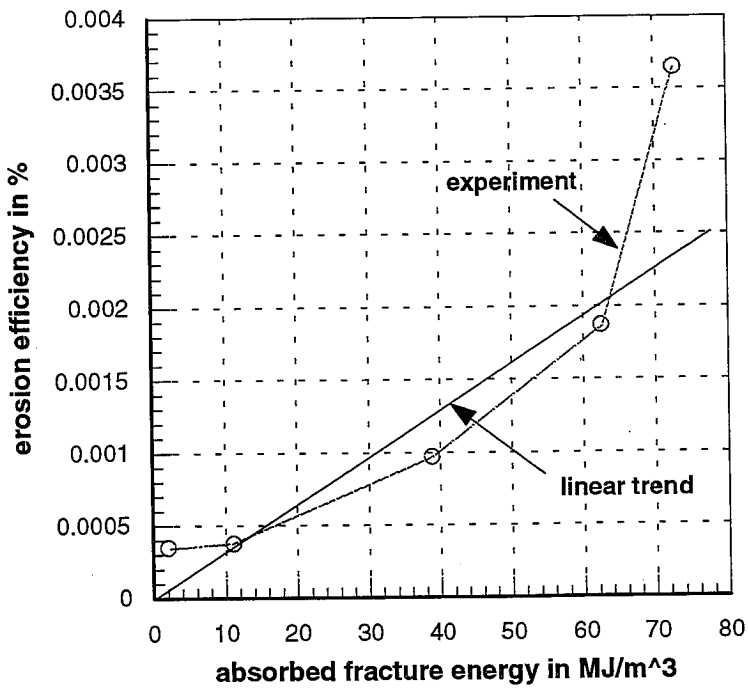

Figure 12. Relation Between Absorbed Fracture Energy and Erosion Efficiency.

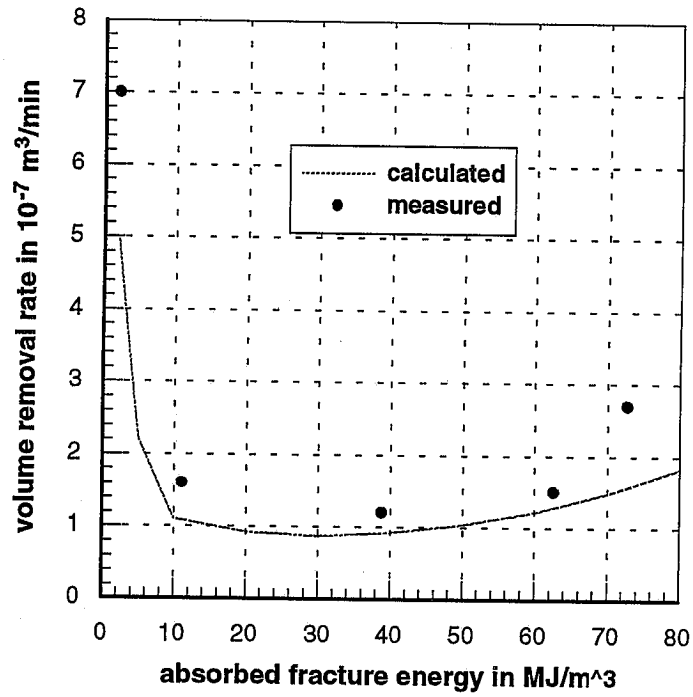

Figure 13. Relation Between Absorbed Fracture Energy and Material Removal Rate.

8th American Water Jet Conference
August 26-29, 1995: Houston, Texas

Paper 61

A SIMPLIFIED MATHEMATICAL ENERGY DISSIPATION MODEL FOR WATER JET AND ABRASIVE WATER JET CUTTING PROCESSES

A. W. Momber*
WOMA Apparatebau GmbH
Duisburg, Germany

ABSTRACT

The paper provides a mathematical model for the estimation of the energy dissipation of materials during water jet and abrasive water jet cutting. The model is based on an energy balance inside the workpiece. An energy dissipation parameter, $\chi(h)$, is defined to describe the energy dissipation process. A mathematical method for the estimation of this parameter is developed based on the structure of the cutting front generated in the kerf walls. Experiments on metallic, ceramic and mineral samples cut by abrasive water jets under different cutting conditions shows that the relation between the depth of cut and the energy dissipation is non-linear. The relation can effectively be described by a second order polynomial $\chi(h)=A\cdot h^2+B\cdot h+C$. This polynomial seems to be sensitive to changes in the specimen materials. It is also shown that the relation between the relative depth of cut, $\Phi=h/h_{max}$, and the energy dissipation parameter, χ, is also a second order polynomial. It seems that the regression parameters of this polynomial are independent of the specimen material as well as of the process conditions.

---

* Feodor-Lynen Scholar of the Alexander von Humboldt Foundation, Bonn, Germany, at the Center for Robotics and Manufacturing Systems, University of Kentucky, Lexington, U.S.A.

Organized and Sponsored by the Water Jet Technology Association.

1. INTRODUCTION

As new manufacturing processes, water jet (WJ) cutting and abrasive water jet (AWJ) cutting have been very effective in machining a wide variety of materials. AWJs are used for cutting a wide range of materials, including ceramics (Hamatani and Ramulu 1990, Hochheng and Chang 1994) and composite materials (Arola and Ramulu 1993, Momber 1994). As shown by Laurinat et al. (1993), AWJs also have potential for milling operations and 3-D-machining. A typical commercial AWJ system consists of a pressure generator, typically an intensifier pump, an abrasive cutting head, a x-y-z-positioning system, and a catcher. On the basis of jet generation, abrasive water jets can generally be categorized as injection jets or suspension jets. For practical applications, injection jets are more commonly used. For this type of jet, the pressure ranges between 100 MPa and 400 MPa. An injection AWJ is formed by accelerating small abrasive particles (garnet, aluminum oxide, silicon carbide) through contact with a high velocity plain water jet. A typical abrasive grain diameter is 400 μm. The plain water jet is formed in an orifice above the abrasive cutting head. The abrasives enter the cutting head at a separate entry. The mixing between abrasive, water and air takes place in a mixing chamber, and the acceleration process occurs in an acceleration tube, or abrasive waterjet nozzle. The abrasive particles leave this nozzle at velocities of several hundred meters per second. A high number of abrasives (10^5 per second) leads to a high frequency impingement on the materials being processed. The intensity and the efficiency of the cutting process depend on several process parameters such as pump pressure, orifice diameter, traverse rate, standoff distance, abrasive flow rate, abrasive type, and mixing chamber geometry.

Water jets and abrasive water jets are streamlike tools, similar to lasers and electron beams, which are characterized by an unsteady material removal process. The most pronounced characteristic of AWJ-generated surfaces is the presence of striation marks which transpire below a region of relatively smooth surface finish as shown in Figs. 1 and 2. It is widely accepted that the striations are a result of the formation of steps on the cutting front. The concept of step formation was introduced in the water jet cutting research by Mohaupt and Burns (1973) who suggested this model based on water jet cutting experiments on plastics. Typical striations generated during the cutting of materials by plain and abrasive water jets are shown in Figs. 1 and 2. It is not clear yet what physical phenomenon may cause the formation of steps and striations. Detailed observations in transparent materials by Hashish (1988) and Blickwedel (1991) during AWJ cutting have revealed that the material removal occurs in two stages. In the first stage the abrasive particles strike the surface at shallow angles producing a relatively smooth surface. The secondary stage, which yields unsteady cutting with striation marks is controlled by erosive wear due to particles impacting at large angles of attack. Arola and Ramulu (1993) and Raju and Ramulu (1994) suggest that the striation formation is related only to the available AWJ energy at a certain depth of cut. In contrast, Chao and Geskin (1993) assumed that the striation formation is independent of the material removal process, and observed a strong relation between machine vibrations and the structure of the generated striations. This may be questionable, because investigations by Hashish (1992), who used a material with very high erosion resistance to filter external effects, showed that external effects do not influence the striation formation.

A part of the AWJ input energy is consumed by the workpiece and contributes to the material destruction. As shown by Momber et al. (1994, 1995), only a small amount of the AWJ energy is used to remove the material. The rest of the energy may be dissipated by different mechanisms, such as friction and heat generation (Kovacevic et al. 1995). An important part of the AWJ energy is contained by the mixture of abrasive, water, and wear particles after it leaves the workpiece (Momber and Kovacevic 1994).

Capello and Groppetti (1992) considered the energy loss during cutting in their energetic model and approximated it by using a negative power function. However, this assumption was not verified by experiments. Also, this function leads to a total energy loss only for an infinite cutting thickness. Serious investigations on the energy absorption capability during AWJ cutting have been carried out by Zeng et al. (1991), Momber and Kovacevic (1994), and Raju and Ramulu (1994). The first two references modeled the shape of the striations using a parabolic function. Based on this model Zeng et al. (1991) estimated the angle between the workpiece and the exiting AWJ and used it as a process control parameter. Momber and Kovacevic (1994) developed a calculation method for the estimation of the AWJ exit energy after cutting a workpiece, which is based on an energy balance and considers the influence of the depth of cut on the energy absorption during the process. Raju and Ramulu (1994) developed a physical model for the striation formation process and found a significant relation between the kinetic energy of the abrasive particles and the transition zone between the smooth cutting zone and rough cutting zone.

The assumption that the formation of the striations is related to the local kinetic energy of the water jet leads to the possibility of modeling the energy dissipation processes in the material by using the geometry of the cutting front. The objectives of the present paper are the development of a simple mathematical model for the quantitative estimation of the energy dissipation capability of the materials during water jet machining, and the mathematical description of the influence of the depth of cut on the energy dissipation process.

2. DEVELOPMENT OF THE ENERGY DISSIPATION MODEL

2.1 Energy Balance During Water Jet Cutting

The general energy situation in a material during cutting with a water jet is shown in Fig. 3. According to this situation the energy which is dissipated during the cutting process, E_{DIS}, can be estimated using Eq. (1).

$$E_{DIS} = E_{IN} - E_L \tag{1}$$

Here, E_{IN} is the input energy of the jet and E_L is the amount of energy in the jet when it leaves the workpiece. Many investigations in jet cutting have shown that a critical minimum energy E_C (critical pump pressure, critical traverse rate) is necessary to destroy a material and to initiate the cutting process. A review of this problem is given by Momber (1993). It

is assumed that this critical situation will also be found at the bottom of the cut in a workpiece ($h=h_{max}$), when the jet does not have enough energy to penetrate the material. This simple assumption leads to Eq. (2).

$$E_{DIS}(h=h_{max}) = E_{IN}-E_C \tag{2}$$

Another critical condition exists in the case $h=0$. Here no energy is dissipated in the workpiece and the total amount of the jet energy goes into the exit jet. This situation leads to Eq. (3).

$$E_{DIS}(h=0) = 0 \tag{3}$$

By introducing a parameter $\chi(h)$ which depends on the depth of cut and using Eq. (1), the situation can be described by Eq. (4) for all cases between these extremums.

$$0<h<h_{max}: \; E_{DIS}(h) = \chi(h)\cdot[E_{IN}-E_C] \tag{4}$$

For the conditions in Eq. (2) one obtains $\chi(h=h_{max})=1$, whereas Eq. (3) leads to the case $\chi(h=0)=0$. So the parameter $\chi(h)$ considers the energy dissipation processes in the material during cutting. Section 2.2 describes how to determine this parameter from the geometry of the cutting front.

2.2 Estimation of the Energy Dissipation Parameter $\chi(h)$

Fig. 4 shows two simplifications of the jet cutting process with and without energy losses due to energy dissipation during cutting. As Fig. 4a suggests, a rectangular area A_1 is generated as the jet moves in the traverse direction without energy loss. This is an ideal case. Realistically one would find a curved cutting front as shown in Fig. 4b, which occupies an area A_0. This area is used to characterize the energy loss in real cutting. The calculation of this area is given by Eq. (5).

$$A_0 = \int_0^x h(x)dx \tag{5}$$

Zeng et al. (1991) have assumed a parabolic curve to describe the shape of an AWJ generated cutting front. A similar relation - a second order polynomial - was found by Chao and Geskin (1993) for the relation between striation peak amplitude and the depth of cut. These findings were developed further by Momber and Kovacevic (1994) who used Eq. (6) to estimate the function h(x).

$$h(x) = a\cdot(x-b)^2 + c \tag{6}$$

Here, a, b and c are constants which can be evaluated by measurements of the cutting front. An approximation for the parameters can be done by assuming $c=h_{max}$ as shown in Fig. 5. If this is valid, it follows that $b=x_{max}$. If $h=0$ and $x=0$, one can write

$$a=\frac{-c}{b^2}=\frac{-h_{max}}{x_{max}^2}. \tag{7}$$

The parameters x_{max} and h_{max} can be easily estimated for every full-cut surface. The role of these parameters is shown in Fig. 5. As the figure shows, for the case $x=b$ the area A_0 can be calculated by Eq. (6).

$$A_0 = b\cdot c - \int_0^b h(x)dx = -\frac{a\cdot b^3}{3} \tag{8}$$

It is assumed that A_0 includes all energy losses during cutting of the material up to a depth of $h=h_{max}$, which is the maximum depth of cut under the given process conditions. A change of the regression parameters a, b and c with the depth of cut is neglected. A_0 is not considered to have the unit of energy, but it represents the energy losses due to energy dissipative processes during cutting. If this parameter is related to other area values from different depths of cut, it can be used to describe the dependence between energy dissipation and depth of cut, $\chi(h)$. Fig. 6 shows that certain areas A(h) exist on certain depth levels. The area A(h) which is occupied by the cutting front during a certain depth of cut, h(x), is shown in Fig. 6 and can be described by Eq. (9).

$$A(h) = x\cdot[h(x)] - \int_0^x h(x)dx = a\cdot\left(\tfrac{2}{3}\cdot x^3 - b\cdot x^2\right) \tag{9}$$

Here x can be calculated using Eq. (10).

$$x=\sqrt{\frac{h-c}{a}}+b \tag{10}$$

The dissipation parameter, $\chi(h)$, can now be estimated for different depths of cut using Eq. (11).

$$\chi(h)=\frac{A(h)}{A_0}=\frac{A(h)}{A(h_{max})} \tag{11}$$

It can be shown that $\chi=1$ and that Eq. (9) is identical to Eq. (8) for the case $x=b$ and for the case $h=h_{max}$. Also, it is easy to see that $\chi=0$ for the case $x=b$, where the amount of

dissipated energy is negligible, and for the case h=0. Using Eqs. (8), (9), and (11), the energy dissipation parameter, $\chi(h)$, can be calculated by Eq. (12).

$$\chi(h)=\frac{2\cdot x^3-3\cdot b\cdot x^2}{(-b)^3} \tag{12}$$

Here, the relation between h and x is given by Eq. (10).

3. EXPERIMENTAL SETUP AND EXPERIMENTAL WORK

For the investigations, reference cuts were generated by abrasive water jets samples from in aluminum, cast iron, concrete, and magnesia chromite under different cutting conditions. The cutting conditions are listed in Table 1. The samples were completely cut through to measure the geometry of the cutting front. That means, the maximum possible depth of cut was not reached in these cases. The abrasive water jet unit consists of an intensifier pump, an abrasive cutting head, an abrasive storage and metering system, a catcher and a CNC-controlled positioning system. The position of the cutting head is controlled using a x-y-z-positioning table.

After cutting, the shapes of the cutting fronts on the cut walls (see Fig. 1) were measured using a video camera for magnification. After this, the cutting fronts were modeled by using the parabolic approximation given in Eq. (6). The parameters of these regressions are listed in Table 2.

4. RESULTS AND DISCUSSION

The modeled shapes of the cutting fronts are given in Fig. 7. Due to the modeling process described in the previous chapter, the heights of the curves are identical to the generated depths of cut. If the progress of the parabola function is zero, the maximum possible depth of cut is reached for the given cutting conditions. Fig. 8 shows results of the calculations based on Eq. (12). The calculated energy dissipation parameters, χ, are plotted against the depth of cut for different cutting conditions and different materials. The relative energy dissipation is $\chi=0$ for non-cutting, and $\chi=1$ for the maximum depth of cut. Between these extremums the function is non-linear and can be approximated very reasonably by a second order equation according to Eq. (13).

$$\chi(h) = A\cdot h^2+B\cdot h+C \tag{13}$$

Interestingly, a similar relation was found by Chao and Geskin (1993) between the depth of cut and the peak amplitudes of the generated striations. Mohan et al. (1995) who used a simplified physical model also found a second order polynomial relation between the depth of cut and the dissipated jet energy. These results may support the validity of Eq. (13). The

regression parameters for the investigated cutting conditions are given in Table 3. It is very striking that the energy dissipation functions for the concrete and the ceramic material are relatively straight lines. Because both these materials are brittle and multiphase, there may be a relation between the material structure and the behaviour of the energy dissipation. Here, a systematic study of this effect is necessary. The absolute values of the dissipated energy, E_{DIS}, can be estimated using Eq. (14).

$$E_{DIS}(h) = [A \cdot h^2 + B \cdot h + C] \cdot [E_{IN} - E_C] \tag{14}$$

In Fig. 9 the relative depth of cut, $\Phi = (h/h_{max})$, is plotted against the relative energy dissipation, χ, for the different cutting conditions applied in this study. It is seen that all plotted points can be fitted by the same line which may be described by Eq. (15).

$$\chi(\Phi) = A_1 \cdot \Phi^2 + B_1 \cdot \Phi + C_1 \tag{15}$$

The regression parameters are given in Table 3. Interestingly, and in contrast to Fig. 8, it seems that the regression parameters A_1, B_1, and C_1 are independent of the cutting conditions as well as on the investigated materials.

5. SUMMARY

The investigations lead to the following summary:

- A model for the calculation of the energy losses due to energy dissipative processes in the material during water jet cutting is developed based on an energy balance inside the workpiece.
- A parameter, $\chi(h)$, is defined to describe and calculate the energy dissipation capability of a material during cutting by a water jet.
- A method which is based on a parabolic model of the cutting front is developed to estimate the energy dissipation parameter, $\chi(h)$.
- The relation between the absolute depth of cut, h, as well as the relative depth of cut, Φ, and the energy dissipation capability parameter, χ, can be described by a second order equation.
- The regression parameters for the second order polynomial describing the relation between relative depth of cut and energy dissipation seems to be independent of the cutting conditions.

6. ACKNOWLEDGEMENTS

The author wishes to thank the Alexander-von-Humboldt Foundation, Bonn, Germany, and the Center for Robotics and Manufacturing Systems, University of Kentucky, Lexington, for financial support.

7. REFERENCES

Arola, D., and Ramulu, M., "Mechanisms of Material Removal in Abrasive Waterjet Machining of Common Aerospace Materials," *Proceedings of the 7th American Water Jet Conference*, pp. 43-64,Water Jet Technology Association, St. Louis, MO, 1993.

Blickwedel, H., "Erzeugung und Wirkung von Hochdruck-Abrasivstrahlen," *Ph.D. Dissertation*, Univ. Hannover, 1990.

Capello, E., and Groppetti, R., "On an Energetic Semi-Empirical Model of Hydro-Abrasive Jet Material Removal Mechanism for Control and Optimization," *Jet Cutting Technology*, pp. 101-120, Kluwer Acad. Publ., Dordrecht, 1992.

Chao, J., and Geskin, E., "Experimental Study of the Striation Formation and Spectral Analysis of the Abrasive Water Jet Generated Surfaces," *Proceedings of the 7th American Water Jet Conference*, pp, 27-41, Water Jet Technology Association, St. Louis, MO, 1993.

Hamatani, G., and Ramulu, M., "Machinability of High Temperature Composites by Abrasive Water Jet," *ASME Transactions, Journal of Engineering Materials and Technology*, Vol. 112, pp. 381-386, 1990.

Hashish, M., "Visualization of the Abrasive-Waterjet Cutting Process," *Experimental Mechanics*, pp.159 to 169, 1988.

Hashish, M., "A Modeling Study of Jet Cutting Surface Finish," *ASME-PED-Vol. 58*, pp. 151-167, 1992,

Hocheng, H., and Chang, K.R., "Material Removal Analysis in Abrasive Waterjet Cutting of Ceramic Plates," *Journal of Materials Processing Technology*, Vol. 40, pp. 287-304, 1994.

Kovacevic, R., Mohan, R., and Beardsley, H., "Monitoring of Thermal Energy Distribution in Abrasive Water Jet Cutting Using Infrared Thermography," *ASME Transactions, Journal of Engineering for Industry*, in review, 1995.

Laurinat, A., Louis, H., and Haferkamp, H., "Werkstücke dreidimensional bearbeiten mit Hilfe des Was- serabrasivstrahlverfahrens'" *Maschinenmarkt*, Vol. 99, pp. 22-27, 1993.

Mohan, R., Momber, A., and Kovecevic, R., 1995, "Detection of Energy Absorbtion During Abrasive Water Jet Machining Using Acoustic Emission Technique," *International Mechanical Engineering Congress and Exhibition*, San Francisco, in review, 1995.

Mohaupt, U. H., and Burns, D., "Machining Unreinforced Polymers With High-Velocity Water Jets," *Experimental Mechanics*, Vol. 14, pp. 152-157, 1974.

Momber, A., "*Handbuch Druckwasserstrahl-Technik,*" Beton Verlag GmbH, Düsseldorf, 1993.

Momber, A., "Schneidversuche an Stahlbeton mit dem Abrasiv-Druckwasserstrahlen," *Beton- und Stahlbetonbau*, Vol. 89, pp. 132-134, 1994.

Momber, A., and Kovacevic, R., "Calculation of Exit Jet Energy in Abrasive Water Jet Cutting," *Manufacturing Science and Engineering*, pp. 361-366, ASME, New York, 1994.

Momber, A., Kwak, H., and Kovacevic, R., "Investigation in Abrasive Water Jet Erosion Based on Wear Particle Analysis," *ASME Transactions Journal of Tribology*, in review, 1994.

Momber, A., Eusch, I., and Kovacevic, R., "The Influence of the Stress-Strain Behaviour of Quasi-Brittle Materials on Their Machinability by Abrasive Water Jets," *International Conference of Solids and Materials Engineering*, accepted for publication, Singapore, 1995.

Raju, S. P., and Ramulu, M., "Predicting Hydro-Abrasive Erosive Wear During Abrasive Water Jet Cutting," *Manufacturing Science and Engineering*, pp. 339-351, ASME, New York, 1994.

Zeng, J., Hines, R., and Kim, T., "Characterization of Energy Dissipation Phenomena in Abrasive Water Jet Cutting," Proceedings of the *6th American Water Jet Conference*, pp. 163-177, Water Jet Technology Association, St. Louis, MO, 1991.

8. NOMENCLATURE

a,b,c	parabola regression parameters
A,B,C	regression parameters
A(h)	area, occupied by the cutting front
A_0	area, occupied by the cutting front at $h=h_{max}$
E_{DIS}	energy, dissipated in the material
E_C	material threshold energy
E_{IN}	jet input energy
E_L	jet exit energy
h	depth of cut

h_{max} maximum depth of cut
p_C material threshold pressure
s standoff distance
v traverse rate
x cutting ordinate
α striation angle
χ energy dissipation parameter
Φ relative depth of cut h/h_{max}

Table 1. Cutting Parameters Used in the Experimental Work.

Specimen	p [MPa]	v [mm/s]	$\dot{m}_p$ [g/s]	abrasive
# 1	250	0.8	8.30	garnet 1
# 2	250	0.8	8.30	garnet 2
# 3	200	8.0	7.41	garnet # 100
# 4	200	8.0	7.41	garnet # 36
# 5	276	0.6	3.40	garnet # 80

Table 2. Regression Parameters of the Parabola Expression $h=a\cdot(x-b)^2+c$.

Specimen	Material	a	b	c
# 1	aluminum	-0.337	8.3	22.0
# 2	aluminum	-0.336	8.0	20.8
# 3	ceramic	-0.200	15.0	45.0
# 4	concrete	-0.221	25.0	75.0
# 5	cast iron	-0173	13.4	41.6

Table 3. Regression Parameters for the Approximation $\chi(h) = A\cdot h^2+B\cdot h+C$.

Specimen	A	B	C	R^2
# 1	0.0023	-0.0069	0.0138	0.999
# 2	0.0026	-0.0076	0.0121	0.999
# 3	0.0060	-0.0050	0.0118	0.999
# 4	0.0020	-0.0028	0.0063	0.999
# 5	0.0070	-0.0050	0.0125	0.999
	$\overline{A_1}$	$\overline{B_1}$	$\overline{C_1}$	
relative depth of cut $\chi(\Phi)$	1.226	-0.277	0.037	0.999

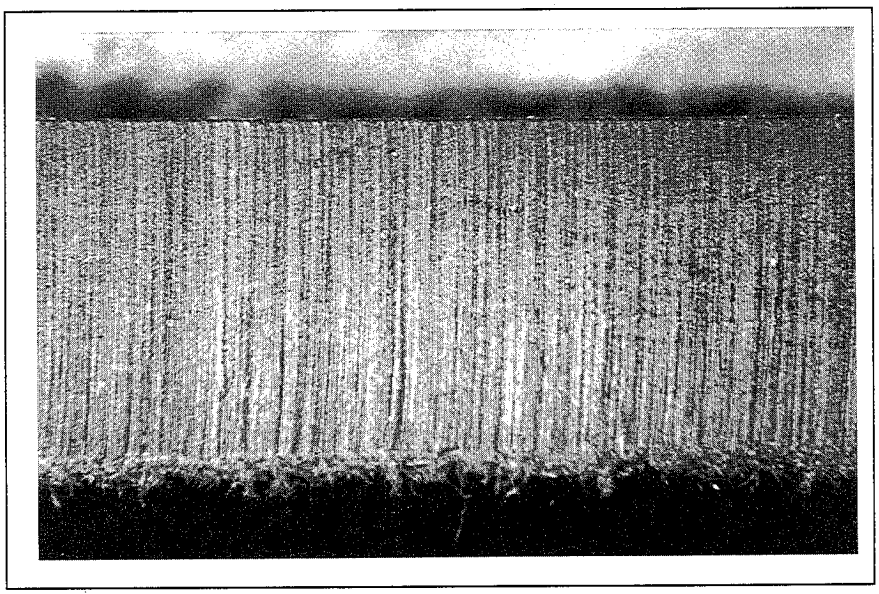

Figure 1. Cutting Front in Thermoplastics During Water Jet Cutting
(Photo: Univ. of Hannover).

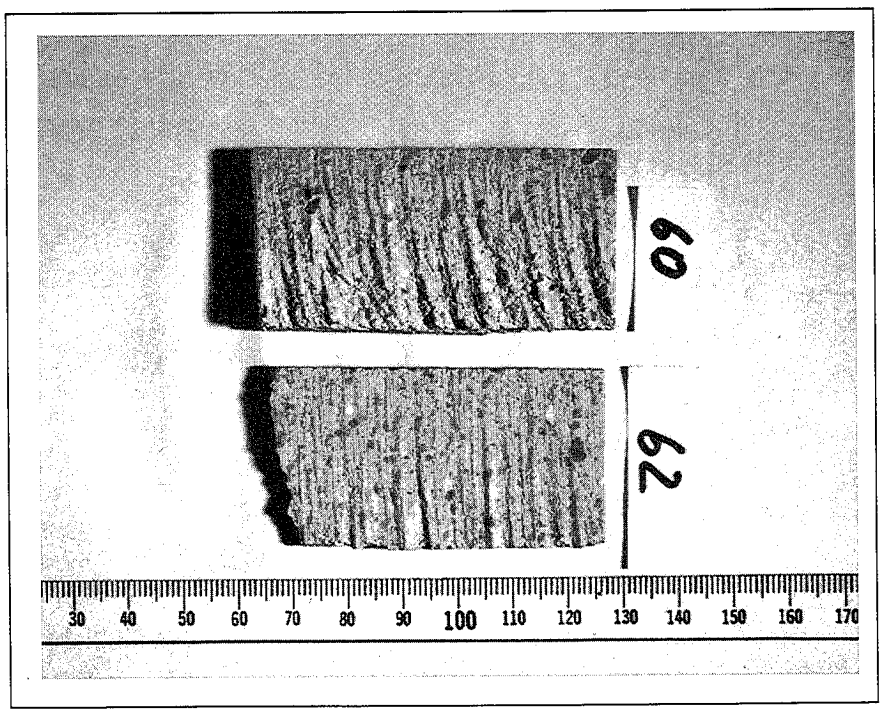

Figure 2. Cutting Front in Ceramics During Abrasive Water Jet Cutting.

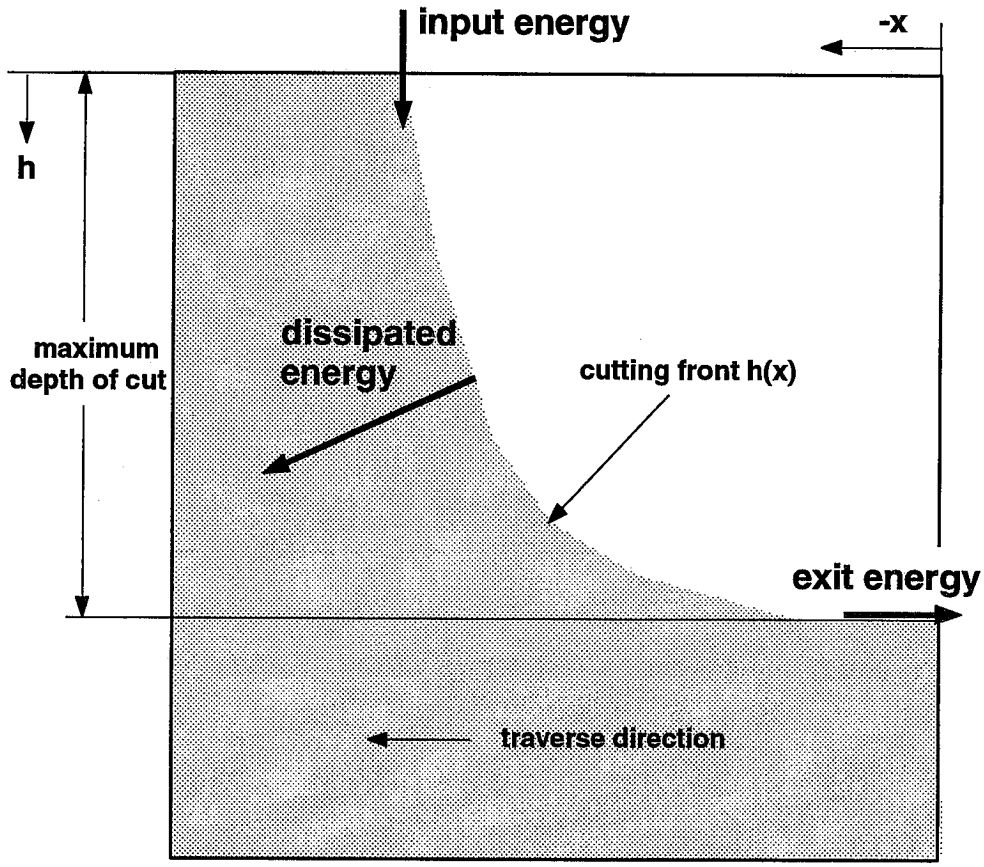

Figure 3. Simplified Energy Balance of the Jet Cutting Process.

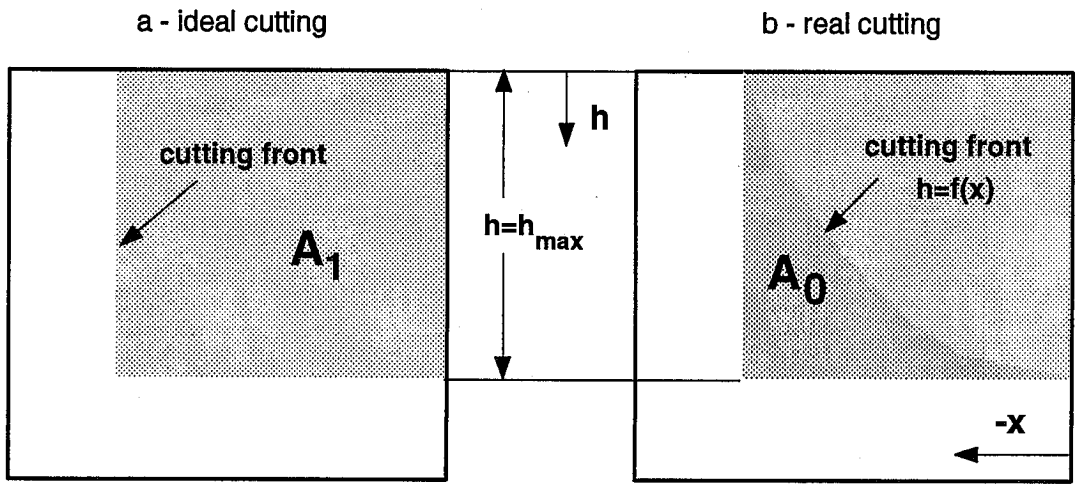

Figure 4. Comparison Between Ideal Cutting Without Energy Losses and Real Cutting with Water Jets.

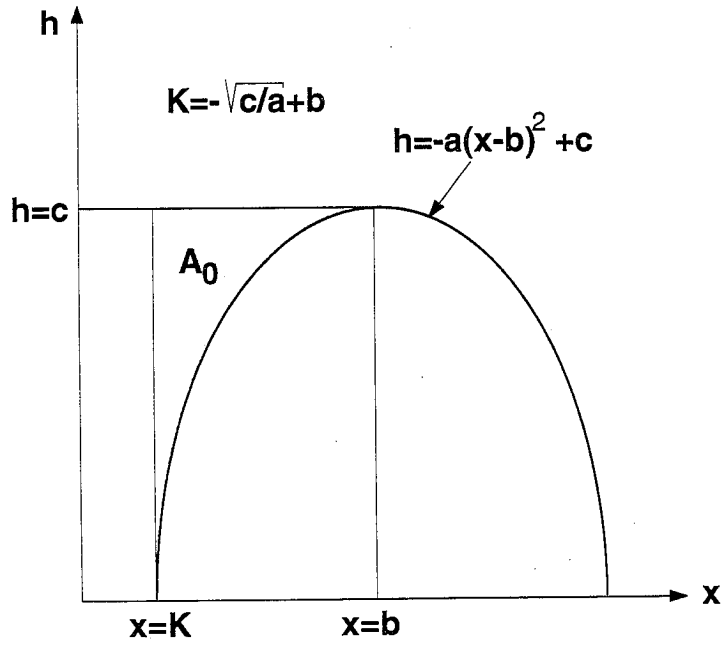

Figure 5. Parabolic Model of the Water Jet Cutting Process.

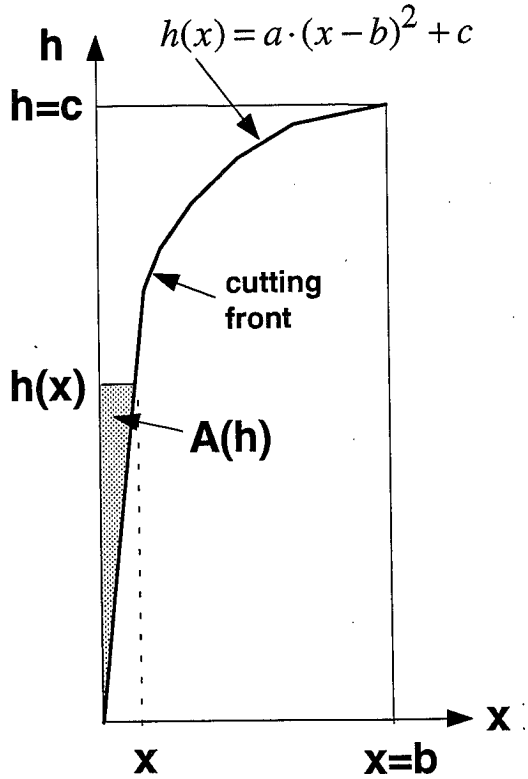

Figure 6. Structure and Partition of the Model Area.

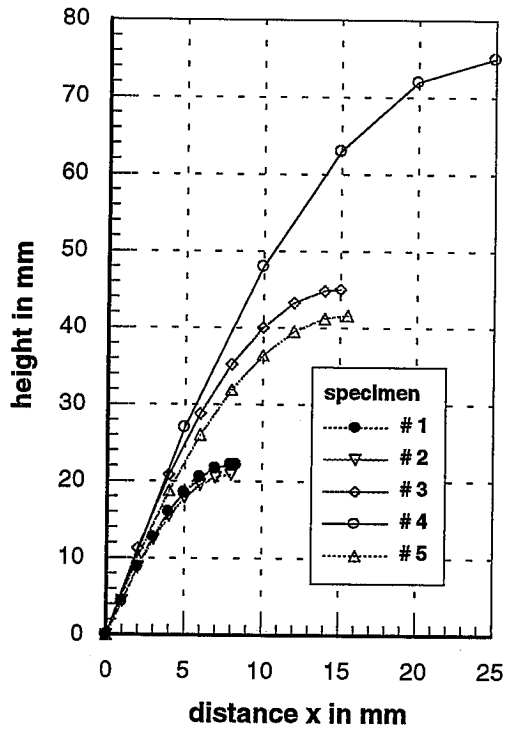

Figure 7. Parabolic Models of the AWJ Generated Cutting Fronts.
(Regression Parameters are Given in Table 2)

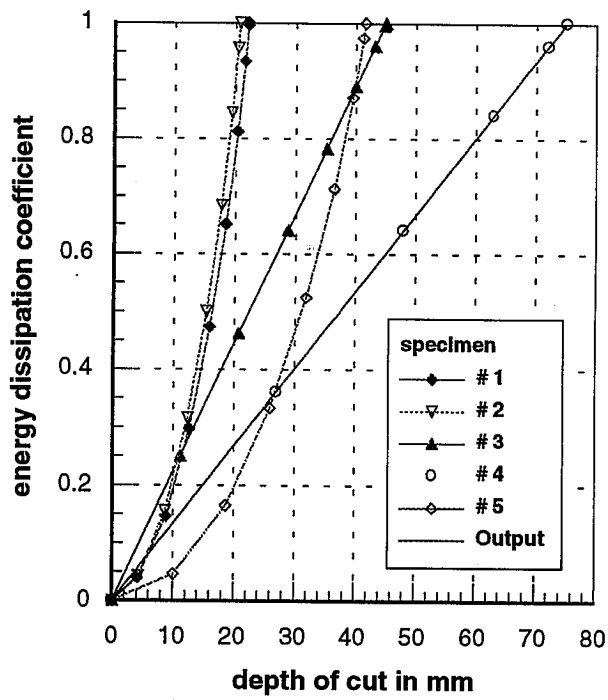

Figure 8. Relation Between Depth of Cut and Relative Energy Dissipation.
(Regression Parameters are Given in Table 3)

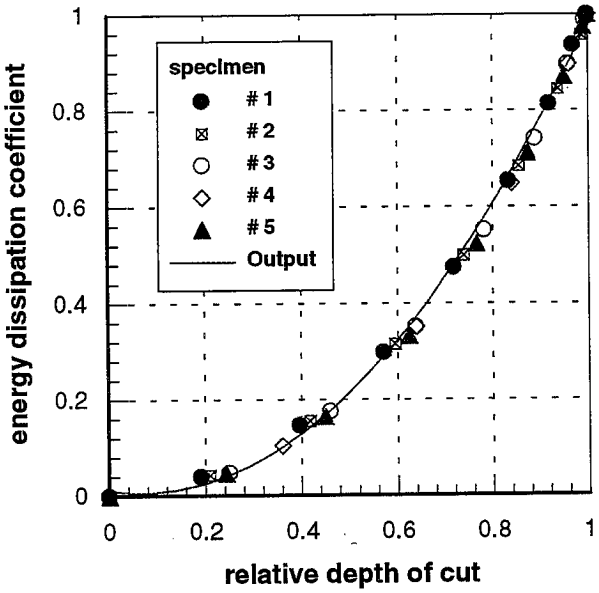

Figure 9. Relation Between Relative Depth of Cut, $\Phi=h/h_{max}$, and Relative Energy Dissipation Parameter, $\chi(\Phi)$. (Regression Parameters are Given in Table 3)

8th American Water Jet Conference
August 26-29, 1995: Houston, Texas

Paper 62

IMPULSIVE WATER JET UNDER WATER

G.A. Atanov and A.N. Semko
Donetsk State University
Donetsk, 340055, Ukraine

ABSTRACT

The paper deals with motion of impulsive water jets and their interaction with the target material under water. The mathematical model of the process is built, calculations are carried out for a real hydro-cannon jet. Distribution of the hydrodynamic parameters on the target material is obtained. Influence of the surrounding water on the jet pressure and the target and hydro-cannon parameters is estimated.

Organized and Sponsored by the Water Jet Technology Association.

1. INTRODUCTION

A compilation of different applications of impulsive water jets were summed up in works by Atanov, 1987; Atanov, 1991; Ljatkher, 1974; Water.., 1971. A number of advantages of the jets have been identified and can be formulated as following:

1. The technique is highly efficient at relatively low power consumption.
2. The need for mechanical tools is eliminated thus making the cost of operations more economical.
3. Since the machine is a non contact tool, no thrust force is involved.
4. Small size and relatively light weight contribute to high mobility and render the device ideal for multitask operations such as, making grooves for drainage or holes for inserting support legs, etc.
5. Simplicity of design makes it possible to mechanize and automate underground mining operations particularly in formations where rocks of high hardness and any abrasiveness are involved.
6. Contributes to the health and safety of the workers by improving the working environment and hence to the overall productivity.

The above investigations are devoted to impulsive water jets in the air. There is series of underwater works where using the jets can give essential effect too. Partially, these questions were considered in work Cooley et al., 1970. But there are no systematic investigations which could give more or less full ideas about motion of impulsive water jets under water and their interaction with the target material.

2. DESCRIPTION OF THE PROCESS

Let us consider an impulsive water jet out flowing from the installation nozzle in a semi-space filled with water (Figure 1). At some distance L from the nozzle outlet is located a flat target. The goal of the investigation is determination of hydrodynamic parameters of impulsive jet moving in water and its influence on the target.

Let us make the following assumptions. Water is considered to be compressive and ideal, the flow is believed to be adiabatic and axis-symmetrical, the target material is considered to be non-deformed. Axis x of a cylindrical coordinates system is directed along the installation axis, the beginning of the coordinates is located in the nozzle outlet. The initial moment is when water starts to outflow.

Under the above conditions the water flow is described with equations of unsteady gas dynamics. Let us write down the governing system of equations in a divergent form:

$$\begin{gathered}\frac{\partial}{\partial t}(\rho r)+\frac{\partial}{\partial x}(\rho u r)+\frac{\partial}{\partial r}(\rho v r)=0,\\ \frac{\partial}{\partial t}(\rho u r)+\frac{\partial}{\partial x}[r(p+\rho u^2)]+\frac{\partial}{\partial r}(\rho u v r)=0,\\ \frac{\partial}{\partial t}(\rho v r)+\frac{\partial}{\partial x}(\rho u v r)+\frac{\partial}{\partial r}[r(p+\rho v^2)]=p,\\ p=B[(\rho/\rho_0)^n-1],\end{gathered} \tag{1}$$

where t is time; x and r are an axial and radial coordinates; u and v are the axial and radial speed; p and ρ are pressure and density of water; B = 300 MPa, n = 7.15, ρ_0 = 1000 kg/m^3 are constants in the water state equation (Teit's equation). The initial conditions are discontinuous. In field G filled with water its velocity is equal to zero:

$$u(0,x,r)=0;\quad v(0,x,r)=0;\quad p(0,x,r)=p_0;\quad x,r\in G; \tag{2}$$

$$u(0,l,r)=u_e;\quad v(0,x,r)=0;\quad p(0,x,r)=p_e;\quad 0<r<r_0; \tag{3}$$

were p_o is the initial water pressure; l is the nozzle outlet coordinate; u_e and p_e are the speed and pressure on the nozzle outlet; r_o is the nozzle radius.

The boundary conditions are:

on the target surface:

$$u(t,L,r)=0;\quad 0<r<\infty; \tag{4}$$

on the installation surface:

$$w_n(t,x_s,r_s)=0; \tag{5}$$

at some large distance from the installation:

$$u(0,x,r)=0;\quad v(0,x,r)=0;\quad p(0,x,r)=p_0;\quad x,r\to\infty. \tag{6}$$

Here w_n is a normal component of water speed, x_s and r_s are coordinates of the installation surface. In the nozzle outlet there are no boundary conditions. Here parameters are found

by jointly solving the above external problem and the internal ballistics problem of the installation.

The above formulated problem is solved numerically with the help of a shock-copturing method (Godunov, et al., 1974) that was spread to fluid flows in the works (Atanov, 1974; Atanov, 1975). The method is considered in detail by Atanov (1987). There is a peculiarity of its application here. It is that the jet surface is not marked out and calculations are carried out in all the field filled with water. The boundaries of this field are given far enough from the jet so that disturbances from the boundaries did not influence the jet. The difference grid was immovable and right-angled. It is shown in Figure 1.

3. RESULTS OF CALCULATIONS

First, let us consider the dependence of the jet pressure on the target as a function of the distance from it. In order to reveal the influence of the surrounding water on the jet parameters, in a clear appearance, let us consider a jet flowing with a constant speed u_o. Below are some results presented for the following parameters: u_o = 1000 m/s, the nozzle outlet diameter d_o = 20 mm, pressure in the surrounding water p_o = 0.1 MPa. In Figure 2, pressure on the target that is located at different distances from the nozzle outlet is shown. If the distance is small ($L < d_o$), the maximum pressure on the target reaches the value of about 850 MPa. This pressure is caused by the impact action. The same pressure will be if the jet moves in the air. Increase of the distance leads to the fast decrease of the pressure to value of 450 MPa that corresponds to the jet dynamic head. Then for $5d_o \le L \le 10d_o$ the pressure remains relatively constant.

Distribution of pressure along the target surface for $L = 2.5d_o$, $5d_o$ and $10d_o$ is shown in Figure 3 (curves 1, 2, 3 respectively). As we can see the diameter of the zone of the heightened pressure is commensurable with the jet diameter. Pressure at distance from the center $r = d_o$ (twice more then the jet radius) is only 5-10% from the pressure in the center.

Below some results of calculations for a real hydro-cannon are shown. Its parameters are: nozzle outlet diameter d_o = 20 mm, barrel diameter d_b = 40 mm, nozzle length l = 135 mm, barrel length L_b = 400 mm, and water discharge mass m = 0.4 kg. Distance from the nozzle outlet to the target L = 200 mm. Water in the hydro-cannon was accelerated and ejected by the products of the powder combustion (Atanov, 1992). In Figure 4, the speed of flow in the nozzle $t \le t_f$ and one of out flowing $t \ge t_f$ for this hydro-cannon is shown. As we see, the speed of out flowing has a pulsating character that is explained by a wave character of the process in the hydro-cannon.

Figure 5 shows dependence of pressure in the target center as a function of time. The maximum pressure is observed at the initial stage of interaction and it is equal to 600 MPa. This is more than the jet dynamic head but less than the impact pressure for the given speed of out flowing (about 850 MPa). Influence of the surrounding water that has to be pierced is apparent in this. Later the pressure on the target follows the speed of out flowing.

Influence of the surrounding water parameters on the internal hydro-cannon ones was estimated. If the pressure was 1 MPa (that corresponds to the depth of 100 m) an appreciable influence was discovered at distance L < 50 mm from the nozzle outlet.

4. CONCLUSION

It is shown that motion of impulsive hydro-cannon jets under water can be calculated by a shock-capturing method without any marking out their surface. Action of the jet on a target is the same approximately as it is in the air at distance to 20 diameters of the nozzle outlet.

5. ACKNOWLEDGMENT

The research described in this publication was made in part by Grant No U96000 from the International Science Foundation.

6. REFERENCES

Atanov, G.A., "Calculation of hydro-cannon pulse by the method of the break disintegration," *Gidrodinamika*, Kyiv, Naukova Dumka, Vol. 30, pp.52-57, 1974 (In Russian).

Atanov, G.A., "Calculation of Hydrodynamic cumulation," *Zhurnal Vychislitelinoj Matematiki i Matematicheskoj Fisiki*. Vol. 3, No. 3, 1975, pp. 258-263 (In Russian).

Atanov, G.A., "The Hydro-impulsive Installation for Breaking Rock Formation in the Mines," Vyshcha Shkola, Kiev, 1987 (In Russian).

Atanov, G.A., "The impulsive water jetter is a qualitatively new machine for rock breaking," *Proceeding of the 6th American Water Jet Conference*, pp. 9:103-126, Water Jet Technology Association, St. Louis, Missouri, 1991.

Atanov, G.A. "The impulsive water jet device: a new machine for breaking rock," *International Journal of Water Jet Technology*, Vol. 1, No. 2, pp. 85-91, 1991.

Atanov, G.A., "Powder impulsive water jetter," *Proceedings of the 11th International Conference On Water Jet Cutting Technology*, pp. 295-303, 1992.

Cooley, W.C., and Clipp, L.L., " High-pressure Water Jets for Undersea Rock Excavation," *J. Eng.Ind* (ASME), Vol. 281, No. 5, pp. 281-287, 1970.

Godunov, S.K., et al., "Numerical solution of the many-dimensional gasdynamics problems," Moscow, Nauka, 1976 (In Russian).

Ljatkher, V.M., "Hydroimpulsive breaking rocks," *Gidrotekhnicheskoe Stroitelstvo*, No. 10, pp. 72-78, 1974 (In Russian).

"Water Jet Mining," *Colliery Guardian*, Vol. 219, No. 11, pp. 524-527, 1971.

7. NOMENCLATURE

B, n	constants of the water state equation
d_b	barrel diameter
d_o	nozzle outlet diameter
G	semi-space filled with water
L	distance to the target
L_b	barrel length
l	nozzle length
$\dot{m}$	water discharge mass
p	pressure
p_e	pressure in the nozzle inlet
p_o	initial pressure
r	radial coordinate
r_s, x_s	coordinates of the installation surface
r_o	nozzle radius
t	time
t_f	time of flowing into the nozzle
x	axial coordinate
u	axial velocity
u_e	velocity in the nozzle inlet
u_o	initial jet velocity
v	radial velocity
w_n	normal component of the water velocity
ρ	water density

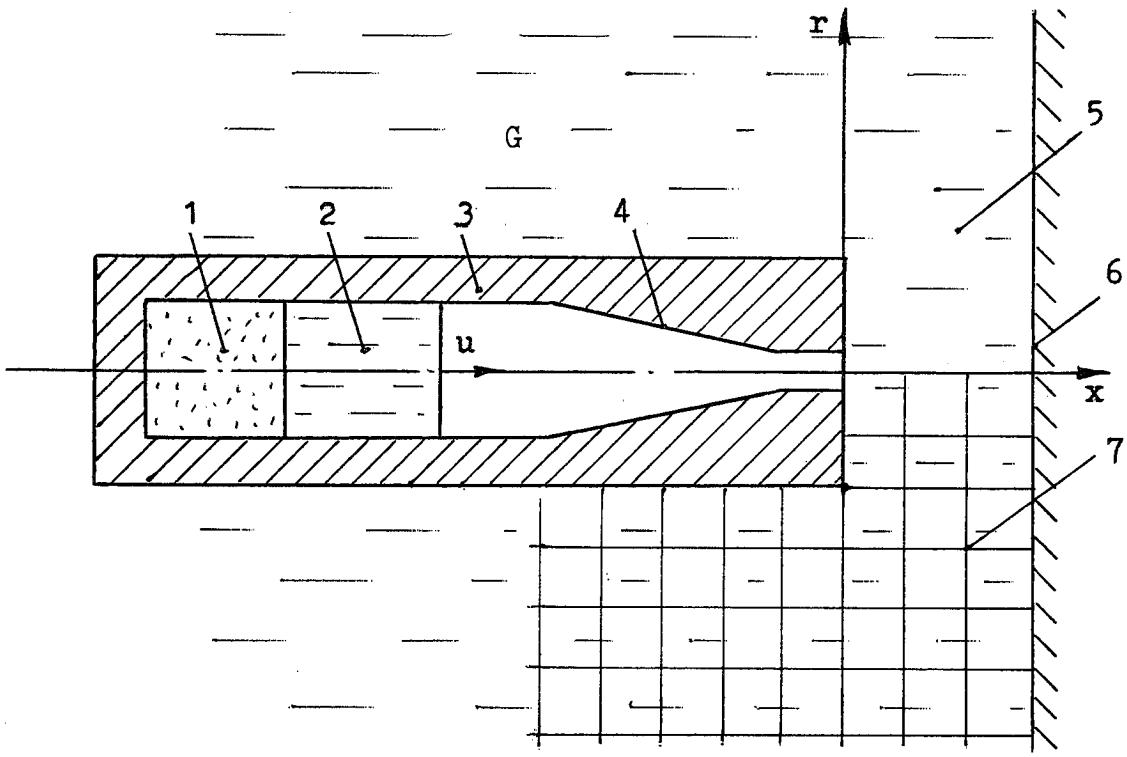

Figure 1. Hydro-cannon under water.
1 - pressured gas; 2 - water discharge;
3 - barrel; 4 - nozzle; 5 - surrounding
water; 6 - target; 7 - difference grid.

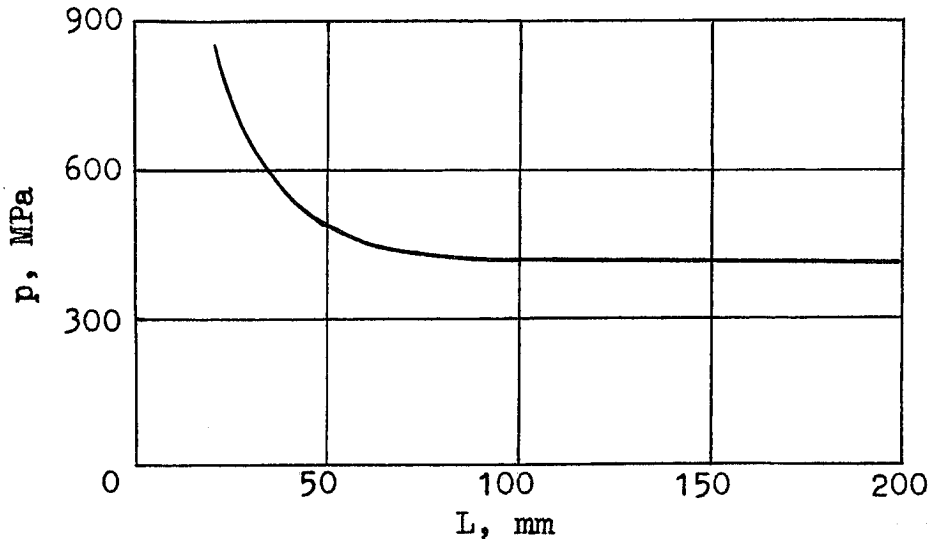

Figure 2. Plot of pressure in the target center as a function of distance to installation.

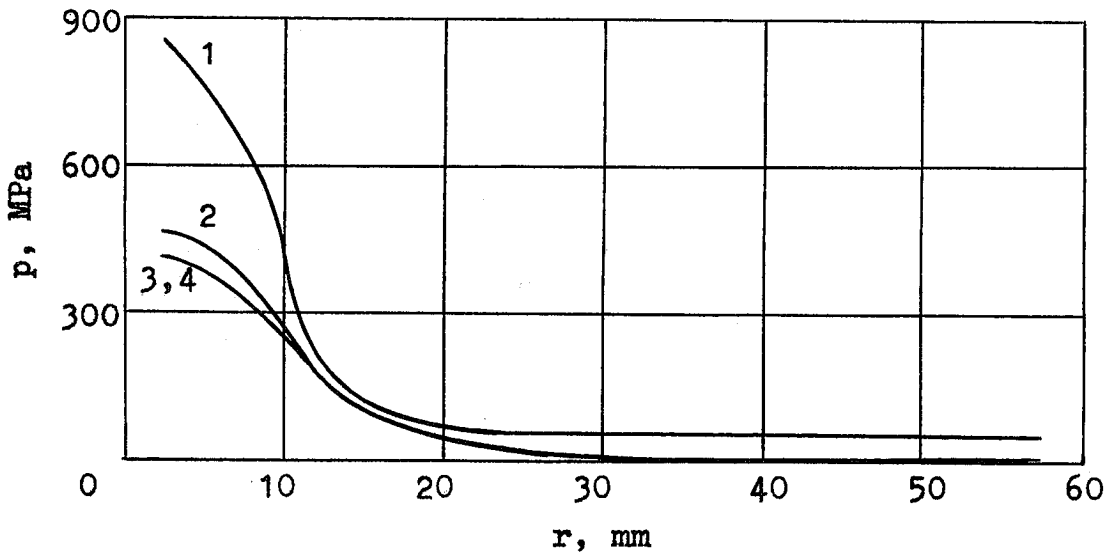

Figure 3. Distribution of pressure along the target.

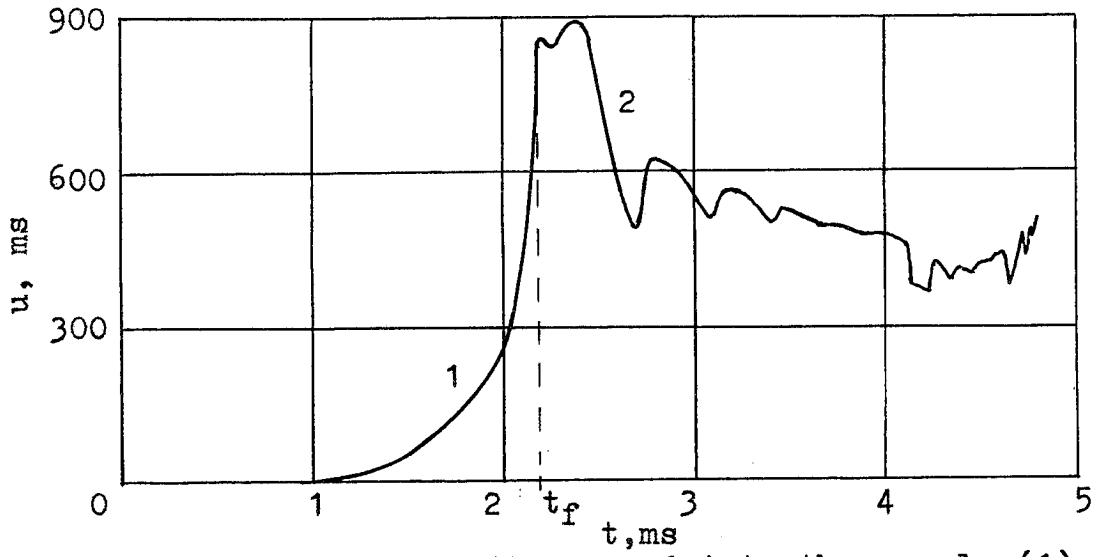

Figure 4. Plot of the flow speed into the nozzle (1) and outlet speed (2).

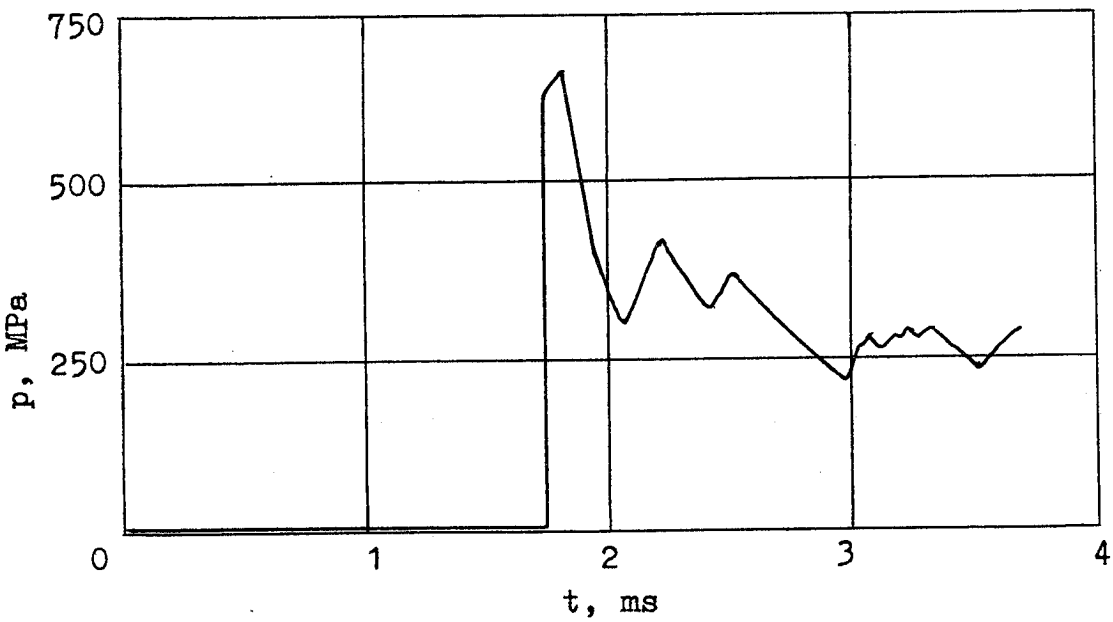

Figure 5. Plot of pressure on the target center as a function of time for the powder hydro-cannon.

8th American Water Jet Conference
August 26-29, 1995: Houston, Texas

Paper 63

PRODUCING IMPULSIVE WATER JETS TO EXTINGUISH UNDERGROUND FIRES

G.A . Atanov, E.G . Evseeva
Donetsk State University
Donetsk, 340055, Ukraine

S.T . Aksentiev, V.A . Egorov
Scientific and Manufacturing Association
for Main Rescuie Work "Respirator"
Donetsk, 340032, Ukraine

ABSTRACT

The analysis of the impulsive water jet devices in which water is ejected by pressured gas is fulfilled. Mathematical models of the pulses are built, results of calculations are given . Results of experimental investigations are described, some properties of the pulse are installed.

Organized and Sponsored by the Water Jet Technology Association.

1. INTRODUCTION

Fires are a dangerous and widespread kind of accidents in the coal mines. Liquidation of a fire is a complex and long-term process. In Ukraine, the average duration of liquidation of a fire was about 65 hours and the average labor-consumption was about 1000 man-hours in 1992.

Extinguishing an underground fire begins with its localization by different means (water-screens, temporary partitions and so on). Then steady water jets are used in the fire zone. In practice, a fire often oversteps the limits of the initial fire zone. That is explained with small efficiency of extinguishing by steady jets because the jet range is small (Guttler, 1972). The last is explained with (i) a low jet pressure (the normative pressure into the water main is equal to 0.5 MPa, the jet length being about 12 m) as well (ii) a limited height of main workings.

As investigations (Abduragimov, 1978) have shown, if jets are steady, only from 5 to 10% of their water are used to put out the fire. The rest of water is lost and it does not take part in the extinguishing. At the same time, there is often deficiency of water in practice.

Dispersion of water increases efficiency of extinguishing, essentially the water jet turns into a short torch of the sprayed water. Its length is less than a permissible distance to the fire place that is determined by the heat radiation.

Thus, in order to increase efficiency and decrease duration of extinguishing a fire by water jets, it is necessary: (i) to increase the jets length, (ii) increase intensity of the sprayed water feed, (iii) decrease the total water consumption. This can be addressed with the help of impulsive water jets.

2. DESCRIPTION OF THE JET PRODUCTION PROCESS

An impulsive water jet is a definite portion of water thrown out from some volume during a short period of time. In that way a pulse takes place. As a rule, water is ejected from the volume by a piston or high pressure gas. This can be achieved by a previously pressured gas, products of combustion of an air-petrol mixture or powder and so on (Atanov, 1987; Atanov, 1992).

Let us consider a schematic of the impulsive water jet device that is simple enough and answers the demands according to reliability and gabarits for underground conditions. It is shown in Figure 1. There is compressed gas in high pressure vessel (1). The gas pressure into buffer vessel (2) is established to be equal to the rated water pressure into barrel (3) with the help of pressure regulator (4). The barrel is filled with water through back valve (5) from the water main. Pneumatic valve (6) is opened and water is ejected from the barrel by pressured gas coming in the barrel from the buffer vessel.

The pulse process has three stages: (1) the working regime stage when water is ejected from the barrel; (2) the exhaust stage when the pressured gas outflows; (3) the filling stage when the barrel is filled with water.

While dilating and ejecting water, gas is decreasing its pressure, therefore pressure in the barrel is decreasing during the pulse too. Let us characterize this pressure decrease by the pressure lowering degree c that is determined as a ratio of the final pressure in the barrel P_f to the initial one P_i for the working regime stage:

$$c = P_f / P_i. \tag{1}$$

Let us take that gas and water are ideal and processes is adiabatic. Then we have:

$$P_f / P_i = (V_{bv} / V_f)^{\kappa}, \tag{2}$$

where V_{bv} is the buffer vessel volume; V_f is the final gas volume, k is adiabat index. The final volume $V_f = V_{bv} + V_b$, where V_b is the barrel volume (that is, the volume of the ejected water). So $c \simeq 1$ a formula follows from formulas (1) and (2) :

$$\frac{V_{bv}}{V_f} = \frac{k}{1 - c}. \tag{3}$$

Values of this ratio are given for a two-atom gas below:

c	0.95	0.90	0.85	0.80
V_{bv} / V_f	28.8	14.0	9.30	7.00

As we see, the buffer vessel volume is much more than the ejected water volume ($V_{bv} \gg V_b$) and this system does not often meet the demands according to gabarits, especially for underground conditions. It is possible to use another system without any buffer vessel and pressure regulator. In this case, pneumatic valve (6) plays a role of a throttle passing a definite gas volume.

First, let us consider the last system. The pressure into the vessel is more than one into the barrel. As gas dilates from the initial pressure in the vessel P_{vo} to the rated water

pressure in the barrel P_r (this process is adiabatic), the number of the pulses that can be made without any recharging is determined by formula

$$N = \frac{V_v}{V_b}\left[\left(\frac{P_r}{P_{vo}}\right)^{1/k} - 1\right], \tag{4}$$

where V_v is the high pressure vessel volume.

Let us denote parameters in the barrel by subscript "1" and ones in the vessel by subscript "2". While describing the adiabatic processes in the barrel and vessel (taking into account that V_2 = const) in a differential form, we have:

$$\frac{dP_1}{dt} = kP_1\left(\frac{1}{m_1}\frac{dm_1}{dt} - \frac{1}{V_1}\frac{dV_1}{dt}\right); \tag{5}$$

$$\frac{dP_2}{dt} = kP_2\frac{1}{m_2}\frac{dm_2}{dt}, \tag{6}$$

where m is the gas mass.

As gas flows from a place to another, we can write down:

$$\frac{dm_1}{dt} = -\frac{dm_2}{dt}. \tag{7}$$

The value of dm_2/dt is determined from expression [5]:

$$\frac{dm_2}{dt} = -F_p\sqrt{\frac{2k}{k+1}P_2\rho_2}\;\lambda\left(1-\frac{k-1}{k+1}\lambda^2\right)^{1/(k-1)}, \tag{8}$$

where F_p is the cross-section area of the pneumatic valve opening,

$$\lambda = \begin{cases} 1, \ for \ \ P_1 / P_2 \geq [(k+1)/2]^{k/(k-1)}, \\ \sqrt{\dfrac{k+1}{k-1}[1-(P_1/P_2)^{(k-1)/k}]}, \ for \ \ P_1 / P_2 < [(k+1)/2]^{k/(k-1)}. \end{cases} \tag{9}$$

$$\rho_2 = m_2/V_2. \tag{10}$$

The first equation (9) corresponds to a super critical flow when gas speed is sonic, the second one applies to a subcritical flow when gas speed is under sonic (Atanov, 1992).

The change of the gas volume in the barrel is determined by the volume flow of water:

$$\frac{dV_1}{dt} = F_o\sqrt{2(P_1-P_a)/\rho_w}, \tag{11}$$

where F_o is the outlet cross-section area, P_a is the atmospheric pressure, ρ_w is the water density.

Thus, from equations (5)-(11), we have a system that describes the working regime stage:

$$\begin{gathered} \frac{dP_1}{dt} = kP_1\left(\frac{1}{m_1}\frac{dm_1}{dt}-\frac{1}{V_1}\frac{dV_1}{dt}\right); \\ \frac{dP_2}{dt} = kP_2\frac{1}{m_2}\frac{dm_2}{dt}; \\ \frac{dm_1}{dt} = -\frac{dm_2}{dt}; \\ \frac{dm_2}{dt} = -F_p\sqrt{\frac{2k}{k+1}p_2\frac{m_2}{V_2}}\ \lambda\left(1-\frac{k-1}{k+1}\lambda^2\right)^{1/(k-1)}; \\ \frac{dV_1}{dt} = F_o\sqrt{2(P_1-P_a)/\rho_w}. \end{gathered} \tag{12}$$

The initial conditions are:

$$P_1(0) = P_m, \quad P_2(0) = P_{vo}, \quad V_1(0) = V_{10},$$
$$m_1(0) = P_m V_{10}/RT, \quad m_2(0) = P_{vo} V_v/RT, \tag{13}$$

where P_m is pressure into the water main; V_{10} is the initial gas volume in the barrel; R is the gas constant; T is temperature. Generally speaking, $V_{10} = 0$, so all the barrel volume is filled with water, and equation (5) cannot be solved. Therefore it is possible to put $V_{10} = (0.01 - 0.05)V_b$.

After all water has been ejected the following stage begins, namely the exhaust stage. There are two special circumstances here: (i) volume V_1 = const; (ii) gas outflow is supercritical. While using equations (8)-(10), we can write down analogous:

$$\frac{dm_1}{dt} = -F_a \left[\frac{2}{k+1}\right]^{\frac{k+1}{2(k-1)}} \sqrt{kP_1\rho_1}; \tag{14}$$
$$\rho_1 = m_1/V_b.$$

On excluding m from system (14) and using the adiabat equation, we get a differential equation for P_1:

$$P_1^{(1-3k)/2k} \frac{dP_1}{dt} = \frac{k}{V_b}\sqrt{kP_{11}^{1/k}/\rho_{11}}. \tag{15}$$

Its solution is as follows:

$$P_1 = P_{11}^{(1-k)/2k} + \frac{k}{V_b}\sqrt{kP_{11}^{1/k}/\rho_{11}(t_1 - t)}, \tag{16}$$

where t_1 is the time at the beginning of the exhaust stage. The time of its end t_2 is found from expression (16) by substitution $P_1 = P_m$. In formulas (15) and (16), the second subscript corresponds to t_1.

At the time t_2, the third stage starts. The back water admission valve opens and water flows into the barrel, ejecting gas. This process is described by a system of equations analogous to system (12) by condition $dm_2/dt=0$:

$$\frac{dP_1}{dt} = kP_1\left(\frac{1}{m_1}\frac{dm_1}{dt} - \frac{1}{V_1}\frac{dV_1}{dt}\right);$$

$$\frac{dm_1}{dt} = -F_b\sqrt{\frac{2k}{k+1}P_1\frac{m_1}{V_1}}\,\lambda\left(1-\frac{k-1}{k+1}\lambda^2\right)^{1/(k-1)}; \qquad (17)$$

$$\frac{dV_1}{dt} = F_0\sqrt{2(P_1-P_a)/\rho_w}.$$

where F_b is the cross-section area of the back valve opening,

$$\lambda = \begin{cases} 1, \ for \ \ P_1/P_a \geq [(k+1)/2]^{k/(k-1)}, \\ \sqrt{\frac{k+1}{k-1}[1-(P_1/P_a)^{(k-1)/k}]}, \ for \ \ P_1/P_a < [(k+1)/2]^{k/(k-1)}. \end{cases} \qquad (18)$$

The initial conditions for system (17) are the parameters' final values at the end of the second stage.

Now the cross-section area of the pneumatic valve opening must be determined. It is found from condition (7) if $P_1 = P_r$, and we have from equations (8) and (11):

$$F_p = \frac{F_a\rho_{10}}{\lambda}\sqrt{\frac{k-1}{k}\frac{2P_{10}}{\rho_w P_{20}\rho_{20}}}\left(1-\frac{k-1}{k+1}\lambda^2\right)^{1/(k-1)}. \qquad (19)$$

where the second subscript corresponds to the pulse beginning. Hence it follows that each pulse of the pulses' succession must be carried out by its own value of F_p.

Some calculations results are shown in Figure 2 for the following parameters: the rated pressure in the barrel $P_2 = 3.0$ MPa, the barrel volume $V_b = 6$ l, the outlet diameter $d_o =$ 20 mm, the initial volume of the high pressure vessel $V_v = 50$ l. The device has no buffer vessel.

The number of pulses without any recharging is 8. The working regime stage lasts 0.26 s, all the pulse does 0.61 s. All the pulses have the same initial pressure in the barrel that is equal to the rated one. During the pulse, pressure in the barrel is decreasing and curve 1 shows the final one for each pulse. This pressure is less for each subsequent pulse.

Curve 2 gives the cross-section area of the pneumatic valve opening as a function of the pulse number. As we see, the following ones increase very fast. This must be secured by the device construction. This is a shortcoming of the system without any buffer vessel.

If the buffer vessel is an organic part of the device, there is $P_1 = P_2$, $P_{10} = P_r$. Then equations (12) for the first stage is reduced to one equation according to V if $P_a \ll P_r$ is neglected:

$$V_1^{k/2} \frac{dV_1}{dt} = F_o \sqrt{2P_r V_{bv}^k / \rho_w}. \tag{20}$$

Its solution is:

$$V_1 = \frac{k+2}{2} \left(\frac{2}{k+2} V_{bv}^{(k+2)/2} + F_o \sqrt{\frac{2P_r V_{bv}^k}{\rho_w}}\, t \right)^{2/(k+2)}. \tag{21}$$

From the adiabatic equation we have:

$$P_1 = P_r (V_{bv} / V_1)^k. \tag{22}$$

The cross-section area of the pneumatic valve opening must be big enough so that there will not be any throttling. This is possible if the following condition is fulfilled:

$$F_p \geq (1 - 1.5) F_o. \tag{23}$$

3. EXPERIMENTAL INVESTIGATIONS

An experimental impulsive water jet device for extinguishing fires has been done. The working device is shown in Figure 3.

As a result of the experiments, sufficient accuracy of the above pulse description was corroborated. But some circumstances, which are not taken into account by the theory, were revealed.

First, only about two thirds of water outflow from the barrel as a continuous jet (a slug regime). Then some pulsations arise with frequency of 40 to 50 Hz and the rest of water outflows as an air-water mixture.

Second, there is an optimum rated water pressure which secures a maximum jet range. In general, the increase of the rated pressure increases the jet range. But other processes proceed in parallel, namely disintegration and dispersion of the jet. These processes are final for any jet. The increase of the rated pressure increases their intensity too. Beginning with same rated pressure value, the disintegration goes out in the foreground and the jet range

stops to rise. This rated pressure is the optimum one. If the rated pressure is more than the optimum one, the jet disintegrates before.

Concrete values of water ejected by the slug regime and the optimum rated pressure depend on concrete parameters of the device. For example, the experimental device has the optimum rated pressure about 1.7 MPa, the jet range being from 31 to 32 m. We think the above mentioned value can be increased with the help of special engineering solutions.

The ability of the device for extinguishing a fire was tested. A round griddle of 1 m diameter was filled with petrol. The griddle was located at distance of 25 m from the device. Petrol was set on fire and the extinguishing was started in 60 seconds. This process was repeated several times. All the tests gave a good result. About 55% ejected water (about 1.3 liter per pulse) took part in the extinguishing. The fire has been put out an average during 2.8 seconds. The power of the water feeding (the water volume taking part in extinguishing per m^2 per second) was twice more than a normative one for steady jets.

4. CONCLUSION

It is shown that the ability of impulsive jets for extinguishing a fire is more than one of steady jets. Methods of theoretical and experimental investigations of impulsive water jet device are elaborated. Further investigations must be directed on increasing the jet range, decreasing the water and energy consumption, and studying thermal processes in underground workings by intensive extinguishing with help of high energy impulsive water jets.

5. ACKNOWLEDGEMENT

The research described in this publication was made possible in part by Grant No U96000 from the International Science Foundation.

6. REFERENCES

Abduragimov, M.M. and Javorskiy, G.Ja., "The increase of the water extinguishing possibility by means of perfection of its feedig to the fire zone," *Protivopozharnaja technika i bezo-pasnost*, No. 4. Moscow, VIPTSH, pp. 75-82, 1978 (In Russian).

Atanov, G.A., "The hydro-impulsive installation for breaking rock formation," Vyscha Shkola, Kyiv, 1987 (In Russian).

Atanov, G.A., "Powder impulsive water jetter," *Proceedings of the 11th International Conference on Water Jet Cutting Technology*, September, St. Andrews, Scotland, pp. 295-303, 1992.

Atanov, G.A., "Gasdynamics," Vyscha Shkola, Kyiv, 1992, (In Russian).

Guttler, E. "Normal pressure and high pressure: a comparison", *Fire International*, Vol. 4, No. 37, pp. 94-101, 1972.

7. NOMENCLATURE

c	pressure lowering degree
F_b	cross-section area of the water back valve opening
F_o	outlet cross-section area of the nozzle
F_p	cross-section area of the pneumatic valve opening
P_a	atmospheric pressure
P_m	water main pressure
P_r	rated water pressure
P_f	final gas pressure
P_1	gas pressure in the barrel
P_2	gas pressure in the vessel
V_b	barrel volume
V_{bv}	buffer vessel volume
V_v	vessel volume
V_1	gas volume in the barrel
V_2	gas volume in the vessel
R	gas constant
T	gas temperature
k	gas adiabat index
m_1	gas mass in the barrel
m_2	gas mass in the vessel
t	time
ρ_w	water density

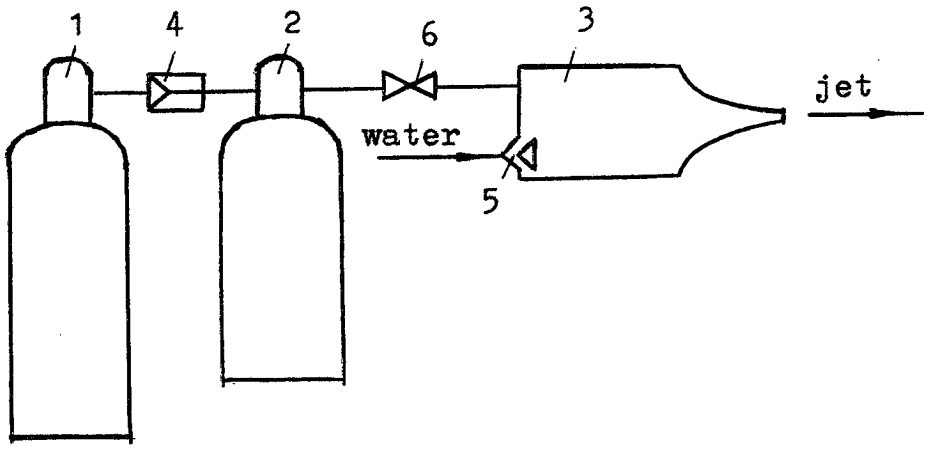

Figure 1. The impulsive water jet device.
1 - high pressure vessel; 2 - buffer vessel;
3 - barrel; 4 - pressure regulator; 5 - water
back valve; 6 - pneumatic valve (throttle).

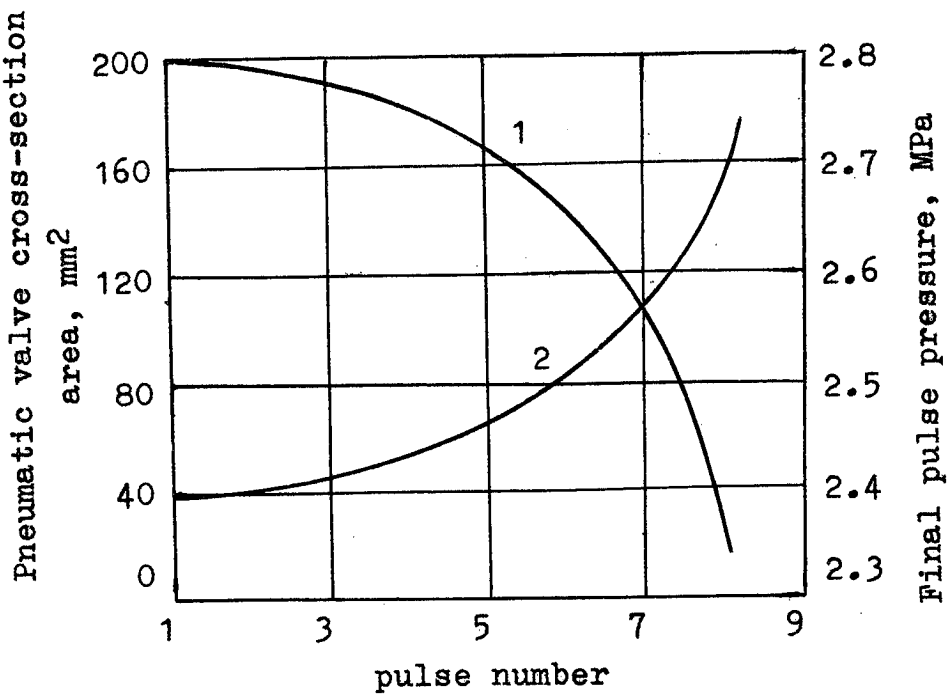

Figure 2. Plot of the final pulse pressure (1) and pneumatic valve cross-section area (2) as a function of the pulse number.

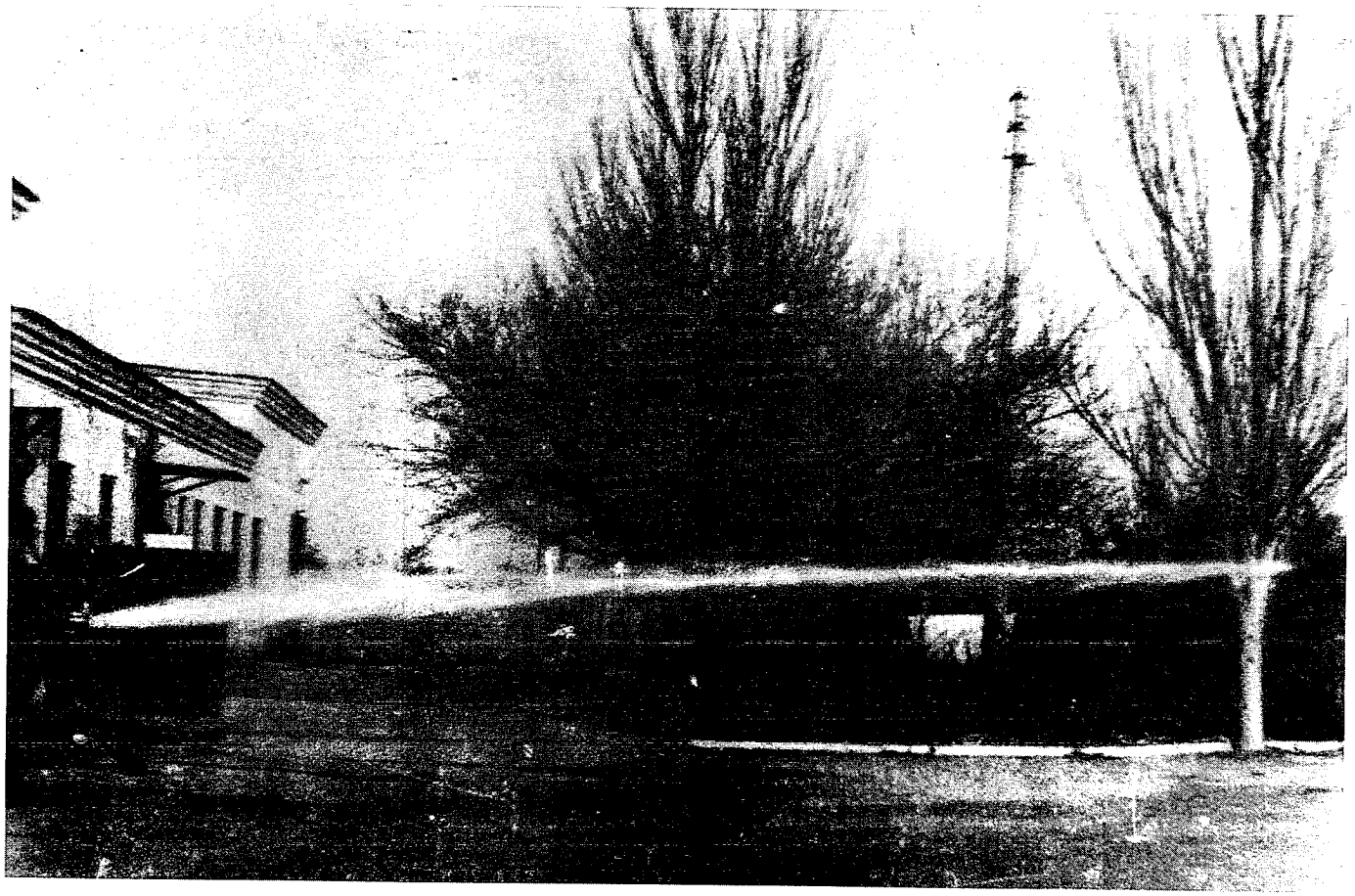

Figure 3. The working impulsive water jet device.

8th American Water Jet Conference
August 26-29, 1995: Houston, Texas

Paper 64

EMPIRICO-ANALYTICAL INVESTIGATIONS OF COAL SEAMS BREAKING PROCESS WITH PLAIN WATER JETS

B.V. Radjko
Ukrainian Research and Design Institute of Coal Hydromining,
Oboronnaya 34, Lugansk 348017, Ukraine

ABSTRACT

Experimental and theoretical studies of coal seam breaking with plain water jets performed in different basins allow constructing a satisfactory method for technological calculations. This problem is also addressed using the empirico-analytical method of statistical phenomena investigations. A mathematical model of a coal face breaking process with plain water jets taking into account their hydraulic parameters, nature factors, interaction between water jets and coal block etc. was constructed. This mathematical model may be used to analyze the influence of some jet hydraulic parameters on the broken coal mass.

Organized and Sponsored by the Water Jet Technology Association.

1. INTRODUCTION

Plain water jets are used in some Donbass basin collieries for coal breaking in pillar mining and entry driving. There are some advantages of underground water jet breaking technology: remotability of coal getting and utilizing of the post breaking water for removal coal mass from a face by gravity in the pulp state. It gives possibility to cut coal from a face without any roof support and using transport equipment, improves safety of work. Nevertheless, there is no expansion of water jet breaking technology to other collieries. Supposed reasons of that are as follows. For cutting coal from a face and transporting it to the surface, the large masses of water are used.

Because of that there are uncomfortable wet conditions in the faces to work. Besides, using such a large volume of head water stipulates a high consumption of energy per ton. To improve an effect of this technology application and make short some negative consequences, it will be useful to get knowledge about water jet breaking mechanism. The experimental and theoretical studies have been performed in different basins to improve an effect of plain water jet breaking process of coal seams in underground mining. Nevertheless, there were shortages of results (Sigaev et al., 1986).

The process of hydraulic breaking of coal seams with plain water jets in underground mining is not yet understood enough because of changeable interaction character between the hydromonitor jet and coal block and also of some obstacles in investigation.

There is a large variety of the physico-mechanical properties of the coal seams depended on the ground condition and complicated non-forecasting dynamics of the massif internal strain. Besides, the coal face is moved off gradually while breaking process is provided and the structure and parameters of the hydromonitor water jet changes constantly in places of contact too. In this connection serious difficulties arise on the way of study.

The laboratory experiments do not allow to make clear the mechanism of coal seams water jet breaking because of the impossibility to model their physico-mechanical properties as in nature. At the same time the large scale experiments in acting mines are very difficult to be performed because of interference into the process of production. Therefore it is necessary to search for other methods to cover all heterogeneity of the effective factors to take into account their interaction and, this way, to know the mechanism of the coal seams hydraulic breaking with plain water jets.

The empirico-analytical method of the statistical data investigation worked out by the other was used to form the mathematical model of coal face hydraulic breaking with plain water jets. The joint effect of the hydraulic jet parameters, character and interval of the water jet action, physico-mechanical properties of the coal seams were taken into account by the mathematical model. That gives possibility to calculate the breaking process rate, to examine influence of different factors, to select the rational parameters of hydraulic breaking etc.

To receive information about the correctness of the affecting factors registration in the constructed mathematical model of face hydraulic breaking one can look at Figure 1. The

symmetrical distribution of the empiric dots relatively to the calculate ones is a basis to judge about that.

The positive experience of the empirico-analytical investigation method for studying of coal seams hydraulic breaking with plain water jets gives a certain hopefulness for its successful use in testing regimes and parameters of water jet cutting technology for rock, concrete, metal and other applications.

2. THE NEW STATISTICAL APPROACH

It is clearly that statistical data formed in the production conditions display technology process special features in full details and they are most accessible for studying the mechanism of coal seams hydraulic breaking with plain water jets. These statistical data may be used to analyze the process of hydraulic breaking as a whole and together with the influencing factors and in different aspects depending on variable conditions. Such statistical data were accumulated for the period of 1959-1984 years by a number of specialists performing investigations in the collieries of Donbass basin. These materials were used by the author.

It is known that considerable efforts are required for decoding statistical data to make clear the mechanism of their forming. Some circumstances cause the statistical data resistance during their processing. Firstly, data processing of the whole statistical population is labor-consuming because of large information volume. More easy it can be made with statistical sample. The less the volume of a sample is the easier its processing is. But at the same time minimizing of the statistical sample volume is limited by the requirements to fit its adequacy to forming conditions and parameters of the examined population. Secondly, statistical data accumulated in production conditions contain non-acceptance errors both in quantity and forming character. Therefore data processing methods have to provide minimum influence of probable errors on the gained results. Thirdly, it is necessary to overcome the formal method limitations when revealing the character of the statistical influence to avoid the quality mistakes in constructing the process mathematical model. At last, statistical data processing methods have to provide obtaining the results useful for technological calculations.

Overcoming of the statistical material resistance is got by using some new ways of data processing. The statistical sample of limited volume and fitted adequacy with forming conditions and parameters of a population is selected according to the requirements of the principle "other things being different." The last one differs from well known principle of the experiment planning "other things being equal" by the possibility to cover uniformly a large statistical population with a small number of key points. The key point is not a concrete empiric dot of the analyzed statistical population but it is used to indicate the position with the definite meanings of the factors. Therefore the key point can be represented with only one or some concrete empiric dots. It is clearly that influence of a random errors is the less the more the number of the empiric dots taken accordingly to the minimum damageis in order to characterize the key point reliably (Figure 2). The statistical sample

volume complying with first two requirements is formed by multiplying together the number of the key points and empiric dots.

Correlation methods limitedness to determine character of twofold (function-independent variable) statistical dependencies are overcome using the analytical investigation methods. Statistical sample data covered with analytical tendencies allow to construct an empirico-analytical model technology process fitted to make their parameters and regimes calculations.

3. PRINCIPAL STATEMENTS OF EMPIRICO-ANALYTICAL METHOD

The method includes a number of steps of statistical data processing and preparing sequently and parallelly to construct empirico-analytical model of the studied phenomena. The main indicators of statistical process, as well as active and probable factors, are revealed by studying early experience, papers, investigations, construction of check empirical influence curves and others. Statistical population data being analyzed are distributed according to their truth, weight, value of active and probable factors with regard for the achieved results.

Further, analytical investigation of the process' physical properties corresponding to changing of one or another factor, as well as its action on the exit dynamic parameter are produced to make clear the influence curves character of the factors taken into account. Corresponding mathematical expressions are selected in accordance with twofold dependencies character determined before. The twofold influence curves fixed with the analytical method are necessary to correlate with concrete statistical data to do then suitable for technological calculations. Correlation is produced easy of access when statistical sample data are used.

Isolation of the statistical sample from a population one is made according to the definite rule. To observe the principle "other things being different," the statistical sample is formed in the way when every key point has a distinct parameters combination. The statistical sample volume is reduced rather mode under this approach. The gain is more the largest are the dimensions of a studying population. Reliability of results is guaranteed by using some concrete empiric dots to map every key point.

Construction of the twofold empirico-analytical dependencies using statistical sample data is made by employing a number of reduction steps to exclude distorting effect of the factors taken into account at early stages. This procedure allows to reduce empiric data variation dozen of times, to come nearer to its value suitable for technological calculations.

This way some twofold dependencies are united by using Brandon method (Brandon, 1959) to form multifactorous empirico-analytical model of a process. Truth of the constructed mathematical model is estimated with the variation coefficient according to the formula taking into account the empiric dots weight

$$V = 100 \sqrt{\Sigma(1-x_i/\bar{x}_i)^2 w_i},$$

where x_i and $\bar{x}_i$ are the empiric and theoretical values of a single dot; w_i is the weight of a single dot in a sample (population). Summation is carried out all over the empiric dots in a sample. The theoretical value of a single dot is calculated with the help of the multifactorous empirico-analytical model.

Sometimes while analyzing the technological process physical distinctions there is a possibility to derive a general equation which allows us to take into account influence of many active factors and there is an opportunity to make clear some twofold dependencies opposite way.

4. CONTENTS OF THE STATISTICAL PROCESS

The mathematical model of hydraulic coal breaking takes into account the character and peculiarities of hydromonitor water jet interaction with coal face, hydraulic parameters of jet, productivity and physico-mechanical properties of coal seams, as well as factors influencing on the dynamics and continuance of coal breaking.

There are some special features of coal water jπt cutting from a face in hydromines. The position of a hydromonitor is not changed while cutting. Therefore the coal face is moved gradually away from a monitor when extracting. It is natural that the performing length of a water jet becomes longer, hydraulic parameters and jet force influencing on the face are changed too. Extracting coal from a face with the help of the hydromonitor water jet is made by sharing it into some parts and breaking those parts one by one using two regimes: cutting and falling. Regime of coal face breaking is chosen to achieve maximum rate of extraction. The constructed mathematical model of coal face breaking with plain water jets allow to calculate winning rate and energy consumption in access road and actual faces under different hydraulic parameters and ground conditions.

The most important factors influencing on a coal face hydraulic breaking efficiency are as follows: water jet structure and its performing length, nozzle design, its diameter, density and pressure of water jet. The mathematical model gives the possibility to take into account these parameters in large scale variation of quantity values. According to dirty estimates it allows to perform calculations in all range of plain water jets physical existence.

The physico-mechanical properties of coal seams are taken into account in mathematical model by using coefficient of coal seam water jet breaking R_o (m/MN). Its quantity values are formed in dependence on coal seams dip angles, ash, gas and volatile matter content, depth of mining, mined-out space influence etc. Increase of dip angles, gas content influence actual mining results by rising the coal hydraulic breaking coefficient. And vice versa its value decreases under rising of ash content and mining depth.

Dependence of coal hydraulic breaking coefficient R_0 on volatile matter content has complex character. To calculate the coefficient R_0 values in different ground conditions, a multifactorous empirico-analytical dependence is constructed, reliability of which is shown in Figure 1. While calculating coal hydraulic breaking coefficient R_0, the value of the random errors estimated with probability 0.943 did not exceed the quantity variation coefficient of the studied statistical population that was equal to 16.3%. When calculation hydraulic breaking rate of coal seams and its energy consumption by using the constructed mathematical model, probable value of random errors in estimation is expected to be on the same level.

5. INFLUENCE OF SOME FACTORS AND PARAMETERS

The mathematical model of coal plain water jets breaking process is constructed to take into account joint influence of a number of hydraulic parameters and other factors. It gives the possibility to analyze both the individual and joint influence of these factors and parameters in different combinations on the hydraulic coal breaking efficiency values and by this way to make the process function optimum. Examples of some factors influence on coal mass broken from actual face with the help of hydromonitor jet are shown in Figure 3.

The mass broken from the coal face decreases fast enough while performing length of water jet increases (Figure 3A). Under that influence curve slopes down when nozzle diameter becomes less. Increasing water jet pressure and nozzle diameter realizes in growing of performing length of jet and coal mass broken. Influence curves shown in Figure 3A agree well enough with right mind. Clearly that structure of hydromonitor jet and its effect on a face for contact become accordingly worse and broken coal mass decreases when performing length of jet becomes longer.

Rise of the water jet pressure makes growing of the broken coal mass (Figure 3B) what is enough clearly. Influence curves shown in the figure give possibility to have additional information about some conditions affecting on hydraulic breaking from coal face.

Increase of the hydraulic breaking period by the constant parameters of water jet (Figure 3C) leads to the proportional increasing of broken mass. The effect of working liquid density on the broken coal mass is multifarious and it depends on the jet forming conditions. Erosion coal mass may increase or decrease in dependence on rising head water density (Figure 3D).

The costructed mathematical model of hydraulic coal breaking process from a face with plain water jets gives the possibility to make the analysis of all factors influencing both quality and qantity.

6. CONCLUSION

The empirico-analytical method of statistical process investigations, worked out by the author, has been used for constructing the mathematical model of hydraulic coal breaking from actual and development faces made by plain water jets.

This mathematical model takes into account the nozzle design features, hydraulic parameters of jets, physico-mechanical properties of coal seams in different ground conditions, interaction character between water jet and coal block, breaking period of coal mass from a face.

The constructed mathematical model gives the possibility to understand influence of the different factors on the coal hydraulic breaking process with plain water jets, to make sure that the brought out dependencies correspond to the understanding of the process being studied from the right minded position, to analyze the influence of taken into account factors and their combinations on the hydraulic coal breaking efficiency, to choose optimal process function parameters, to produce technological calculations under different jet parameters and ground conditions, to perform numerical experiments in range of parameters and conditions both corresponding to and out of limits of available technique level.

The influence curves of coal mass broken from faces calculated in dependence on water jet parameters and shown in figures as examples allow to have more knowledge depth about hydraulic breaking mechanism, to see how taking into account joint influence of the acting factors important is. Individual effect of separate factor may be displayed in different ways in dependence on degree of the other factors influence (Figure 3B and 3D).

7. ACKNOWLEDGMENTS

The author is thankful to those specialists who have performed experiments and observations on coal seams hydraulic breaking in Donbass basin collieries to accumulate statistical data in different ground conditions that has given the possibility to construct the empirico-analytical model of studied process. Special thanks to Prof. G. A. Atanov for the inspiration to write this paper and help in its preparation.

8. REFERENCES

Brandon, D.B., "Developing mathematical model for computer control," *GSAI.* No. 7, 1959.

Sigaev, E.A., and Teodorovich, B.A., "State and development of the scientific gouds of the hydraulic coal getting calculation," *Fisiko-technicheskie Problemy razrabotki poleznych iskopaemych*, Vol. 2. Moscow, pp. 80-85, 1986.

9. NOMENCLATURE

d diameter of nozzle
D relative damage
E water jet energy

H/C	hydromining colliery
H/L	local hydromining colliery
L	stand-off distance
n	number of testing
p	probability
P	pressure of water
Q	flow rate of head water
R	statistical coefficient of coal seam water jet breaking
R	theoretical coefficient of coal seam water jet breaking
s	coal seam
V	coefficient of variation
V	variation coefficient of nature indeterminacy

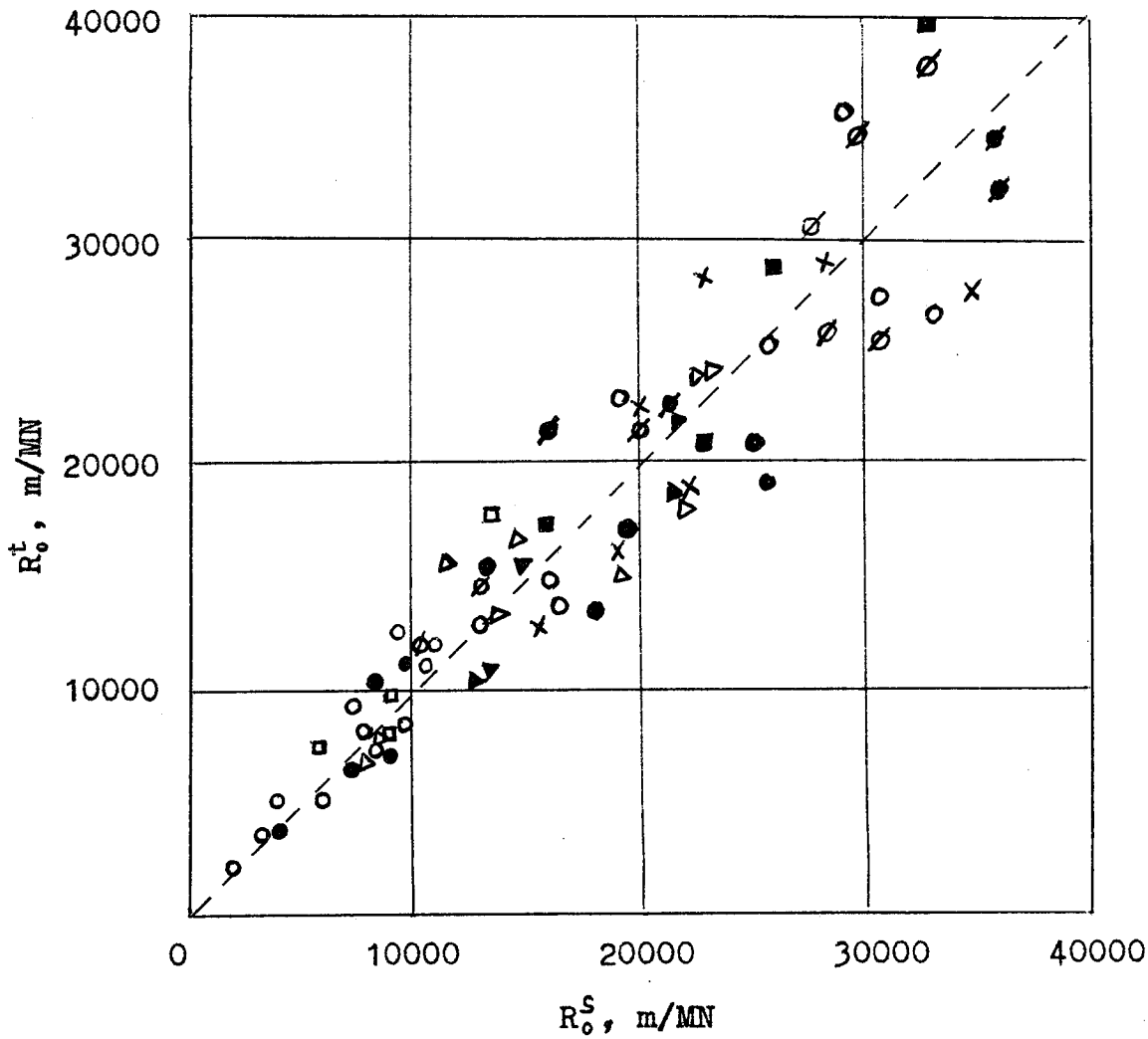

Figure 1. Theoretical (R_o^t) and statistical (R_o^s) coefficients of coal seam erosion with plain water jets.

- ● - H/C "Krasnoarmeiskaya", s.m_5^1;
- o - H/C "Novodonetskaya", s.l_3;
- x - H/C "Pioneer", s.l_7;
- ▲ - H/C "Pioneer", s.m_1^o;
- △ - H/C "Pioneer", s.m_4^2;
- ■ - H/L N7 "Belyanka", s.h_7;
- ▫ - H/L N63 "Simogorye", s.m_3;
- ◖ - H/L N4 "Privolnyanskaya-Severnaya", s.m_3;
- ⌀ - H/C N4 "Alexandrovckaya", s.h_{10}.

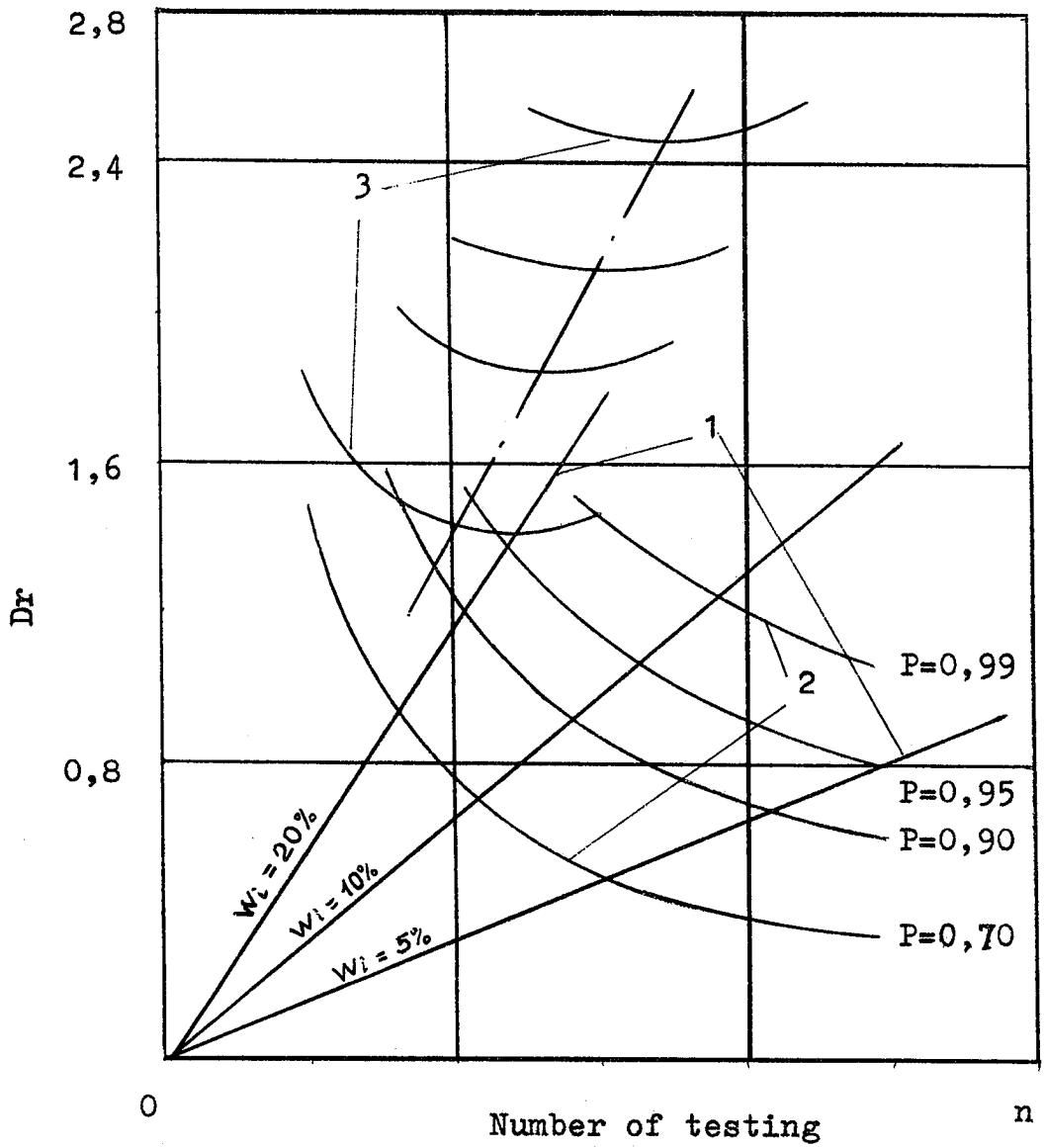

Figure 2. Relative damage Dr from random errors while testing.

1 - error accumulation;
2 - error reduction;
3 - sum relative damage.

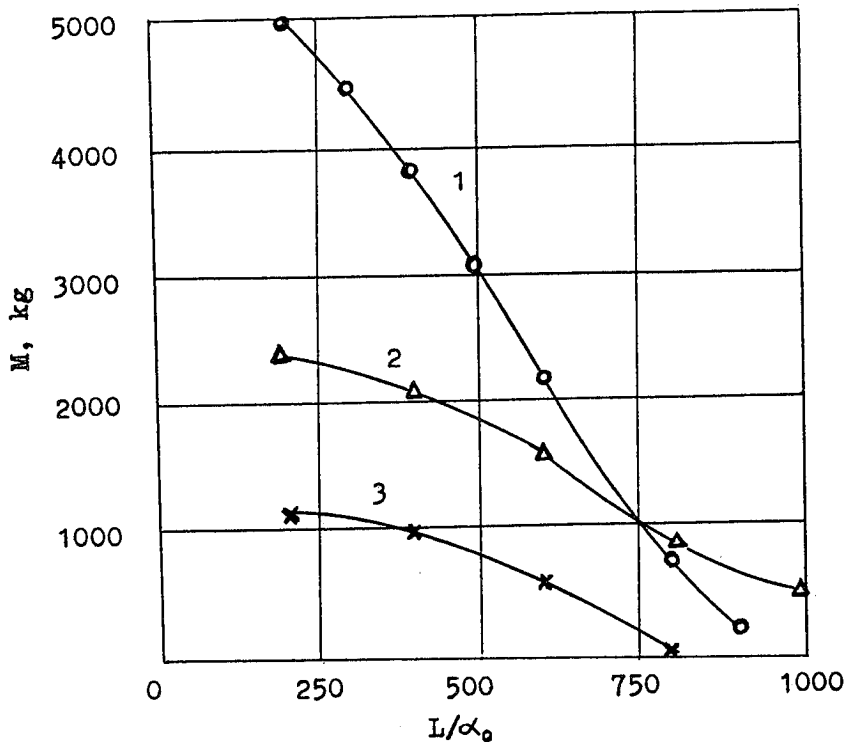

A. t=180 s;
2 - P_0=15 MPa, d_0=10 mm;
1 - P_0=10 MPa, d_0=20 mm;
3 - P_0=10 MPa, d_0=10 mm;

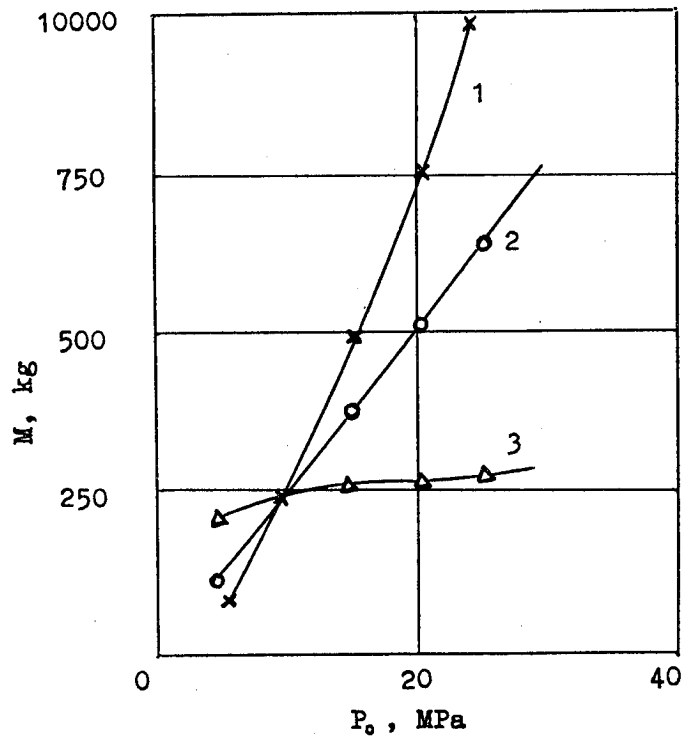

B. t=180 s; L/d_0=200;
1 - d_0=const; 2 - Q=const; 3 - E=const;

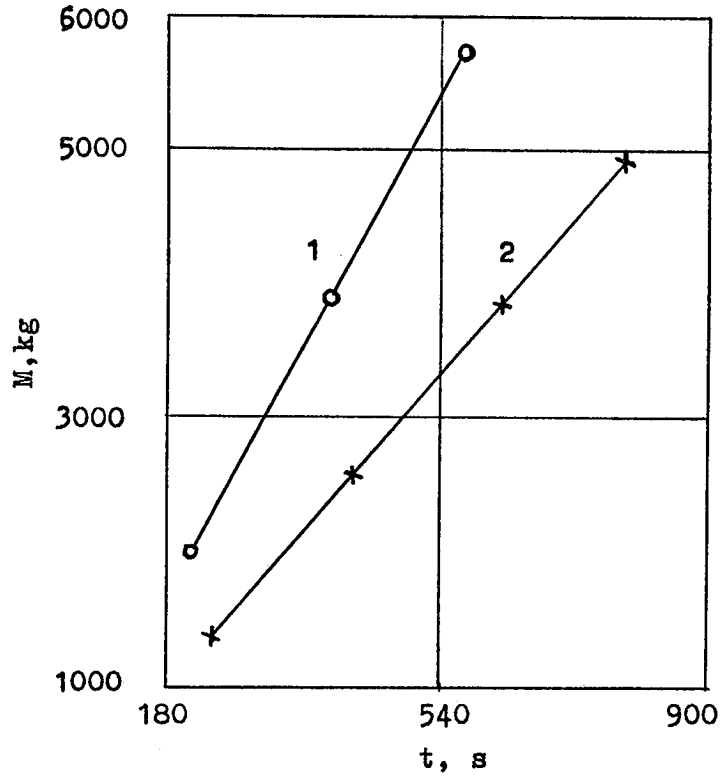

C. Q=const; L/d_o=100; 1 - P =15 MPa; 2 - P =10 MPa.

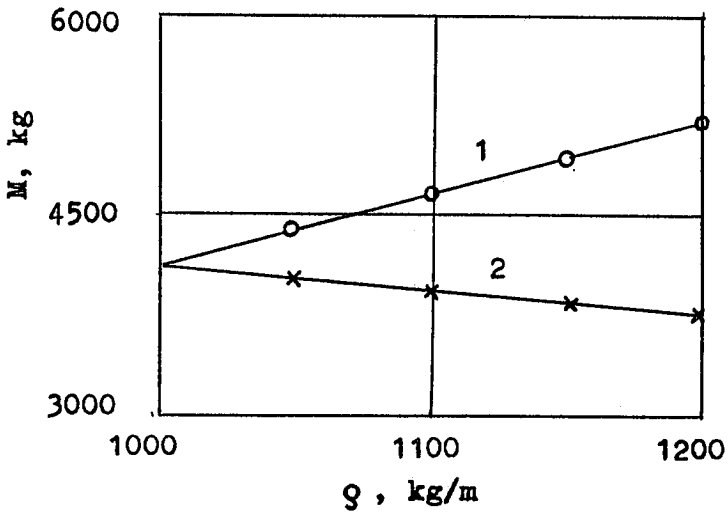

D. t=180 s; L/d_o=200; 1 - Q=const; 2 - P =const, d =const.

Figure 3. Erosion of coal face M with plain water jets. d_o - nozzle diameter, Dr - relative damage, E - water jet energy, L - stand-off distans, n - number of testing, P_o - water pressure, Q - water flow rate, ϱ - water density, H/C - hydromining colliery, H/L - local hydromining collieri.

8th American Water Jet Conference
August 26-29, 1995: Houston, Texas

Paper 65

REDUCTION OF WASTE TIRES WITH HIGH PRESSURE WATER JETTING

Lydia M. Frenzel, Ph.D.
Box 850
Sutter Creek CA 95685 U.S.A.

ABSTRACT

The results of a feasibility study, funded by the California Integrated Waste Management Board in 1993-94, for the processing of waste tires with high pressure water jetting will be presented.

Water jet processing of tires has not been practiced in solid waste management, but it will become a reality in the next few years. Water jetting is found to be a completely general procedure to separate the tire rubber cleanly from the cord and wire. It produces clean bead wire, tread mesh, and pure rubber powders which can be used in value added applications. The feasibility study covered pressures from 35 MPa up to 280 MPa (5,000 up to 40,000 psi). The process is perceived as an environmentally friendly process.

Organized and Sponsored by the Water Jet Technology Association.

1. INTRODUCTION

In 1993-94, the California Integrated Waste Management Board through the California Tire Recycling Management Fund provided a grant for a feasibility study involving water jetting. The objective of the project was to examine the feasibility of transferring the technology of high and ultra-high pressure water jetting to waste tire processing to avoid adverse environmental effects and to reduce processing costs. The plan included a literature survey of existing patents and applications, site demonstrations to document the effectiveness of the tire processing, with and without abrasive entrained in the stream, and preparation of initial pro forma economics.

The technology of processing large quantities of waste tires involves the use of massive feeders with chopper blades to mangle the tires and finally produce chips[1]. These chips consist of the bead wire and tread mesh imbedded in the solid rubber and find limited commercial application. Other technologies to produce tire powders involve rubbing (abrading) and cryogenics to freeze the tires and then form powders. By its very nature, rubber is an elastomeric, resilient, energy absorbing, material which resists ordinary cutting operations. Freezing the rubber in order to abrade the material and crack the rubber is energy intensive.

It is desirable to produce clean, finely divided rubber powders and chips for recycling into value-added products and for re-vulcanization. There exists a need for selective removal to cleanly separate the rubber from the wires and cords. High Pressure Water Jetting meets the need for the selective removal.

Water jetting is a one step process to separate the rubber from the cord and wire. It produces clean bead wire and tread mesh for resale. It produces pure rubber granules which can be used in value added applications. Water pressures as low as 35 MPa (5,000 psi) with only 14 horsepower can be used to process tire side walls. As the volume and pressure increase, the throughput rate increases. Pressures of 140-280 MPa (20,000- 40,000 psi) are practical for higher production rates.

Water jetting can reduce the impact on the environment by using closed loop systems with water reclamation.

2. LITERATURE SURVEY

There were several hundred pages of citations located on waste tire handling and on water jetting. It is significant that the water jet industry has known for a long time that water jetting will separate rubber and elastomeric polymers from surfaces such as steel. Depending on the orifice configuration, water jetting systems can be designed to cut rubber or reduce rubber to powder. This integrated knowledge is found in the application literature of various manufacturers, but not in technical publications. Consequently, solid waste management companies and governmental agencies who are dealing with waste tires do not recognize water jetting as a processing tool.

There was one citation which combined water cleaning with tire processing, US Patent 5,115,983, issued May 26, 1992 to Darrell Rutherford, Sr. of Hamilton Ohio[2]. As a patent, it claimed the idea of processing of whole and partial waste tires from pressures starting at 14 MPa (2,000 psi) with separation of the rubber from the cord and steel belts.

3. SITE SELECTION AND DEMONSTRATION

Many of the water jet pump manufacturers had worked and continue to work with individual clients to investigate the use of water jetting to reduce waste tires.

Site visits were conducted at

NLB Corporation in Wixom, Michigan;
Butterworth Jetting Systems in Houston, Texas;
Aqua-Dyne Inc. in Houston, Texas; and
Flow International Corporation, Kent, Washington.

Additional field trips were made to Total Tire Recycling in Sacramento and S.F. Royster at Tracy, California for background information into the perceived difficulties of on-going tire recycling operations.

As the demonstrations progressed, each company recognized the potential of water jetting to produce crumb rubber and to handle the large off-the-road tires. Candid discussions centered on the effectiveness, handling of the tire themselves, or tire chips which had been passed once through a tire shredder, and the potential of a value-added market for crumb rubber. Each of the water jetting sites presented unique opportunities for processing of waste tires.

NLB Corporation had a complete robot arm and controls for adjusting the pressure, flow rates, stand off distance, production rates, and other parameters. At NLB Corporation, all the standoff distances were kept relatively close to get maximum effectiveness of the cutting pattern. Abrasive was added to the stream to cut the tread metal mesh. The tires were clamped onto a fixture with a half-hub. The tire was held tightly under compression. The fixture could be rotated via a gear and chain driven mechanism.

Butterworth Jetting Systems demonstrated the difference between an efficient tapered nozzle and a nozzle which has an abrupt choke in the water stream. At Butterworth Jetting Systems, the effectiveness of fan jet was compared to the self-propelled dual sapphire nozzle system. Standoff distances were varied from 2.54 to 46 cm (1 to 18 inches). The tires were clamped onto a sawhorse to provide a steady base.

Aqua-Dyne demonstrated nozzles which were cut in triangle, star, diamond, and rectangular shapes as well as the straight circular pattern. The tungsten carbide nozzles were tapered in a cone and terminated in the desired shape. Aqua-Dyne demonstrated an air powered rotating lance (barrel) for the dual sapphire nozzles as compared to the self propelled nozzles.

Abrasive was added to the stream at Aqua-Dyne to cut the tires. The tires were clamped into a vise with a solid backing to provide a steady base.

Flow International Corporation manufactures hydraulically driven water jetting pumps. The pressures range from 245-385 MPa (35,000 to 55,000 psi) and above with flow rates in the 3.8-7.6 Li/minute (1-2 gallons per minute) range. At Flow the emphasis was on cutting. The cutting operations, with and without abrasive, were mechanically manipulated with robotic controls. The rotating, multiple nozzle "cleaning" operations were conducted with hand-held guns. The tires were laid flat and the head was moved relative to the tire body. Cutting rates for side wall rubber were successful up to 10 meters (33 feet) per minute. The cutting of the steel tread and bead wire were accomplished at rates up to 1.3 Meters (50 inches)/minute with abrasive added.

The removal of rubber from the cord and tread was demonstrated with hand held guns with a rotating nozzle. As at the other sites, there were 2 streams of water at different angles for particulate removal. In another configuration, all the orifices were plugged except for a single orifice rotating at an angle so that the power would be concentrated within a single stream. The steel fan jet was demonstrated in a non-rotating configuration, as in earlier trials, in an effort to slice the rubber from the tread mesh. The fan jet was also rotated for a comparison with the rotating coherent jet streams.

3.1 Demonstration of Effectiveness

In total, fifteen tires were processed during the demonstrations at the various sites. The tires ranged from light automobile and truck tires, to recreational vehicle tires with much rubber still left at the edges, to large truck tires with deep tread patterns.

Findings

- Standoff distances from 1.3 - 46 cm (0.5 to 18 inches) were demonstrated to be effective.
- Production rates from 0.13 cm (0.05 inches)/second to 13 cm (5.0 inches) per second were demonstrated to be effective.
- Pressures from 35 to 245 MPa (5,000 to 35,000 psi) were demonstrated.
- Horsepower from 7 horsepower to 118 horsepower was demonstrated.
- Abrasive from two different manufacturers were added into the jet stream at 4 pounds/minute.
- The manipulation of the water jet lance by robotics, vise-held, and hand-held was demonstrated.

Without the addition of abrasives into the stream, water jetting will selectively produce granulated rubber without cutting the steel mesh. The addition of abrasive allows the clean cutting of the cord, steel, and rubber. This will be useful in the processing of the large off-road (mining) tires.

The site visits demonstrated that water jetting can be used to selectively remove the tire rubber for the production of crumb rubber from the cord and the metal at a threshold

pressure around 49 MPa (7,000 psi). Depending on the pressure, stand-off distance, volume, and rate of progression, the cord will remain intact or can be cut as part of the tire processing.

3.2 Slicing and Cutting of Side Walls

One process application of water jetting is as a selective cutting device to remove the bead wire from tires ranging from automobile to "off the road" (OTR) mining tires. This would utilize pressure ranging from 70- 280 MPa (10,000 to 40,000 psi), without the addition of abrasive. Removing the bead wire removes much of the problem of producing wire-free rubber. This cutting was demonstrated at rates up to of 10 meter (33 feet) per minute in an ordinary tire.

Water jetting can cut 5 cm (2 inches) of tire rubber at 46 cm (18 inches) per minute and can cut 15-25 cm (6-10 inches) thick material. This water jetting can also literally cut the side wall into usable strips from the steel belted tread and the bead. The side wall can be shaped into any form. The availability of clean side walls should make split tire applications more feasible.

Because the head does not contact the tire, it can be positioned for any size of tire on a rotating platform. It is practical now to process OTR tires.

With the selection of a proper angle, the cutting jet is able to cut the nearest side wall, pass through the air space, and penetrate to the opposite wall and cut the bottom half in the same pass.

3.3 Cutting of Steel Belts and Bead Wire

A second application is the cutting of the bead wire in tires using abrasive. In smaller tires, this cutting can be accomplished economically with mechanical shears. However, the bead wire in the OTR tires is like a twisted wire cable 5-7.5 cm (2 - 3 inches) thick. OTR tires do present a large problem in recycling and clean-up operations. Large shears cannot cut the cable- subsequently the tires are difficult to cut up in order to feed to the shredder. Water jetting with abrasive can cut the large bead wire and then remove the bead wire so the OTR tires can be handled.

The demonstration showed abrasive water jetting can cut the smaller bead wires at 51 cm (20 inches)/minute. This presented no problem as abrasive water jetting is used commercially to cut half inch steel plate.

The tread splitting can be accomplished with an abrasive water jet operating at 49 MPa (7,000 psi) and above. At NLB, the production rate of 30 cm (12 in)/minute was limited by the demonstration equipment. The tire was passed in front of the cutting head. At Flow the cutting rates were 50-127 cm (20-50 inches) per minute. Both the NLB and Flow companies have cut tires and bead wires for other companies very successfully. Flow International provides a commercial tire cutting assembly for research purposes.

The water jet cutting of the rubber side walls, bead wire, and tread mesh leaves a very smooth surface with no jagged wires. This is very desirable if the rubber pieces are to be used in applications where they should present a surface which won't catch. Flow International manufactures a specialty tire cutter for quality control in tire research labs.

3.4 Production of Clean Granulated Rubber

A third application, and the one with the most economic incentive, is the production of granulated rubber in a fine mesh form. The feasibility study literally shows that a tire can be rotated in front of a high pressure water jet and the rubber is removed in 0.08 cm (1/32") particles leaving the cord and wire intact. This opens the possibility of producing rubber powder directly from the tires or for putting a water jet pass-through at the end of the current shredding equipment. It eliminates the costs of multiple passes through shredders. It eliminates the high capital costs and energy requirements for cryogenic freezing and cracking of tires- estimated at 2-3 million dollars for a single installation.[1] It is a clean technology. It eliminates the problem of rubber left on the steel which devalues the steel from a secondary market. It effectively allows for nearly 100% reduction of the tire rubber into reusable products. In fact, in the production of granulated rubber by water jetting, the bead wire does not have to be removed as the rubber can be cleanly removed during the process.

The head was moved past the surface at a rate of 76 cm (30 inches) per minute to remove all of the rubber from the tread mesh. In the hand-held demonstrations, the gun was moved past a stationary tire at variable rates.

4. TIRE PROCESSING

In the Market Status Report for Tires[3], Lin Lindert noted the expense of producing crumb rubber without wire, the need for value added products, and the reluctance of the public to accept tire derived fuel or incineration as a viable consumption of tires.

There is a growing awareness in the United States that used tires must be recycled into value added products rather than being used for tire derived fuel or as fillers in asphalt rubber. The public does not perceive that incinerating tires for fuel is "recycling" or desirable without regard to the technical merits. To the public, recycling is reuse; it is not shredding the tires and placing them into a landfill or sending them to be burned.

Using the properties of elasticity and energy absorption requires the production of granulated rubber particles free from wire or cord. The manufacturers of molded plastic products, the waste recovery industry, and the transportation departments are all being affected by mandates to use recovered tire rubber. The waste tire industry has inappropriately adopted machinery from the lumber industry.

People are trying to produce "pure" rubber from tires by shredding together the wire, cord, and rubber, or by rubbing it into powder, or by freezing the tires with nitrogen and cracking the rubber using hammer mills. These processes are working against the physical properties

of the tire rubber. The carbon black is hard on the shredder blades. Tire rubber naturally resists cracking into smaller pieces. Tire rubber is resistant to rubbing mechanisms.

4.1 Comparison of Waste Tire Processing with Current Technology and Economics

Without any optimization, the product resulting from water jet processing and cleaning of tires is fine crumb rubber or rubber powder. The throughput for a single pump is estimated in the one to two ton per hour range. The water jetting process is not likely to replace the mechanical shredders which provide high throughput with a wire-in chip. It can provide the feed stock to other grinding technology. It can be used to provide the value added fine powder. Water jetting can also be used to cut the side wall from the tread and the bead wire from the side wall at rates up to 10 m (400 inches) per minute. This reduces transportation volume and processing problems.

Shredders are capitalized at 400,000 - 500,000 dollars. An ambient grind system to produce 30-40 mesh powder is capitalized at 3.5 - 5.5 million dollars. A cryogenic process to produce 60-80 mesh rubber is capitalized at 3.5 million dollars. The capital cost to provide a water jetting tire processing system is estimated at 250,000 to 350,000 dollars, once integration and development is completed. Complete integration, development, and fabrication of a prototype is estimated at 1.5 million dollars.

Operating costs are estimated at 50 to 140 dollars per hour. Costs to produce 80 mesh powder are reported at 140 dollars per ton.

The close loop recycling system consists of a high pressure pump subsystem, the tire conveying subsystem, and the effluent recovery subsystem. Zero waste discharge can be obtained.

4.2 Characteristics Of Rubber Product Resulting From Water Jetting

In the demonstrations, a single pass by the tire was performed. The rubber powder fell to the floor. The smaller particles were carried away by the water down the drain. The rubber which was left was collected with a whisk brush. It was difficult to make larger chunks of rubber because the rubber remained on the tire cord or tread mesh after an initial cut. The water would then go through the cord or mesh.

At the Butterworth site, we specifically tried to cut larger pieces from the tires and peel the rubber back from the tire. We continued to get small pieces and powders. The water literally drills holes in the rubber and then passes through the cord and wire.

The rubber which was collected at the various sites was consolidated and sieved for a general sizing. This collection is not believed to be a typical distribution as the finer particles were swept away during the demonstrations.

The largest pieces were typically 0.6 cm (.25 inch) width and 1.2-2.5 cm (0.5-1 inch) long. Approximately 110 grams were recovered which were greater than 12 mesh.

The under 12 mesh powder was sieved gently through a 30 mesh screen. Rubber powder < 12 mesh and > 30 mesh weighed 19.1 grams.
The under 30 mesh rubber powder weighed 58.4 grams.

The weight distribution of this rough collection was:

> 12 mesh	59%	Typical size 1/4" wide by 1/2'- 1" long.
< 12 mesh	10%	
< 30 mesh	31%	

Without any optimization of the size or any special grinding or cracking techniques, the rubber product from water jetting far surpasses the results from shredders in terms of size. All of the rubber (100 %) comes off the tire and can be collected using commercial sieves, vacuum, and centrifugal separators.

The product from water jetting systems will be competing in the manufacture of powders in the under 40 mesh range or in providing the feed stock to grinders, pulverizers, and crackers, rather than in competition with the tire shredders.

4.3 Shredders

Various shredding machines and techniques are available for processing car and truck tires into rubber chips which still include the wire and cord. This product finds limited uses.

The shredders typically have a high throughput to produce 5 cm (2") chips at a cost of $25-50 per ton. Waste Recovery Inc. in Oregon will supply a 3.2 cm (1 1/4") chip with 90% of the wire removed at approximately $35/ton fob Oregon.

Some manufacturing companies of shredders are:
Saturn Shredders- $375,000 capitalization for production of 5 cm (2") chips at 15 tons per hour.
Tri-C Manufacturers- $500,000
Columbus McKinnon- $410,000 capitalization for production of 5 cm (2") chips at 10 tons per hour.

The capital requirements for a water jetting process is estimated at $250,000 to $350,000 depending on whether one or two high pressure water pumps are utilized. While the capital equipment requirement may be less, the cost to operate a water jetting process is more than the shredding systems.

4.4 Grinders/Crackers

In processing waste tires, a major difficulty is getting the rubber freed from the wire and cord so that it may be processed by grinders, pulverizers, or cryogenic crackers. A water jetting system certainly can produce the feed stock for the grinders, pulverizers, or crackers in a single pass system.

The water jetting processing also appears that it can produce the finer, value added powders if the throughput is sufficient. In order to be competitive for crumb rubber production at least one ton per hour of rubber must be produced.

4.5 Capital Equipment Costs

The capital equipment costs for a water jetting system is around $100,000. Allowing for a tire conveying system, liquid solid separation, and water reclamation, the capital equipment costs are estimated at 250,000 - 350,000 dollars.

The shredder systems cost approximately 400,000- 500,000 dollars.

An ambient grind system to produce 30-40 mesh rubber powder is estimated at 3.5 - 5 million dollars.

An cryogenic process to produce 60- 80 mesh rubber is estimated at 3.5 million dollars for installation.

There is an additional cost of technology transfer, development, and system integration to be considered for a state-of-the-art water jetting process. In estimating the costs for integrating the components, the Office of Naval Research Ship ARMS™ development is a good example as it addresses many of the problems of close loop requirements. This ONR system includes a sophisticated standoff and travel system which is not required in the tire process, but which would be replaced in costs by the tire conveying equipment.

The Office of Naval Research has just integrated a completely automated water jetting system with a rotating head containing 22 orifices, a newly designed and fabricated water jet pump operating at 280 MPa (40,000 psi) and 38 liters (10 gallons) per minute flow, a full robotics system and new 6 axis manipulator, solids separator and reclamation, water reclamation and deionization unit. There is no technical reason why this same system could not be used to process water tires in an automated fashion.

Equipment costs for a water jet unit for cutting can be as low as $17,000 for a used pump which is reconditioned or up to $150,000. The head does not touch the tire so it can be used to cut auto, truck, and off the road tires equally well. A complete low flow, hydraulic driven pump and 6 axis robot is available for $85,000 in a used condition with 300 hours use, when the same equipment would cost an estimated $300,000 in a new condition.

Cost of Water Jetting Systems (100 hp)

High Flow (crankshaft driven)	Low Flow (hydraulic driven)
$90,000	$150,000 (new)
	$ 48,000 (used)

Maintenance costs are relatively inexpensive and have been estimated from industry sources.

expendable parts $2-3.00/ hour	$15-20/hour- expendable parts
expendable parts $8.00/hour	$25.00/hour- (second source)

In addition, the operating costs should include diesel consumption at 10 gallons per hour or the equivalent electrical output of running a 75 to 100 hp motor with 460/3 phase, 125 AMP maximum.

Very good used equipment is readily available in the commercial market. The high volume, low pressure pumps last for several years.

4.5 Rubber Powder Production Costs

The manufacturing costs of the rubber powders vary with the production method.

Single pass through a tire shredder - production costs[1]	$15 - 20 /ton
Producing a 5 cm (2") chip (wire in)[1]	$ 25-35 /ton
Producing a 5 cm (2") chip (Wire in) (independent source)	$22-50 /ton
Producing crumb rubber (wire out?) (independent source)	$160-$220/ton
Producing a 10-30 mesh ground particle[1]	$150-$240 /ton
Producing granulated rubber (cryogenic)[1]	$240-$400/ton
Producing of 60-80 mesh rubber	$200/ton
Producing 80 mesh rubber (water jetting)	**$140/ton**

Wire out Material
Selling prices of crumb rubber vary with the fineness of grind. There is not much, if any, demand for rubber powders in a greater than 30 mesh.

Selling price of 2.5 cm (1") chip (independent source)	$31/ton (95% wire out, cord in)
Selling price 10 mesh rubber (independent source)	$260-$320/ton
Selling price 10 mesh rubber (independent source)	$100-200/ton
Selling price 30 mesh rubber (independent source-buffing)	$360-$400/ton
Selling price 40 mesh rubber	$300 / ton
Selling price for 80 mesh rubber	$560- 700 /ton
Selling price for 100 mesh rubber	$700-1000 /ton

4.6 Production Rates

The production rates vary for side wall cutting, tread cutting, side wall cleaning, and tread cleaning. Side walls were cleaned from 14 hp to 140 horsepower with pressures ranging from 35-140 MPa (5,000 to 20,000 psi).

There is a compromise in ease of operation, maintenance, linear production speed between the centrifugal driven pumps and the hydraulic driven pumps. There is also a compromise

between the use of lower pressure and higher volumes with the higher pressures and lower volumes. The less volume of water, the less separation, and the less water recovery is involved.

For example, the 35 MPa (5,000 psi), 14 HP demonstration gives a very clean separation, but slow. However, several heads can be run with the same pump and there is very little stress on the equipment. At 140 MPa (20,000 psi) and 120 HP, the cleaning throughput is at least 30 times faster than the 35 MPa (5,000 psi) demonstration. Only one rotating head can be driven.

The time to process the individual tire will vary depending on whether the rubber is thick or thin, whether you are working on the side wall or the tread, or on a completely solid rubber tire.

4.6.1 Side wall Cutting

The maximum rate demonstrated to cut the side walls free from the tread was 10 m (400")/minute or six tires per minute on an ordinary auto tire. Equipment can be designed to move the head past the tire or to rotate the tire past a stationary head. This same type of design can be used to cut Off-The- Road (OTR) side walls free of the tread. With the setup of two cutting heads, the bead wire could be cut free in the same pass.

4.6.2 Side wall and Tread Cleaning

The throughput for rubber powder production from the side walls is estimated at least 2.3-4 linear meters (90-150 inches) per minute at 140 MPa (20,000 psi).

For side wall cleaning at a linear feed rate of 76 cm (30 inches) per minute and a width of 61 cm (24 inches), the calculated throughput is: 30 inches * 1/2 inch thick * 24 inches wide = 360 cubic inch/minute; 13 pounds/minute; 780 pounds per hour.

The feasibility demonstration showed that the linear rate can be 3-5 times faster for reduction of side walls to crumb rubber, implying that production rates of one-two tons per hour are achievable.

The rubber can be removed cleanly, leaving the bead wire ready for separation and sale.

The linear rate for the tread cleaning is slower, but the rubber is generally thicker so that the production rate remains relatively the same. A calculated throughput of two tons of rubber tires per hour with an operating cost of $50 per hour per water jet pump is a cost of 0.25$ per tire.

4.6.3 Tread Cutting

The water alone will not cut through the wire mesh or the bead wire. When abrasive is added to the stream, the tread or bead wire can be cut cleanly. The abrasive water jetting is

feasible to cut the OTR bead wire or cable as it is commonly used to cut steel or stainless steel plate. A mechanical shearer would be faster and more economic to cut the tread mesh rather than use abrasive water jetting.

4.7 Components of a Close Loop Water Recycling System

- The components of a complete integrated tire processing system consist of:
- **High Pressure Pump Subsystem**

- **Tire Conveying Subsystem**
- Tire side wall cutting system
- Tread cutting/shearing system
- Side wall processing by water jet
- Tread processing by water jet

- **Effluent Recovery Subsystem**
- Liquid solid separator
- Vacuum Unit
- Water Reclamation unit
- Optional diesel-powered electric generator for mobility

4.7.1 High Pressure Pump Subsystem

Depending on whether the whole tire is processed or if there is a cutting of the side wall from the tread, there may be one or two high pressure water pumps. The high-pressure water pump is self-contained, may be driven by diesel or electric power. Depending on the size, it will provide water to the cutting and cleaning heads. It may have maximum pressures of 175-280 MPa (25,000 or 40,000 psi).

All pressure lines and fittings are ultrahigh-pressure tubing. Bursting pressures are generally at least twice the operating pressure. Cabinets are soundproofed to reduce the operating noise. Pumps are chosen and mounted for ease of access and maintenance.

Remote programmable logic controllers are typical to provide remote operation with a minimum of personnel. The pumps can be also be manually operated. An automatic feature to monitor pump functions and shut down the unit if abnormal conditions are detected is highly desirable.

4.7.2 Tire Conveying Subsystem Designs

The cleaning head can be a self-contained nozzle and shroud. Commercial nozzles are available to cover 10 to 15 cm (4" to 6") wide strips with hydraulically or air controlled rotation rates. The design should include the stand off rate, and complete effluent capture of the process water and rubber.

The selection of a tire conveyance system, whether or not the side wall cutting can be done more efficiently with a mechanical cutter or a water jet head, and the decision to separate the stream into side wall and tread components are simply technical details which a good manufacturing engineer can select.

The rubber target must be firmly supported or flattened to maintain efficiency. A major decision point is whether to reduce the whole tire to powder or to cut the side walls from the tread before reduction.

If you are working with the whole tire, or with the side wall and the treads as two separate entities, then the cord is removed intact and the wire mesh is removed essentially as a single piece. This makes the separation process easier to automate rather than have small bits of wire intermingled with cord.

4.7.3 Off-The-Road Tire Design

It is equally effective to move the head past the tire or the tire past the head. One can easily design for the large Off-The-Road (OTR) tires a four to six inch bar placed against the tread wall with a firm standoff mechanism. The head is shrouded to contain the water and may be fitted with a vacuum system. The inner rim is shrouded to collect the rubber and water. The head is then moved slowly along the tire to reduce the tread to crumb rubber. The shroud may be nothing more than an impermeable rubberized tarpaulins material.

For the Off-The-Road tires, the tire is placed horizontally on a rotating plate. There is a bar to the inside which keeps the tire from rebounding away from the water jet operating at >140 MPa ($>20{,}000$ psi) and high horse power. The tire rotates past the plate so that the tread rubber is stripped.

The OTR tire is then cut with a water jet or abrasive water jet to remove the bead wire and to cut the side wall from the tread. The side wall is then processed past rotating heads.

4.7.4 End of Shredder Design

One option is to integrate the water jetting process at the discharge end of a shredder. Envision a shredder whose objective is to make a mangled tire and large strips, rather than 5 cm (2") chips. These shredders do not need the classifier options. The output goes to the conveyer belt which is fed into a two layered metal conveyer with open wire mesh on top and 80 mesh wire on the bottom. This presses the mangled tire flat. The flattened tire pieces then pass under a rotating fixed water jet orifice or series of water jets. The rubber and water are collected immediately under the open 80 mesh conveyer. The wire and cord are carried along the conveyer which then opens and discharges the mangled skeleton.

This design allows the production of 80 mesh rubber to be integrated into the high volume of the shredder without much of a classifier and without regards to a "cleanly cut" chip. The disadvantage is the tire skeleton is chopped into pieces so more equipment is needed to separate cord and wire.

4.8 Effluent-Recovery Subsystem

Notes for this section are excerpted from discussions with the Office of Naval Research Ship ARMS™ Robotic System as these concepts are general for any closed-loop system involving water jetting, separation of particles, and water reclamation. The closed loop system was integrated from existing technology. These proposed recycling requirements are very stringent as they are designed for a mobile unit with maximum protection to the environment and zero waste water discharge requirement.

An air compressor may be required to operate pump, valves, and utility equipment.

An integrated liquid/solid separator is used to separate the rubber powder from the process water. The liquid/solid separator is conceived to be a continuous membrane filter or a vibrating screen. The rubber particles collected on the top of the separator are removed by a doctor knife arrangement.

Located under the liquid/solid separator membrane or sieve, a high-powered vacuum unit can recover 95% of the process water after the rubber passes through the liquid/solid separator.

A modular water reclamation unit will filter and condition the used process water to return it to the high-pressure pump. As the water is cycled in the system, dissolved ions will build up. These ions may precipitate or plate out inside the pumps so it may be necessary to provide a deionization unit. Piston driven pumps generally are more tolerant of the water conditions than the hydraulically driven pumps.

A sump pump directs the water to a centrifugal separator. The centrifugal separator will remove the majority of the remaining rubber particles. The discharge water is then directed to a 20 micron filter and into a raw water tank. The level in the tank is kept constant by addition of potable water. This accounts for evaporative losses. This raw water is pumped through a series of filters, an oil separator, and an ozone generator and finally into a clear well tank. The clear well water is passed through deionization units to remove ions, and then through 0.35 micron filters before returning to the high-pressure water pump.

5. CONCLUDING REMARKS

Demonstration of the feasibility of ultra-high water jetting for waste tire processing has been successfully completed.

The advantages of the water jet processing are:

- Separation of 100% rubber from cord and Tread
- Economic Production of Rubber Powder
- Close Loop Recovery System Potential
  - no toxic effluent
  - no toxic vapors

no dust particulates
- Significantly reduced particulate contamination and worker exposure
- Low manpower requirement
- Process controls allow for processing of whole tires into clean powder streams with easy separation of cord, wire, and rubber.
- The production of rubber powders for value added products rather than placement of rubber chips into land fills.

The water jetting process will eventually compete with the current use of tires for tire derived fuel by the economic manufacture of powdered rubber. Tires will indeed be turned into a valuable product stream, not a waste stream.

Two companies have solicited firms to use water jet technology to produce rubber powders in the United States. Both companies claim manufacturing of rubber powders in the 80 mesh range at a substantial savings over grinding, shredding, and cracking technology. A market research survey completed by a Northern California firm indicates that value added applications for finely divided tire rubber does exist in such a magnitude that all tires could be used in other products, not just used as tire derived fuel.

The key to this technology transfer is to find companies who are large enough to accept development as a means for leaping ahead of the competition. When a company purchases a mature process, they gain the safety net of knowing that most problems are already worked out, but they lose any advantage in implementing a more efficient process. The production costs are essentially already fixed and known within the industry. Many companies express a desire to have new technology but their management is not prepared to take a long term view. Short term considerations have priority. In addition to commercial firms, federal agencies such as NASA and the Small Business Innovative Research Programs (SBIR), and individual state agencies are funding this development as state agencies are finding that they do not have the answer to waste tire management.

Technology is being transferred from foreign countries into the USA as the USA has the large volume of waste tires but other countries have already faced conservation of resources. The attention of solid waste management of tires within the US must turn from how to process the tires to new value-added market recognition and development.

6. ACKNOWLEDGMENTS

This feasibility study was funded by the California Integrated Waste Management Board for the period July, 1993 through June 1994 under the California Tire Recycling Management Fund. The statements and conclusions of this report are those of the Grantee and not necessarily those of the California Integrated Waste Management Board, its employees, or the State of California. The State neither endorses or promotes nor makes any warranty, express or implied, and assumes no liability for the information contained in the text.

A heartfelt thanks and gratitude is extended to the companies who participated and donated in kind to the feasibility study. The water jetting manufacturers are fierce competitors, but do cooperate together to develop new applications. Many hours of conversation with governmental agency personnel, private individuals, and companies have contributed greatly to this study.

7. REFERENCES

1. "Tires as a Fuel Supplement: Feasibility Study, Report to the Legislature," January, 1992, California Integrated Waste Management Board

2. Rutherford, Sr. Darrel, "Process for Recycling Vehicle Tires," US Patent No. 5,115,983, May 26, 1992

3. Lindert, Lin, "Market Status Report, Tires," California Integrated Waste Management Board, July 17, 1993

8th American Water Jet Conference
August 26-29, 1995: Houston, Texas

Paper 66

MEASUREMENT OF SURFACE DISPLACEMENTS BY MOIRÉ IN ABRASIVE WATERJET PIERCING PROCESS

Z. Guo and M. Ramulu
Department of Mechanical Engineering, Box 352600
University of Washington, Seattle, WA 98195

ABSTRACT

A Moiré interferometry, optical experimental setup is developed to study the strains in the material due to an abrasive waterjet impacting and piercing. Moiré interferometry has the unique advantage of portraying the full field of displacements. During abrasive waterjet piercing of polycarbonate and ceramic materials, moiré fringe patterns for both U- and V-displacement fields are recorded simultaneously by a high speed camera system. Preliminary experimental results indicate that the Moiré technique is a viable method in the field of abrasive waterjet machining to study the fundamental mechanisms by measuring microstrains.

Organized and Sponsored by the Water Jet Technology Association.

1. INTRODUCTION

The abrasive waterjet (AWJ) machining process involves wave propagation, tensile and shear fracture, erosion, cratering and large scale cracking enhanced by pressure. However, very limited research on the mechanics of the abrasive waterjet and workpiece materiel interaction has been reported [1-4] to date. Dynamic photoelasticity [5-10] was used to study the waterjet and AWJ impacting and machining, respectively, using birefringent transparent brittle polymeric materials. The stress distributions associated with jet penetration process were calculated from the photoelastic fringe patterns. The stress distributions and the fracturing behavior of the material under dynamic conditions were found to be less than the static loading stress fields.

Even though AWJ machining technique has been used widely for industrial applications, the micromechanisms of material removal in the abrasive waterjet machining of hard-to-cut materials has not yet been very well understood. Thus, a full understanding of the machining phenomena is urgently needed for more successful application of abrasive waterjet in tough materials like structural ceramics.

For opaque material like ceramics, photoelasticity can not be applied. Furthermore, much less deformation induced by the AWJ machining is expected in ceramic material due to its hard and brittle nature. Thus a new technique, moiré interferometry, is needed to investigate the strain state in the material during AWJ piercing. The surface displacement field in any material can be obtained by using the moiré interferometry method while the specimen is being pierced by a high pressure abrasive waterjet. The purpose of this research is an attempt to develop and apply an optical technique, moiré interferometry, to determine the jet-material interfacial strains at the onset of machining.

2. EXPERIMENTAL SETUP AND PROCEDURE

The abrasive waterjet system used in the research is a POWERJET 20-35 model pump. It consists of a high pressure pump, a nozzle assembly, a catcher unit, and an abrasive supply hopper. The nozzle assembly is adjustable in the vertical direction. A milling machine transport the workpiece in the X and/or Y directions horizontally. A twenty horsepower motor drives a hydraulic pump which outputs high pressure hydraulic oil, which pushes an intensifier pump. Thus, output water can be pressurized to as high as 241 MPa. The maximum water flow rate is approximately 25 liters per minute. Inside the abrasive waterjet nozzle there is a waterjet orifice of size 0.30 mm in diameter and a tungsten carbide focusing tube of internal dia 1.02 mm. Garnet abrasive #80 was chosen for both economy, longer nozzle life, and its proven performance with regard to metal cutting.

The specimen materials used in the piercing experiment are polycarbonate and a ceramic alumina AD99 , plates of the size 76 x 19 x 6.4 mm. The surface facing the optical setup is polished and cleaned. A specimen grating is transferred to this surface by using PC-10 epoxy adhesives and then is cured. A glue is used to seal the gap between the splash shroud and the specimen. A specimen holder is designed and machined from an aluminum block of 100 x 100 x 25 mm. Seven threaded holes were drilled and tapped. The holes are used to fasten the splash shroud to the specimen holder. Protection of the optical setup and the optical specimen gratings glued to the specimen was accomplished by installing a specially designed and built water splash shield. Figure 1 is a photograph showing the abrasive waterjet system with the specimen system mounted. AWJ piercing parameters used for the experiment are: 1) supply pressure for the abrasive water jet was 240 MPa; 2) standoff distance was 1 mm; 3) the abrasives used were garnet abrasive #50; 4) the piercing duration was 3 seconds; and 5) the abrasive flow rate 25 gram/sec.

Figure 2 is an abrasive waterjet optical experiment setup schematic, using a four beam moiré interferometry . The density of the specimen moiré gratings used in the moiré interferometry experiments on the polycarbonate specimen is 600 lines/mm. Moiré grating density of 1200 lines/mm were used for ceramic (alumina) specimen, due to its smaller deformation. These arrangements provide a moderate sensitivity for measuring the in-plane displacement. The light source used in the optical experiment is a 20 mW polarized He-Ne laser generator (wavelength 632.8 nm). The laser beam is expanded by a spatial filter which also filters the laser light noises. The expanded light is collimated by the collimating lens. With the help of a self made U-V mirror set, two moiré patterns in the orthogonal displacement field are produced. In these experiments, special optical setup is arranged, so that both U- and V-displacement fields can be recorded simultaneously. Two Nikon F3PH 35 mm cameras with MD-4 motor drive, of maximum speed of 5 frame per second, were used to record the moiré fringe patterns. These fringes are the real time response of displacement in the workpiece. A control box designed to synchronize the timing of the abrasive waterjet system and moiré fringe recording system (two Nikon cameras) is also utilized. The control box triggers the abrasive waterjet system and the two cameras simultaneously, which makes the real time recording of the displacement fringe patterns possible.

3. RESULTS AND DISCUSSIONS

Typical frames of moiré fringe patterns of the displacement fields recorded during the abrasive waterjet piercing of polycarbonate material are shown in Figures 3 and 4. At the beginning of the drilling process, the U field has a few fringes, while the V field only shows obscure fringes. As the pierced hole gets deeper, clearer fringes appear on both U and V fields, and more and more fringes appear. When the AWJ system starts, vibration causes the blur fringe patterns, and the V field tends to be affected more than the U field. Stress waves in the specimen induced by the impingement of the AWJ is another factor causing this problem. After a short while (300 microseconds) the system becomes stabilized, good fringe images can be seen. It is also interesting to observe that the recorded fringe patterns in the V- field shown in Figure 4 look like a skeleton and were terminated at or near the vicinity of the bottom of a hole.

Figure 5 shows a sequence of the moiré fringe patterns photographed as the AWJ penetrates the Alumina AD99 specimen. Moiré interferometry experiments on Alumina AD99 ceramic materials were conducted with garnet abrasive #80, a supply pressure 180 MPa; standoff distance 1 mm; and abrasive flow rate 18 gram/sec. The jet exposure to

piercing was 1 second. However only the U-field displacement fringes were recorded successfully in this experiment due to the reasons cited above.

Figure 6 shows the transient surface displacements U and V plotted against width and height, respectively. All the data shown in Figure 6a and 6b corresponds to Figure 4. Note that the displacements at a given location near the jet decreased with the time. and variations in the displacement with respect to time are not linear, as expected. Strains were calculated using linear elasticity by assuming quasi-static loading conditions and equivalent strain was calculated to see the effect of triaxiality. Figure 7 shows the parallel (y) and perpendicular (x) strains and equivalent strain associated with the penetrating jet at the root of a pierced hole. Note that the strains also decreased with time. The magnitude of displacements and strains clearly demonstrates that the actual pressures at the impact site are a lot less than the supply pressures used in this set of experiments. Although these results are preliminary, they are nonetheless a first attempt to study the microstrains in the material during abrasive waterjet machining. The sampled results from moiré are consistent with our dynamic photoelasticity observations of stress fields [8-10]. This could be due to frictional losses in the pipes and stress relief after crack nucleation, micromachining and erosion.

4. CONCLUSIONS

A moiré experimental setup was developed to measure the displacement fields for hard-to-cut material under the impingement of abrasive waterjet machining. Moiré interferometry technique has been applied to both transparent polycarbonate and ceramics materials. The preliminary results presented demonstrated the feasibility of this technique in studying the jet-material interaction and the associated microstrains in real engineering and engineered materials.

5. ACKNOWLEDGMENTS

The authors wish to acknowledge the financial support of the National Science Foundation, Grant No. MSS-895864.

REFERENCES

1. Hashish, M., "Visualization of the Abrasive Waterjet Cutting Process," Experimental Mechanics, Vol. 24, 1986, pp. 159-169.

2. Hashish, M., "Machining of Advanced Composites by Abrasive Waterjet," Manufacturing Review, vol. 2, 1989, pp. 142-150.

3. Zeng, J., "Mechanisms of Brittle Material Erosion Associated with High Pressure Abrasive Waterjet Processing -- A Modeling and Application Study," Ph.D. Dissertation, University of Rhode Island, 1993.

4. Raju, S., "Modeling of Hydro-Abrasive Erosive Wear during Abrasive Waterjet Machining," Ph.D. Dissertation, University of Washington, 1994.

5 Daniel, I. M., Rowlands, R. E. and Labus, T. J., "Photoelastic Study of Water Jet Impact," Proceedings of the 2nd International Symposium on Jet Cutting Technology, 2nd-4th April, 1974, Cambridge, UK.

6. Daniel, I. M., "Experimental Study of Water Jet Impact on Rock and Rocklike Materials," Proceedings of the 3rd International Symposium on Jet Cutting Technology, 11th-13th May, 1976, Chicago.

7. Ramulu, M., "Dynamic Photoelastic Investigation on the Mechanics of Waterjet and Abrasive Waterjet Machining," Optics and Lasers in Engineering, 19, 1993, pp. 43-65.

8. Ramulu, M., and Wong, K. P., "Preliminary Investigations of Abrasive Waterjet Piercing process by Dynamic Photoelasticity," International Journal of Water Jet Technology, Vol. 1, No. 2, Sept. 1991, pp. 53-63.

9 Ramulu, M., Yeh, H., and Raju, S.P., Photoelastic Investigation of Jet Piercing Process," Proceedings of the 6th American Waterjet Conference, 1991, pp. 1-15.

10. Yeh, H., Wang, F.X, and Ramulu, M., " An Optical Investigation on the Abrasive Waterjet Penetration Process," Proceedings of the 7th American Waterjet Conference, Vol. 1, 1993, pp. 65-70.

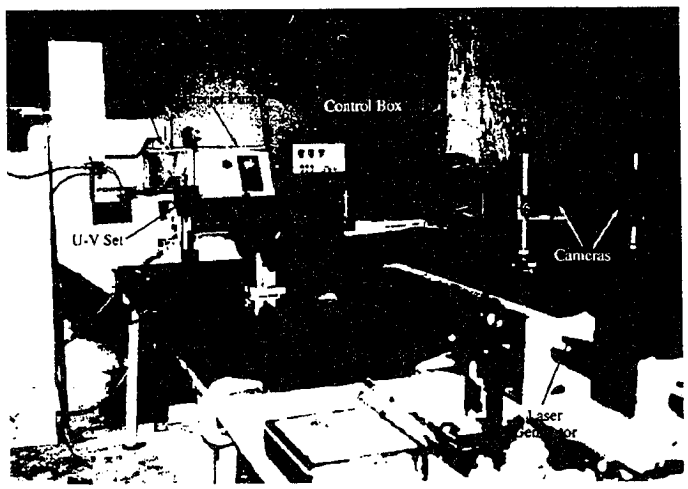

Figure 1 Photograph of the Experimental Setup

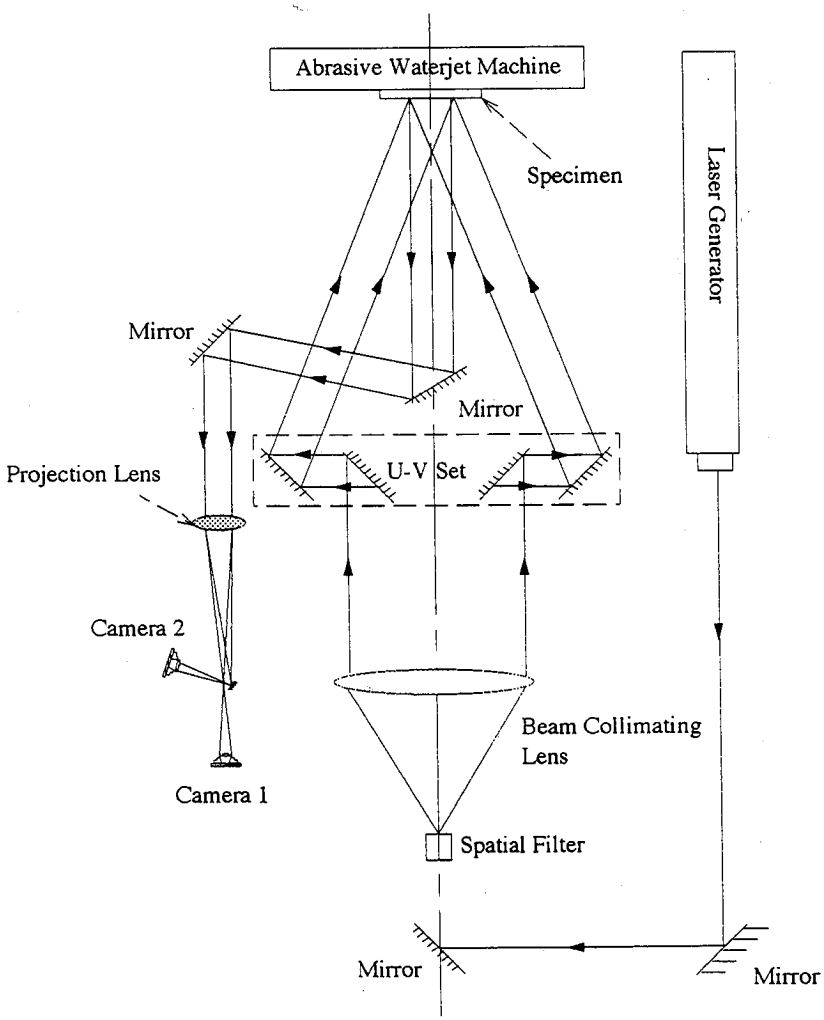

Figure 2 Schematic Diagram of the Abrasive Waterjet Optical Experiment Setup

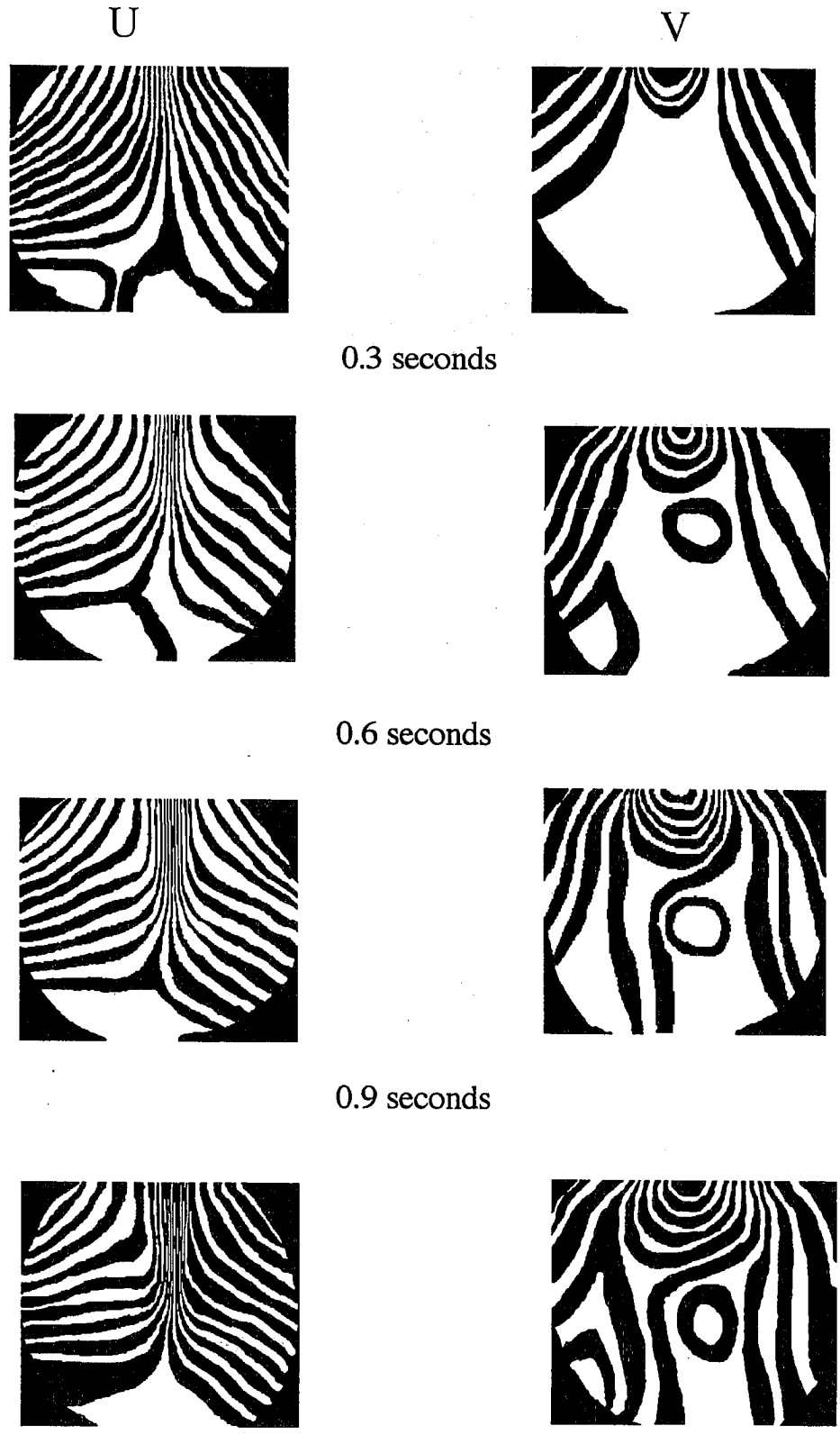

Figure 3 Typical Moire Fringe Patterns of the Displacement Fields in Polycarbonate Material

0.3 seconds

0.5 seconds

0.7 seconds

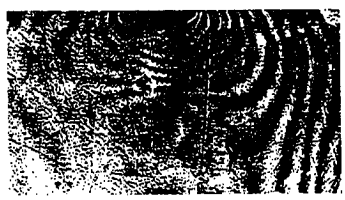

0.9 seconds

1.3 seconds

Figure 4 Typical Moire Fringe Pattern of V-Displacement Fields in Polycarbonate Material

t=0.75 sec.

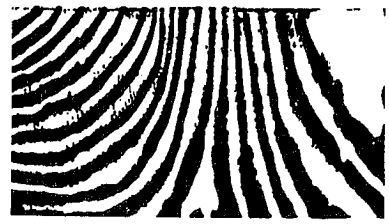

t=1.5 sec.

t=2.5 sec.

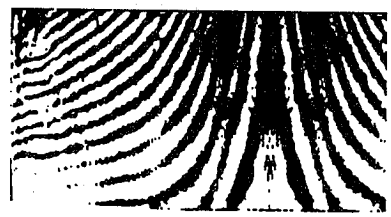

t=3.0 sec.

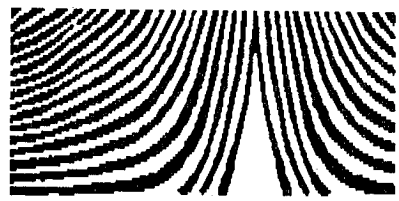

Figure 5 Typical Moire Fringe Pattern of U-Displacement Fields in Alumina AD99

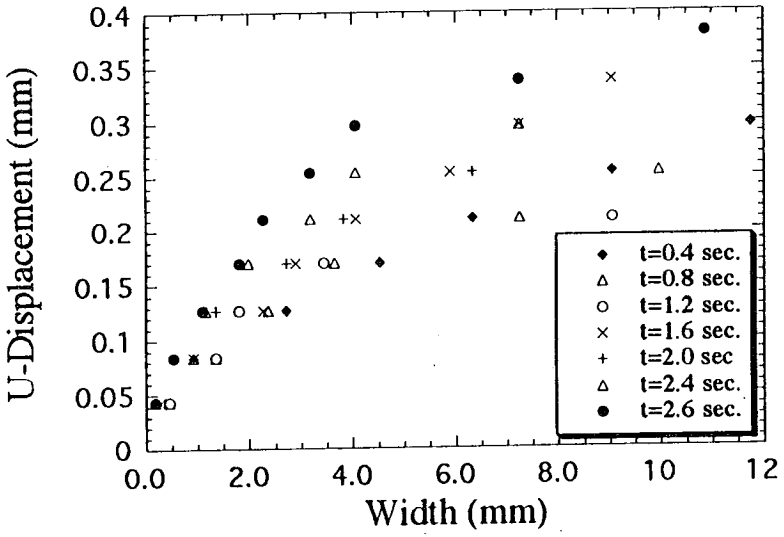

a) U field Displacement vs. width

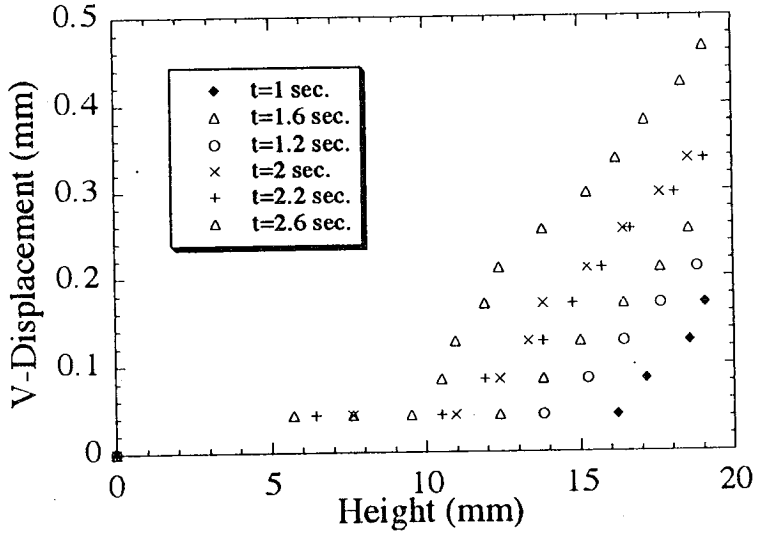

b) V Field Displacement vs. height

Figure 6 U and V fields in polycarbonate

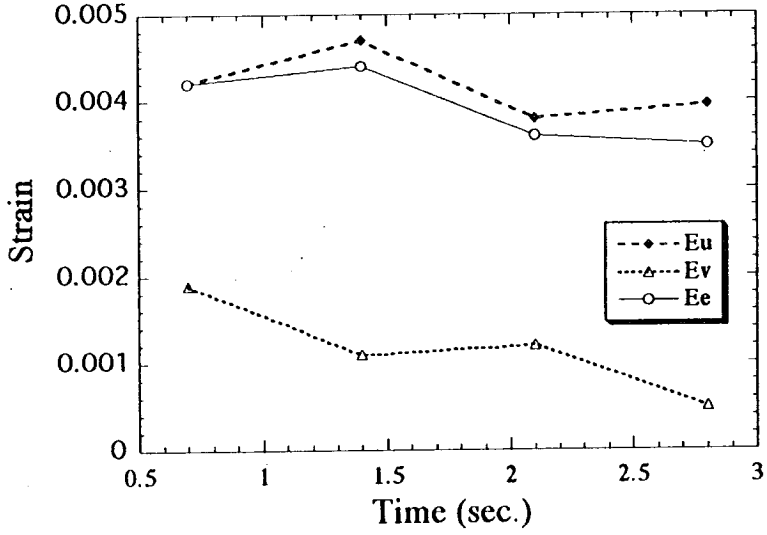

Figure 7 Strains associated with jet penetration process

Index Of Authors